Generation of coordination architectures from dynamic covalent ligand libraries

Jan Holub

▶ **To cite this version:**

Jan Holub. Generation of coordination architectures from dynamic covalent ligand libraries. Other. Université de Strasbourg, 2016. English. NNT : 2016STRAF060 . tel-01531327v2

HAL Id: tel-01531327

https://theses.hal.science/tel-01531327v2

Submitted on 6 Jun 2017

HAL is a multi-disciplinary open access archive for the deposit and dissemination of scientific research documents, whether they are published or not. The documents may come from teaching and research institutions in France or abroad, or from public or private research centers.

L'archive ouverte pluridisciplinaire **HAL**, est destinée au dépôt et à la diffusion de documents scientifiques de niveau recherche, publiés ou non, émanant des établissements d'enseignement et de recherche français ou étrangers, des laboratoires publics ou privés.

UNIVERSITÉ DE STRASBOURG

ÉCOLE DOCTORALE DES SCIENCES CHIMIQUES

INSTITUT DE SCIENCE ET D'INGÉNIERIE SUPRAMOLÉCULAIRE

UMR 7006

THÈSE présentée par :

Jan Holub

soutenue le : **28 Septembre 2016**

pour obtenir le grade de : **Docteur de l'Université de Strasbourg**

Discipline/ Spécialité : CHIMIE

Generation of Coordination Architectures from Dynamic Covalent Ligand Libraries

THÈSE dirigée par :
[M. LEHN Jean-Marie] Professeur Émérite, Université de Strasbourg

RAPPORTEURS :
[Mme. FROMM Katharina M.] Professeur, Université de Fribourg
[M. ALBRECHT Markus] Professeur, Université de RWTH Aachen

EXAMINATEUR :
[M. SAUVAGE Jean-Pierre] Professeur Émérite, Université de Strasbourg

TABLE OF CONTENTS

ACKNOWLEDGEMENT

I would like to thank to Prof. Jean-Marie Lehn for accepting my candidacy and giving me the opportunity to do my PhD in his group. It was great experience and good lesson which considerably broadened my horizons and went beyond the frontiers of science. I would like in particular highlight his never fading enthusiasm, inspiring guidance and his boundless way of thinking.

Rád bych poděkoval a tuto práci věnoval mým dvěma dědům, kteří ve mě probudili lásku k přírodě a vědě jako takové.

Rád bych poděkoval i zbytku rodiny za podporu, zázemí a tu trochu teplých motivačních slov.

The special acknowledgement goes to my high school chemistry teacher Mgr. Poštová for she has the biggest credit in my choice of the chemistry as a field of study.

I would like to thank Petr and Katka Kovaříčkovi for their big help and guidance in my beginnings. I cannot imagine it without you. Dokonce ti Petře odpouštím i tu poznámku ve tvém poděkování.

My special thanks, acknowledgement and respect goes to Prof. Jack Harrowfield, Dr. Jean-Luis Schmitt, Dr. Sebastian Dhers, Dr. Petr Kovaříček, Dr. Jean-Francois Ayme and Dr. Karolína Flídrová for dealing with my gibberish and giving this work beginning and end. It was never my plan to have it so long.

ABSTRACT

This thesis in four chapters describes the employment of Dynamic Combinatorial Chemistry (DCC) of imine-based dynamic covalent bonds (-C=N-) under the governance of coordination chemistry to form different metallosupramolecular architectures and responsive functional systems.

The first introductory chapter talks about the principles of DCC and basic characteristics of imine based dynamic bonds. The short historical excursion reveals joint historical path of combinatorial chemistry and imines which contributed to the establishment of DCC. This chapter also exposes close relationship between imines and coordination chemistry, a common element of all three following chapters. As the reversibility of the imine condensation reaction is a central mechanism in imine-based DCC, the mechanism of the imine formation is discussed, as well as factors influencing it, such as catalysis and kinetic/thermodynamic/factors.

The second chapter describes the assembly of rectangular metallosupramolecular arrays or *grids*. At the beginning of the chapter the work focuses on the introduction of suitable functional groups on the periphery of the ligand backbone. The substitution was chosen with special regards to imine chemistry and the potential application in assembly of large 2D arrays of grids. A short study focuses on the description of photophysical properties of a bishydrazone family of grids ligands. The rest of the chapter describes unintendedly discovered molecular grids which offer interesting directionality of the functional groups on the grids periphery. The research here focused especially on the preparation of the suitable building block for the "grid of grids" assembly, a special type of grid array.

The third chapter talks about another evergreen architecture in coordination chemistry - *helicates*. The chapter starts with the description of our search for simple and easily tuneable dynamic precursors for helicate ligands. The focal point was to have easy access to various helical architectures from both octahedral and tetrahedral coordinating metal cations. The basic dynamic studies concerning the constitution of the ligands as well as shape of the helicate are also included. The second part present attempts at obtaining the right imine ligands for dynamic assembly of trinuclear helicates. We envisaged that such ligands could be used as model

compounds to study "*supramolecular programming"*, a principle which allows to access different structures starting from the same ligand depending on the presence and/or ratios of different metals.

The fourth chapter deals with the response of complex mixtures of imines in regard to the presence of complexing metal cation(s). Different metal cations can have different impact on the library distribution. When this impact causes strong amplification of some constituents, in comparison to the initial metal-free state and providing that this new distribution is stable even after removal of the metal, it is possible to talk about information processing operations: training, storage, recall, and erase. Our goal was to design a system which would be able to store the information about two orthogonally coordinating metalo-effectors. After this was achieved, the relationships between the individual members of the library were subjected to mechanism investigation, providing interesting insight to the relationships between individual constituents in the mixture. Even though this chapter is highly conceptual it holds great significance in the field for future studies of the systems under thermodynamic governance.

Conclusions and suggestions for future work are presented in chapter five. This work provided several interesting compounds suitable for future studies, such as aldehyde functionalized grids (chapter two), dynamic building block for trinuclear helicates (chapter three) and a novel multi responsive system able to be trained for information storage (chapter four).

Final chapter six consists of the experimental part where analytical data for individual compounds prepared are summarized together with their respective synthetic procedures.

ABBREVIATIONS

AcCN	Acetonitrile
Bipy	2,2'-Bipyridine
CDC	Constitutional Dynamic Chemistry
CDN	Constitutional Dynamic Network
CITS	Current-imaging-tunneling spectroscopy
COSY	Correlated spectroscopy
Da	Dalton (g/mol)
DCC	Dynamic Combinatorial Chemistry
DCL	Dynamic Combinatorial Library
DMSO	Dimethylsulphoxide
DOSY	Diffusion-ordered spectroscopy
EDTA	Ethylenediaminetetraacetic acid
Eq.	Equivalent
ESI-MS	Electrospray ionisation mass spectrometry
HOPG	Highly oriented pyrolytic graphite
mM	Millimolar, 10^{-3} mol/l
Mw	Microwave irradiation
NMR	Nuclear Magnetic Resonance
NOE	Nuclear Overhauser effect
NOESY	Nuclear Overhauser effect spectroscopy
Paphy	Pyridine-2-carbaldehyde-2-pyridylhydrazone
ppm	Parts per million
STM	Scanning Tunneling Microscope
Terpy	2,2′:6′,2″-Terpyridine
TFA	2,2,2-Trifluoroacetic acid
TfO^-	Triflate = Trifluoromethanesulfonate ($CF_3SO_3^-$)
Uv-VIS	Ultra-violet-visible

RESUME

PROJET DE « LA GRILLE DE GRILLES »

Les grilles moléculaires ont montré leur utilité dans divers domaines de recherche: réponse à des stimulus chimiques ou physiques, dispositifs électroniques/spintroniques à l'échelle nanométrique et applications biologiques.[1] L'exemple le plus simple d'un complexe de type grille est un complexe bidimensionnel où quatre ions métalliques sont liés à quatre ligands dans un arrangement perpendiculaire noté grille [2x2] (*Figure 1, gauche*).

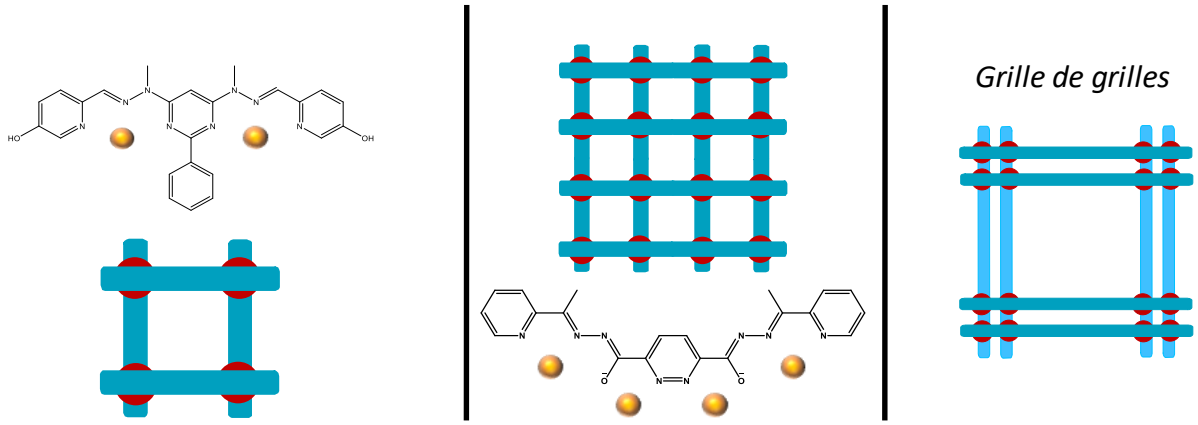

Figure 1. *vue schématique de (gauche) grille [2x2] ; (milieu) grille [4x4] ; (droite) grille de grilles*

Lorsque des ligands avec n sites de coordination (n>2) sont utilisées en conjonction avec n^2 ions métalliques, l'architecture est une grille d'ordre élevé de dimension [*n* x *n*]. Ces grilles d'ordre élevé peuvent aussi être vu comme l'assemblage de n/2 grilles $[2x2]^2$, aussi appelé « grille de grilles » (*Figure 1, droite*).

L'utilisation de ces grilles d'ordre élevée dans la conception de dispositif nanoélectronique est limitée par la trop grande proximité des ion métalliques entre eux dans ce type d'architecture. Pour pallier à ce problème ce travail de thèse propose d'intégrer des jonctions plus longues entre le motif [2x2] dans des grilles d'ordre élevé.

Le motif de base [2x2] de notre grille de grilles a été conçu à partir de travaux antérieurs effectués par notre groupe,[3] combinés à des diols simples tels que 1,4-butanediol (**GR7a**), 1,5-pentanediol (**GR7b**), éthylèneglycol (**GR7c**), 1,3-propandiole (**GR7d**) et hydroquinone

(**GR7e**), qui seront utilisés comme jonction (*Figure 2*). La synthèse de la première génération de ligands est décrite sur le *Figure 2*.

A partir du modèle du ligand **GR7** une bibliothèque de ligand contenant diverses jonctions a été préparée. Dans le cas du **GR7x**, des diols appropriés ont été choisis au lieu du butane-1,4-diol. La formation des « grilles de grilles » correspondantes aux ligands mentionnés ci-dessus a été étudié dans l'acétonitrile *via* l'addition de triflate de zinc à 70°C.

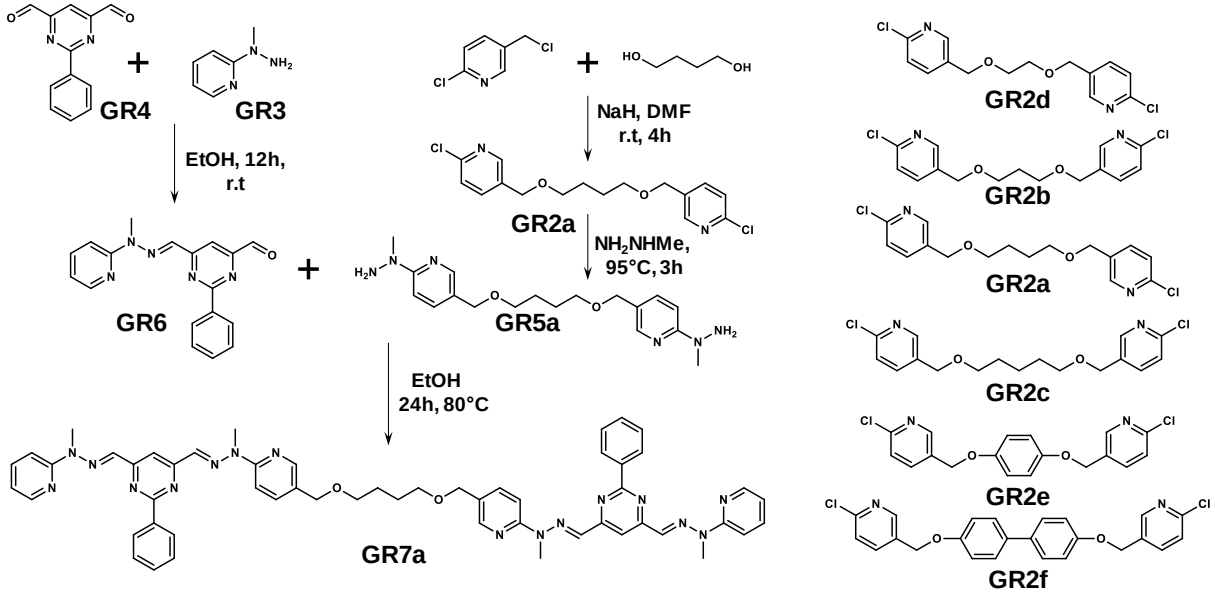

Figure 2*: La voie de synthèse générale pour des ligands du projet « la grille des grilles ».*

Les complexes résultant ont été caractérisé par diffraction des rayons-X, spectroscopie RMN et spectroscopie de masse (ESI-MS). Même si les complexes fournissent des spectres ^{1}H RMN relativement clairs, suggérant une haute symétrie du complexe, leur caractérisation non ambiguë n'a pas été possible malgré l'utilisation d'une combinaison de plusieurs techniques de RMN (expériences 2D, DOSY) et de spectrométrie de masse. Seule la diffraction des rayons X pourrait nous donner une réponse définitive sur la forme du complexe (*Figure 3*). Des monocristaux adaptés à la diffraction des rayons X ont été obtenu dans le cas des grilles **GR7c** et **GR7e**, montrant la formation de simples grilles [2x2] dans lequel deux ligands sont repliés sur eux même au lieu de la « grille de grilles » attendue.

À partir de ces structures cristallines, il est clair que l'utilisation d'une jonction flexible -O-CH_2- ne permet pas la formation d'une grille de grilles (*Figure 3*). Néanmoins, la technique RMN de diffusion DOSY indique la présence d'une espèce plus volumineuse que la grille [2x2] observée dans le cristal. Les structures **GR7c** et **GR7e** nous ont donné de précieuses indications quant aux exigences en termes de rigidité de la jonction entre les sites de coordination du ligand.

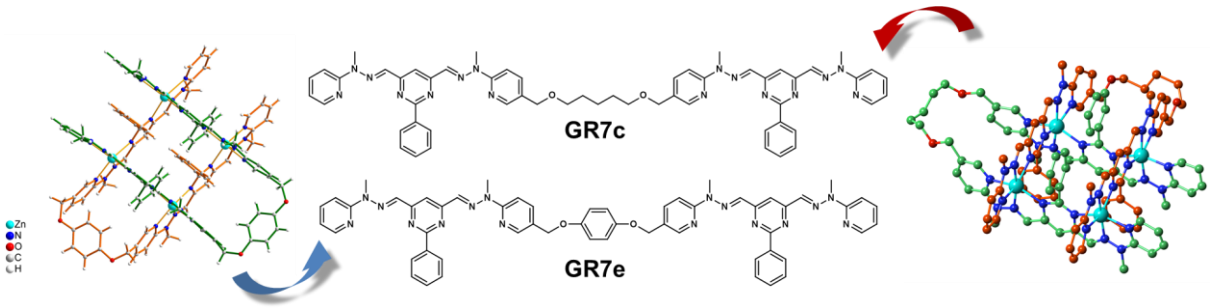

Figure 3: *Les structures obtenues du type "Bend" du projet «grille des grilles ».*

Une seconde génération de ligands a été préparés en utilisant des jonctions plus rigides (F*igure 4*). Malheureusement, ces composés se révélés très peu soluble et par conséquent aucun des ligands de cette génération n'a pu être utilisé pour former des grilles.

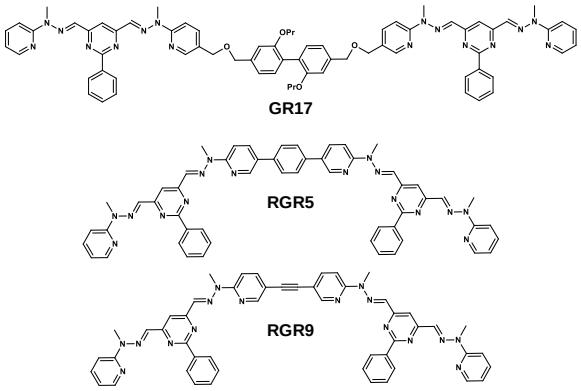

Figure 4*: La deuxième génération de ligands*.

En conclusion, une bibliothèque de ligands variant en termes de flexibilité et de solubilité a été préparée. Néanmoins, les grilles de grilles attendues n'ont pu être obtenues, seul des grilles [2x2] contenant deux ligands repliés sur eux même ont pu être isolées. L'utilisation de ligands plus rigides a été infructueuse. Pour cette raison, une approche différente a été choisie récemment et est actuellement étudiée.

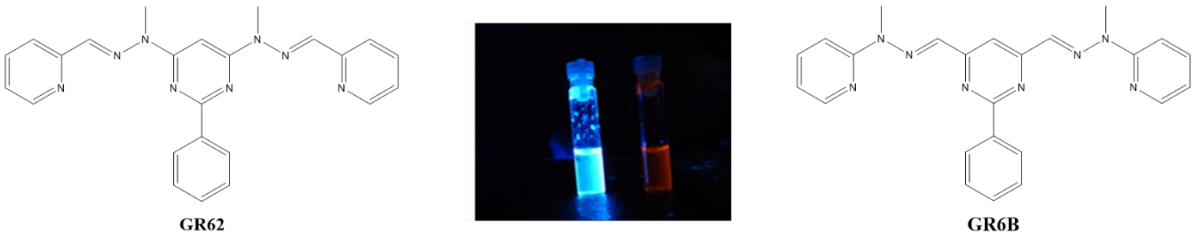

Figure 5: *Les couleurs différentes de lumière émise par deux grilles simples avec une symétrie différente de la liaison hydrazone.*

De plus au cours de ce travail certaines des grilles de zinc synthétisées (**GR62**, **GR6B**) ont démontrées une fluorescence modérée en solution dans l'acétonitrile (*Figure 5*). Un changement intéressant de la lumière émise, du bleu au rouge, est observé lorsque la 2-phenyl-4,6-N-methylpyrimidine hydrazine (**GR62**) est utilisée au lieu de la 2-phenyl-4,6-pyrimidinedicaroxaldehyde (**GR6B**) (*Figure 5*). Les dérivés de **GR62** fournissent une émission bleue avec une efficacité allant jusqu'à 60% et les dérivés du **GR6B** ont quant à eux une émission orange-rouge avec une efficacité faible d'environ 2%.

HELICES

Les hélices simples

Au cours du travail sur le projet « grille de grilles » un autre projet intéressant a émergé. Lorsque les jonctions du projet précédant sont substituées de part et d'autre par un simple aldéhyde de pyridine, des ligands potentiellement intéressant pour la formation d'hélices sont obtenus. En variant la rigidité et la longueur de la jonction plusieurs types de ligands ont été synthétisés et étudiés pour la formation d'hélices (*Figure 6*).

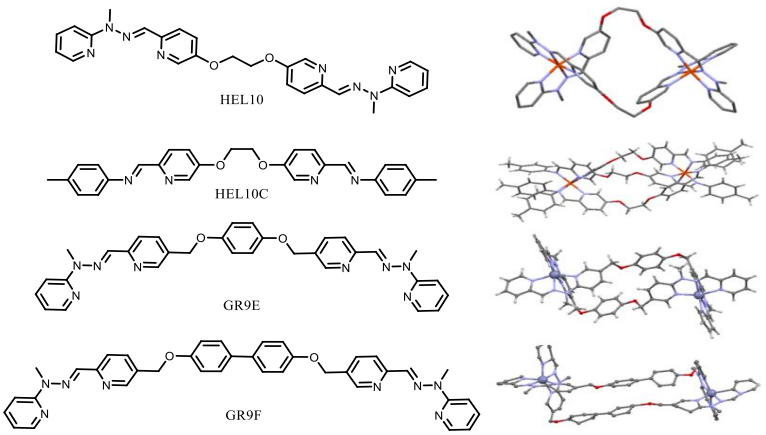

Figure 6*: Les ligands simples et les structures cristallines correspondants*

Les hélices composées

L'objectif de ce projet est d'étudier l'assemblage dynamique d'hélices hétérométalliques dans lequel les ligands contiennent deux sites de coordination différents, l'un tridentate (**T**), et l'autre bidentate (**B**). Les sites tridentates sont basés sur des dérivés de terpyridine tels que PAPHY (*Figure 7*) et les sites bidentates sont basés sur des dérivés de bipyridine tels que des imines de pyridine.

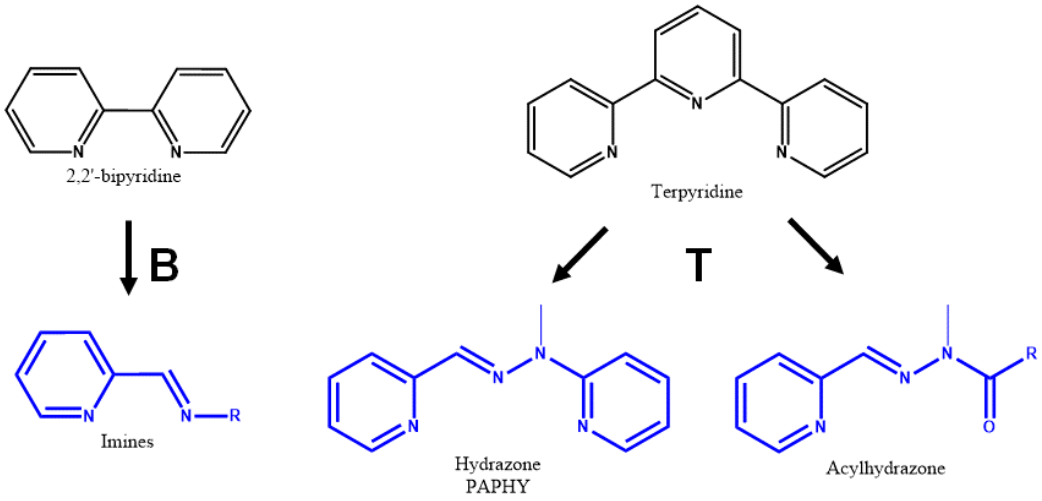

Figure 7: *Les motifs de coordination des groupes **T** (terpyridine) et **B** (bipyridine) et leurs analogues dynamiques.*

On s'attend à ce que différentes architectures soient obtenues en fonction du type d'ion métallique utilisé. Un ligand (**CN13**, *Figure 8*) portant deux sites de coordination différents a été préparé à partir de deux équivalents de carboxaldéhyde de pyridine et d'une jonction contenant à la fois un groupement amine et un groupement hydrazine de pyridine, donnant respectivement le site de coordination **B** et **T**. La chimie de coordination du ligand **CN13** a été étudié avec diverses métaux tels que Cu(II)/Cu(I), Fe(II), Pb(II), Zn(II) et Ag(I).

Malgré l'existence dans la littérature d'exemples intéressants d'architecture formées avec des ligands similaires (mais non dynamiques) avec du Cu(II) et Fe(II),[4] nous n'avons pas obtenu de résultats concluants avec ces métaux. Malheureusement dans ces différents exemples, la spectroscopie RMN ne s'est montrée d'aucune utilitée pour identifier les complexes formés. Seule la présence d'espèces $\mathbf{L_2M_2}$ a pu être prouvée par spectrométrie de masse. Cette espèce pourrait correspondre au cas où deux ligands sont positionnés tête-bêche autour de deux ions métalliques.

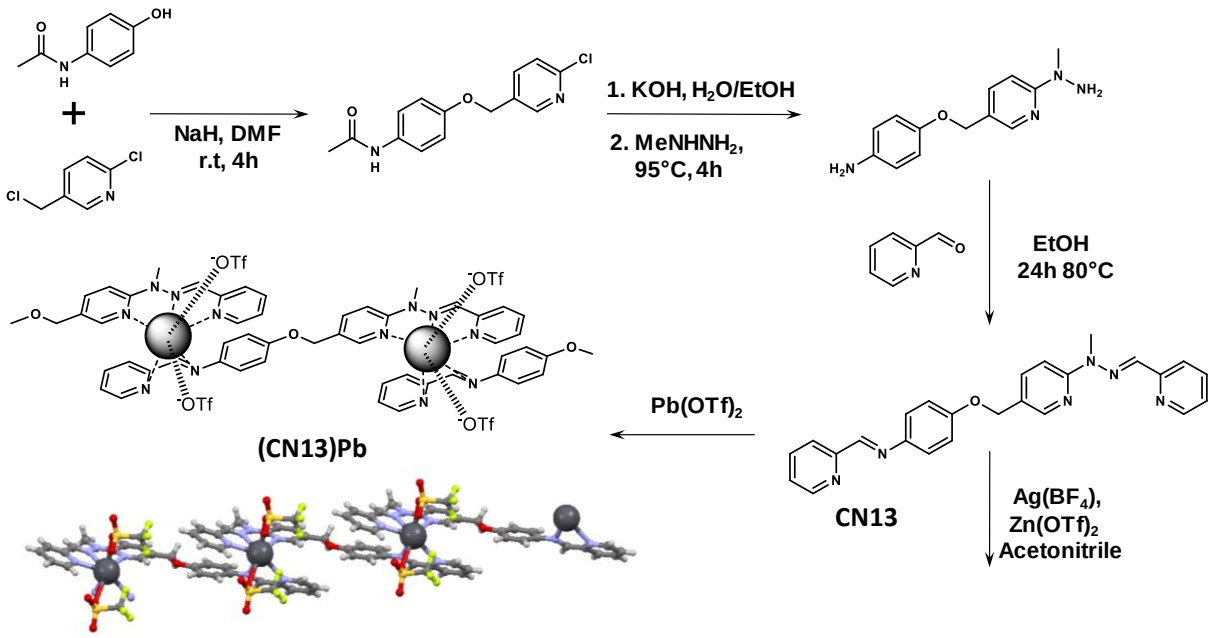

Figure 8: *Le chemin synthétique du ligand **CN13** avec les unités **T** et **B** et la structure cristalline de son polymère en coordination avec le Pb(II).*

Dans le cas de Pb(II), le complexe formé (*Figure 8*) n'est pas une hélice, mais un polymère de coordination où le Pb(II) est coordiné á sept atomes, trois N du motif paphy d'un ligand, deux N du motif imine de la pyridine d'un l'autre ligand, et deux O provenant de contre-ions trifaltes.

En parallèle la formation de complexes bimétalliques a été étudiée. Plusieurs combinaisons de métaux ont été testées, Zn(II) et Fe(II) pour le site **T** et Ag (I) et Cu(I) pour le site **B**. Jusqu'à présent, seul la combinaison Zn(II) et Ag(I) a été étudiée en détails. Les spectres RMN de cette

structure suggèrent la présence d'une seule espèce correspondant au complexe **$L_2M_2M'_2$**, ce qui est aussi confirmé par spectrométrie de masse et RMN DOSY. Toutefois, les spectres de masse montrent aussi la présence d'une faible quantité de **$L_4M_2M'_2$**. Cependant, la confirmation indéniable de la structure du complexe nécessiterait la résolution structurale par rayons X des complexes.

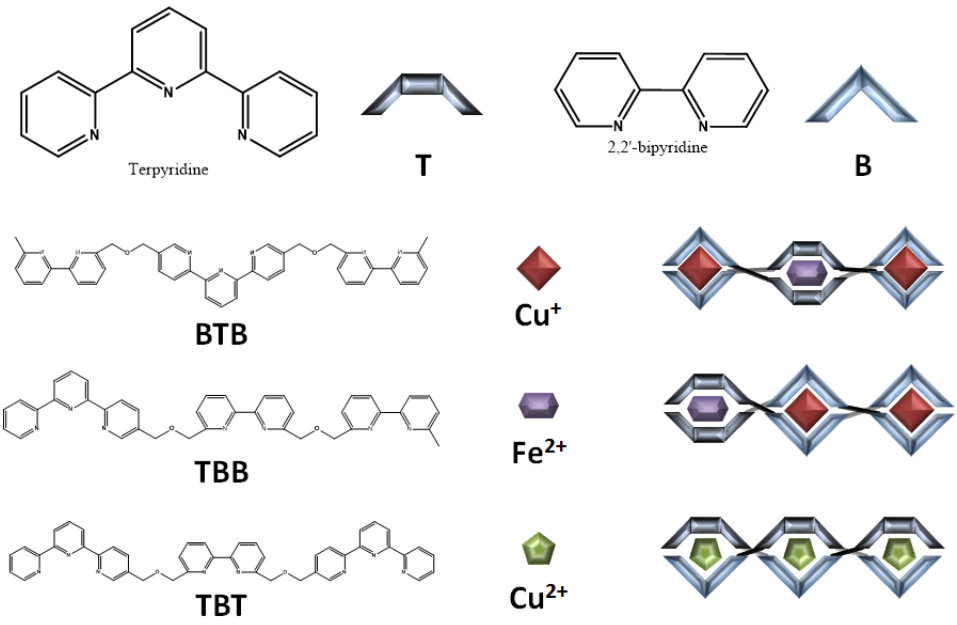

Figure 9: *Précédents travaux de notre groupe sur les mélanges complexes à base de complexes de coordination.*

En s'appuyant sur les résultats ci-dessus et les travaux précédant de notre groupe (*Figure 9*) nous envisageons d'étendre cette stratégie à des double hélices hétérometalliques à trois centres métalliques.[5] Pour cela nous prévoyons de remplacer les deux sites de coordination aux extrémités des ligands originaux par des sites dynamiques (DCC). Ainsi les terpyridines des ligands originaux seront remplacés par des pyridines hydrazones (PAPHY) et les bipyridines seront remplacées par les pyridines imines. Pour des raisons pratiques les sites centraux des ligands originaux ne seront pas changés car les unités PAPHY sont asymétriques, ce qui conduirait à un mélange compliqué d'isomères.

Deux ligands dynamiques ont été synthétisés et caractérisés, l'un contenant deux imines de pyridine **CN26** et l'autre contenant deux motif PAPHY **AS53** (*Figure 10*). Dans le cas du ligand **AS53** il a été possible d'assembler la double hélice de Zn(II) et de Cu(I) correspondante lorsque le ligand terpy-core est mélangé avec un équivalent de Zn(II), deux équivalents de Cu(I) et deux équivalents de 2-pyridinecarboxaldéhyde dans l'acétonitrile à 70 °C. Dans le cas du ligand **CN26** il n'a été possible d'assembler que l'hélice de Zn(II) et de Cu(I) correspondante à partir du ligand préformé et deux équivalents de Zn(II) et un équivalent de Cu(I). La structure de cette

hélice a été confirmée par diffraction des rayons X (*Figure 10*). Néanmoins, l'hélice de **AS53** ne peut pas être obtenu à partir de ses composants puisqu'il a été prouvé que les hydrazines de pyridine libres se lient au Cu(I) et catalysent très fortement son oxydation en Cu(II). Ce phénomène se manifeste par un changement de couleur de la solution du violet au vert. Pour cette raison, nous avons dû modifier le design de ligand.

Cette nouvelle génération de ligands **TBT** et **BTB** contient les mêmes noyaux terpyridine et bipyridine que la première génération mais les groupements sur les côtés ont été modifiés pour des aldéhydes de pyridines. Cela évite ainsi l'utilisation d'hydrazine de pyridine et permet de le substituer par son analogue l'acyle hydrazine ou le 8-aminoquinoléine.

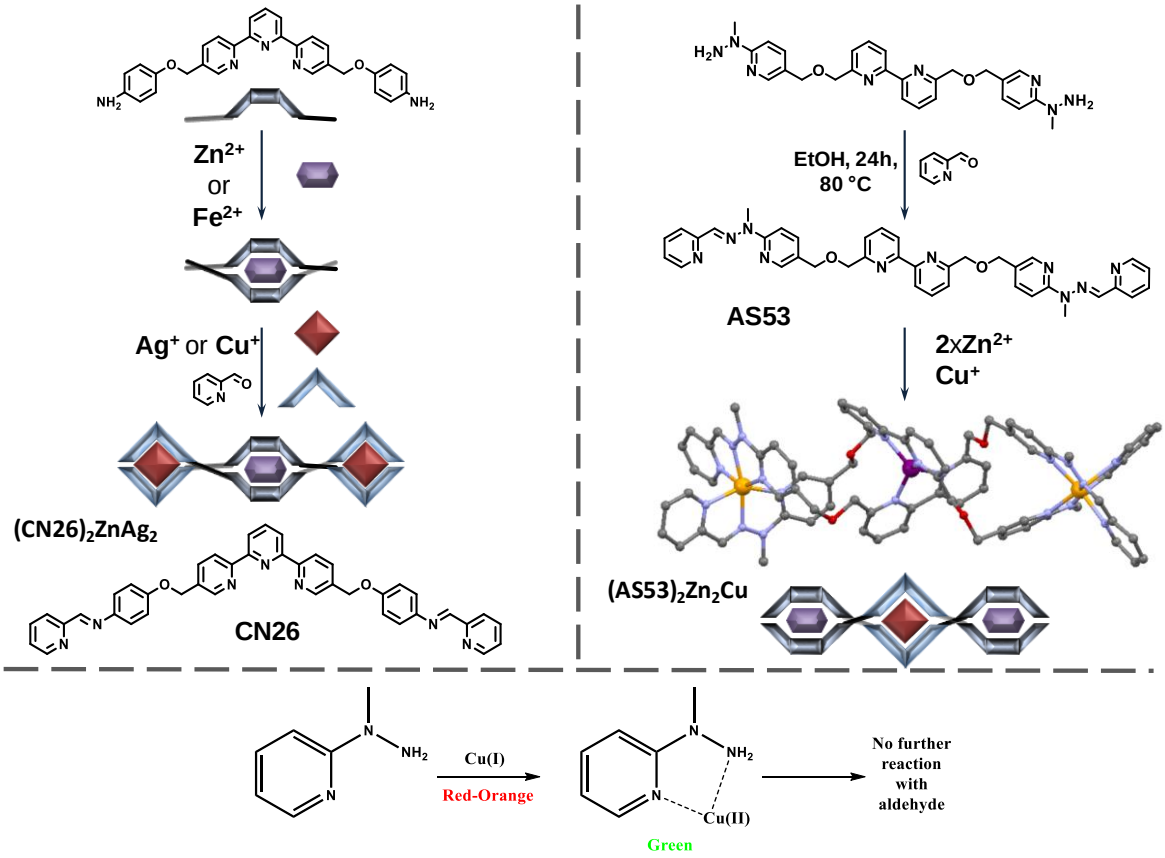

Figure 10*: L'idée initiale du projet d'hélices de coordination dynamiques et les raisons pour lesquelles elle ne fonctionne pas.*

A partir de cette nouvelle génération de ligand il a été possible de former les doubles hélices **MAF13**, **MAF10** et **GEN2BBB, GEN2BTB** (*Figure 11*) non seulement à partir des ligands préformés, mais aussi de façon dynamique à partir des composants. Pour cela, les noyaux centraux terpyridine ou bipyridine ont été mélangés avec respectivement l'acyle hydrazide pour former les sites dynamiques **T** et la *p*-toluidine pour former les sites dynamiques **B**, puis ce mélange a été traité avec différentes combinaisons de cations métalliques (Cu(I), Ag(I) et Zn(II), Fe(II)). La caractérisation exacte des hélices ainsi obtenues est en cours.

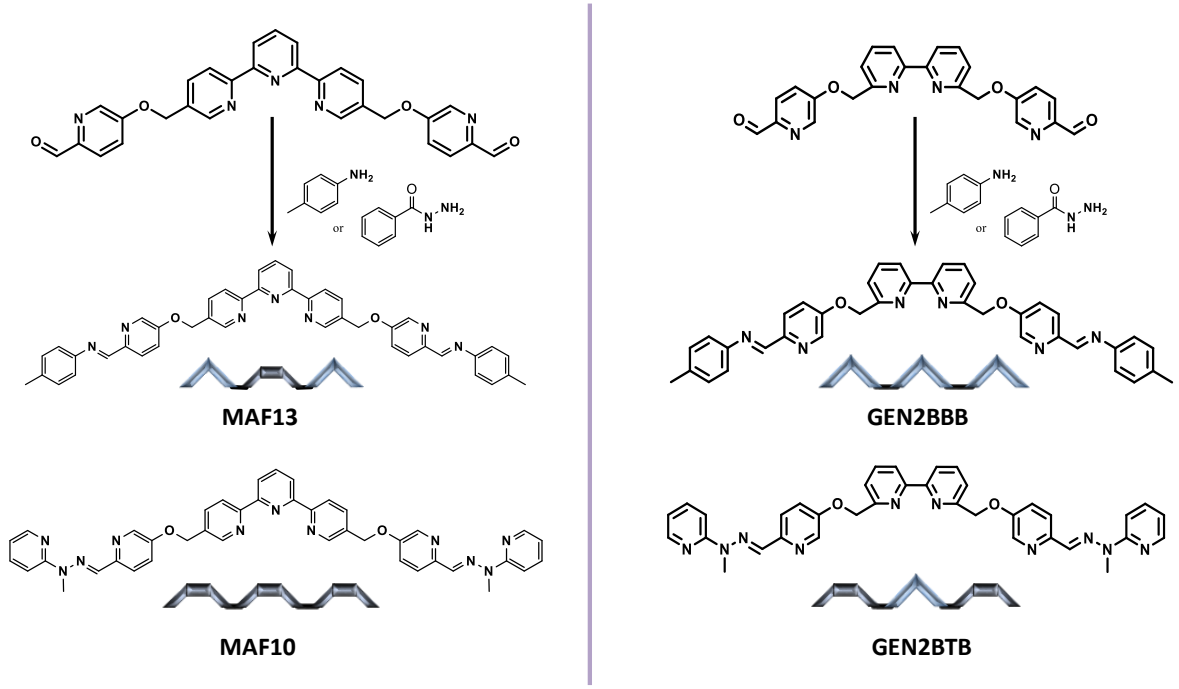

Figure 11: *La deuxième génération des ligands pour les mélanges dynamiques de coordination.*

DOUBLE FORMATION DE SYSTEME DYNAMIQUE

Les processus d'auto-assemblage permettent de produire des architectures fonctionnelles où l'information moléculaire de l'assemblée est stockée dans la structure covalente des composants et exprimée au niveau supramoléculaire à travers des algorithmes d'interaction spécifiques.[6] Une nouvelle étape consiste à la création de systèmes chimiques capable d'apprendre, autrement dit qui ne sont pas simplement programmés pour s'auto-assembler, mais qui sont aussi capable d'être entrainés à se souvenir d'un agent ayant causé leur assemblage au préalable.

Les membres d'une DCL (Dynamic Combinatorial Library/Libraire Combinatoire Dynamique) sont liés pour former un réseau constitutionnel dynamique qui interconnecte les constituants de la DCL à travers des relations agoniste/antagonist. Les opérations de formation du DCL sont accessibles via les changements entre les paires de constituants agonistes/antagonistes dans le CDN (Constitutional Dynamic Network). Les antagonistes sont les constituants (par exemple le **50AB** et le **50AB'**, *Figure 13*) qui partagent un composant (**50A**) et qui sont donc des

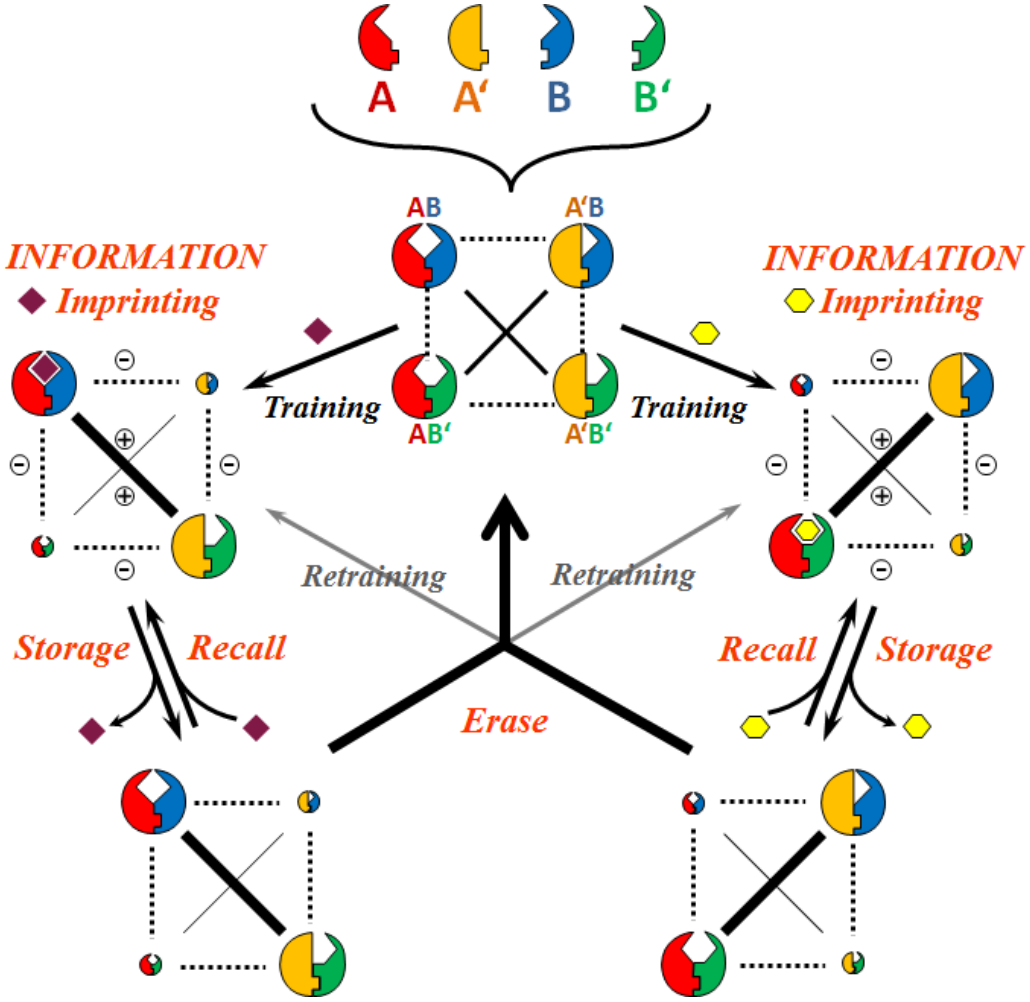

Figure 12: *Le modèle de « Double Dynamic Combinatorial Library » de deux paires orthogonales agonistes créées et recréées par la sélection des composants en réponse à deux cations.*

concurrents. La formation de l'un (**50AB**) se traduit par la réduction de l'autre (**50AB'**). De plus, les agonistes (par exemple le **50AB** et le **50A'B'**, *Figure 13*) sont des constituants sans composant commun. Ils ont une relation synergique, donc l'augmentation de l'un (**50AB**) implique également la formation de l'autre (**50A'B'**).[6 c, d] Les relations agoniste/antagoniste en réponse à l'interaction avec un effecteur (ici un cation métallique) est la clé du mécanisme de régulation permettant au DCL d'ajuster sa composition a l'équilibre.[7,8,9] Un tel DCL peut aussi s'adapter à deux (ou plusieurs) effecteurs différents (des cations métalliques).

En outre, la suppression de l'effecteur conduit à un état constitutionnel hors équilibre[10] conservant les informations sur l'effecteur dans sa distribution inchangée. On peut aussi dire que la mémoire du réseau correspond à un état hors équilibre. Les informations ainsi stockées pourront ultérieurement être effacées par la ré-équilibration des composants. De plus, des ions métalliques ayant des préférences de coordination différentes pourront entrainer une distribution différente des composants du DCL (*Figure 12*).

Le système doit combiner : i) la capacité à équilibrer les constituants du DCL en réponse à un effecteur(s) par un échange des composants ; ii) une stabilité suffisante pour retenir la distribution des constituants après le retrait de l'effecteur(s). Au moins l'un des constituants doit présenter ces caractéristiques. Dans notre système, les constituants à base d'imines utilisés échangent très facilement leurs composants. Les autres constituants à base d'acyle hydrazone sont quant à eux beaucoup plus résiliant à subir un échange de leurs composants mais sont toujours capables de répondre à un effecteur. La présence d'acyle hydrazone est donc d'une importance capitale pour fournir la barrière cinétique nécessaire à stabiliser les états hors équilibre générés après l'élimination du cation métallique, empêchant ainsi la ré-équilibration du système et permettant de conserver la mémoire/les informations du cation métallique.

a) *Équilibration* (*Figure 13) :* Notre CDL est générée à partir d'un mélange équimolaire ($1.25x10^{-5}$ mole, 25 mM) de quatre composants: du 6-phénylpyridine-2-carboxaldéhyde (**50A**), du 4-chlorobenzaldéhyde (**50A'**), du benzhydrazide (**50B**) et de la p-toluidine (**50B'**) dans l'acétonitrile. Le mélange est chauffé à 60 °C pendant 12 heures pour atteindre l'équilibre. Quatre constituants **50AB**, **50A'B'**, **50A'B**, et **50AB'** sont obtenus avec une distribution de 34/23/16/13 % respectivement ainsi que 14 % d'hydrolyse. (*Figure 13*) L'hydrolyse **50A'B'** fait partie de l'équilibre et ne peut pas être évité. De plus, il faut noter la présence de deux isomères du constituent **50AB**: E-**50AB** et Z-**50AB**, présent respectivement à hauteur de 40 % et 60 %. Cette observation est confirmée par la RMN 2D et les deux isomères sont comptés pour un dans la distribution globale des constituants de la DCL. La même distribution des constituants est obtenue dès que l'on commence depuis un mélange des quatre composants ou des paires de constituantes agonistes.

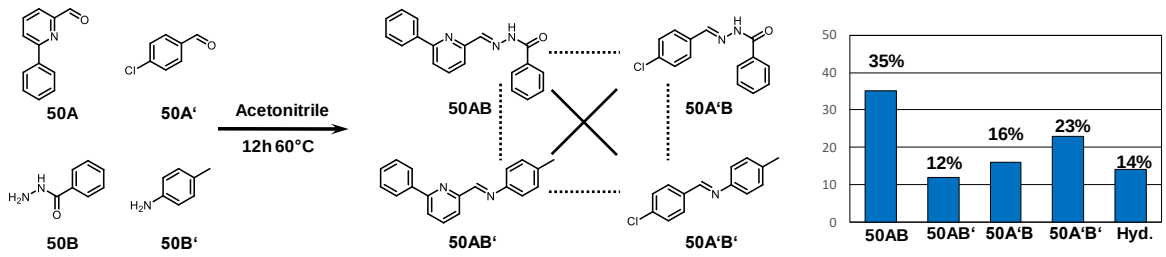

Figure 13*: La distribution des constituants du DCL à partir des composants en l'absence des cations métalliques.*

b) *Mémorisation/Formation (Figure 14) :* le système s'adapte très bien à l'ajout de cations Zn(II) malgré un certain niveau d'hydrolyse. La réaction est assez lente à température ambiante mais à 60 °C la réaction se termine en trois heures (*Figure 14*). Le Zn(II) peut être enlevé du milieu réactionnel par l'ajout de $(Et_4N)_2EDTAH_2$. Lorsque le zinc est enlevé il ne reste que des quantités négligeables de **50A'B** et de **50AB'** mais E-**50AB** reste formé.

c) Rappel (Figure 14) : après l'élimination des cations de Zn(II), le système est instruit et pourra se rappeler du zinc s'il est à nouveau ajouté. Cela devrait rendre l'organisation du réseau beaucoup plus rapide que lors du premier ajout de zinc (moins de 5 min. lors du second ajout contre 3 h lors du premier ajout) (*Figure 14*).

d) *Effacement (Figure 14) :* suite au retrait du cation métallique le système est hors équilibre mais conserve sa distribution pendant 12 heures à 23 °C en raison de la lenteur de l'échange de l'acyle hydrazone du constituent **50AB** de la bibliothèque (voir ci-dessus). En

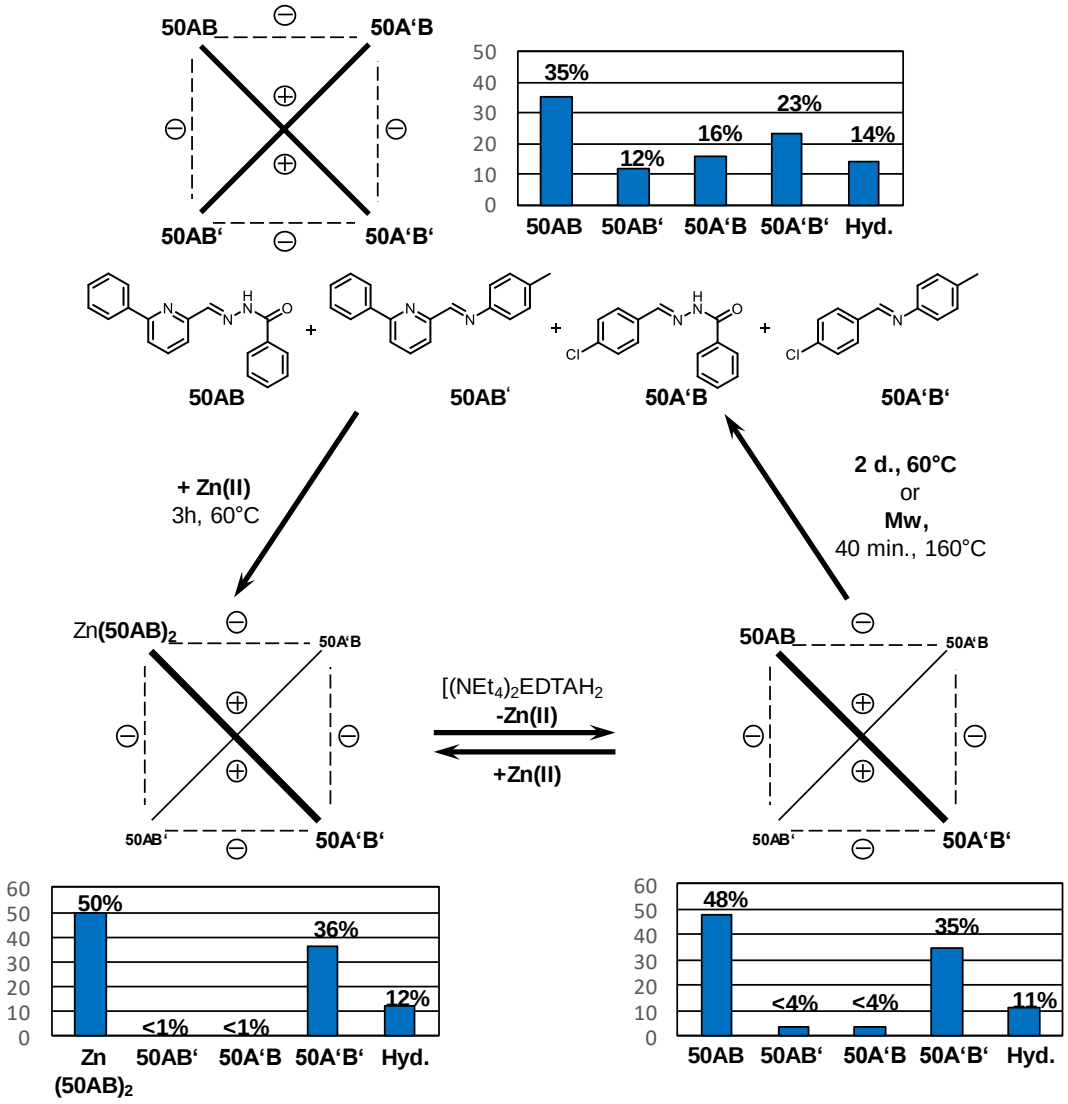

Figure 14 : *La formation du Zn entraîne la DCL et la distribution après l'addition du $Zn(OTf)_2$ à un mélange de quatre constituants,* ***50AB***, ***50A'B'***, ***50A'B***, ***50A'B'*** *(formation, en haut à gauche vers le bas), qui lors de l'enlèvement des cations conserve essentiellement sa composition de DCL-métal-libre (stockage de l'information, en bas à gauche à droite); le rappel par l'addition du zinc(II) (en bas de droite à gauche) et l'effacement de DCL-sans-métal par l'échauffement (de bas à droite en haut); le retour au conduit thermodynamiquement á l'état initial.*

effet, des conditions plus vigoureuses sont nécessaires pour effacer toute l'information du système et retourner à un état thermodynamiquement stable correspondant au mélange qui peut être obtenu suite au chauffage de la bibliothèque pendant plusieurs jours à 60 °C en l'absence d'effecteur (ou pendant 40 min à 160 °C dans un four à micro-ondes 270 W) (*Figure 14*).

e) *Rééducation* : si du triflate (TfO^-) de Cu(I) est ajouté à l'état hors équilibre obtenu suite au retrait du Zn(II) et que le système est chauffé à 60 °C pendant 12h on passe directement de

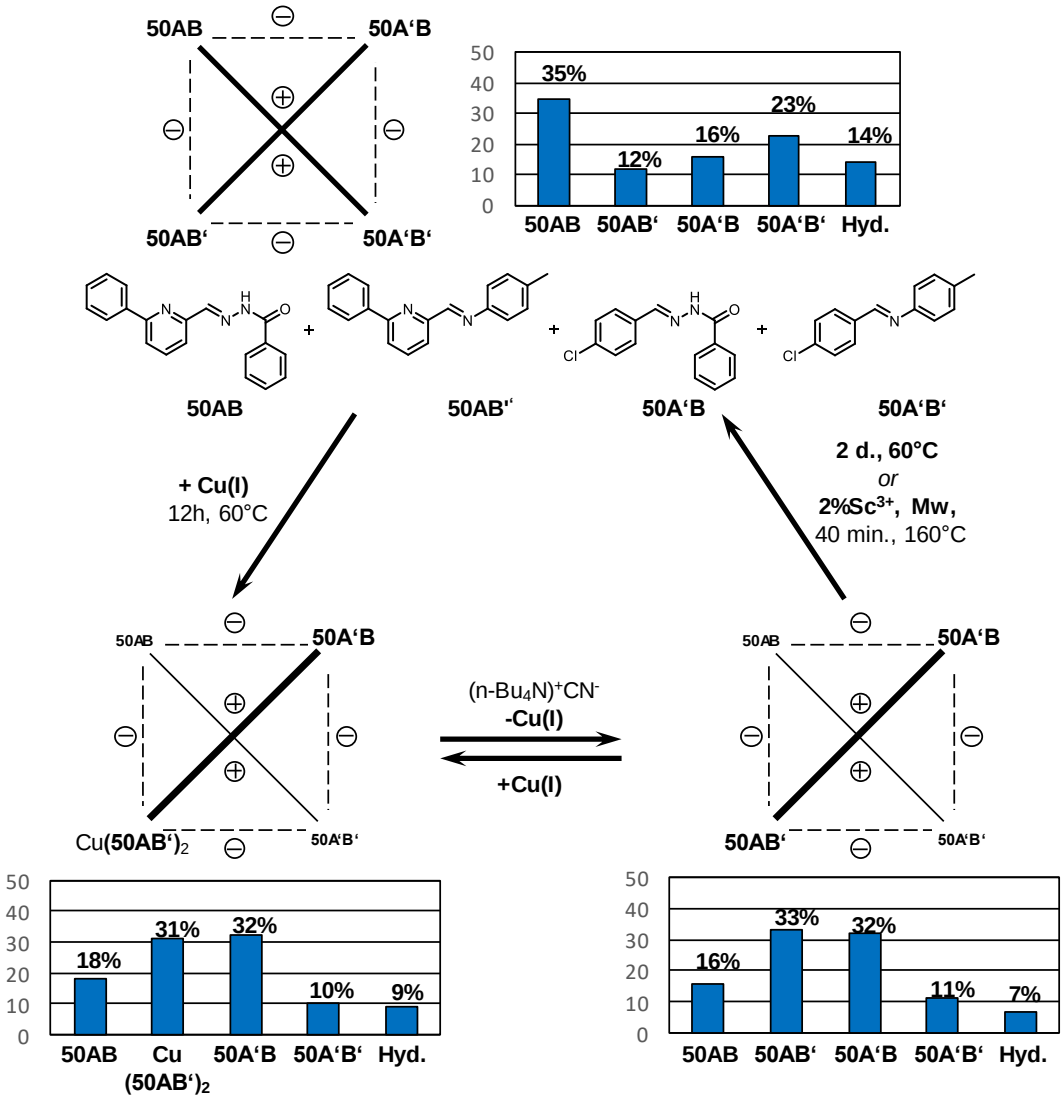

Figure 15: *La formation du Cu entraîne le DCL et la distribution après l´addition du CuOTf à un mélange de quatre constituants* ***50AB, 50A'B', 50A'B*** *et* ***50AB'*** *(formation, en haut à gauche vers le bas), qui lors de l'enlèvement de cations conserve essentiellement sa composition dans le métal -libre DCL (stockage de l'information, en bas à gauche à droite); le rappel par l´addition du Cu(I) (en bas de droite à gauche) et l'effacement du DCL sans métal par le chauffage (de bas à droite en haut); le retour au conduit thermodynamiquement á l'état initial.*

la distribution typique du zinc à la distribution typique du cuivre sans qu'il soit nécessaire de passer par une étape d'effacement (*Figure 16*).

f) *Deuxième effecteur - Cu(I) (Figure 15) :* au lieu d'utiliser un cation Zn(II) comme effecteur on peut utiliser un cation Cu(I) (*Figure 15, 16*). Le traitement du mélange de départ avec du CuOTf ($0.625x10^{-5}$ mole, 12.5 mM) suivi de son équilibration à 60 °C pendant 12 h conduit à un changement marqué de la distribution du réseau, qui se distingue cette fois par la formation du complexe tétraédrique Cu(**50AB'**)$_2$. Lorsque le cuivre est utilisé comme effecteur le ligand du Cu(I) **50AB'** et son agoniste **50A'B** sont amplifiés. Il s'agit de constituants antagonistes à ceux obtenus avec le zinc. La distribution obtenue est 10/18/31/32/9 %

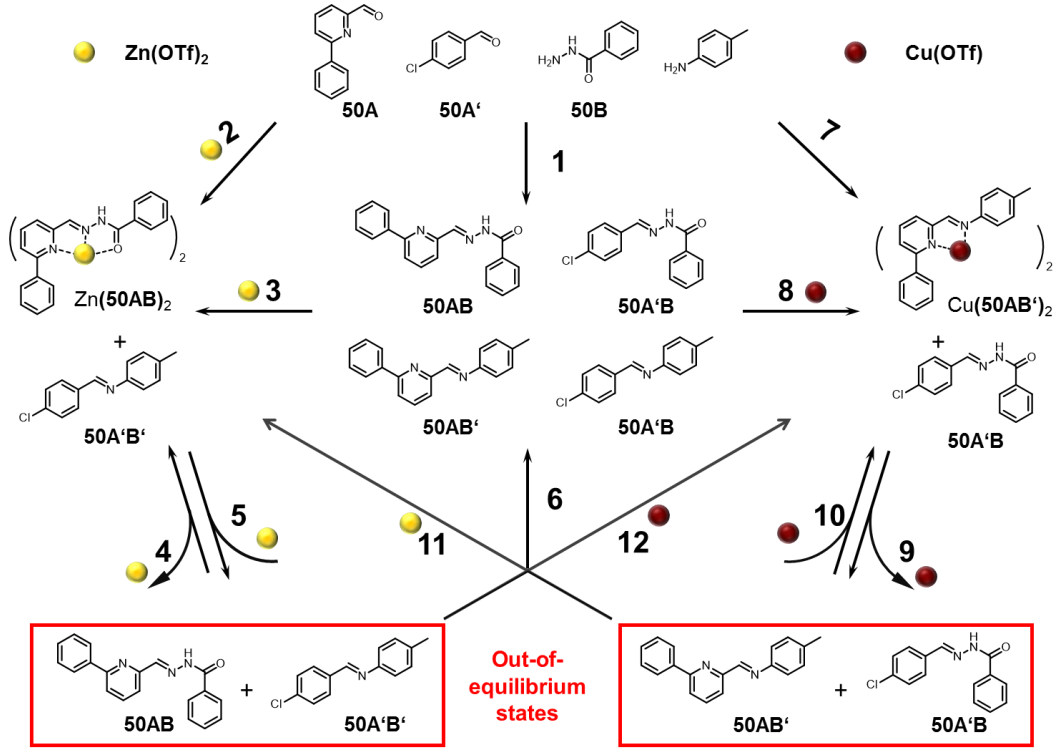

Figure 16: *La représentation de toutes les transformations effectuées par le système DCL réactif en fonction de la DCL* ***50AB***, ***50A'B'***, ***50AB'*** *et* ***50A'B***: (**1**) *la génération de la DCL à partir des composants; 12 h, 60 °C, AcCN;* (**2**), (**3**) *l'adaptation / la formation du système au Zn(II) effecteur; 0.5 eq., du Zn(OTf)*$_2$, *3 h 60 °C;* (**4**) *Le Zn(II) complexé par du [(Et*$_4$*)N]*$_2$*EDTAH*$_2$*; la mémorisation de la distribution / information, à la température ambiante pendant 12 h;* (**5**) *Un rappel rapide de l'information; la re-addition de 0.5eq Zn(OTf)*$_2$*;* (**6**) *l'effacement d'information / d'impression; Mw, 1 h, 160 °C;* (**7**), (**8**) *l'adaptation / formation du système du Cu(I); 0.5 eq. du CuOTf, 12h, 60 °C;* (**9**), *Le precipitation du Cu(I) par (n-Bu)*$_4$*NCN; la mémorisation de la distribution / du stockage de l'information à la température ambiante pendant 12 h;* (**10**) *Un rappel rapide d'information; La re-addition de 0.5eq Zn(OTf)*$_2$*;* (**11**) *La re-formation directe au Zn(II); 0.5 eq. de Zn(OTf)*$_2$*, 3 h, 60 °C;* (**12**) *La re-formation directe au Cu (I); 0.5 eq. CuOTf, 12 h, 60 °C. Le [****50AB***, ****50A'B'****] (en bas à gauche) et le [****50AB'***, ****50A'B****] en bas à droite) représentent des formations constitutionnelles, des états hors d'équilibre.*

pour respectivement **50AB /50A'B'**/Cu(**50AB'**)$_2$/**50A'B**/hydrolyse. Le retrait du Cu(I) peut être effectué par l'addition de NBu_4CN, conduisant à la précipitation de CuCN sans changer la répartition des constituants. A ce point si on ajoute à nouveau du Cu(I) la même distribution que précédemment est immédiatement obtenue sans nécessiter de temps de chauffe. L'effacement de l'empreinte du Cu(I), peut être obtenue suite au retrait du cation métallique par l'irradiation de la solution dans un four micro-ondes (40 min, 160 °C, de 270 W + 1 % de $Sc(OTf)_3$). Enfin, l'addition de triflate de zinc à l'état hors équilibre obtenu suite au retrait du cuivre résulte en la formation directe (sans temps de chauffe) de la distribution typique du zinc le système a été rééduqué (*Figure 16*).

REFERENCES

1. Hardy, J. G. *Chem. Soc. Rev.* **2013**, 42, 7881–7899.
2. Ruben, M.; Rojo, J.; Romero-Salguero, F. J.; Uppadine L. H.; Lehn, J.-M. *Angew. Chem. Int. Ed.*, **2004**, 43, 3644-3662
3. Stadler, A.; Burg, Ch.; Ramırez, J. R.; Lehn, J.-M. *Chem. Commun.* **2013**, 49, 5733–5735.
4. a) Cardona-Serra, S.; Coronado, E.; Gaviña, P.; Ponce, J.; Tatay, S. *Chem. Commun.*, **2011**, 47, 8235–8237; b) Coronado, E.; Galan-Mascaros J. R.; Gaviña P.; Romero F. M.; Tatay S. *Inorg. Chem.*, **2008**, 47, 5197-5203
5. Annie Marquis, A,; Smith, V.; Harrowfield, J.; Lehn, J.-M.; Herschbach, H.; Sanvito, R.; Leize-Wagner, E.;Van Dorsselaer, A. *Chem. Eur. J.* **2006**, 12, 5632 – 5641
6. Lehn, J.-M. *Chem. Eur. J.* **2000**, *6*, 2097-2102.
7. a) Lehn, J.-M. *PNAS*, **2002**, 99, 4763-4768 b) Lehn, J.-M. *Chem. Soc. Rev*. **2007**, *36*, 151-160. c) Lehn, J.-M. in Barboiu M. *Constitutional Dynamic Chemistry*, *Topics Curr. Chem.* **2012**, *322*, 1-32. d) Lehn, J.-M. *Angew. Chem., Int. Ed.* **2013**, *52*, 2836-2850.
8. Lehn, J.-M. *Chem. Eur. J.*, **1999**, *5*, 2455-2463.
9. Chaur, M. N.; Collado, D.; Lehn, J.-M. *Chem. Eur. J.* **2011**, *17*, 248-258.
10. Lehn, J.-M. *Angew. Chem., Int. Ed.* **2015**, *54*, 3276-3289

1. Combinatorial chemistry and Imines

1.1. Combinatorial chemistry – Behind the curtain

The traditional approach in classical chemistry towards synthesis is to prepare one desired compound per reaction in the highest yield possible per reaction. To achieve such a goal, synthetic chemists use a variety of protective groups, study numerous retrosynthetic ways to choose the right sequence of reactions and employ sophisticated methods of analysis to prove that they obtained the compound they had envisaged. In order to accurately predict the reaction outcome, generations of devoted chemists since the times of Lavoisier, the father of modern chemistry[1], have studied reaction mechanisms, relentlessly optimized reaction conditions and invented ingenious purification methods. All this has greatly contributed to not only the progress of chemistry as a field, but shaped the development of our society. Thanks to this, we are able to produce fine chemicals such as effective drugs and almost all articles of daily use (clothes, cosmetics, etc.), but there is a cost to this traditional approach. This cost is the time needed to prepare individual compounds separately, snowballing the cost of solvents and other equipment necessary for the process. This cost is justifiable if one specific compound is targeted, but in some cases, e.g., during the search for new drugs, a large pool of different chemical species is desirable. Therefore, when libraries of hundreds or thousands of compounds are wanted the one-at-a-time approach is not suitable.

As classical chemistry has moved from the synthesis of simple compounds to the synthesis of complex biological systems (DNA, peptides) and from testing individual analytes to broad-range screening of libraries of thousands of species, chemists started to develop new synthetic approaches focusing more on gaining a diversity of newly formed species rather than optimising the yield of one particular compound. Thus, combinatorial chemistry came to light as a complement to the traditional synthetic approach. Combinatorial chemistry is a method that enables the preparation of complex mixtures of individual compounds and also paves the way

to compounds with a complex constitution. Incorporating covalently dynamic properties into combinatorial chemistry has enabled the preparation of diverse chemical structures and assemblies in areas spanning from dynamic covalent chemistry to supramolecular chemistry.

Although this method is powerful, the first examples of combinatorial methods provided only a limited control over the reactions and transformations taking place in the reaction mixture. Therefore, shortly after the establishment of the methods of covalent combinatorial chemistry, which still relied on irreversible covalent organic reactions, a new branch called Dynamic combinatorial chemistry (DCC) appeared.[2]

Dynamic combinatorial chemistry employs reversible reactions to generate complex mixtures, for example mixing various aldehydes and amines creates a mixture (a library) of different imines. The imine bond of any individual constituent in this library repeatedly forms and breaks while exchanging parts of the molecule (components) with other constituents in the mixture. This ensures that the final distribution of the constituents in the library is the result of a thermodynamic equilibrium. This means that any change in conditions can be translated into a shift of the equilibrium leading to a different final composition starting from the same initial mixture. This is a crucial factor that allows the dynamic library to respond to external stimuli.[2] Application of the right impulse can alter the system's distribution of products or entirely change the outcome of the reaction between components/reactants.[3]

In achieving such changes, dynamic combinatorial chemistry utilizes a wide range of reversible connections and reactions ranging from noncovalent interactions (H-bonds, electrostatic interactions) through coordination bonds to covalent bonds. This has given rise to the term Constitutional Dynamic Chemistry (CDC)[4] for its description. As the name suggests, the essence of this chemistry is the reversibility of bonds which can break, form and exchange components. A mixture of compounds obtained in this way is termed a Dynamic Constitutional library (DCL) and its special characteristic is that it is able to respond by constitutional variations to physical stimuli or chemical effectors. In some cases, the whole set of possible

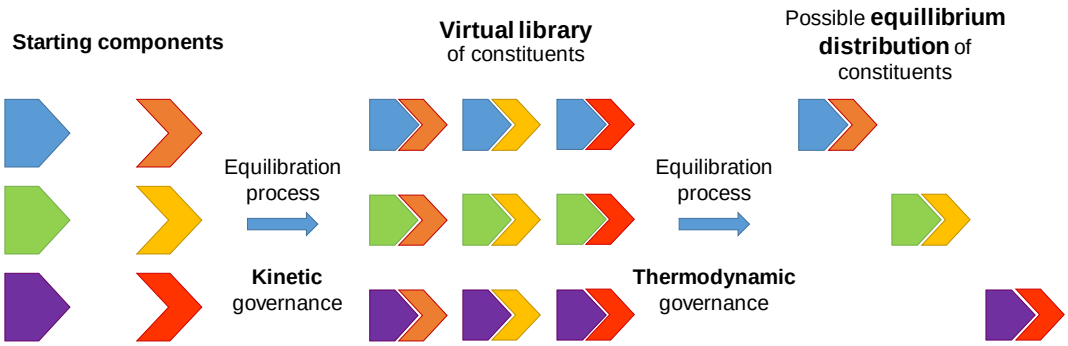

Figure 1.1: *Possible different states of DCL's equilibration process*

combinations of exchange products from given starting units/components is called a virtual library - virtual because not always will all the possible products be formed in the mixture.[5] (*Figure 1.1*)

In order to study and exploit all the appealing features of CDLs, our research group employs the family of C=N dynamic bonds. From the number of described examples, it is one of the most frequently applied dynamic covalent connections. The family of C=N bonding arises from the condensation of an amine (H_2N-X) with a carbonyl (RR'C=O) group and includes imines, hydrazones, acylhydrazones and some other derivatives which are not considered in this work. (*Figure 1.2*) From all the suitable bonds available, this connection has several advantageous characteristics. There are many commercially available starting blocks (aldehydes, amines...), the dynamic behaviour is well described in the literature and it is easily tuneable. Above all, the outstanding coordination properties of constituents assembled from pyridine-containing building blocks will be repeatedly highlighted through this whole work. In the case of dynamic ligands of this type, a cation can also promote formation of its own favourite constituent/binder via templating. An additional level of dynamicity is added by conformational processes defining the E/Z isomerization of the C=N bond.[6,7]

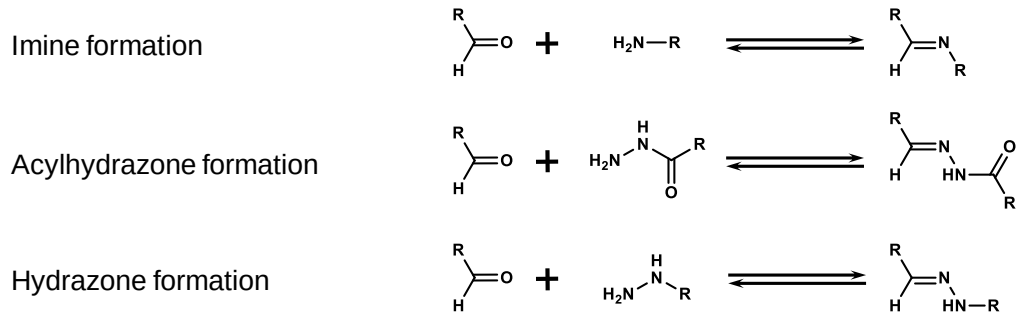

Figure 1.2*: Dynamic -C=N- bonds which were used in this work*

CDC has features from both its parent fields: combinatorial chemistry and supramolecular chemistry. Supramolecular chemistry contributes with self-assembly, molecular recognition (templating) and responsiveness to an external stimulus (chemical or physical). Accomplishing this in a multi-component system is a feature brought by combinatorial chemistry (selection/evolution of the fittest and adaptation).

Even though this is not an aspect of this work, it is important to note that today, with all the development in the whole field of combinatorial chemistry, the creation of libraries is no longer the key factor in the studies and applications. Nowadays, the general problem lies at the opposite end of the process, in the analysis of the complex mixtures. Constantly equilibrating mixtures impose critical challenges to analytical methods and a huge effort is being made to improve analysis and enable rigorous study of chemical transformations within the library,

accurate final composition determinations and establishment of the nature of the products formed.[8]

1.1.1. History

Combinatorial chemistry probably started shortly after the first seas appeared on Earth. The ancient sea represented one large pool of chemical compounds which reacted in a random combinatorial fashion.[9,10,11] In the course of time, a set of the most optimal reactions under given conditions emerged. Some of their products could then catalyse or auto-catalyse the formation of another set of different chemical species and this complicated network of transformations eventually led to life itself. [12,13,14,15]

Much later, people learned how to prepare new chemical compounds, which answered their needs and had been previously unknown to nature. Many of them were prepared in a way which could be considered combinatorial as well.

However, the combinatorial methods as applied in modern chemistry appeared only at the end of 19th and beginning of the 20th century. The experimental procedures of early pioneers such as Emil Fischer, with his work on carbohydrates[2,16], and Alfred Werner[2,17], with his work on coordination compounds clearly contain principles of combinatorial chemistry, even though the authors did not describe them in this way yet. For example, the synthesis of phthalocyanines reported in 1932 is clearly a dynamic and combinatorial process, although this fact had to wait a few more decades for its recognition.

In 1953, Watson and Crick published their now legendary work clarifying the structure of DNA and marking a new era of natural sciences. Shortly thereafter, the principles of DNA replication and transcription were explained based on *Templation theory*. The theory states that all proteins are synthesised on a basis of template called gene, which is entirely made of a sequence of nucleotides. The order of nucleotides in a sequence then encodes the order of amino acids in the final protein. At first, Crick introduced this idea only to the small group of molecular biologists in a draft called "*On Degenerate Templates and the Adaptor Hypothesis*". Interestingly, this important paper has never been published. It was two years later in 1957 when Crick finally summarized his ideas in another ground-breaking paper "*On Protein Synthesis*".[2,18]

The universal role of a template was quickly recognised and articulated by Todd[19] and soon adopted by chemists across all specializations. For coordination chemistry, one of the first pioneers of intentional use of templated synthesis was Busch in 1962. (*Figure 1.3*) In the

introduction of his communication he clearly describes the role of the metal cation in Schiff base formation:

"*The metal ion brings the reactants together in the product form that is most favourable for complexation.* "[20]

Another interesting work is Nelson's study in the early 80's on the formation of imine macrocycles. Some of the principles that are taken for granted today were for the first time clearly formulated and put into context by him. He pointed out that transamination (in this context amine exchange on carbonyl) is an important process in formation of novel macrocycles from basic imines, acknowledging the thermodynamic control of this phenomenon. Based on this knowledge he correctly identified open-chain imine complexes as intermediates in the formation of the macrocycles (*Figure 1.3a*) and used them in the synthesis of previously inaccessible unsymmetrical imine macrocycles.[21] (*Figure 1.3b*)

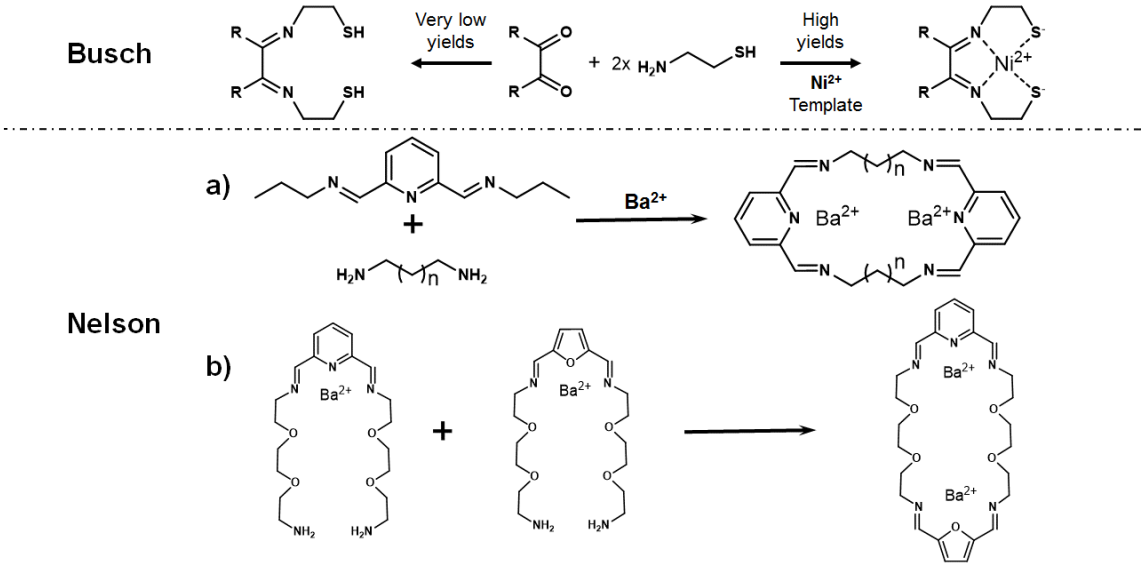

Figure 1.3: *Early works of Busch and Nelson. Top: Busch's dynamic assembly of otherwise hard to obtain imine ligand. Bottom: a) Nelson's prove of transamination step during the macrocycle formation; b) Successful use of the transamination in preparation of otherwise inaccessible unsymmetric macrocycles.*

Nowadays, chemists are very familiar with the use of a template to shift an equilibrium in favour of an otherwise non-favoured product. However, to advance the concept from how to produce a single compound to the manipulation of complex mixtures, the crucial input of combinatorial chemistry was required. Just as *template theory* emerged from biochemistry, combinatorial chemistry was also originally developed for the synthesis of peptides and oligonucleotides.

The method published in 1963 by R. B. Merrifield was an innovative way of synthesising peptides in high yields. It is based on anchorage of the first amino acid onto a polymeric carrier

and sequential attachment of different amino acids via the terminal -NH_2. The chain is then cleaved from the polymer at the end of the synthesis by a simple chemical reaction. The advantage was not only the simplified purification after each step of the synthesis, but also the possibility of division of the carriers for different fragment syntheses. The individual batches could be split, reaction sequences altered for each of them and different shorter fragments later combined to provide longer sequences, increasing the efficacy of this method.[22,23] These aspects were later improved and developed by others (Furka - Split & mix concept[24], Geyhen-Multipin synthesis[25], Houghten-Tea bag[26]) making it a standard method of choice anytime when a defined sequence of building blocks in a molecular backbone is needed.

An interesting combination of thermodynamically controlled dynamic bonds and a template was employed for imine-mediated synthesis on a DNA template. Goodwin and Lynn (1992) used a DNA template in order to shift the equilibrium of imine condensation of two DNA fragments. (*Figure 1.4*) With this simple approach, which does not require any polymerases, they achieved the first chain-length and sequence-specific template-directed polymerization.[27,28]

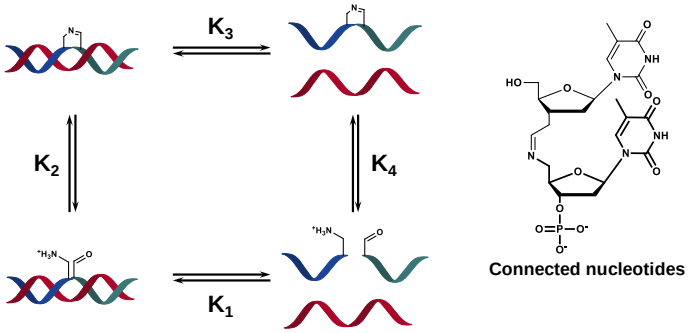

Figure 1.4: *The work of Goodwin and Lynn on templated dynamic ligation of DNA fragments. K_1 = 0.8 (DNA Ternary complex); K_2 = ~40 (Imine formation in ternary complex); K_3 = 5x10^5(DNA Duplex dissociation); K_4 = 10^{-4} (Imine hydrolysis). After the equilibration period, the imine product was reduced to a secondary amine by $NaBH_3CN$ and the products were analysed by HPLC.*

Shortly afterwards, in the mid-90s, the first publications describing a dynamic combinatorial approach appeared. Rideout used assembly of originally non-toxic precursors to form highly cytotoxic hydrazones in order to take advantage of differences in nutrition uptake between normal and tumor cells.[29] In 1995, Hamilton used a combinatorial approach to prepare artificial receptors using terpyridine derivatives coordinated around Ru(II) cation in the presence of a target.[30] (*Figure 1.5*) In the same year, Harding followed with a work describing an amplification of a suitable host induced by π-π stacking between a metallo-macrocylic host and an appropriate aromatic guest.[2,31] The general principles behind these examples are still widely used.

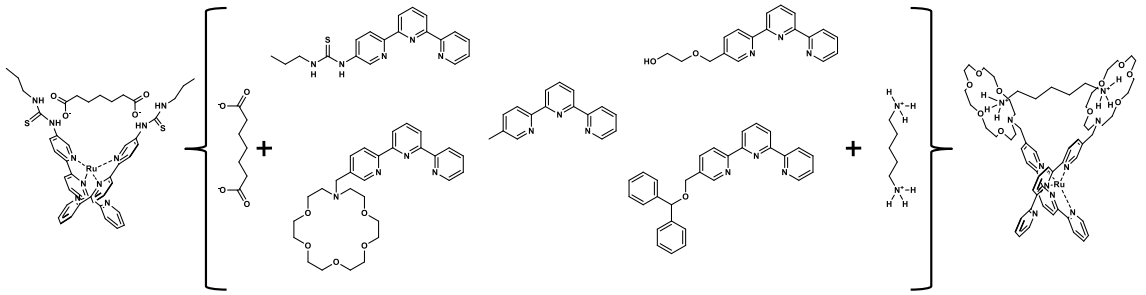

Figure 1.5: *Different outcomes of equilibration of a terpyridine based receptor library in response to a different host. (Hamilton)*

Right after these promising pioneering works, Sanders published a study utilising base-catalysed transesterification. It was not the ideal choice of dynamic linkage due to several significant limitations of this reaction, such as rather slow equilibration and the necessity to work under strictly anhydrous conditions. Nevertheless, the work described successful thermodynamically controlled lactonisation of steroidal building blocks to assemble macrocycles. Moreover, the work not only described product formation, but also reported the exchange of building blocks between macrocycles.[27,32] (*Figure 1.6*) Shortly after, Sanders' group turned to dynamic disulphide bonds, which were easier to handle and provided a valuable extension of the general approach.

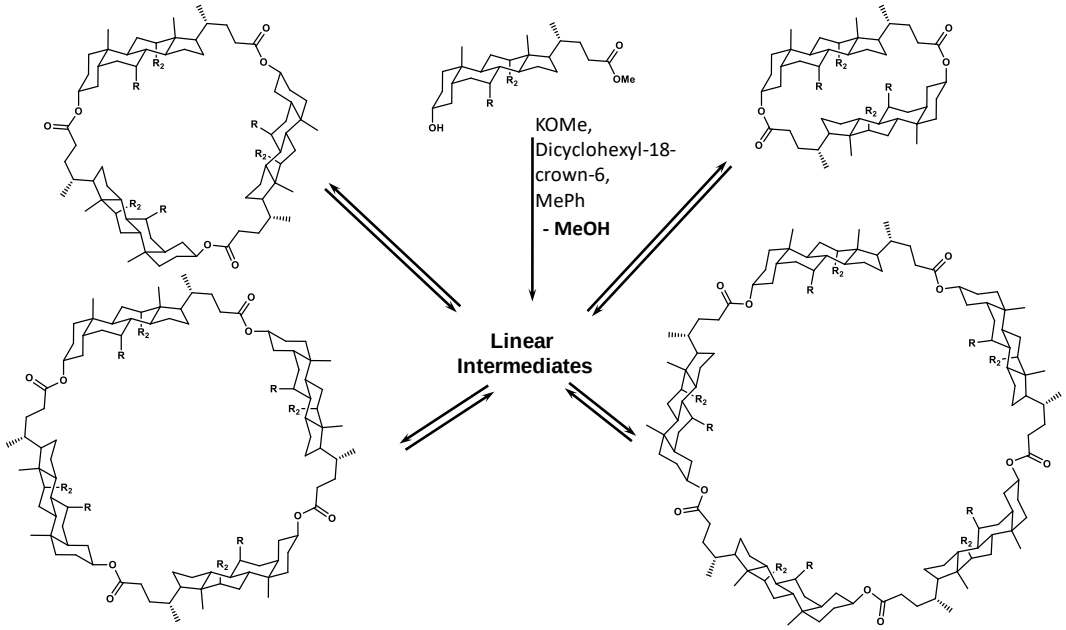

Figure 1.6: *Sanders's dynamic formation of different macrocycles via reversible transesterification. A thermodynamic mixture of different macrocycles is accessible starting from the monomer as well as by the equilibration of any individual macrocycle.*

The field of dynamic covalent chemistry has been greatly influenced by work emanating from the Lehn laboratory. An initial contribution was the description of coordination assemblies where a ligand bearing three bipyridine units forms circular helices, the size of which depends

on the counter anion of the Fe(II) cation. [33] Lehn also presented one of the first dynamic systems openly advocating the idea of DCC.[2,34] In this work, an aldehyde/amine library was created from components structurally similar to fragments of a molecule already known as a potent inhibitor of carbonic anhydrase. From all possible combinations, the amplified constituent was also the one with best inhibition properties. It was consequently structurally the most similar one to the already known inhibitor. (*Figure 1.7*) The pioneering works of this group are summarized in the reference [5].

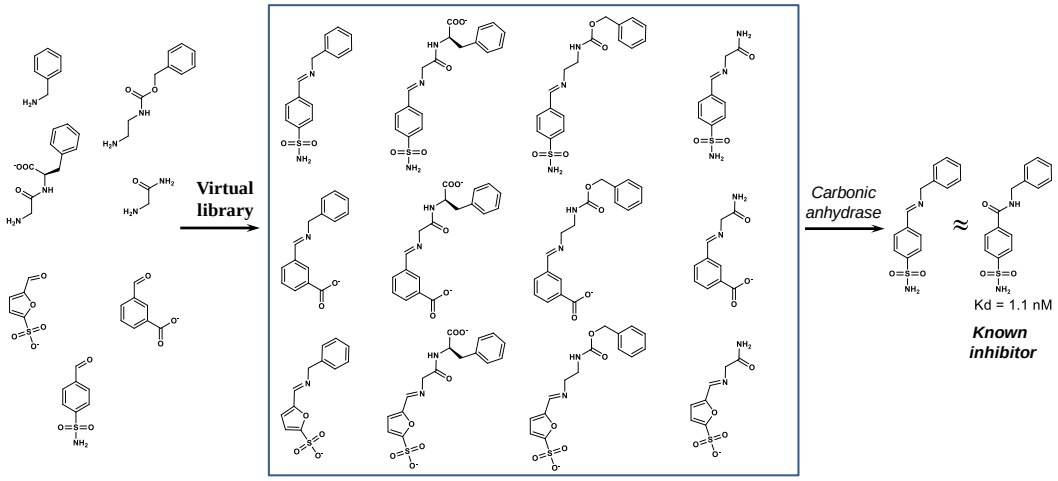

Figure 1.7: *Dynamic amplification of the best enzyme inhibitor form in a constantly exchanging imine library.*

The field underwent rapid development and many publications have now appeared. However, due to the strict focus of this thesis on imine chemistry, other dynamic covalent reactions (e.g. disulfides, metathesis, boronic esters) will not be discussed here. Nevertheless, these dynamic connections represent valuable complements, replacements or orthogonal motifs to -C=N- bonds. [2,3,35]

1.1.2. Description of basic reversible reactions used in this work: Imines, Acyl-Hydrazones, Hydrazones

1.1.1.1. Imines

The condensation of amines and carbonyl compounds to form imines is a well-known reversible reaction widely used in dynamic systems. The reaction was described for the first time in the year 1864 by the German chemist Hugo Schiff[36], thus the name "Schiff bases" came to light. In 1920, the first transamination exchange reaction was described by Reddeline.[37]

The reaction offers several advantages, the most significant being: *a) accessibility of building blocks*, as numerous aldehydes, ketones and amines are commercially available; *b)*

cost friendliness and in the case where synthesis is inevitable *c) knowledge of many synthetic procedures* leading to the desired derivatives.

However, although this reaction may seem simple on paper, it is actually quite complicated. (*Eq. 1*) The nucleophilic addition of the amine to the carbonyl compound is just the first step, as the successful condensation is accomplished only after elimination of water (or amine in the case of exchange).

Equation 1

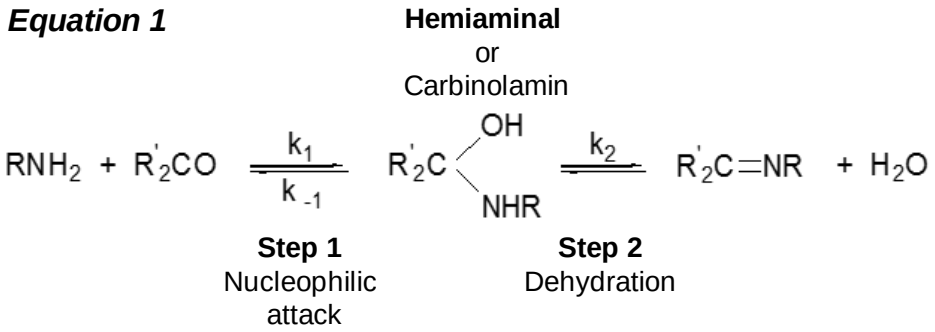

In aqueous solutions, imine condensation may be subject to opposing factors. Acid accelerates the course of the reaction by protonation of carbonyl-O, but the amine is protonated as well, which ultimately leads to a lower conversion. On the other hand, addition of a base will increase the conversion due to liberation of free amine, but regarding kinetics it can lead both to deceleration or enhancement of the reaction rate versus neutral pH depending on the particular case. The hydrolysis and exchange of imines is to large extent governed by the electrophilicity of the imine (carbonyl) bond, which in turn is determined by the substituents attached to both parts of the molecule.[2]

Hydration of aldehydes also competes with the formation of imines. The hydration is in fact also a nucleophilic attack to the carbonyl group by a water molecule. In this case however, generally the same correlation between the structure of the aldehyde and equilibrium constants is expected for hydration as well as for imine formation. Indeed, the same trends were observed in cases of equilibrium constants for water, semicarbazide and hydroxylamine addition to several carbonyl compounds, with N nucleophiles having constant values several orders higher than that of water (O nucleophile).[38]

A useful relationship between the imine formation equilibrium constant and structural properties of amines and carbonyl compounds has been provided by Lehn.[39,40,41] The rate of imine formation varies only moderately with the amine used. With a difference of 6 pK_a units between aniline (pK_a = 5.3) and isopropyl amine (pK_a = 11.47), the difference in equilibrium constants (logK) for formation of their imines is only 2 units. This is probably due to the higher

values of $E_{(Homo)}$ of weakly basic amines (low pK_a) which increases the covalent contribution to the bonding, those of higher pK_a favouring an electrostatic contribution, similarly to effects on reactivity in other nucleophilic reactions. [39,40]

Analysing the mechanism of the reaction, the nucleophilic attack (Eq. 1, step 1) of an amine to carbonyl results in zwitterionic intermediate which is transformed to hemiaminal. This is caused by intramolecular or water mediated intermolecular transfer of a proton from hemiaminal ($-NH_2^+-$) to carbonyl ($-O^-$). In cases where the zwitterionic intermediate is relatively stable, the initial amine attack on carbonyl is the rate determining step.

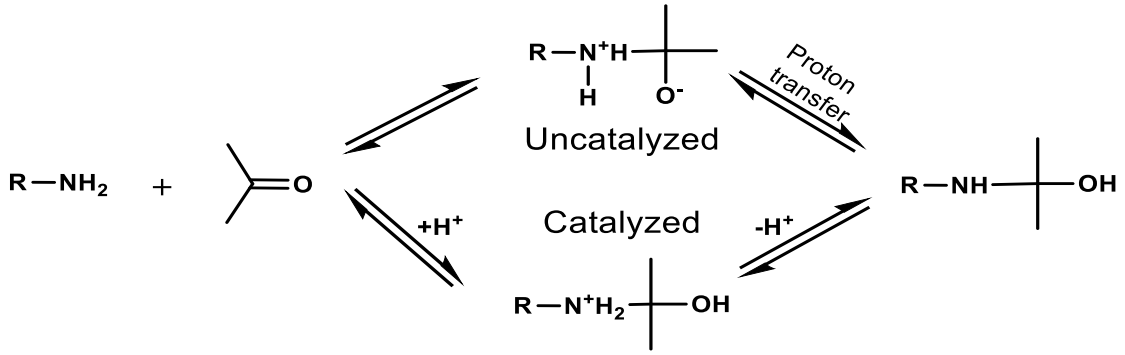

Figure 1.9: *Two possible routes of amine addition to carbonyl. Top: The uncatalysed nucleophilic attack of amine to carbonyl followed by intramolecular or medium mediated intermolecular proton transfer. Bottom: Attack of amine onto acid activated carbonyl the first step of imine formation.*

For strongly basic amines the hydrolysis of the zwitterionic intermediate can be extremely fast, much faster than the proton transfer which then becomes the rate determining step. In such cases, proton transfer and also the stability of hemiaminal can be increased by the addition of an acid.[42] (*Figure 1.9*)

The second step (*Eq. 1, step 2*), dehydration, is acid catalysed up to pH 9. Below this value the catalysis can proceed via two limiting cases: a) general acid catalysis[43,44] (by the conjugate acids of strongly basic amines and semicarbazones), where the hydroxyl is protonated before elimination (*Figure 1.10A*); b) specific acid catalysis[45,46] (benzophenone phenylhydrazone) where water elimination proceeds via a concerted mechanism with a contribution of the protonated solvent (e.g. water, *Figure 1.10B*) c). In most cases it goes through combination of both. At a pH in the range 8-12 the dehydration of the hemiaminal (from strongly basic amines and hydroxylamine, *Figure 1.10C*) can proceed without catalysis via expulsion of OH^-. [44,47,48] Most commonly, the mechanism above pH 8 involves general base catalysis[44] (general

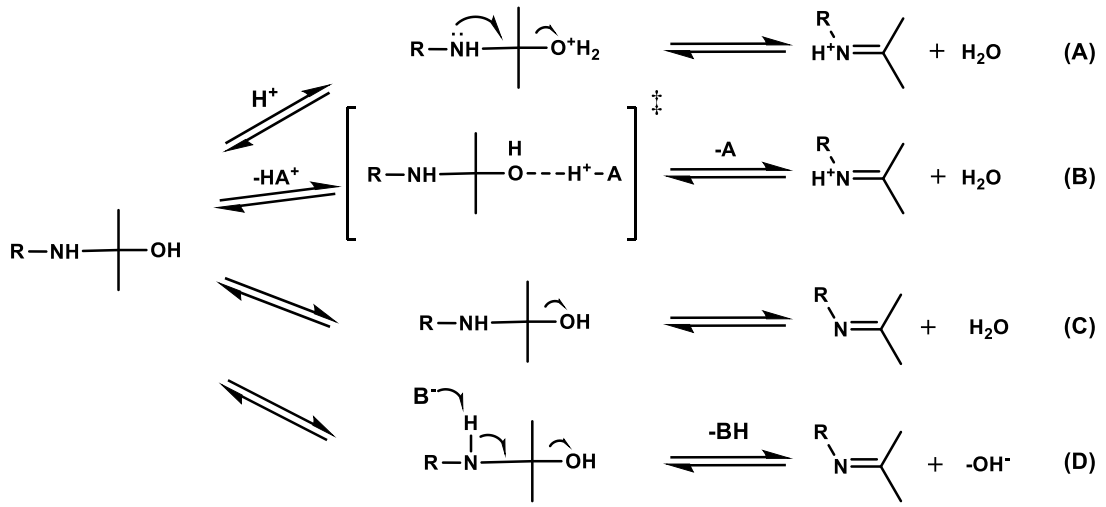

Figure 1.10: *All the possible ways of water elimination, the second and final step of imine formation. From the top:* ***A)*** *General acid catalysis;* ***B)*** *Specific acid catalysis (HA^+ is protonated solvent e.g. H_3O^+); C****)*** *uncatalyzed dissociation;* ***D****) General basic catalysis.*

mechanism, *Figure 1.10D*) accompanied in special cases by specific base catalysis[44,49] (N-hydroxymethylanilinium).

Because amines are readily protonated in acid and the protonated species cannot attack carbonyl-C, the first step is slow and rate-determining under pH 4. However, the second dehydration step is slow in a weakly acidic or neutral pH above 6. Considering both steps, the imine formation proceeds best in pH between 4 and 6.[50] (*Figure 1.11*)

For a start, simple mixing of an amine and an aldehyde proceeds to a thermodynamic equilibrium of starting compounds and the condensed product. Often this equilibrium does favour the products, but sometimes it is necessary to apply azeotropic distillation or molecular sieves to remove water and shift the equilibrium in the desired direction. Acid catalysis is often recommended to promote the reaction, but it can be omitted in the case of reactive aldehydes and amines or in cases where side reactions may occur. The condensation provides the imine product even under neutral or basic conditions. [2,51]

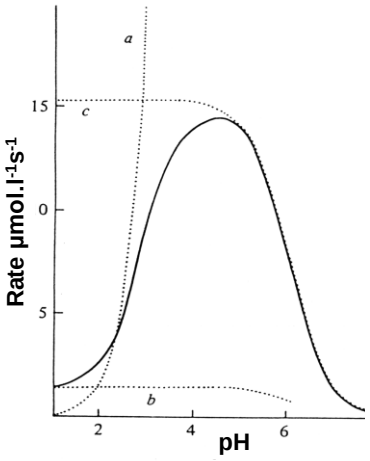

Figure 1.11: *A pH dependence of the overall imine formation rate*

Although the reversible nature of this reaction may be troublesome from the point of view of synthetic chemists, it is essential for the construction of dynamic combinatorial libraries. Imine formation is one of a few reactions where there can be simple and efficient control of both forward and backward paths of the reaction, which in turn renders the system

adaptable to a stimulus. Different concepts such as "proof-reading" and "error checking" which can be often found in scientific texts[52,53,54,55,56] describe the thermodynamically regulated association and dissociation of imine products.

Imines can undergo three types of thermodynamically controlled reactions (*Figure 1.12*):

a) *Hydrolysis:* Dissociation of an imine to its building blocks, an amine and a carbonyl compound, requires the presence of water to establish the equilibrium.

b) *Exchange:* Substitution of another amine for that initially held within the -C=N- is called transamination or imine exchange, not to be confused with the biochemical process of keto acid to amino acid transformation, also called transamination but there because it involves the transfer of one N-centre between two C-centres.

c) *Metathesis:* Sometimes denoted as transimination or imine exchange, this is a process of exchange of amine parts between two imines. The term metathesis reflects the fact that it is formally a double exchange of groups. There are various possible mechanisms for this reaction, the most simple being that of a double hydrolysis which leaves the various components able to condense in the alternate manner.

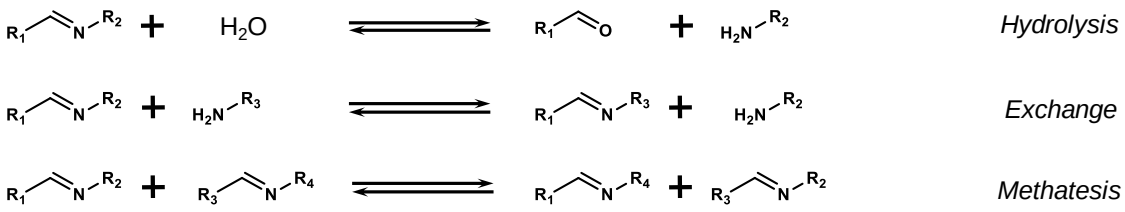

Figure 1.12: *Reversible reactions of -C=N- connection.*

As mentioned above, the imine condensation is an acid-catalysed reaction and so is its reverse. Under basic conditions, exchange and hydrolysis can be slowed down, but in order to stop them entirely it is necessary to alter the imine bond. This can be done via reduction of the imine to a secondary amine[57] or via the Ugi reaction[58]. Both methods prevent further equilibration and freeze the actual distribution of constituents in the library. This approach is frequently used for analytical purposes because it allows preservation of the library composition in the form of amines (reduction) or amides (Ugi r.), which can be then easily analysed by standard methods. For the purpose of kinetic self-sorting and studies of the evolution of an

imine DCL it is possible to prevent exchange via imine oxidation. This approach provides another level of control over the outcome of the DCL's equilibration. Oxidation, however, can be slower than imine exchange so that the final distribution of oxidized products does not reflect the distribution of constituents in the imine DCL. It rather corresponds to the rate at which the individual imines are oxidised.[59] (discussed in chapter 3.1.2.1 dealing with kinetic self-sorting)

As stated above, acid catalysis is an often recommended tool to promote the dynamic exchange in imine libraries, but nucleophilic catalysis is equally important. In the presented work, amine nucleophilic catalysis served as the rate enhancing element for hydrazone and acylhydrazone formation in cases when both imines and other dynamic -C=N- bond types were mixed together. The mechanism involves as an intermediate a relatively labile -C=N- derivative, which is attacked by and exchanged for a more stable hydrazine, liberating a protonated amine.[60,61,62]

In the same way, the exchange can by catalysed by the presence of Lewis acids. This catalysis often occurs in libraries equilibrated in a presence of metal cations.[6] In fact, in organic solvents and in cases where protonation decreases the reactivity of amines, Lewis acid catalysis can be even more effective than Brønsted acid catalysis. Scandium triflate was found to be the most efficient catalyst, followed by lanthanides, but also other more common metals such as Zn(II) can be used.[63] The mechanism starts with the formation of an imine/metal complex followed by a nucleophilic attack of the amine as the rate determining step, meaning that amines with the highest affinity toward the metal will react the most efficiently.[2,64] (*Figure 1.12*)

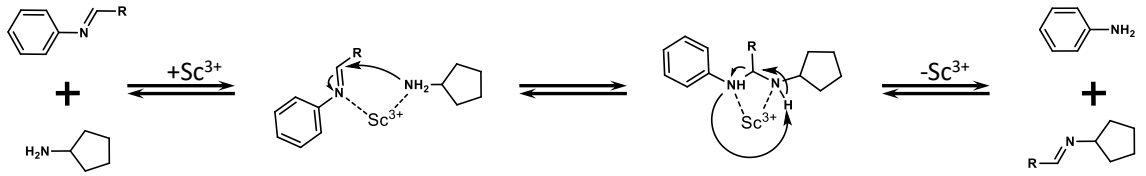

Figure 1.12: *Simplified mechanism of the role of Sc^{3+} in Lewis acid catalysed imine exchange.*

These facts illustrate the complexity and challenges connected with imine chemistry. Even though it is not always of obvious importance, it is important to keep in mind the various mechanistic subtleties, especially in cases where standard procedures provide unexpected results.

1.1.1.2. Hydrazones and Acylhydrazones

Figure 1.13: *Selected members of -C=N- family.*

Hydrazone and acylhydrazones are siblings of imines in terms of formation and structural characteristics. The main difference is that the equilibrium is very strongly shifted towards the products and despite the slow reaction rates, the overall stability of products towards hydrolysis is much higher than that of imines. The other members of this family - oximes and semicarbazones - were not used in this work and will not be discussed here. (*Figure 1.13*)

Regarding hydrazines and hydrazides, the reacting -NH_2 is markedly more nucleophilic due to the alpha effect of the adjacent nitrogen. This effect is mainly responsible for the higher stability of the corresponding condensation products as it renders the -C=N- resistant to nucleophilic attack of water or simple amines. An acyl group or another electron withdrawing group linked directly to the hydrazine decreases the alpha effect, thus increasing the rates of hydrolysis and exchange.

In a recent study, Nguyen and Huc demonstrated that hydrazines bearing electron-withdrawing substituents can form hydrazones that are sufficiently activated for hydrolysis and exchange to occur even at neutral pH.[2,51,65] The same principles can also be applied to the aldehyde part, because hydrazones built from aldehydes with electron withdrawing groups (*p*-carboxybenzaldehyde) have higher equilibrium constants than the ones without substitution. (In general the equilibrium constant increases in the order: imine < acylhydrazone <hydrazone)

1.2. References

1. McKie, D. *Antoine Lavoisier: The Father of Modern Chemistry;* J. P. Lippincott Company: Philadelphia, 1935.
2. Corbett, P. T.; Leclaire, J.; Vial, L.; West, K. R.; Wietor, J.-L.; Sanders, J. K. M.; Sijbren, O. *Chem. Rev.* **2006,** *106,* 3652-3711.
3. Herrmann, A. *Chem.Soc.Rev.* **2014,** *1899-1933,* 43.
4. Lehn, J.-M. *Chem. Soc. Rev.* **2007,** *36,* 151-160.
5. Lehn, J.-M. *Chem. Eur. J* **1999,** *9* (5), 2455-2463.
6. Vantomme, G.; Jiang, S.; Lehn, J.-M. *J. Am. Chem. Soc.* **2014,** *26,* 9509-9518.
7. Kovaříček, P.; Meister, A. C.; Flídrová, K.; Cabot, R.; Kovaříčková, K.; Lehn, J.-M. *Chem. Sci.* **2016,** *7,* 3215-3226.
8. Misuraca, M. C.; Moulin, E.; Ruff, Y.; Guiseppone, N. *New J. Chem.* **2014,** *38,* 3336-3349.
9. Jortner, J. *Phil. Trans. R. Soc. B.* **2006,** *361,* 1877-1891.
10. Philip, G. K.; Freeland, S. J. *Astrobiology* **2011,** *11,* 235-240.
11. Grover, M. A.; He, C. Y.; Hsieh, M.-C.; Yu, S.-S. *Processes* **2015,** *3,* 309-338.
12. Kuppers, B.-O. *Information and theOrigin of Life;* MIT Press: Cambridge, 1990.
13. Lehn, J.-M. *Angew. Chem., Int. Ed.* **2013,** *52,* 2836-2850.
14. Ludlow, F. R.; Otto, S. *Chem. Soc. Rev.* **2008,** *37,* 101-108.
15. Kauffman, S. A. *The origins of order;* Oxford University Press: Oxford, 1993.
16. Kunz, H. *Angew. Chem. Int. Ed.* **2002,** *41* (23), 4439–4451.
17. Constable, E. C.; Housecroft, C. E. *Chem. Soc. Rev* **2013,** *42,* 1429-1439.
18. Medicine, U. S. N. L. o. The Francis Crick papers - The Discovery of the Double Helix, 1951-1953. https://profiles.nlm.nih.gov/ps/retrieve/Narrative/SC/p-nid/143 (accessed Aug 13, 2016).
19. Todd, A. R. *Perspectives in Organic Chemistry;* Interscience Publishers: London, 1956, p 263.
20. Thompson, M. C.; Busch, D. H. *J. Am. Chem. Soc. 1962* **1962,** *84,* 1762.
21. Nelson, M. S.; Knox, V. C.; McCann, M.; Drew, M. G. B. *J. Chem. Soc., Dalton Trans.* **1981,** 1669-1677.
22. Merrifield, R.B. *J. Am. Chem. Soc* **1963,** *85* (14), 2149-2154.
23. Gutte, B.; Merrifield, R. B. *The Journal of Biological Chemistry* **1971,** 1922-1941.
24. Furka, A.; Sebestyen, F.; Asgedom, M.; Dibó, G. *Int. J. Peptide Protein Res.* **1991,** 37, 487-493.
25. Meaji, N. J.; Bray, A. M.; Geysen, H. M. *J. Immunol. Methods.* **1990,** *134,* 23-33.
26. Houghten, R. A. *PNAS* **1985,** *82,* 5131-5135.
27. Beeren, S. R.; Sanders, J. K. M. History and Principles of Dynamic Combinatorial Chemistry. In *Dynamic Combinatorial Chemistry;* Wiley-VCH Verlag GmbH & Co. KGaA: Weinheim, 2010; pp 1-22.
28. Goodwin, J. T.; Lynn, D. C. *J. Am. Chem. Soc.* **1992,** *114,* 9197-9198.
29. Rideout, D. *Science* **1986,** *233,* 561.
30. Goodman, M. S.; Jubian, V.; Linton, B.; Hamilton, A. D. *J.Am.Chem.Soc.* **1995,** *117,* 11610.
31. Bilyk, A.; Harding, M. M. *J.Chem.Soc., Chem. Commun* **1995,** 1697.

32. Brady, P. A.; Bonar-Law, R. P.; Rowan, S. J.; Suckling, C. J.; Sanders, J. K. M. *Chem. Commun* **1996,** 319-320.
33. Hasenknopf, B.; Lehn, J.-M.; Boumediene, N.; Dupont-Gervais, A.; Van Dorsselaer, A.; Kneisel, B.; Fenske, D. *J. Am. Chem. Soc.* **1997,** *119,* 10956-10962.
34. Huc, I.; Lehn, J.-M. *Proc. Nat. Acad. Sci. USA* **1997,** *94,* 2106-2110.
35. Jin, Y.; Yu, C.; Denman, R. J.; Zhang, W. *Chem. Soc. Rev.* **2013,** *42,* 6634-6654.
36. Schiff, H. *Ann. Chem(Paris)* **1864,** *131,* 118.
37. Reddelin, G. *Bey. Bunsenges. Phys. Chem.* **1920,** *53B,* 355.
38. Malpica, A.; Calzadilla, M. *J. Phys. Org. Chem* **2003,** *16,* 202-204.
39. Godoy-Alcantar, C.; Yatsimirsky, A. K.; Lehn, J. M. *J. Phys. Org.* **2005,** *18,* 979.
40. Edwards, J. O.; Pearson, R. G. *J. Am. Chem. Soc.* **1962,** *84,* 16.
41. Appel, R.; Mayr, H. *J. Am. Chem. Soc.* **2011,** *133,* 8240-8251.
42. Sayer, J. M.; Pinsky, B.; Schonbrunn, A.; Washtien, W. *J. Am. Chem. Soc.* **1974,** *96,* 7998-8009.
43. Cordes, E. H.; Jencks, W. P. *J. Am. Chem. Soc.* **1962,** *84,* 4319-4328.
44. Sayer, J. M.; Peskin, M.; Jencks, W. P. *J. Am. Chem. Soc.* **1973,** *95,* 4277-4287.
45. Powers, J. C.; Westheimer, F. H. *J. Am. Chem. Soc.* **1960,** *82,* 5431-5434.
46. Capon, B.; Perkins, M. J.; Rees, C. W. *ORGANIC REACTION MECHANISMS - 1966;* John Wiley & Sons Ltd.: London, 1967.
47. Jencks, W. P. In *Progress in physical organic chemistry vol. 2;* Interscience Publishers, Inc.: New York, 1965; pp 96-98.
48. Williams, A.; Bender, M. L. *J. Am. Chem. Soc.* **1966,** *88,* 2508-2513.
49. Abrams, W. R.; Kallen, R. G. *J. Am. Chem. Soc.* **1976,** *98,* 7777-7789.
50. Clayden, G. W. W. *Organic Chemistry;* Oxford University Press: New York, 2001.
51. Belowich, M. E.; Stoddart, J. F. *Chem. Soc. Rev.* **2012,** *41,* 2003-2024.
52. Simpson, M. G.; Pittelkow, M.; Watson, S. P.; Sanders, J. K. M. *Org. Biomol. Chem.* **2010,** *8,* 1173-1180.
53. Sauvage, J. P.; Gaspard, P. *From Non-Covalent Assemblies to Molecular Machines;* John Wiley & Sons: Weinheim, 2011.
54. Schalley, C. A.; Vogtle, F.; Dotz, K. H. *Tamplates in chemistry I;* Springer-Verlag: Berlin, 2004.
55. Furlan, R. L.; Otto, S.; Sanders, J. K. M. *Proc. Natl. Acad. Sci. U.S.A.* **2002,** *99,* 4801-4804.
56. Au-Yeung, H. Y.; Pantos, G. D.; Sanders, J. K. M. *PNAS* **2009,** *106,* 10466-11047.
57. Ziach, K.; Jurczak, J. *Org. Lett.* **2008,** *10,* 5159-5162.
58. Wesjohann, L. A.; Rivery, D. G.; León , F. *Org. Lett.* **2007,** *9,* 4733-4736.
59. Osowska, K.; Miljanić, O. Š. *J. Am Chem. Soc.* **2011,** *133,* 724.
60. Cordes, H.; Jencks, W. P. *J. Am. Chem. Soc.* **1962,** *84,* 826-831.
61. Crisalli, P.; Kool, E. T. *J. Org. Chem* **2013,** *78,* 1184.
62. Dirksen, A.; Dirksen, S.; Hackeng, T. M.; Dawson , P. E. *J. Am. Chem. Soc.* **2006,** *128,* 15602-15603.
63. Giuseppone, N.; Schmitt, J.-L.; Lehn, J.-M. *Angew. Chem. Int. Ed.* **2004,** *43,* 4902-4906.
64. Guiseppone, N.; Schmitt, J.-L.; Schwartz, E.; Lehn, J.-M. *J. Am. Chem. Soc.* **2005,** *127,* 5528-5539.
65. Nguyen, R.; Huc, I. *Chem. Commun.* **2003,** 942-943.

2. Training a Constitutional Dynamic Network

2.1 Introduction

2.1.1 Functional dynamic covalent chemistry

2.1.1.1 Self-sorting systems

Recently the focus of many chemists has shifted from compounds to systems, many of which are intended to mimic natural processes (self-sorting, adaptation) or/and process simple information operation (multi-sensing, responsiveness, information storage). In fact, both features are closely connected because the assembly in a system can take place through combination of *self-sorting* (internal properties/information of the building blocks) and the *interaction way* (template) or *organizational way* (cooperation in the framework, e.g. agonist/antagonist relationships in DCL).[1,2,3]

The progress of a DCL towards thermodynamic equilibrium depends on three basic factors: *(a)* the overall distribution of constituents in the mixture depends on the formation of each single compound in the library (*self-sorting*); *(b)* if the formation/stability constant of one constituent changes, the whole library reflects it in an increased/decreased availability of building blocks and as a result the overall equilibrium changes as well *(organizational way)*; *(c)* such change can be induced by different templates or external chemical/physical stimuli like pH or light (*interactional way*).

Inherent differences in stability constants of individual members of a virtual library leads to the deviation from statistical distribution even in libraries with structurally similar building blocks and without any external stimulus. Such behaviour, where differences in stability of individual member of library leads to amplification of specific constituents is called thermodynamic self-sorting[4] and it is important for the description of the present work. The

problems with a markedly deviant distribution (biased distribution) are only accentuated in systems with dynamic bonds of different stability (e.g.: imine and acylhydrazone). This sometimes overlooked factor was articulated by Lehn:[5]

"To this end, it is desirable to achieve an unbiased, isoenergetic DCL, whose equilibrating constituents be of similar free energy, so as to generate a Boltzmann distribution displaying comparable populations for its different states/constituents. With a biased library, where one or a few constituents would be highly favoured, the preferred interaction of a minor constituent with the target may not be strong enough to overturn the equilibrium situation."[5]

Self-sorting can also occur by kinetic means in cases where the back reaction is hindered either by subsequent transformation (hydrogenation) of the product or its ultimate stability. Sanders observed one such example during formation of hydrazone based macrocycles.[6] To re-equilibrate in such mixture, the macrocycle must break in the first place, react with the free hydrazine and then disengage from the macrocycle in order to be replaced but because the concentration of free hydrazines in such libraries is rather low, the reverse intra-molecular closing of the disrupted macrocycle is more probable, thus hampering any possible re-equilibration. To avoid such kinetic trap, the Sanders's group used a high excess of monoacylhydrazine to attack and exchange with acylhydrazones inside the macrocycle. Monoacylhydrazone formation enables re-equilibration through formation of a stable open chain intermediate which provides enough time for component disengagement and subsequent exchange. Finally, the exchange of this monoacylhydrazone for the diacylhydrazone results in the closure of the macrocycle.[6]

Kinetic self-sorting together with conformity to Le Chatelier's principle gives chemists an interesting opportunity to obtain a series of defined products from large complex mixtures. It is possible to take advantage of this feature and to isolate only a specific product or a set of products from the complex virtual library. A constant re-equilibration of the mixture leads to the formation of a given product as long as there are its building blocks available. Such kinetic self-sorting was nicely demonstrated by Osowska and Miljanić.[7,8] In their most advanced experiment, they mixed five aldehydes and five amines and let them equilibrate. This virtual library comprises 25 possible imines. (*Figure 2.1*) They then subjected this mixture to vacuum distillation to remove gradually particular products from the library based on their boiling point.

The **A1** (77 %) with the lowest boiling point (70 °C) of all imines was first distilled off. Together with it, imines **A2-A5**, and **B1-E1** bearing the same building blocks disappeared from

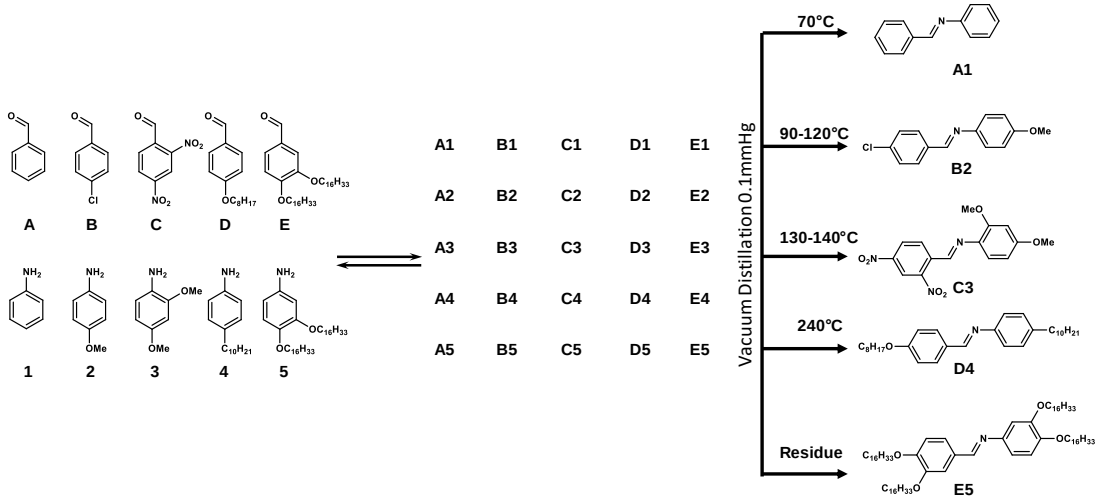

Figure 2.1: *The most complex example of self-sorting based on Le Chatelier principle. A mixture of imines constantly re-equilibrates, allowing quantitative isolation of pure imines according their boiling point.*

the mixture as well. Following the same principles, the following isolated imines according their boiling point were: **B2** (80 %, 90-120°C), **C3** (73 %) (130–140 °C), **D4** (80 %, 240 °C) which left **E5** (80 %) as the last imine in the flask. The gradual depletion of building blocks, caused by the removal of imines, enabled the stepwise access to five pure products from one reaction/mixture.[8] (*Figure 2.1*)

2.1.1.2 Adaptation to an external stimulus

The thermodynamic control of the assembly in dynamic combinatorial libraries allows/forces the system to adapt in response to changes of the environment. So-called adaptation can be triggered by physical stimuli (temperature, light, electric current), chemical stimuli (H^+, template) or environmental changes (solvent, phase change). The hydrazones and acylhydrazones presently studied can participate in three dynamic processes: 1) conformational dynamics by shape switching on cation coordination to the tridentate coordination site; 2) configurational dynamics during isomerization from E to Z configuration stabilized by internal hydrogen bonding to the pyridine group; 3) constitutional dynamics, by component exchange

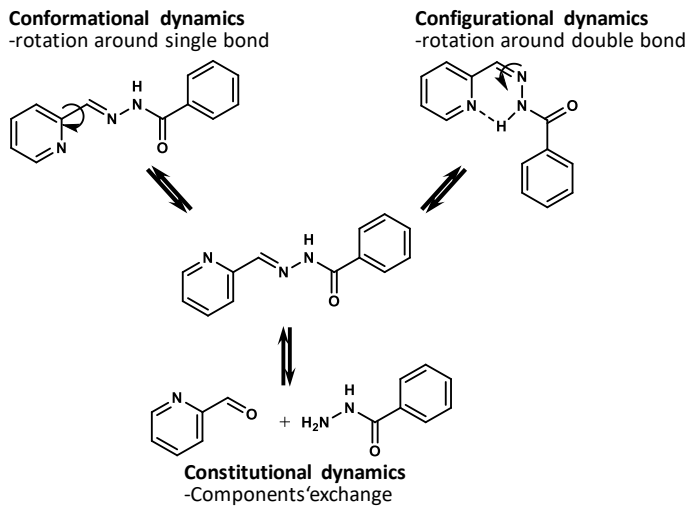

Figure 2.2: *Triple dynamics of pyridyl acylhydrazones observed in this work.*

of the reversible -C=N- bond.[2,3] (*Figure 2.2*) An access to multiple dynamics is especially interesting for building multi-responsive systems adaptable to several orthogonal stimuli. Possibly the best example of such behaviour is the system described by Vantomme and Lehn, which can be modulated via metalloselection and photoselection.[9] The group of Lehn has built systems adaptable to many kind of stimuli and under a wide range of conditions. These have already been reviewed in ref. [2, 3] and accessible through resources mentioned therein. A few examples of adaption to some less common stimuli are discussed below.

Lehn and Giuseppone showed that it is possible to modulate the distribution in a dynamic library by an electric field. In their work, an equilibration between two imines depended on dielectric anisotropy. One imine was designed to be liquid crystalline with a negative dielectric constant (**MBBA**, **EBBA**, *Figure 2.3*). This imine, which couples better with an electric field, is amplified while the other is suppressed probably through an electrohydrodynamic process. The coupling of liquid crystals with an electric field also resulted in liquid to nematic phase transition.[10] (*Figure 2.3*)

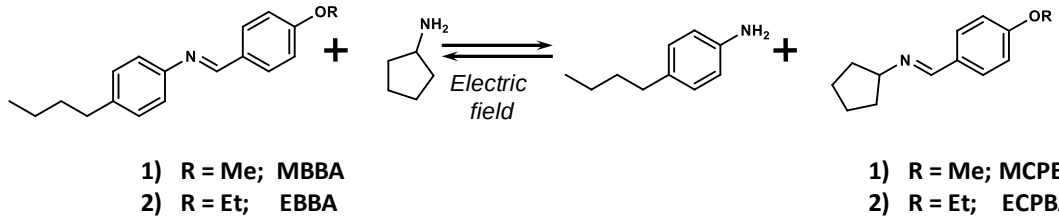

1) R = Me; MBBA
2) R = Et; EBBA

1) R = Me; MCPBA
2) R = Et; ECPBA

Figure 2.3: *Imine based exchange reaction which was used during the study of the impact of electric field. Liquid crystalline **MBBA** and **EBBA** which couple with electric field are amplified while the **MCPBA** and **ECPBA** are suppressed.*

Response to a phase transition, e.g. from liquid to solid (crystallization), is another form of adaptation to environmental changes. One such example is a chiral reorganization of Cu(I) phenanthroline complexes during crystallization described by Nitschke. When a phenanthroline dialdehyde, Cu(I) and (±)-1-amino-2,3-propanediol were mixed together in methanol, it gave rise to a complicated mixture of different diastereomers. (*Figure 2.4*) However, upon crystallization only one of these diastereomers, that of the highest symmetry (D_2), was found in the crystals in which the lattice contained columnar arrays of both its Δ and Λ enantiomers. It was assumed that the high level of symmetry might have been a consequence of the formation of four hydrogen bonds per molecule in the lattice, a situation unlikely to be maintained with the lower symmetry diastereomers and thus causing them to be more soluble, so that the constant re-equilibration of the mixture in solution resulted in the deposition of a single species.[11]

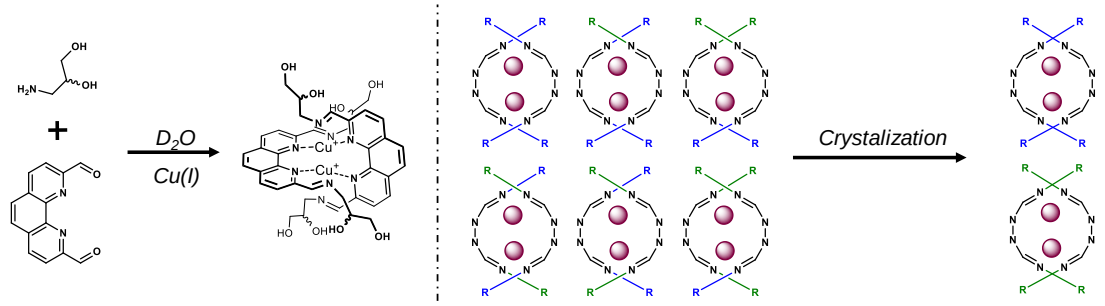

Figure 2.4: *Adaptation to phase change.* ***Left:*** *Illustration of the structure of studied double helical copper(I) complex.* ***Right:*** *A part of the virtual library of individual diastereomers and dynamic chiral resolution during the liquid to solid transition (crystallization).*

An interesting example of adaptation to environmental changes is that to the ionic strength of the solution. (*Figure 2.5*) An equilibration of a pseudopeptidic thiol library of macrocycle precursors was studied while increasing the salt concentration. The change in ionic strength of a solution corresponds to a shielding effect on the electrostatic forces between charged species. An increase of ionic strength amplified previously disfavoured species: homodimeric macrocycles with twice the same charge were amplified on the expenses of the macrocycle bearing both positive and negative charges.[12]

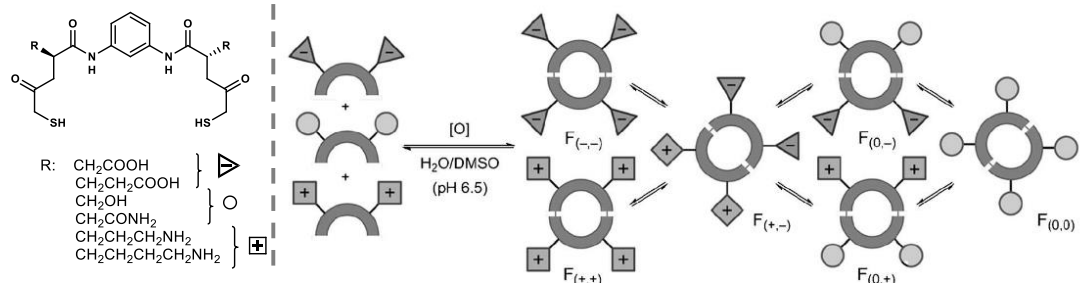

Figure 2.5: *Adaptation of disulphide library in response to change in ionic strength of the environment. Ref. [12]*

2.2 Key terms, concepts and ideas

Before I present the actual data, I would like to introduce the goal, concepts and key terms which are used throughout this work.

Learning and training can be seen as interesting examples of dynamic processes. Without going into details, when our brain encounters new stimulus, it sends an impulse into the network of neurons where the information is stored in a unique pattern of neural connections. This pattern is responsible for storage of memories or skills. Repeating the memory or practising the skill strengthens the dynamic connection so that on every following encounter the recall (time to express the information) is shorter. On the other hand, when the connections are not used,

they break and re-arrange until the original information is lost, being equivalent to erasure of the information.[13,14,15,16]

The goal of the present work was to design, assemble and test a system to which specific information can be imprinted, stored in, recalled and erased. Some of these features have been reported in individual examples[9,17,18,19], but no system integrating all the functions with multiple entries has been found yet. Herein, we wanted to prepare a system which is able to store information about multiple entries (metallo-templation) using ability of DCL to organize itself in different ways as a response to different stimuli.

In order to address all these features on molecular level, C=N based DCLs are very promising systems. To clarify the following text, all starting compounds such as aldehydes, amines and acylhydrazones will be called *components* and the products of their condensation will be called *constituents*.

To explain and describe the behaviour of a system, one can imagine a simple four component setup: **A**, **A'**, **B**, **B'**, where **A**s (aldehydes) can react with **B**s (amines). Ideally, in an equilibrated mixture of all four components in equimolar amounts, all constituents (**AB**, **A'B**, **AB'**, **A'B'**) are present in equal amounts.

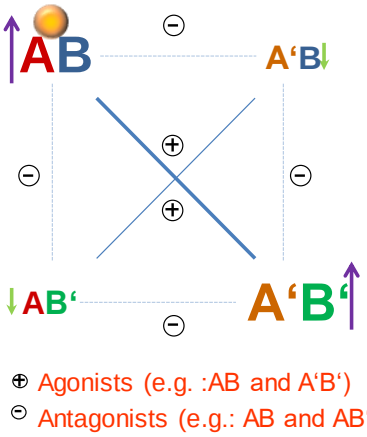

Figure 2.6: *Schematic illustration of the agonist/antagonist relationship.*

Upon addition of a metal cation (e.g. hexa-coordinating Zn(II)), its superior binder (e.g. **AB**) is complexed and therefore to large extent removed from the equilibrium mixture. As a consequence, the equilibrium of the rest of the library change accordingly. Now, the equilibrium of the mixture is changed and new relationships between constituents become evident. As free **AB** is removed by complexation, amounts of the free components **A** and **B** in the mixture decrease. In a constantly equilibrating (dynamic) mixture, this decrease/increase is directly reflected in the amount of constituents which contain the same components (e.g. **A'B** and **AB'**). Constituents that compete directly with **AB** for building blocks, **A'B** and **AB'**, are called *antagonists*. The result is such that when the amount of **AB** increases, the amount of its *antagonists* proportionally decreases. (*Figure 2.6*)

In the ideal case, all **A** and **B** are fully converted into **AB** and the only components left in the solution are **A'** and **B'**. These can then only form **A'B'** which is called an *agonist* (to **AB**)

implying a synergistic relationship between them. An amplification of one *agonist* causes increase of the amount of the other one. (*Figure 2.7*)

Addition of the metal causes adaptation of the library and this adaptation is called *training* of the DCL by a (particular) metal cation. When the new equilibrium is established and new distribution of the constituents is settled, it can be said that the metal imprinted its own fingerprint into the distribution of the library.

Provided that the re-equilibration is slow under given conditions and the removal of the metal ion does not affect the constituents, an imprinted distribution of constituents is conserved, still *storing* the information about the influence of the effector. (*Figure 2.7*) Clearly, this system is *out-of-equilibrium* because the metal-free library would thermodynamically provide four equally represented constituents. The information in this kinetically locked distribution can be understood as a different form of pre-organization towards effector. Therefore, when the same metal cation is re-added, the library does not need to rearrange leading to a much faster

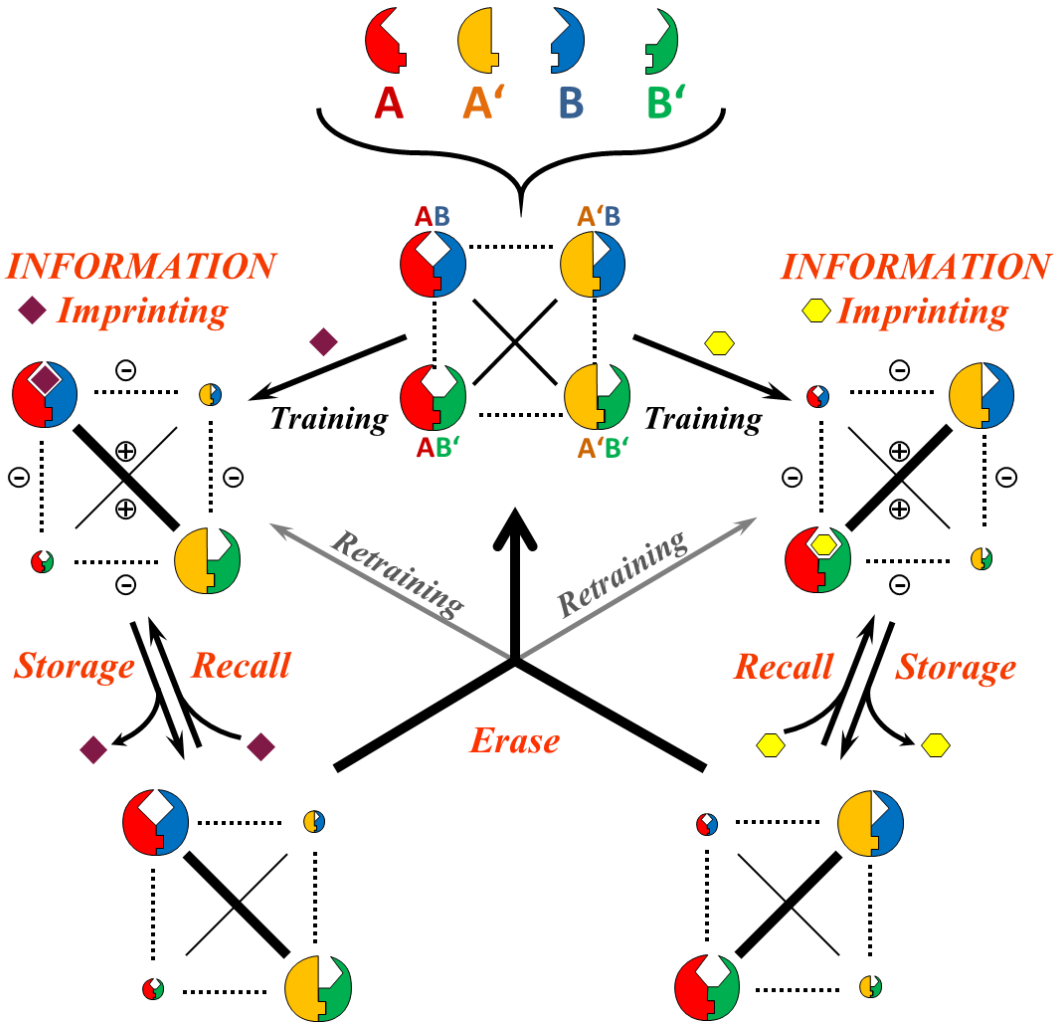

Figure 2.7: *Schematic illustration of a doubly responsive/trainable system, with the equivalent informatics operations identified"*

complexation/return to the second state than during the initial adaptation. The process is described as (fast) *recall*. (*Figure 2.7*)

Due to the thermodynamically out-of-equilibrium nature of metal-free state, the restoration of the initial distribution of the constituents should be possible via a change of conditions (e.g. high temperature) and thus effectively *erase* the information about effector. (*Figure 2.7*)

The goal of this work was to achieve doubly responsive systems. This means that two orthogonally acting metals are needed, each of them affecting a different pair of agonists. As may be seen in *Figure 2.7*, the second metal cation (e.g. tetra-coordinating copper(I)) amplifies **AB'.** This species is in an antagonist relationship to **AB** and **A'B',** the amounts of which now decrease while that of its agonist **A'B** increases. Now, the same set of operations as described above: *training*, removal of the metal ion, *storage* of information, *fast recall* upon re-addition of the metal ion and *erasure* of the imprint can be performed in the same manner. The out of equilibrium state can be also directly re-trained just by the addition of the orthogonal metal cation without the explicit need to erase the information beforehand.

The following sections will describe proposed libraries, encountered problems and a final successfully operating system.

2.3 Results and discussion

2.3.1 First steps: Introduction to the problems

With the goal set and the general concept defined as above, the first system was designed and practically tested. The four-component system comprised 6-methyl-2-pyridinecarboxaldehyde (**27A**, methylpyral), salicylaldehyde (**27A'**, salal), benzhydrazide (**27B**) and bis(2-aminoethyl)ether (**27B'**).

The first system was designed in order to balance fast equilibration and selection for specific metals on one side and stability on the other side. Both pairs of agonists consist of one acylhydrazone and one imine compound. The formation of an acylhydrazone is of crucial importance because its stability towards hydrolysis serves as the kinetic barrier, which stabilizes the out of equilibrium states and blocks re-equilibration. Such behaviour can be described by the term "agonist inhibition". The re-equilibration of the agonist pair (e.g. **27AB**, **27A'B'**) requires their hydrolysis and formation of new constituents which share one component from each agonist (**27AB'**, **27A'B**). Since one agonist (acylhydrazone, **27AB**) shows very limited hydrolysis its building blocks are not readily available for the exchange. Therefore, building

blocks of the other agonist (imine, **27A'B'**), despite of being available for exchange can only reform the same imine and as a result the distribution in the system does not change.

When all four components were mixed in a NMR tube in d_3-acetonitrile (**27A**, **27A', 27B** $1.25x10^{-5}$ mol, 25 mM, **27B'** $0.625x10^{-5}$ mol, 12.5 mM), the only components found in the mixture after 3 h at 23 °C were **27AB** and **27A'B'**, exposing a truly biased system. The origin of this bias is probably of kinetic origin and can be attributed to the favoured formation of the acylhydrazone **27AB** (compared to **27A'B**) and to the stabilization of its agonist **27A'B'** by hydrogen bonding between the phenolic –OH and the imine –N=.[20] Combination of both factors drives the selection between constituents towards strong amplification of the agonists **27AB** and **27A'B'** in a synergistic fashion even in the absence of any metal cation. However, from thermodynamic point of view, not even extensive heating (48 h, 70 °C) could effectively overturn this bias. (*Figure 2.8, Figure E1.1*)

After heating this system at 60 °C for a few hours (3-5 h), a new set of peaks emerges. These peaks were identified as the E and Z isomers of acylhydrazone **27AB**. This problem of the presence of several configurational isomers of pyridyl acylhydrazones[9,21,22] will be explained in detail later in the chapter together with other more detailed examples.

Another unforeseen problem appeared after addition of 0.5 eq. of $Zn(OTf)_2$ (compared to **27A**, $0.625x10^{-5}$ mol) which led to extensive hydrolysis of the imine **27A'B'**. (*Figure 2.8, Figure E1.2*) Nevertheless, the expected acylhydrazone **27AB** was formed almost quantitatively and complexed in a form of Zn(**27AB**)$_2$. Its agonist **27A'B'** formed only in 14% with the rest in form of non-condensed components (30 %). This behavior was observed to affect only non-complexing imines (**27A'B'**, **27A'B'**, **27A'B'**). In the following text, it is referred to as hydrolysis and its amount was always determined by integration of **A'** aldehyde peak in ^{1}H NMR spectra of respective system.

At this point, the removal of Zn was attempted but another problem was encountered. Acidic hydrogen atoms (N-H, O-H) on the components and constituents create complex acid-base equilibria under the basic conditions involved in the use of a polyamine (hexacyclen) for this purpose. As a result, the NMR spectra of the product mixtures showed both broad peaks and peaks indicative of the presence of new species, so that their full analysis was impossible.

On the other hand, a dramatic effect of Cu(I) on the components mixture was observed. Addition of 0.5 eq. of CuOTf ($0.625x10^{-5}$ mol, compared to **27A**) caused after 12 h at room temperature pronounced amplification of **27AB'** and its agonist **27A'B**

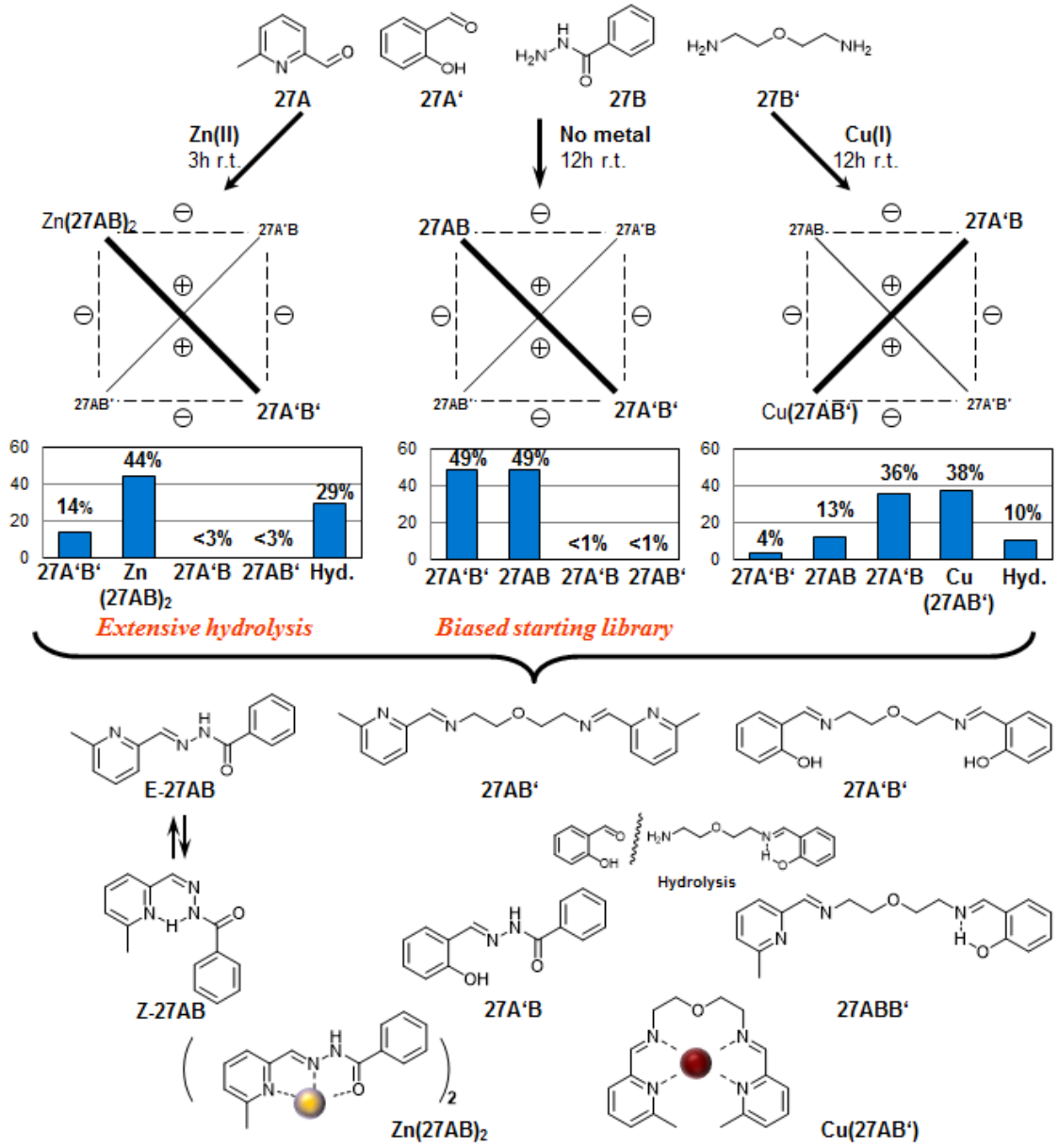

Figure 2.8: *The very first tested system, with marked encountered problems (noted in red text) and illustrative example of the whole virtual library of possible constituents. Distribution of the four constituents of the DCL **27AB**, **27A'B'**, **27AB'** and **27A'B**: without any metal (**middle**), after Zn(II) addition (**left**) and Cu(I) addition (**right**) showing the biased initial distribution (**middle**) and extensive hydrolysis of **27A'B'** (**bottom left**). **27AB** exists in E and Z forms.*

(**27A'B'**/**27AB**/**27A'B**/Cu(**27AB'**)/hydrolysis = 3/13/36/38/10 %). (*Figure 2.8, Figure E1.3*) The hydrolysis was quantified based on the amount of free salicylaldehyde. In all the above mentioned cases, the same distribution was reached starting from both agonist pairs/diagonals as well as from the mixture of components. The formation of metal complexes of the different constituents in the **DCL** was deduced from the marked chemical shift of resonances for the respective complexes (Zn(**27AB**)$_2$ or Cu(**27AB'**)) in comparison to the free constituent (**27AB** or **27AB'**). The peaks of the remaining non-complexing constituents were almost unaffected

and found with same chemical shifts as in their individual solutions in d_3-acetonitrile. The adaptation in the DCL was then quantified by integrating the characteristic peaks of each constituent. In cases where one constituent was found as different isomers, all isomers were integrated separately and their amount sum up to afford final herein reported value.

Thus, in the system described above marked changes in constituents' expression was observed together with a significant difference between the effects of the two different cations. However, considering both the initial bias of the DCL and the extensive hydrolysis caused by the addition of the Zn(II), the performance of the system was not satisfying enough. In order to address these issues, further exploration was conducted.

For this purpose, several different combinations of aldehydes and amines were tested. Among the examined systems one is worthy of closer description, even though it was found to be unsatisfactory for our purposes in the end.

First, instead of 6-methyl-2-pyridinecarboxaldehyde (**35A**), 6-phenyl-2-pyridinecarboxaldehyde (**35A**) was taken. This was inspired by the work of J.-P. Sauvage whose study on substituted 2,2'-bipyridines demonstrated that bulky groups in position 6 stabilized Cu(I) complexes making the copper almost un-removable.[23]

Another improvement was replacing the aliphatic diamine with *p*-toluidine (4-methylaniline), which shows, as do aniline imines in general, higher resistance/stability towards hydrolysis in the presence of Zn(II). The *p*-methyl derivate was chosen for its simpler NMR spectrum compared to that of aniline. In this regard, it is worth mentioning that benzylamine was also tested, but some interfering reaction (decomposition/side reaction) was observed and thus this amine was abandoned.

When 6-phenyl-2-pyridinecaboxaldehyde, salicylaldehyde, benzhydrazide and p-toluidine (1.25×10^{-5} mol, 25 mM) were mixed in d_3-acetonitrile and heated for 12 h at 60 °C, again a strongly biased distribution was observed (**35AB**/**35A'B'**/**35A'B**/**35AB'**/hydrolysis = 49/34/3/2/12 %) This distribution did not change even after prolonged heating. (*Figure 2.9, Figure E1.4*)

Compared to the previous case, this system showed improved resistance to Zn(II). As expected, after addition of 0.5 eq. of Zn(II) a total amplification of **35AB** was observed. Interestingly, the level of hydrolysis in this mixture even decreased to 5 % (from 12 % in the plain library) and as a consequence the amount of **35A'B'** increased up to 46 %. (*Figure 2.9, Figure E1.5*)

In contrast, the amplification of the copper agonists was rather low. After addition of 0.5 eq. of Cu(I)OTf (0.625×10^{-5} mol) and subsequent heating for 12 h at 60 °C, an almost equimolar

distribution of components (**35AB**/**35A'B'**/**35A'B**/**35AB'**/hydrolysis = 26/25/23/23/4 %) was found in the mixture. This distribution still reflects amplification of desired **35A'B**/**35AB'** by more than 20 %, but this is not enough for the outlined goal to demonstrate training of a system via explicit amplification of a given agonist pair. (*Figure 2.9*, *Figure E1.6*)

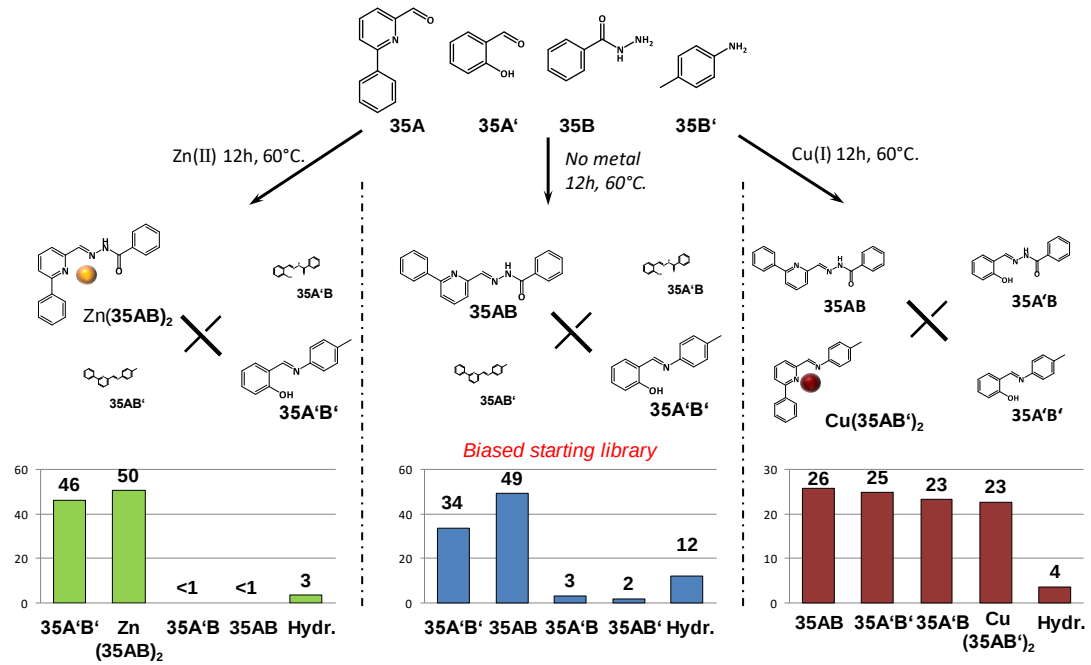

Figure 2.9: *Improved DCL with unresolved bias and loss of selectivity for Cu(I). Distribution of the four constituents of the DCL **35AB**, **35A'B'**, **35AB'** and **35A'B**: without any metal (middle), after Zn(II) addition (left) and Cu(I) addition (right) **35AB** exists in E and Z forms.*

At this point, it is necessary to stress out that this distribution still bears information about the specific effector. The characteristically changed distribution between constituents directly points to the presence of Cu(I) cation. In a hypothetical case of a series of different metal cations, each of them with characteristic fingerprint in a form of defined distribution, such dynamic systems could turn into an analytical tool for metal cation identification.

The abovementioned examples illustrate major problems encountered during this project: strong initial bias towards one diagonal and extensive hydrolysis in the presence of Zn(II). Solving these issues while keeping the selectivity for both orthogonally performing metals turned out to be a major challenge.

2.3.2 Dual responsive and information processing system

Numerous optimizations and investigation of different starting components finally provided a system which comprised all the desired challenging features of the trainable multi-responsive dynamic covalent system.

The final DCL was generated from the following four components ($1.25x10^{-5}$ mol each, 25 mM): 6-phenylpyridine-2-carboxaldehyde, 4-chlorobenzaldehyde, benzhydrazide and p-toluidine were mixed in acetonitrile and heated at 60 °C for 12 h to achieve thermodynamic equilibration. Four constituents **50AB, 50A'B', 50A'B** and **50AB'** were obtained with a distribution of **34**/**23**/**16**/**13 %** respectively, accompanied with 14 % of non-condensed species (i.e. hydrolysis). (*Figure 2.10, Figure E1.7*) The degree of hydrolysis of **50A'B'** is a part of the equilibrium and cannot be avoided. Moreover, the presence of the two configurational isomers of **50AB** (E-**50AB** (40 %) and Z-**50AB** (60 %)) was observed and their interconversion was taken into account.

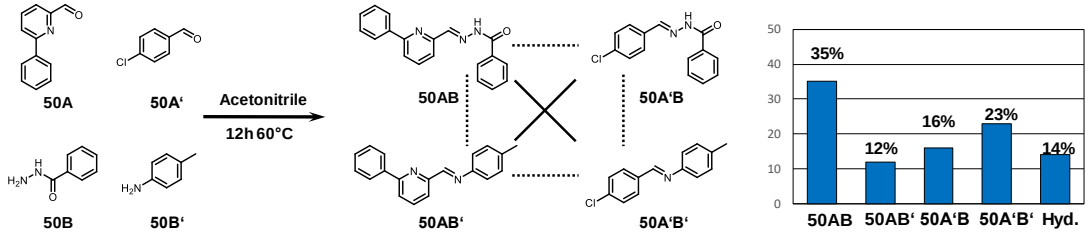

Figure 2.10: *Distribution of the constituents of the optimized DCL generated from the components in the absence of metal cations in acetonitrile. The amount of **50AB** indicated is the sum of the E and Z forms of this constituent.*

Even though the system still shows some initial bias, the actual level allows effective induction and demonstration of the amplification to both diagonals as was anticipated at the beginning as the project.

Taking into account various kinetic and thermodynamic processes accompanying the component exchanges, starting from free components is desirable. It simplifies the preparation of the library as well as allowing a more accurate study of the dynamic behavior of the system. However, in order to exclude any discrepancy, all the transformations described below were carried out starting from both component and constituent mixtures, with the same results being obtained regardless of the path.

2.3.3 Dual responsive information processing within a CDL Training, Storage, Recall, Erasing and Re-training

2.3.3.1 Operating with the first effector: Zinc(II)

Training: When the initial mixture of four components was subjected to the addition of $Zn(OTf)_2$, ($0.625x10^{-5}$ mol, 12.5 mM, 0.5 eq. in respect to **50A**), the preference for an octahedral coordination environment with tridentate ligands promoted formation of the constituent/complex Zn**(50AB)**$_2$ and as a consequence the amount of its agonists **50A'B'** increased as well. Equilibration of the library after addition of Zn(II) requires heating at 60 °C

for 3 h allowing total amplification of only one diagonal/agonist pair **(**Zn**(50AB)**$_2$ **/50A'B'/50A'B/50AB'/**hydrolysis = 50/39/<1/<1/11). (*Figure 2.11, Figure E1.10*)

Once the information about the Zn(II) cation was imprinted in the new distribution of the constituents, in the next step it was necessary to remove the metal cation and thus prepare the system for subsequent operations of recall, re-training or erasure.

The removal of the zinc turned to be particularly challenging because of the presence of N-H group in the acylhydrazone moiety and Lewis acid nature of zinc cation. Acylhydrazone N-H, only weakly acidic in the free ligand, turns out to be easily ionizable upon complexation, which resulted in a complex acid-base equilibrium and hard-to-analyze mixtures upon decomplexation. Further, some demetalation reagents (e.g. hexacyclen) can interfere with one of the following steps (re-training, recall, erasure), some are insoluble in pure acetonitrile (e.g. $K_3[Fe(CN)_6]$) and some catalyze fast re-equilibration. Finally, after extensive optimization, the best reagent proved to be $[(NEt_4)_2]EDTAH_2$ (bis-(tetraethylammonium) dihydroethylenediaminetetraacetate). It forms a strong $ZnEDTAH_2$ (LM) complex, which precipitates out from the mixture. However, a slight excess is needed to ensure that no zinc remains in the solution. These leftover traces of Zn(II) were found to catalyse re-equilibration of the metal-free state and substantially decrease the lifetime of the out-of-equilibrium state. Therefore, slightly elevated levels of **50AB'** and **50A'B** observed after demetalation are consequences of the zinc-catalyzed equilibration during the demetalation/precipitation step. (*Figure 2.11, Figure E1.11*)

Recall: At this point, the system has been trained and prepared for the repeat zinc recognition (recall), which should be presumably much faster than the initial complexation/equilibration. Indeed, the re-addition of the zinc cations results in direct return to the previous state (recall) and the overall time of restoration of the complex state is much shorter (minutes) than the first adjusting step (hours). (*Figure E1.11)*

In the training step, the DCL needs time not only for complexation of the cation, but mainly for a change in distribution, which in all cases presented herein takes several hours. The removal of the metal cation does not affect the distribution. Therefore, after the re-addition of the cation, the system does not need to change an already pre-organized distribution and the resulting time is only that needed for complexation. This re-complexation of Zn(II) is complete within the time of mixing the solution and measuring the ^{1}H NMR spectrum (minutes).

Storage and Erasure: The metal–free state (out-of-equilibrium state) does not change by more than 10 % from the originally amplified distribution for at least 12 h at 23 °C, meaning

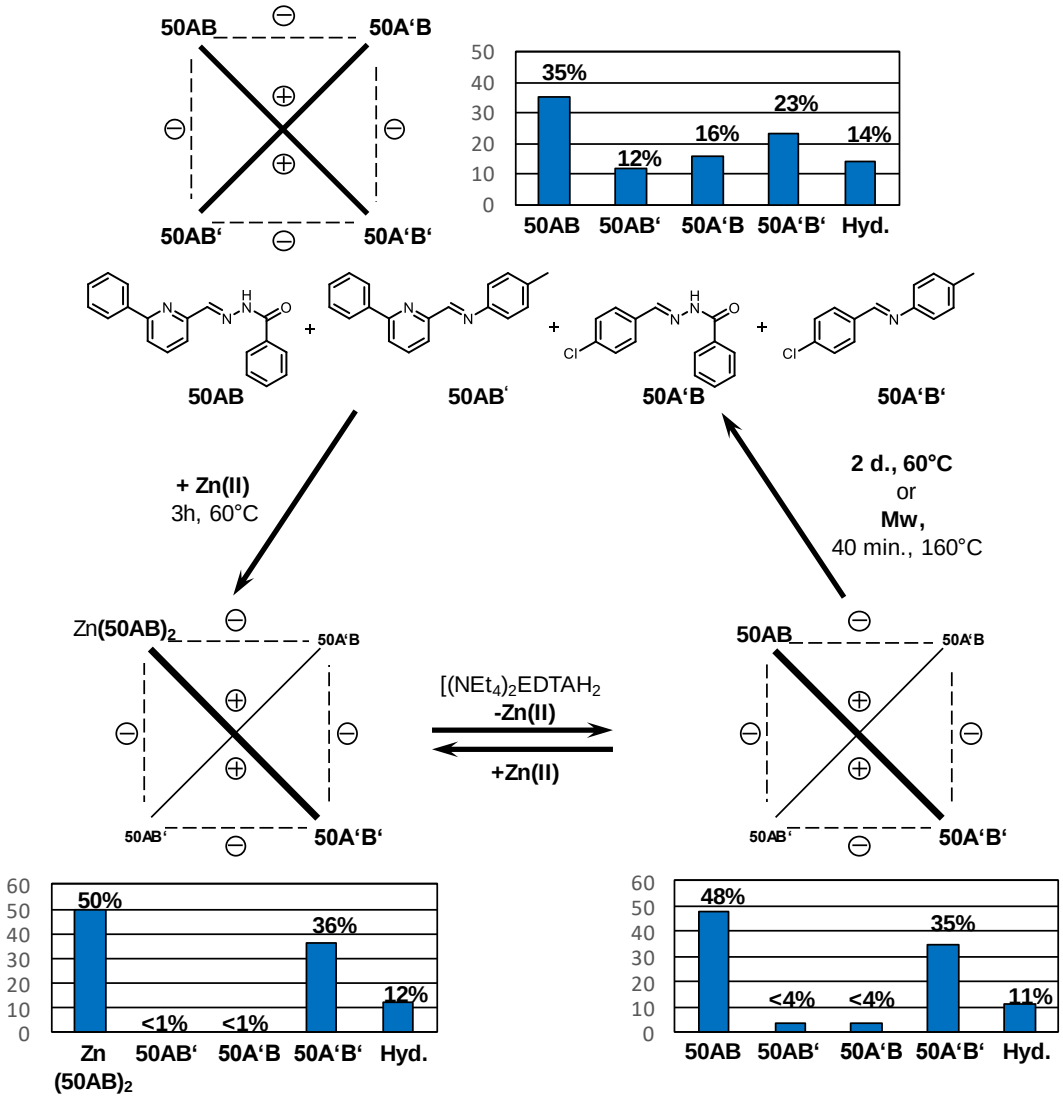

Figure 2.11: *Formation of the Zn-trained DCL distribution by addition of $Zn(OTf)_2$ to the mixture of the four constituents **50AB**, **50A'B'**, **50A'B** and **50AB'** (training; left top to bottom), which on cation removal retains its composition in the metal-free DCL obtained (information storage; bottom, left to right); recall by addition of zinc(II) (bottom, right to left) and erasing of the metal-free DCL by heating (right bottom to top) with return to the thermodynamically driven initial state. Mw = microwave irradiation*

that the information is stable and efficiently recallable in this period of time. As described above, the distribution is given by the stability of the acylhydrazone **50AB** via agonist inhibition. The remarkable stability is demonstrated by the harsh conditions needed for the erasure and return to thermodynamic state. To achieve this, it is necessary to heat the system for two days at 60 °C or apply microwave irradiation (40 min, 160 °C). (*Figure 2.11, Figure E1.12, E1.13*)

Re-training: Finally, the addition of Cu(I)OTf to the out-of-equilibrium state and subsequent heating at 60 °C for 12 h re-trains the system from the zinc-trained/selected directly into copper-

trained/selected (described below) without the need of any particular erasing step. (*Figure 2.13, Figure E1.13)*

2.3.3.2 Operating with the second effector: Cu(I)

Training (*Figure 2.12*)*:* As a second step, the starting mixture was treated with copper(I) triflate (CuOTf, 0.625×10^{-5} mol, 12.5 mM, 0.5 eq. in respect to **50A**) and left to equilibrate at 60 °C for 12 h. A change in the composition of the library was expected due to the amplification of **50AB'** as the tetrahedral complex Cu(**50AB'**)$_2$ and of its agonist **50A'B**, which represents complementary result to the previous zinc-selected diagonal. The distribution obtained for **50AB /50A'B'**/Cu(**50AB'**)$_2$/**50A'B** /hydrolysis was **10/18/31/32/9 %** respectively. This led to

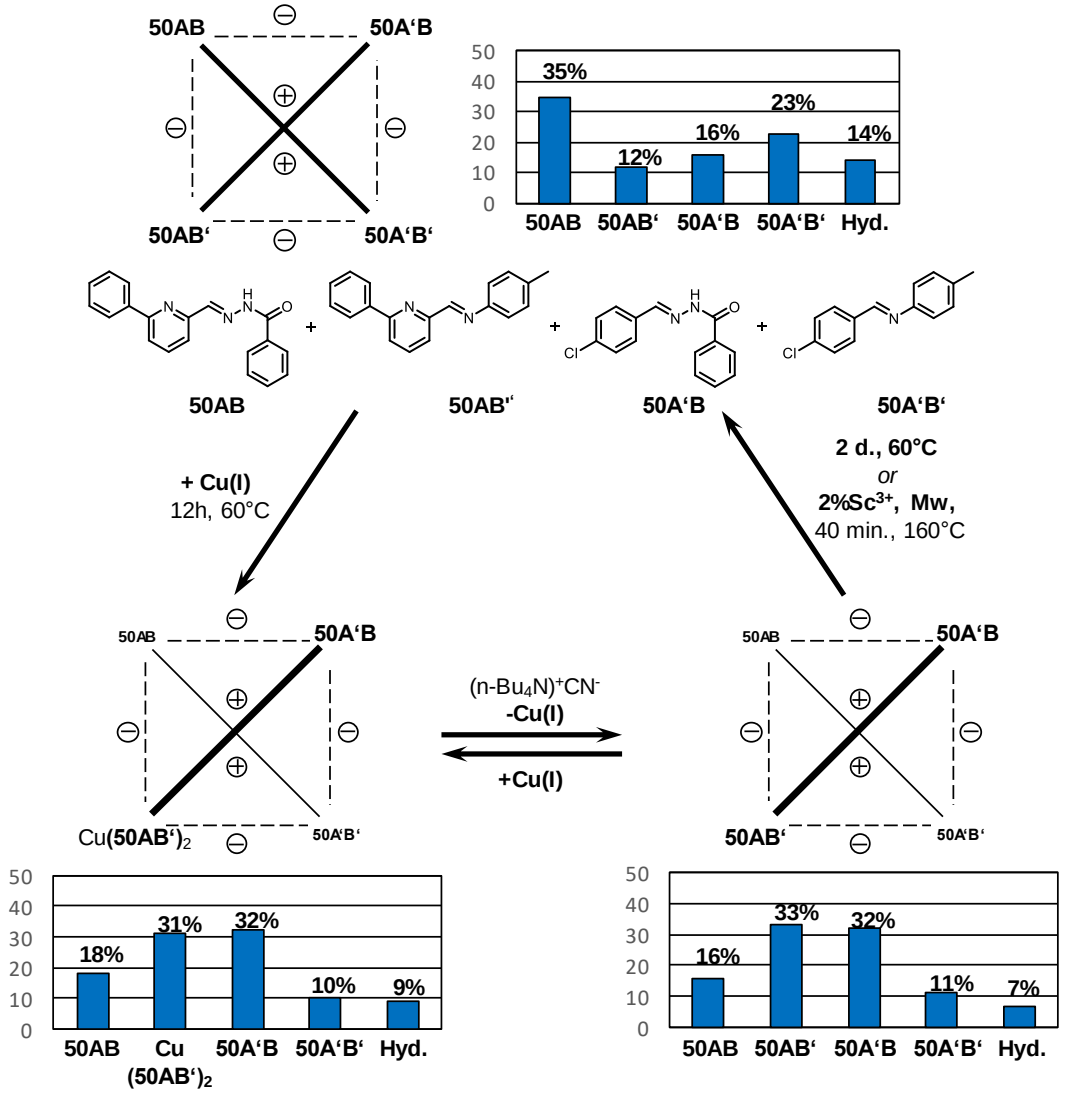

Figure 2.12: *Formation of the Cu(I)-trained DCL distribution by addition of CuOTf to the mixture of the four constituents **50AB**, **50A'B'**, **50A'B** and **50AB'** (training; left, top to bottom), which on cation removal retains its composition in the metal-free DCL (information storage; bottom left to right); recall by addition of Cu(I) (bottom right to left) and erasing of the metal-free DCL by heating (right, bottom to top) with return to the thermodynamically driven initial state. Mw = microwave irradiation*

amplification of 16 % in the case of **50AB'** and 19 % in the case of its agonist **50A'B** compared to the initial metal-free distribution.

Storage, Recall, Erasure *and* ***Re-training*** (*Figure 2.12, Figure E1.14-E1.18):* In a case of Cu(I), commercially available NBu_4CN precipitated CuCN from the mixture without any change in the distribution of the constituents. The return to the complexed state after the re-addition of Cu(I) is complete almost immediately (the time between mixing and measuring an NMR spectrum) and is also manifested by a profound colour change of the solution from colourless back to dark red, which is a result of MLCT charge transfer between the Cu(I) cation and pyridine-imine ligand. Thermodynamic equilibration and erasure of the imprint can be

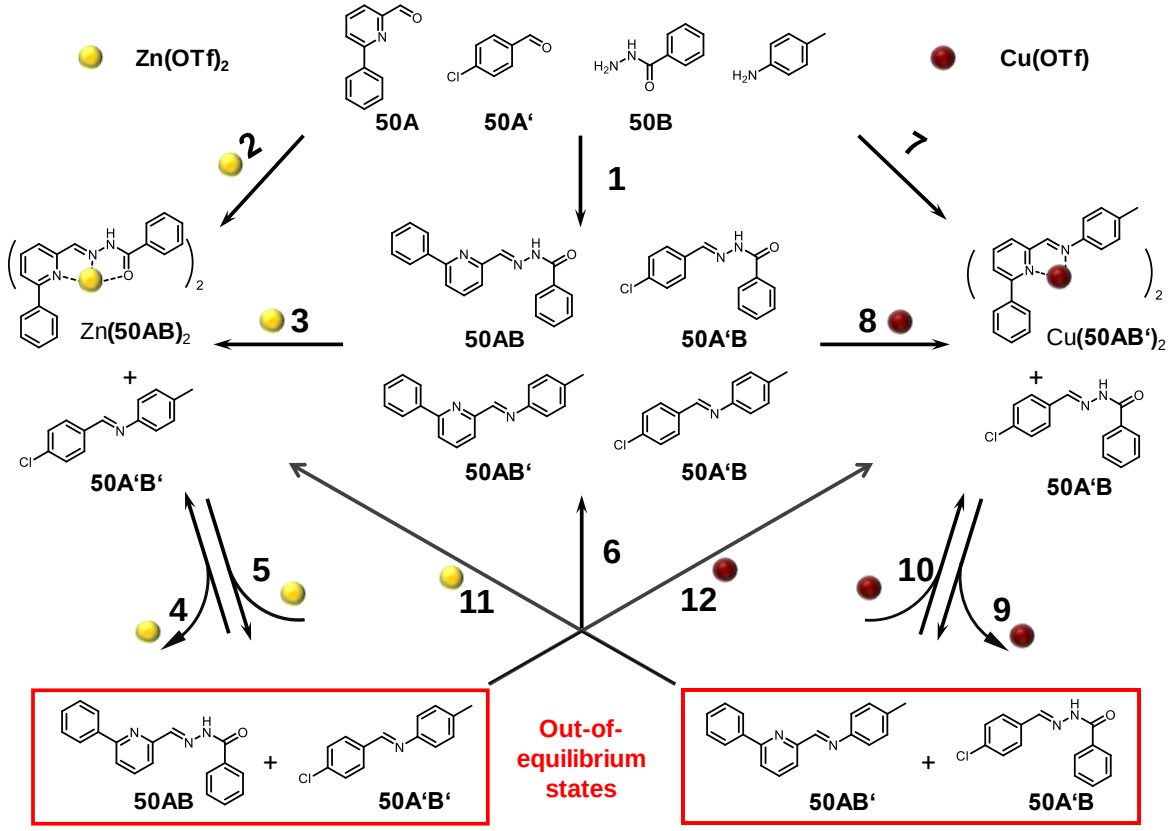

Figure 2.13: *Synoptic representation of all the transformations performed by the dual responsive dynamic covalent system based on the DCL* ***50AB***, ***50A'B'***, ***50A'B*** *and* ***50AB'****. (1) DCL generation from the components; 12 h, 60 °C, CD_3CN. (2), (3) Adaptation/training of the system on the Zn(II) effector; 0.5 eq. of $Zn(OTf)_2$, 3 h, 60 °C. (4) Storage of information/imprint: retention of the Zn-distribution for more than 12 h at r.t. after Zn(ll) removal by $[(Et_4)N]_2EDTAH_2$. (5) Fast information recall on re-addition of 0.5 eq. $Zn(OTf)_2$. (6) Erasing of information/imprint by regeneration of the initial DCL distribution, MW, 40 min, 160 °C. (7), (8) Adaptation/training of the system on Cu(I); 0.5 eq. of CuOTf, 12 h, 60 °C. (9) Storage of information/imprint: retention of the Cu-distribution for more than 12 h at r.t. after Cu(l) removal by $(n\text{-}Bu)_4CN$. (10) Fast information recall on re-addition of 0.5 eq. CuOTf. (11) Direct re-training of the Cu-DCL on Zn(II); 0.5 eq. of $Zn(OTf)_2$, 3 h, 60 °C. (12) Direct re-training of the Zn-DCL on Cu(I); 0.5 eq. CuOTf, 12 h, 60 °C. [****50AB***, ****50A'B'****] (bottom left) and [****50AB'***, ****50A'B****] (bottom right) represent constitutional engrams, out-of-equilibrium states.*

achieved by microwave irradiation (40 min, 160 °C, Mw, 2 % of $Sc(OTf)_3$)[24]. Addition of Zn(II) to the out-of-equilibrium Cu(I)-free system results in the imposition of Zn(II) preferences and complete re-training (change of the distribution). This also completes the full circle of transformations, thus demonstrating the interconvertibility of all paths. (*Figure 2.13*)

2.3.4 Thermal isomerization of two model pyridyl acylhydrazones

The E/Z isomerization of **27AB** and **50AB** was studied in detail. All four isomers were observed and characterized by NMR spectroscopy (1D and 2D). E-**27AB** and Z-**50AB** were isolated in pure forms and their transformation from one isomer to the other was achieved by different methods. The other two isomers were prepared from their counterparts in solution and studied without isolation.

2.3.4.1 E/Z isomers of 27AB

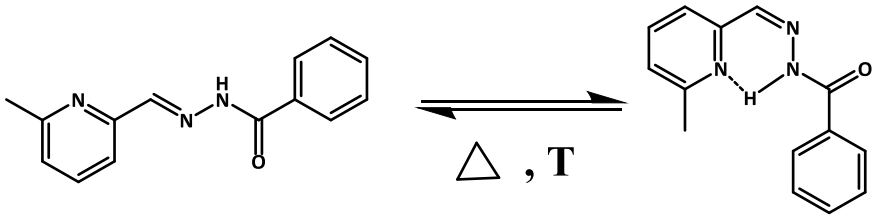

Figure 2.14: *Illustration of E/Z isomerization of the constituent 27AB*

Initially, the 6-methylpyridine-2-carboxaldehyde was mixed with benzhydrazide in EtOH and the reaction mixture was heated for 12 h at 70 °C. After this period, the solvent was evaporated under vacuum at room temperature, providing a viscous oil. Hexane was added and mixture was briefly sonicated. A white precipitate was formed and collected by filtration in ~90 % yield.

The desired acylhydrazone **27AB** was obtained as almost pure E isomer (>95 %). The configuration around the double bond was deduced from the chemical shift (10.34 ppm) of the NH proton, which is significantly lower than that of the Z-isomer (15.75 ppm) and was further confirmed by the 2D NOESY spectrum. (*Figure 2.14, 2.15, See also Figure E1.19-E1.22*)

The transformation between E/Z is slow at room temperature but becomes faster at higher temperatures. At 70 °C, the system reaches equilibrium in 12 h. The formation of the Z isomer leads to the appearance of a new set of peaks in the proton NMR spectrum. The equilibrium of pure **27AB** in acetonitrile contains 55 % of the Z isomer and 45 % of the E isomer. In this case, 2D NOESY was used to assign the signals of both species in the mixture. (*Figure 2.15*)

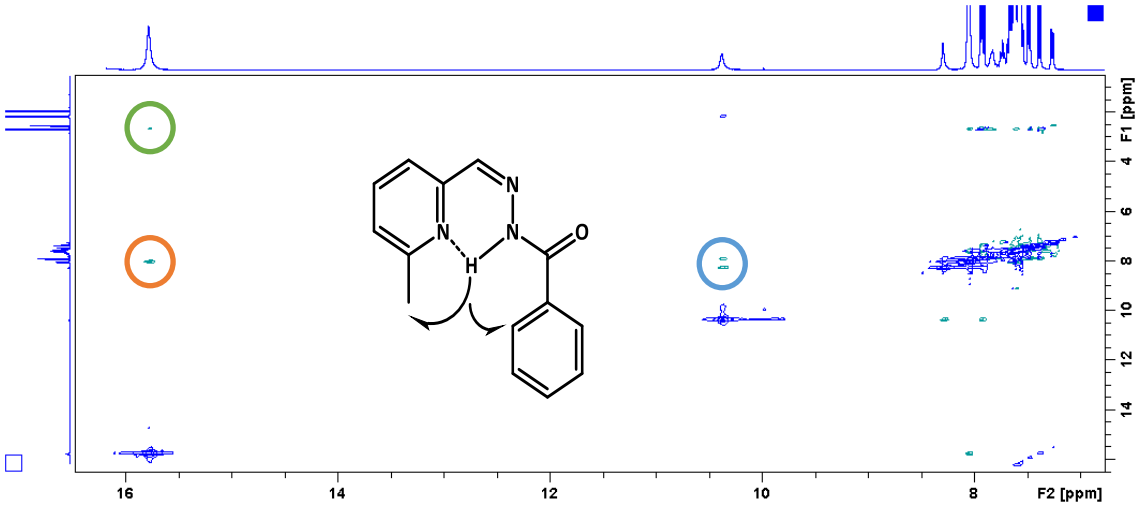

Figure 2.15: *2D NOESY of the mixture of **27AB** E and Z isomers. For Z isomer, the N-H is hydrogen bound to the pyridine nitrogen atom and has NOE interaction with benzhydrazide C-H (purple circle) and interaction with -CH_3 of pyridine (orange circle). There are also visible NOESY signals of E isomer (blue circle) which has only the N-H to aromatic C-H interaction.*

In the case of **27AB,** the Z isomer was never isolated as a pure compound and all the studies and characterization were performed in an acetonitrile solution of an equilibrated mixture of E and Z isomer.

The formation of **27AB** in the training system is significantly faster than in the case of formation from a pure **27A** and **27B** mixture. When the equilibration was done at room temperature only the formation of E-isomer was observed. The faster formation rate in the full system can be attributed to nucleophilic catalysis by the amines present. Concerning the mechanism of E and Z isomerization, it is assumed that the E- isomer is the first formed isomer after the elimination of a proton and -H_2O (amine in the case of nucleophilic catalysis) during the dehydration (deamination) step of the condensation. The isomerization step takes places after the formation and is significantly accelerated at higher temperatures. The final ratios of E and Z isomer in the full library are the same as in the case of isolated **27AB**.

2.3.4.2 E/Z isomers of 50AB

A mixture of 6-phenylpyridine-2-carboxaldehyde and benzhydrazide was heated at 70 °C for 12 h in ethanol. Upon cooling to room temperature, a white precipitate formed. This precipitate was identified as acylhydrazone **50AB** comprised of than 95 % of the **Z**-isomer and only traces of **E**. (*Figure 2.18, See also Figure E1.23-E1.27*)

When dissolved in acetonitrile, this isomer starts to isomerize slowly into E isomer. When heated at 70 °C, the equilibrium between E and Z is reached within 48 h. The equilibrated mixture contains 65 % of Z and 35 % of E isomer. This ratio is consistent with the ratio observed in the training system after equilibration in the absence of any metal cation. (*Figure 2.16*).

The pure E isomer can be obtained through two different approaches. The first one is a complexation and decomplexation method. Zn(II) cation templates the formation of the E isomer because it is more suitable for complexation. The fast removal of Zn(II) by $(Et_4N)_2EDTAH_2$ at room temperature liberates the E isomer in the solution. As in the case of structurally analogous terpyridine ligands, the complexed **50AB** has *cisoid* orientation of the pyridine- and imine-N donor atoms. Therefore, the release of free E isomer is followed by the configurational change around this bond providing the opposite *transoid* rotamer. This is a consequence of the repulsion of the nitrogen lone pairs and it is characteristic for all the components bearing asimilar structural motif. The subsequent heating for 24 h at 70 °C

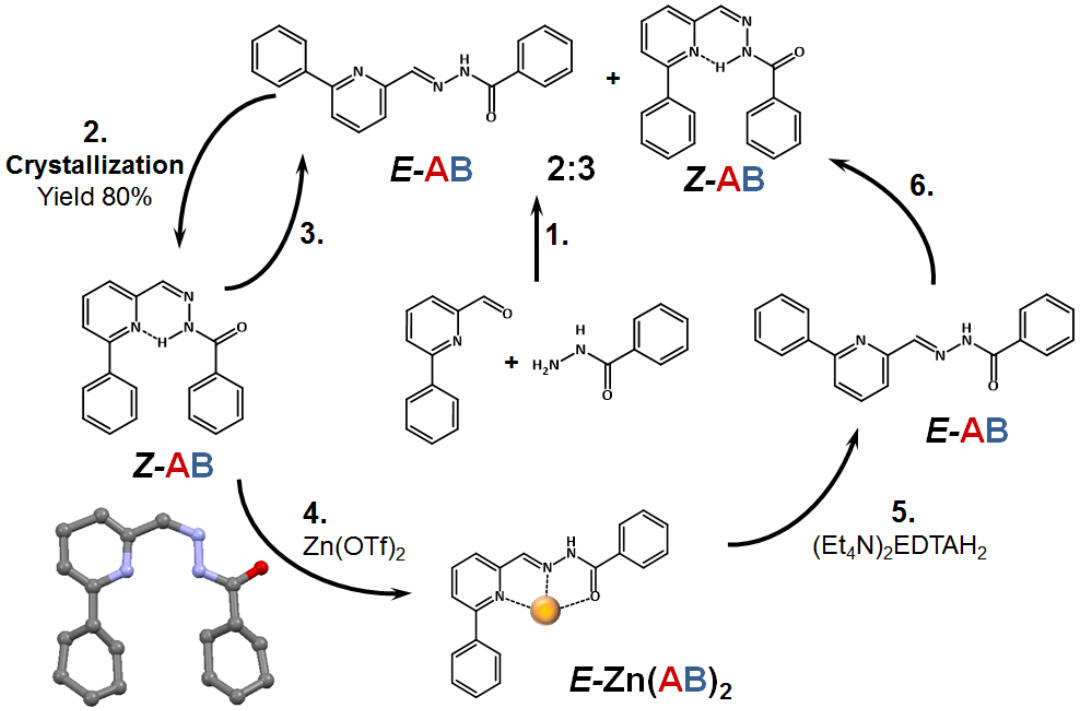

Figure 2.16: *Full circle of **50AB** transformations. 1) 72 h, 70 °C, Acetonitrile. Formation of the mixture of isomers; 2) Adaptation to phase change (liquid to crystal); 3) 3 d, 70 °C, Acetonitrile. Repeated isomerization to the initial E/Z mixture; 4) 0.5 eq. of $Zn(OTf)_2$, 3 h, Acetonitrile; Adaptation to external stimulus (Training), Configurational change of Z to E; 5) 0.55 eq. of $(Et_4N)_2EDTAH_2$, Removal of Zn(II), conformational change (Cisoid to Transoid); 6) 3 d, 70 °C, Acetonitrile. Repeated isomerization to the initial E/Z mixture.*

provided approximately the same distribution of isomers as in the case of pure Z-**50AB** equilibration (Z = 62 %, E = 38 %) and <5 % of hydrolysis. (*Figure 2.16*)

A second approach was to let the aldehyde react with benzhydrazide at room temperature with ~10 mol. % of p-toluidine present as a catalyst. The formation of the acylhydrazone in acetonitrile is very slow even at elevated temperatures but the presence of the catalyst[25] (0.1 eq. of *p*-toluidine) enables the E isomer to be obtained in 12 h at room temperature.

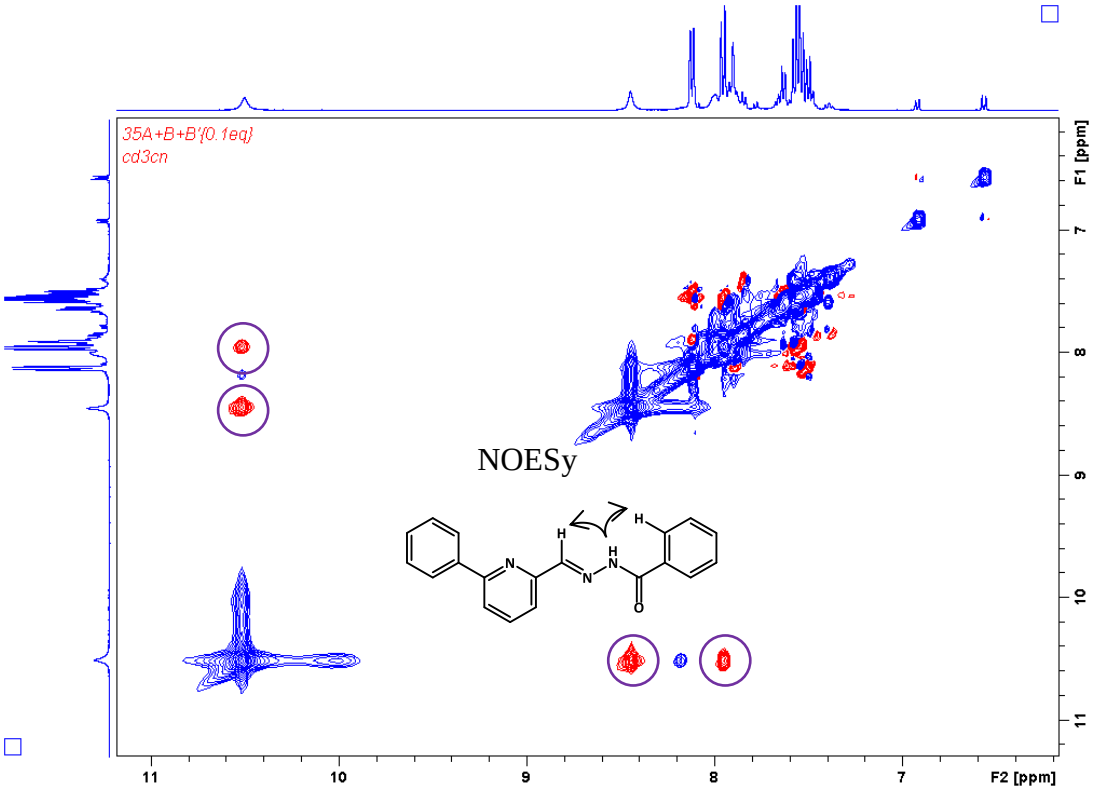

Figure 2.17: *2D NOESY spectrum of the E-**50AB** showing an interaction of the N-H with two hydrogens (imine and aromatic). It is in agreement with the structure of E*

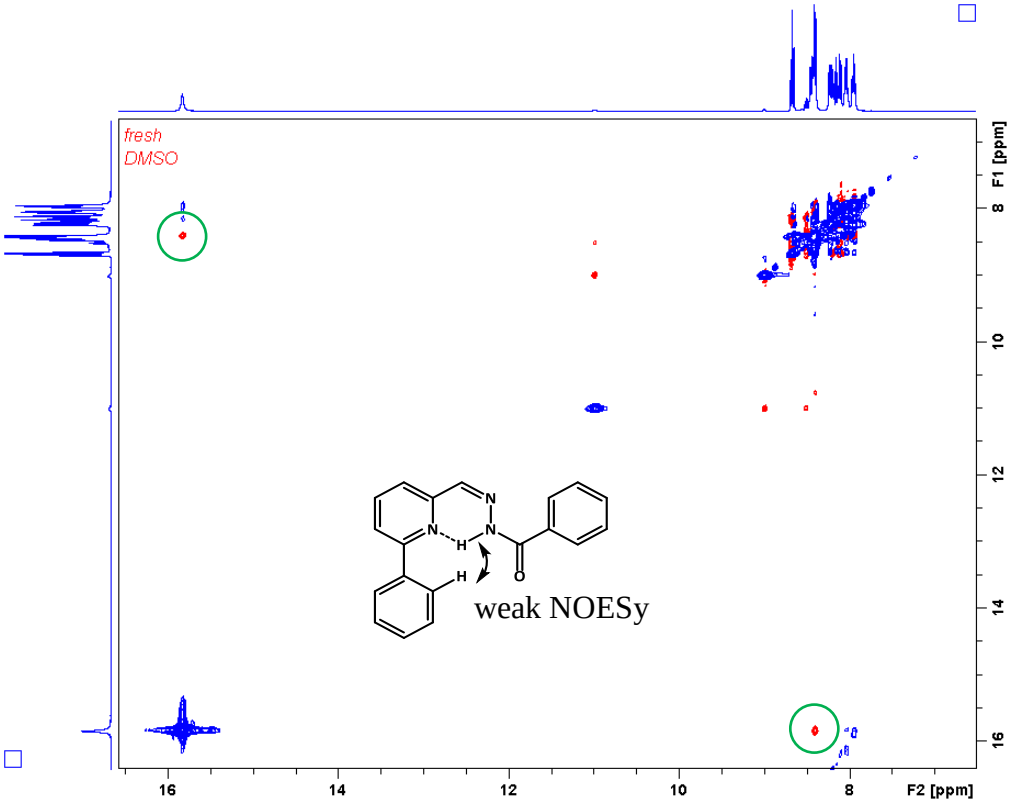

Figure 2.18: *2D NOESY spectrum of Z-**50AB** showing an interaction of the N-H with only one aromatic hydrogen. It is in agreement with for the structure of Z isomer of **50AB**. (The signal approximately at 11 ppm belongs to traces of E isomer).*

Both isomers were again identified by ^{1}H NMR. The E isomer exhibits an N-H chemical shift of 10.64 ppm, which is below the range of hydrogen-bonded N-H protons. In the 2D NOESY spectrum, the N-H signal shows two through-space interactions with the benzhydrazide moiety and the azomethine N=CH proton (*Figure 2.17, See also Figure E1.23-E1.27*). It is also important to point out that E-**50AB** was not isolated as a pure isomer and all studies were conducted on the mixture with the Z isomer in solution. The N-H proton of the Z isomer has a chemical shift of 15.31 ppm, which is indicative of a hydrogen-bonded N-H…N proton. Moreover, only one interaction of this N-H proton with a signal of an aromatic C-H can be seen in the NOESY spectrum. (*Figure 2.18*) The Z configuration of the C=N bond was finally confirmed by X-ray crystallography, even though the data quality did not allow full refinement of hydrogen atoms (R = 25 %).

2.3.5 A rationale of the equilibration process in systems with two -C=N- dynamic bonds with substantially different stability constants.

In order to gain further insight into the mechanistic relationships in interconnected dynamic covalent systems, a series of experiments with three-component "subsystems" was performed.

A very interesting result was obtained with an equimolar mixture of 6-phenyl-pyridine-2-carboxaldehyde (**50A**), benzhydrazide (**50B**) and p-toluidine (**50B'**). In this mixture, the amines have to compete for the aldehyde, revealing the influence of an effector on the equilibrium of components **50AB** and **50AB'**. It was assumed that the coordination preferences of these two constituents would be the driving forces shifting the CDL's distribution in either direction.
When the components (**50A**, **50B**, **50B'**) were mixed in 1:1:1 ($1.25x10^{-5}$ mol, 25 mM) ratio and heated for 12 h at 60 °C, the expected **50AB** formed quantitatively as two isomers E and Z in a 1:1.8 ratio. (*Figure 2.19*). It is worth emphasizing the effect of *p*-toluidine as a catalyst of acylhydrazone formation[26,27,28]. Even though there is no **50AB'** present when the equilibrium of the reaction is reached, it is clearly there at the beginning of the reaction and disappears with the increasing amount of **50AB** formed. The nucleophilic catalysis is reflected in the considerably faster formation of acylhydrazone **50AB** in the mixture than when just 6-phenylpyridine-2-carboxaldehyde and benzhydrazide are mixed under the same conditions.

Further, the impact of the presence of Zn(II) or Cu(I) cations was studied. Again, the components (**50A**, **50B**, **50B'**) were mixed in 1:1:1 ($1.25x10^{-5}$ mol, 25 mM) ratio, but this time also of 0.5 eq. of $Zn(OTf)_2$ or Cu(OTf) ($0.625x10^{-5}$ mol, 12.5 mM) was added and the resulting

mixture was heated for 12 h at 60 °C It was assumed that each metal would amplify its respective constituent, **50AB** for Zn(II) and **50AB'** for Cu(I). While the zinc provided the expected result, giving Zn(**50AB**)$_2$ as the sole product, the presence of Cu(I) did not lead to any of the desired Cu(**50AB'**)$_2$. The only product observed after equilibration of this subsystem was again **50AB**, except with an inverted ratio of E:Z (1.6:1). This can be attributed to the preferential coordination of Cu(I) to the **E-50AB** isomer. (*Figure 2.19, See also Figure E1.28-E1.30*).

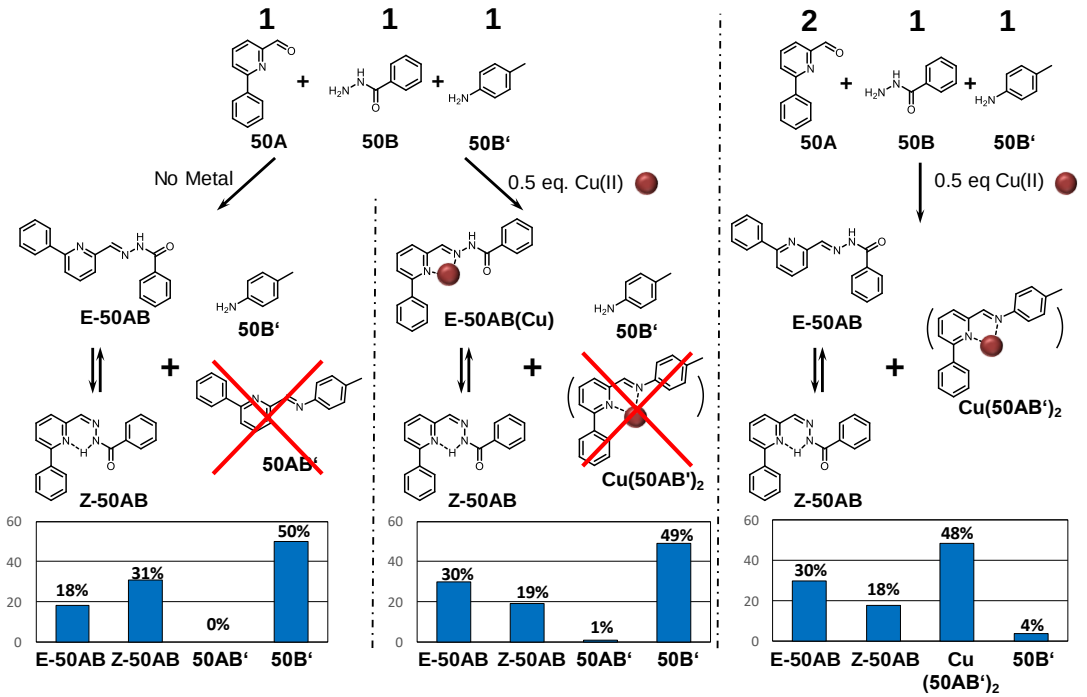

Figure 2.19: *(**Left**) Subsystem **50A**:**50B**:**50B'** (1:1:1) equilibrated without metal cation; **50AB** and **50AB'** form in substoichiometric amounts, not in a 1:1 ratio; (**Middle**) subsystem **50A**: **50B**: **50B'** (1:1:1) equilibrated in a presence of Cu(I) cation; (**Right**) subsystem **50A**:**50B**:**50B'** (2:1:1) equilibrated in a presence of 0.5 eq. of Cu(I) cation; **50AB** and **50AB'** form in 1:1 ratio. (Table E1.1)*

To establish the preference of Cu(I) for binding either to **50AB** or **50AB'**, the same mixture of 6-phenylpyridine-2-carboxaldehyde, benzhydrazide and p-toluidine was prepared in a 2:1:1 ratio. This setup not only allows comparison of the coordination preferences of **50AB** and **50AB'**, but also takes in account both kinetic and thermodynamic aspects of constituent formation (too slow formation, hydrolysis, coordination to components, etc.). After equilibration of the system at 60 °C for 12 h in acetonitrile in the presence of Cu(I), the following distribution was observed: 43 % of **Cu(50AB')$_2$**, 50 % of **50AB** with E:Z = 1:1 and 7 % of hydrolysis. This result illustrates the strong preference of Cu(I) cation for **50AB'** over the acylhydrazone. (*Figure 2.19*) This result, however, did not clarify the counter-intuitive distribution of the previously described subsystem with copper.

The observation can be explained in terms of factors operative in the systems where there is a big difference in thermodynamic stability of individual dynamic bonds (acylhydrazone vs. imine) in that the templating effect simply is not enough to turn the tables. In a case of the entire four-component system (**A**, **A'**, **B**, **B'**) there is one imine (e.g. **50AB**') and one acylhydrazone (**50A'B**) on each diagonal of the whole library. Only when both agonists pairs bear approximately the same overall thermodynamic stability, as happens to be true in the functioning four-component system, can the templating provide an additional impulse to amplify the diagonal with otherwise disfavored constituents. The less stable ligand (**50AB'**) alone is not sufficiently strongly bound to cause displacement of the system and its agonist **50A'B** is ineffective also. Only their concerted orchestration, together with the help of Cu(I), can result in a shift of equilibrium as was observed in the training DCL described above.

2.3.6 Agonistic/antagonistic competitive coevolution and dynamic ratiometry in a DCL

The adaptability of the dynamic system discussed here can also be employed to probe mixtures of effectors. In the present case, the ratio between the two antagonists **50AB** and **50AB'** in the DCL of the four constituents directly correlates with the ratio between the Zn(II) and Cu(I) in the test mixture.

Thus, a series of samples was prepared in which the amount of Cu(I) gradually decreased from 0.5 eq. to 0 eq. and the amount of Zn(II) correspondingly increased from 0 eq. to 0.5 eq. All components (**50A**, **50A'**, **50B**, **50B'**) including metal cations in appropriate ratios (*a*Cu(I) and *b*Zn(II), $a + b = 1/2$x**50A**) were heated at 60 °C for 12 h to achieve thermodynamic equilibration. In the resulting mixtures, the ratio of antagonists **50AB** and **50AB'** was calculated from the signal integration of all species (free, bound in complex, E and Z isomer) of a given constituent. (*Figure 2.20, 2.21*).

The observed co-evolution originates from the differential amplification effects of these two effectors on the antagonists **50AB** and **50AB'**, both containing the aldehyde **A**, and their direct competition for this constituents (in order to form their respective complexes). Therefore, increasing the ratio of Zn(II) in the Cu(I)/Zn(II) mixture amplifies proportionally the formation of **50AB.**This correlation is shown on the graph in *Figure 2.21*, further illustrating the concept of coevolution.

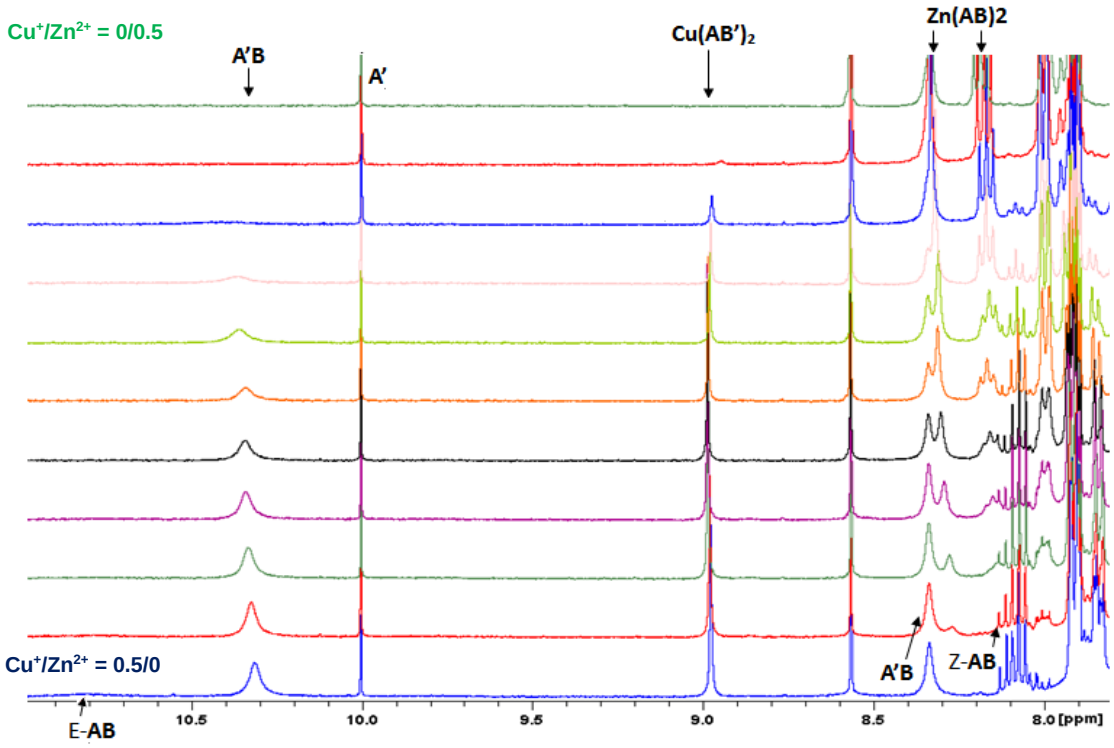

Figure 2.20: *^{1}H NMR spectra of the solutions corresponding to the ratiometry experiments performed by addition of mixtures of Cu(I) and Zn(II) cations to the DCL of constituents **50AB**, **50A'B**, **50AB'** and **50A'B'**. All systems were formed from equimolar mixture of **50A**, **50A'**, **50B**, **50B'** (1.25x10^{-5} mol, 25 mM) with addition of a mixture of Cu(I) and Zn(II). The ratio of Cu(I) decrease from 0.5 eq. (in respect to **50A**, bottom spectrum) for 10 % for each spectrum (0.45, 0.40…0 eq.) to 0 eq. (top spectrum). The ratio of Zn(II) increased from 0 eq. (bottom spectrum) for 10 % for each spectrum to spectrum (0.05, 0.10…0.5 eq.) to 0.5 eq. (in respect to **50A**, top spectrum).*

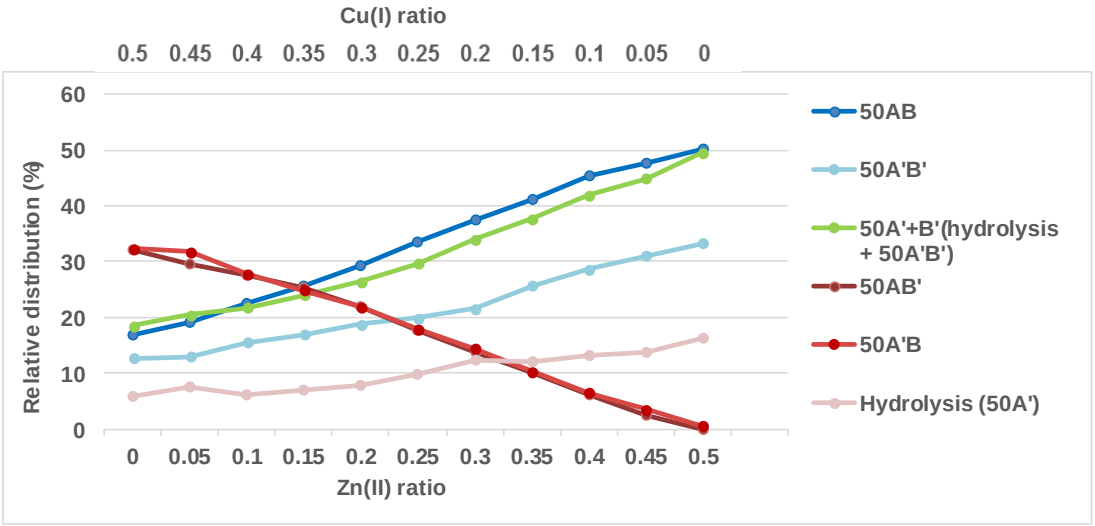

Figure 2.21: *Constitutional dynamic ratiometry: Graph representing the evolution of the relative amounts of the antagonists **50AB** and **50AB'** and their counter parts **50A'B'** and **50A'B** against the Cu(I)/Zn(II) ratio (numerical representation of Figure 2.20).*

From the graph in *Figure 2.21* it is possible to directly relate the ratio of antagonists to the ratio of the metals (Cu/Zn) present, hence to use this system as a way to analyse a mixture of the metal cations by measuring the ratio of constituents. In view of the dynamic component exchange between the cation sensors **50AB** and **50AB'**, the behaviour observed can be described as constitutional *dynamic ratiometry*. This is in reference to the analytical method called *ratiometry* where an effector produces a different effect on two sensors, usually displayed as a change in a given macroscopic observable (like an optical effect). Two significant points can be seen in the graph: the 0.7:0.3 Cu/Zn ratio which gives a 1:1 ratio of **50AB** and **50AB'** (25 % each) and the 0.5:0.5 Cu/Zn ratio giving a 0.33:0.17 **50AB**/**50AB'** ratio. These value are in agreement with the stronger amplification caused by the Zn(II) observed during previous studies of the system. (F*igure 2.21*)

The individual percentages in *Figure 2.21* were obtained from the ^{1}H NMR spectra as a sum of integrals of all species belonging to particular constituent. The values reported in the graph are an average of three individual experimental values. There is a clearly visible agonist/antagonist relationship between **50AB**/**50A'B'** and **50A'B**/**50AB'**. The agonist pair follows in both cases the same trend while antagonist pairs have a negative correlation. It is obvious that the correlation for **50A'B'** (light blue) and hydrolysis (pink) is somewhat variable compared to that for other constituents, and this is ascribed to its higher sensitivity to the environment, therefore its amount fluctuates more than others. It is also important to note that hydrolysis in this system under all circumstances almost exclusively concern components **50A'** and **50B'**, thus being the natural counter partners of **50A'B'**. Indeed, if the values for hydrolysis and **50A'B'** are summed, the resulting correlation is in nice agreement with the expected trend and gives a direct positive correlation with its agonist constituent **50AB**.

At this point it is important to note that this approach requires stoichiometric ratios between components of the mixture in order to obtain a linear response.

2.4 Conclusions

For all investigated DCLs, different equilibrium distributions were reached in response to different metal cations. Each of these different distributions characterizes a different constitutional state which can be then attributed to one of the informatics operations (training, information storage, recall, erasure). Moreover, all the operations were successfully combined in one simple system for two orthogonally acting effectors (metal cations).

The system exhibits a long re-equilibration time at room temperature, thus allowing retention of the metal-free state and the information about the effect of the particular metal effector. These out-of-equilibrium states allow fast re-complexation/detection of the given metal effector, as the DCL is already in the pre-organized state, producing fast recall. Introduction of another effector/metal cation in this step leads to the adaptation of the constituents' distribution and pre-organization of the system for the recognition of the other effector. Finally, subjecting an out-of-equilibrium informed distribution to elevated temperatures leads to restoration of the initial equilibrium, effectively erasing the information stored in the DCL concerning any previously applied effector.

The versatility of the DCL was also demonstrated by probing it with a mixture of effectors, i.e. the ratio between Zn(II) and Cu(I) cations was directly reflected in the ratio between two competing antagonists. The change in this case can be described in terms of constitutional dynamic coevolution involving cooperative agonistic and antagonistic relationships between all constituents in the DCL. Herein, the results obtained lead to several specific conclusions: a) increasing the complexity of the system can actually lead to a more selective output through dynamic competition; b) agonist/antagonist competition gives rise to a process that may be described as dynamic ratiometry, directly relating the ratio of antagonists to the ratio of two different effectors (here the Cu(I)/Zn(II) ratio) using a simple calibration curve; c) finally, the full DCL, i.e. the system of higher complexity, is required for the concerted operation of both pairs of agonists eventually manifested by subtle but precise adjustment to external influences.

2.5 References

1. Corbett, P. T.; Leclaire, J.; Vial, L.; West, K. R.; Wietor, J.-L.; Sanders, J. K. M.; Sijbren, O. *Chem. Rev.* **2006,** *106,* 3652-3711.
2. Lehn, J.-M. *Angew. Chem., Int. Ed.* **2013,** *52,* 2836-2850.
3. Lehn, J.-M. *Angew. Chem. Int. Ed.* **2015,** *54,* 3276-3289.
4. Osowska, K.; Miljanić, O. Š. *Synlett* **2011,** *12,* 1643-1648.
5. Lehn, J.-M. From supramolecular chemistry towards. *Chem. Soc. Rev.* **2007,** *36,* 151-160.
6. Beeren, S. R.; Pittelkow, M.; Sanders, J. K. M. *Chem. Commun.* **2011,** *47,* 7359-7361.
7. Osowska, K.; Miljanić, O. Š. *J. Am Chem. Soc.* **2011,** *133,* 724.
8. Osowska, K.; Miljanić, O. Š. *Angew. Chem. Int. Ed.* **2011,** *50,* 8345.
9. Vantomme, G.; Jiang, S.; Lehn, J.-M. *J. Am. Chem. Soc.* **2014,** *26*, 9509-9518.
10. Guiseppone, N.; Lehn, J.-M. *Angew. Chem.* **2006,** *118,* 4735-4740.
11. Hutin, M.; Cramer, C. J.; Gagliardi, L.; Shahi, A. R. M.; Bernardinelli, G.; Cerny , R.; Nitschke, J. R. *J.A.C.S.* **2007,** *129,* 8774-8780.
12. Atcher, J.; Moure, A.; Bujons, J.; Alfonso, I. *Chem. Eur. J.* **2015,** *21,* 6869-6878.
13. Hormuzdi, S.; Filippov, M. A.; Mitropoulou, G.; Monyer, H.; Bruzzone, R. *BBA – Biomembranes* **2004,** *1662,* 113-137.
14. Bassett, D. S.; Wymbs, N. F.; Porter, M. A.; Mucha, P. J.; Carlson, J. M.; Grafton, S. T. *PNAS* **2011,** *108,* 7641-7646.
15. Gupta, M.; Jin, L.; Homma, N. *Static and Dynamic Neural Networks: From Fundamentals to Advanced Theory;* John Wiley & Sons: New Jersey, 2004.
16. Wagner, A. D.; Schacter, D. R.; Michael, R.; Koutstaal, W.; Maril, A.; Dale, A. M.; Rosen, B. R.; Buckner, R. L. *Science* **1998,** *281,* 188-1191.
17. Fujii, S.; Lehn, J.-M. *Angew. Chem. Int. Ed.* **2009,** *48,* 7635-7638.
18. Ulrich, S.; Lehn, J.-M. *Chem. Eur. J.* **2009,** *15,* 5640-5645.
19. Campbell, V. E.; de Hatten, X.; Delsuc, N.; Kauffmann, B.; Huc, I.; Nitschke, J. R. *Natur. Chem.* **2010,** *2,* 684-687.
20. Kovaříček, P.; Lehn, J.-M. *J. Am. Chem. Soc.* **2012,** *134*, 9446-9455.
21. van Dijken, D. J.; Kovaříček, P.; Ihrig, S. P.; Hecht, S. *J. Am. Chem. Soc.* **2015,** *137,* 14982-14991.
22. Chaur, M. N.; Collado, D.; Lehn, J.-M. *Chem. Eur. J.* **2011,** *17,* 248-258.
23. Dieatrich-Buchecker, C. O.; Marnot, P. A.; Sauvage, J. P.; Kintzinger, J. P.; Maltese, P. *Nouveau Journal de Chimie* **1984,** *8*, 573-582.
24. Guiseppone, N.; Schmitt, J.-L.; Schwartz, E.; Lehn, J.-M. *J. Am. Chem. Soc.* **2005,** *127,* 5528-5539.
25. Ciaccia, M.; Di Stefano, S. *Org. Biomol. Chem.* **2015,** *13,* 646-654.
26. Dirksen, A.; Dirksen, S.; Hackeng, T. M.; Dawson , P. E. *J. Am. Chem. Soc.* **2006,** *15602-15603,* 128.
27. Crisalli, P.; Kool, E. T. *J. Org. Chem* **2013,** *1184,* 78.
28. Cordes, H.; Jencks, W. P. *J. Am. Chem. Soc.* **1962,** *84,* 826-831.

3.
Metallosupramolecular grid complexes:
Peripheral substitution/decoration and assembly

3.1 Introduction

3.1.1 Grids in general

Multidentate ligands bridge the metal ions in a linear fashion, lying to either side of the metal ion plane, so that A demand for ordered grid-like structures can be found in various fields and on various scales. In architecture, a grid motif serves as a basic and versatile framework for support or functional space partitioning. A grid of platinum wires has proven to be an efficient platform for information storage[1,2]. In materials chemistry, grid-like assemblies on surfaces are of interest for nanoscale electronic devices[3]. Of particular appeal is the idea that grids might be used as "quantum cellular automata", where information storage could be based on an array of different redox states rather than of points capable of current transmission.[1, 4]

In a line with our interest in a dynamic covalent chemistry and coordination chemistry, we focus on a family of grids formed by organic ligands and metal cations called metallosupramolecular grids. The term "metallosupramolecular grid" defines a multi-nuclear metal complex where the metal ion array is either square or rectangular and essentially planar. orthogonal ligand binding sites each provide an equal number of donor atoms to the metal ion coordination sphere. [5] Using a ligand with *n* coordination sites and n^2 metal cations, it is possible to assemble square arrays of [*n* x *n*] dimensionality. [6] (*Figure 1*) Using two different ligands *n* and *m* with a different number of coordination sites, it is possible to assemble heteroleptic rectangular [*n* x *m*] grids.[7] (*Figure 1 middle*) According to these rules, the simplest grid is formed by a ligand with two coordination pockets (n = 2). Indeed, mixing four metal cations (n^2 = 4) and four of the mentioned ligands results in assembly of a [2x2], M_4L_4

metallosupramolecular grid. (*Figure 3.1*) As the simplest obtainable grid with its regular arrangement of metal centres, it has been widely used to study various properties of metallosupramolecular arrays (magnetic susceptibility [8], conductance [9], ion encapsulation [10], sensing [11], assembly processes[12]) as well as for bottom-up building of larger multinuclear coordination arrays [13,14].

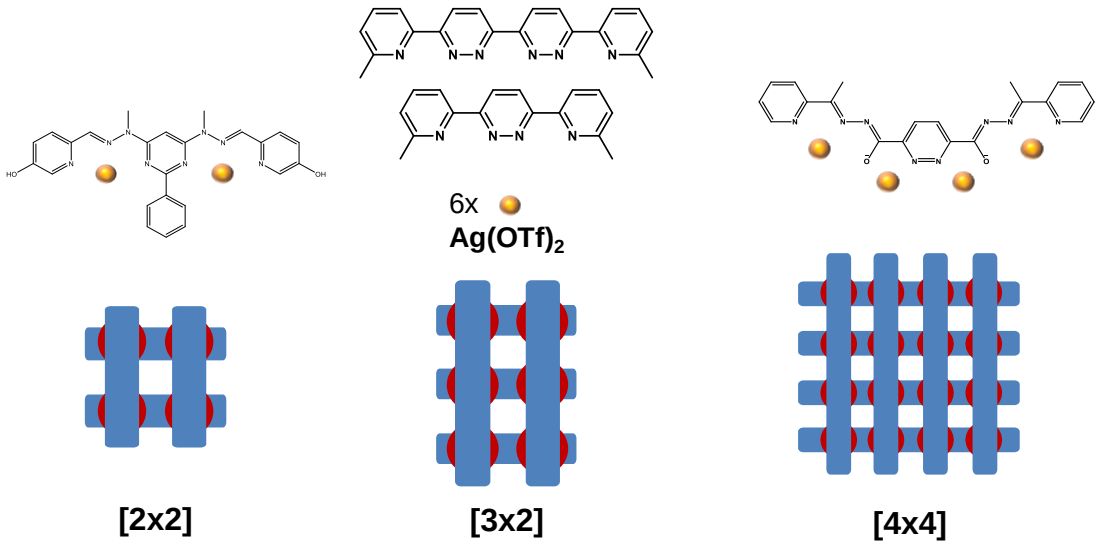

Figure 3.2: *General examples of grids with different dimensionalities and their ligands. 1) [2x2] – Ref.* 18 *and this work; 2) [2x3] – Ref. 7; 3) [4x4] – Ref.* 6

The first rationally designed grid was prepared by Osborn, et al. in 1992[15], shortly followed by Lehn [7, 16, 17,18], Thompson [6, 19] and others, resulting in more than two decades of fruitful development. [5, 20, 21, 22]

The Osborn grid was a tetranuclear Cu(I) [2x2] grid ($[Cu_4\mathbf{1}_4]^{4+}$). Complexation of tetrahedrally coordinating Cu(I) by an extended double bipyridine ligand (3,6-di-2-pyridinyl pyridazine, **1**) resulted in a novel tetranuclear square [2x2] structure.[15] (*Figure 3.2 left*)

Another motif was introduced shortly after by Lehn.[17] Just as a tetrahedral array of donor atoms can be considered as formed from pairs of donors in orthogonal planes, an octahedral array can be considered as generated from two orthogonal planes in which there are three donor atoms each. Thus, double-terpyridine ligands were used to form [2x2] grids with octahedrally coordinating metal ions (**2**, $[Co_4\mathbf{2}_4]^{8+}$, *Figure 3.2 middle*). The synthesis of such ligands is relatively tedious and an important subsequent development[5] was that of the facile synthesis of isomorphic ligands derived from hydrazones[18] (*e.g.* **GR6B**, *Figure 3.2*), acylhydrazones [23] and imines[24]. Such ligands are not only easy to prepare and good mimics of terpyridine derivatives but are also more readily functionalised. Given the reversibility of their formation, they have also proved very useful in studies of dynamic covalent chemistry. The following chapter will present my work on dynamic hydrazone grid ligands, particularly on their peripheral

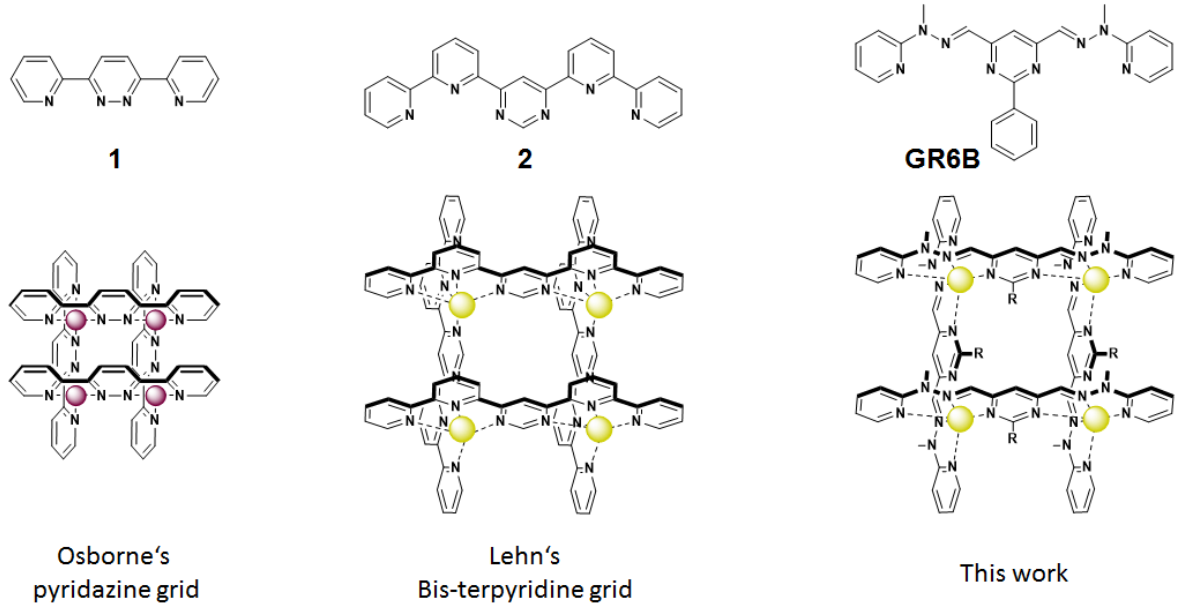

Figure 3.1: *Structural motives of ligands relevant for this work and their grid assembly.*

functionalization with special regard to possible extension of the isolated [2x2] grid units into large assemblies and arrays.

The tetrahedral (Osborn) and octahedral (Lehn, Thompson) geometries were not chosen by chance. As noted above, the idealised geometries both can be considered to involve equal groups of donor atoms lying in orthogonal planes, so that planar ditopic ligands should enforce the grid form of the metal ion array on their 1:1 complexes.[20] In reality, many complexes classified as metallogrids show significant distortions from true planarity of the M_n arrays and precise orthogonality of the opposing ligands[6, 15, 23, 25]. There are also examples of grids incorporating metal centres with coordination number 5 (trigonal bipyramid)[27, 28]. There also exceptional cases, for example in catenated [2x2] acylhydrazone grids, where space restrictions do not allow full octahedral coordination and the ligand is bound in a unit of trigonal bipyramid geometry. [29]

The stability of grids is influenced by many factors such as the conformational flexibility of the ligands, different coordination preferences of cations, and solvation. From the thermodynamic point of view, the grid assembly competes with the formation of small oligomeric and polymeric species. These assemblies are, however, enthalpicaly disadvantageous as they do not have all the possible binding sites filled by the strong donor atoms of the ligands and instead have some coordination sites occupied by (generally) weaker donor atoms of the solvent. Nonetheless, for transition metal ions where ligand field stabilisation energy (LFSE) can make a contribution depending upon both the donor atom and

the coordination geometry to the overall enthalpy change, there can be exceptions to this generalisation. (*Figure 3.19*) [1, 20]

An entropic contribution to assembly then lies in the number of released solvating molecules from the cation. This may be important especially for metal cations which do not have strong contribution from LSFE (e.g.: Mn(II)). Of course, enthalpic supramolecular interactions (π-π stacking, H-bonding, etc.) can further contribute to stabilization or destabilization a grid structure.[1, 20]

Regarding the terpyridine-derived hydrazone ligands studied herein, there is a subtle aspect in their formation which should not be overlooked. Their complexation and subsequent grid formation must be preceded by a change in conformation. (*Figure 3.3*) In the free state, the terpyridine ligands (bipyridine as well) are present in a *transoid* conformation with the N-donors oppositely oriented. The cost of energy required to turn from unproductive *trans*- to useful *cis*- conformations must be paid by the metal cation upon binding. For the simple bisterpyridine (**2**) ligand which forms a [2x2] grid the cost is about 100 kJ mol^{-1} per ligand (25-30 kJ mol^{-1} per bond, four turns, *Figure 3.3*) and can easily reach up to 1500 kJ mol^{-1}. This aspect then easily becomes limiting for assembly of grids with higher dimensionalities[1, 20, 25].

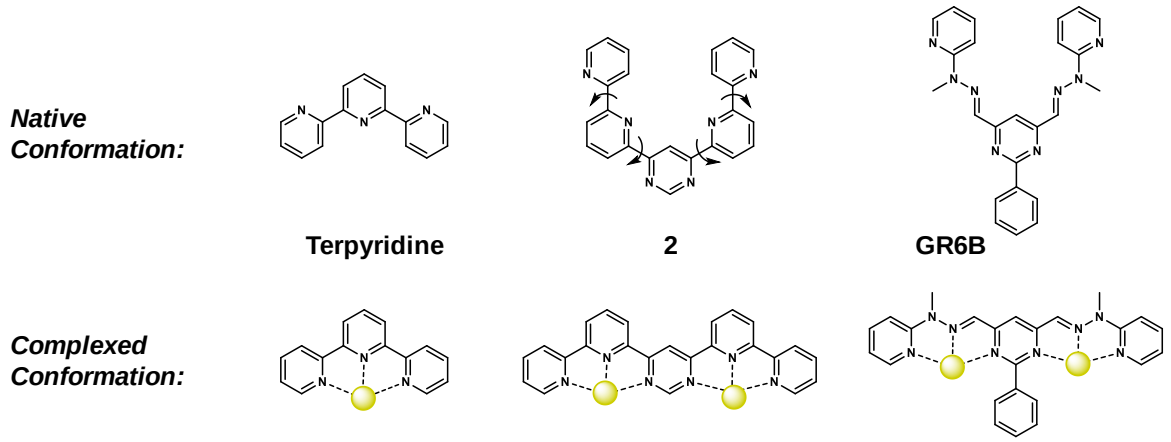

Figure 3.3: *Conformational changes of different terpyridine ligands upon complexation*

Interestingly, in attempting electrospray deposition of the Co(II) grid ([2*x*2]Co^{II}_4) on Au(1,1,1), several conformers of the free ligand were observed. Their existence was explained by decomposition of the [2*x*2]Co^{II}_4 grid during the deposition on the surface. Surprisingly, the presumably thermodynamically most stable all-*transoid* **T** conformer (10 %) was only the second most abundant conformer, far behind the **TC** conformer (75%). (*Figure 3.4*) Except for the **T** conformer, all others shown are probably only trapped states formed during the short time between grid decomposition and adsorption of the free ligand which was not long enough to

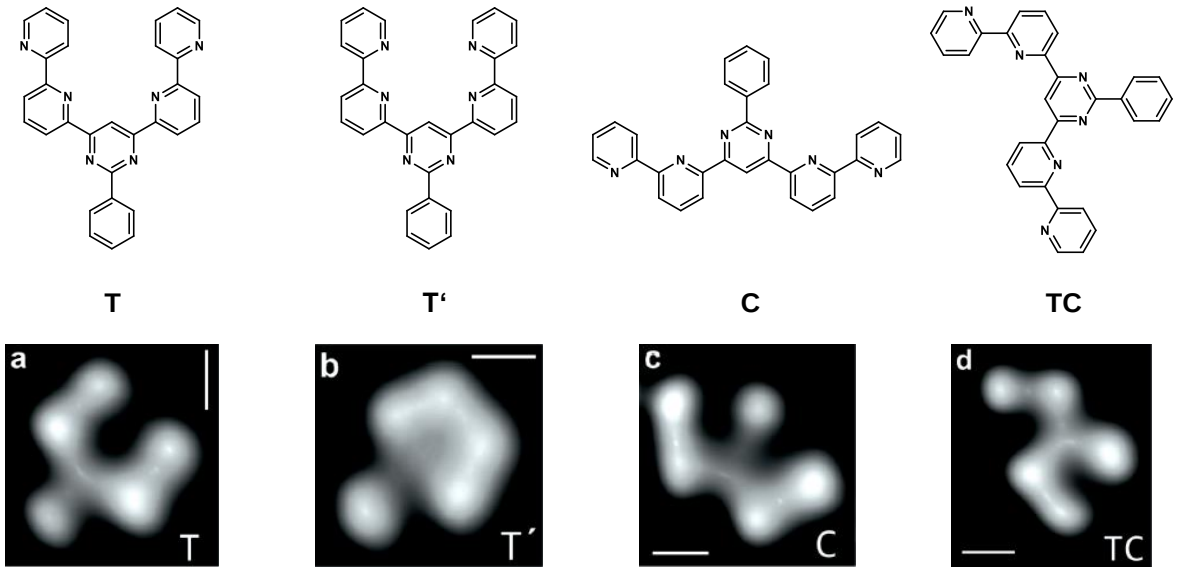

Figure 3.4: *The on-surface observed conformation of bisterpyridine ligand. The most abundant was not the thermodynamically most stable **T** but instead **TC**.*

complete all the necessary turns. This also gave birth to some exotic interactions previously unseen in a solution, such as formation of N…HC-bonded dimers and trimers.[29]

However, very little is actually known about the stability constants of higher grid arrays as well as about a mechanism of their assembly. Even the studies carried out on the simple [2x2] (bishydrazine) grids, showed very complicate equilibria of many different species. [30] Many parametres and factors are in play including the solvent and counter-anions, thus it is not possible to judge on the outcome of the grid formation just from one structural aspect.

Despite of this, the assembly of a grid is usually not the major task. From the point of view of the organic chemist, everything comes down to structural factors and rational design of the ligand backbone. By applying subtle tuning of the ligand scaffold, one can dramatically influence the selectivity of the formation in a presence of specific metal cation and disfavour certain species [21, 31, 32]. It is possible to influence spin-spin interaction of certain metals [33] or access a higher intermolecular assembly leading to hierarchical 2D or 3D organization [34]. There exists a plethora of different families of ligands with different organization of the coordinating sites[18, 20, 22], but since this work is strictly oriented to ligands derived from terpyridine backbone, these will not be discussed here.

3.1.2 Bis-terpyridine grids on surfaces

As interesting as a grid may be, any single molecule/complex will rarely find real-world applications. There is strength in numbers, and macroscopic properties usually arise from beneficial interactions between molecules in an assembly. The same applies for grid

applications where nanoscale electronic or spintronic devices require a deposition of 2D or 3D ordered arrays. Indeed, a lot of effort has been put into their preparation/assembly.

One approach has been to prepare a long, multi-chelating ligand. With the right design, higher grids ranging from [3x3] up to [5x5] can be successfully prepared. [20, 35] This approach has, however, some disadvantages: a) the *solubility* of long and rigid structures tends to be very low. One way to overcome this is the introduction of solubilizing groups [36], but it is not always desirable for assembly and characterization reasons; b) the *synthesis* of such ligands is usually very demanding on resources and time, making them unsuitable for any application above pure research studies.

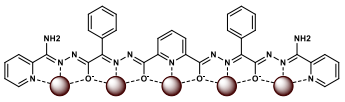

4

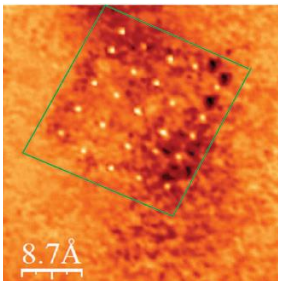

Figure 3.5: *Illustrative example of a ligand forming [5x5] grid and CITS picture proving the grid-like alignment of Mn(II) cations in the assembly.*

Characterization of large grids is indeed problematic. Mass spectrometry and NMR are very often inconclusive and even application of other analytical methods sometimes cannot give the final proof of the shape and size of the structure. So far, the most conclusive way to unequivocally prove a successful grid assembly is to obtain single crystal suitable for X-ray diffraction. However, the bigger the assembly is, the more difficult becomes to crystallize it and/or solve the final structure. All this was evident in the case of the [5x5] grid in which case all standard techniques provided only inconclusive hints of a big assembly. (*Figure 3.5*) The definite proof of successful formation of the [5x5] grid $(Mn_{25}(\mathbf{4})_{10}](ClO_4)_{20}x65H_2O)$ was provided using CITS (current image tunnelling spectroscopy), an alternative STM technique which allows topographical and spectroscopic data to be obtained simultaneously. [35]

Higher grid assemblies provide unique possibilities due to the regular and defined positioning of metal nods. However, assembly where even individual subsets of grids can be distinguished and precisely targeted (e.g. by STM) could provide structures with interesting properties for information processing, memory storage and other electronic devices. Such higher grids which are formed of covalent ligands but with clearly distinguishable subunits of smaller grids are called "grids of grids". [25] (*Figure 3.6*)

One of the first examples can be seen in the incomplete silver(I) [4x5] grid $(Ag_{20}(\mathbf{5})_9(OTf)_{20})$. [25] (*Figure 6*) Here, probably in order to reduce the strain in the structure, one central ligand is missing. This results in formal 2x[2x5] grid assembly with two clearly distinguishable subunits. Unfortunately, again in order to release the strain in the assembly, the *cisoid* orientation of the

pyrazines in the middle of five ligands which lie perpendicularly to the missing one, is changed to *transoid*. Consequently, the planes of the two [2x5] subunits are not the same and the structure as a whole is no longer planar.

A better example, which directly illustrates our approach to a grid of grids, is the [4x4](**6**)$_8$Pb$_{16}$ grid (Pb$_{16}$(**6**)$_8$(CF$_3$SO$_3$)$_6$(H$_2$O)$_5$](OTf)$_{10}$·23H$_2$O).[37] (*Figure 3.6*) Its ligand contains four coordination pockets separated by a pyrimidine core, which in the final assembly clearly creates a groove between individual [2x2] subunits and effectively creates a 4x[2x2] grid of grids. Later in the chapter, our approach towards a similar 4x[2x2] grid, with an intended wider separation of [2x2] subunits will be described in detail.

If any grid array can be divided into [2x2] subunits, then it is not implicitly necessary to synthetize large ligands. Instead, one can imagine assembly of an array of basic [2x2] grids connected through supramolecular interactions or with help of dynamic covalent chemistry. Therefore, another approach to ordered arrays of grids lies in the assembly of appropriate [2x2] grids.

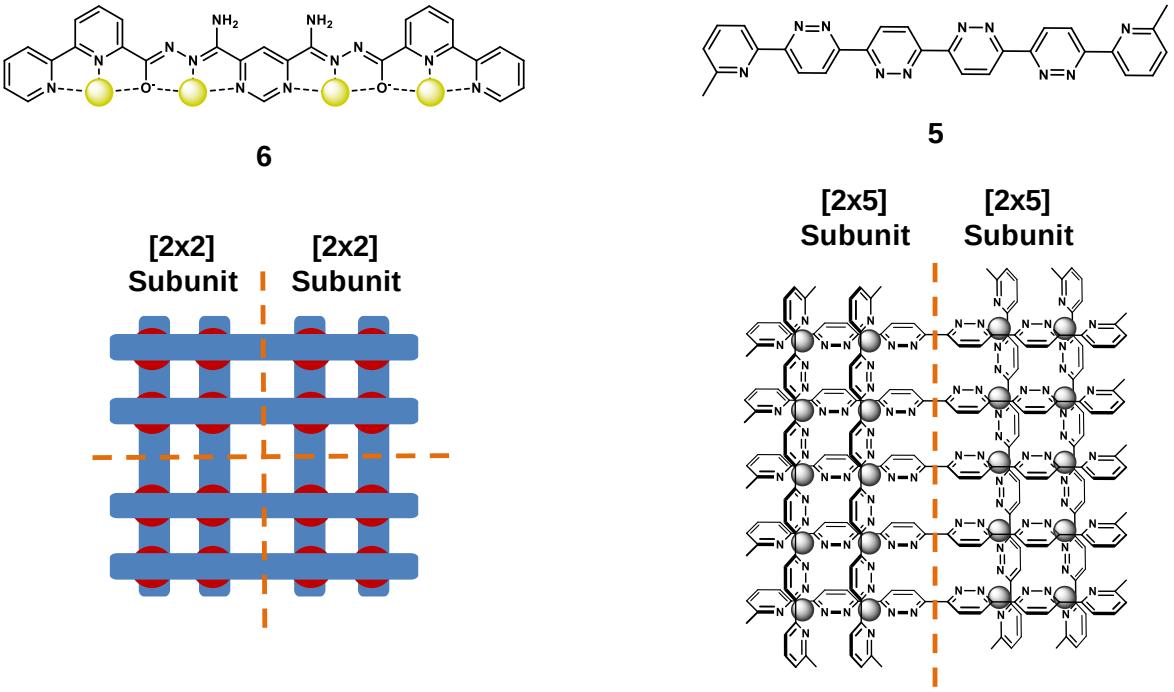

Figure 3.6: *Illustrative examples of "grid of grids" assemblies with their respective ligands*

In fact, a 2D assembly on a surface is actually highly desirable as any practical application such as in spintronics or memory storage needs molecules to be easily accessible and to maintain an exact position for repeated access/reading. This is a condition which is naturally impossible to achieve in solution or in an amorphous solid state. The importance of this approach is illustrated by the fact that the first STM study on electrochemically deposited [2x2]

grids on gold(111) was reported only one year after the first preparation of bisterpyridine grid $[Co_4\mathbf{2}_4]^{8+}$.[38]

Encouraging results were obtained in case of $[Co_4\mathbf{7}_4]^{8+}$and $[Co_4\mathbf{8}_4]^{8+}$ grids. (*Figure 3.7*) Evaporation of their acetone solution (C_s = 0.1g/1) over the surface of highly ordered pyrolytic graphite (HOPG) yielded a defect-free ordered assembly over areas up to 0.5μm^2. Two different orientations of the grid complex relative to the surface were observed depending on the substitution of the ligand. The ligand **7** with -CH_3 on the central pyrimidine adopted a parallel orientation to the surface. Application of a short negative pulse (V_{tip} = -0.5 V, 1 ms) on such an assembly resulted in removal of just one cationic grid moiety. The missing piece appears on the STM image as regular and well-defined hole in the array. The mobility of this hole was measured to be 200 times slower than of a similar defect in a monolayer of cycloalkenes. The positive pulse on the other hand had no visible impact on the assembly. This was a very important study as it demonstrated the possibility of selective targeting of single grid molecule in a large 2D array and the comparatively stable position of the change. The other ligand **8** with two -CH_3 groups on the ligand edges was observed to adopt only the undesired almost perpendicular orientation to the HOPG surface. [1, 13, 39]

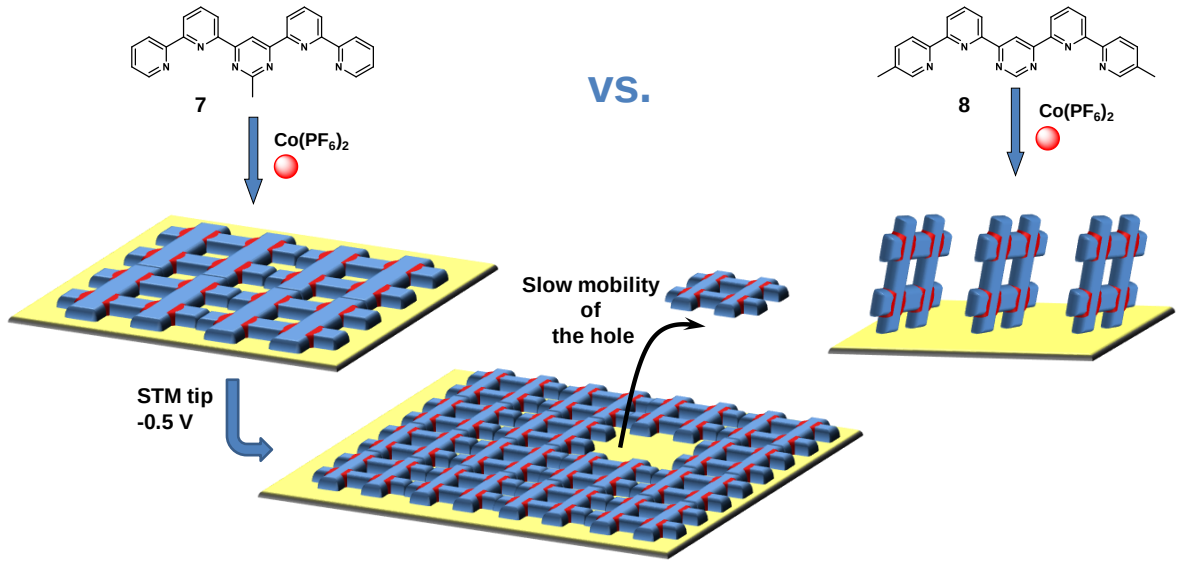

Figure 3.7: *Different orientation of $[Co_4\mathbf{7}_4](PF_6)_8$ and $[Co_4\mathbf{8}_4]$ $(PF_6)_8$ grids adsorbed on HOPG surface and illustrative removal of one $[Co_4\mathbf{7}_4]^{8+}$ grid moiety from the array of grids by application of a short negative pulse (V_{tip} = -0.5 V, 1 ms).*

The substitution of the ligand backbone of the middle terpyridine pyridine with 4-pyridyl[40] or n-propylthiol groups led only to a decrease in the adsorption strength and sped up the mobility of the grids in the array.[1, 40, 41] To improve the adsorption properties and try to force the grid to lie parallel to the surface, long alkyl chains were added on the sides of the bisterpyridine backbone. This substitution was previously shown to improve interactions with

HOPG and lead to very ordered and reproducible STM patterns. [42] In the previous case, the orientation of the grids depended on the substituents but each derivative adopted only either a parallel or a perpendicular position. In one case, the C_{16} alkyl substituted $[Fe_4\mathbf{9}_4](BF_4)_8$ grid (*Figure 3.8)* accommodated both orientations. Moreover, both domains were stable enough not to be transformed one into another by use of the STM tip.[44]

The analogous bishydrazone ligand **10** was also decorated with two long alkyl chains ($[Fe_4\mathbf{9}_4](BF_4)_8$, *Figure 3.8*). In this case, only the perpendicular orientation of the grid was observed. This was attributed to the BF_4^- counter anions being wedged on the face of the grid.[44] The grid also showed only low affinity towards HOPG, probably due to its polar nature.[40] To identify the exact cause of perpendicular assembly it is necessary to eliminate the effect of the counter anion by working with neutral complexes. The deprotonation of hydrazine based grids has only limited effect on properties of the grid, so observed changes should be attributable to anion elimination.[44]

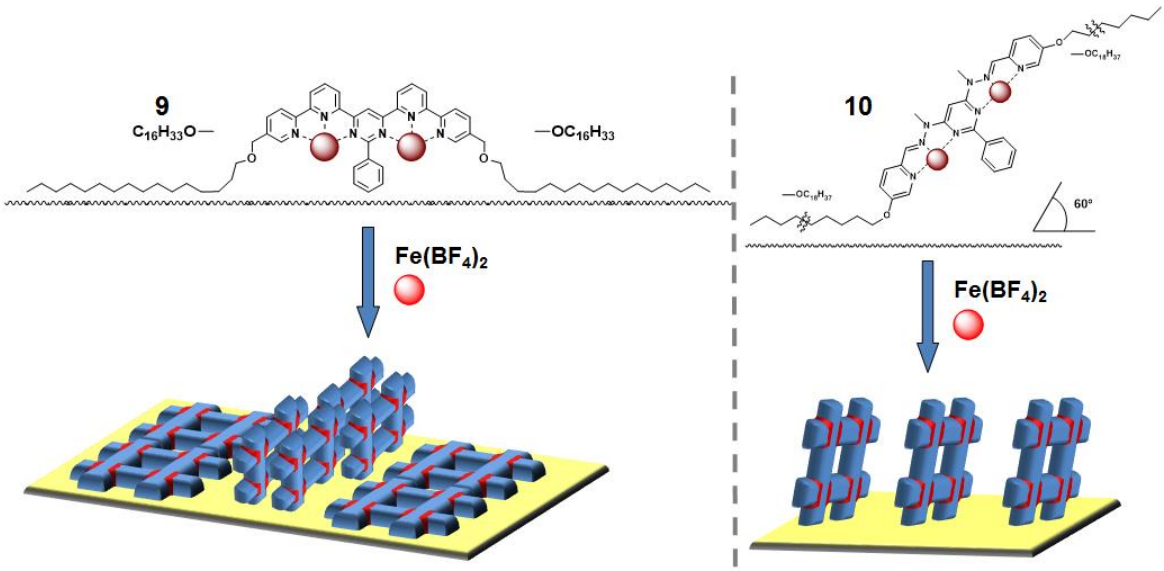

Figure 3.8: ***Left:*** *Illustration of perpendicular orientation of* $[Fe_4\mathbf{9}_4]^{8+}$ *(**Top**), and schematic illustration of both perpendicular and parallel orientations observed on HOPG surface (**bottom**). **Right:** Illustration of perpendicular orientation of the* $[Fe_4\mathbf{10}_4]^{8+}$ *grid. Only perpendicular orientation was observed in this case.*

3.1.3 Axial and lateral substitution and possible applications of [2x2] grids

As for all metallo-complexes, the behaviour of the grids is greatly influenced by the metal centres, especially when it comes to the building of the functional nano-devices. Despite of this, the substitution of the ligand backbone is not less important. Electron-donating or -accepting groups can affect the energy transfer between the metal centre and the ligand or the spin-spin transition energy, subtly tuning the performance of the complex.[45] Different substituents also

play an important role during the assembly of arrays, as in the abovementioned case of the relative orientation of the different grid derivatives during adsorption. Multivalence capacity and external substrate binding are further examples of where the modification of the ligand is more important than choice of the cation. [11, 46]

The desire to build a supramolecularly connected 2D array of grids led to a design of a bisterpyridine ligand (**11**) capable of self-complementary hydrogen bonding. (*Figure 3.9*) The approach was only half successful as the X-ray data showed continuous hydrogen bonding only along one axis, while the units in the perpendicular direction were connected through π-π stacking[14]. Other attempts to functionalize the bisterpyridine scaffold other than those mentioned above for surface adsorption, include the case of a hybrid NNO derivative. [46] In this derivative, two peripheral pyridines are transformed into an ester or an amide. The third donor atom is thus carbonyl oxygen (C=O). The utility of such ligands lies in their presumably simpler functionalization via alteration of the ester or amide units. Although this direction was not further pursued for covalent ligands, it was successfully implemented for acylhydrazone-based ligands, which can be viewed as a dynamic expression of the NNO motif.[46]

It has already been stated that the focus of this work is exclusively on the dynamic analogues of bisterpyridine ligands. The appearance of the first hydrazone derivatives dates back to 2003.

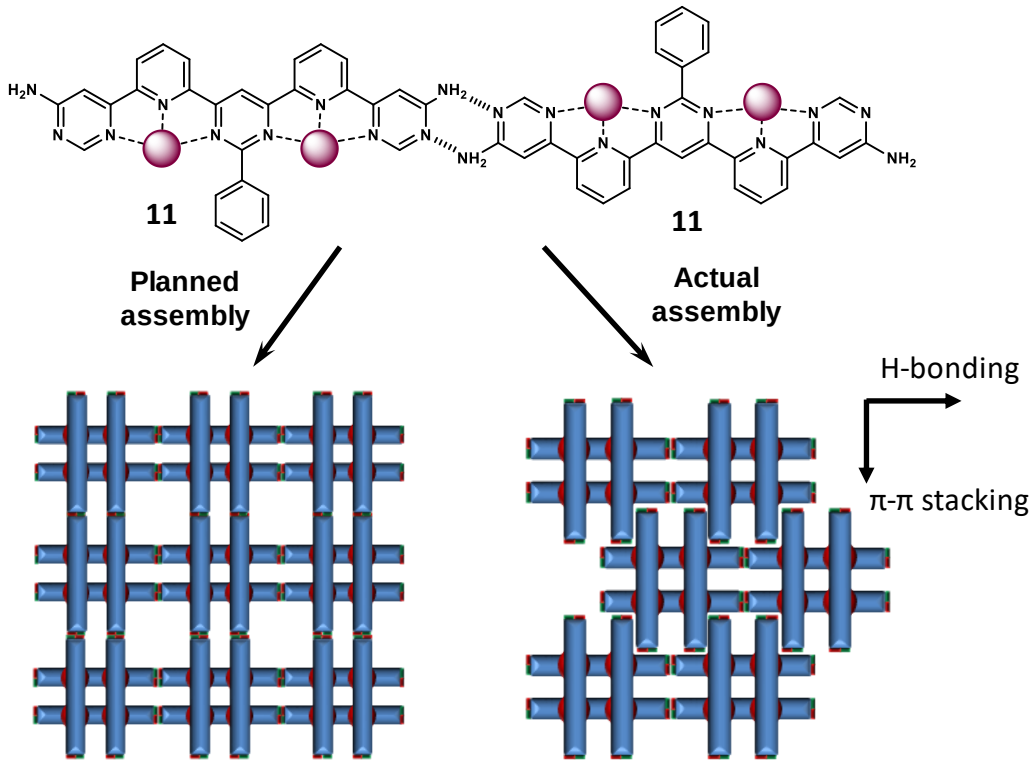

Figure 3.9: *Assembly (crystal) of bisterpyridine ligand with self-complementary H-bonding motif. Expected 2D array (**Left**) and obtained array (**right**). The X-ray data showed formation of the parallel linear H-bond connected chains which are connected between each other by π-π interactions.*

The same (2,4')-pyridine-pyrimidine (pyr-pym, **12**) motif was used in the same year by the Lehn group to generate helical structures.[21, 47, 48] as well as to assemble dynamic and ionisable [2x2] $[Co_4(\mathbf{JHA})_4](BF_4)_8$.[18] (*Figure 3.10*) Their ease of the preparation renders them especially appealing and following years brought extensive development along the same axes as for the parental bisterpyridine based grids.

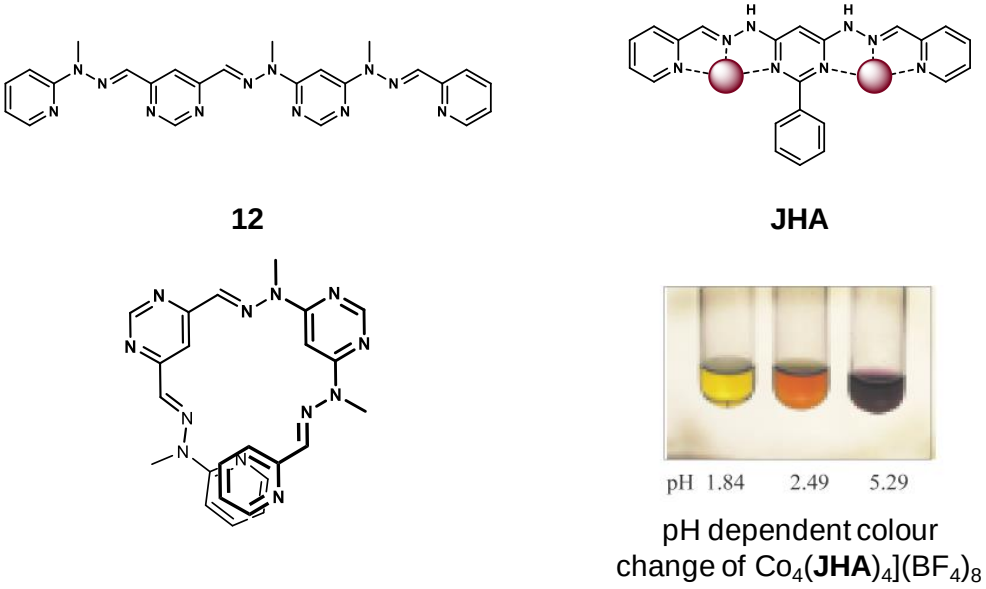

Figure 3.10: *Illustration of characteristic helical folding of poly(pyr-pym) ligands and early example of ionisable [2x2] bishydrazine grid with pH modulated optical properties [18].*

With just two synthetic steps to a pyrimidine derivative (Dialdehyde **GR4** or dihydrazine **GR4B**, *Figure 3.13*) and a wide commercially available pool of different 2-halopyridines (1 step to pyridine hydrazine) or 2-pyridinecaboxaldehydes, one can create a diverse library of ligands. The first approach to decorate these ligands targeted onto the ionisable and thus reactive N-H in the bridge between the pyridine and pyrimidine.[11] Copper(II) complexes of such laterally substituted derivatives (**13**, **14**, *Figure 3.11 top*) were examined, for example, to see if there was significant ferromagnetic coupling between their Cu(II) centres. The bulky aliphatic units attached to the central nitrogen atoms served in this case to prevent intermolecular interactions between grid cores in the solid as well as in solution.[8]

Another study assessed the possible use of these grids for sensing and external substrate binding.[11] (*Figure 3.11 bottom*) However, most of the derivatives prepared either failed to readily assemble in a grid or failed to provide any defined complex at all.

Concerning lateral substitution, a broad-ranging study was done in case of bisacylhydrazone-based analogues. [23] The trimethylammonioacetylhydrazide derivative, readily soluble in water as the chloride, was suggested on the basis of a preliminary study to have possible application as an acetylcholine esterase inhibitor. [49] The attachment of a urea-containing alkyl chain

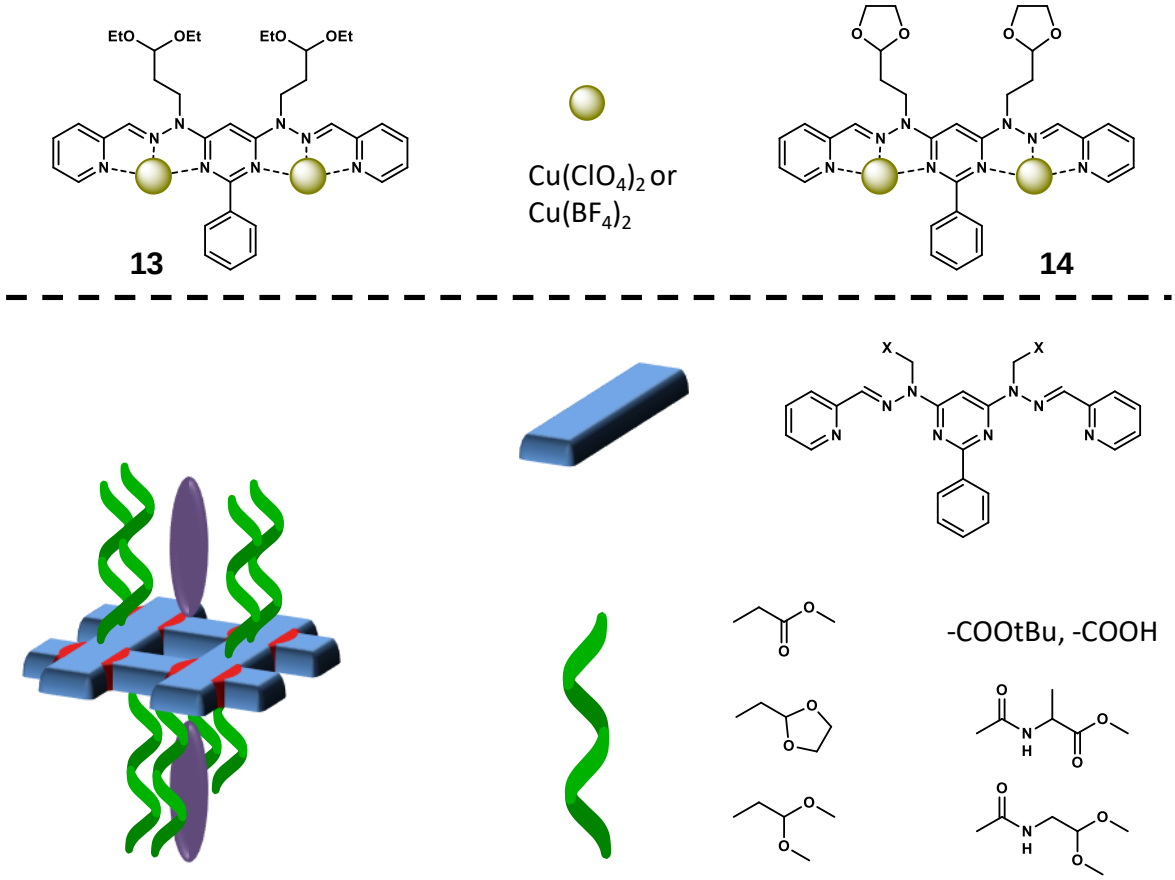

Figure 3.11: ***Top****: Derivatives exhibiting ferromagnetic coupling between Cu(II) cations.* ***Bottom****: Some of the originally prepared derivatives with aim providing external substrate binding in the newly created cavities.*

provided a metallosupramolecular gelator (**15**). (*Figure 3.12*) Here the grid is just neutral scaffold which bears several active substituents, thus multiplying their effect.[51] The grid as a dynamically assembling scaffold bearing active auxiliary groups was later advantageously used in a binding study on Concanavalin A. (*Figure 3.12*) At first, the alkyl-acylhydrazide chain was attached to glucose (**16**) and mannose (**17**) units. Then this acylhydrazide moiety was reacted with pyrimidine-4,6-dicarboxaldehyde in the presence of Zn(II) cations to form the multi-saccharide decorated [2x2] grid. This multivalent oligosaccharide grid demonstrated strong affinity for concavalin, mannose performing much better than glucose. A very interesting property is that this grid is stable in water at physiological pH, while at a slightly more acidic pH it readily dissociates. This feature is especially significant in that it is indicative of a possible biological application, for example, in detecting differences in pH between healthy and pathological cells.[51]

On bishydrazone ligands the only axial substitution/decoration done so far is, as already mentioned, the introduction of a the long alkoxy-chain (in **10**) in order to stabilize grids on HOPG.[44] (*Figure 3.8*)

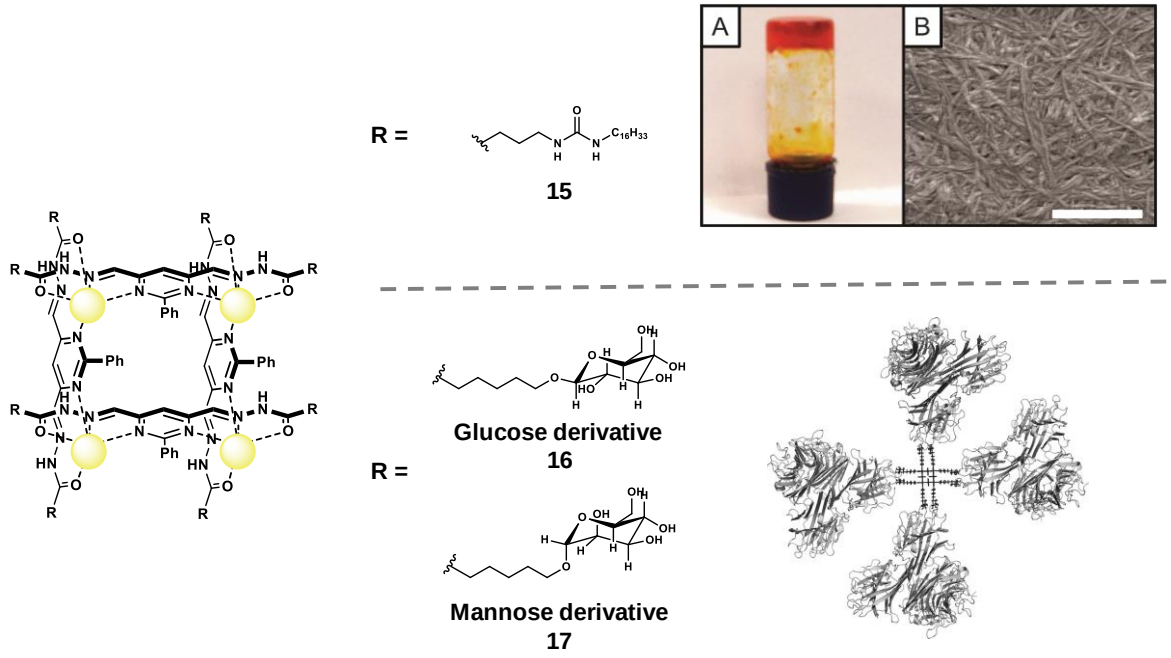

Figure 3.12: *Illustration of the acylhydrazone based grid employed as toluene gelator [45] (**Top**) or as multivalent receptor for concavalin A and idealized illustration of such assembly (**Bottom**)*

From a chemical point of view, the choice of right method for an introduction of a substituent onto a bisterpyridine ligands is simple. The aromatic cores are rather inert so almost all synthetic methods are viable. Although, multistep and demanding synthesis of even simple derivatives make the bisterpyridines heavy-footed.

In contrast, functionalization of dynamic ligands based on reactive imine (-C=N-) bonds must be handled with care. Acidic conditions readily hydrolyse the -C=N- bond to aldehyde and hydrazine. Reductive conditions can convert the imine to an amine, thus changing the intrinsic properties of the ligand, while oxidative conditions may either oxidise the imine or even completely destroy the ligand. The -C=N- bond also takes place in some specific reactions such as the Ugi reaction, which excludes use of reactive reagents such as isocyanates.

All these obstacles left us with just a handful of basic methods, mostly applicable under basic conditions. Luckily, of all the varieties of -C=N- derivatives, hydrazones contain the strongest bond thus no exchange was observed to occur in basic or neutral solution, despite literature evidence of this reaction in mixtures containing Lewis acids (e.g.: $Zn(BF_4)_2$).[52] The hydrazone bond is also very resistant to basic conditions; thus ester hydrolysis could be readily achieved even under strongly basic conditions (KOH/Ethanol/water mixture). Nucleophilic substitution is also theoretically available but the limited solubility of most of the ligands hinders its use. An important step forward in the present work was the discovery that the Dess-Martin periodinane does not attack the ligand skeleton and was thus readily applied to oxidise primary

alcohols to aldehydes. This method was successfully used even for the ligands with limited solubility. In respect to aldehyde synthesis, acetal hydrolysis was previously found to work on specific substrates.[11] However, facile hydrolysis during reaction was considered unsuitable for the multistep synthesis of our ligands.

3.2 Results and Discussion

3.2.1 [2x2] grids: ligand substitution, extension and decoration towards arrays of grids

To synthetize the simplest derivatives of a bishydrazone ligand is a matter of three basic steps, no chromatography needed, no special skills required (**GR6B**, **GR62**, *Figure 3.13*). However, right from the beginning, it is important to realize that the terpyridine motif, which hydrazone ligands mimic, is accessible by two different strategies which result in two different ligands of the same formula (constitutional isomers). The two isomers have a different orientation of the hydrazone bond. (*Figure 3.13*) This structural factor plays an important role not only for synthesis but also for coordination performance and spectroscopic properties, as will be described later in the chapter.

The isomers are accessible via two different strategies. The preparation of **GR6B** is based on 2-phenyl-4,6-pyrimidinedicarboxaldehyde (**GR4**) and the final ligand (**GR6B**) is formed via reaction with 2-(1-methylhydrazinyl)-pyridine. [23] The starting material for the other isomer (**GR62**) is 4,6-bis(1-methylhydrazino)-2-phenylpyrimidine (**GR4B**) and the sequence is completed by the reaction with 2-pyridinecarboxaldehyde. [48] (*Figure 3.13*)

Even though the reaction setup is not difficult in either case, it is necessary to say a few words about the synthesis of **GR4**. (*Figure 3.13*) Its precursor 2,4-dimethyl-6-phenyl pyrimidine (**GR1**) is obtained in form of fine white needles from a mixture of benzamidine, acetylacetone and K_2CO_3 in water upon standing at room temperature for 4-5 days. The reaction is time demanding, but gives a reasonable yield ~60 %, proceeds under mild conditions (room temperature, water) and the simple isolation (filtration) of pure product makes it appealing. However, the following oxidation has to carried out with care. The yield for oxidation of the methyl groups to aldehyde units strongly depends on the reaction conditions. Before the reaction, all solvents must be thoroughly degassed and the apparatus must be kept under inert gas for the whole time of heating. Attention has to be paid especially on the possible build-up of pressure in the apparatus caused by gaseous Me_2S produced as a side product during the reaction. Least dangerous is when any overpressure only breaks the seal and the following

influx of air decreases the yield. In worse cases, the whole setup blows up. When the reaction proceeds without problems, subsequent basification, extraction with dichloromethane and provides a crude product which has to be extracted into ether. The extraction has to be repeated until the colour of the extract changes from dark orange to very light yellow. Slow evaporation of ethereal fractions (diethyl ether or diisopropylether) gives the dialdehyde **GR4** analytically pure as orange-yellow crystals in a yield of 80 %.

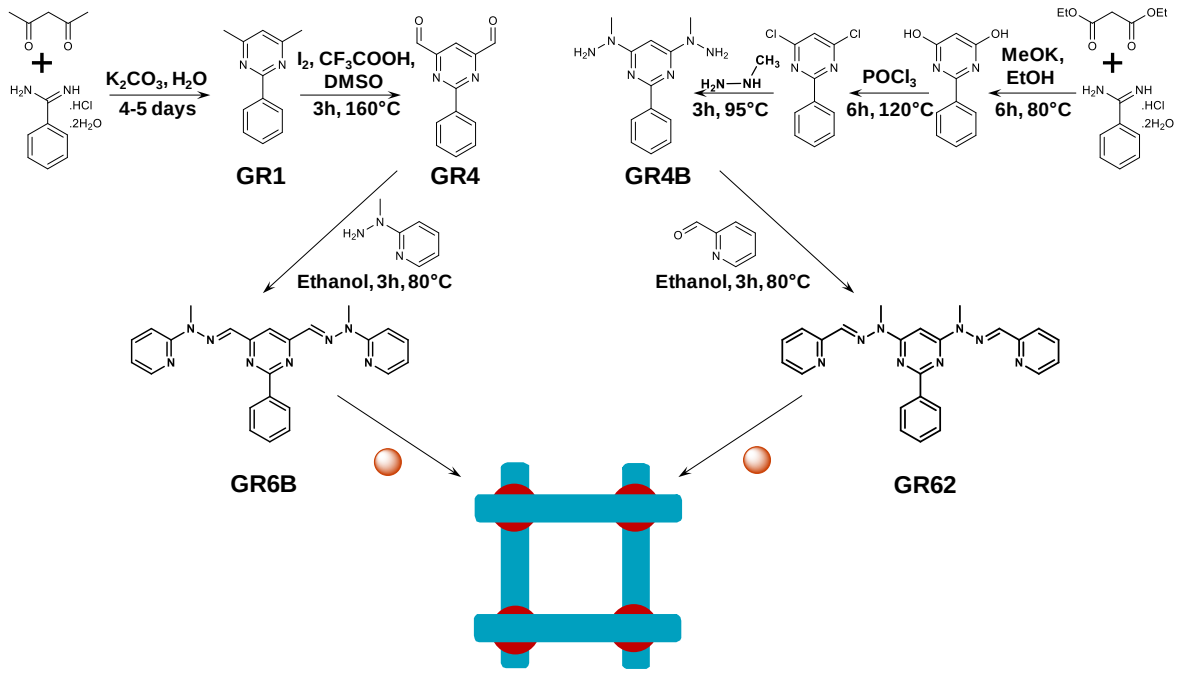

Figure 3.13: *Synthesis of ligands **GR6B** and **GR62**. If mixed with cations with octahedral coordination preferences, both ligands provide [2x2] grid assembly.*

When the ligands (**GR6B**, **GR62**) are formed, the addition of 1 eq. of $Zn(OTf)_2$ per ligand provide the desired [2x2] grid in quantitative yield in both cases. The structures of complexes of both isomers with different metals have already been reported in the literature [48, 53].

Our goal in this project was to assemble larger arrays of grids either by connection of basic [2x2] units or via preparation of "grids of grids". The grid of grids approach is based on two covalently linked ligands which should assemble into double square array of 4x[2x2] grids' array and will be described later.

The assembly of [2x2] units described herein was based on dynamic covalent linkages between individual grids. For this purpose, several ligands with aldehydes and amines on the periphery of the ligand were designed, prepared and tested.

Due to the considerably better accessibility of diamines to serve as linkers and the inherent instability of aliphatic dialdehydes, effort was mainly devoted to the introduction of aldehydes into the position "5" of peripheral pyridines. As already mentioned, the presence of an imine bond in the ligand backbone considerably reduce the choice of synthetic methods. Ultimately,

the aldehyde insertion was achieved by Dess-Martin oxidation. This method oxidizes primary alcohols to aldehydes with excellent yields as well as, somewhat sluggishly, secondary alcohols to ketones.

The key was therefore to prepare suitable derivatives bearing hydroxymethyl groups. The chemical pathway to dialdehyde ligand (*Figure 3.14*) started from (5-hydroxymethyl)-2-chloropyridine, which after boiling in N-methylhydrazine and subsequent condensation in ethanol provided ligand **GR32**. Overnight reaction with Dess-Martin periodinane in dichloromethane at room temperature afforded dialdehyde **GR33** in 85 % yield.

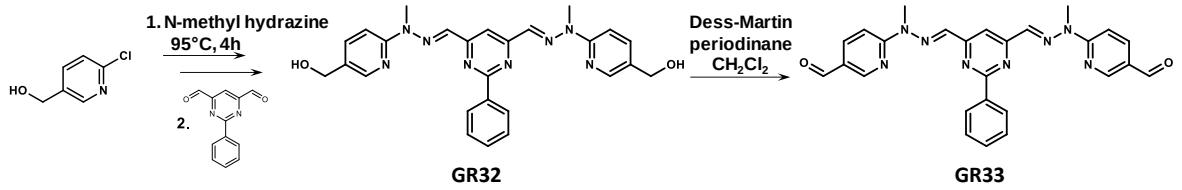

Figure 3.14: *The synthetic path to first prepared dialdehyde ligand.*

Surprisingly, neither one of these two ligands (**GR32-GR33**) provided a [2x2] grid complex with $Zn(CF_3SO_3)_2$ ($Zn(OTf)_2$, used everywhere if not specified otherwise). The fact that the grid formation fails in both cases points to some interactions of the oxygen either with Zn(II) cations or between the ligands themselves but the true nature of these interactions is unknown. Unpublished results of Dr. Stadler on a similar compound indicate the formation of either a helical structure or a rack-type complex. In the case of ligand **GR33**, things are complicated by its insolubility in common solvents. It is illustrated by the fact that its ^{1}H NMR spectrum could only be measured in DMSO at 70 °C. Additionally, neither variation of the metals cations (Cd(II), Pb(II)) nor addition of *n*-butylamine (imine formation) increased the solubility nor led to formation of the [2x2] grid complex, thus forcing us to adjust the design of the ligand.

It was postulated that the obstructive interactions could be disrupted by putting a distance between the ligand (cation) and the aldehyde. Therefore, a new design was proposed. (*Figure 3.15*) Starting with substitution of commercially available (5-chloromethy)-2-chloropyridine by Hydroxymethylbenzyl acetate, followed by acetyl deprotection under strongly basic conditions with KOH, subsequent boiling with methylhydrazine afforded the final building block for condensation of the extended ligand **GR47** (90 % yield). An encouraging result was the clear observation of formation of a [2x2] grid by this extended bis-hydroxyl ligand, which contrasts with the failure of its short analogue **GR32**. The sequence was again finished by Dess-Martin oxidation to finally obtain extended dialdehyde ligand **GR48** (73 % yield**)**.

Surprisingly, the assembly of ligand **GR48** with Zn(II) does not provide the grid as the sole product. The ^{1}H NMR spectrum shows a complex mixture of a grid and another species that

could not be separated. In this case we attribute this disappointing result to the weaker binding strength of ligands based on pyrimidine dicarboxaldehyde, as the aldehyde/imine groups reduce the electron density on the pyrimidine nitrogens decreasing their affinity for a cation. However, the successful grid formation with **GR47** indicates that with an improved design this approach should be fruitful.

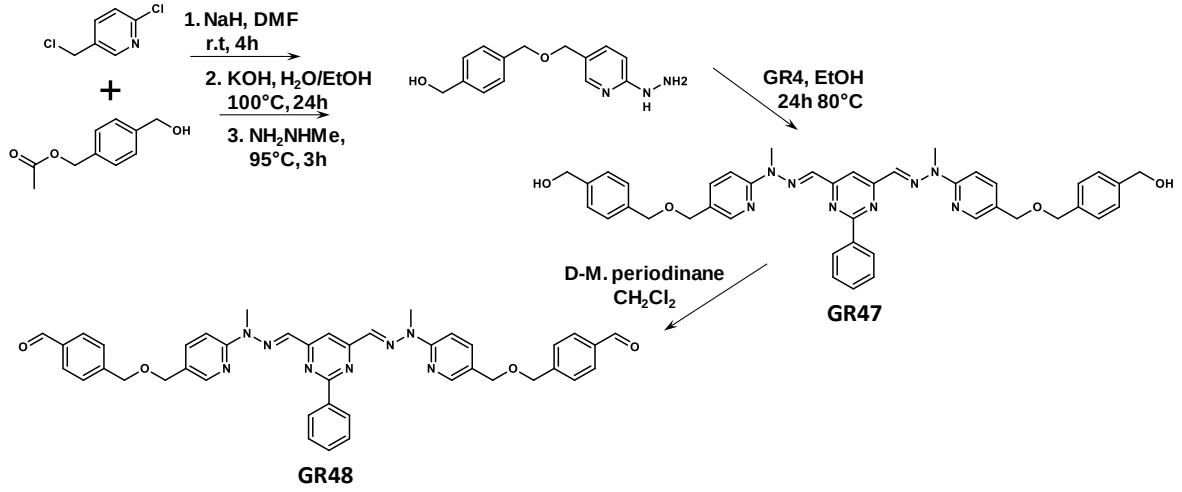

Figure 3.15: *The synthetic path to the extended dialdehyde ligand. At first the hydrazine building block forms through sequence of nucleophilic substitution, deprotection and aromatic nucleophilic substitution. This block then easily condensed with* ***GR4*** *to form* ***GR47*** *(90%). The peripheral hydroxymethyl group were then oxidized to aldehyde* ***GR48*** *(73 %) which, however, failed to assemble a clean grid.*

Contemporaneously, further research on the ligands with the reverse direction of hydrazine bond (analogues of **GR62,** *Figure 3.13*) was in process. These ligands are supposed to have higher affinity towards metal cations and also allow slightly different synthetic approach.

In contrast to above described work, our initial aim was to build a complementary bis-amine ligand. Here, a classic Gabriel synthesis was chosen attach the amine group via short aliphatic linker. The key compound for this and also for the rest of the chapter became 5-hydroxy-2-pyridinecarboxaldehyde, a simple compound of not so simple a preparation.

Condensation of this aldehyde with **GR4B** by heating at reflux for 12 h in ethanol provided the yellowish ligand **GR23** in almost quantitative yield (96 %). Subsequent complexation of $Zn(OTf)_2$ in acetonitrile gave clean grid assembly. The nature of the **GR23Zn** grid was later confirmed by a single crystal X-ray structure determination (R1 = 11.27 %). Suitable crystals were prepared by the vapour diffusion of diethylether into an acetonitrile solution. The structure of the grid showed the expected simple highly symmetric [2x2] form with eight -OH groups pointing out from the sides of the complex. (*Figure 3.16*)

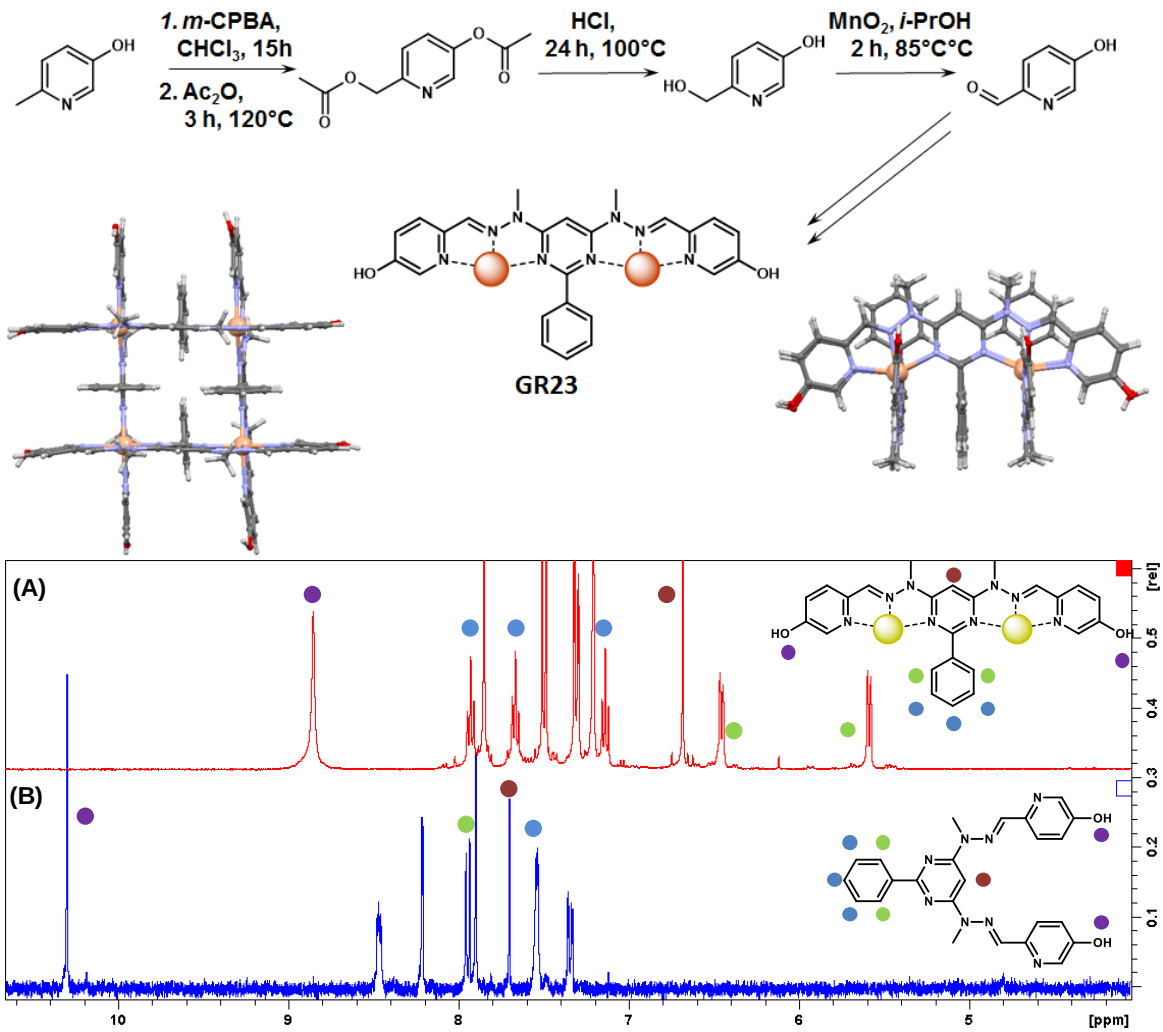

Figure 3.16: Top: *The preparation of important pyridine building block - 5-hydroxy-2-pyridinecarboxaldehyde and its octahydroxyl grid* $[Zn_4(\mathbf{GR23})_4](OTf)_8$*.(**GR23Zn**) Its crystal structure nicely illustrates the highly ordered and rigid structure of the grids based on bisterpiridine complexing motive.* ***Bottom (A):*** ^1H *NMR* (CD_3CN) *of **GR23Zn** characteristic peaks for grid formation marked with dots.* ***Bottom (B):*** ^1H *NMR (DMSO) of free ligand **GR23** for comparison.*

The formation of all grids in this work was evaluated based on their ^1H NMR spectrum. One of the very characteristic features of the bishydrazone ligands which are built from phenyl pyrimidine is very typical shift of its phenyl proton signals. When compared to the free ligand, it is possible to see that all five protons of the phenyl ring are different. On a model spectrum of **GR23Zn** (*Figure 3.16 Bottom (A)*) these signals are marked with colour dots. The characteristic splitting is caused by the restricted rotation of the phenyl due to the tight packing of the complex. From the crystal structure it is possible to see that the phenyls are tightly intercalated between ligands. The protons marked green feel the shielding of surrounding ligands much more than the blue signals which in final assembly already point out of the grid. As a consequence, these green signals appear at much lower ppm than the other aromatic

protons of the complex typically in the range of 5.5-6.5 ppm. Even though there are cases of grid assemblies where the rotation is allowed and these characteristic signals do not appear [23] in a case of our ligands it is safe to judge on the formation of the grid just from the presence of these split signals. Examples where the split signals played important role for the identification of grid structure will be seen through the whole chapter. (*Figures 3.22 and 3.37*)

The hydroxyl group provided an important starting point, and could be decorated through nucleophilic substitution. Our attempt to attach aliphatic amino groups to the ligand periphery started with the reaction of the *N*-(2-bromoethyl)phthalimide and 5-hydroxy-2-pyridinecarboxaldehyde. Subsequent condensation of this aldehyde building block (**GR25**) with **GR4B** successfully provided ethylphthalimide-decorated ligand **GR26**. (*Figure 3.17*) The assembly of the [2x2] **GR26Zn** grid proceeded very well. In spite of the lack of a good quality X-ray structure, the grid assembly was established by the combination of NMR and ESI-MS measurements. Unfortunately, all attempts to deprotect the amine were disappointing. The classic deprotection method with hydrazine completely destroyed the ligand, while prolonged (2 days) reflux with KOH afforded only partially hydrolyzed phthalimide (**GR27,** *Figure 3.17*) with one carboxyl hydrolysed and the other still attached as the amide. Interestingly this ligand is soluble in slightly acidic and basic aqueous solutions, while the neutral form is soluble in organic solvents but does not form any soluble complex with Zn(II). Again, it may be noted that Dr. Stadler found similar ligands with pendant amine groups very insoluble and unsuitable for grid formation.

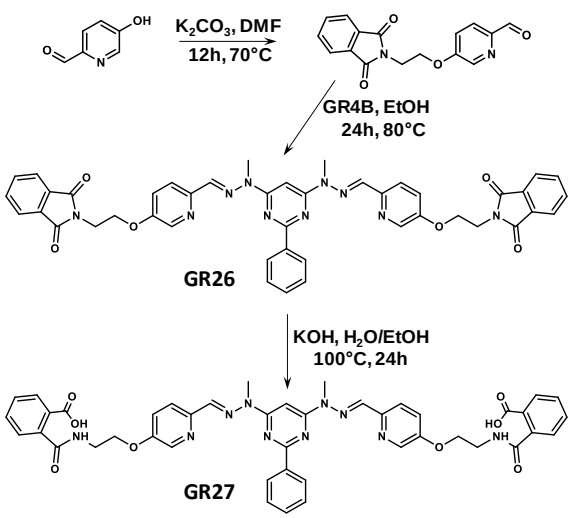

Figure 3.17: *The attempt to synthetize the amino- decorated grid. The phtalimide derivative* ***GR26*** *was successfully synthesized. Unfortunately, the subsequent deprotection failed.*

In the same time, in attempts to introduce various functional groups on the periphery of a bis-hydrazone ligand, we prepared two ligands **GR30** and **GR31** bearing carboxylic groups. (*Figure 3.18*) Even though this set of ligands has the potential to create an aldehyde, the reaction conditions are not compatible with a hydrazone bond. The ligands bearing ester groups can

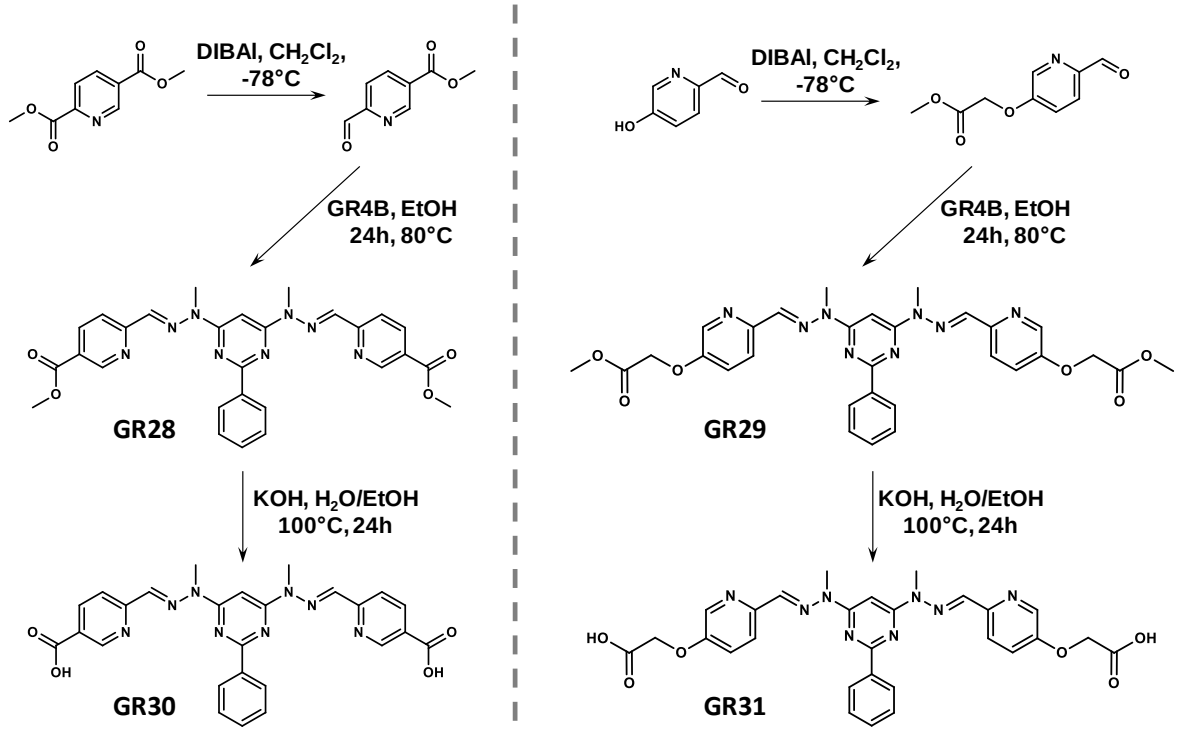

Figure 3.18: *Two examples of the grid ligands with carboxylic groups. Esters **GR28** and **GR29** were observed to form the grid structure, while the structures formed in cases of carboxylic acids **GR30** and **GR31** could not be clearly elucidated.*

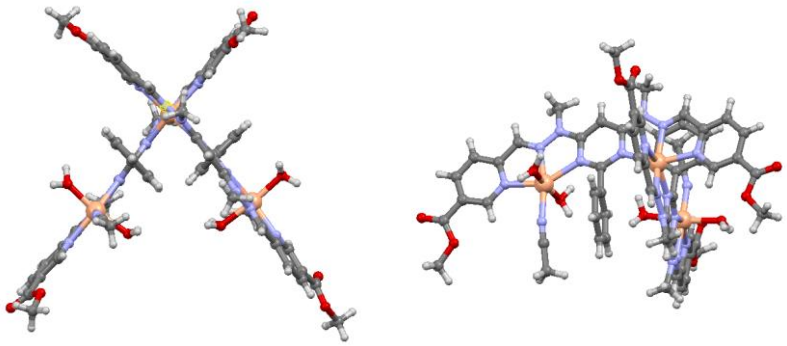

Figure 3.19: *Crystal structure of corner complex obtained from the solution of **GR28** and $Zn(OTf)_2$. The complex is formed from two ligands and three Zn(II) One Zn(II) connects the ligands while the other two satisfies the octahedral coordination with three donor atoms pf ligand two oxygens from water and one acetonitrile.*

assemble a regular [2x2] grid. However, the complex **GR28Zn** always contained some amount of a corner complex **GR28Zn(corner)**. The crystal structure of this corner complex (R1 = 7.87 %) shows two ligands connected via one Zn(II), with two other Zn(II) cations occupying the second coordination sites but completing their coordination spheres with molecules of acetonitrile and water. (*Figure 3.19*) The single crystals for the structure determination were grown by the vapour diffusion of the diethyl ether into an acetonitrile solution of **GR28** and $Zn(OTf)_2$. The second ester ligand **GR29** forms the Zn(II) grid cleanly but no suitable crystals were obtained in this case.

Overnight boiling of esters **GR28** and **GR30** in an ethanol/water solution of KOH provided, after acidification, the carboxylic acids in quantitative yield. This experiment nicely demonstrates the perfect stability of hydrazones under basic conditions. The resulting ligands are, however, very insoluble and the addition of Zn(II) did not give clean grid formation, probably due to the interactions of the carboxylate groups with Zn(II). For these reasons further steps in this direction were abandoned.

Even though at this point we were not any closer to our desired aldehyde or amine grid, thanks to these derivatives (**GR23**, **GR26**, **GR28**, **GR30**) we became aware of a previously neglected feature of Zn(II) grid assemblies and that was their fluorescence.[54] All the ligands and Zn(II) grids described here show some level of fluorescence, details of which will be given later in the chapter.

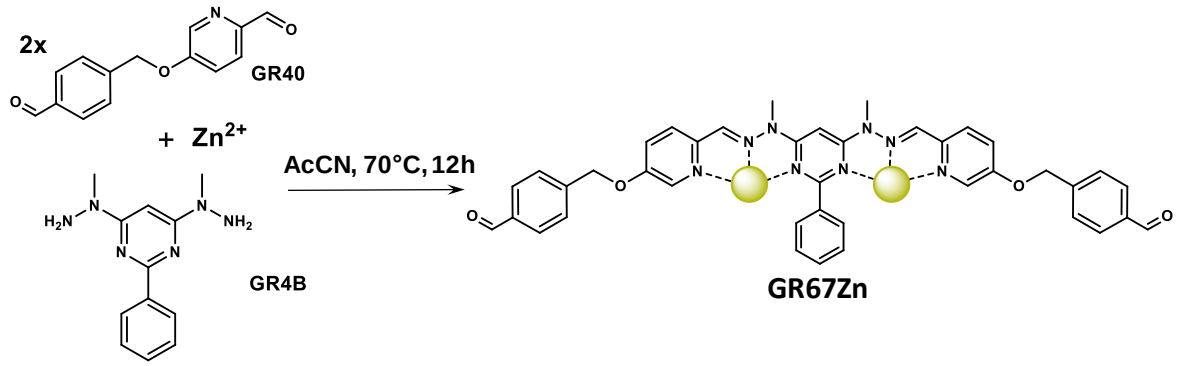

Figure 3.20: *Dynamic approach towards dialdehyde ligand **GR67**. The condensation between dialdehyde building block and **GR4B** was templated by Zn(OTf)$_2$. Its coordination preference helps to distinguish between pyridinecarboxaldehyde and benzaldehyde.*

Due to the difficulties encountered with basic ligands, on our way to the aldehyde functionalised grid we also tested the possibility of assembling a grid directly via template dynamic covalent chemistry. (*Figure 3.20*) Even though it was far from perfect, this experiment proved that it is indeed possible to assemble such grid and it also justified the shift to hydrazinopyrimidine (**GR4B**) based grids. When dialdehyde **GR40**, was mixed in an NMR tube together with **GR4B** and Zn(II) cation and heated overnight at 60°C in acetonitrile, the desired grid **GR67Zn** was undoubtedly present in the mixture. (*See Figure E2.3 in Exp. p.*) This grid must possess eight aldehyde groups protruding from the complex. However, despite the grid being a major product, the mixture also contained considerable amounts of another species. Instead of trying a complicated purification or optimization of the formation conditions, we decided to directly prepare this ligand via classic bottom-up synthesis.

The retrosynthetic path was centred on introduction of benzyl alcohol (**GR66**) at the extremities of our extended ligand. (*Figure 3.21*) Combining all the knowledge obtained in

above cases, the acetyl ester (**GR65**) was seen as an ideal protecting group. With this logic, methyl 4-(bromomethyl)benzoate was chosen as a starting material. The rest of the actual synthesis was then straightforward and is described in the *Figure 3.21*. The final ligand **GR67** is rather insoluble in CH_2Cl_2 which is used for Dess-Martin oxidation. Therefore, it could be directly collected as an off-white precipitate from the reaction mixture.

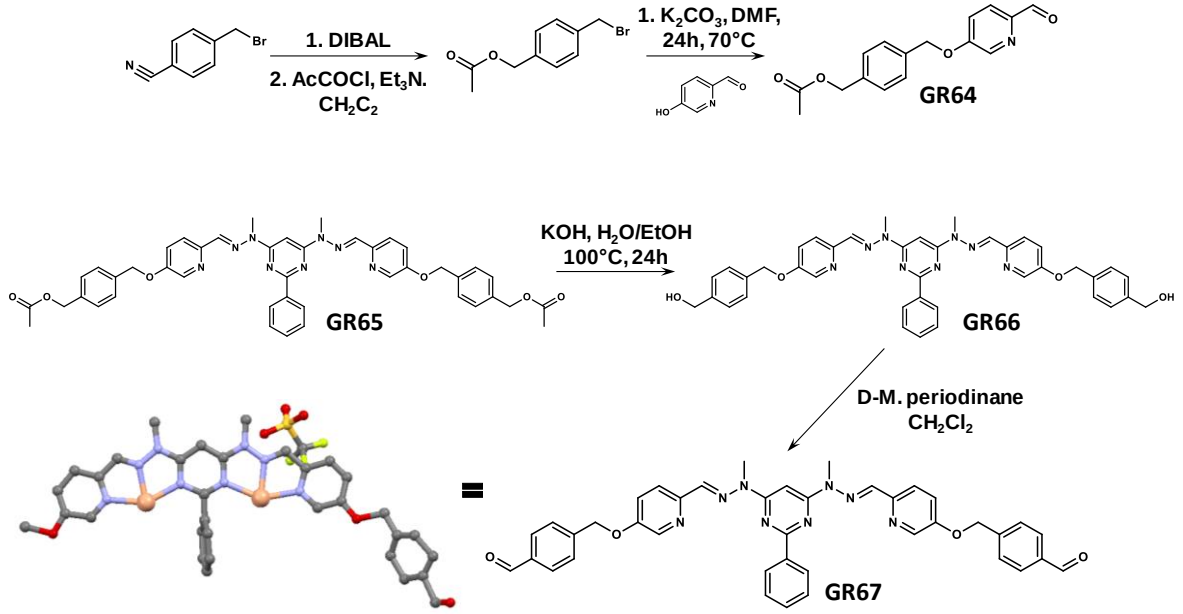

Figure 3.21: *Synthetic path to dialdehyde ligand **GR67**. **Bottom left**: Depiction of a half of the ligand from incomplete crystal structure of the grid $[Zn_4(\mathbf{GR67})_4](OTf)_8$ (**GR67Zn**). It shows formation of the grid and attachment of the benzaldehyde on the side. Nevertheless, the structure of **GR67Zn** was confirmed with the complementary analysis from ^{1}H NMR and ESI-MS.*

The complete **GR67** ligand assembled in the presence of Zn(II) into the grid. Although an X-ray structure determination did not provide a satisfactory residual (R1 = 20.40 %), it clearly defined the eight pendant aldehyde groups on the grid unit. (*Figure 3.21*)

The long-desired grid was finally obtained! At this point it is only appropriate to say something about its ^{1}H NMR as most of the successes or failures of grid assembly mentioned so far, were decided on the basis of this method. The ^{1}H NMR spectrum (*Figure 3.22*) is very simple, indicating the formation of a highly symmetric complex. The most readily assigned peak is that of the aldehyde proton at 9.94 ppm. Its relative integration is in agreement with the presence of two aldehyde units per ligand. Much more significant in relation to establishing successful grid assembly were already mentioned small doublets **B** (6.44 ppm) and **C** (5.65 ppm). Observation of two doublets in the range between 5.5-6.5 ppm is indeed a very characteristic sign for the assembly of our grids and even here it was general criterion for identification of a successful grid formation. [54, 55] The peaks **B** and **C** were assigned to the inner and outer protons of the pyrimidine phenyl ring whose rotation was blocked due to the

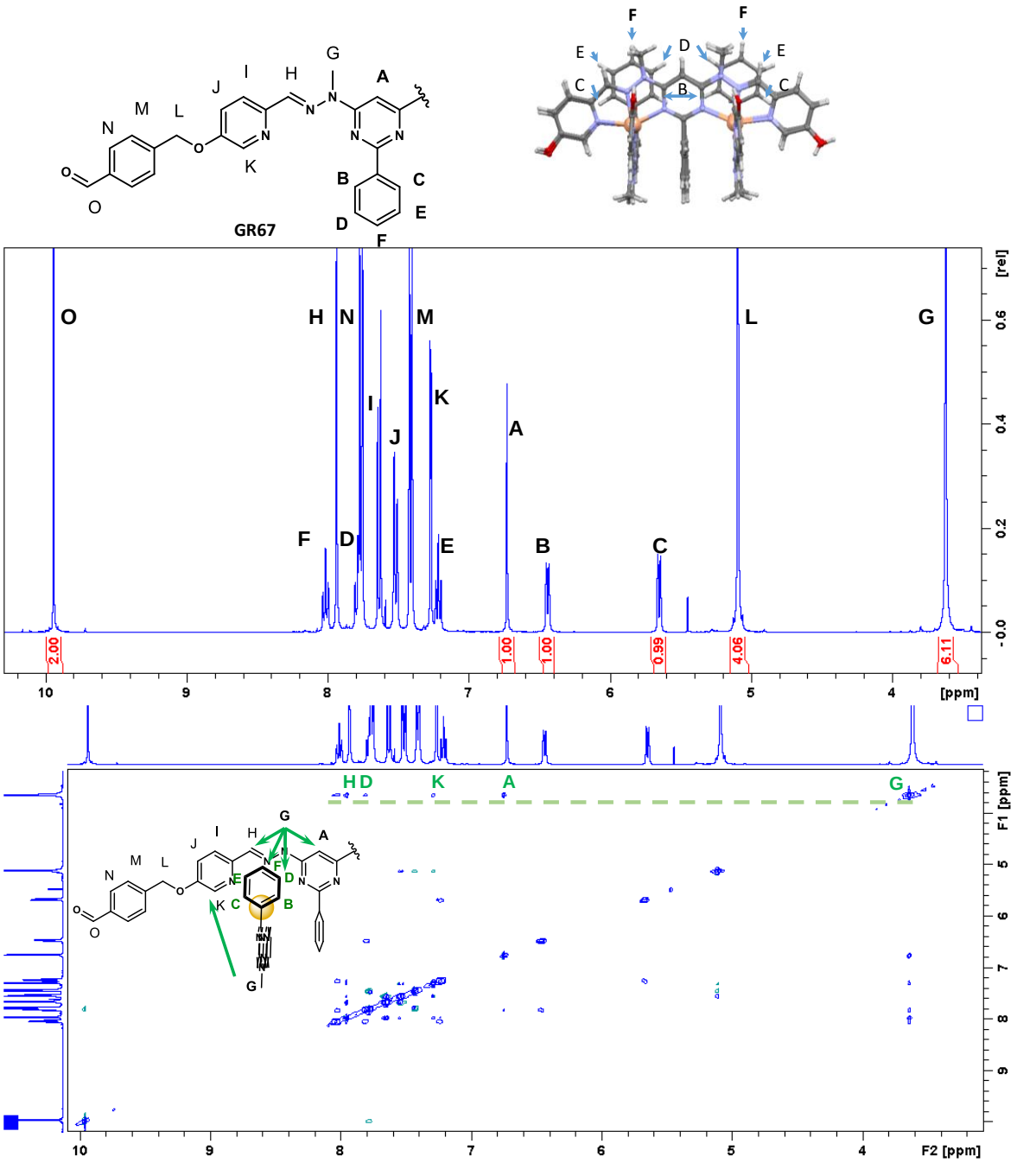

Figure 3.22: ***Top****: The* ^{1}*H NMR spectrum of the grid showing characteristic peaks of grid formation (**B** and **C**) and also aldehyde functional group (**O**). The crystal structure of **GR23Zn** was taken to illustrate the close packing and important interactions within grid core.* ***Bottom****: 2D NOESy spectrum showing some NOE interactions important for the assignment of the signals.*

close packing of the structure. (*Figure 3.16 and 3.22*) Close analysis of the NOESY (*Figure 3.22 bottom*) and COSY 2D NMR spectra revealed their coupling with three triplets **D**, **E**, **F** which belong to the rest of the phenyl protons. The fact that all five protons provide unique and sharp signals is nice demonstration of the rigidity of the grid structure.

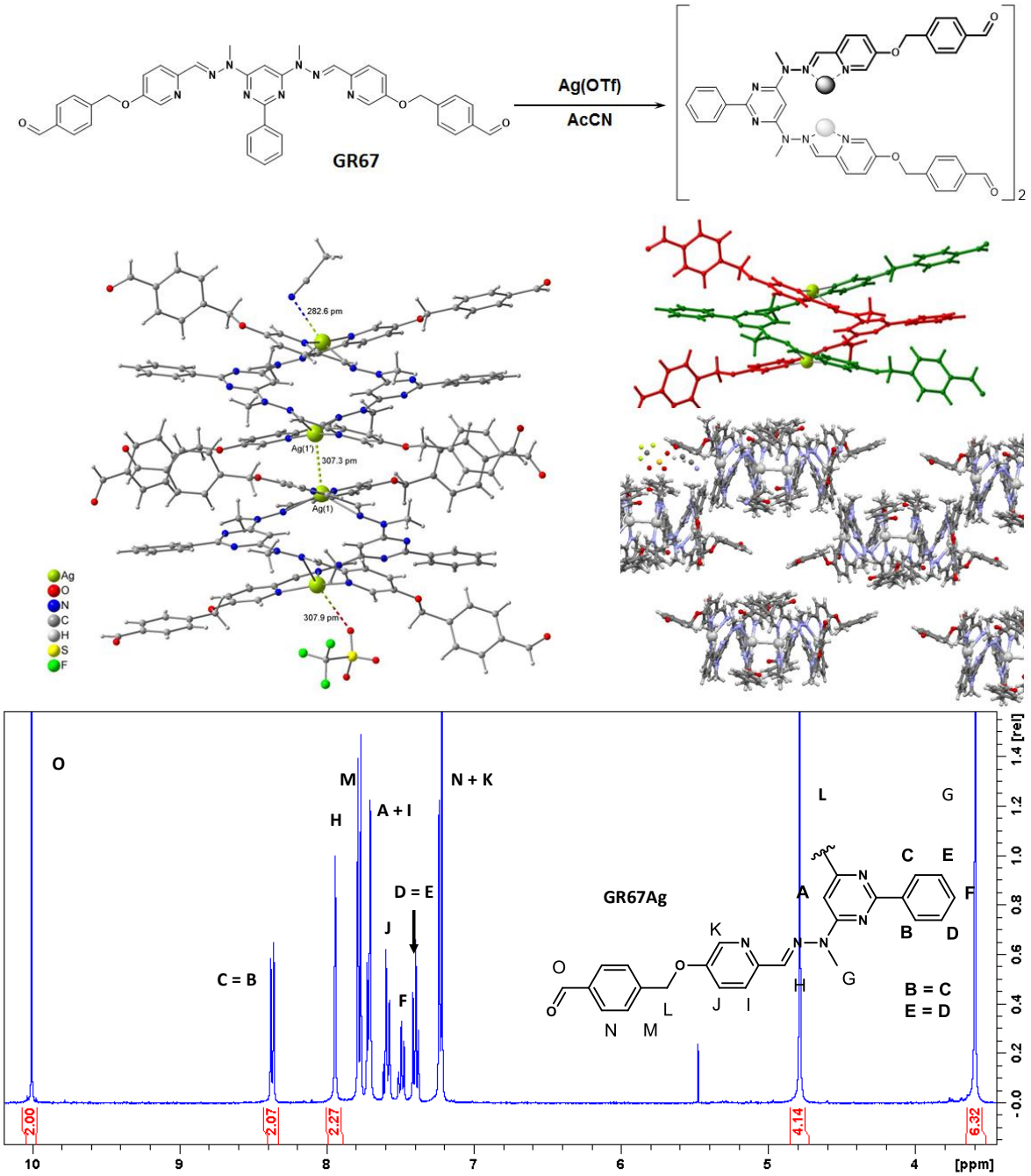

Figure 3.23: ***Top****: The illustration of the ligand configuration in the [Ag$_2$(**GR67**)$_2$](OTf)$_2$ (**GR67Ag**). **Middle left**: The crystal structure of dimeric double helicate **GR67Ag**. **Middle right**: Illustration of the double helical nature of **GR67Ag** and its crystal packing. Bottom: Assigned ^{1}H NMR spectrum of **GR67Ag**. Noteworthy is absence of any signals between 5.5 – 6.5 ppm.*

This ligand is not only a very interesting building block for arrays of grids but also with the right choice of metal cation can assemble into helixes. Stadler and Lehn recently published several interesting articles on the interconversion of grids into helices. [21, 31] Herein, only the assembly of a helicate was attempted. Adding an acetonitrile solution of Ag(I) to the ligand **GR67** successfully provided double helix **GR67Ag**, the structure of which was subsequently

proved by X-ray crystallography (R1 = 7.23 %). Interestingly, the helix crystalizes in a form of a dimer connected through an Ag-Ag bond. However, the simple nature of its ^{1}H NMR spectrum indicates that no dimerization occurs in the solution. (*Figure 3.23*) It is worth pointing out the absence of any peaks in a range of 5.5-6.5 ppm and subsequent equivalency of **B**, **C** and **D**, **E** phenyl peaks which indicates that structure of helicate is flexible, allowing free rotation of all parts of the structure. In the crystal, the dimeric double helicates are arranged in layers interconnected by counter anions, molecules of acetonitrile and via π-π interactions of benzaldehydes at the periphery.

Next, we probed the reactivity of the aldehydes of **GR67Zn** and their willingness to form imines. The first trials were rather encouraging. A short series of different amines was tried. It was possible to successfully prepare the imines of **GR67Zn** with *n*-butylamine, *p*-toluidine, 1-(methyl)-1-phenylhydrazine, and benzhydrazide probably formed an imine as well but it precipitated from the solution. Surprisingly, no reaction was observed between the grid and 3- and 4-aminopyridine. It was possible to obtain a single crystal of the 1-(methyl)-1-phenylhydrazine derivative (**GR67ZnHydr**) but only an unsatisfactorily precise structure could be obtained from the X-ray diffraction measurements (R1 = 26.66 %). Nevertheless, it was possible to see the newly formed hydrazone on the periphery of the ligand. (*Figure 3.24*)

In an extension of this approach we also tried the reaction with diamines. 2-(2-aminoethoxy)ethylamine, 2-[2-(2-aminoethoxy)ethoxy]ethanamine and 2,2'-dimethoxy benzidine were tested. In all cases a large quantity of precipitate was formed which could not be re-dissolved in hot acetonitrile. This behaviour was not surprising as the diamine would be expected to form an extended network of interconnected grids in a way that resembles covalent organic frameworks (COF). What was interesting, in the case of aliphatic diamines, was that it was possible to observe a defined grid structure in the supernatant solution above the precipitate. The shorter 2-(2-aminoethoxy)ethylamine provided a remarkably clean ^{1}H NMR spectrum of this newly formed grid species **GR67ZnIm1,** for which a symmetric four times interconnected grid structure is proposed. (*Figure 3.24 and Figure S1.4-S1.5. in Exp. p.*) Further support for this idea was provided by HR-ESI-MS, the mass of 1347.6256 Da closely corresponding to the calculated mass of (**GR67ZnIm1**)$^{5+}$ which is 1347.6333 Da. All crystallization attempts failed so far, thus the structure still awaits confirmation.

Despite a rather cold start, we were able to prepare a grid complex bearing eight aldehydes on its periphery. We also successfully decorated this grid with various imine derivatives which gives high hopes for future attempts to create covalently linked arrays of [2x2] grids.

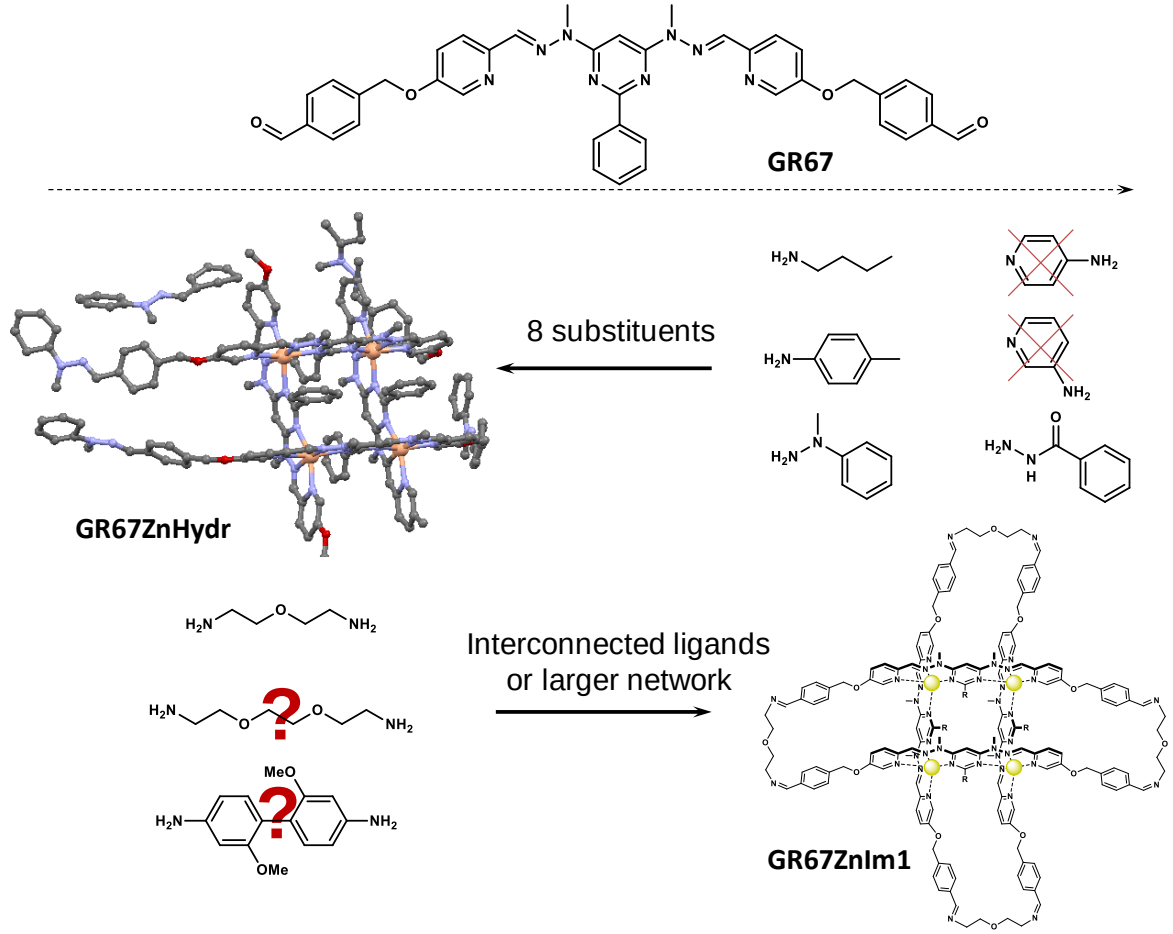

Figure 3.24: *The illustration of attempted decoration of **GR67Zn** with various imines. Crossed compounds failed to provide any defined structure. The incomplete structure obtained from the single crystal X-ray analysis of 1-(methyl)-1-phenylhydrazine derivative (**GR67ZnHydr**) proves the viability of this approach. **Bottom**: The possible structure of interconnected **GR67Zn** obtained from the reaction of 2-(2-Aminoethoxy)ethylamine (**GR67ZnIm1**). The nature of the structure obtained from other diamines will be subject of further studies.*

3.2.2 Fluorescence observations on bishydrazone ligands and grids

While structural knowledge is of basic importance, in contemporary chemistry there is also a strong interest in measurable physical properties which may be of practical applicability like magnetism, conductivity or spectroscopic properties.

The fluorescence of Zn(II)/hydrazone complexes has been known for a long time. In 1972, a comparative study on various hydrazine ligands with NNN chelating motifs was published.[57] The measurements were carried out at pH 8 in order to ionize the -NH- and obtain a fully conjugated system in the ligand. All the ligands in this study were chosen to be planar, conjugated and ionisable. Therefore, the observed difference in the relative fluorescence (R.f) was hard to explain just by structural differences, especially between structurally similar ligands

like **QAPH** (R.f. = 2) and **PAQH** (R.f. = 660), which differ only in the direction of the hydrazone bond. (*Figure 3.25*) It was observed, that fluorescence depends on the preferred resonance form and length of the conjugated system. The form with double bond at imine -C=N- rather than in diazo -N=N-. The ligands where both factors meet should then have stronger fluorescence than the others, including the symmetric ligands where neither -C=N- or -N=N- is preferred. Therefore, the **PAQH** (R.f. = 660) and **BAQH** (R.f. = 2000), which fulfil these requirements the best have strong fluorescence. The symmetric ligands **PAPH** (R.f. = 1) and **QAQH** (R.f. = 20) without preference for the position of the double bond in deprotonated state and those which prefer the-N=N- have weak fluorescence.[56] (*Figure 3.25*)

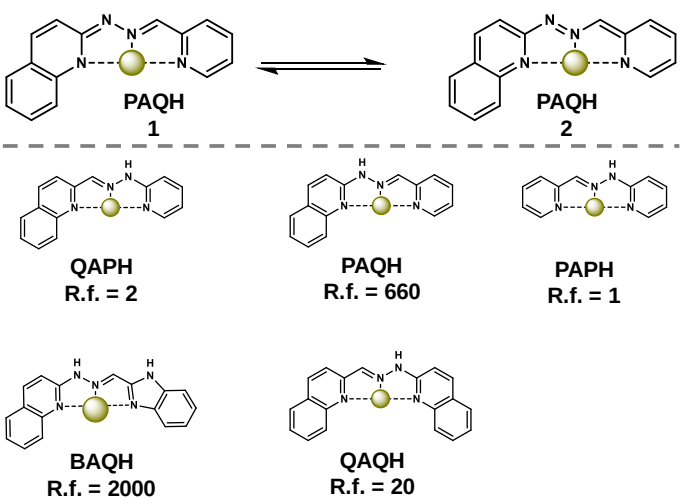

Figure 3.25: ***Top****: Two resonance forms* ***QAPH****. The form 1 is favoured, due to the aromatic system being broken at quinoline and double bond -C=N-.* ***Bottom****: Relative fluorescence of chosen Zn(II) complexes.*

There are also many reports of fluorescent Zn(II)-terpy complexes (terpy = 2,2';6',2''-terpyridine) and their study for applications in supramolecular polymers or as sensors for various analytes. The dissociation of the bis(terpyridine)Zn(II) complex to the monoterpyridine species provides a sensor for pyrophosphate due to fluorescence quenching.[57] Another study describes the fluorescence of a perylene bisimide substituted with two divergent terpyridine units. Complexation of Zn(II) afforded a fluorescent coordination polymer having a quantum yield 61 %. Here, the fluorescence is a property of the ligand, but the binding of Zn(II) proved to have no quenching effect.[58]

The spectroscopic features of bishydrazone grids were already mentioned in the first publication on ionisable bishydrazone ligands also reported reversible pH-dependent colour changes.[18] The colour of the Co(II) grid of **JHA** ligand goes from pale yellow at pH ~1, to orange at pH ~3 and to deep violet above pH 7. (*Figure 3.10*)

In an early review of grid chemistry, there is also a reference to unpublished results from our group (M. Ruben) regarding the emission of the Zn(II) grid of the same **JHA** ligand.[1] Here the emission was supposed to be modified by π-π interactions of the phenyl substituents intercalated between two ligands. This is probably only partially true, because other unpublished work by

Stadler indicates that even the derivatives without any substitution on pyrimidine show some emission. There are several further references in doctoral theses of the other members of our group to the fluorescence of hydrazone helicates and polymers (J.-L. Schmitt) or acylhydrazone grids (X. Y. Cao) but in no case was a detailed study completed.

The structurally closest ligand to the present examples for which photoluminescence has been studied is ligand **18**.[59] (*Figure 3.26*) This ligand has substitution of the central pyrimidine which prevents grid formation. With $ZnCl_2$ it forms trinuclear complex similar to the corner observed in case of **GR28** (*Figure 3.19*). The study reports strong fluorescence of this Zn complex, even though no value of quantum yield is given. Since Zn(II) itself is spectroscopically inactive in the visible region, the fluorescence of the complex was assigned to an intra-ligand charge transfer (ILCT) π-π* transition. The fact that the ligand is non-emissive while the complex is strongly luminescent was attributed to the enhanced rigidity of the ligand backbone upon complexation. This conclusion was taken to be supported by the fact that Cd(II) complex with its folded shape has no fluorescence whatsoever.[59]

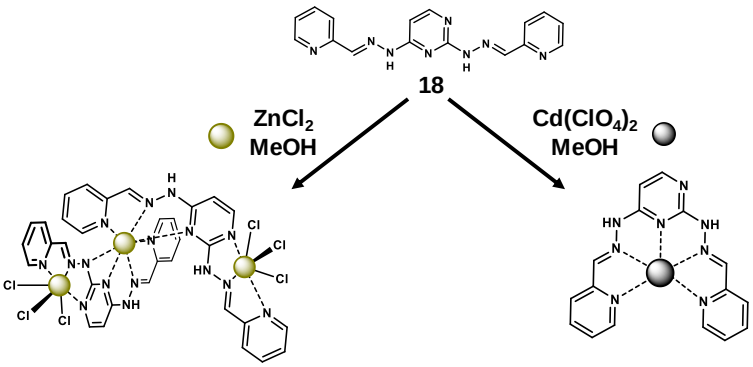

Figure 3.26: *The depiction of fluorescent trinuclear Zn(II) complex with ligand **18** and non-emissive Cd(II) complex.*

In the present work, all absorption and emission spectra of grid complexes were measured in HPLC grade acetonitrile. In such a coordinating solvent and at the very low concentrations normally necessary for luminescence measurement, there is the probability of solvolysis of the complex, that is, of some extent of ligand dissociation. Grids formed from the derivatives of ligand **GR6B**, in particular, were observed to dissociate fully at the concentration of ~10^{-6} M. Their relative fragility when compared to complexes of **GR62** can be attributed to the already mentioned lower affinity towards the metal ion, due to the lower electron density on the pyrimidine nitrogens. All the emission spectra were measured at the excitation wavelength 365 nm. This wavelength is slightly below that of the absorption maxima of our complexes but it is one of the wavelengths of the usual laboratory UV lamp (365 nm) so the lamp was used for the initiall assessment of the complexes before measurements. All the quantum yields were measured at 360 nm using integrating sphere.

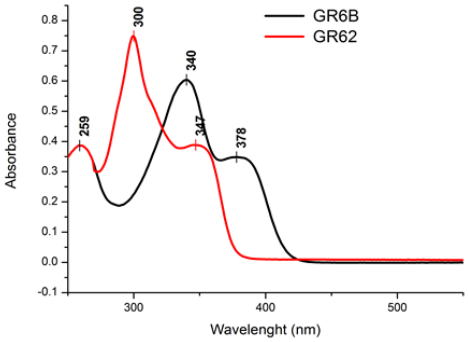

Figure 3.27: *The UV-VIS of the ligands **GR62** and **GR6B** in $CHCl_3$. ($1.6x10^{-5}$ mol/dm^3)*

The absorption spectra of ligands **GR6B** and **GR62** were measure in chloroform at a concentration of $1.6x10^{-5}$ M. (F*igure 3.27*) **GR62** has three bands with maxima at 259 nm ($\varepsilon = 24125$ M^{-1} cm^{-1}), 300 nm (46750 M^{-1} cm^{-1}) and 347 nm (24250 M^{-1} cm^{-1}), and the ligand **GR6B** has also three maxima at 259 (24125 M^{-1} cm^{-1}), 340 nm (40000 M^{-1} cm^{-1}) and 378 nm (21750 M^{-1} cm^{-1}). All the observed bands of both **GR62** and **GR6B** can be attributed to ligand π-π* transitions.

The basic ligands **GR6B** and **GR62** are insoluble in acetonitrile and show no fluorescence in chloroform or DMSO but do show emission in the solid state pointing to the presence of aggregation enhanced emission. (*Figure 3.28*) The ligand **GR6B** exhibits orange-yellow fluorescence, though with rather low quantum yield of ~2 %. (λ_{ex} = 360 nm). The other ligand **GR62** which differs only in the direction of the hydrazone bond, shows a weak white-blueish fluorescence of quantum yield ~1 % (λ_{ex} = 360 nm). The quantum yields for powdered crystals of the Zn(II) grids grids are approximately twice as great at 4 % for **GR6BZn** and ~3 % in case of **GR62Zn**. (*Figure 3.28*) This can be attributed to the conformational change from the folded structure of the free ligand to a planar, fully conjugated one in the complex with increased rigidity due to the inhibition of rotational motion due to binding within the grid. Another reason for enhanced fluorescence could be also elimination of photoinduced electron transfer (PET) process caused by the presence of a lone electron pairs on nitrogens. This process is again eliminated by the complexation with Zn(II). [60]

The red shift of the emission maxima is usually attributed to the influence of metal ion binding on the levels involved in the intra-ligand charge transfer absorption. Some influence might also have π-π stacking in the complex between ligands and intercalated phenyl rings. Further analysis is needed to explain the especially large shift of 95 nm in case of **GR6B**. (*Figure 3.28*)

An acetonitrile solution of the grid **GR6BZn** has an orange colour while a solution of **GR62Zn** is completely colourless. Despite their similar structures, the differences in their absorption spectra are marked. (*Figure 3.29*) Especially interesting is the absence of a second peak in a spectrum of **GR6BZn**, its generally broader bands and the pronounced red shift of its

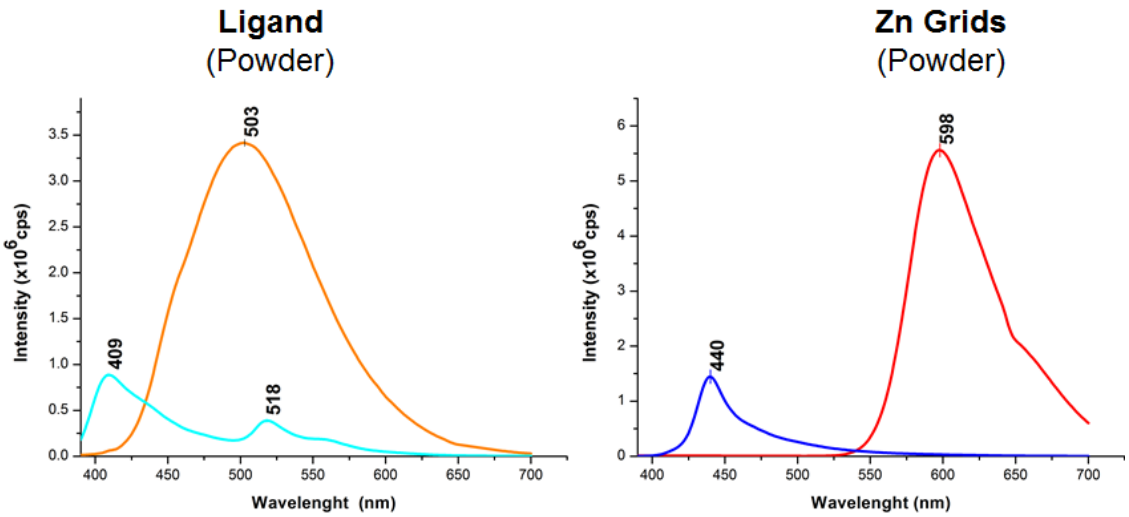

Figure 3.28: *Left: The powder emission of ligands **GR6B** (orange) and **GR62** (turquoise) at λ_{ex} = 365 nm. Right: The powder emission of grids **GR6BZn** (red) and **GR62Zn** (blue) at λ_{ex} = 365 nm.*

visible region maximum (465 nm). The second peak is characteristic for all the derivatives of **GR62** and the absorption of **GR62Zn** closely resembles that of related complexes already described in a literature.[61]

To see if the fluorescence of Zn grids is a unique property, grids with different metal cations (Cu(I), Cu(II), Pb(II), Fe(II), Co(II), Ag(I), Cd(II)) were prepared and exposed to the UV lamp at 365 nm. Only the Cd(II) grid showed fluorescence. Its emission was relatively intense and of pale blue colour similar to that from the Zn(II) grid. The electronic spectrum of **GR62Cd** showed about a 2/3 stronger absorption than the analogous Zn(II) grid, while both grids share the same maxima at 373 nm and 390 nm. (*Figure 3.29*) In the spectrum shown, the second maximum of **GR62Cd** is reduced to a shoulder on the first but at a concentration two times higher the peaks are resolved and of the same intensity. In contrast, the spectra of the **GR67Zn** grid assembly are unchanged over the concentration range 10^{-6}-10^{-7} M, with apparent dissociation starting only below 10^{-7} M. (*Figure 2.29*)

Excitation at 365 nm of **GR62Zn** and **GR62Cd** produced intense blue emission. (*Figure 3.30*) The blue emission can be also seen by the naked eye even in daylight. The quantum yield of the **GR62Zn** emission was measured to be around 60 %, relatively high for Zn(II) complex without any auxiliary sensitizing units.[58] In contrast, **GR62Cd** has a low quantum yield of approximately 8 % and the counter partner **GR6BZn** shows even weaker orange fluorescence (quantum yield 1 %) with a maximum at 585 nm. The red shift of the maximum in comparison with the free ligand (503 nm) is probably due to the effect of the metal ion binding. The excitation spectra of **GR62Zn** and **GR6BZn** as expected mirror their absorption spectra.

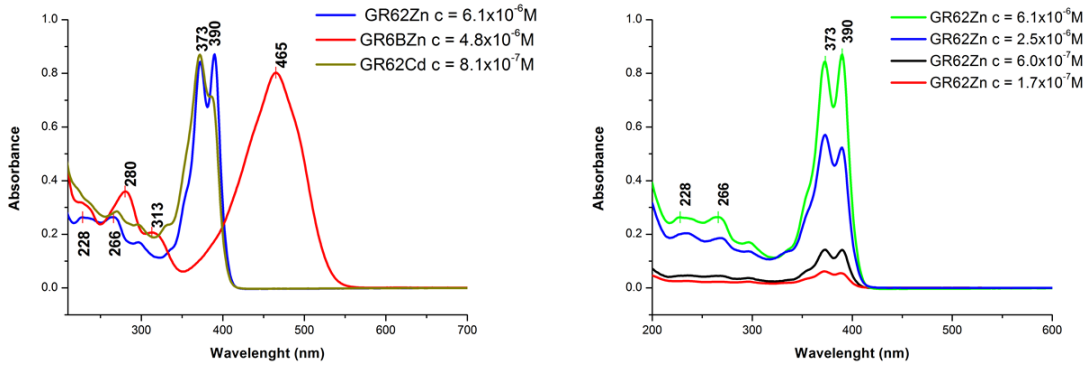

Figure 3.29: ***Left****: Absorption spectra of* ***GR62Zn*** *(blue),* ***GR62Cd*** *(green) and* ***GR6BZn*** *(red).* ***Right****: Absorption spectra of* ***GR62Zn*** *at various concentrations.*

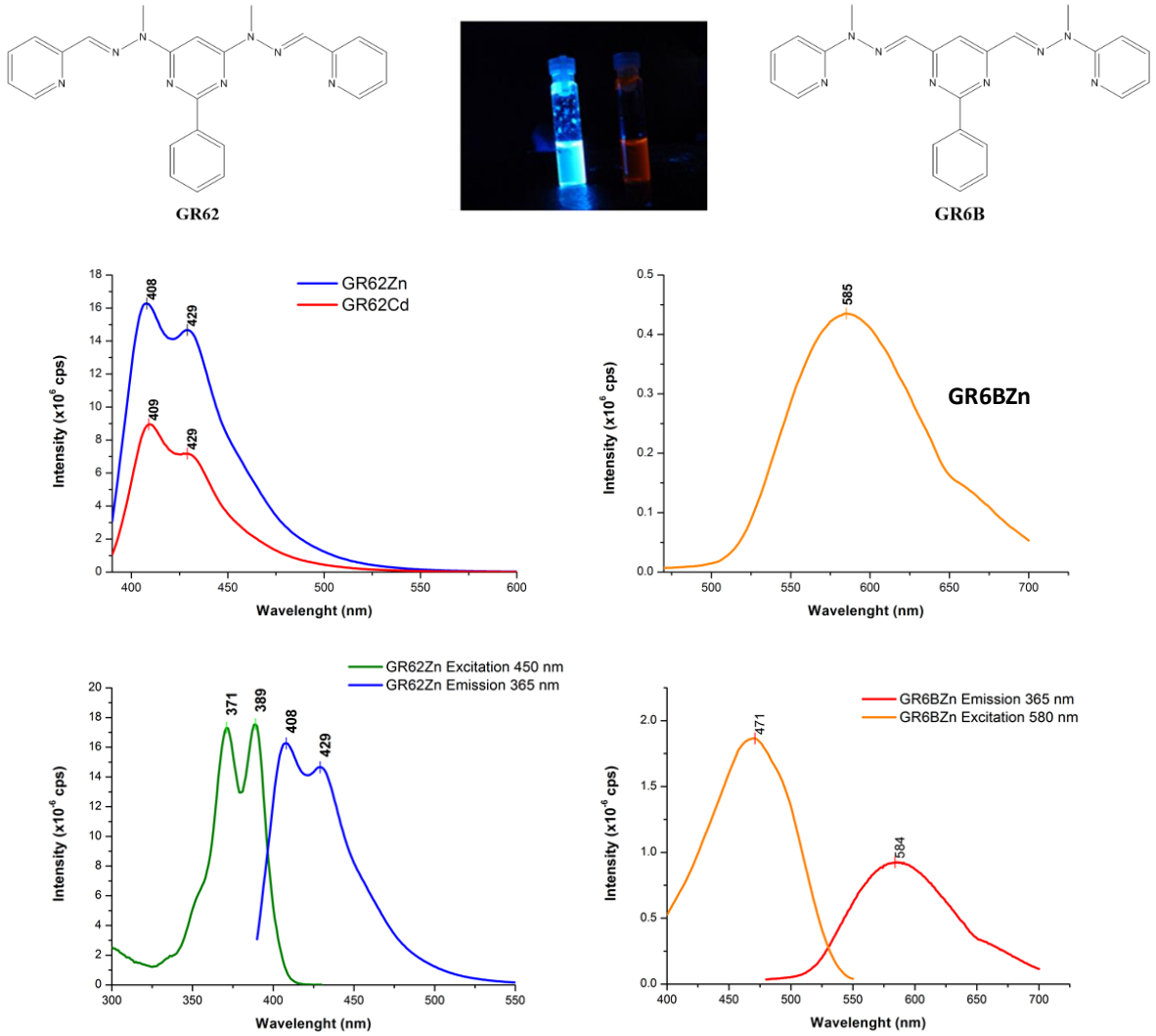

Figure 3.30: ***Top****:* ***GR62Zn*** *(Blue),* ***GR62Cd*** *(Red) and* ***GR6BZn*** *(Orange) and visual comparison of their emission at* λ_{ex} *= 365 nm.* ***Middle left****: The emission spectra of* ***GR62Zn*** *(*$6x10^{-7}$ *mol/dm*^{3}*),* ***GR62Cd*** *(*$6x10^{-7}$*mol/dm*^{3}*) at* λ_{ex} *= 365 nm;* ***Middle right****: The emission spectra of* ***GR6BZn*** *(*$4x10^{-6}$ *mol/dm*^{3}*) at* λ_{ex} *= 365 nm;* ***Bottom left****: Symmetry of excitation and emission spectra of* ***GR62Zn****;* ***Bottom right****: Symmetry of excitation and emission spectra of* ***GR6BZn****;*

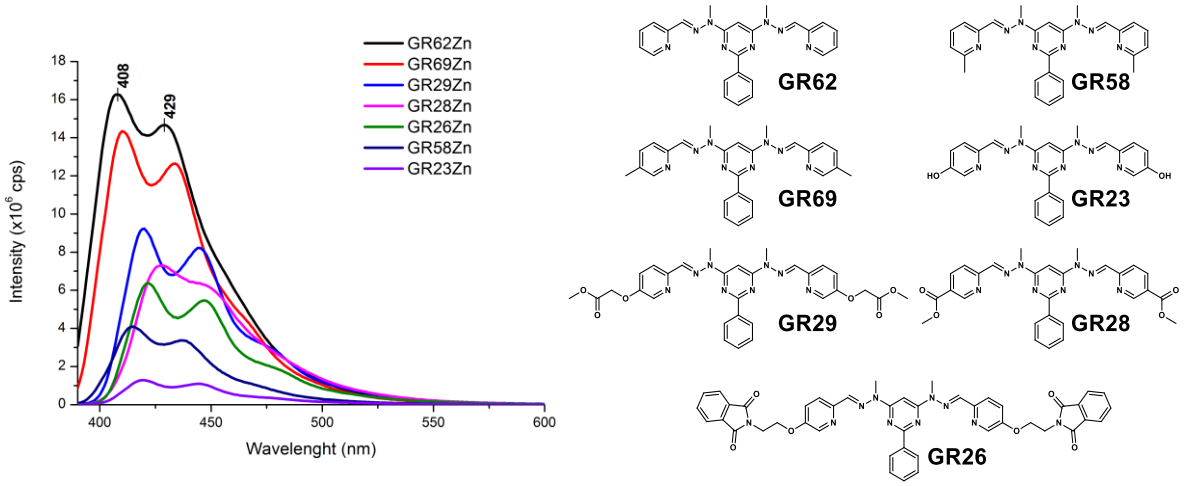

Figure 3.31: ***Left:*** *The emission spectra of selected Zn(II) grids of the ligands from the* ***GR62*** *derivatives (****GR69, 62, 58, 29, 28, 26, 23; Right****) in acetonitrile. (each c = 6x10^{-7} mol/dm^3 of grid)*

The synthesis of various substituted grids was described in the previous chapter. All the grids were observed to be more or less emissive. A summary of measured quantum yields of a representative sample of derivatives is shown in *Table 3.1*. The relative emission intensities of several grid complexes are depicted in *Figure 3.31*. In several cases, the quantum yield was also measure by a comparative method. At first, two standards, quinine sulphate and 9,10-diphenyl anthracene, were calibrated against each other. Subsequently, the grids were measured at several concentrations for which the absorbance was not greater than 0.1 at λ_{ex} = 365 nm. The values obtained agreed with those obtained by use of the integrating sphere.

The quantum yields in *Table 3.1* show that the simplest derivative, **GR62,** gives the strongest fluorescence. The ionisable derivative **JHA** has a very low quantum yield, probably due to the quenching by ionisable hydrogen. The same applies for **GR23**. The substitution of the hydroxyl in **GR26** and **GR30** again increases the values of quantum yield by over 30 %. The quantum yields of "5"-substututed pyridines (**GR69**) are much higher than "6"-substituted ones (**GR58**), possibly due to the steric interactions of methyl groups of the ligand when it is forced into its metal-ion binding form as in **GR58Zn**. Indeed, the grid **GR58Zn** was observed to be somewhat less stable than

Table 3.1: Quantum yields of chosen grids

Sample	λ_{exc}/nm	Quantum Yield (φ)
GR62Zn	360	0.606
GR69Zn	360	0.405
GR26Zn	360 (365)[a]	0.373 (0.33)[a]
GR62Cd	360	0.079
GR23Zn	360 (365)[a]	0.075 (0.08)[a]
GR6BZn	360	0.059
GR58Zn	360	0.053
JHA	360	0.003
GR28Zn	365	0.36
GR30Zn	365	0.41

[a]Values obtained by comparative method

GR69Zn. In a case of **GR62Cd** it is probably the heavy metal effect which reduces the intensity of the emission, as the d^{10} Cd(II) cation cannot otherwise influence the ligand fluorescence. The last metal in the II.B group, mercury(II), has no observable fluorescence at all.

3.2.3 On the way to "grids of grids".

In fact, what is described above actually grew on the shoulders of another project. Our original goal was to assemble a so-called "grid of grids". Some examples have been already described in the introduction. Our design lay in the covalent connection of four [2x2] grids by linkers. Such an array could provide a path to physical manipulation of individual small grids, which are however, still arranged in defined positions.

A grid of grids can be seen as transitional between incomplete multinuclear grids [25] and polymeric "grids of nodes"[22] The first case refers to multinuclear grids with some empty coordination places, such as in the case of polypyrazine ligands with five possible coordination centres (incomplete silver(I) 2x[2x5] grid (Ag_{20}(**5**)$_9$($OTf)_{20}$)), already mentioned in the introduction. (*Figure 3.6*) There, the separation was unintentional and subsequently hard to predict. Also the front-side/back-side out-of-plane placement of the separate grids is rather inconvenient for surface applications.

The second case concerns grid polymers linked via hydrogen or coordination bonds, an example already described being the hydrogen bond interconnected network of the grid from the bisterpyridine ligand (**11**). [14] (*Figure 3.9*)

The design of the grid of grids presented here was proposed by Stadler. The synthetic pathway is as simple and straightforward as possible (*Figure 3.31*). As a result, in a whole sequence there were only two chromatographic purification steps required (only one for **GR7E, F**), other products precipitating or crystallizing in sufficient purity for direct use.

The synthesis of **GR4** was described earlier as part of the synthesis of **GR6B** (*Figure 3.13*). The next step in our convergent synthetic path was the preparation of 1-methyl-1-phenylhydrazine (**GR3**), which involved addition of 2-bromopyridine into a large excess of methylhydrazine and subsequent heating of the mixture at reflux (95 °C) for 3 h. Extraction into $CHCl_3$ from aqueous $NaHCO_3$ provided **GR3** as a colourless oil in sufficient purity for further use in close to quantitative yield. All *N*-methylhydrazines must be stored in a freezer since they slowly decompose at room temperature, as marked by a colour change (colourless to dark red).

The last step in this synthetic branch was the formation of the monohydrazone (**GR6**). (*Figure 3.31*) Both components **GR3** and **GR4** were added in 1:1 ratio to ethanol and stirred

overnight at r.t. During this time, a yellow powder precipitated from the solution. This precipitate was **GR6B** and simple filtration led to isolation of some of this ligand in analytical purity. The supernatant solution was slowly evaporated under vacuum at 30 °C and chromatographed first on alumina in EtOAc/petrolether (1:5) and subsequently on silica EtOAc/petrolether (1:3). The chromatographic separation was not easy and sometimes needed to be repeated. The yield was rather low, usually in a range of 30-40 %.

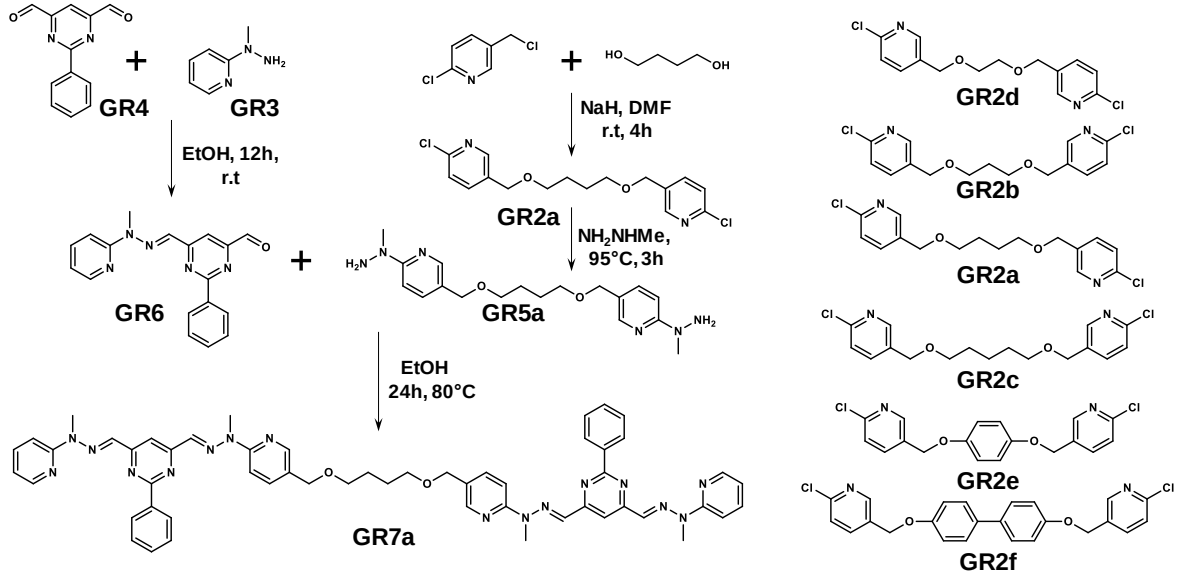

Figure 3.31: *Synthetic path for the **GR7** family of ligands for grid of grids. In the case **GR7(a, b, c, d, e, f)** instead of butan-1,4-diole an appropriate diole was taken.*

A second branch involved the synthesis of a bridging unit (**GR2x**). As parts of the bridging unit, simple diols such as 1,4-butanediol **(GR2a**), 1,5-pentanediol (**GR2b**), ethyleneglycol (**GR2c**), 1,3-propandiol (**GR2d**) and hydroquinone (**GR2e**) were used (*Figure 3.31*). The synthetic path started with standard nucleophilic substitution of commercially available 2-chloro-5-chloromethylpyridine with the appropriate diol in dry DMF in the presence of NaH at room temperature for 12 h. The yields of different bridging units were between 40-50 % for aliphatic groups (**GR2a-d**) and 30-40 % for phenyl and biphenyl units (**GR2e-f**). The phenyl units could be advantageously purified by simple repeated trituration in H_2O and MeOH. Subsequent transformation into hydrazines (**GR5x**) was carried out in the same way as for **GR3** with the difference that the crude products (aliphatic) were dissolved in CH_2Cl_2, solid K_2CO_3 was added, the suspension was stirred for few minutes and filtered. This protocol was repeated three times, before the organic phase was evaporated to give the product in sufficient purity to be used in the next step. Compounds **GR5E, F** are, however, insoluble in $CHCl_3$. These were suspended in saturated aqueous K_2CO_3 solution, filtered, dried in air and used as such in the next step. The analytically pure products can be in this case be obtained also by cooling down

the hydrazine solution, filtering the crystalline precipitate and washing it on the sinter with aqueous K_2CO_3 solution. This treatment reduced the yield from ~90 % to ~70 %, but provided superior purity.

The last step of whole synthesis was the formation of the final bridged ligand (**GR7x**). Both, **GR5 (**1 eq.) and **GR6** (1.1 eq. excess) components were mixed in ethanol and refluxed overnight. The ligand usually precipitated in a pure state from this solution. If not, an additional portion of **GR6** was added and the mixture was refluxed again. In general, the reaction proceeded well even in cases where the **GR5** components seemed insoluble in EtOH.

All metal complexes described below were made by mixing the appropriate ligand and metal cation in a 1:2 ratio in acetonitrile and heating overnight at 70 °C. It is important to mention that the efficiency of the complex formation is dependent on the exactitude of the ligand to metal ratio. Several metal cations were tested (Zn(II), Fe(II), Pb(II), Co(II)) but the only metal salt that provided readily interpreted results was $Zn(O_3SCF_3)_2$ ($Zn(OTf)_2$).

The addition of $Zn(OTf)_2$ resulted in assembly of the grid, as seen in the development of an orange colouration of the solution. The ^{1}H NMR spectrum the of the recrystallized **GR7aZn** showed characteristic peaks for the grid in the region between 5.5 and 6 ppm. (*Figure 3.32*) Again, these peaks belong to phenyl substituent on pyrimidine which is intercalated between ligands so that its rotation is blocked. Close inspection of the spectrum showed that most of the peaks were doubled. (*Figure 3.32*) This was expected as in the grid of grids assembly the inner and outer parts of the ligands experience different chemical surroundings. However, these observations proved to be misleading, because no other analytical method provided any proof of the grid of grids formation. (For the ^{1}H NMR comparison of **GR7xZn** grids see *Figure E2.1* in Experimental part)

As noted, formation of the complex was accompanied by the appearance of bright orange colour. The DOSY NMR spectra of the complexes with different alkyl-chain bridges (**GR7a**, **b**, **c**) suggested the presence of more than one species, supported by findings in their ESI-MS spectra. Unfortunately, none of the observed peaks could be attributed to the desired grid of grids ($[\mathbf{L_8M_{16}}]^{32+}$). Instead, peaks corresponding to smaller species of the constitution $\mathbf{L_4M_8^{16+}}$ and $\mathbf{L_2M_4^{8+}}$ were found. The longer the bridge, the more $\mathbf{L_2M_4^{8+}}$ that could be observed in the sample. In the case of **GR7c** (-$(CH_2)_5$- linker) $\mathbf{L_2M_4^{8+}}$ was found exclusively. This $\mathbf{L_2M_4^{8+}}$ grid, which also corresponds to a smaller species visible in the DOSY spectrum was later unequivocally established by an X-ray structure determination on a suitable crystal (vapour diffusion of diisopropyl ether into acetonitrile or nitromethane solution of the complex, R1 = 30.02 %). (*Figure 3.33*)

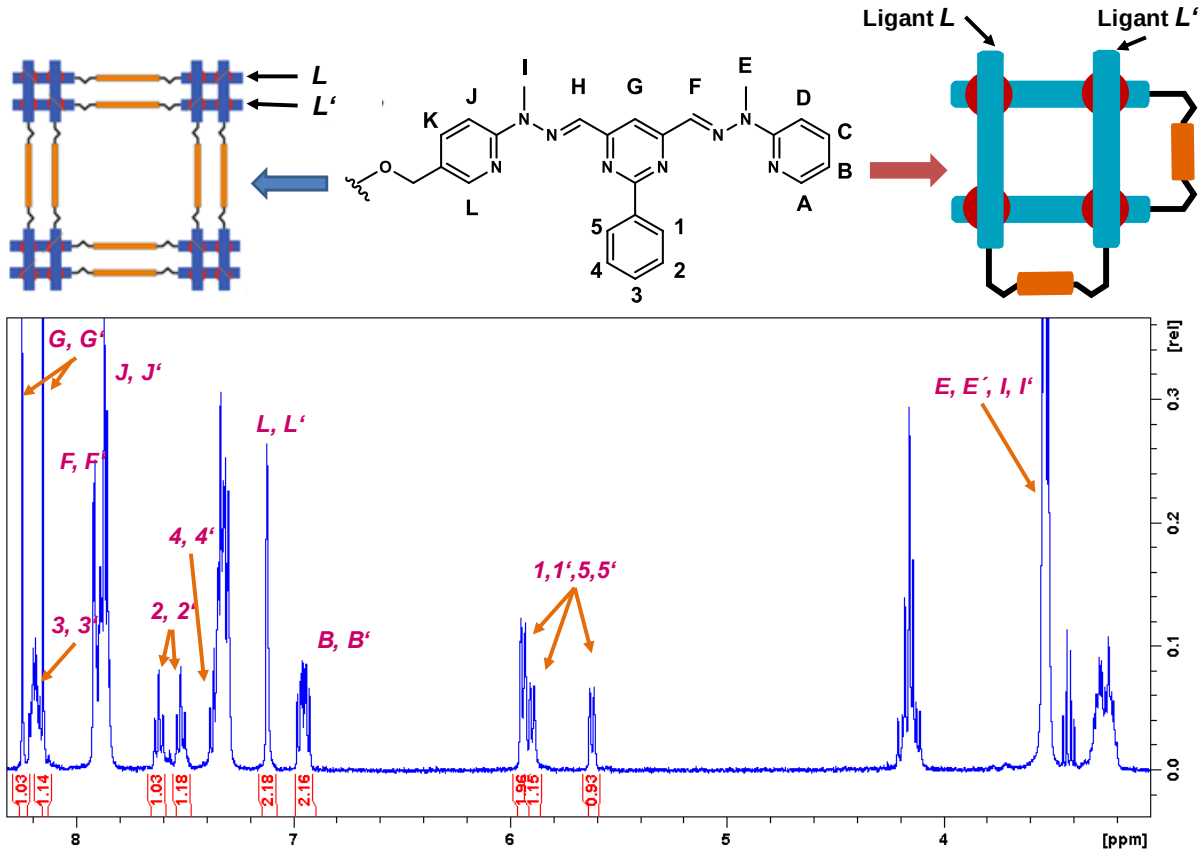

Figure 3.32: ***Bottom****: The assignment of* ^{1}*H NMR of recrystallized sample of* ***GR7aZn****. It is possible to identified grid assembly from characteristic peaks 1 and 5. It is also possible to observe two sets of signals of most of the protons.* ***Top****: Two possible structures which could provide the* ^{1}*H NMR spectrum with doubling of the signals due to inequality of the ligands. The recrystallized sample was used due to its better resolution, the spectra of the complex after assembly are identical.*

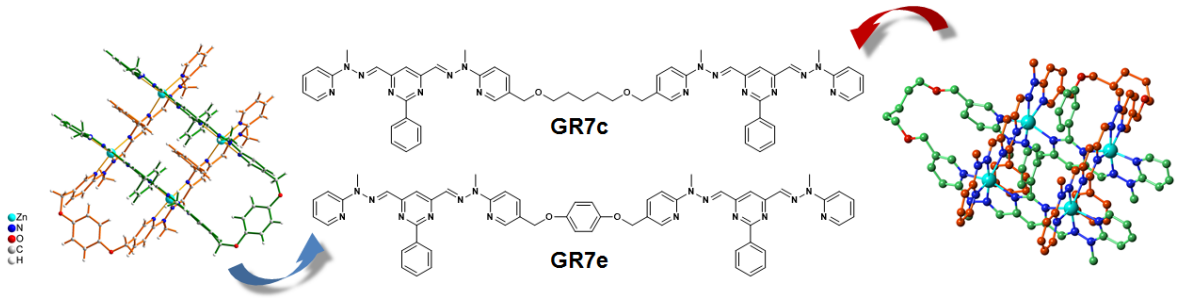

Figure 3.33: *The folded nature of the Zn(II) grids formed from ligands* ***GR7c*** *and* ***GR7e*** *and their respective crystal structures.*

The crystal structure revealed that the grid consists from two molecules of the ligand which are bent around the -O-CH_2- joint of their linker. Unfortunately, attempts to obtain higher assemblies found in DOSY and ESI-MS failed.

Similar results were obtained with the **GR7e** ligand. (For its ^{1}H NMR see *Figure E2.2* in Exp. p.) This ligand has phenyl ring which was introduced in order to hinder the folding. However, this ligand can still bend into an $\mathbf{L_2M_4}$ complex as was again proved by an X-ray

structure determination. (v.d. of diisopropylether into $MeNO_2$, R1 = 13.21 %). To make folding even harder, the ligand **GR7f** with the 4,4'-biphenol bridging unit was prepared. In contrast to all previous ligands, the ^{1}H NMR spectrum of its Zn(II) complex is very broad and ESI-MS showed just the presence of two undesired $\mathbf{LM^{2+}}$ and $\mathbf{L_2M_2^{4+}}$ species.

To promote assembly with a biphenyl-containing ligand, the more flexible and more soluble ligand **GR17** was designed and synthesized. (*Figure 3.34*) Unfortunately, not even this ligand formed any defined complex. Its ^{1}H NMR spectrum after addition of Zn(II) was again broad. Although the biphenyl unit is apparently large enough to thwart formation of folded complexing moieties, at the same time the ligand also lost its ability to form a defined assembly.

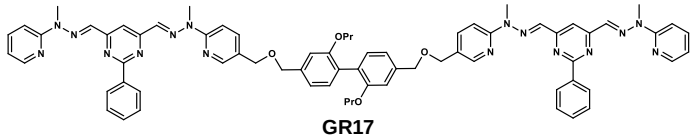

GR17

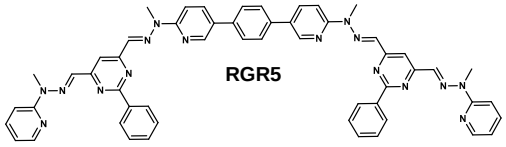

RGR5

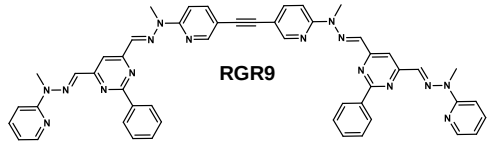

RGR9

Figure 3.34: *The second generation of the ligands intended for the formation of the grid of grids assembly.* ***GR17*** *is more flexible and more soluble than similar* ***GR7F****. In contrast to that, the ligands* ***RGR5*** *and* ***RGR9*** *have a more rigid backbone. Unfortunately, neither one provides a defined grid complex.*

In another attempt to prevent folding into a [2x2] grid, two ligands **RGR5** (phenyl bridge) and **RGR9** (acetylene bridge) with non-flexible rigid bridges were synthesized. (*Figure 3.34*) Unfortunately, both ligands were very insoluble, and moreover the broad proton NMR spectra in the presence of Zn(II) indicated that desired complexes did not form efficiently.

After these results, we decided to change our strategy once again. The formation of grid of grids with covalently bridged ligands proved to be above our capability but there is more than one way to connect units in chemistry. Our next strategy was directed at using dynamic covalent bonds. The ligands which gave folded grids had termini open to further functionalization. Thus, it was considered that four units could organize and interconnect to form a square structure which would closely resemble to our initially desired grid of grids. (*Figure 3.35*) With this twist

we came back to the principles outlined in the previous chapter and our efforts to obtain ligands bearing either aldehyde or amine groups. The challenge here is complicated by the need to prepare monohydrazones from either from **GR4** (similar to **GR6**) or **GR4B**.

A lot of effort was devoted to preparing monohydrazones based on **GR4**, but in all attempts we failed to isolate the desired product in sufficient purity. A breakthrough came only recently

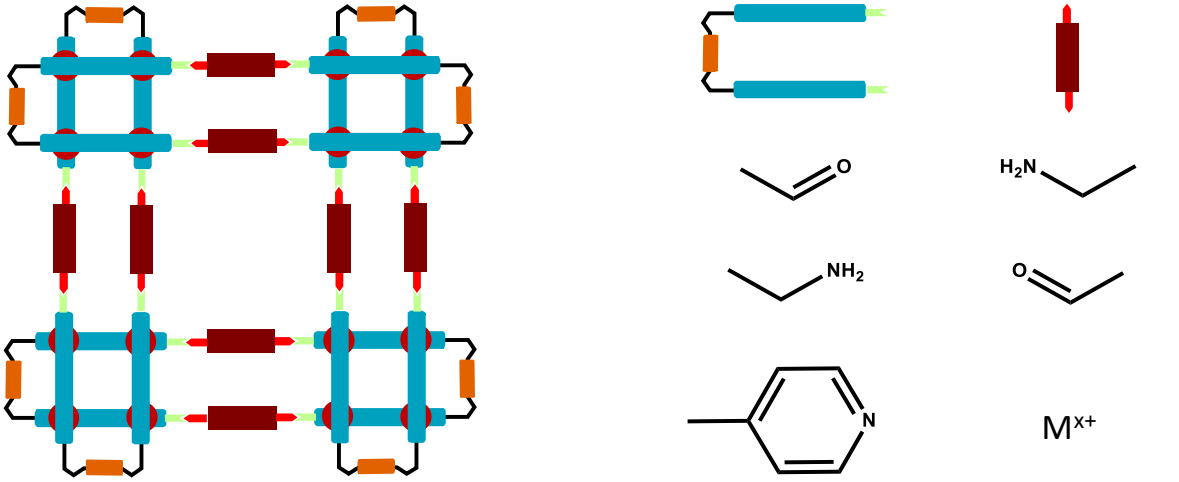

Figure 3.35: *The structure of the grid of grids assembled from above prepared folded grids and set of possible dynamic connections which could interconnect individual units.*

with our turn to derivatives of **GR4B.** Parallel to the synthesis of the ligand **GR65** (intermediate for **GR67**, *Figure 3.21*), the preparation of its half ligand (**GR65B**, with one free hydrazine, *Figure 3.36*) was carried out. In this case, a tedious purification was overcome thanks to the use of reverse-phase chromatography which is a very useful technique for purification of compounds bearing highly polar groups. Next, the monohydrazine **GR65B** was condensed with dialdehyde **HEL9** which was prepared for different project and will be introduced later. Even though the ethylene bridge is rather short and the coordination moieties are in an inconvenient orientation, based on ^{1}H NMR spectroscopy complemented by ESI-MS it was possible to establish the formation of the folded grid complex **GR70Zn**. (*Figure 3.36*)

Similar procedures were adopted with ligands **GR65**, **GR66**, **GR67**. The products were all rather insoluble in all organic solvents but dissolved in acetonitrile in the presence of Zn(II) providing surprisingly clean folded [2x2] grids **GR71Zn** and **GR72Zn**. (*Figure 3.36*, ^{1}H NMR comparison in *Figure E.2.6-E2.7*)

The previous case taught us the importance of the right orientation of the complexing moieties and the length of the linker for the success of assembly and crystallization. Therefore, another ligand with an odd number of atoms from a 1,5-dibromopentane bridge was prepared by the same procedure. (*Figure 3.37*)

The condensation of **GR65B** with dialdehyde **HEL9b** (*Figure 3.37*) gave ligand **GR70B**. This time it was possible to successfully prepare the crystals of its Zn(II) complex (**GR70BZn,** *Figure E2.8*) by vapour diffusion of diethyl ether into its acetonitrile solution but at the time of writing the results are not known yet. Subsequently, the acetyl was deprotected with KOH in ethanol/water mixture under reflux for 48 h to give the alcohol. The last step was a Dess-Martin oxidation which successfully led to the preparation of dialdehyde ligand **GR72B**. In the ^{1}H

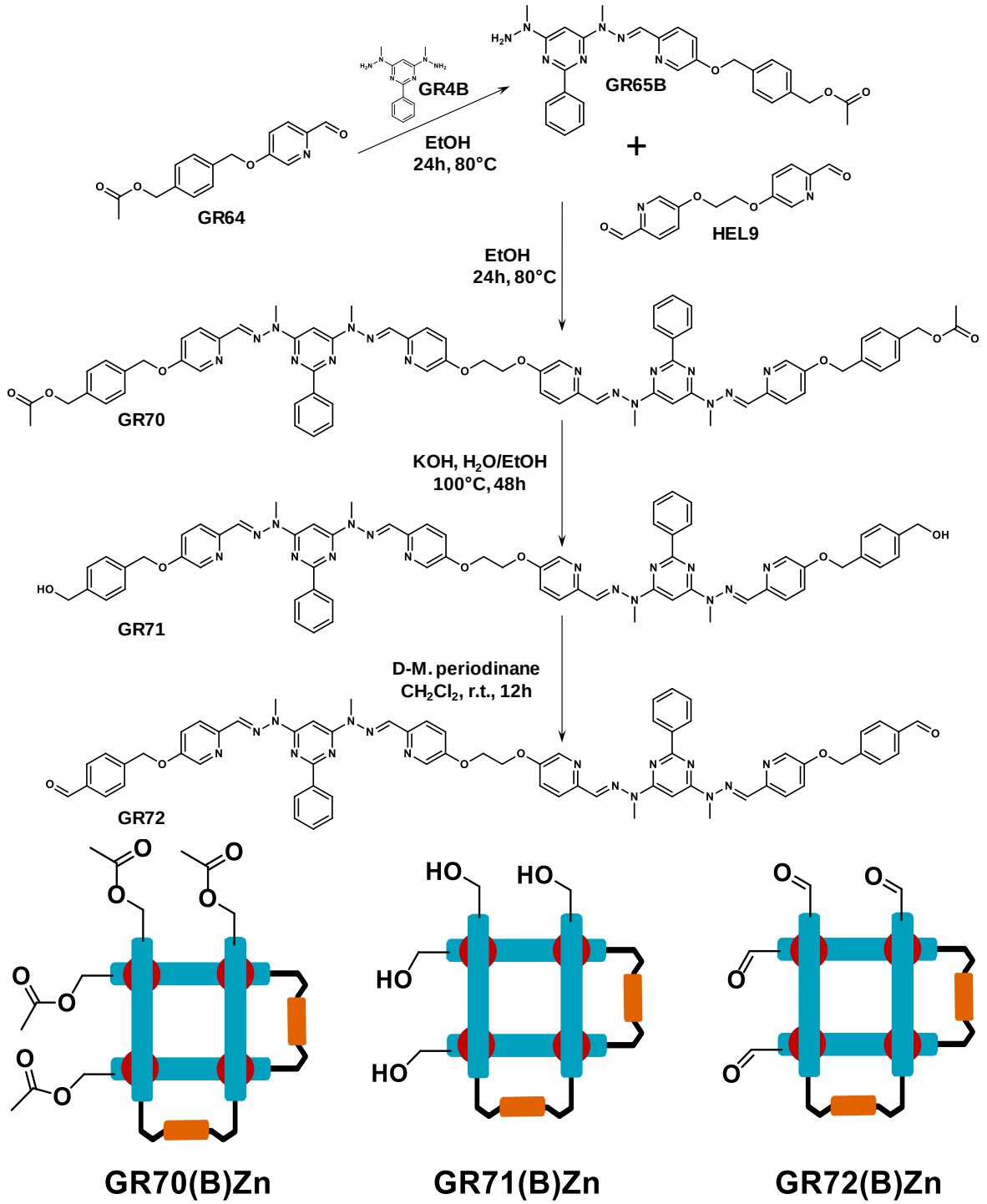

Figure 3.36: *The final sequence of the synthesis of ligand **GR72**. It was envisaged that this ligand should formed the folded grid with four aldehydes pointing from two neighbouring sides and therefore should be able to form grid of grids via dynamic imine connections.*

NMR spectrum of its Zn(II) complex (**GR72BZn**) it was again possible to distinguish signals of two different ligands. (*Figure 3.37* and *Figure E2.9*) The frozen rotation of phenyl rings provided again a characteristic and well defined signal of grid formation. Finally, the formation of a folded [2x2] grid of $[Zn_4(\mathbf{GR72B})_4]^{8+}$ formula was proved by ESI-MS. This grid has two

sides connected via an alkyl bridge in the same way as **GR7CZn** but this grid also has four aldehyde units pointing out from orthogonal sides of the square structure. Attempts to crystallize this complex as well as attempts to decorate the aldehydes are currently in progress. This effort should then result in the dynamic assembly of the grid of grids.

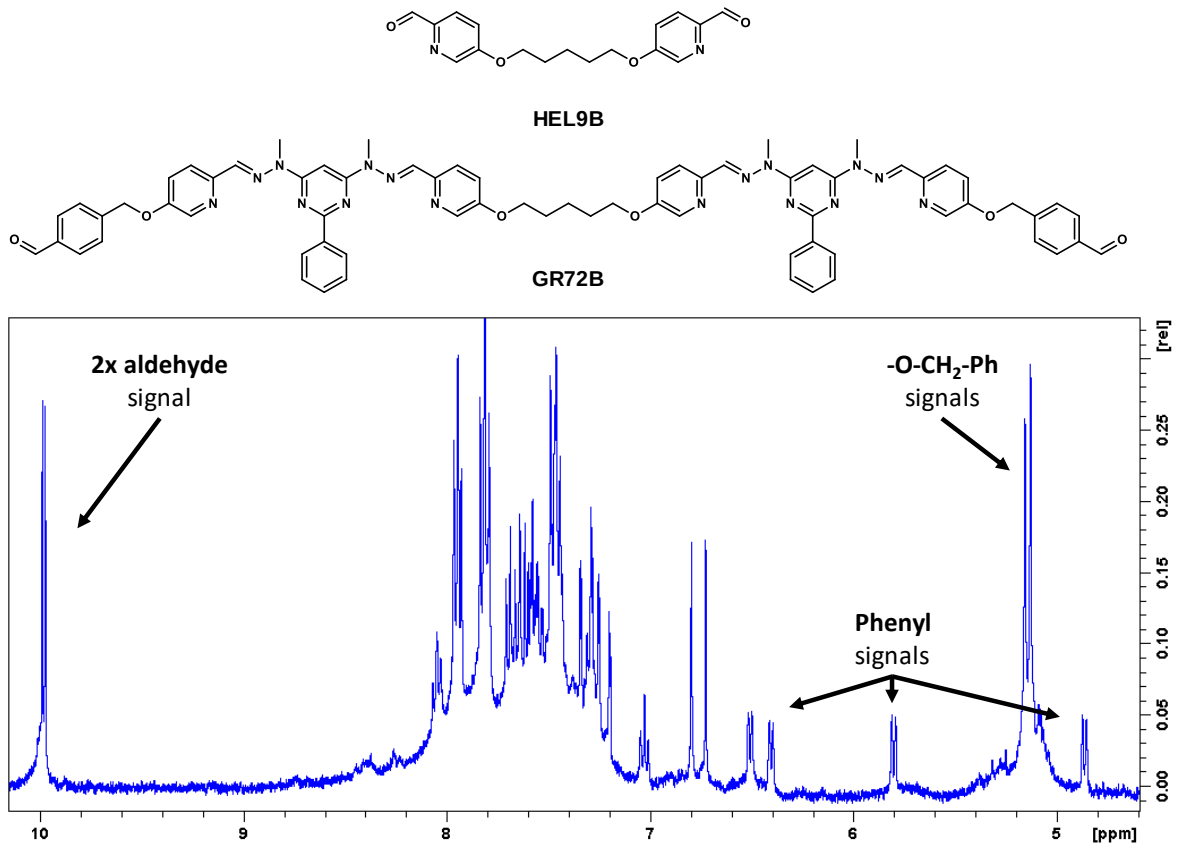

Figure 3.37: *The structure of new ligand **GR72B** which provides the folded [2x2] grid [Zn4(**GR72B**)2](OTf)8. Below is the ^{1}H NMR of this grid (**GR72BZn**), the grid assembly is proved by characteristic split of phenyl protons and by the presence of different inner and outer ligands which is proved by the two signals of aldehyde.*

3.3 Conclusion

Even though our goal to assemble large array of grids was not reached it was still possible to obtain several interesting derivatives of bishydrazone-based grids.

The grid **GR67Zn** with its eight aldehyde units is an ideal candidate for dynamic interconnection with various amines. This interconnection could result in a 2D array in the case of diamines, or in novel and functional derivatives. The grid is also an ideal candidate for application in studies of multivalent receptors similar to the saccharide-decorated acylhydrazide grid described in the introduction.[51] (*Figure 3.12*)

In our attempt to prepare grid of grids assembly we accidentally obtained several folded grids of general formula $[\mathbf{L_2Zn_4}]^{8+}$ the structures of which were determined by single crystal X-ray diffraction (**GR7cZn**, **GR7eZn**, *Figure 3.33*). After much effort we also successfully prepared aldehyde-decorated folded grids **GR72Zn** and **GR72BZn**, which could be further used to assemble our desired grid of grids in a dynamic fashion.

In adding to the previously limited studies of luminescrnce of Zn(II) grids, we obtained an interestingly high quantum yield (60 %, **GR62Zn**) with ligands of relatively simple preparation. Special note should be given to the fact that the simplest derivative performed the best. Finally, the grids which were built on 4,6-bis(1-methylhydrazino)-2-phenylpyrimidine (**GR4B**) had substantially more intense emission than those from the ligand which was built on 2-phenyl-4,6-pyrimidinedicarboxaldehyde (**GR4**).

The synthetic achievements of this part have the potential to lead to preparation of functionalized grids or even more interesting higher supramolecular assemblies. Research along these lines is still in progress.

3.4 References

1. Ruben, M.; Rojo, J.; Romero-Salguero, F. J.; Uppadine, L. H.; Lehn, J.-M. *Angewandte Chemie: Intermational Edition* **2004,** *43,* 3644-3662.
2. Service, R. F. *Science* **2003,** *302,* 556-559.
3. Pulizzi, F. *Nat. Mater.* **2012,** *11,* 367.
4. Lent, C. S.; Tougaw, P. D. *Proc. IEEE* **1997,** *85,* 541.
5. Hardy, J. G. *Chem. Soc. Rev.* **2013,** *42,* 7881-7899.
6. Dey, S. K.; Thompson, L. K.; Dawe, L. N. *Chem. Commun* **2006,** 4967-4967.
7. Baxter, P.; Lehn, J.-M.; Kneisel, B. O.; Fenske, D. *Angew. Chem. Int. Ed.* **1997,** *36,* 1978-1981.
8. Madalan, A. M.; Cao, X. Y.; Rogez, G.; Lehn, J.-M. *Inorganic Chemistry* **2014,** *53,* 4275-4277.
9. Osorio, E. A.; Ruben, M.; Seldenthuis, J. S.; Lehn, J.-M.; van der Zant, H. S. *Small* **2010,** *6,* 174-178.
10. Manzano, B. R.; Jalón, F. A.; Ortiz, I. M.; Soriano, L. M.; Goméz de la Torre, F.; Elguero, J.; Maestro, M. A.; Mereiter, K.; Claridge, T. D. W. *Inorg. Chem.* **2008,** *47,* 413-428.
11. Tielman, P.; Marchal, A.; Lehn, J.-M. *Tetrahedron Letters* **2005,** *46,* 6349-6353.
12. Breuning, E.; Hanan, G. S.; Romero-Salguero, F. J.; Garcia, A. M.; Baxter, P. N. W.; Lehn, J.-M.; Wegelius, E.; Rissanen, K.; Nierengarten, H.; van Dorsselaer, A. *Chem. Eur. J.* **2002,** 3458-3466.
13. Semenov, A.; Spatz, J. P.; Moller, M.; Lehn, J.-M.; Sell, B.; Schubert, D.; Weidl, C. H.; Schubert, U. S. *Angew. Chem. Int. Ed.* **1999,** *38,* 2547-2550.
14. Breuning, E.; Ziener, U.; Lehn, J.-M.; Wegelius, E.; Rissanen, K. *Eur. J. Inorg. Chem* **2001,** 1515-1521.
15. Youinou, M.-T.; Rahmouni, N.; Fischer, J.; Osborn, J. A. *Angew. Chem. Int. Ed. Engl.* **1992,** *31*, 733-735.
16. Baxter, P. N. W.; Lehn, J.-M.; Fischer, J.; Youinou, M.-T. *Angew. Chem. Int. Ed. Engl.* **1994,** *33,* 2284.
17. Hanan, G. S.; Volkmer, D.; Schubert, U. S.; Lehn, J.-M.; Baum, G.; Fenske, D. *Angew. Chem. Int. Ed. Engl.* **1997,** *36,* 1843-1844.
18. Ruben, M.; Lehn, J.-M.; Vaughan , G. *Chem. Comm.* **2003,** 1338-1339.
19. Zhao, L.; Zhiqiang, X.; Thompson, L. K.; Heath, S. L.; Miller, D. O.; Ohba, M. *Angew. Chem. Int. Ed.* **2000,** *39,* 3114-3117.
20. Dawe, L. N.; Shuvaev, K. V.; Thompson, L. K. *Chem. Soc. Rev.* **2009,** *38,* 2334-2359.
21. Barboiu , M.; Stadler, A.-M.; Lehn, J.-M. *Angew. Chem. Int. Ed.* **2016,** *55,* 2-27.
22. Stadler, A.-M. *Eur. J. Inorg. Chem* **2009,** 4751-4770.
23. Cao, X.-Y.; Harrowfield, J.; Nitschke, J.; Ramírez, J.; Stadler, A.-M.; Kyritsakas-Gruber, N.; Madalan, A.; Rissanen, K.; Russo, L.; Vaughan, G.; Lehn, J.-M. *Eur. J. Inorg. Chem.* **2007,** 2944-2965.
24. Nitschke, J. R.; Lehn, J.-M. *PNAS* **2003,** *100,* 11970-11974.
25. Baxter, P. ; Lehn, J.-M.; Baum, G.; Fenske, D. *Chem. Eur. J* **2000,** *6*, 4510-4517.
26. Bao, X.; Liu, W.; Mao, L.-L.; Jiang, S.-D.; Liu, J.-L.; Chen, Y.-C.; Tong, M.-L. *Inorg. Chem.* **2013,** *52,* 6233-5235.
27. Han, Y.; Chilton, N. F.; Li, M.; Huang, C.; Xu, H.; Hou, H.; Moubaraki, B.; Langley, S. K.; Batten, S. R.; Fan, Y.; Murray, K. S. *Chem. Eur. J.* **2013,** *19,* 6321-6328.
28. Giri, C.; Topić, F.; Cametti, M.; Rissanen, K. *Chem. Sci.* **2015,** *6,* 5712-5718.

29. Karan, S.; Hamann, C.; Tang, H.; Stefankiewicz, A. R.; Lehn, J.-M.; Berndt, R. *Chem. Phys. Chem.* **2015,** *16,* 1370-1373.
30. Stefankiewicz, A. R.; Harrowfield, J.; Madalan, A.; Rissanen, K.; Sobolev, A. N.; Lehn, J.-M. *Dalton. Trans.* **2011,** *40,* 1320-1332.
31. Stadler, A.-M.; Burg, C.; Ramírez, J.; Lehn, J.-M. *Chem. Commun.* **2013,** *49,* 5733-5735.
32. Bassani, D. M.; Lehn, J.-M.; Fromm, K. M.; Fenske, D. *Angew. Chem. Int. Ed.* **1998,** *37,* 2364-2367.
33. Breuning, E.; Ruben, M.; Lehn, J.-M.; Renz, F.; Garcia, Y.; Ksenofontov, V.; Gutlich, P.; Wegelius, E.; Rissanen, K. *Angew. Chem. Int. Ed.* **2000,** *39,* 2504-2507.
34. Ruben, M.; Ziener, U.; Lehn, J.-M.; Ksenofontov, V.; Gutlich, P.; Vaughan, G. B. M. *Chem. Eur. J.* **2005,** *11,* 94-100.
35. Dey, S. K.; Abedin, T. S. M.; Dawe, L. N.; Tandon, S. S.; Collins, J. L.; Thompson, L. K.; Postnikov, A. V.; Alam, M. S.; Muller, P. *Inorg. Chem.* **2007,** *46,* 7767-7781.
36. Schmittel, M.; Kalsani, V.; Fenske, D.; Wiegrefe, A. *Chemm. Commun.* **2004,** 490-491.
37. Onions, S. T.; Frankin, A. M.; Horton, P. N.; Hursthouse, M. B.; Matthews, C. J. *Chem. Comm.* **2003,** 2864-2865.
38. Schubert, U. S.; Lehn, J.-M.; Hassman, J.; Hahn, C. Y.; Hallschmid, N.; Muller, P. In *Functional Polymers;* ACS Symposium Series; American Chemical Society: Washington, 1998; pp 248-260.
39. Semenov, A.; Spatz, J. P.; Lehn, J.-M.; Weidl, C. H.; Schubert, U. S.; Moller, M. *Applied Surface Science* **1999,** *144/145,* 456-460.
40. Ziener, U.; Lehn, J.-M.; Mourran, A.; Moller, M. *Chem. Eur. J* **2002,** *8,* 951-957.
41. Ziener, U. Self-Assembled Nanostructures of Oligopyridine Molecules. *J. Phys. Chem. B* **2008,** *112,* 14698-14717.
42. Rabe, J. P.; Buchholtz, S. *Science* **1991,** *253,* 424-427.
43. Mourran, A.; Ziener, U.; Moller, M.; Breuning, E.; Ohkita, M.; Lehn, J.-M. *Eur. J. Inorg. Chem.* **2005,** 2641-2647.
44. Pace, G.; Stefankiewicz, A.; Harrowfield, J.; Lehn, J.-M.; Samori, P. *Chem. Phys. Chem* **2009,** *699-705,* 10.
45. Wang, Y.-T.; Li, S.-T.; Wu, S.-Q.; Cui, A.-L.; Shen, D.-Z.; Kou, H.-Z. *J. Am. Chem. Soc.* **2013,** *135,* 5942-5945.
46. Patroniak, V.; Baxter, P. N. W.; Lehn, J.-M.; Kubicki, M.; Nissinen, M.; Rissanen, K. *Eur. J. Inorg. Chem.* **2003,** 4001.
47. Schmitt, J.-L.; Lehn, J.-M. *Helvetica Chimica Acta* **2003,** *86,* 3417-3426.
48. Schmitt, J.-L.; Stadler, A.-M.; Kyrytsakas, N.; Lehn, J.-M. *Helvetica Chimica Acta* **2003,** *86,* 1598-1624.
49. Cao, X.-Y. *PhD thesis;*, 2009.
50. Hardy, J. G.; Cao, X.-Y.; Harrowfield, J.; Lehn, J.-M. *New. J. Chem.* **2012,** *36,* 668-673.
51. Chmielewski, M. J.; Buhler, E.; Candau, J.; Lehn, J.-M. *Chem. Eur. J.* **2014,** *20,* 6960-6977.
52. Guiseppone, N.; Schmitt, J.-L.; Lehn, J.-M. *Angew.Chem.Int.Ed.* **2004,** 4902-4906.
53. Stadler, A.-M.; Kyritsakas, N.; Graff, R.; Lehn, J.-M. *Chem. Eur. J.* **2006,** *12,* 4503-4522.
54. Rojo, J.; Romero-Salguero, J.; Lehn, J.-M.; Baum, G.; Fenske, D. *Eur. J. Inorg. Chem.* **1999,** 1421-1428.
55. Barboiu, M.; Ruben, M.; Blasen, G.; Kyritsakas, N.; Chacko, E.; Dutta, M.; Radekovich, O.; Lenton, K.; Brook, D. J. R.; Lehn, J.-M. *Eur. J. Inorg. Chem.* **2006,** 784-792.
56. Ryan, D. E.; Snape, F.; Winpe, M. *Analytica Chimica Acta* **1972,** *58,* 101-106.
57. Liang, L. J.; Zhao, X. J.; Huang, C. Z. *Analyst* **2012,** *137,* 953-958.

58. Dobrawa, R.; Lysetska, M.; Ballestar, P.; Grune, M.; Wurthner, F. *Macromolecules* **2005,** *38,* 1315-1325.
59. Das, K.; Jana, A.; Konar, S.; Chatterjee, S.; Mondal, T. K.; Barik, A. K.; Kar, S. K. *Journal of Molecular Structure* **2013,** *1048,* 98-107.
60. Konar, S.; Jana, A.; Das, K.; Ray, S.; Chatterjee, S.; Golen, J. A.; Rheingold, A. L.; Kar, S. K. *Polyhedron* **2011,** *30,* 2801-2808.
61. Stefankiewicz, A. R.; Rogez, G.; Harrowfield, J.; Drillon, M.; Lehn, J.-M. *Dalton Trans.* **2009,** 5787-5802.
62. Davis, K. M. C. *Nature* **1969,** *223,* 725.
63. Tran-Thi, T.-H.; Prayer, C.; Millié, P.; Uznanski, P.; Hynes, J. T. *J. Phys. Chem. A.* **2002,** *106,* 2244-2255.

4
Dynamic helicates

4.1 Introduction

In our universe helical geometry can be found in formations as big as galaxies, in living creatures around us, such as on the shells of snails, or even on a molecular level in our body in DNA or α-Amylose.[1] Helical geometry has also fascinated mankind since ancient times due to its appealing aesthetics. The helix as a geometric motif has always been in the centre of human art and architecture. Lines and structures which wrap around a central axis have been used as a decoration since ancient times: pictures of the ancient god Ningishidzu, a god associated with healing, fertility and the afterlife who was depicted as two serpents entwined around an axis, have been dated to as far back as 2000 B. C. (*Figure 4.1*). The helical motif later inspired Greeks to represent Hermes (Mercury), the messenger of gods, in the form of a herald's staff (*Caduceus*).[2] In Greek mythology, Hermes was a guide for dead souls to the afterlife, but he was also a protector of merchants. Therefore, in modern times Caduceus is found mostly in places connected with commerce. Caduceus is sometimes confused with the rod of Asclepios, the Greek god of healing and medicine, which has only one serpent wrapped about the stick (*Figure 4.1*). It is believed that the snake was originally a worm causing dracunculiasis (Guinea worm disease), a disease treated by slowly pulling the worm out of the wound and winding it on a stick.[3,4]

There are many geometric and entangled shapes which have attracted people's imagination. Another example of entities which crossed the boundaries between aesthetics, symbolism and chemistry are "*knots*" and "*links*".[5,6,7] In general, a knot is an entangled strand that cannot be untangled to one loop without cutting the strand. A link consists of several entangled loops which again cannot be separated without cutting them. An example of a link is the *Borromean rings*, three interlocked rings which can be found on the coat of arms of one of the most prominent Italian aristocratic families, (*Figure 4.1*) and which besides representing the unity of Borromean family, were also used to represent inseparability of the holy trinity.[8] *King*

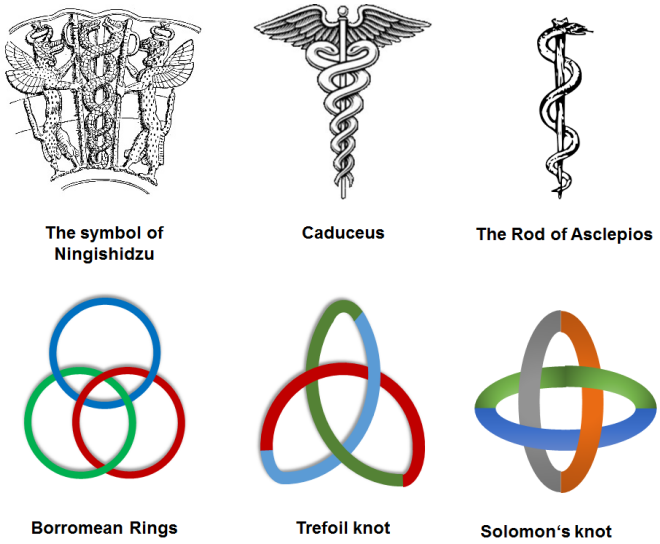

Figure 4.1: *Illustration of shapes, links and knots which have symbolic meaning and which have connections with helixes and helicates.*

Solomon's knot was widely used as a decorative motif across all ancient Mediterranean cultures (*Figure 4.1*). It was also used as a symbol of knowledge and wisdom, in some African societies it even symbolized the royal status and served as a reminder of the power of pagan gods.[9] In order to be precise, it is necessary to note that *Solomon's knot* is not a knot in terms of the mathematical definition, but it is just a link.[5] An example of a true knot is the so-called "*Trefoil knot*" which is indeed formed by three-times-interwoven loops (*Figure 4.1*). As a symbol, the *Trefoil knot* was attributed to Odin. Celts used it as a decorative ornament which was later taken by Christians as a symbol for the Holy Trinity.

Some of these motifs can be found in nature even at the molecular level (e.g. the protein Trefoil fold[10]) although such examples are scarce. Over the past decades, chemists have worked hard to mimic these aesthetic motifs. Several cases of successful synthesis have been reported, including in particular the use of coordination complexes for the formation of helicates and circular helicates.[8,11,12,13,14]

Before describing individual cases it is necessary to explain the term *helicate*. This word was introduced by Lehn in 1987 in order to distinguish between molecules where the helicity is intrinsic (DNA, proteins) and molecules where the helicity is a result of the interactions between a ligand and a metal cation.[15] The word is derived from the Greek *helix* with a suffix *-ate* which implies the host-guest nature of the assembly in the same manner as does the term *cryptate* (macrocyclic host with encapsulated guest).[16] The term helicate is now used to describe coordination complexes containing two or more metal cations complexed and connected by one or more covalent ligands.[17,18,19,20,21,22]

Nevertheless, the history of helical complexes started long before the term helicate was known. In 1937, Morgan and Burstall prepared coordination complexes of various polypyridines with Ag(I).[23] Chemists at that time had very limited analytical tools and depended largely on studies of chemical reactivity and elemental analyses. While studying the complex of Ag(I) and quarterpyridine (**H1**) they noticed an unusual resistance of the complex towards oxidation which they attributed to the helical orientation of the ligand and its shielding of Ag(I) (*Figure 4.2*). However, their proposed structure was composed of a single ligand wrapped around one metal (**H3**). Later, this structure was questioned by other scientists but the answer came only in 1992, when Constable prepared a similar complex of quarterpyridine (**H1**) with $Ag(BF_4)$. The X-ray structure determination of a single crystal proved that the structure is double helicate (**H2**) (*Figure 4.2*).[23,24,25,26]

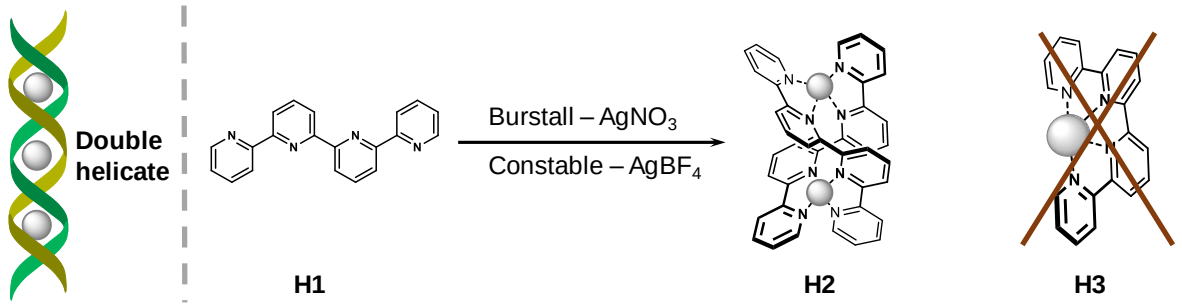

Figure 4.2: ***Left****: Illustration of (Three-centred) double helicate.* ***Right****: Burstall and Constable double helicate (**H2**) and depiction of originally proposed structure (**H3**).*

The first triple helicate was probably prepared by Stratton and Busch in late 1950s, although they were not yet aware of the helicity in their binuclear triplestranded complex ($[M_2(\mathbf{H4})_3]^{2+}$).[27] Along the line of Busch's research on imine based organometallic complexes[28], he prepared pyridinaldazine ligand (**H4**, *Figure 4.3*), an imine analogue to Osborne's pyridazine ligand[29,30] mentioned in chapter 3 of this thesis. (*Figure 3.2.*) Pyridinaldazine ligand, however, can freely rotate around the N-N single bond.[31] This flexibility, together with octahedral metal cations (Co(II), Fe(II), Ni(II)), leads to the triple helical structure in contrast to the perpendicular arrangement of the Osborne's grid complex. Busch and Stratton also noticed that their binuclear triple stranded complex ($[M_2(\mathbf{H4})_3]^{2+}$) was only a kinetic product and that over a certain period of time (with or without heating) it transformed into a monomolecular complex where two ligands coordinate one metal centre.[27] The triple helicate was later proved by the single crystal X-ray structure determination of the structurally very similar pyridylmethylketazine ligand (**H5**)[30,32] (*Figure 4.3*). The number of reported examples of double and triple helicates quickly increased and there is a large number of ligands suitable to the formation of different types of helicates. [4,17,18,19,20,21,22,33]

The plasmid DNA of some bacteria and eukaryotes can have the shape of a circular double helix.[34] In the same way, there are examples in the literature of circular coordination structures with helical arrangement of ligand strands. These circular helicates recently attracted

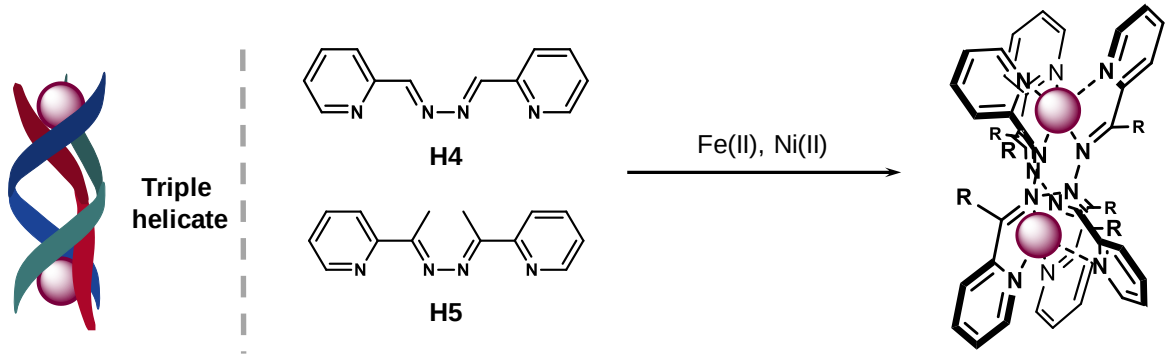

Figure 4.3: ***Left****: Illustration of (Binuclear) triple helicate.* ***Middle:*** *pyridinaldazine ligand (**H4**) and pyridylmethylketazine ligand (**H5**) triple helicate.* ***Right****: the triple helical nature of the complex with Co(II) was confirm by X-ray determination.*[32]

a lot of attention for the interconnection of the individual ligands, giving access to topologically interesting structures (*Borromean rings*[35], *Trefoil knot*[11], *Solomon knot*[8], *Pentafoil knot*[12,13]).

Arguably one of the most complicated structures obtained so far is Leigh's *Pentafoil knot*[12,13], known as "*Solomon's seal*". The design was based on Lehn's assembly of pentameric bipyridine-based circular helicate.[36] Lehn's ligand (**H6**) was originally designed to produce a triple helicate with three coordination centres using Ni(II) metal ions.[37] However, under very vigorous conditions (170 °C in ethylengylcol) when mixed with $FeCl_2$ the ligand did not provide a single triple helicate structure, instead it assembled into a circular double helicate containing five Fe(II) metal ions and five ligands (**H7**) (*Figure 3.4*). The crystal structure showed the

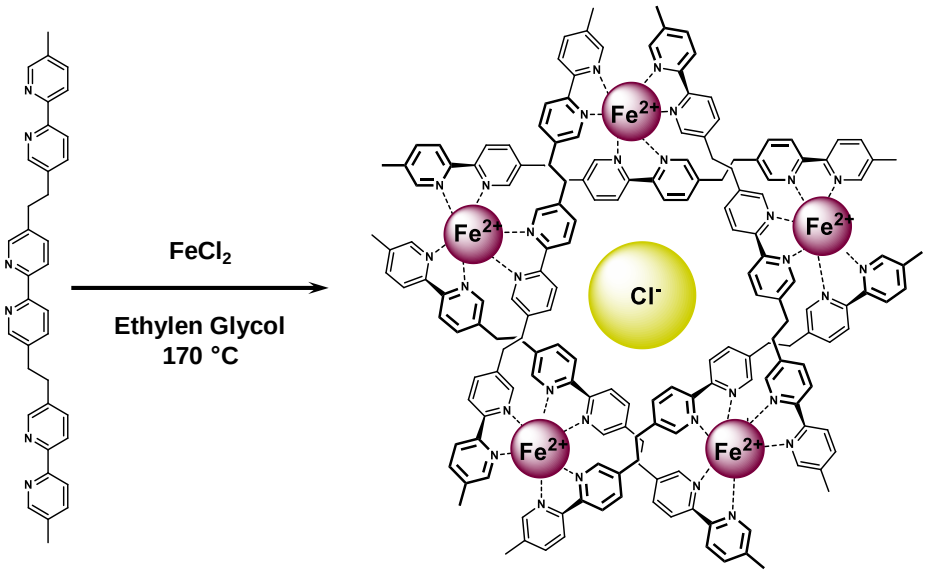

H6 **H7**

Figure 4.4: *Lehn's pentameric circular helicate*

presence of a cavity in the middle of the ring which appears to a crucial role during the assembly. The formation of **H7** was found to be dependent on the ability of the Fe(II) counteranion to fit in this cavity, with Cl^- being the anion found to be the best templating counterion to form the pentameric structure.[19,38] (*Figure 4.4*)

Leigh used an analogous half-dynamic ligand prepared by connecting the central bipyridine unit with two 2-pyridinecarboxaldehydes (**H8**) to form his *Pentafoil knot*. Heating ligand **H8** in DMSO (60 °C) with $FeCl_2$ and the diamine 2-(2-aminoethoxy)ethylamine provided the interconnected pentameric circular helicate (**H9**) in excellent yield (>98 %).[12] Following the ligands along their interconnections, one can "travel" through the structure back to the initial point, hence showing the whole structure is in fact one inseparable strand (*Figure 4.5*).[12,13,39]

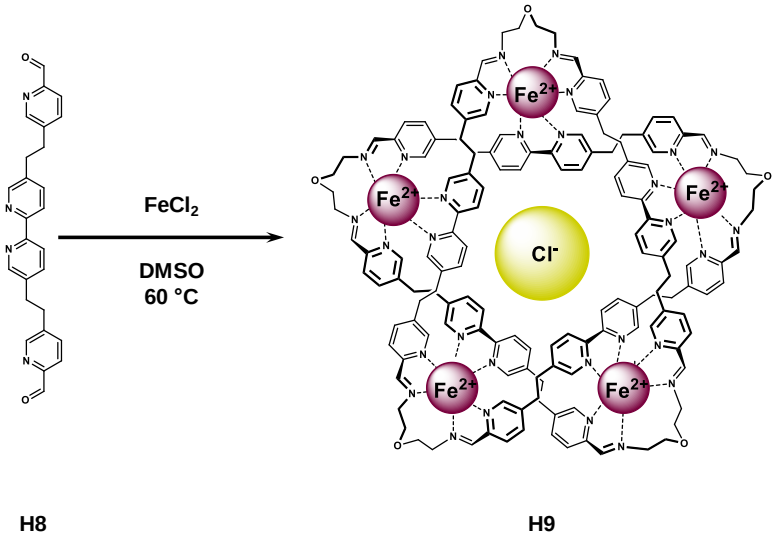

Figure 4.5: *Leigh's Pentafoil knot (**H9**).*

The introduction of an additional oxygen atom between the bipyridine and pyridine aldehyde units (giving $-CH_2-O-CH_2-$ links) gives the ligand (**H10**) more flexibility. (*Figure 4.6*) This ligand can now support more strained structures such as a four-stranded circular helicate. Use of the same reaction conditions as applied for the pentafoil knot resulted in the formation of the Solomon knot (**H11**). In this case though the choice of amine is critical, as different amines were observed to provide formation of either a circular helicate or a simple triple helicate.[40]

Results presented in this chapter were obtained whilst working towards the synthesis of dynamic helicates. Initially, we investigated dependence of the helical assembly on the directionality of hydrazone/imine bond. Later, in order to study supramolecular programming[17] and to extend a previously reported study on trinuclear helices[41] the work focused on the assembly of dynamic trinuclear helicates with different coordination motifs. As a result, several types of helicates were obtained, including double helicates, triple helicates and circular

helicates.

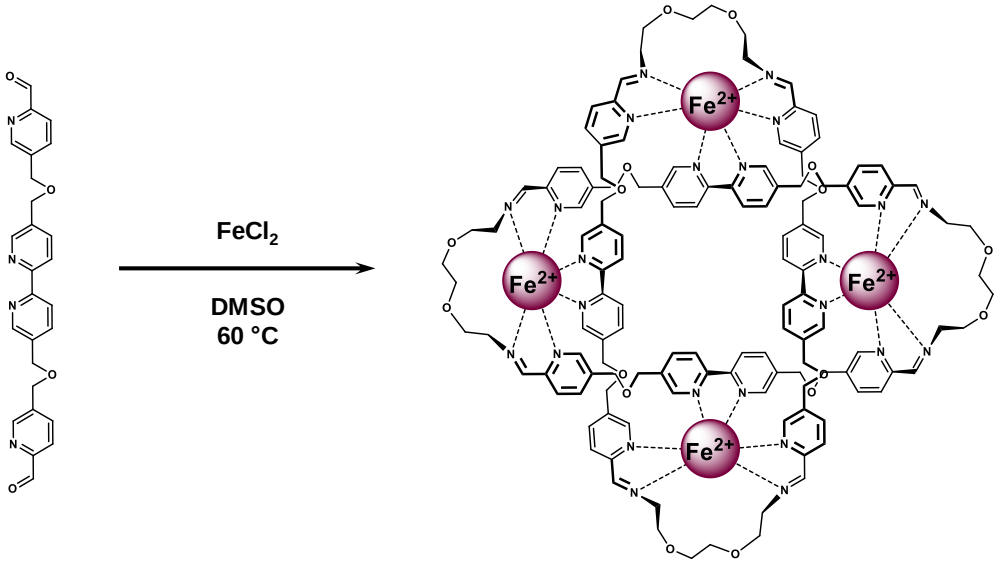

H8 **H9**

Figure 4.6: *Leight's Solomon link*

4.2 Results and Discussion

4.2.1 Hydrazone and imine based helicates

One of the first ligands (**JRHel7**) synthesized in this project was prepared with the help of Janane Rahbani (*Figure 4.7*). Its coordination moieties comprise two **MePaphy** units (pyridine-2-carbaldehyde-(*N*-methyl)-2-pyridylhydrazone, *Figure 4.7*) connected with a -CH_2OCH_2- linker. The ^{1}H NMR spectrum of the mixture of 1 eq. of **JRHel7** with 1eq. of $Zn(OTf)_2$ provided sharp signals with a characteristic AB splitting for the -CH_2- protons, consistent with the diastereotopicity expected in a helical complex. However, contrary to our expectations, a subsequent X-ray structure determination (R1 = 4.83 %) showed a single-stranded species with two Zn(II) centres, of general formula **LM_2**, the complex **(JRHel7)Zn_2** (*Figure 4.7*). Both Zn(II) metal ions are coordinated to three hydrazine nitrogens; two triflate anions fill the vacant coordination sites. The two Zn(II) metal ions are different with an extra acetonitrile molecule coordinated to one giving it an octahedral geometry. The other pentacoordinated Zn(II) ion has a distorted square pyramidal geometry (*Figure 4.7*).

Based on this result, it was concluded that the connection in position "*6*" of the 2-pyridinecarboxaldehyde moiety is not suitable to build helicates with ligands based on a **Paphy** unit, probably due to the lack of flexibility and subsequent incapability to adopt a suitable geometry for helical assembly (*Figure 4.7*).

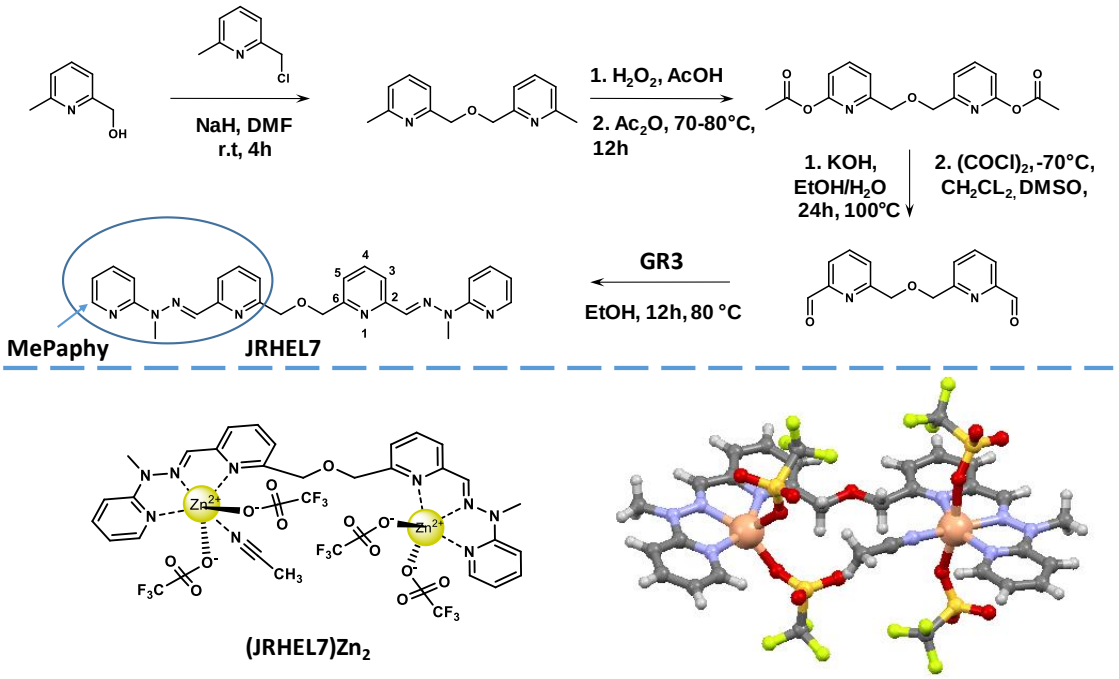

Figure 4.7: ***Top:*** *Synthetic path towards ligand* ***JRHEL7****.* ***Bottom:*** *Crystal structure of the Zn(II) complex of* ***JRHEL7****.*

While working on new ligands for helicates, the contemporaneously ongoing grid of grids project produced the family of dihydrazines **GR5x** (*Figure 3.31*, Chapter 3), which also possessed the structural preconditions suitable for formation of dynamic helicates. By just mixing these ligands with aldehydes, it is possible to form hydrazone coordination pockets and their linker connects two pyridines in position "*5*" of the 2-pyridinecarboxaldehyde moiety (*Figure 4.7*). We hoped that this would provide more favourable conditions to form helicates.

Despite our expectations, these ligands were not ideal for assembling helicates. All ligands from this series tended to form mixtures of two species. The observations are analysed in detail in the following for the model ligands **GR9e, f** (F*igure 4.8A, 4.9*).

The ligand bears a phenyl bridge connected through -CH_2O- link to the **MePaphy** unit and was observed to provide slightly different outcomes in the presence of different metal ions. Mixing 1 eq. $Fe(BF_4)_2$ with 1 eq. of **GR9e** gives almost exclusively the $\mathbf{L_2M_2}$ type complex ($\mathbf{(GR9e)_2Fe_2}$) (9:1 ratio estimated by integration of the NMR spectrum). ESI-MS also showed only peaks belonging to $\mathbf{L_2M_2}$ complexes (459.1133 $[(\mathbf{GR9e})_2Fe_2(BF_4)]^{3+}$ and 763.1371 $[(\mathbf{GR9e})_2Fe_2(BF_4)_2]^{2+}$) (F*igure 4.8B, Figure E3.6*).

The ^{1}H NMR spectrum of the complex with $Cd(OTf)_2$ clearly shows two species in 4:1 ratio. Based on ESI-MS (major peak 771.1324 $[(\mathbf{GR9e})Cd(OTf)]^+$) and the 2D NMR spectrum, the

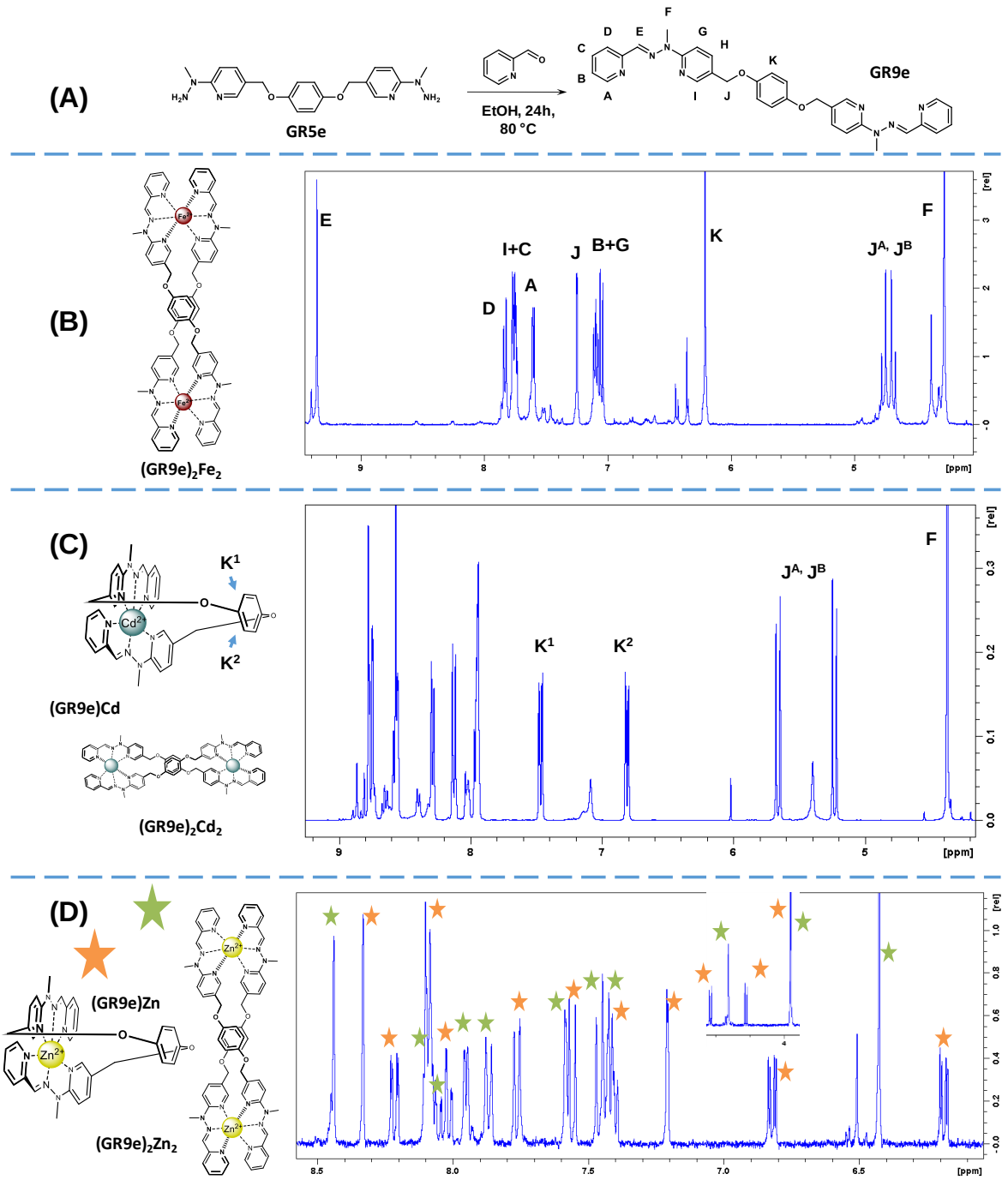

Figure 4.8: *(A) Synthesis of ligand **GR9e**. (B) ^{1}H NMR spectrum of the Fe(II) double helicate. (C) ^{1}H NMR spectrum of mixture of double helicate (minor) and simple complex (major) in case of Cd(II). (D) ^{1}H NMR spectrum of 1:1 mixture of double helicate and simple complex in case of Zn(II) complex of **GR9e.***

structure of the main complex was assigned to the **LM** (**(GR9e)Cd**) structure while the minor species was assigned to a double helicate **L_2M_2** (**$(GR9e)_2Cd_2$**) (F*igure 4.8C*).

The most complex mixture arose when $Zn(OTf)_2$ was used. Signals for two species in a roughly 1:1 ratio could be seen in the ^{1}H NMR spectrum (F*igure 4.8D*). In this case, the presence of a helical species (**$(GR9e)_2Zn_2$**) was proved by a single crystal X-ray structure

determination (R1 = 8.56 %). F*igure 4.9*). Therefore, by re-dissolving these crystals it was possible to unequivocally identify the peaks belonging to the double helicate. However, even right after the re-dissolution of the recrystallized material it was possible to observe peaks of both species and after one day the system reached the previously observed distribution. This shows that both helicate and simple complex (**(GR9e)Zn**) species are in a dynamic equilibrium. (Figure E3.2-E3.3)

Currently, the actual form of the other complex is still uncertain. Molecular volumes obtained from DOSY experiments are in agreement with the simple $\mathbf{L_2M_2}$ (3737 Å^3, calc. from crystal 4200 Å^3, $\mathbf{(GR9e)_2Zn_2}$) and **LM** (1370 Å^3, (**GR9e)Zn**) mixture. Based on examples known in the literature [42,43] the formation of a mesocate was expected, but all analytical data point rather to the formation of a monometallic complex. The assessment based on ESI-MS is further complicated by the presence of the peaks which were identified as those of $\mathbf{L_3M_3^{x+}}$ (**GR9e** + Cd(II), Zn(II)). However, due to the dynamic nature of the mixture no further effort was put into purification and isolation and instead efforts were focused on designing and synthesizing new ligands.

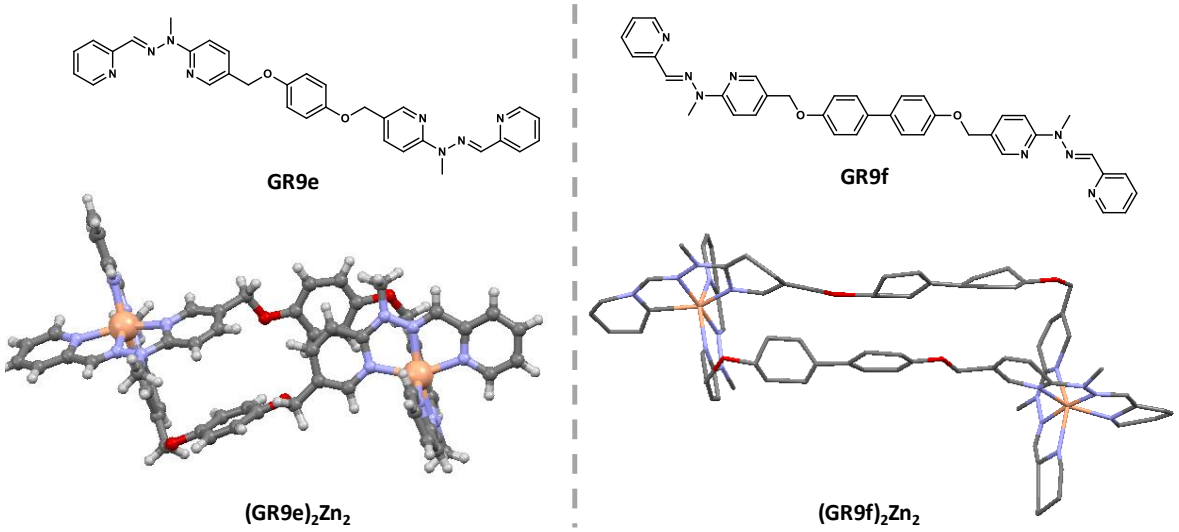

Figure 4.9: ***Left****: representation of the ligand* ***GR9e*** *and the crystal structure of the corresponding Zn(II) complex.* ***Right****: representation of the ligand* ***GR9f*** *and unsatisfavtory crystal structure of the corresponding Zn(II) complex.*

In contrast to **GR9e**, the analogous ligand with a biphenyl bridge (**GR9f**, *Figure 4.9*) provided a clean ^{1}H NMR spectrum of a double helicate with all tested metals (Zn(II), Cd(II), Fe(II)) and ESI-MS showed only binuclear species to be present. In the case of the Zn(II) complex ($\mathbf{(GR9f)_2Zn_2}$, *Figure 4.9*) it was possible to grow crystals suitable for an X-ray structural determination, which unfortunately provided only a poorly refined structure. In spite of the low quality of the dataset, it is still possible to identify the up and down double helical

winding of the ligands around the Zn(II) centres (*Figure 4.9*), therefore proving the existence of a double helicate.

At this point, for further referencing, it is necessary to note that even the ligands bearing aliphatic linkers of different length (from **GR5x** series, *Figure 3.31*, Chapter 3) provided only mixtures of different species. However, in contrast to **GR9e** and **GR9f**, even their ESI-MS spectra were inconclusive and therefore no reliable conclusions could be made about the shape of the complexes in the mixture.

Furthermore, it was found that **GR5x** cores were suitable only for construction of octahedrally coordinating ligands. The possible transformation to tetra coordinated imine was hindered by the fact that the hydrazinopyridine motif is incompatible with four coordination of Cu(I) (F*igure 4.10*); when starting from components rather than from preformed ligands, Cu(I) was quickly complexed by the hydrazinopyridine and oxidized to Cu(II). The oxidation was proved by the disappearance peaks for the diamagnetic Cu(I) complex from the ^{1}H NMR spectrum of the mixture. The same behaviour, even though slower, was also observed in the cases of preformed ligands. It is probably due to the slow hydrolysis of hydrazones and subsequent interaction between released hydrazine and Cu(I) cation. Again, this transformation is manifested by the change of the colour of the solution from dark red to yellow-green. In order to find a replacement for the dihydrazine core and to render our starting block more versatile a new core based on pyridine dialdehyde (**HEL9**) was synthesized (*Figure 4.11*). This ligand is analogous to the above-mentioned ligands, but compared to **JRHEL7** it is connected in position "5" and in contrast to the **GR9e** the dialdehyde core can be easily adjusted for complexation of different metals with both tetrahedral or octahedral preferences just by changing the amine used in the condensation reaction.

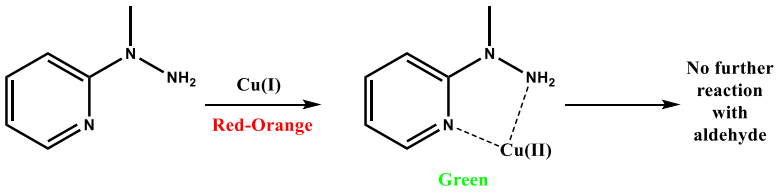

Figure 4.10: *Illustration of the observed interaction of Cu(I) with 2-pyridylhydrazones and 2-(aminomethyl)pyridine*

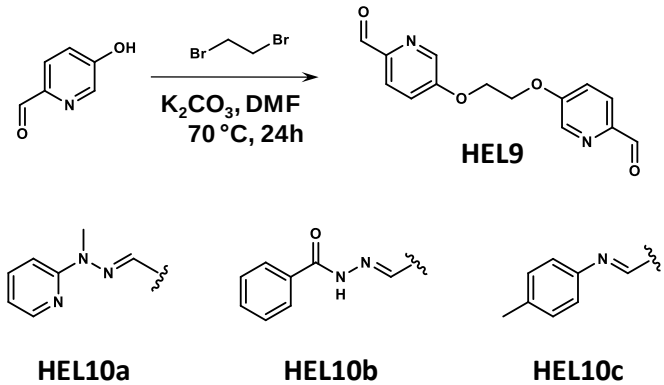

Figure 4.11: *A synthesis of the ligand **HEL9** and three model ligands prepared by using different capping units.*

First, to probe the complexation of octahedral metal cations, the ligand

HEL10a was formed by the reaction of aldehydes with 2-(1-methylhydrazinyl)pyridine (**GR3**) (*Figure 4.11*). All octahedral metals (Zn(II), Cd(II), Fe(II)) reacted with ligand **HEL10a** gave the expected double helicate structure, which was proved by an X-ray crystal structure determination of the Fe(II) complex (**(HEL10a)$_2$Fe$_2$**, R1 = 17.75 %, *Figure 4.12*). The acylhydrazone ligand **HEL10b** was prepared as a possible alternative to **HEL10a** (*Figure 4.11*). However, all tested benzhydrazides provided only insoluble ligands which did not solubilize even in the presence of metal salts. Therefore, the ligand **HEL10b** was abandoned.

Next, we looked at synthesizing a double helicate using Cu(I), to obtained tetrahedrally coordinated helicates. Previous experience with similar coordination motifs showed the good coordination properties of aniline-based imines. To simplify analysis of the NMR spectra, *p*-toluidine was chosen and ligand **HEL10c** resulted (*Figure 4.11*). The results obtained were again encouraging. Indeed, in the case of Cu(I) the ^{1}H NMR spectrum and ESI-MS showed the formation of a double helicate (**(HEL10c)$_2$Cu$_2$)**. Unfortunately, no X-ray structure could be obtained due to the low quality of the crystals. On switching to octahedral cations (Zn(II), Cd(II), Fe(II)), clean assembly of triple helicates (**L$_3$M$_2$**) was observed, proved, in the case of Fe(II), by an X-ray structure determination (**(HEL10c)$_3$Fe$_2$,** R1 = 7.95 %, *Figure 4.12*).

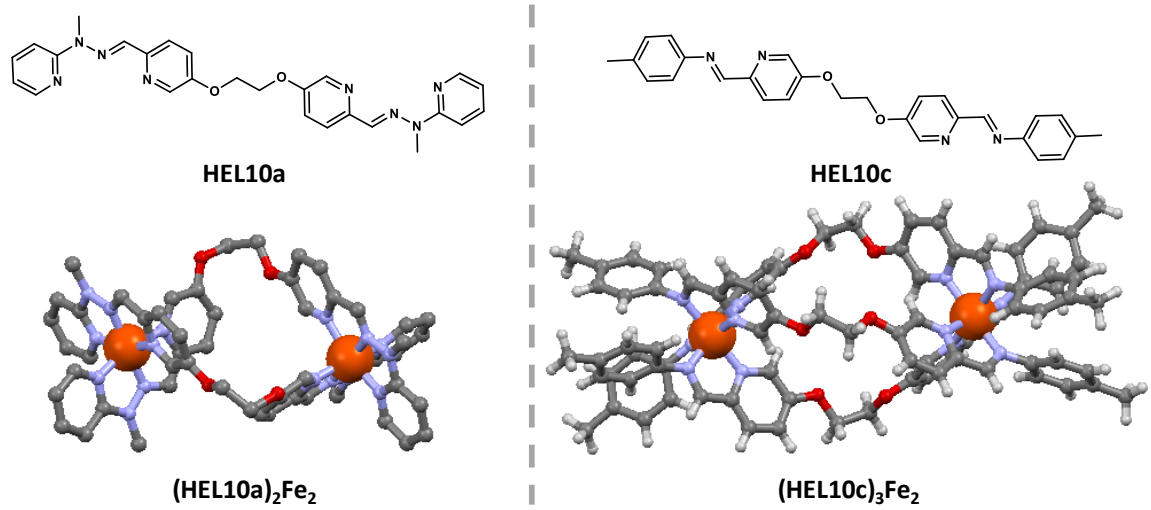

Figure 4.12: ***Left****: representation of the ligand* ***HEL10a*** *and the crystal structure of the corresponding Fe(II) complex.* ***Right****: representation of the ligand* ***HEL10c*** *and the crystal structure of its corresponding triple helical Fe(II) complex (****(HEL10c)$_3$Fe$_2$****).*

Because the assembly of **HEL10a** and **HEL10c** helicates proceeded well starting from both the preformed ligand as well as from components it was also appropriate to test the dynamic transformations between various complexes. Ligand **HEL10c** then provided a good starting point for the imine exchange reactions.

First, the exchange with different amines was studied. Based on similar examples in the literature[44,45] *p*-methoxybenzylamine was chosen to exchange for *p*-toluidine in the Zn(II) triple helicate (**((HEL10c)$_3$Zn$_2$**, *Figure 4.13, Figure E3.9*). The exchange reaction was complete within 30 min at room temperature, giving a sharp ^{1}H NMR spectrum of a new Zn(II) complex (**((HEL10c2)$_3$Zn$_2$)** and free *p*-toluidine (F*igure 4.13*). Interestingly both tri(aminoethyl)amin and 2-(aminomethyl) pyridine failed to provide fully exchanged product, probably due to the direct interactions between the amines and metal cation.

Even though the exchange of *p*-toluidine and p-methoxybenzylamine was successful, the starting and final products were both triple helicates. In order to increase the complexity of the exchange also the transformation of a triple helicate into a double helicate was tried. The addition of **GR3** to the acetonitrile solution ((**HEL10c)$_3$Zn$_2$**) furnished in 2 h at room temperature an exchanged double helicate **(HEL10a)$_2$Zn$_2$** instead of the imine triple helicate (F*igure 4.13, Figure E3.10*).

A similar change in the constitution of the helicate was also triggered by metal ion exchange: starting with the Cu(I) double helicate of **HEL10c** (**(HEL10c)$_2$Cu$_2$**), the addition of Cd(II) forces the complex to rearrange from double helicate to triple helicate with full displacement of the tetrahedral Cu(I) from the complex. This reaction was found to be reversible: the opposite transformation from triple helicate back to starting double helicate could then be triggered simply by preferential binding of the Cd(II) to [2,2,2] cryptand and recomplexation of the Cu(I) from the solution (F*igure 4.13, Figure E3.11*).

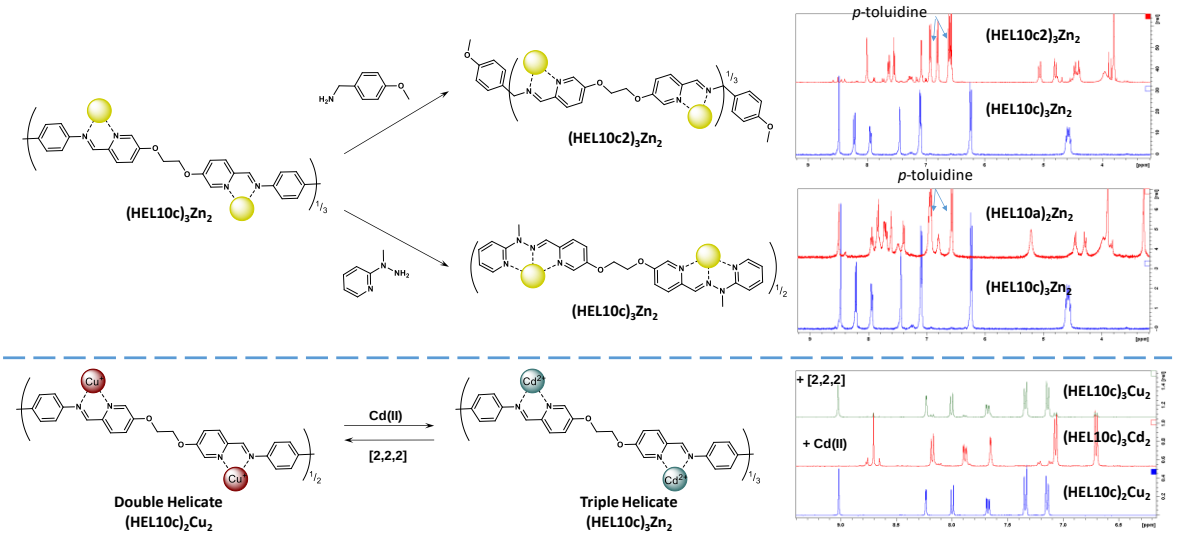

Figure 4.13: ***Top (Top)****: the first reaction depicts the exchange of p-toluidine with p-methoxybenzylamine in Zn(II) complex of* ***HEL10c****, while keeping a triple helical constitution.* ***Top (Bottom)****: The second reaction depicts the exchange p-toluidine with* ***GR3****, while changing the constitution from triple- to double helicate.* ***Bottom****: The metal triggered change from double helicate to triple helicate and back.*

Reading the literature, it is easy to fall prey to the impression that nothing is easier than assembling a helicate. Herein we have shown the importance of careful ligand design. Starting from an unsuitable ligand which did not provida a helicate at all, by iterative rational design we managed to successfully prepare compound **HEL9** which proved to have an ideal core for helicate ligands. Structures of double-helical **(HEL10a)$_2$Fe$_2$** and triple-helical **(HEL10c)$_3$Fe$_2$** were established by X-ray diffraction. The imine bond in **HEL10c** provided us with the possibility to perform various exchange reactions with amines and hydrazines. Moreover, reversible shape switching was achieved by metal exchange, going from the double helical **(HEL10c)$_2$Cu$_2$** to triple helical **(HEL10c)$_3$Cd$_2$** and back. Next, we tried to take advantage of these findings in the construction of ligands for trinuclear helicates.

4.2.2 Heterotopic ligands and multi-metal helicates

Helicates can be divided according to the nature of their ligand strand. A helicate that is made from the identical strands is called *homostranded* helicate, while the one possessing different ligands is called *heterostranded* helicate.[17,19] When the ligand contains only one type of coordination motif it is referred to as *homotopic*, and if it contains different binding pockets it is referred as *heterotopic.*[17,19] All helical ligands mentioned in the first part of this work were *homotopic* and have provided *homostranded* helicates

Their coordinating pockets can be divided into two groups based on the number of donor atoms. For example, in the case of **HEL10a** the coordination site is made of **Paphy** groups with three donor atoms which mimic the coordination behaviour of a terpyridine. This type of coordination motif will be referred to as "**T**". (*Figure 4.14*) The second type, which can be found in **HEL10c** has only two donor atoms and thus will be referred to as "**B**". (*Figure 4.14*)

The goal in this part was to prepare and study dynamic heterotopic ligands containing both **T** and **B** binding motifs in one ligand strand and study their assembly with different metal cations. Such ligands are interesting for the so-called *supramolecular programming* principle, a term describing the information hidden within the structure of the components of the mixture (ligand structure, coordination of metal, etc…) and its processing which results in specific *self-assembly* and *self-organization.* (*Figure 4.14*)[17,41,46]

Molecular self-recognition (selective interaction between components) is indispensable for self-assembly. The recognition of a suitable coordination pocket by metal cation is then demonstrated through the stability and selectivity of the assembly. For example, octahedral cations choose ligand(s) which can provide overall six coordination centres in a suitable geometry. In contrast, tetrahedral metals prefer bidentate ligands which can offer four

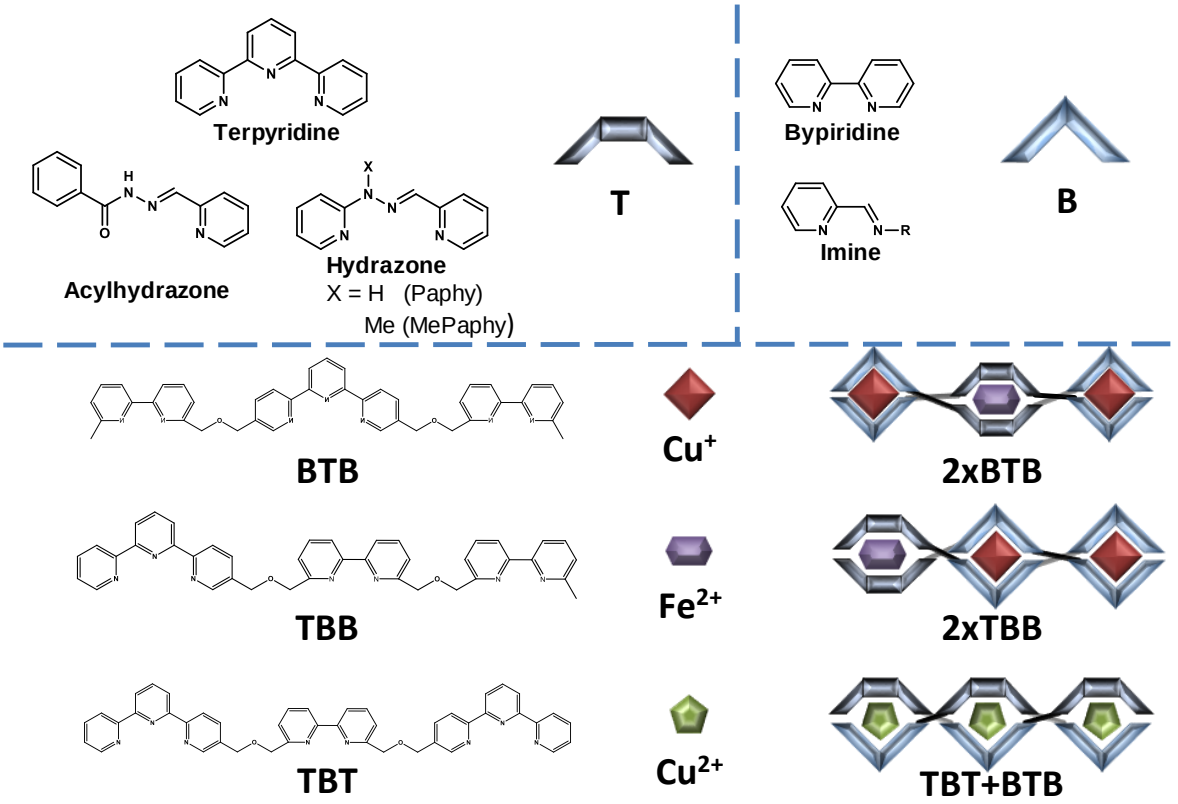

Figure 4.14: ***Top left****: various* ***T*** *units with three donor atoms which were used in this work.* ***Top right****:* ***B*** *units with two donor units which were used in this work.* ***Bottom****: three ligands with different order of* ***B*** *and* ***T*** *units and the assembly of their mixtures in the presence of various metals.* [41]

coordination atoms. In this regard, it is possible to talk about the information/code hidden within the structure of the ligand and read by the metal coordination preferences. The information is expressed upon "meeting" of the ligand and the metal. The satisfaction of their requirements is then manifested by the assembly of a particular structure.[47]

This concept was already tested on a series of homotopic and heterotopic helicates containing three coordination pockets.[41] The ligands were made of connected bipyridine (**B**) and terpyridine (**T**) units with different order of **B** and **T** units in each ligand. When mixed with metals of different coordination properties (Cu(I), Cu(II), Zn(II)) or with their mixtures, different complexes were observed as the ligands tried to satisfy the coordination preferences of different metals. Several examples have already been described in the literature, where different sophisticated structures were generated from one heterotopic ligand upon its exposure to different mixtures of metals. (*Figure 4.14*)[41,48,47,49,50]

In this regard, the aim was to try to go one step further than the above-mentioned study on **B** and **T** helicates[41] and try to assemble different heterotopic ligands in a dynamic combinatorial fashion starting from the ligand subunits. This could be of interest for example in designing a

supramolecular analogue of polymerase chain reaction[51], where the coordination units would play the role of base pairs. Initially the subunits would assemble on the primer strand in the control of a chosen metal cation in respect to the order of **T** and **B** units in the primer. Later, the dynamic connections between subunits (e.g. imines) would be transformed to irreversible, a new strand removed from the primer and circle of transformations could be repeated.

In the initial search for the right model compound the simple ligand **CN13** was designed. The double nature of this compound is based on the presence of amine and hydrazine substituents which can both react with 2-pyridinecarboxyaldehyde providing **B** and **T** binding sites, respectively. (*Figure 4.15*)

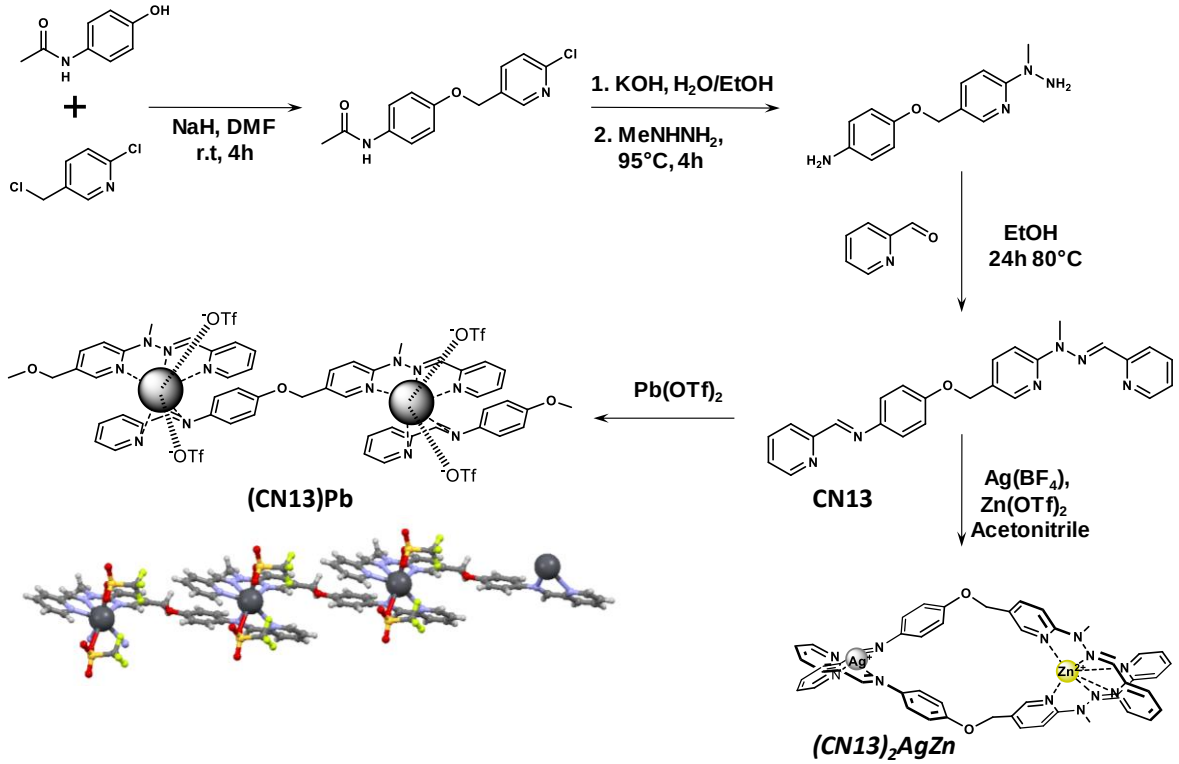

Figure 4.15: ***Top:*** *synthesis of ligand* ***CN13****.* ***Middle left****: Illustration of the coordination polymer formed in the presence of Pb(II) and the resulting crystal structure.* ***Right bottom****: Illustration of probable shape of the observed complex* ***[(CN13)$_2$AgZn]$^{3+}$****.*

At first, the coordination behaviour of metals that are able to accommodate five coordinating atoms in their coordination sphere was studied. There are interesting examples in the literature of similar non-dynamic ligands and their assemblies with Cu(II) and Fe(II).[52,53] Due to the paramagnetic nature of Cu(II) and Fe(II) complexes, our conclusion about the structure of complexes is based on mass spectrometry. In both cases, the presence of a simple **L$_2$M$_2$** complex was evidenced, most likely in a head-to-tail arrangement. Unfortunately, no suitable crystals for X-ray diffraction could be obtained to further support this conclusion.

However, it was possible to prepare a crystal of the $Pb(OTf)_2$ complex of **CN13** (**(CN13)Pb**, R1 = 2.79 %, *Figure 4.15*). This compound is made of two head-to-tail connected ligands and is a coordination polymer where Pb(II) has a coordination number of seven. The Pb(II) is surrounded by one **T** and one **B** group which are complemented by two triflates (*Figure 4.15*).

Nevertheless, the focal point of heterotopic ligands is their ability to accommodate metals with different coordination preferences. Therefore, in the next phase, bimetallic complexes were explored. A few combinations of Zn(II) or Fe(II) with preferences for **T** site and Ag(I) or Cu(I) for **B** site were tested. From all tested combinations, the combination Zn(II)/Ag(I) was found to be the best due to the sharp and very well resolved ^{1}H NMR spectra which indicated the presence of only one complex. ESI-MS spectra showed the presence of a very minor amount of $\mathbf{L_4M_2N_2}$ complex ($[(\mathbf{CN13})_4Zn_2Ag_2]^{x+}$), but the main peaks belonged to the $\mathbf{[(CN13)_2AgZn]^{x+}}$ complex ($\mathbf{L_2MN}$). DOSY analysis showed a volume consistent with the expected $\mathbf{L_2MN}$ (**(CN13)$_2$AgZn**) complex (2873 Å^3, calculated 3300 Å^3) (*Figure 4.15*). Again no single crystals could be grown for this compound, leaving conclusions about the constitution and shape of the complex solely based on other indirect techniques. Even though no structure of **(CN13)$_2$AgZn** could be obtained it was possible to confirm that the paphy **T** unit and imine **B** unit are selective towards different metals according their coordination properties.

In order to advance our attempt to extend the scope of previous study[41] on *supramolecular programming* the first ligand with three coordination pockets was designed and prepared. To facilitate the beginning, it was decided to start with the terpyridine as the core to which aniline units were attached. The preparation of the ligand **CN26** was finished by condensation with 2-pyridinecarboxaldehyde. Even though the preformed ligand **CN26** (1 eq.) is totally insoluble in acetonitrile, the addition of Zn(II) (0.5 eq.) and Ag(I) (1 eq.) provided a clean yellow solution. The ESI-MS spectrum indicated the presence of an $\mathbf{L_2MN_2}$ complex (**(CN26)$_2$ZnAg$_2$**, *Figure 4.16*) and DOSY analysis showed a volume consistent with the expected value for the helicate structure (measured 6959 Å^3, calcul. 7200 Å^3 from cryst. of **(MAF13)$_2$Zn$_3$**, *Figure 4.18*). Unfortunately, the peaks in ^{1}H NMR spectrum were broad and therefore no NOE interactions were visible in the 2D NOESY spectra. The broadening of the spectra is connected with the addition of Ag(I). It was possible to assemble only the middle cross section by addition of 0.5 eq. of Zn(II) to the ligand **CN26** (1 eq.) which exhibited sharp and well resolved NMR spectra. Subsequently, the use of Cu(I) provided even more inferior resolution than that of Ag(I) (*Figure 4.16*).

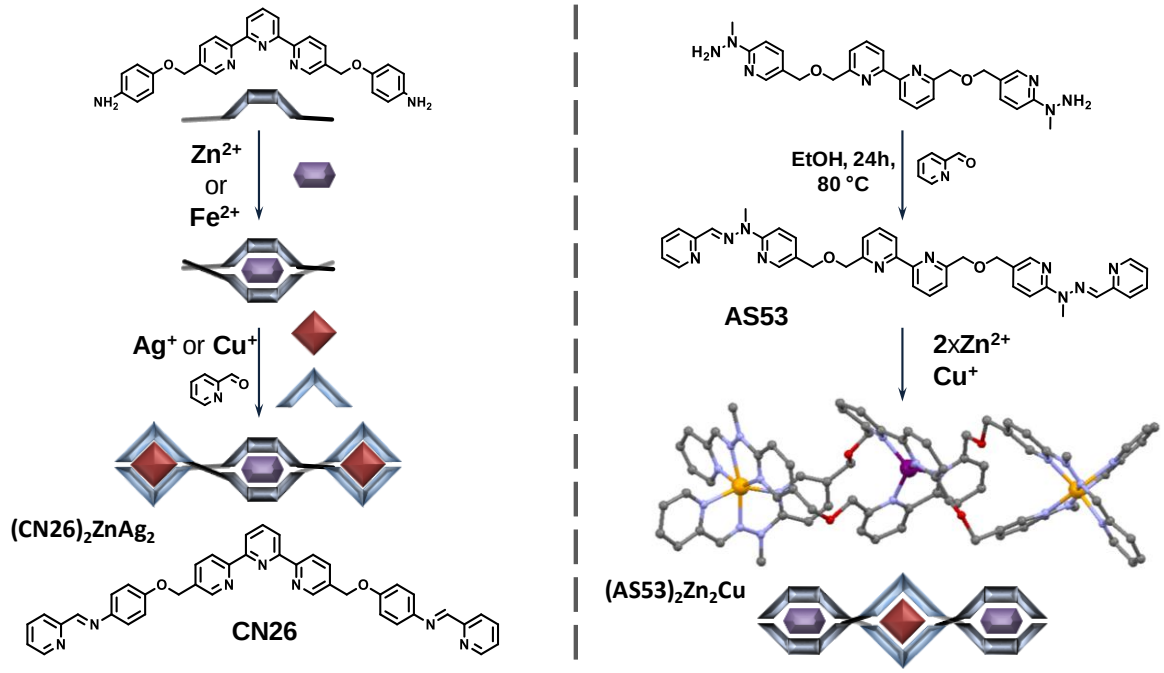

Figure 4.16: ***Left****: illustration of the stepwise dynamic assembly of the ligand **CN26** with various combination s of metals.* ***Right****: preparation of the ligand **AS53** and the crystal structure obtained with Cu(I) and two Zn(II).*

To have a complementary ligand to **CN26**, another ligand was synthesized with a bipyridine core, **AS53**, in collaboration with Dr. Antonio Santoro. The peripheral **T** units were prepared via attaching pyridine hydrazine and subsequent condensation with 2-pyridinecarboxyaldehyde. In contrast to the broad ^{1}H NMR spectrum of **(CN26)$_2$ZnAg$_2$** this new ligand provided a sharp and nicely resolved spectrum when complexed with one Cu(I) and two Zn(II) (**(AS53)$_2$Zn$_2$Cu**). In this case, it was also possible to grow a crystal suitable for X-ray diffraction. The X-ray structure determination indeed showed the expected double helicate **(AS53)$_2$Zn$_2$Cu** (R1 = 9.85 %) with one tetrahedral Cu(I) in the middle and two octahedral Zn(II) on the sides (*Figure 4.16*). Unfortunately, the dynamic assembly of the helicate failed due to the already mentioned interactions of the pyridine hydrazine with Cu(I) and its subsequent oxidation to Cu(II) (*Figure 4.10*). Interestingly, in the case of the ligand **AS53** two different crystals were obtained from the same crystallization setup. Liquid diffusion of diisopropyl ether into an acetonitrile solution of **AS53**, Cu(I) and Zn(II) provided orange crystals of the described three centred double helicate, as well as colourless needles which were identified as the circular helicate **(AS53)$_4$Zn$_6$** (R1 = 7.65 %, *Figure 4.17*). This circular structure consists of four ligands entangled around six Zn(II) cations. The coordination motif of the Zn(II) cations in the central bipy unit is quite interesting: the linker which consists of -CH_2OCH_2- connects to the bipy at position six. Such proximity to the coordination centre allowed the oxygen to coordinate the Zn(II) metal ion in the position which is occupied by the

central bipy in the structure of **(AS53)$_4$Zn$_6$**. Therefore, the binding motif around Zn(II) is five nitrogens (Bipy and MePaphy) and one ether oxygen (linker) (*Figure 4.17*). Further study of the properties and direct assembly of this circular helicate is still in process. We are hoping to find the right conditions to isolate each helicate during the crystallization process, in order to fully characterize both compounds.

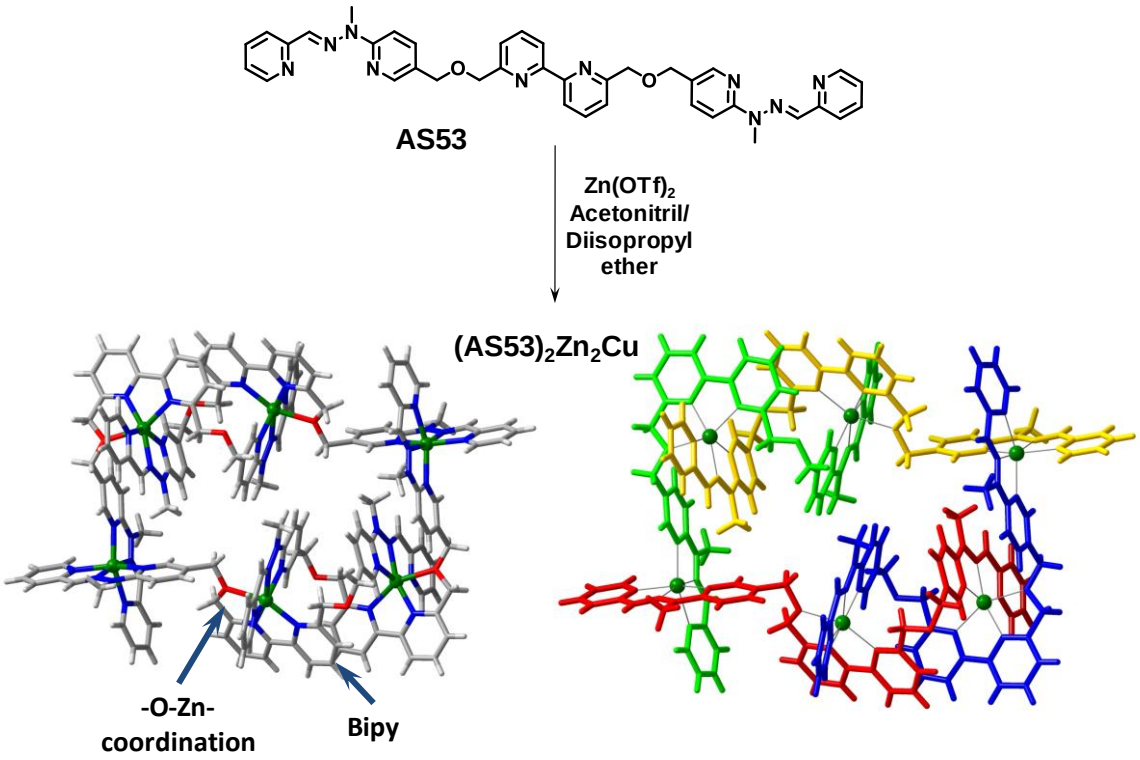

Figure 4.17: ***Top:*** *representation of the circular helicate of **AS53**.* ***Bottom left****: Visible interaction of one oxygen from the linker to the Zn(II) in the central Bipy unit.* ***Bottom right****: Visualization of entanglement between four ligands and six Zn(II) in the complex.*

Even though at this point we had two complementary ligands, they were not suitable for further study on the dynamic mixture. The helical nature of **(CN26)$_2$ZnAg$_2$** could not be unequivocally proved and ligand **AS53** had only limited use for the complex mixtures (incompatibility with Cu(I)).

For our last attempt to prepare a suitable dynamic helicate with three coordination centres, we again turned to aldehydes as core ligands. In collaboration with Marta Fik, a new terpyridine core bearing 2-pyridinecarboxaldehyde moieties was prepared (**MAF9**) (*Figure 4.18*). So far, only preliminary investigations of its coordination behaviour have been made. Condensation of dialdehyde **MAF9** with hydrazine **GR3** (**MAF10**) and with benzhydrazide (**MAF11**) provided ligands with three **T** motifs (*Figure 4.18*). Both ligands provided nice ^{1}H NMR spectra when mixed with 1.5 eq. of Zn(II), Cd(II) or Fe(II) and ESI-MS confirmed the presence of trinuclear double helicates. For **MAF10,** encouraging results from ^{1}H NMR and ESI-MS were supported

by a single crystal X-ray structure determination of **(MAF10)$_2$Zn$_3$** (R1 = 7.65 %, *Figure 4.18*). It showed the expected double helical structure where the ligand folds around the central axis which interconnects three Zn(II). (*Figure 4.18*)

In contrast to this result, the ligand with imine based **B** units at the periphery (**MAF13**, *Figure 4.18*), was mixed with 0.5 eq. Zn(II) and 1 eq. Cu(I) and formed only a mixture of different species shown by multiple peaks in the ^{1}H NMR spectrum. Nevertheless, ESI-MS still showed a presence of a species of **L$_2$MN$_2$** composition (**(MAF13)$_2$ZnCu$_2$)**.

Combining all these results and comparing with others already known from the literature[12,36,40,41] it was concluded that it is necessary to introduce a -CH_2OCH_2- linker between the covalent cores (bipy, terpy) and the 2-pyridinecarboxaldehyde,either in position "6" or position "5". The work on such ligands will be undertaken in the near future.

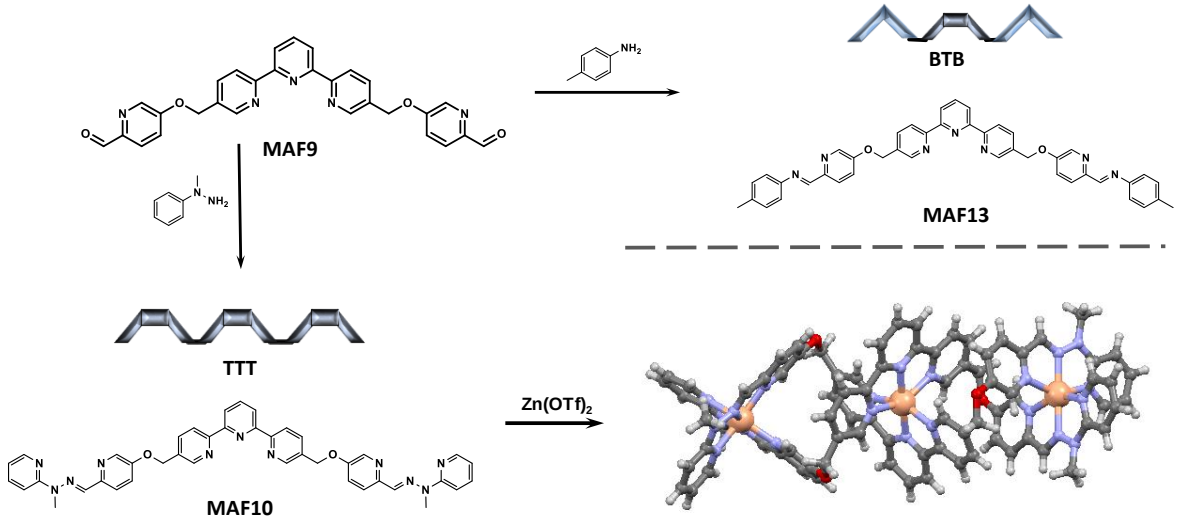

Figure 4.18: *The synthesis of various ligands based on dialdehyde core **MAF9** with terpyridine in the centre. **Bottom**: the structure of **MAF10** with hydrazones on the periphery and the crystal structure of the three-centred double helicate* ***(MAF10)$_2$Zn$_3$.***

4.3 Conclusion

Despite initial struggles to find the ideal dynamic ligand to complex both octahedral and tetrahedral cations, we managed to prepare and successfully test the dynamic behaviour of a small series of ligands based on dialdehyde **HEL9**. Meanwhile, the structures of binuclear single stranded complex **(JRHEL7)Zn$_2$** and two binuclear double helicates **(GR9e)$_2$Zn$_2$** and **(GR9f)$_2$Zn$_2$** were determined by single crystal X-ray diffraction. Unfortunately, the double helicate **(GR9e)$_2$Zn$_2$** formed only in the mixture with simple **(GR9e)Zn** complex and **(GR9f)$_2$Zn$_2$** could be used only to complex cations with octahedral preferences. The pyridine

hydrazine motif, which forms the core of **GR9x** ligands was observed to lead to facile oxidation of Cu(I) to Cu(II).

In attempts to improve previous work from our group[41], we managed to prepare a series of ligands with three coordination pockets. The core of these ligands is made of classic terpyridine and bipyridine units, which provided easier analysis and simplified the work with the ligands. The coordinating units at the periphery were made of either **T** (hydrazone, acylhydrazone) or **B** (imine) units. The different combination of **T** and **B** units in the ligands furnished several triple nuclear hetero- and homotopic helicates. Moreover, single crystals were grown for two of them, ((**MAF10)$_2$Zn$_3$** and **(AS53)$_4$Zn$_6$**), allowing us to determine their X-ray structures.

In addition, it was also possible to obtain and determine the structures of one **1D** coordination polymer **CN13Pb** and one circular helicate **(AS53)$_4$Zn$_6$.** The structure of **(AS53)$_4$Zn$_6$** showed an unusual coordination motif where one oxygen from the linker between coordination moieties participated in the coordination of the Zn(II) metal ion.

All the above described results provide a good basis for further research which is already in progress, notably with our different collaborations that could be seen throughout this chapter.

4.4 References

1. Wu, H.-C. H.; Sarko, A. *Carbohydr. Res.* **1978,** *61,* 27-40.
2. Tyson, S. L. The Caduceus. *The Scientific Monthly* **1932,** *34,* 492-498.
3. Despommier, D. chapter 7. In *People, Parasites, and Plowshares: Learning from Our Body's Most Terrifying Invaders;* Columbia University press: New York, 2016; pp 147-163.
4. Boiocchini, M.; Fabbrizzi, L. *Chem. Soc. Rev.* **2014,** *43,* 1835-1847.
5. Rolfsen, D. *Knots and Links;* Publish or Perish: Berkeley, 1976.
6. Adams, C. C. *The Knot Book;* Freeman: New York, 1994.
7. Andrae, D. *New. J. Chem.* **2006,** *30,* 873-882.
8. Pentecost, C. D.; Chichak, K. S.; Peters, A. J.; Cave, G. W. V.; Cantrill, S. J.; Stoddart, J. F. *Angew. Chem. Int. Ed.* **2007,** *46,* 218-222.
9. Rose, L. R. *Seeing Solomon's Knot;* Lois Rose Rose: Los Angeles, 2005.
10. Mallam, A. L.; Jackson, S. E. *J. Mol. Biol.* **2006,** *359,* 1420-1436.
11. Dietrich-Buchecker, C. O.; Sauvage, J.-P.; De Cian, A.; Fischer, J. *J. Chem. Soc. Chem. Commun.* **1994,** 2231.
12. Ayme, J.-F.; Beves, J. E.; Leigh, D. A.; McBurney, R. T.; Rissanen, K.; Schultz, D. *Nat. Chem.* **2012,** *4,* 15.
13. Ayme, J. F.; Beves, J. E.; Leigh, D. A.; McBurney, R. T.; Rissanen, K.; Schultz, D. *J. Am. Chem. Soc.* **2012,** *134,* 9488.
14. Albrecht, M. *Chem. Eur. J.* **2000,** *6,* 3485-3489.
15. Lehn, J.-M.; Rigault, A.; Siegel, J.; Harrowfield, J.; Chevrier, B.; Moras, D. *Proc. Natl. Acad. Sci. U.S.A.* **1987,** *84,* 2565-2569.
16. Dietrich, B.; Viout, P.; Lehn, J.-M. *Macrocyclic chemistry;* VCH: Weinheim, 1993.
17. Piguet, C.; Bernardinelli, G.; Hopfgartner, G. *Chem. Rev.* **1997,** *97,* 2005-2062.
18. Albrecht, M. *Chem. Rev.* **2001,** *101,* 3457-3497.
19. Hannon, M. J.; Childs, L. J. *Supramol. Chem.* **2004,** *16,* 7-22.
20. Caulder, D. L.; Raymond, K. N. *Acc. Chem. Res.* **1999,** *32,* 975-982.
21. Bilbeisi, R. A.; Olsen, J.-C.; Charbonniere, L.; Trabolsi, A. *Inorganica Chimica Acta* **2014,** *417,* 79-108.
22. Albrecht, M. *Chem. Soc. Rev.* **1998,** *1998,* 281-288.
23. Morgan, G.; Burstall, H. *J. Chem. Soc.* **1937,** 1649-1655.
24. Burstall, F. H. *J. Chem. Soc.* **1938,** 1672.
25. Brandt, W. W.; Dwyer, F. P.; Gyarfas, E. C. *Chem. Rev.* **1954,** 959.
26. Constable, E. C.; Hannon, M. J.; Martin, A.; Raithby, P. R.; Tocher, D. A. *Polyhedron* **1992,** *11,* 2967.
27. Stratton, W. J.; Busch, D. H. *J. Am. Chem. Soc.* **1958,** 1286-1289.
28. Thompson, M. C.; Busch, D. H. *J. Am. Chem. Soc. 1962* **1962,** *84,* 1762.
29. Youinou, M.-T.; Rahmouni, N.; Fischer, J.; Osborn, J. A. *Angew. Chem. Int. Ed. Engl.* **1992,** *31*, 733-735.

30. Xu, Z.; Thompson, L. K.; Miller, D. O.; Clase, H. J.; Howard, J. A. K.; Goeta, A. E. *Inorg. Chem.* **1998,** *37,* 3620-3627.
31. Hamblin, J.; Jackson, A.; Alcock, N. W.; Hannon, M. J. *J. Chem. Soc. Dalton. Trans.* **2002,** 1635-1641.
32. Boyd, P. D. W.; Gerloch, M.; Sheldrick, G. M. *J. Chem. Soc. Dalton. Trans.* **1974,** 1097.
33. Albrecht, M.; Kotila, S. *Angew. Chem. Int. Ed.* **1995,** *34,* 2134-2137.
34. Thomas, C. M.; Summers, D. Bacterial Plasmids. *Encyclopedia of Life Sciences* **2008**.
35. Chichak, K. S.; Cantrill, S. J.; Pease, A. R.; Chiu, S.-H.; Cave, G. W. V.; Atwood, J. L.; Stoddart, F. J. *Science* **2004,** *304,* 1308-1312.
36. Hassenknopf, B.; Lehn, J.-M.; Kneisel, B. O.; Baum, G.; Fenske, D. *Angew. Chem., Int. Ed. Engl* **1996,** *35,* 1838-1840.
37. Kramer, R.; Lehn, J.-M.; De Cian, A.; Fischer, J. *Angew. Chem. Int. Ed.* **1993,** *32,* 703-706.
38. Hasenknopf, B.; Lehn, J.-M.; Boumediene, N.; Dupont Gervais, A.; Van Dorsselaer, A.; Kneisel, B.; Fenske, D. *J. Am. Chem. Soc.* **1997,** *119,* 10956.
39. Beves, J. E.; Cambell, C. J.; Leigh, D. A.; Pritchard, R. G. *Angew. Chem., Int. Ed. Engl.* **2013,** *52,* 6464.
40. Beves, J. E.; Campbell, C. J.; Leigh, D. A.; Pritchard , R. G. *Angew. Chem. Int. Ed.* **2013,** *52,* 6464-6467.
41. Marquis , A.; Smith, V.; Harrowfield, J.; Lehn, J.-m.; Herschbach, H.; Sanvito, R.; Leize-Wagner, E.; van Dorsselaer, A. *Chem. Eur. J.* **2006,** *12,* 5632-5641.
42. Bilyk, A.; Harding, M. M.; Turner, P.; Hambley, T. *J. Chem. Soc. Dalton. Trans.* **1994,** 2783-2790.
43. Bilyk, A.; Harding, M. M. *J. Chem. Soc. Dalton. Trans* **1994,** 77-82.
44. Schultz, D.; Nitschke, J. R. *J. Am. Chem. Soc.* **2006,** *128,* 9887-9892.
45. Meng, W.; Ronson, T. K.; Clegg, J. K.; Nitschke, J. R. *Angew. Chem. Int. Ed.* **2013,** *52,* 1017-1021.
46. Lehn, J.-M. *Supramolecular Chemistry;* VCH: Weinheim, 1995.
47. Funeriu, D. P.; Lehn, J.-M.; Fromm, K. M.; Fenske, D. *Chem. Eur. J.* **2000,** *6,* 2103-2111.
48. Funeriu, D. P.; Lehn, J.-M.; Baum, G.; Fenske, D. *Chem. Eur. J.* **1997,** *3,* 99.
49. Smith, V.; Lehn, J.-M. *Chem. Comm.* **1996,** 2733.
50. Cambell, V. E.; De Hatten, X.; Delsuc, N.; Kauffmann, B.; Huc, I.; Nitschke, J. R. *Nature Chemistry* **2010,** *2010,* 684-687.
51. Griep, M.; Whitney, S.; Nelson, M.; Viljoen, H. *AIChE J.* **2006,** *52,* 384.
52. Cordona-Serra, S.; Coronado, E.; Gavina, P.; Ponce, J.; Tatay, S. *Chem. Comm.* **2011,** *47,* 8235-8237.
53. Coronado, E.; Galan-Mascaros, J. R.; Gavina, P.; Romero, F. M.; Tatay, S. *Inorg. Chem.* **2008,** *47,* 5197-5203.

5 CONCLUSION

Herein presented work reported preparation of diverse compounds, architectures and functional systems which all shared common element in the coordination properties of imines. The template effect is universal and was used to assemble grid and helical architectures, as well as the driving force of equilibrium changes in complex imine mixtures.

Even though our goal to assemble large array of grids was not reached, it was still possible to obtain several interesting derivatives of bishydrazone-based grids. The grid **GR67Zn** containing eight aldehyde units is an example of such compound which offers potential for future research. The aldehydes could be interconnected via imine, in order to obtain 2D grid arrays. Furthermore, the eight functional groups are appealing for potential multivalency studies. Additionally, the interconversion between grid and helicate could be applied in studies of molecular motion.

The other molecular grids prepared along the way were used to probe overlooked photophysical properties of bishydrazone grids. Interestingly, from all tested Zn(II) grids the most basic one **GR62** demonstrated the best photophysical properties and relatively high quantum yield of ~60%.

In our attempt to prepare *grid of grids* array we serendipitously obtained several folded grids of general formula $[\mathbf{L_2Zn_4}]^{8+}$. In order to take advantage of the directionality of their functionalization the aldehyde-functionalized folded grids **GR72Zn** and **GR72BZn** were prepared. The dynamic combinatorial assembly of the *grid of grids* will be one of the future tasks.

The search for a universal building block for binuclear helicates yielded compound **HEL9** which can be easily tuned to provide ligands for the complexation of both octahedral and tetrahedral cations. Compared to other compounds tested in this study, **HEL9** slectively formed either double or triple helicates, according to the amine/hydrazone and metal used.

The same approach was undertaken also in the case of triple helicates. As a result, several interesting structures were obtained. The trinuclear helicates $\mathbf{(MAF10)_2Zn_3}$ and $\mathbf{(AS53)_2Zn_2Cu}$ could be used for extension of previously reported study on information storage in the oligo-

bypiridine and oligo-terpiridine strands. Both the circular helicate **(AS53)$_4$Zn$_6$,** which showed two different coordination modes, and the coordination polymer **(CN13)Pb** with its head-to-tail formation, provided interesting and unexpected structural coordination modes which will be further exploited and studied in the development of this project.

Two DCLs were investigated during this work. Two different equilibrium distributions of constituents characterizing different constitutional states (Zn-DCL and Cu-DCL) were reached according the applied metal cation (stimulus). When the metal cation was removed, the system exhibited long re-equilibration time at room temperature, allowing it to retain the related metal-free states, i.e. the information induced by metal-training. These out-of-equilibrium states allow for fast re-complexation/detection of the metal effector, as the DCL is already in the pre-prepared state. Repeated introduction of the other orthogonal effector/metal cation forced the distribution of the constituents to adapt for the recognition of this other effector (re-training). Finally, subjecting an out-of-equilibrium informed distribution to equilibrating conditions leads to the restoration of the initial equilibrium thus erasing any information about metal cation stored in the DCL's distribution.

The versatility of a DCL was also demonstrated by probing it with a mixture of effectors, i.e. the ratio between Zn and Cu cations was directly reflected in the ratio between two competing antagonists. Herein, the results could be summarized into several points: a) increasing the complexity of the system can lead to a more selective output through dynamic competition; b) agonist/antagonist competition gives rise to a process that may be described as dynamic ratiometry, directly relating the ratio of antagonists to the ratio of two different effectors (here the Cu(I)/Zn(II) ratio) using a simple calibration curve; c) finally, the full DCL, i.e. the system of higher complexity, is required for the concerted operation of both pairs of agonists manifested by subtle but precise adjustment to external influences.

6 EXPERIMENTAL PART

Instrumentation

NMR spectra were recorded on Bruker Avance 400 (400.14 MHz for ^{1}H and 100.62 MHz for ^{13}C), Bruker Avance III plus 400 (400.34 MHz for ^{1}H and 100.67 MHz for ^{13}C), and Bruker Avance III 600 (600.13 MHz for ^{1}H and 150.90 MHz for ^{13}C) NMR spectrometers. All the collected spectra were referenced on residual solvent signal according to Nudelman et al.[*]

Mass spectra were obtained on Bruker MicroTOF and HRMS on Bruker MicroTOF-Q, both with electrospray ionization. Nominal precision of the HRMS analysis is 10 ppm.

UV-VIS spectra were recorded on a JASCO V670 dual beam Spectrophotometer.

Elemental analysis was performed at the Service de Microanalyse, University of Strasbourg at ThermoFisher Scientific Flash 200 with absolute precision of 0.3 %.
Deuterated solvents were purchased from EurisoTOP and used without further purification.

Reagents and solvents were purchased from Sigma-Aldrich, Alfa Aesar, and STREM and were used without further purification.

Melting points were measured on a Buchi Melting Point B-540 apparatus and temperature data are uncorrected.

X ray crystallography was performed at the Service de Radiocrystallographie, University of Strasbourg and by Dr. O. Fuhr and Prof. D. Fenske at Karlsruhe institute of Technology.

At University of Strasbourg crystallographic data were collected on a Bruker Kappa Apex II diffractometer using graphite-monochromated Mo-Ka radiation (λ = 0.71073 Å). Note that the structures presented here have not yet been refined to publication standards.

*Gottlieb, H. E.; Kotlyar, V.; Nudelman, A. *J. Org. Chem.*, 1997, **62** (21), 7512-7515.

General Procedures

General methods for preparation of imines and acylhydrazones:

1.05 eq. of aldehyde (0.39 mmol) and 1 eq. of amine or acylhydrazide (0.37 mmol) were weighted in a round bottom flask equipped with a stirrer. After addition of ethanol, the mixture was heated to reflux overnight. Analytically clean product precipitated from the reaction mixture upon cooling. In cases where the product did not precipitate itself, the ethanol was evaporated, petroleum ether was added and the solution was sonicated until the desired product precipitated. If needed, a recrystallization from ethanol was done to purify obtained constituents. In cases where the procedure diverges from the general one, the modified procedure is indicated.

Standard procedure for alkylation of aliphatic alcohols:

A given aliphatic alcohol (1 eq. of -CH_2OH, 12 mmol) was dissolved in dry THF (25 ml) and NaH (2eq per -CH_2OH, 24 mmol) was added to the solution. After 15 min. of stirring a required alkyl reagent (1 eq. per -CH_2OH, e.g.: 2-chloro-5-chloromethyl-pyridine, 12 mmol) was added to the reaction mixture, which was subsequently stirred for 12-15 h at room temperature. The mixture was then poured to water and extracted 3x with dichloromethane. The organic phases were collected, evaporated and crude product purified by flash chromatography on alumina (DCM/Petrol ether gradient 1:2 -2:1) or silica (EtOAc/Petrol ether gradient 4:1 to 2:1) were performed.

Standard procedure for alkylation of aromatic alcohols:

A given aromatic alcohol (1 eq. of ArOH or PyOH, 6.2 mmol), required alkylating reagent (1 eq. per -CH_2OH, 6.2 mmol) and K_2CO_3 (4 eq. per -CH_2OH, 24.8 mmol) were dissolved in dry DMF (20 ml) and resulting mixture was heated at 70 °C for 24 h. During this time the reaction mixture changed colour from orange to dark brown. The solvent was then evaporated and crude product suspended in the hot water, filtered, suspended in methanol (r.t) and filtered. Repeating the cycle two times it was possible to purify most of the aromatic alkylated compounds. In cases, where the compound was soluble in methanol or the purity was not satisfactory a chromatographic purification on silica was done (EtOAc/Petrol ether gradient 1:2 -2:1).

Standard procedure for the preparation of hydrazine reagents:

The given halopyridine was dissolved in large excess of pure Methyl hydrazine (2 ml per 100 mg Pyr-X). The resulting solution was refluxed for 4-8 h. After that, the methyl hydrazine was taken away by high vacuum. The crude product was then taken in CH_2Cl_2 and solid K_2CO_3 was added. The suspension was shortly stirred and filtered over the wool. Subsequently, two rounds of suspension and filtration were repeated. Evaporation of the CH_2Cl_2 provided crude hydrazino derivatives which were used directly without further purification. In cases when hydrazine derivative precipitated from the reaction mixture upon cooling, this precipitate was filtred off and washed on the sinter glass with saturated aqueous solution of $NaHCO_3$. Such obtained hydrazines were of analytical purity.

Standard hydrazone formation (Formation of the bishydrazone grid ligand):

The 1 eq. of dialdehyde **GR4** (2-Phenyl-4,6-pyrimidinedicarboxaldehyde, 180 mg, 0.85 mmol) was added to the round bottom flask and dissolved in ethanol (30 ml). Then the hydrazine reagent was added (2.1eq., 219 mg, 1.78 mmol) and the resulting reaction mixture was heated at reflux (80 °C) for 12h. In special cases of hydrazones or aldehydes with very low solubility, the mixture was refluxed up to 48 h. After that the solution was allowed to cool to room temperature and precipitated product was collected by the filtration, washed with ethanol and used without further purification. The same procedure was applied also in reverse case when starting from dihydrazine **GR4B**.

Standard ester deprotection procedure:

The given carboxylic ester was added into the mixture of water/ethanol 1:1 with 20x weight of KOH or NaOH. This reaction mixture was then refluxed for 24-48 h and concentrated on vacuo by careful evaporation of ethanol. The precipitated product was filtered off and repeatedly washed with distilled water until the pH of rinsed water reached 7. The same procedure was used in some case to successfully hydrolyse even amide group. The yield was usually close to quantitative.

Standard procedure for grid formation:

The weighted amount of prepared ligand (1 eq., **GR6B**, 3 mg, $7.1x10^{-6}$ mol) was introduced into the NMR tube. In cases of regular grids 1 eq. of the metal cation was added ($Zn(OTf)_2$, 2.55 mg, $7.1x10^{-6}$ mol). The grid of grids then requires 2 eq. of metal cation. The metal was usually added in the form of acetonitrile solution of given concentration (0.06 M). Then the acetonitrile was filled up to 0.5 ml, the tube closed and solution heated at 70 °C for 3-24 h.

Standard procedure for Dess-Marten oxidation:

The aliphatic alcohol derivative (1 eq. of $-CH_2OH$, 0.18 mmol) and Dess-Marten periodinane (3 eq. per $-CH_2OH$, 0.54 mmol) were put into a round bottom flask. The flask was equipped with septum and three rounds of classic Schlenk evacuation and Argon/Nitrogen re-filling was done. Then dry CH_2Cl_2 (10 ml) was added through septum by syringe. The reaction mixture was stirred for 3-12h depending on the solubility of the starting alcohol in CH_2Cl_2. After that period, the saturated solutions of $Na_2S_2O_3$ (5 ml) and $NaHCO_3$ (5 ml) were added. The reaction mixture was than vigorously stirred for 12 h. The mixture was then filtered through the fine sinter glass (size 3, 4). Collected product was washed with large amount of water. The purity of obtained ligands was >90 % and they were used as such without further purification. Another crop of less pure product could be obtained by evaporation of the dichloromethane phase after the filtration. However, the various purification methods of this crude crop so far did not lead to the analytically pure compound.

Standard procedure for the decoration of octa-aldehyde grid GR67Zn:

The grid GR67Zn was assembled according the standard procedure for grid formation. Then its acetonitrile solution was taken from the NMR by Pasteur pipet and filtered through wool stucked in the neck of another one. It was filtered directly to the clean NMR tube. To this filtered sample a solution of given monoamine amine/hydrazine/acylhydrazide (2 eq. per ligand!!!) or diamine (1 eq. per ligand!!!) in acetonitrile was added. NMR tube was closed and heated for 2-12 h at 60 °C according the formation speed and then studied by the ^{1}H NMR.

Standard procedure for preparation Cu(OTf).

The $Cu(OTf)_2$ (28 mg, $7.75x10^{-5}$ mol) was dissolved in 0.2 ml of CD_3CN in small vial providing blue coloured solution. Next, excess of powder Cu^0 (50 mg) was added to the solution after brief shaking the initial blue colour disappeared indicating formation of Cu(I)(OTf). This solution was found to be stable over period of several weeks and was used for all Cu(I) complexes.

6.1 Training a Constitutional Dynamic Network

6.1.1 Compounds:

Synthesis of 6-Phenylpyridine-2-carbaldehyde*:

To a suspension of 6-bromo-2-pyridinecarboxaldehyde (2.05 g, 11.0 mmol) and $Pd(PPh_3)_4$ (0.30 g, 0.3 mmol) in toluene (20 mL), aqueous 2.0 M Na_2CO_3 (10 mL) and phenylboronic acid (2.0 g, 16.5 mmol) dissolved in methanol (8 mL) were subsequently added. After refluxing the suspension for 10 h, a 2.0 M aqueous solution of Na_2CO_3 (40 mL) and CH_2Cl_2 (100 mL) were added to the solution after cooling to room temperature. The aqueous phase was separated and extracted with CH_2Cl_2 (25 mL), and the combined organic extracts were dried overnight using Na_2SO_4. Further purification by a silica gel column chromatography gave the title compound. Pale yellow oil, yield 68 %. TLC R_f = 0.39 (hexane : ethyl acetate = 5:1).

^{1}H NMR (400 MHz, CD_3CN): δ 10.11 (d, J = 0.78, 1H); 8.18-8.15 (m, 2H); 8.13 (dd, J=1.2, J=7.8, 1H); 8.05 (dt, 1H); 7.89 (dd, J = 1.2, J = 7.4, 1H); 7.58-7.49 (m, 3H).

*Arai, T.; Suzuki, K.; *Synlett*, 2009, **19**, 3167-3170.

Synthesis of [Et$_4$N]$_2$EDTAH$_2$ *

Bis-(tetraethylammonium) dihydroethylenediaminetetraacetate ([Et$_4$N]$_2$EDTAH$_2$) was

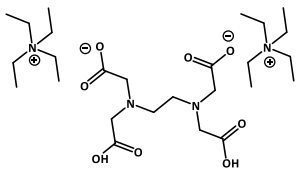

prepared by addition of 1 eq. of EDTA to the solution of 2eq of tetraethylammonium hydroxide in the ethanol/water (1/1) mixture. The mixture was stirred at room temperature until the EDTA was dissolved. The solution was then filtered through the wool and evaporated under reduced pressure to obtain a colorless syrup. This syrup was then dried in the desiccator over P_2O_5 affording quantitative yield of [Et$_4$N]$_2$EDTAH$_2$ as an off-white solid which was directly used without further purification. The compound is strongly hygroscopic.

^{1}H NMR (400MHz, CD_3CN): δ 3.34 (s, 8H); 3.19 (q, J=7.3, 16H); 2.85 (s, 4H); 1.21 (tt, 24H);

^{13}C NMR (100MHz, CD_3CN): δ 174.73; 59.78; 52.097;52.067; 52.036; 51.06; 6.74.

ESI-MS: 551.4032, calc. 551.4014 ($M+H^+$).

* Moon, S. C. *Review of Polarography (Japan)*, 1971, **17**, 94.

E-27AB: Compound was prepared by mixing 6-methyl-2-pyridinecarboxaldehyde and

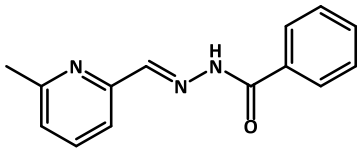

benzhydrazide (1:1) in ethanol. The mixture was left standing at room temperature for 12h. Then, the solvent was evaporated to provide oily crude product. Hexane or petroleum ether were added to the oil and the mixture was sonicated until the precipitation of white product. Such product always comprises both E (~90%) and Z (~10%) isomers. Pure E was obtained through recrystallization from cyclohexane with few drops of ethanol at lower temperature (5°C).

^{1}H NMR (400MHz, CD_3CN): δ 10.33 (brs, 1H); 8.26 (brs, 1H); 7.90 (d, J = 7.0, 2H); 7.80(brd, 1H); 7.69 (t, J = 7.8, 1H); 7.61 (t, J = 7.3, 1H); 7.53 (t, J = 7.4, 2H); 7.23 (d, J = 7.6, 1H); 2.53 (s, 3H);

^{13}C NMR (100MHz, CD_3CN): δ 164.64; 159.50; 153.72; 149.30; 137.95; 134.30; 133.04; 129.62; 128.54; 124.75; 24.39;

ESI-MS: 240.1135, Calc. 240.1131 ($M+H^+$);

M.p.: 151-152°C

27AB': This compound was prepared by mixing 2eq. of 6-methyl-2-pyridinecarboxaldehyde with 27B'q. of 2-(2-Aminoethoxy)ethylamine in acetonitrile. This compound was never isolated and all the analysis were done on acetonitrile solution. Fresh sample was prepared in standard NMR tube prior to every new experiment.

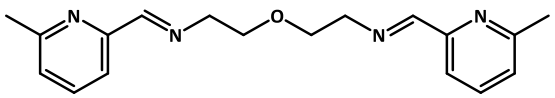

^{1}H NMR (400MHz, CD_3CN): δ 8.23 (s, 1H); 7.67 (d, J= 7.4, 1H); 7.62 (t, J = 7.6, 1H); 7.22 (d, J = 7.0, 1H); 3.75 (m, 4H); 2.49 (s, 3H);

^{13}C NMR (100MHz, CD_3CN): δ 164.42; 159.14; 154.99; 137.78; 125.14; 118.58; 70.86; 61.43; 24.36;

ESI-MS: 311.1896, Calc. 311.1186 ($M+H^+$);

27A'B = 35A'B: This compound was prepared according to general procedure.

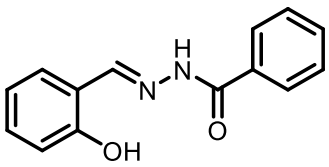

^{1}H NMR (400MHz, CD_3CN): δ 11.57 (s, 1H); 10.39 (s, 1H); 8.45 (s, 1H); 7.91 (d, J = 7.3, 2H); 7.62 (m, 1H); 7.54 (m, 2H); 7.38 (dd, J = 1.5, J = 7.9, 1H); 7.34 (m, 1H); 6.96 (m, 1H);

^{13}C NMR (100MHz, CD_3CN): δ 164.16; 159.35; 150.80; 133.58; 133.18; 132.56; 132.04; 129.65; 128.48; 120.34; 118.85; 117.63

ESI-MS: 241.0976, Calc. 241.0972 ($M+H^+$);

Elemental Analysis**:** (%): N 11.62, C 69.82, H 4.92; (Calc.: N 11.16, C 69.99, H 5.03)

M.p.: 180.3-181.9°C.

27A'B': This compound was prepared by mixing 2eq. of salicylaldehyde with 27B'q. of 2-(2-

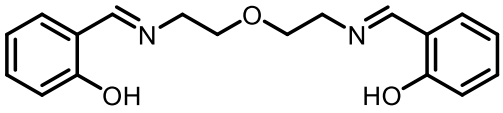

Aminoethoxy)ethylamine in acetonitrile. This compound was never isolated and all the analysis were done on acetonitrile solution and were in accordance with previous reported preparation[3]. Fresh sample was prepared in standard NMR tube prior to every new experiment.

^{1}H NMR (400MHz, CD_3CN): δ 13.46 (s, 1H); 8.38 (s, 1H); 7.29 (m, 1H); 7.23 (dd, J = 1.6, J = 7.8, 1H); 6.84 (m, 2H); 3.74 (m, 4H);

^{13}C NMR (100MHz, CD_3CN): δ 167.86; 162.07; 133.14; 132.60; 119.51; 118.31; 117.50; 70.84; 59.44

ESI-MS: 313.1556, Calc. 313.1547 ($M+H^+$);

*Wu, H.; Pan, G.; Bai, Y.; Zhang, Y.; Wang, H.; Shi, F.; Wang, X.; Kong, J. J. Photochem. Photobiol. B., 2014, **135**, 33-43

Cu(27AB'): 1 eq. of a Cu(I)(OTf) solution of known concentration (prepared via

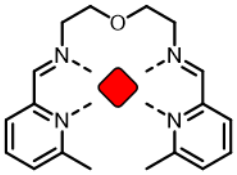

synproportionation of $Cu(II)(OTf)_2$ and Cu(0) in CD_3CN) was added to 1 eq. of 27AB'. The solution immediately turned dark, but to ensure full complexation the mixture was left to stand 30min at room temperature (~23 °C). The complex was never isolated, all the present experiments and analysis were done in acetonitrile solution. The complex was always freshly prepared prior to every new experiment.

^{1}H NMR (400MHz, CD_3CN): δ 12.74 (brs, 1H); 8.94 (s, 1H); 8.17 (t, J = 7.9, 1H); 7.96 (m, 3H); 7.44 (t, J = 7.0, 1H); 7.60 (d, J= 7.9, 1H); 7.56 (t, J = 7.9, 2H), 2.22 (s, 3H)
^{13}C NMR (100MHz, CD_3CN): 163.17; 159.00; 151.26; 139.26; 128.76; 125.29; 73.95; 60.73; 25.09

ESI-MS: 373.10, Calc. 373.11 (LM^+);

Zn(27AB)$_2$: 0.5 eq. of $Zn(OTf)_2$ in a form of acetonitrile solution was added to 1 eq. of **50AB**

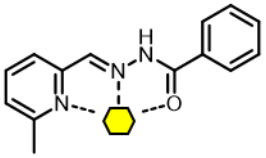

(regardless the isomer) and was heated for 12 h at 70 °C. The complex was always freshly prepared prior to every new experiment. The complex was never isolated, all the present experiments and analysis were done in acetonitrile solution.

^{1}H NMR (400MHz, CD_3CN): δ 12.74 (brs, 1H); 8.94 (s, 1H); 8.17 (t, J = 7.9, 1H); 7.96 (m, 3H); 7.44 (t, J = 7.0, 1H); 7.60 (d, J= 7.9, 1H); 7.56 (t, J = 7.9, 2H)

^{13}C NMR (100MHz, CD_3CN): 168.99, 162.02, 146.54, 145.48, 143.25, 135.91, 131.033, 130.23, 129.37, 127.49, 23.97

ESI-MS: $C_{28}H_{25}N_6O_2Zn$ 541.1343, Calc. 541.1325 (L_2M^+);

Z-35AB = Z-50AB: This compound was prepared and isolated according the general

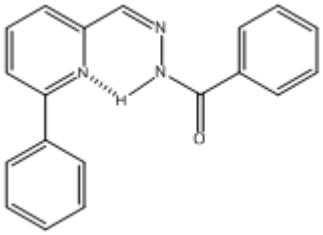

procedure. Upon cooling to room temperature, white amorphous precipitate formed. This precipitate was 95 % pure Z isomer of acylhydrazone and was used as such in all experiments herein described.

^{1}H NMR (400MHz, CD_3CN): δ 15.31 (brs, 1H); 8.08 (t, J = 8.0, 1H); 7.87-7.80 (m, 5H); 7.65-7.51 (m, 4H); 7.45 (t, J = 7.2, 2H); 7.36 (t, J = 7.6, 2H);

^{13}C NMR (100MHz, CD_3CN): δ 165.35; 158.15; 153.46; 140.16; 139.96; 139.64; 134.61; 132.97; 130.62; 130.04; 129.77; 128.64; 128.54 ; 125.97; 123.40;

ESI-MS: 324.1089, Calc. 324.1107, ($M+Na^+$);

Elemental Analysis**:** $C_{19}H_{15}N_3O$ (%) : N 13.92, C 75.84, H 5.09 (Calc.: N 13.94, C 75.74, H 5.02)

M.p.: 153-154.8°C.

E-35AB = E -50AB: The Zn cation templates the formation of the E isomer as it has more suitable conformation for the metal complexation. Therefore, the fast removal of Zn(II) from the complex by addition of $(Et_4N)_2EDTAH_2$ (**27B'** compared to Zn(II)) at room temperature leaves the E isomer free in the solution. The subsequent heating for 24 h at 70 °C provides approximately the same distribution of isomers as described above (Z = 62 %, E = 38 %) and <5 % of hydrolysis.

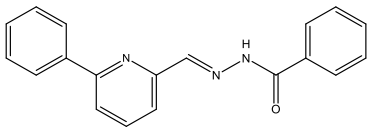

The second approach is based on the direct reaction of aldehyde **50A** with benzhydrazide **50B** in acetonitrile at room temperature in a presence of *p*-toluidine (~10 %) which acts as a nucleophilic catalyst. The uncatalyzed formation of acylhydrazone **50AB** in acetonitrile is very slow even at elevated temperature, but the presence of catalyst allows to obtain the E isomer in 12h at room temperature in acetonitrile. In this case however, traces of Z isomer were still observed in the reaction mixture.

It is needed to mention that isomer E-**50AB** was never isolated as a pure compound. All herein described studies and transformations were done in acetonitrile solution obtained through the complexation/decomplexation method.

^{1}H NMR (400MHz, CD_3CN): δ 10.64 (brs, 1H); 8.43 (brs, 1H); 8.09 (d, J=6.8, 2H); 7.98 (brm, 1H); 7.93 (d, J=7.2, 2H); 7.88 (t, J=8.3, 2H); 7.61 (t, J=7.3, 1H); 7.55-7.44 (m, 5H);

^{13}C NMR (100MHz, CD_3CN): δ 157.78; 154.40; 149.25; 139.71; 138.75; 134.31; 133.08; 130.26; 130.05; 129.80; 129.65; 128.61; 127.76; 121.89; 119.81;

35A'B': This compound was prepared according the general procedure as off-yellow powder.

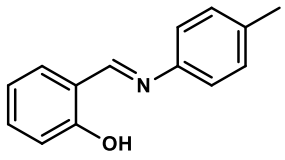

^{1}H NMR (400MHz, CD_3CN): δ 13.33 (s, 1H); 8.80 (s, 1H); 7.52 (dd, J = 1.7, J = 7.6, 1H); 7.37-7.42 (m, 1H); 7.31-7.26 (m, 4H); 6.99-6.95 (m, 2H);

35AB' = 50AB': This compound was prepared according the general procedure as off-yellow powder.

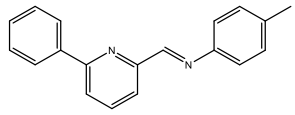

^{1}H NMR (400MHz, CD_3CN): δ 8.69 (s, 1H); 8.15-8.11 (m, 3H); 7.97-7.95 (m, 2H); 7.55-7.45 (m, 3H); 7.27 (s, 4H); 2.38 (s, 3H);

^{13}C NMR (100MHz, CD_3CN): δ 161.25; 157.84; 155.76; 149,44; 139.73; 138.84; 137.89; 130.30; 130.30; 129.83; 127.79; 122.73; 122.12; 120.59; 21.06;

ESI-MS: 273.1353, calc. 273.1386 ($M+H^+$);

Elemental Analysis: $C_{19}H_{16}N_2$ (%) : N 10.35, C 84.13, H 5.93 (Calc.: N 10.29, C 83.79, H 5.92)

M.p.: 109-110°C.

Zn(35AB)$_2$ = Zn(50AB)$_2$: 0.5 eq. of $Zn(OTf)_2$ in a form of acetonitrile solution was added to 1 eq. of **27AB** (regardless the isomer) and was heated for 12 h at 70 °C. The complex was always freshly prepared prior to every new experiment. The complex was never isolated, all the present experiments and analysis were done in acetonitrile solution.

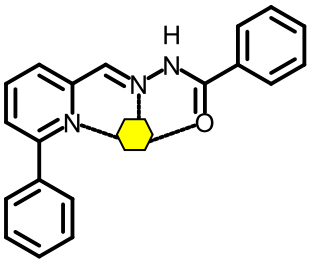

^{1}H NMR (400MHz, CD_3CN): δ 12.50 (brs, 1H); 8.33 (s, 1H); 8.22 (t, J = 7.8, 1H); 7.99 (dd, J = 1.3, J = 8.5, 2H); 7.78-7.74 (m, 2H); 7.69 (dd, J = 0.8, J = 7.9, 1H); 7.61 (t, J = 7.9, 2H); 7.54 (t, J=7.6, 1H); 7.28 (t, J = 7.8, 2H); 6.98 (d, J = 7.2, 2H);

^{13}C NMR (100MHz, CD_3CN): δ 168.77; 161.71; 146.86; 143.81; 143.19; 139.17; 136.02; 131.47; 130.28; 130.13; 129.94; 129.42; 128.98; 128.42; 128.16;

HR ESI-MS: 665.1714, calc. 665.1638 (L_2HZn^+); 815.1290, calc. 815.1236 ($[L_2H_2ZnOTf]^+$).

Cu(35AB')$_2$ = Cu(50AB')$_2$: 1 eq. of Cu(I)(OTf) solution of known concentration in CD_3CN was added to 2 eq. of **50AB**. The solution immediately turned dark, but to ensure full complexation the mixture was left to stand 1 h at room temperature (~23 °C). The complex was never isolated, all the present experiments and analysis were done in acetonitrile solution. The complex was always freshly prepared prior to every new experiment.

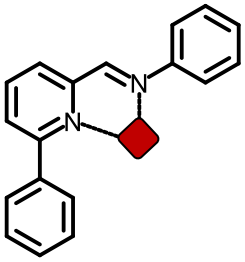

^{1}H NMR (400MHz, CD_3CN): δ 8.99 (s, 1H); 8.05 (t, 1H); 7.87 (d, 1H); 7.76 (d, 1H); 7.49 (br, 2H); 7.41 (d, 2H); 7.22 (d, 3H); 7.17-7.12 (m, 2H); 2.36 (s, 3H);

^{13}C NMR (100MHz, CD_3CN): δ 158.80; 158.48; 152.44; 145.46; 140.58; 139.72; 139.55; 131.14; 130.24; 128.79; 128.37; 127.69; 126.91; 123.41; 21.11

HR ESI-MS: 607.1897, calc. 607.1917 (L_2Cu^+)

50A'B: This compound was prepared according to general procedure as off-white crystalline powder.

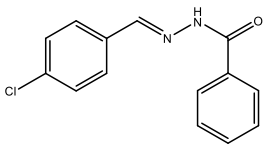

^{1}H NMR (400MHz, CD_3CN): δ 10.30 (brs, 1H); 8.34 (brs, 1H); 7.92-7.9 (m, 2H); 7.78-7.75 (m, 2H); 7.63 (t, J = 7.3, 1H); 7.55 (t, J = 7.6, 2H); 7.49 (d, J = 8.3, 2H);

^{13}C NMR (100MHz, CD_3CN): δ 164.65; 147.39; 136.37; 134.42; 134.29;132.94; 129.96; 129.65;128.50;

ESI-MS: 259.0633, calc. 259.0633 (M+H+)

Elemental Analysis: $C_{14}H_{11}ClN_2O$ (%): N 10.84, C 65.09, H 4.28 (Calc.: N 10.83, C 65.00, H 4.29)

M.p.:175.3-177.1 °C.

50AB': This compound was prepared according the general procedure as off-yellow powder.

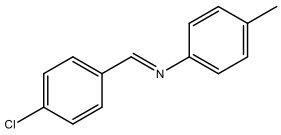

^{1}H NMR (400MHz, CD_3CN): δ 8.54 (s, 1H); 7.89 (d, J = 8.5, 2H); 7.51 (d, J = 8.5, 2H); 7.23 (d, J = 8.5, 2H); 7.16 (d, J = 8.2, 2H); 2.35 (s, 3H);

^{13}C NMR (100MHz, CD_3CN): δ 158.29; 149.02; 136.49; 136.25; 135.38; 129.80; 128.98; 120.88; 20.00;

ESI-MS: 230.0709 (calc. 230.0731, $M+H^+$)

Elemental Analysis: $C_{14}H_{12}ClN$ (%): N 6.15, C 73.27, H 5.26 (Calc.: N 6.10, C 73.20, H 5.27)

M.p.: 126.1-127.1 °C.

6.1.2 Double Training of a Dynamic Covalent Library of imines and acylhydrazones towards two different Effectors

System 27

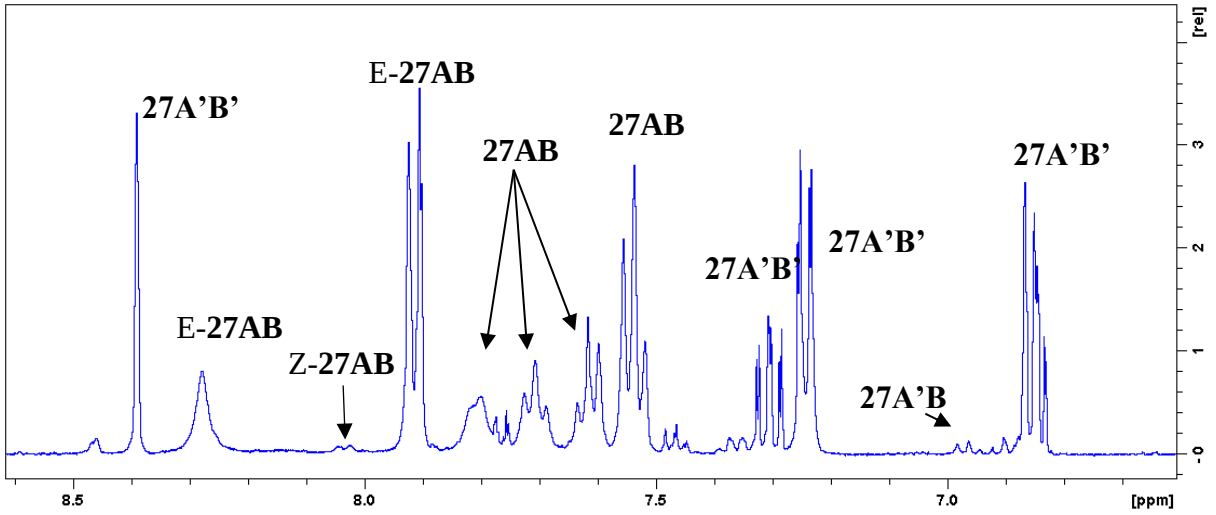

Figure E1.1: Strong bias - Equilibrated mixture of the components **27A**, **27A'**, **27B** and **27B'**. A portion of the 400 MHz ^{1}H NMR spectrum of a mixture of components **27A**, **27A'**, **27B** and **27B'** equilibrated at room temperature (23 °C) for 12 h. The mixture is formed almost exclusively from components **27AB** and **27A'B'**.

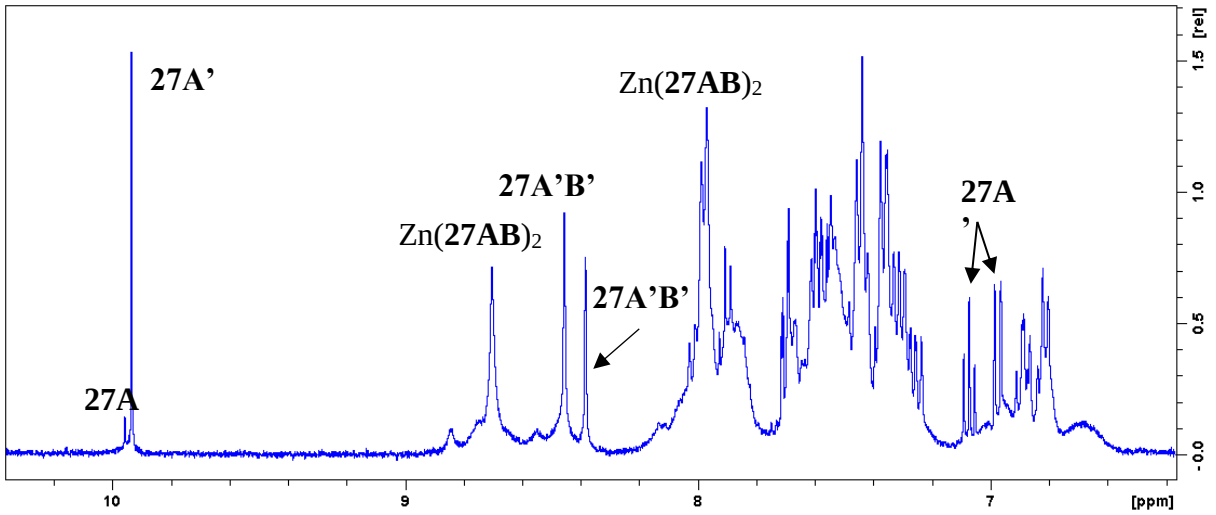

Figure E1.2: Partial destruction - Influence of Zn(II) on a library of **27A**, **27A'**, **27B** and **27B'**. A portion of the 400 MHz ^{1}H NMR spectrum of a mixture of components **27A**, **27A'**, **27B**, **27B** equilibrated in presence of 0.5 eq. $Zn(OTf)_2$ at room temperature (23 °C) for 12 h. There is apparent extensive hydrolysis of **27A'B'** manifested by free salicylaldehyde (**27A'**) and partially hydrolysed constituent **27A'B'** (one free amine group). The acylhydrazone **27AB** is present as a complex $Zn(\mathbf{27AB})_2$.

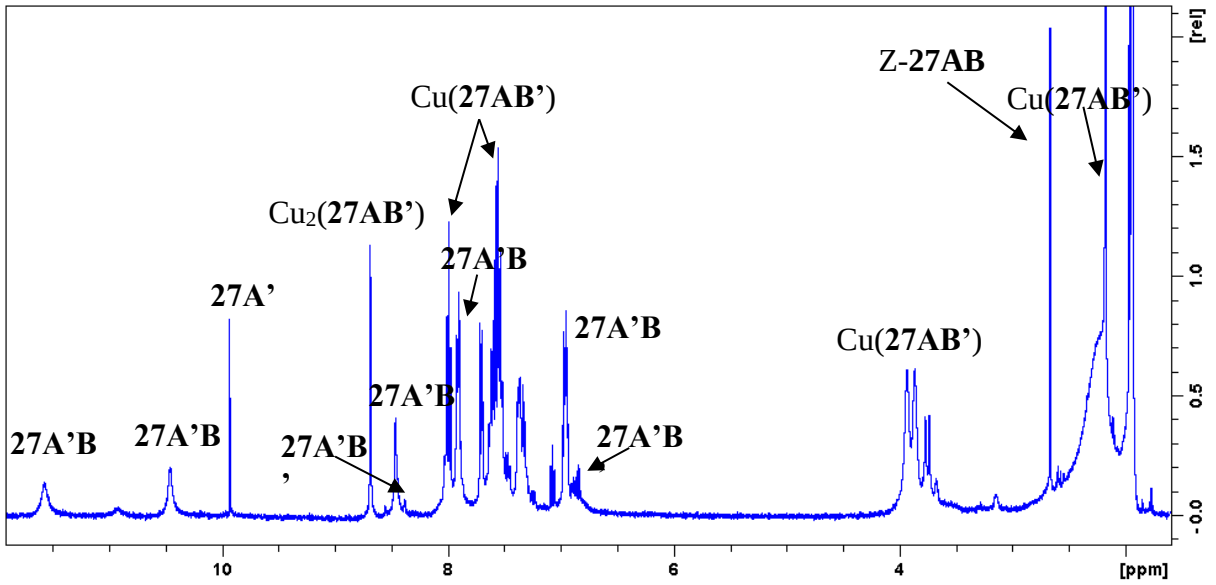

Figure E1.3: Training of the library of **27A**, **27A'**, **27B** and **27B'** on Cu(I). A portion of the 400 MHz 1H NMR spectrum of a mixture of components **27A**, **27A'**, **50B** and **27B'** equilibrated in presence of 0.5 eq. Cu(I)OTf at room temperature (23 °C) for 12 h. The system adapts very well to the Cu(I) cation and amplifies constituents/agonists Cu(**27AB'**) and **27A'B**. The antagonists **27AB** and **27A'B'** are visible as well, nevertheless in considerably smaller amount. (**27AB**/**27AB'**/**27A'B**/**27A'B'**/hydrolysis = **13/38/36/4/10** %)

System 35

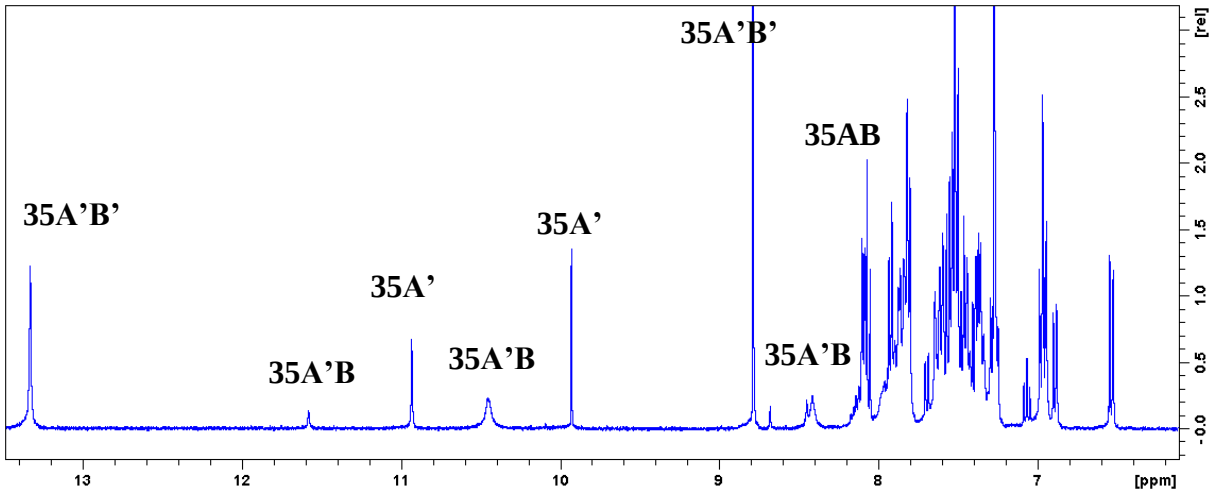

Figure E1.4: Biased distribution - Equilibrated mixture of the components **35A**, **35A'**, **35B** and **35B'**. A portion of the 400 MHz ^{1}H NMR spectrum of an equilibrated mixture of components **35A**, **35A'**, **35B** and **35B'** in absence of any metal cation after 12h at 60°C: Four constituents **35AB**, **35AB'**, **35A'B** and **35A'B'** were obtained with a distribution of **49**/**3**/**2**/**34** % respectively together with 14 % hydrolysis. The values were obtained as an average of three experiments with about ±2 % error.

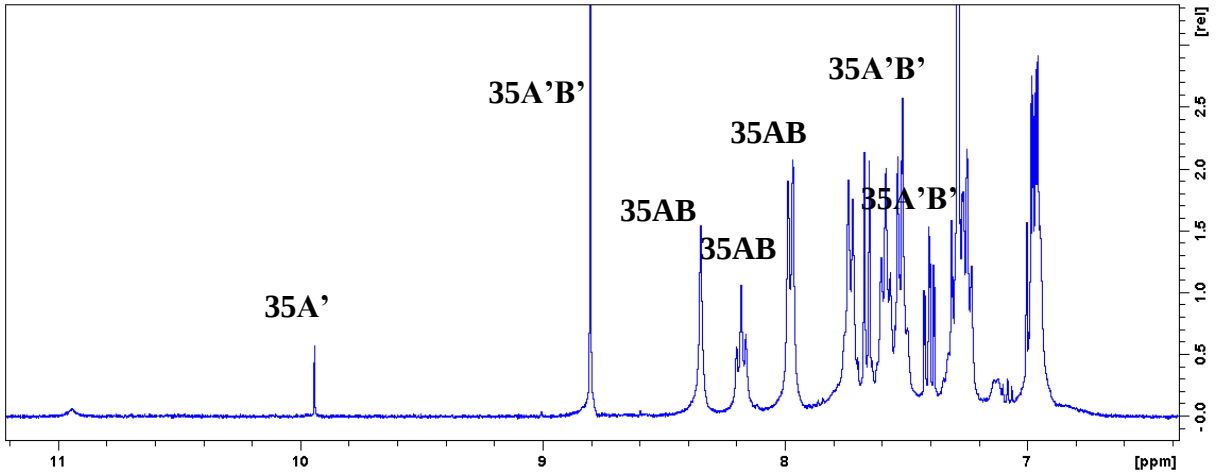

Figure E1.5: Training of the library of **35A**, **35A'**, **35B** and **35B'** on Zn(II). A portion of the 400 MHz ^{1}H NMR spectrum of a mixture of components **35A**, **35A'**, **35B**, **35B** equilibrated in presence of 0.5 eq. $Zn(OTf)_2$ at room temperature (23 °C) for 12 h. The resulting distribution is $Zn(\mathbf{35AB})_2$/**35AB'**/**35A'B**/**35A'B'**/hydrolysis = **49**/**<1**/**<1**/**48**/**3**. The values were obtained as an average of three experiments with about ±2 % error.

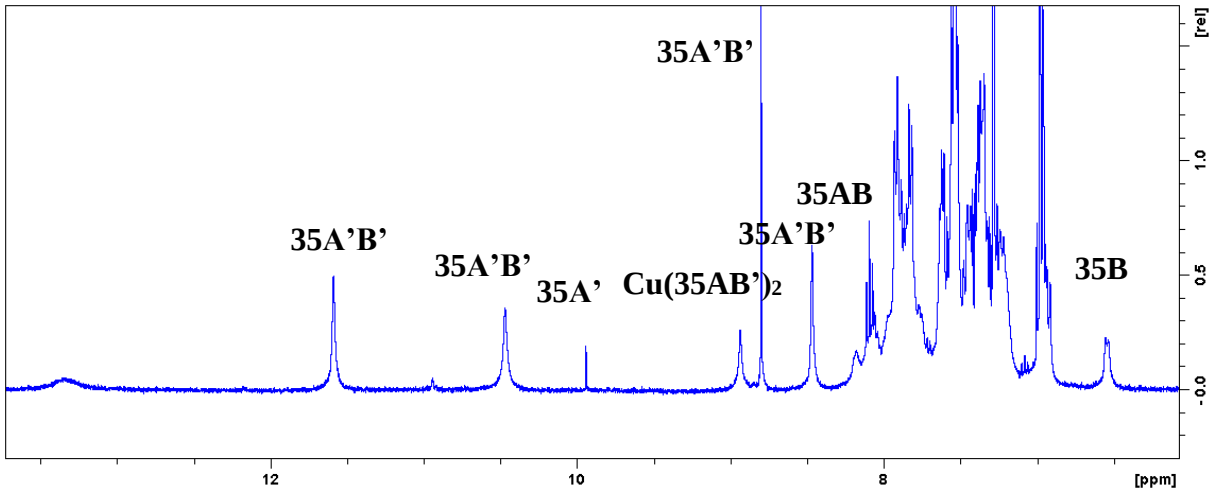

Figure E1.6: Training of the library on Cu(I). A portion of the 400 MHz ^{1}H NMR spectrum of the mixture of components **35A**, **35A'**, **35B** and **35B'** equilibrated in presence of 0.5 eq. of Cu(I)OTf at 60 °C for 12 h. The resulting distribution is **35AB**/Cu(**35AB'**)$_2$/**35A'B**/**35A'B'**/hydrolysis = **25**/**26**/**23**/**23**/**4**. The values were obtained as an average of three experiments with about ±2 % error.

System 50

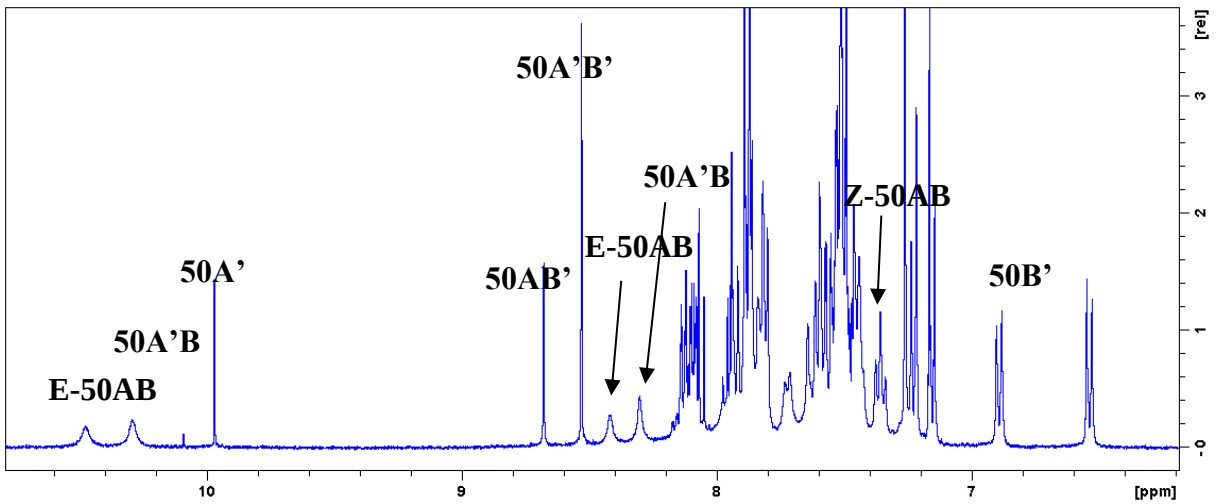

Figure E1.7: Equilibrated mixture of **50A**, **50A'**, **50B** and **50B'**. A portion of the 400 MHz ^{1}H NMR spectrum of an equilibrated mixture of components **50A**, **50A'**, **50B** and **50B'** in absence of any metal cation after 12 h at 60 °C: Four constituents **50AB**, **50AB'**, **50A'B** and **50A'B'** were obtained with a distribution of **35**/**12**/**16**/**23** % respectively together with 14 % hydrolysis. The values were obtained as an average of three experiments with about ±2 % error.

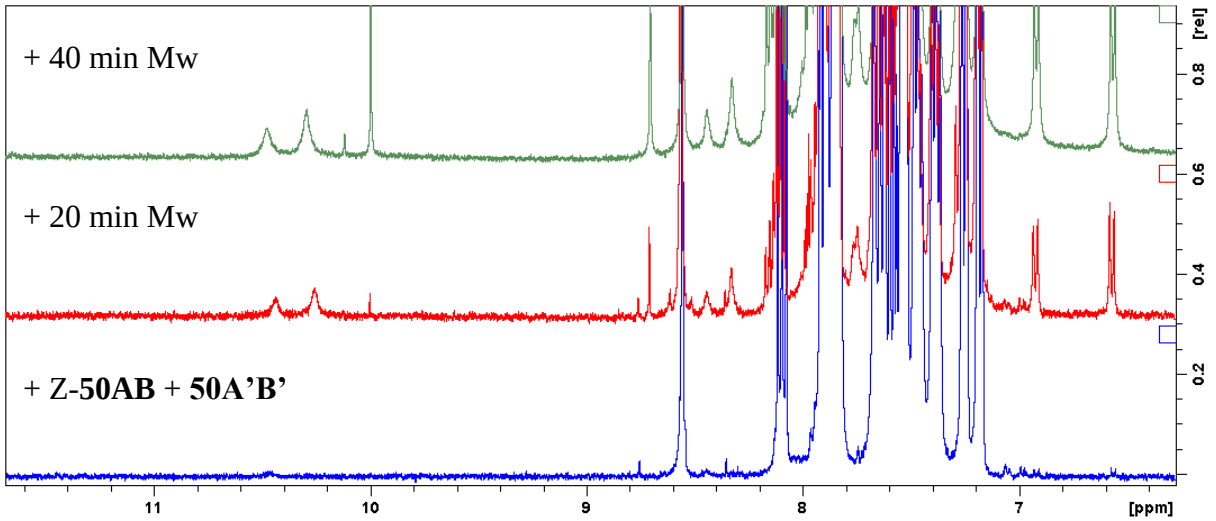

Figure E1.8: Equilibration of the pair of agonists Z-**50AB** and **50A'B'** – Simulation of the erase process. A portion of the 400 MHz ^{1}H NMR spectrum of: 1) Mixture of two preformed agonists Z-**50AB** and **50A'B'**; 2) Spectrum of the same mixture after 20 min of the microwave irradiation (160 °C, 270 W); 3) Spectrum of the same mixture after 40 min of the microwave irradiation (160 °C, 270 W);

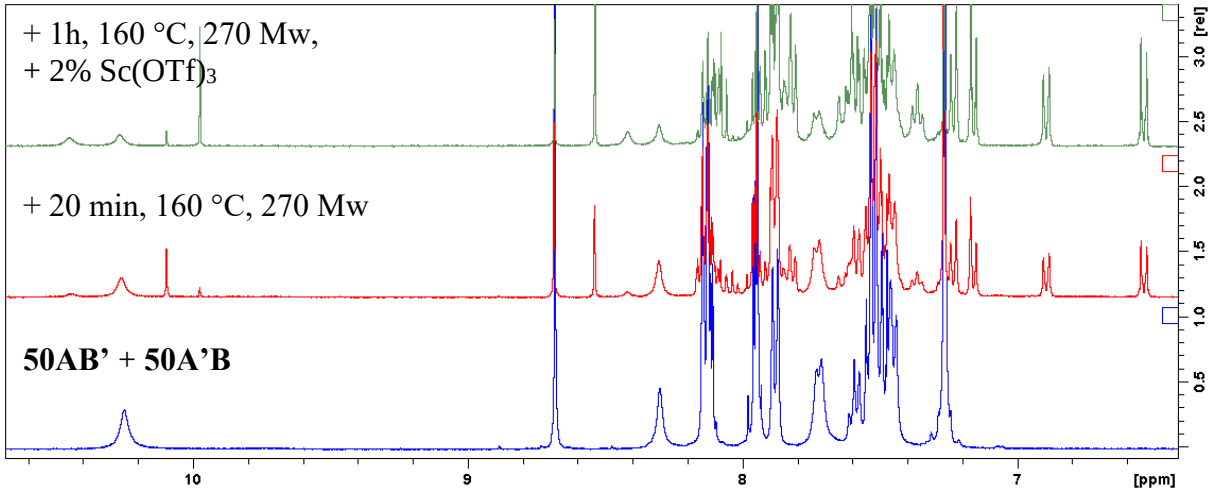

Figure E1.9: Equilibration of the pair of agonists **50AB'** and **50A'B** – Simulation of the erase process. A portion of the 400 MHz ^{1}H NMR spectrum of: 1) Mixture of two preformed agonists Z-**50AB'** and **50A'B**; 2) Spectrum of the same mixture after 20min of the microwave irradiation (160 °C, 270 W); 3) Spectrum of the same mixture after 1h of the microwave irradiation (160 °C, 270 W) in a presence of Sc(III) catalyst (+2 % $Sc(OTf)_3$);

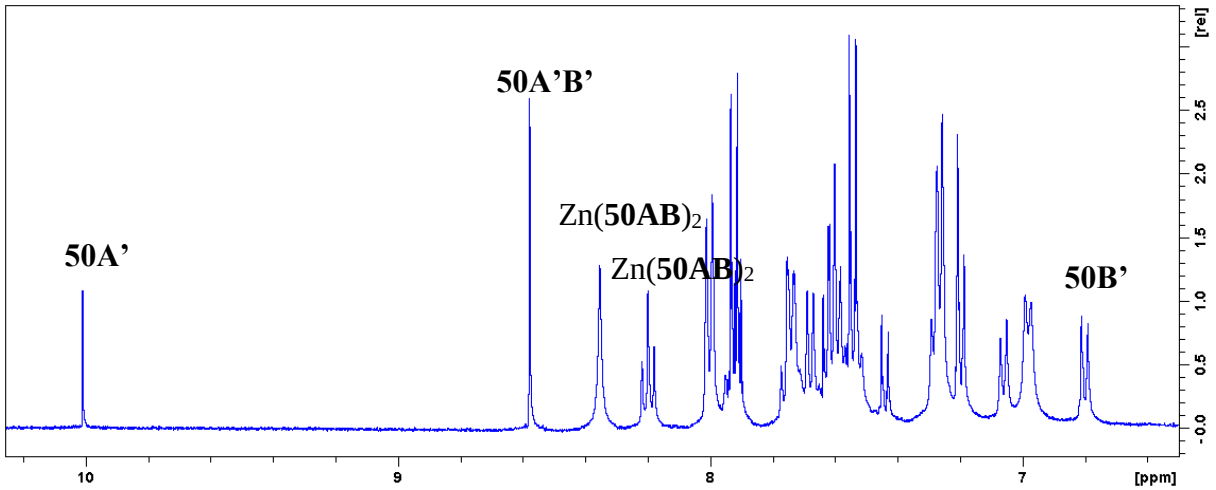

Figure E1.10: Training of the library of **50A**, **50A'**, **50B** and **50B'** on Zn(II). A portion of the 400 MHz ^{1}H NMR spectrum of the equilibrium in the presence of Zn(II). The mixture of components **50A**, **50A'**, **50B** and **50B'** was equillibrated in presence of 0.5 eq. $Zn(OTf)_2$ at 60 °C for 3 h. The resulting distribution is $Zn(\mathbf{50AB})_2$/**50AB'**/**50A'B**/**50A'B'**/hydrolysis = **50**/<**1**/<**1**/**36**/**12**. The values were obtained as an average of three experiments with about ±2 % error.

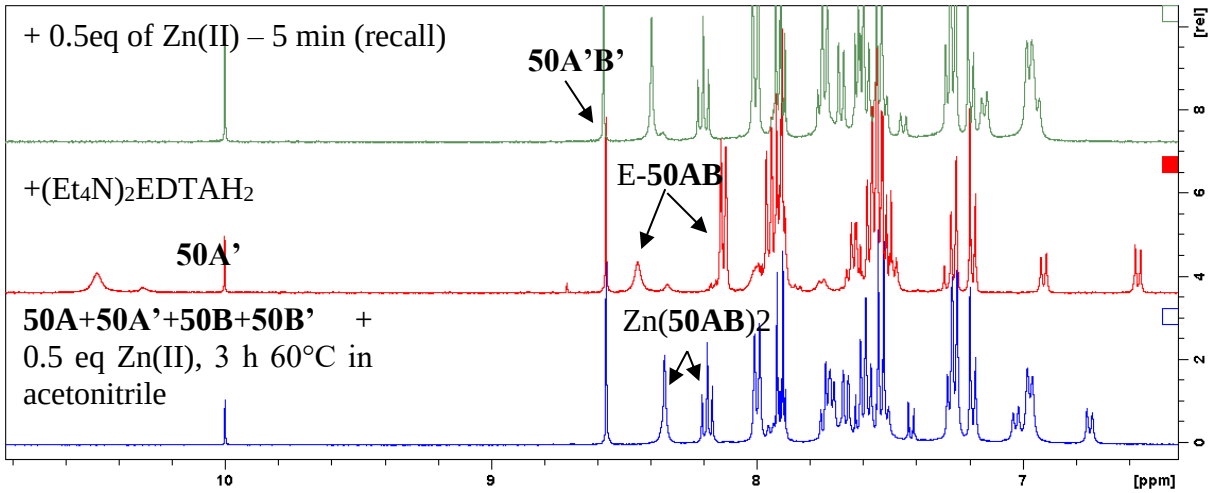

Figure E1.11: Information storage and recall in Zn trained system. A portion of the 400 MHz ^{1}H NMR spectra of the removal of Zn(II) with $(Et_4N)_2EDTAH_2$ and subsequent recall. 1) **Training**: the mixture of components in presence of 0.5 eq. of $Zn(OTf)_2$ at 60 °C for 3 h (*bottom*); 2) **Storage**: removal of Zn(II) with $(Et_4N)_2EDTAH_2$, while the distribution is kept. The resulting distribution is: E-**50AB**/**50AB'**/**50A'B**/**50A'B'**/hydrolysis = **48**/<**4**/<**4**/**35**/**11** (*middle*); 3) **Recall**: the re-addition of Zn(II) resulting in an immediate return to the trained library. The values were obtained as an average of three experiments with about ±5 % error.

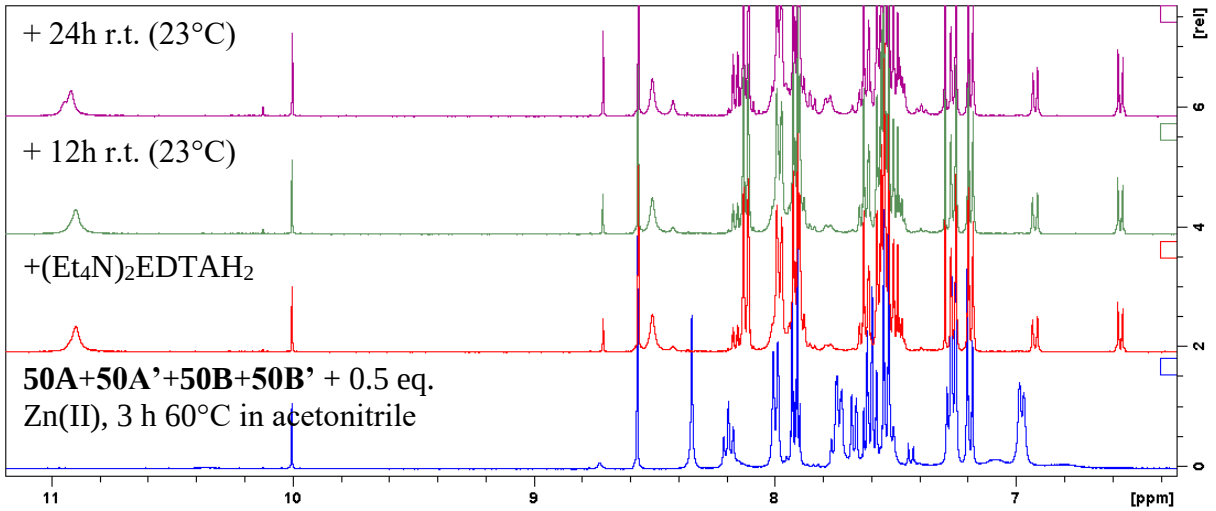

Figure E1.12: Stability study in Zn(II) free out-of-equilibrium system – Time frame of Information storage in Zn trained system Portions of the 400 MHz ^{1}H NMR spectra of the removal of Zn(II) with $(Et_4N)_2EDTAH_2$ and subsequent stability study of the metal free, out-of-equilibrium state. 1) **Training**: the mixture of components in presence of 0.5 eq. of $Zn(OTf)_2$ at 60 °C for 3 h; 2) **Storage**: removal of Zn(II) with $(Et_4N)_2EDTAH_2$, while the distribution is kept. The resulting distribution is: E-**50AB/50AB'/50A'B/50A'B'**/hydrolysis = **48**/<**4**/<**4**/**35**/**11**; 3) **Stability**: After 12 h at room temperature (23 °C) the distribution still does not differ for more than 10 % from the freshly prepared metal free state; 4) After 24 h at room temperature the equilibration process starts to be well visible.

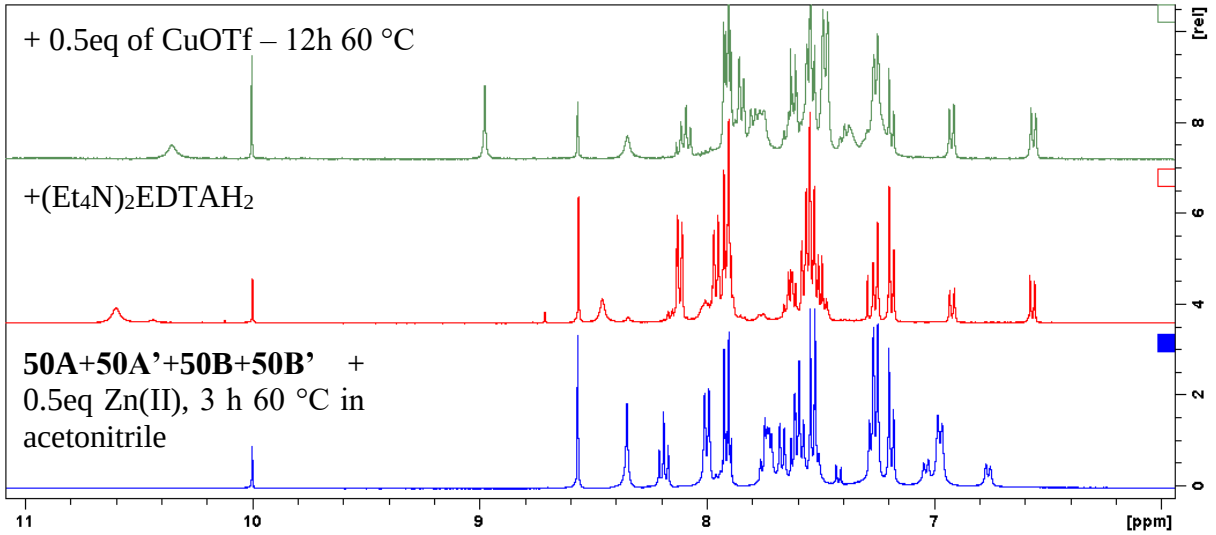

Figure E1.13: Retraining of Zn state to Cu trained state. A portion of the 400 MHz ^{1}H NMR spectra of Zn(II) removal with $(Et_4N)_2EDTAH_2$ and Cu(I) re-training. 1) **Training**: the mixture of components in presence of 0.5 eq. of $Zn(OTf)_2$ at 60 °C for 3 h (*bottom*); 2) **Storage**: removal of Zn(II) with $(Et_4N)_2EDTAH_2$, while the distribution is kept. (*middle*); 3) **Retraining**: the addition of Cu(I) and subsequent heating for 12 h at 60 °C. the system was re-trained and the distribution changed from Zn(II) preferred to Cu(I) preferred system.

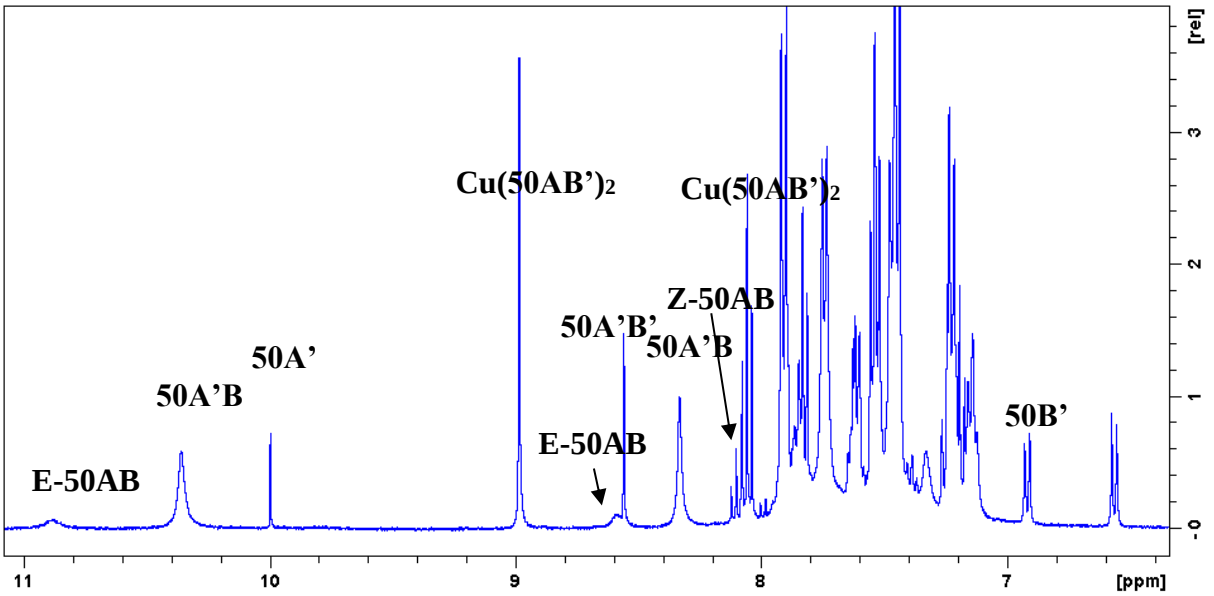

Figure E1.14: Training of the library of **50A**, **50A'**, **50B** and **50B'** on Cu(I). A portion of the 400 MHz ^{1}H NMR spectrum of the mixture of components **50A**, **50A'**, **50B** and **50B'** equilibrated in presence of 0.5 eq. of Cu(I)OTf at 60 °C for 12 h. The resulting distribution is **50AB**/Cu(**50AB'**)$_2$/**50A'B**/**50A'B'**/hydrolysis = **10**/**31**/**32**/**18**/**9 %**. The values were obtained as an average of three experiments with about ±2 % error.

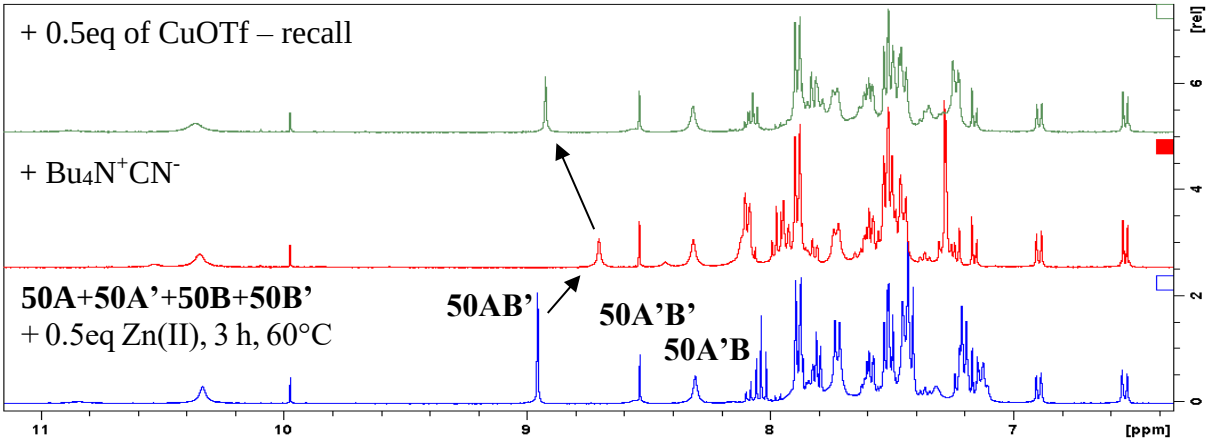

Figure E1.15: Information storage and recall in Cu(I) trained system: A portion of the 400 MHz ^{1}H NMR spectra of the removal of Cu(I) with NBu$_4$CN and subsequent recall. 1) **Training**: the mixture of components in presence of 0.5 eq. of Cu(I)OTf at 60 °C for 12 h (*bottom*); 2) **Storage**: the removal of Cu(I) with NBu$_4$CN, while distribution is kept. The resulting distribution is **50AB**/**50AB'**/**50A'B**/**50A'B'**/hydrolysis = **16**/**33**/**32**/**11**/**7 %** (*middle*); 3) **Recall**: the re-addition of Cu(I) resulting in an immediate return to trained library (*top*). The values were obtained as an average of three experiments with about ±2 % error.

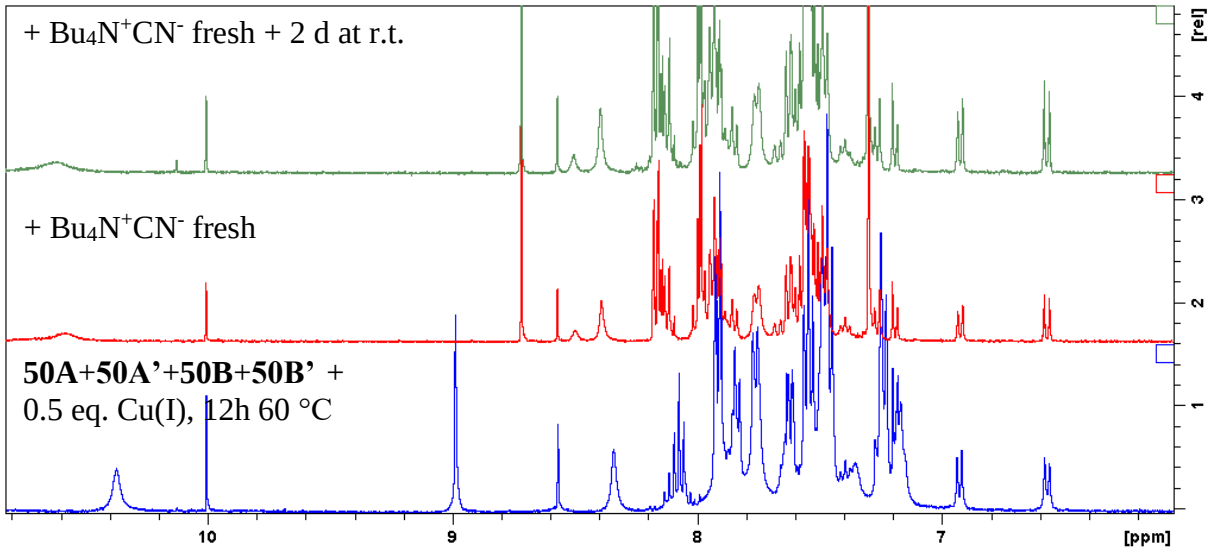

Figure E1.16: Stability study in Cu(I) free out-of-equilibrium system. Portions of the 400 MHz ^{1}H NMR spectra of the removal of Cu(I) with NBu_4CN and subsequent stability test of metal free out of equilibrium state. 1) **Training**: the mixture of components in presence of 0.5 eq. of Cu(I)OTf at 60 °C for 12 h; 2) **Storage**: the removal of Cu(I) with NBu_4CN, while distribution is kept. The resulting distribution is **50AB/50AB'/50A'B/50A'B'**/hydrolysis = **16/33/32/11/7 %**. This state is kept for at least 12 h at room temperature without any visible change in the spectra.; 3) If left at room temperature, the equilibration process starts to be visible only after several days of standing.

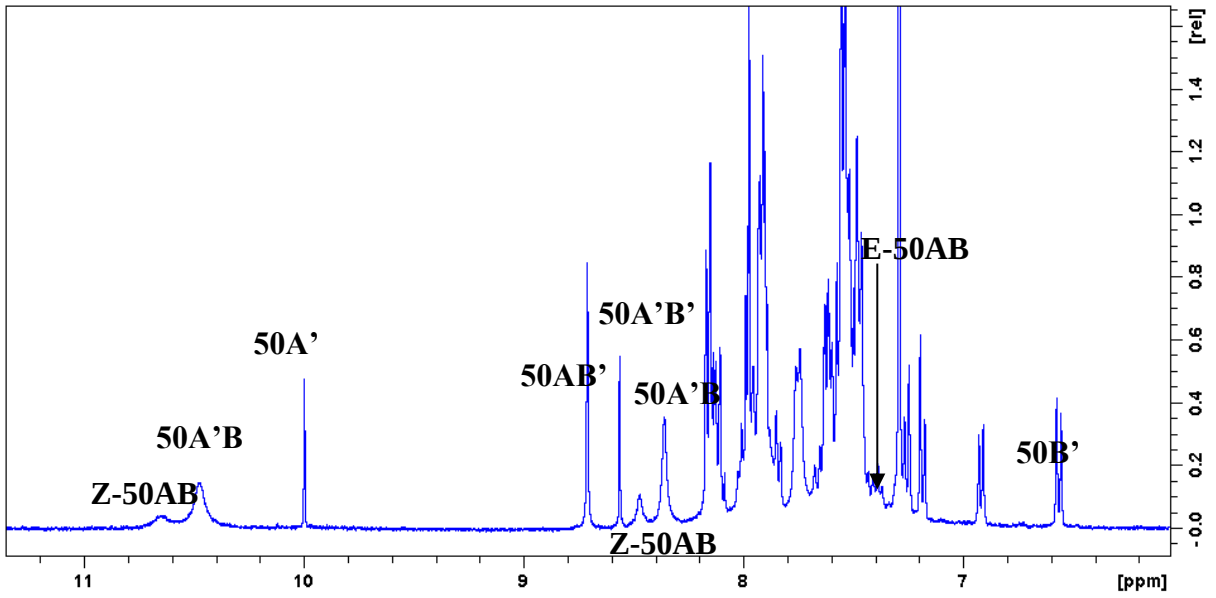

Figure E.1.17: Assignment of ^{1}H NMR spectra in Cu(I) free out-of-equilibrium state. A portion of the 400 MHz ^{1}H NMR spectrum of the removal of Cu(I) with $NBu_4^+CN^-$ and assignment of the peaks to their respective components.

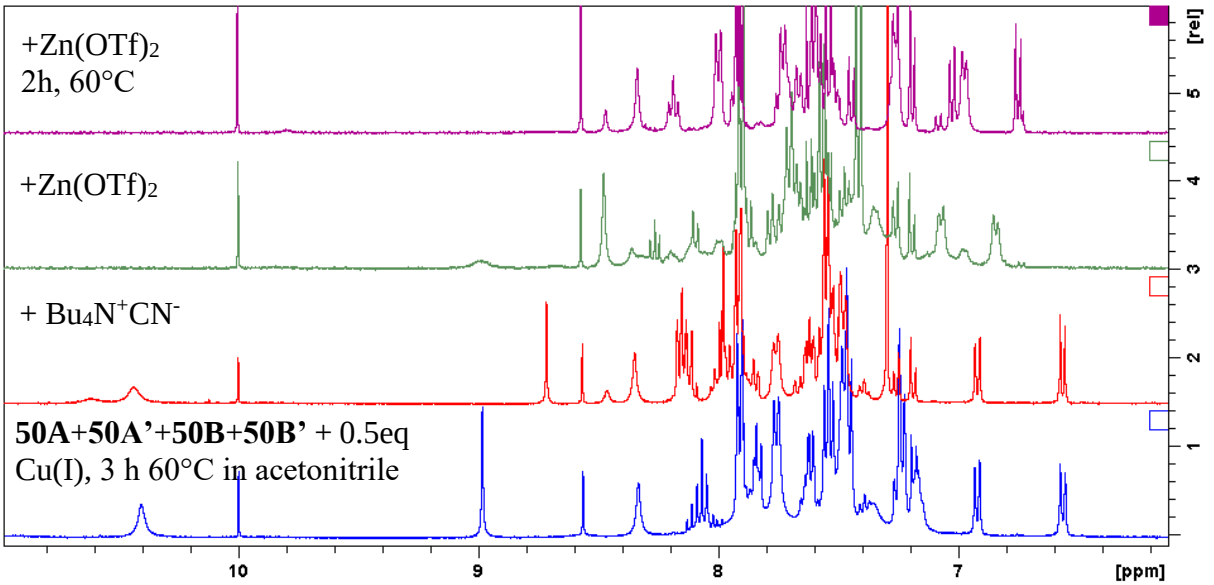

Figure E1.18: Retraining of Cu state to Zn trained state. A portion of the 400 MHz ^{1}H NMR spectra of the removal of Cu(I) with NBu_4CN and subsequent Zn(II) retraining. 1) **Training**: the mixture of components in presence of 0.5 eq. of Cu(I)OTf at 60 °C for 12 h (*bottom, blue trace*); 2) **Storage**: the removal of Cu(I) with NBu_4CN, while the distribution is kept. (*red trace*) 3) **Retraining**: immediately after the addition of 0.5 eq. of Zn(II) (*green trace*) resulting in a retrained library (*top, purple trace*).

6.1.3 E/Z isomerization of 27AB and 50AB Compounds:

E/Z isomerization of 27AB

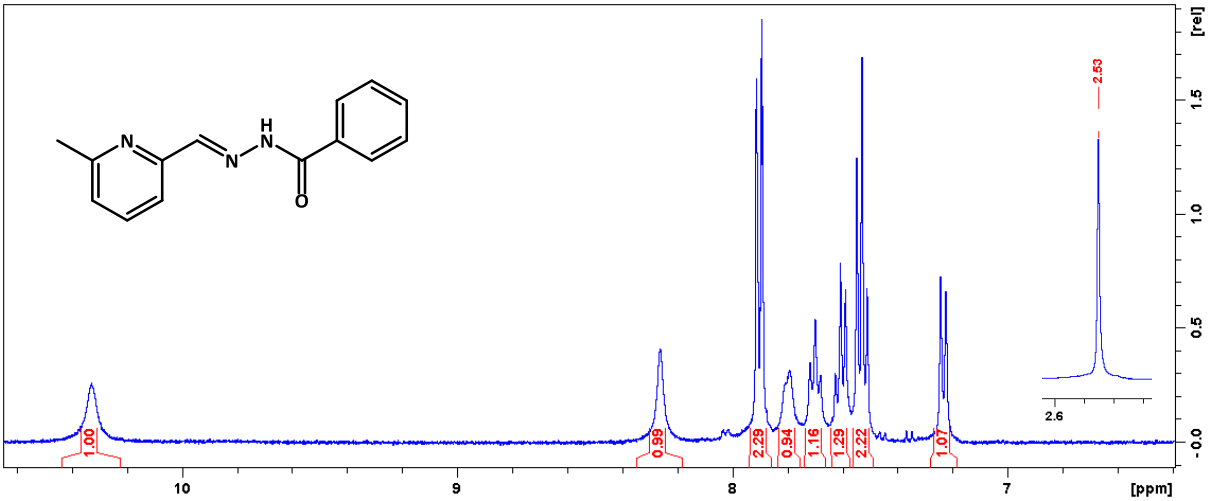

Figure E1.19: ^{1}H NMR spectrum of E-**27AB**

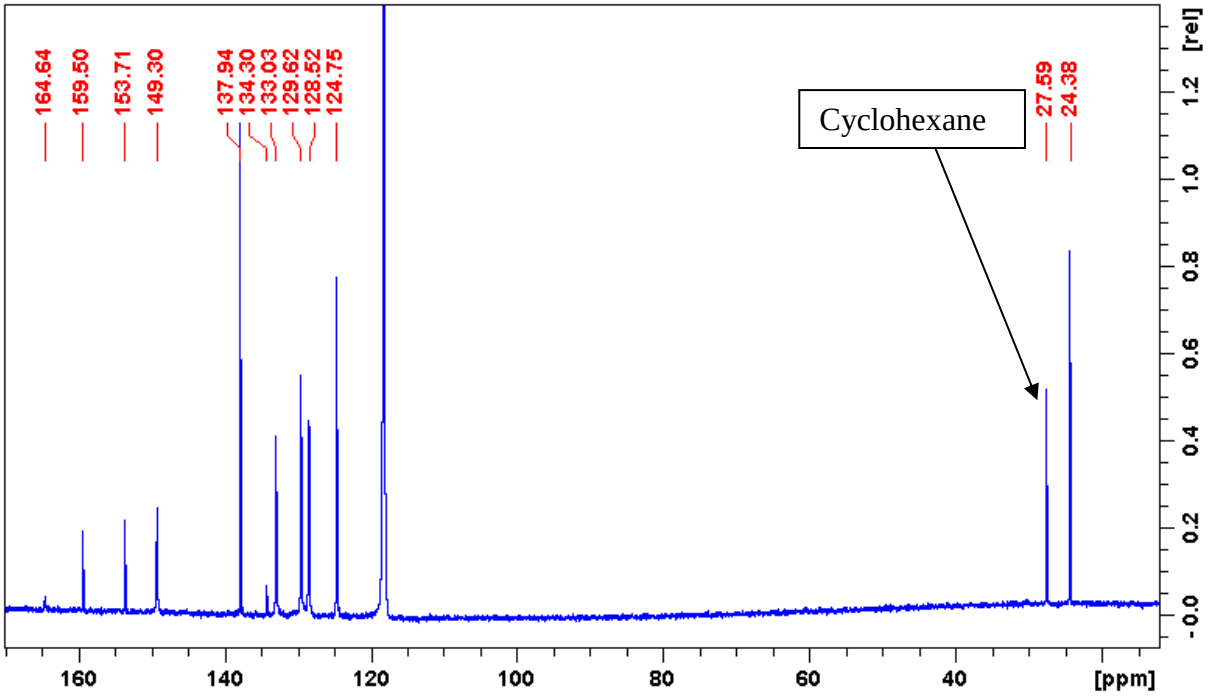

Figure E1.19: ^{13}C NMR spectrum of E-**27AB**

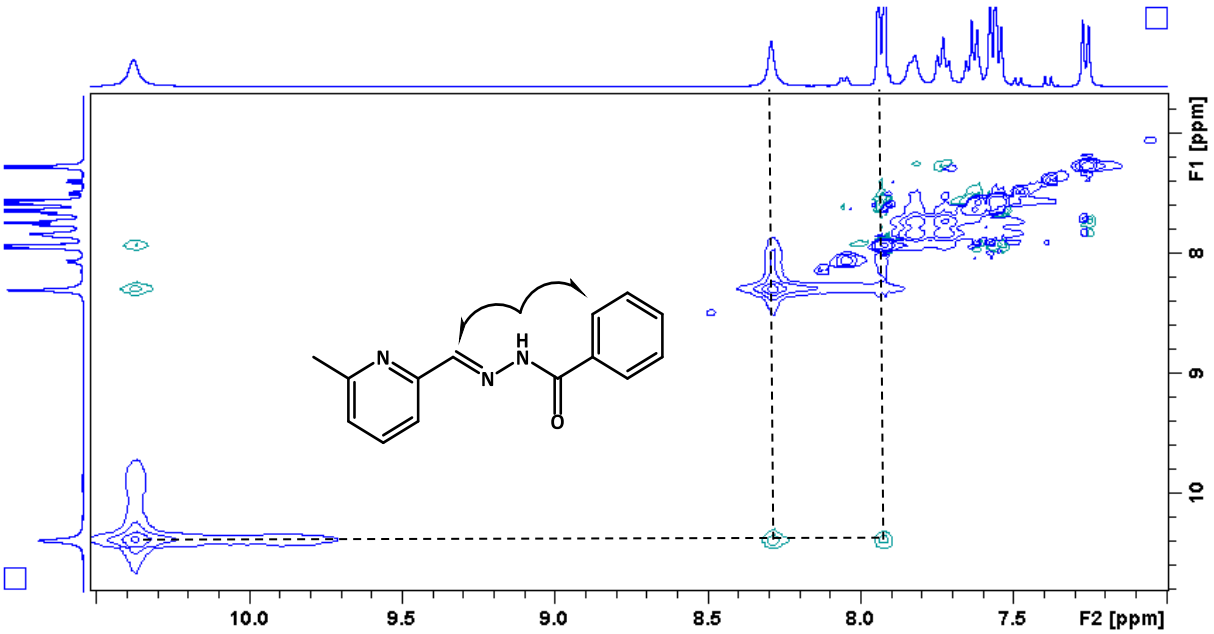

Figure E1.20: 2D NOESY NMR spectrum of E-**27AB**. Interactions between N-H and C-H of benzhydrazide and imine protons are visible. NMR spectrum was taken on the E-**27AB** as it was obtained from ethanol.

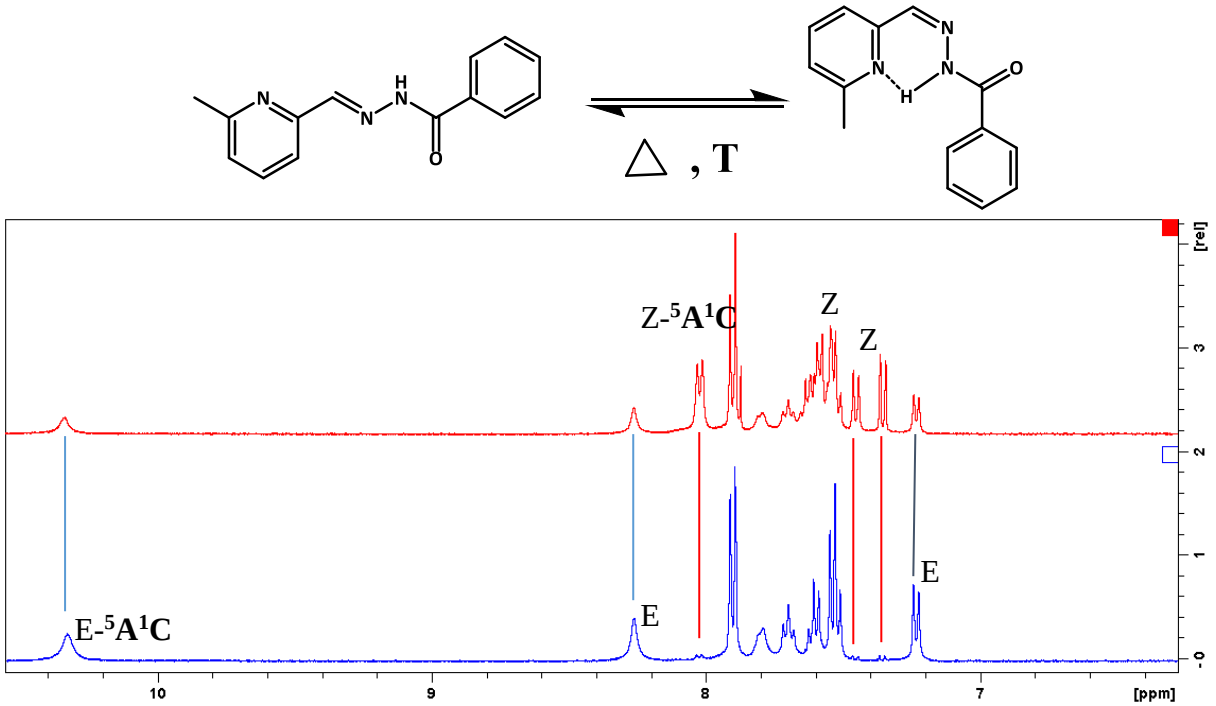

Figure E1.21: Isomerization of **27AB** (^{1}H NMR). ^{1}H NMR spectra of E-**27AB**isolated from ethanol (*bottom*) and its transformation into Z-^{5}**A**^{1}**C** upon heating for 4 days at 60 °C in acetonitrile (*top*). (in equilibrium E/Z = 45/55 %)

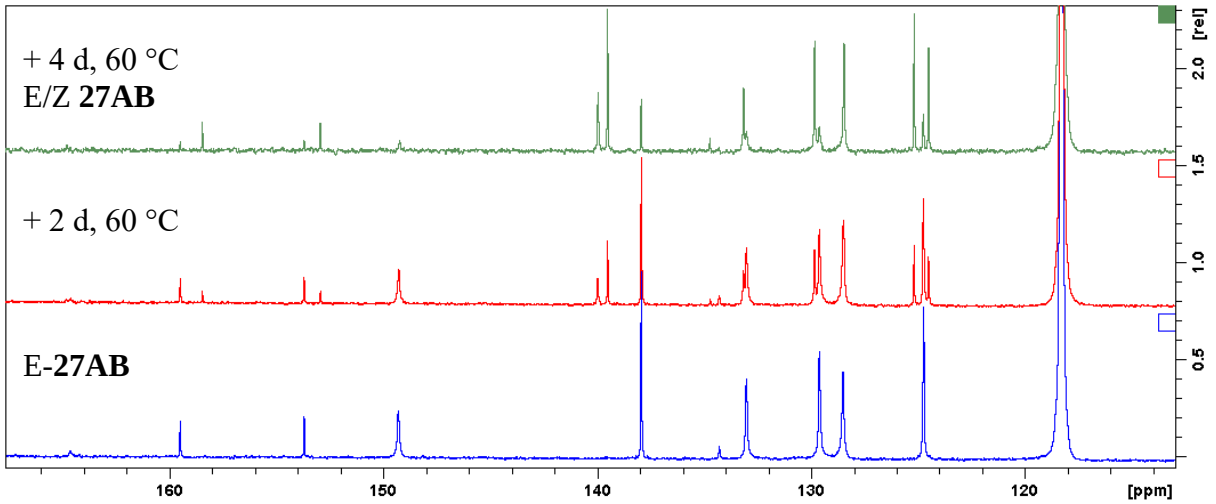

Figure E1.22: Isomerization of **27AB**. ^{13}C NMR spectra of a transformation from E-**27AB** to E/Z mixture upon heating for 4 days at 60 °C in acetonitrile (*top*).

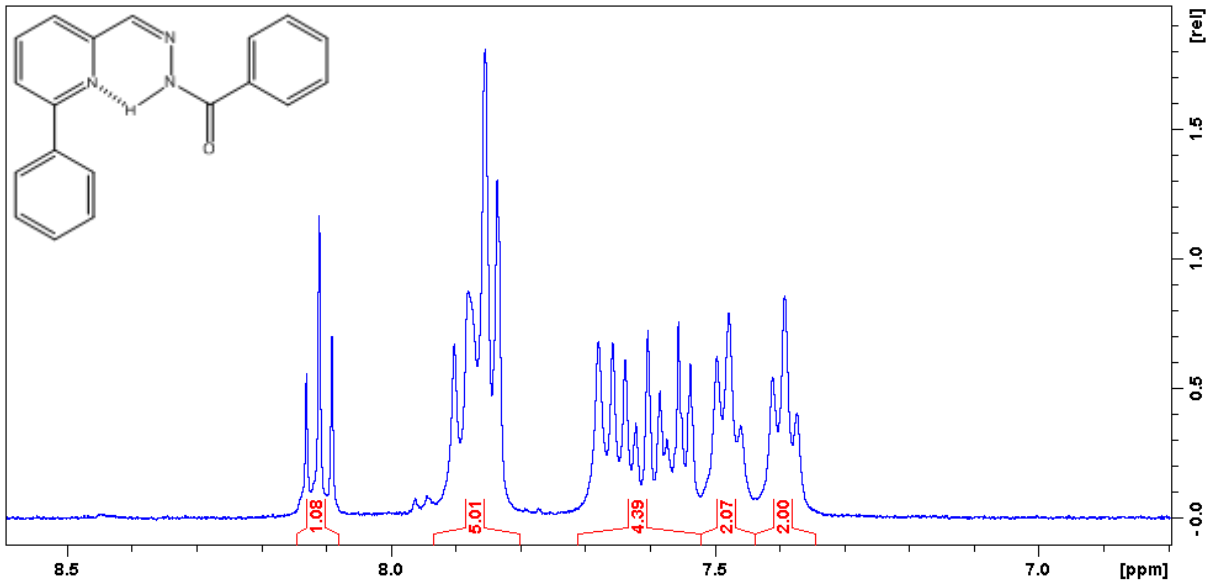

Figure E1.23: Aromatic region of ^{1}H NMR spectrum of Z-**50AB**. The impurity is in fact only the other isomer E-**50AB**.

E/Z isomerization of 50AB

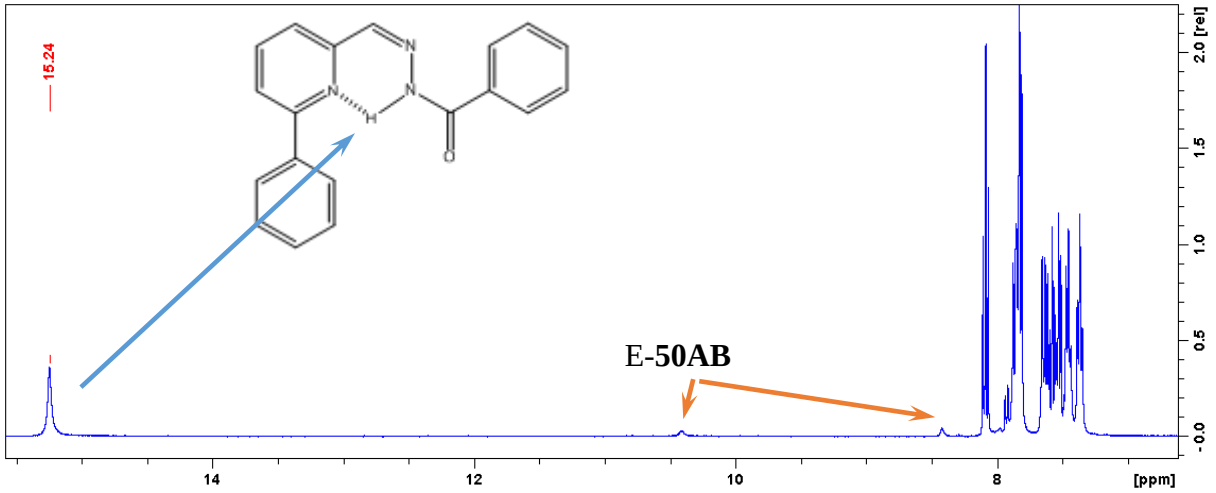

Figure E1.24: Overall ^{1}H NMR spectrum of Z-**50AB**. The N-H signal is shifted to 15.27 ppm due to the hydrogen bonding with the nitrogen of the pyridine unit. The impurity is in fact only the other isomer E-**50AB**

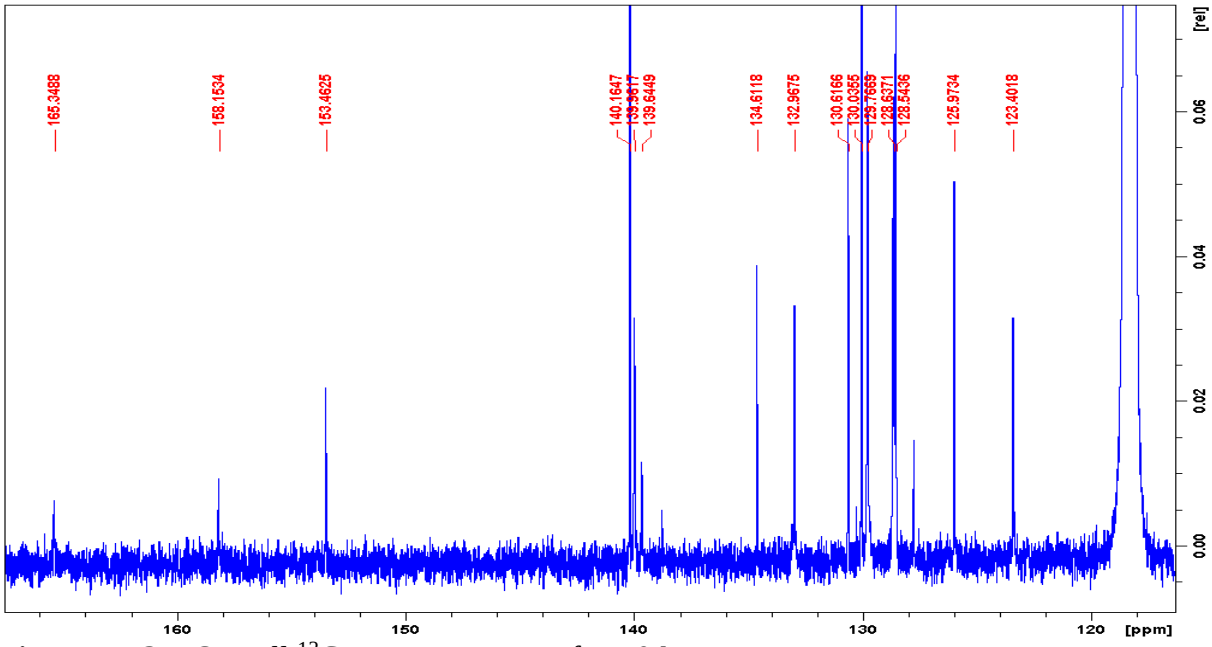

Figure E1.25: Overall ^{13}C NMR spectrum of Z-**50AB**.

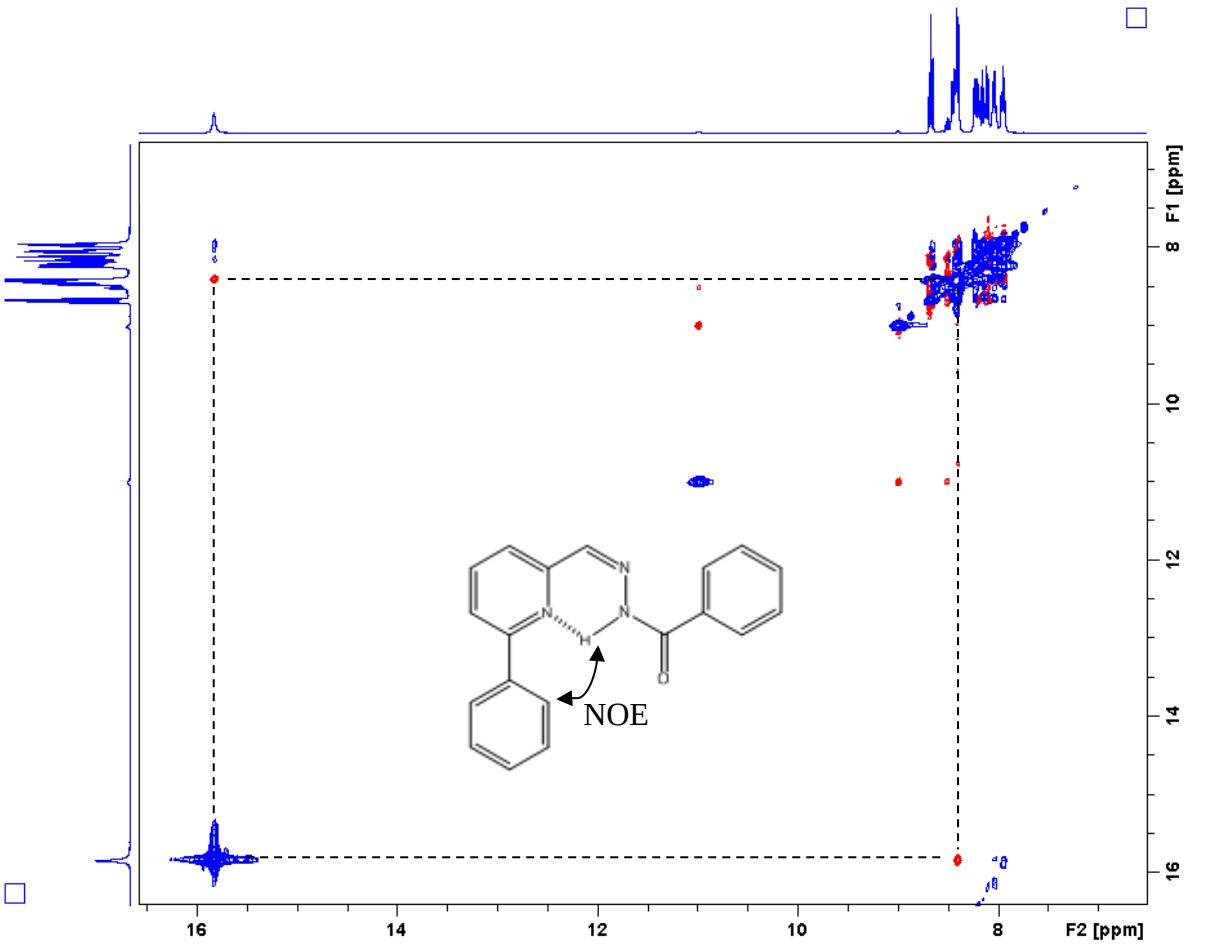

Figure E1.26: 2D NOESY spectrum of Z-**50AB** showing an interaction of the N-H with only one aromatic hydrogen. It is in agreement with our assumption for Z isomer of **50AB**. (The signal around 11 ppm belongs to the small amount of E isomer)

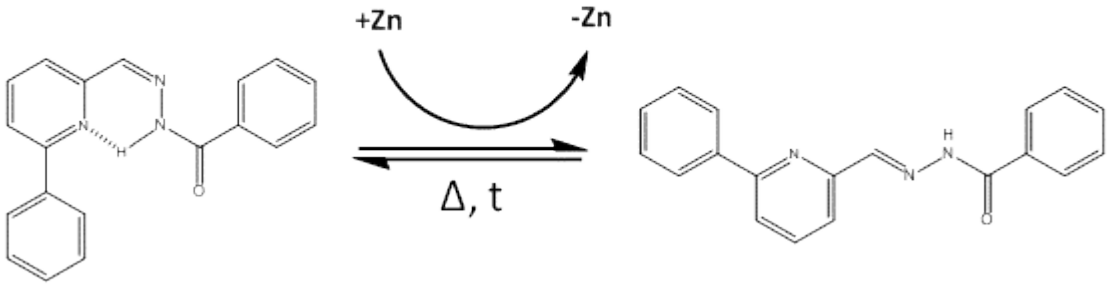

Figure E.1.27: Configurational isomers of **27AB** The Z isomer can be obtained as a precipitate from ethanol. The E isomer can be obtained either through complexation/decomplexation process or through direct reaction of components with 10 % of *p*-toluidine as catalyst at room temperature, 23 °C (the reaction is too slow at room temperature without catalyst). Upon heating both isomers equilibrate to the 3/2 = E/Z mixture.

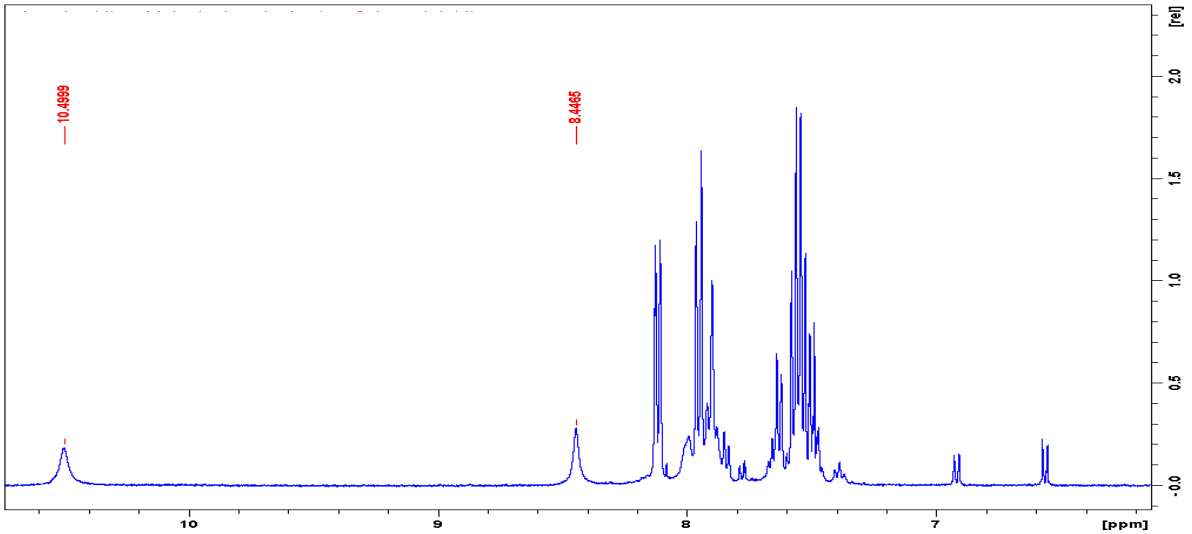

Figure E1.27: ^{1}H NMR spectrum of E-**50AB**. The shift of the N-H proton is at 10.49 ppm, which indicates an absence of hydrogen bonding with the pyridine unit. This compound was never isolated and all the studies were done in acetonitrile solution. (The peaks below 7 ppm belong to the *p*-toluidine used as a catalyst and the marked peak at 8.44 ppm belongs to the E-acylhydrazone)

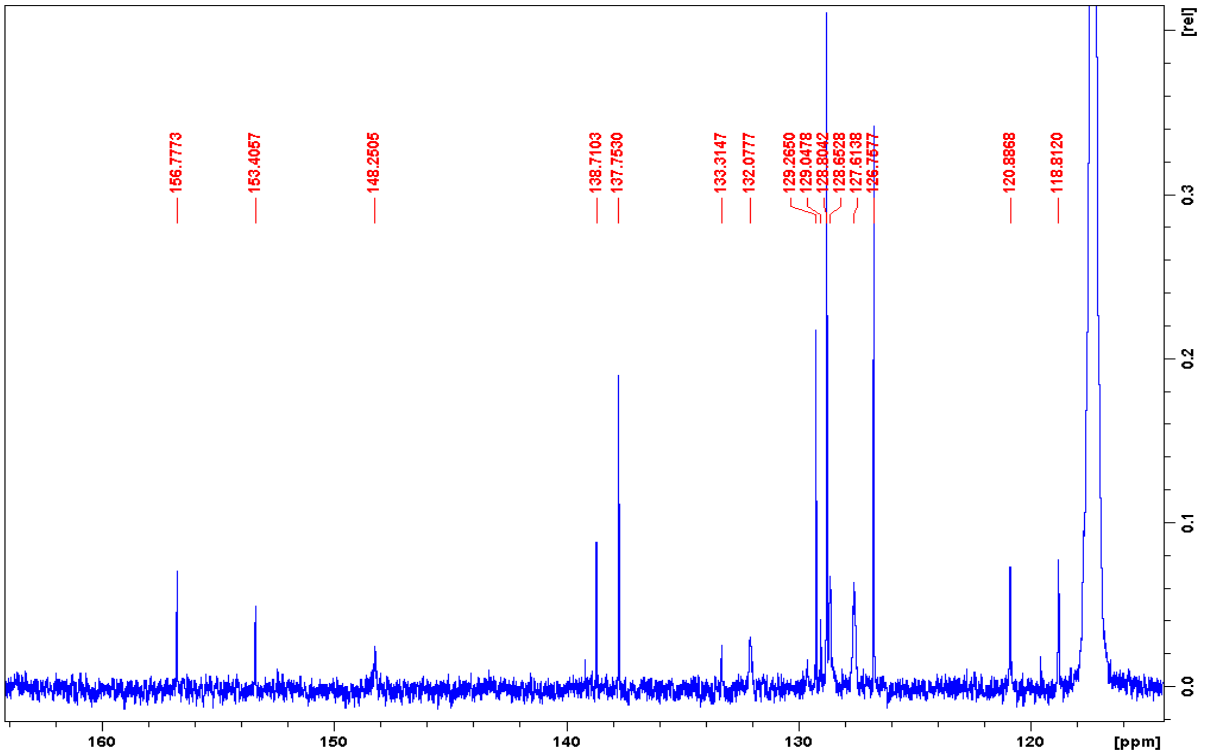

Figure E1.28: ^{13}C NMR spectrum of E-**50AB**

6.1.4 A rationale of the equilibration process in systems with two -C=N- dynamic bonds with substantially different stability constants.

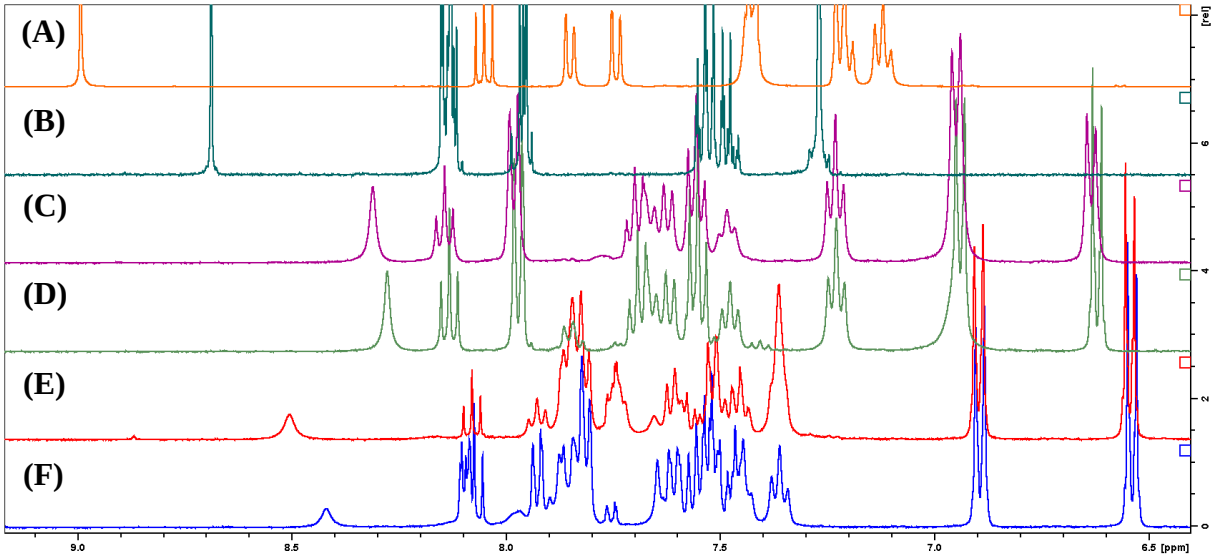

Figure E1.29: ^{1}H NMR (CD_3CN) spectra of the: **(A)** Cu(**50AB'**)$_2$; **(B) 50AB'**; **(C)** A mixture of **50A** + **50B** + **50B'** + Cu(I) 0.5 eq. +Zn(II) 0.5 eq., 12 h, 60 °C; **(D** A mixture of **50A** + **50B** + **50B'** + Zn(II) 0.5 eq., 12 h, 60 °C; **(E)** A mixture of **50A** + **50B**+ **50B'** + Cu(I) 0.5 eq., 12 h, 60 °C; **(F)** A mixture of **50A** + **50B**+ **50B'** + 12 h, 60 °C; Spectra show no formation of **50AB'** or its complex even in the presence of Cu(I).

Table E1.1

	AB-E (%)	**AB-Z** (%)	**AB'** (%)	**A** (%)	**B'** (%)
50SABB' (F)	**18**	**30**	**0**	**0**	**52**
50SABB'Cu (E)	**29**	**17**	**1**	**0**	**53**
50SABB'Zn (D)	**49**	**0**	**4**	**0**	**47**
50SABB'CuZn (C)	**51**	**0**	**0**	**0**	**49**
50S2ABB‘ Fig. E1.30	**30**	**18**	**48**	**4**	**4**

Distribution of individual constituents in the different cases in Figure E1.29.

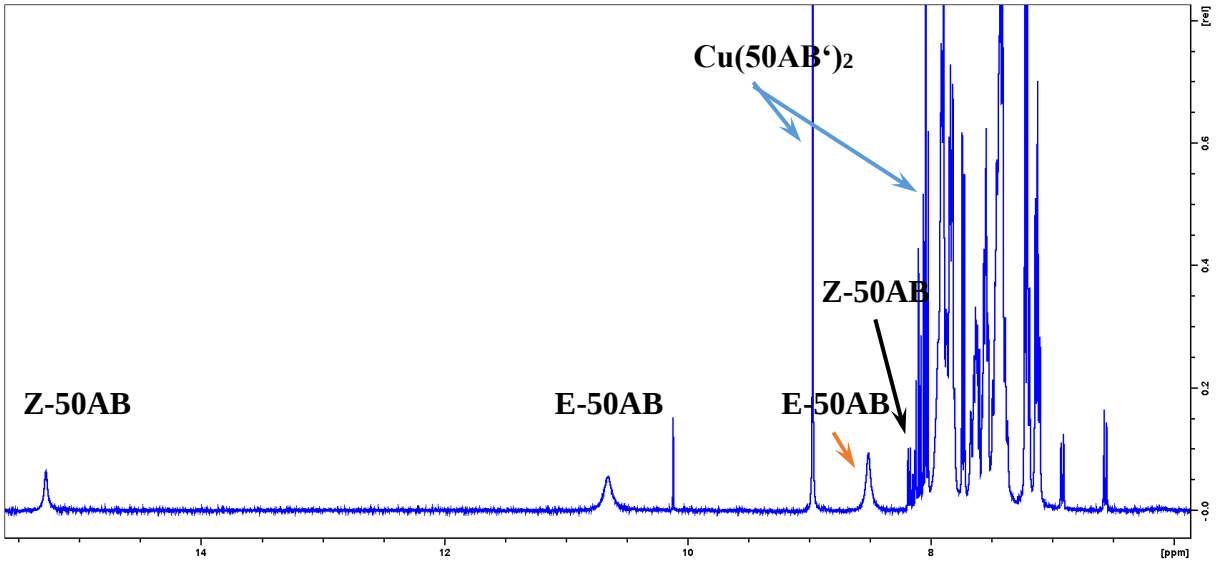

Figure E1.30: ^{1}H NMR (CD_3CN) spectra of the **50A**:**50B**:**50B’** (2:1:1) equilibrated in a presence of 0.5 eq. of Cu(I) cation; **50AB** and **50AB’** form in 1:1 ratio.

6.2 Metallosupramolecular grid complexes: Peripheral substitution/decoration and assembly

6.2.1 Synthesis of the GR7x family of ligands and their $Zn(OTf)_2$ complexes.

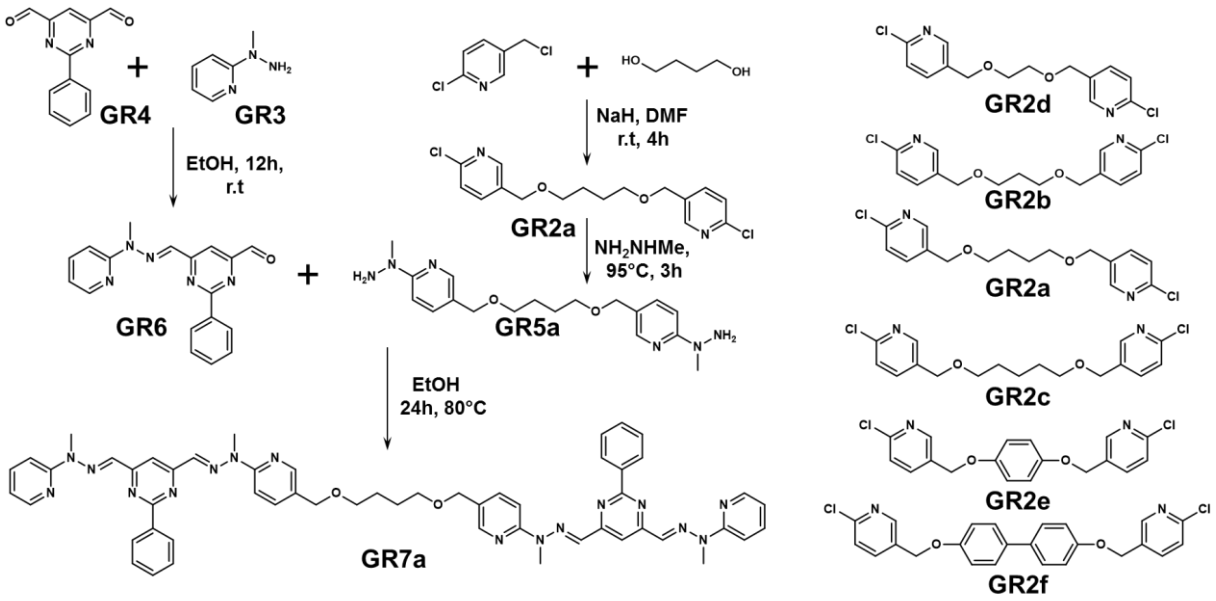

4,6-dimethyl-2-phenylpyrimidine (GR1)*:

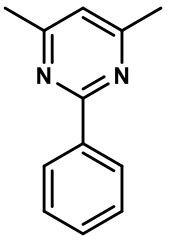

3.86 g (25 mmol) of benzamidine hydrochloride hydrate and 5.6 g (40 mmol) of K_2CO_3 was dissolved 25 ml of water and 3 ml (30 mmol) of acetylacetone was added. The solution was briefly shaken and left to stand for 4-5 days at room temperature. During this time, white needle crystals appeared. Filtration and repeated washing with water provided product **GR1**. This product was used without further purification.

^1H NMR (400MHz, $CDCl_3$): δ 8.42-8.39 (m, 2H); 7.47-7.42 (m, 3H); 6.90 (s, 1H); 2.52 (s, 6H);

*C. A. C. Haley and P. Maitland *J. Chem. Soc.*, **1951**, 3155-3174

Compounds GR2x:

The compounds **GR2a, b, c, d** were all prepared according the standard procedure for alkylation of aliphatic alcohols. The final purification was done one alumina (DCM/Petrol ether gradient 1:2 -2:1).

GR2a: Off-white solid. Yield 55 %.

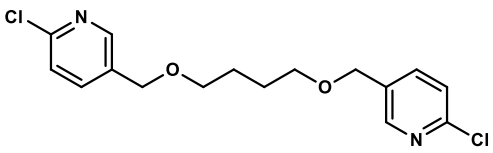

^{1}H NMR (400MHz, $CDCl_3$): δ 8.33 (d, J=1.96, 2H); 7.63 (dd, J=2.5, J=8.0, 2H); 7.31 (d, J=8.21, 2H); 4.48 (s, 4H); 3.51 (t, 4H); 1.70 (m, 4H);

^{13}C NMR (400MHz, $CDCl_3$): 150.71, 148.78; 138.14; 132.97; 124.11; 123.91; 70.58; 69.52; 26.45

MS ESI: 363.061, calc.: 363.064 ($M+Na^+$)
M.p.: 71-73.6 °C

GR2b: Yellowish oil. Yield 58 %

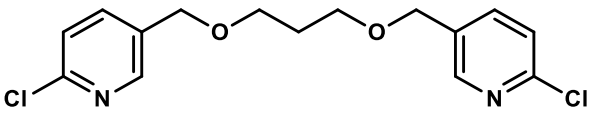

^{1}H NMR (400MHz, $CDCl_3$) δ: 8.33 (d, J = 2.3, 2H); 7.61 (dd, J = 8.2, J = 2.3, 2H); 7.30 (d, J = 8.2, 2H); 4.48 (s, 4H); 3.59 (t, J = 6.2, 4H); 1.92 (p, J = 6.2, 2H);

^{13}C NMR: 150.76; 148.81; 138.13; 132.84; 124.10; 69.63; 67.53; 29.97;

ESI MS: 349.50, calc.: 349.48 ($M+Na^+$)

GR2c: Colourless oil. Yield 48 %.

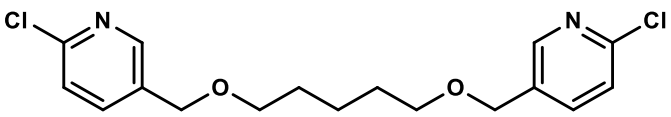

^{1}H NMR (400MHz, $CDCl_3$) δ: 8.33 (s, 2H); 7.64 (d, J = 7.9, 2H); 7.3 (d, J = 8.8, 2H); 4.48 (s, 4H), 3.48 (t, J = 6.2, 4H); 1.64 (p, J = 6.9, 4H); 1.45 (m, 2H);

^{13}C NMR: 150.68; 148.80; 138.16; 133.03; 124.10; 70.78; 69.53; 29.47; 22.87

ESI MS: 377.082, calc. 377.079 ($M+Na^+$)

GR2d: Yield 42 %

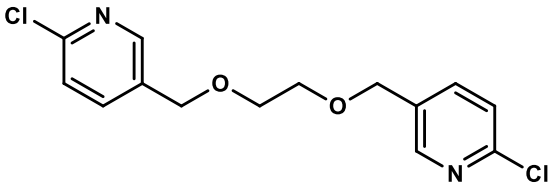

^{1}H NMR (400MHz, $CDCl_3$) δ: 8.34 (d, J=2.3, 2H); 7.64 (dd, J=2.5, J=8.0, 2H); 7.31 (d, J=8.2, 2H); 4.56 (s,4H); 3.68 (s,4H);

^{13}C NMR: 150.84; 148.82; 138.19; 132.51; 124.13; 69.97; 69.93;

ESI MS: 335.032, Calc.: 335.030 ($M+Na^+$)

The compounds **GR2e, f** were prepared according the standard procedure for alkylation of aromatic hydroxyls. The final purification was done by suspension and filtration.

GR2e: Yield 35 %.

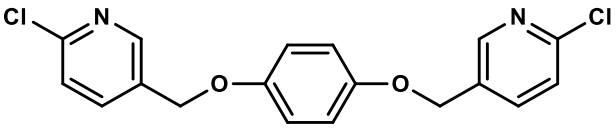

^{1}H NMR (400MHz, $CDCl_3$) δ: 8.44 (s, 2H); 7.75 (dd, J=7.9, J=8.2, 2H); 7.36 (d, J= 8.2, 2H); 6.90 (s, 4H);

^{13}C NMR: 152.87; 151.14; 148.73; 138.05; 131.63; 124.25; 116.02; 67.44;

ESI-MS: 361.051, calc.: 361.051 (M+H)

Elemental analysis: (%): N 7.63, C 58.24, H 3.81; (Calc.: N 7.76, C 59.85, H 3.86

GR2f: Yield 33 %

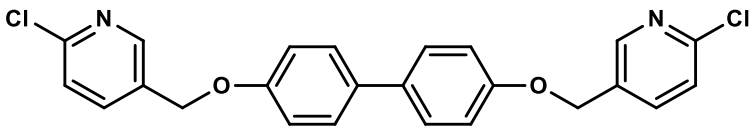

^{1}H *NMR* (400MHz, $CDCl_3$) δ: 8.50 (d, J=2.3, 2H); 7.80 (dd, J=2.3, J=8.2, 2H); 7.51 (d, J=8.6, 4H); 7.40 (d, J=8.2, 2H); 7.04 (d, J=8.6, 4H); 5.12 (s, 4H)

^{13}C *NMR*: 157.37; 151.22; 148.75; 138.09; 134.12; 131.55; 127.95; 124.31; 115.13; 66.85;

ESI-MS: 459.0614, calc.: 459.0638 ($M+Na^+$)

Compounds GR5x:

All compounds **GR5a-f** were prepared according the standard procedure for the preparation of hydrazine reagents. Compounds **GR5e** and **GR5f** precipitated from the cold reaction mixture and therefore could be purified by alternative filtration/washing procedure.

GR5a:

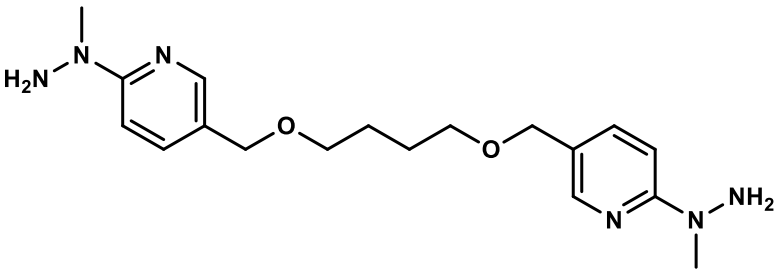

^{1}H *NMR*: 8.07 (d, J=1.9, 2H); 7.47 (dd, J=2.3, J= 8.6, 2H); 6.93 (d, J=8.6, 2H); 4.35 (s, 4H), 3.41 (m, 4H); 3.25 (s, 6H); 1.64 (m, 4H);

^{13}C *NMR*:160.96; 147.05; 137.83; 122.60; 107.26; 70.31; 69.66; 41.27; 26.47;

ESI MS: 361.232, calc.: 361.235 ($M+H^+$)

GR5b:

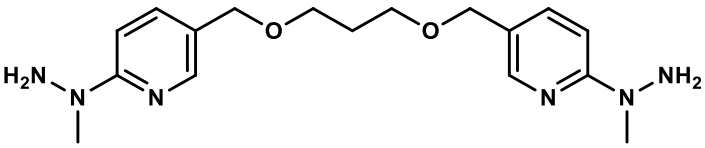

^{1}H *NMR*: 8.06 (d, J = 2.2, 2H); 7.44 (dd, J = 8.8, J = 2.2, 2H); 6.92 (d, J = 8.6, 2H); 4.34 (s, 4H); 3.98 (brs, 4H, $-NH_2$); 3.50 (t, J = 6.3, 4H); 3.24 (s, 6H); 1.85 (m, 2H);

^{13}C NMR: 146.36; 140.01; 138.38; 122.52; 107.55; 70.26; 66.77; 41.35; 30.06;

ESI MS: 347.221, calc.: 347.218 (M+H)

***GR5c*:**

^{1}H NMR (400MHz, $CDCl_3$) δ: 8.10 (s, 2H); 7.51 (dd, J = 2.3, J = 8.6, 2H); 6.93 (d, J = 9.0, 2H); 4.36 (s, 4H); 3.42 (t, J = 6.5, 4H); 3.30 (s, 6H); 1.59 (p, J = 6.9, 4H); 1.41 (m, 2H)

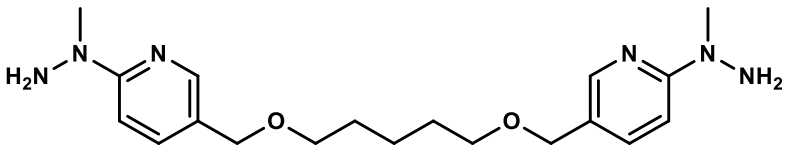

^{13}C NMR:146.31; 145.86; 138.40; 122.66; 107.57; 70.14; 69.94; 41.36; 29.48; 22.88;

ESI MS: 397.232, calc.: 397.232 ($M+Na^+$)

GR5d:

^{1}H NMR (400MHz, $CDCl_3$) δ: 8.08 (d, J=1.9, 2H); 7.49 (dd, J=2.2, J=8.8, 2H); 6.93 (d, J=8.6, 2H); 4.43 (s, 4H); 4.05 (s, 4H); 3.58 (s, 4H); 3.26 (s, 6H);

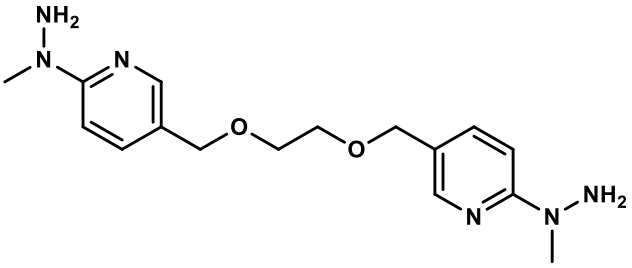

^{13}C NMR: 161.09; 147.36; 137.82; 122.21; 107.14; 70.77; 69.01; 41.19;

ESI MS: 333.202; calc.: 333.203 ($M+H^+$)

GR5e:

^{1}H NMR (400MHz, $CDCl_3$) δ: 8.20 (d, J=1.9, 2H); 7.59 (dd, J=2.2, J=8.8, 2H); 7.29 (s, 2H); 7.00 (d, J=9.0, 2H); 6.92 (s, 2H); 4.90 (s, 4H); 3.31 (s, 6H)

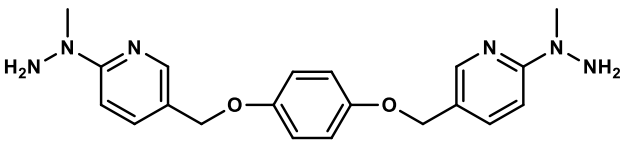

^{13}C NMR: 161.11; 153.07; 147.33; 137.64; 121.19; 116.00; 107.21 68.57; 41.12;

ESI-MS: 381.203, calc.: 381.203 ($M+H^+$)

Elemental analysis: $C_{20}H_{24}N_6O_2$ (%): N 22.09, C 62.82, H 6.33; (Calc.: N 22.09, C 63.14, H 6.36)

GR5f:

^1H *NMR* (400MHz, DMSO) δ: 8.12 (s, 2H); 7.51-7.57 (m, 2H+4H); 7.16 (d, J=9.0, 2H); 7.05 (d, J=8.6, 4H); 4.97 (s, 4H); 4.58 (s, 4H); 3.21 (s, 6H);

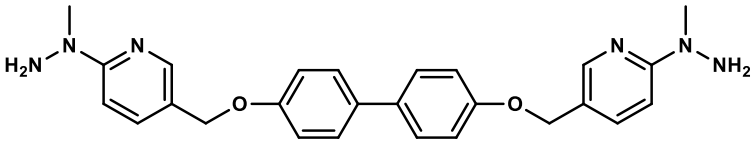

ESI -Ms: 457.2353, calc.: 457.2347 ($M+H^+$)

1-Methyl-1-(2-pyridyl)hydrazine (GR3):*

To 2-bromopyridine was added a large excess of methylhydrazine and the mixture was subsequently heated at reflux (95°C) for 3h. Extraction into $CHCl_3$ from aqueous Na_2CO_3 provided **GR3** as a colourless oil in sufficient purity for further use in close to quantitative yield.

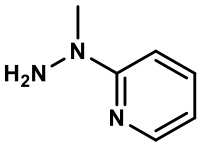

^1H *NMR* (400MHz, $CDCl_3$): δ 8.15-8.11 (m,1H); 7.48-7.44 (m, 1H); 6.93 (dd, J = 0.8, J = 8.6, 1H); 6.61-6.58 (m, 1H); 4.05 (brs, 2H); 3.25 (s, 3H) ;

*M. A. Baldo, G. Chessa, G. Marangoni, B. Pitteri, *Synthesis*, **1987**, 720

2-Phenyl-4,6-pyrimidinedicarboxaldehyde (GR4)*:

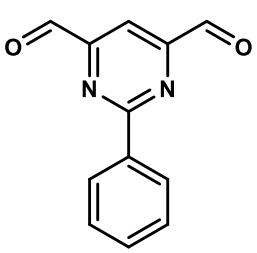

To a solution of 4,6-dimethyl-2-phenylpyrimidine (5.08 g; 27.6 mmol) in dry and degassed DMSO, the iodine (14.02 g; 53.2 mmol) and trifluoroacetic acid (8.0 mL; 103.8 mmol) were heated under inert atmosphere at 150 °C for 3h. After cooling to room temperature, the aqueous solution of $Na_2S_2O_3 \cdot 5H_2O$ (31.6 g; 127.3 mmol) was added. During the addition, the solution change the colour from violet to orange. After that, the solution was neutralized by the addition of saturated aqueous $NaHCO_3$ solution after which the aqueous phase was repeatedly extracted with CH_2Cl_2. The organic phases were collected, dried over Na_2SO_4 or $MgSO_4$ and evaporated to dryness. Crude solid was then repeatedly triturated with diethyl ether or diisopropyl ether. The process has to be repeated until the colour of the etheric solution changes from dark orange to light yellow. Slow evaporation furnished orange crystalline material in 70 % yield which was sufficiently pure to be used for further steps.

^{1}H NMR (400MHz, $CDCl_3$): δ 10.18 (s, 2H); 8.60 (d, J = 7.9, 2H); 8.12 (s, 1H); 7.58 (m, 3H)

*X.-Y. Cao, J. Harrowfield, J. Nitschke, J. Ramirez, A.-M. Stadler, N. Kyritsakas, A. Madalan, K. Rissanen, L. Russo, G. Vaughan, J.-M. Lehn, *Eur. J. Inorg. Chem.* **2007**, 2944-2965

Synthesis of GR6 and GR6B*:

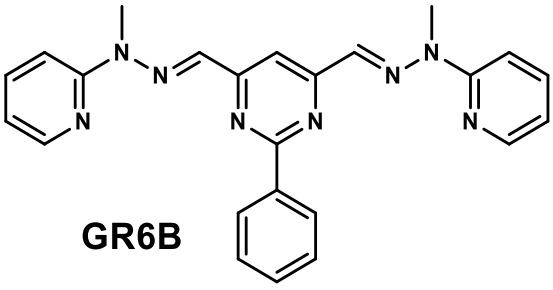

GR6B

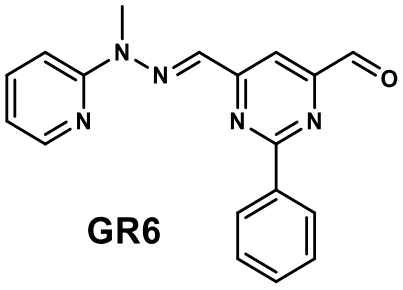

GR6

The dialdehyde **GR4** (1 eq.) was dissolved in EtOH and **GR3** was then added dropwise (in EtOH, 0.9 eq. for **GR6B** or 2.1 eq. for **GR6**) into the flask. Reaction was then stirred overnight at room temperature, during this period a yellow precipitate appeared. Then, about ¾ EtOH were evaporated with water bath kept bellow 35 °C and a yellow precipitate was filtered off (**GR6B**). In case of the preparation of **GR6B** the filtrate was evaporated to dryness and the

residue was purified by flash chromatography on alumina (DCM/heptane gradient 1:3 to 2:1) or on silica (EtOAc/heptane gradient 1:4 to 1:1) yielding yellow solid in 40 %.

GR6

^{1}H NMR (400MHz, $CDCl_3$): δ 10.18 (s, 1H); 8.58 (m, 2H); 8.3 (m, 1H); 8.26 (s, 1H); 7.84 (d, J=8.22, 1H); 7.79 (s, 1H); 7.75 (m,3H); 6.97 (m, 1H); 3.80 (s, 3H)

^{13}C NMR: 193.89; 165.76; 164.65; 158.08; 156.33; 146.43; 138.59; 136.82; 132.64; 131.32; 128.75; 128.40; 117.60; 111.03; 109.18.

ESI MS: 318.136; calc.: 318.135($M+H^+$)

M.p.: 118-121°C

GR6B

*Schmitt, J.-L.; Stadler, A.-M.; Kyritsakas, N.; Lehn, J.-M. *Helv. Chim. Acta*, **2003**, 86, 1598-1624.

^{1}H NMR (400MHz, $CDCl_3$): δ 8.52-8.50 (m, 2H); 8.36 (s, 1H); 8.30-8.28 (m, 2H); 7.87 (d, J = 8.2, 2 H); 7.77 (s, 2H); 7.69-7.65 (m, 2H); 7.55-7.47 (m, 3H); 6.92-6.89 (m, 2H); 3.77 (s, 6H).

General procedure for the GR7x compounds:

The standard procedure for hydrazone formation was used for all **GR7x** compounds.

GR7a:

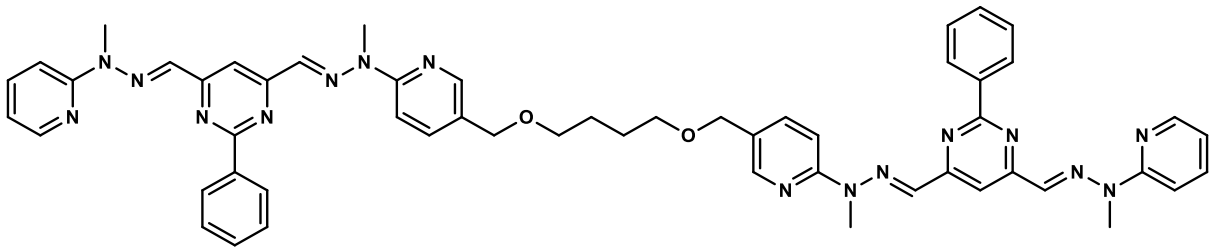

^{1}H NMR (400MHz, $CDCl_3$): δ 8.57 (m, 2H); 8.35 (s, 1H); 8.31 (d, J = 4.3, 1H); 8.26 (d, J = 1.6, 1H); 7.86 (d, J = 9, 2H); 7.74 (d, 2H), J = 12.5, 2H); 7.69-7.63 (m, 2H); 7.58-7.55 (m, 4H); 6.90 (1H), 4.52 (s, 2H); 3.77 (s, 3H); 3.76 (s, 3H); 3.58 (t, J = 5.4, 2H); 1.79 (t, J= 5.4, 2H);

ESI MS: 959.466; calc.: 959.469 ($M+H^+$)

***GR7b*:**

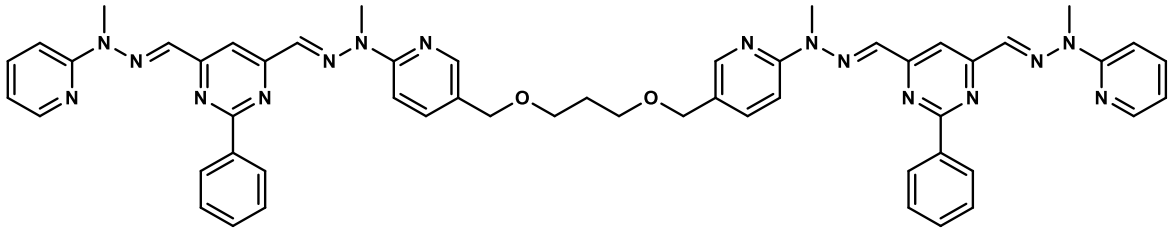

^{1}H NMR (400MHz, $CDCl_3$): δ: 8.57-8.5 (m, 2H); 8.31-8.25 (m, 2H); 8.21 (d, J=4.3, 1H); 7.79 (m, 2H); 7.74 (s, 2H); 7.64-7.53 (m, 6H); 6.89 (t, J=5.6, 1H), 4.51 (s, 2H); 3.79 (t, J=5.5, 2H); 3.73 (s, 3H); 3.69 (s, 3H); 1.99 (t, J= 5.7, 2H);

^{13}C NMR: 30.02; 30.08; 66.53; 70.06; 70.2; 107.52; 110.04; 110.19; 110.31; 110.79; 116.80; 116.93; 126.80; 128.21; 125.55; 130.59; 132.76; 137.51; 137.86; 146.26; 146.98; 156.61; 156.93; 161.87

ESI MS: 945.454; calc.: 945.453 ($M+H^+$)

***GR7c*:**

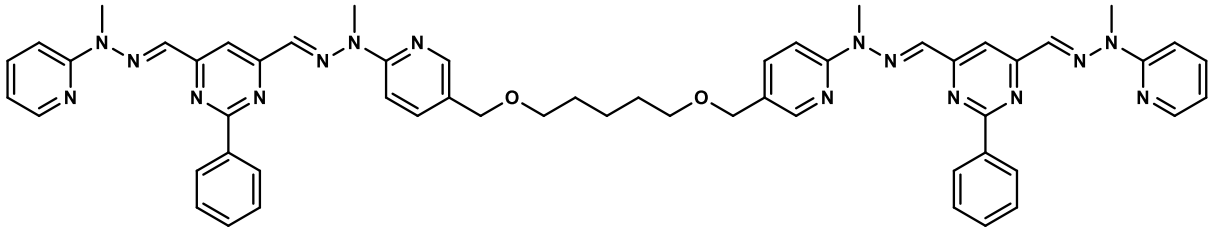

^{1}H NMR (400MHz, $CDCl_3$): δ: 8.50-8.48 (m, 2H); 8.27 (s, 1H); 8.17 (d, J=1.6, 1H); 7.51-7.49 (m, 3H); 7.78 (d, J=11.3, 2H); 7.68 (d J=8.9, 2H); 7.66-7.58 (m, 2H); 7.58-7.55 (m, 4H); 6.86 (dd, J=5.2, 1H), 4.44 (s, 2H); 3.73 (s, 3H); 3.70 (s, 3H); 3.51 (t, J=6.2, 2H); 1.68 (p, J= 6.9, 2H); 1.56-1.49 (m, 1H)

ESI MS: 973.482; calc.: 973.484 ($M+H^+$)

GR7d:

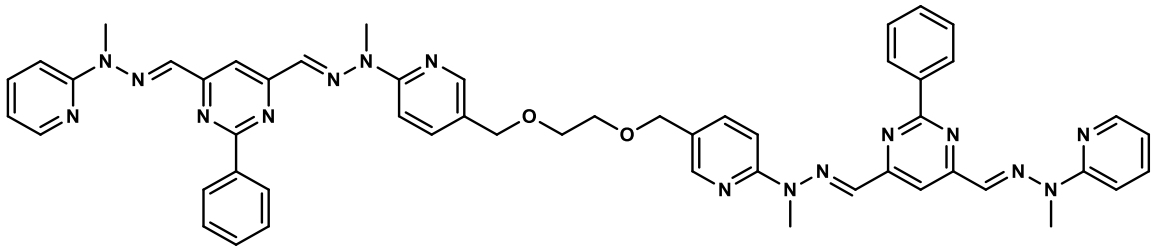

^{1}H NMR (400MHz, $CDCl_3$): δ: 8.51-8.49 (m, 2H); 8.24 (s, 1H);8.23-8.22 (m,1H); 8.20 (d, J=2.3, 1H); 7.81 (d, J=8.6, 1H); 7.73-7.69 (m, 2H); 7.60 (s,1 H); 7.51-7.54 (m, 4H); 7.48-7.43 (m, 1H); 6.77 (dd, 1H); 4.56 (s, 2H); 3.74 (s, 3H); 3.65 (s, 3H); 3.61 (s, 3H);

ESI MS: 931.438; calc.: 931.438 ($M+H^+$)

GR7e:

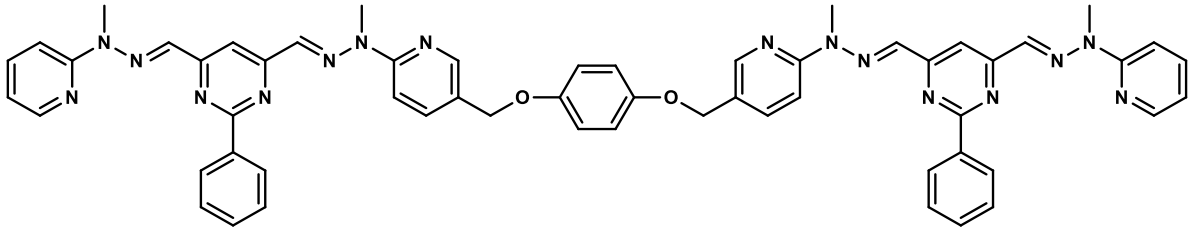

^{1}H NMR (400MHz, $CDCl_3$) δ: 8.53-8.50 (m, 2H); 8.33 (s, 1H);8.31 (d, J=1.9, 1H); 8.27 (d, J=4.6, 1H); 7.87-7.81 (m, 3H); 7.76-7.72 (m, 2H); 7.60 (m,1 H); 7.51-7.54-7.52 (m, 4H); 6.92 (s, 1H); 5.01 (s, 2H); 3.76 (s, 3H); 3.75 (s, 3H);

ESI MS: 979.438; calc.: 979.438 ($M+H^+$)

GR7f:

^{1}H NMR (400MHz, $CDCl_3$) δ: 8.54-8.52 (m, 2H); 8.36 (s, 1H); 8.29 (d, 1H); 7.90 (d, J=8.6, 1H); 7.86 (d, J=8.6, 1H); 7.8-7.76(m, 2H); 7.67 (m,1H); 7.54-7.49 (m, 6H); 7.05 (d, J=8.6, 2H); 6.90 (m, 1h); 5.09 (s, 2H); 3.8 (s, 3H); 3.79 (s, 3H);

ESI MS: 1055.4698; calc.: 1055.4688 ($M+H^+$)

The folded grids of GR7xZn series:

All complexes were prepared according the standard procedure for grid formation. The metal salt of choice was $Zn(OTf)_2$. Crystallization of grids was achieved by vapour diffusion of diethylether or diisopropylether into Acetonitrile or $MeNO_2$ solution of the complex.

***GR7aZn*:**

^{1}H NMR (400MHz, CD_3CN): δ 8.25 (s, 1H); 8.21-8.16 (m, 2H); 8.15 (s, 1H); 7.92-7.84 (m, 8H); 7.62 (t, J= 7.4, 1H); 7.52 (t, J=7.2, 1H); 7.38-7.29 (m, 8H); 7.12 (s, 2H); 6.98-6.92 (m, 2H); 5.94 (d, J=7.4, 2H); 5.89 (d, J=7.4, 1H); 5.62 (d, J=7.4, 1H); 4.21-4.10 (m, 4H); 3.54-3.51 (4 x s, 12H); 3.32-3.19 (m, 4H); 1.54-1.42 (m, 4H).

^{13}C NMR: 26.79; 26.85; 34.51; 34.65; 34.74; 34.90; 68.44; 70.77; 112.18; 112.36; 112.40; 120.23; 121.57; 121.72; 122.42; 122.57; 122.77; 124.19; 125.32; 127.71; 128.25; 129.05; 129.37; 129.69; 130.06; 130.45; 130.76; 130.82; 133,37; 133.52; 134.28; 134.43; 135.33; 135.72; 143.39; 143.44; 143.64; 143.67; 145.26; 145.35; 147.12; 147.22; 149.41; 149.45; 149.98; 150.02; 158.31; 158.34; 158.54; 158.58; 166.31; 166.42;

ESI MS: 1537.22 $[L_2M_4]^{2+}$, calc.: 1537.18 ($[(C_{54}H_{54}O_2N_{16})_2(CF_3SO_3)_6Zn_4]^{2+}$)

GR7bZn:

^{1}H NMR (400MHz, CD_3CN) δ: 8.26 (s, 1H); 8.21-8.15 (m, 2H); 7.97 (s, 1H); 7.95 (s, 1H); 7.92-7.83 (m, 6H); 7.66 (t, J= 7.4, 1H); 7.48 (t, J=7.3, 1H); 7.42-7.29 (m, 6H); 7.25 (t, J = 7.55, 1H); 7.15 (s, 2H); 6.99-6.92 (m, 2H); 5.99 (d, J = 7.6, 1H); 5.96 (d, J=7.3, 2H); 5.89 (d, J=7.7, 1H); 5.45 (d, J=7.4, 1H); 4.20-4.05 (m, 4H); 3.55-3.52 (4 x s, 12H); 3.33-3.23 (m, 2H); 3.18-3.09 (m, 2H); 1.75-1.68 (m, 1H); 1.62-1.54 (m, 1H).

^{13}C NMR: 167.34; 166.81; 166.77; 159.09; 158.94; 150.49; 150.40; 150.20; 150.12; 147.67; 147.54; 146.17; 146.12; 144.81; 144.77; 144.11; 144.05; 136.20; 135.59; 134.89; 134.76; 133.23; 133.09; 131.29; 131.23; 131.02; 130.43; 130.39; 130.17; 129.79; 129.57; 128.75;

125.71; 124.69; 124.50; 123.16; 122.98; 122.16; 120.61; 113.12; 112.87; 112.81; 112.63; 68.22; 68.05; 35.27; 35.17; 35.03; 34.96.

ESI MS: 1523.16, calc.: 1523.16 $[(C_{53}H_{52}O_2N_{16})_2(CF_3SO_3)_6Zn_4]^{2+}$

***GR7cZn*:**

^{1}H NMR (400MHz, CD_3CN): δ 8.33 (s, 1H); 8.32-8.20 (m, 2H); 8.18 (s, 1H); 8.02 (s, 1H); 7.95-7.87 (m, 6H); 7.85 (s, 1H); 7.71 (t, J = 7.2, 1H); 7.59 (t, J = 7.6, 1H); 7.49 (t, J = 7.4, 1H); 7.40-7.29 (m, 6H); 7.15-7.17 (m, 2H); 6.99-6.95 (m, 2H); 6.37 (d, J=7.4, 1H); 6.00 (d, J=7.4, 1H); 5.93 (d, J=7.4, 1H); 5.67 (d, J = 7.8, 1H); 4.15-4.07 (m, 4H); 3.54-3.62 (m, 14H); 3.32-3.26 (m, 2H); 1.53-1.23 (m, 6H).

^{13}C NMR: 167.02; 166.72; 158.90; 158.88; 151.12; 150.38; 150.27; 150.05; 149.94; 147.66; 147.30; 146.11; 145.99; 144.83; 144.66; 144.14; 144.09; 136.27; 135.89; 134.87; 134.72; 133.11; 131.45; 131.13; 130.77; 130.43; 130.37; 129.94; 129.87; 129.81; 129.72; 128.58; 128.48; 125.73; 124.99; 124.47; 123.18; 122.92; 122.54; 122.10; 121.98; 120.64; 112.88; 112.75; 112.66; 112.57; 71.76; 69.19; 35.27; 35.18; 34.97; 34.87; 30.41;

ESI MS: 1551.20, calc.: 1551.19 ($[(C_{55}H_{54}O_2N_{16})_2Zn_4(CF_3SO_3)_6]^{2+}$)

X-Ray single crystal structure in appendice.

***GR7dZn*:**

^{1}H NMR (400MHz, CD_3CN) δ: 8.26 (s, 1H); 8.24 (s, 1H); 8.22-8.13 (m, 2H); 8.04 (s, 1H); 7.96-7.85 (m, 8H); 7.72 (t, J = 7.2, 1H); 7.50-7.32 (m, 9H); 7.26-7.17 (m, 3H); 7.05-6.97 (m, 2H); 6.13 (d, J=7.4, 1H); 5.98 (d, J=7.4, 1H); 5.91 (d, J=7.4, 1H); 5.07 (d, J = 7.4, 1H); 4.28-4.17 (m, 4H); 3.59-3.54 (m, 12H); 3.44-3.34 (m, 4H);

Comparison of ^{1}H NMR spectra of GR7x Zn grids (Figure E2.1)

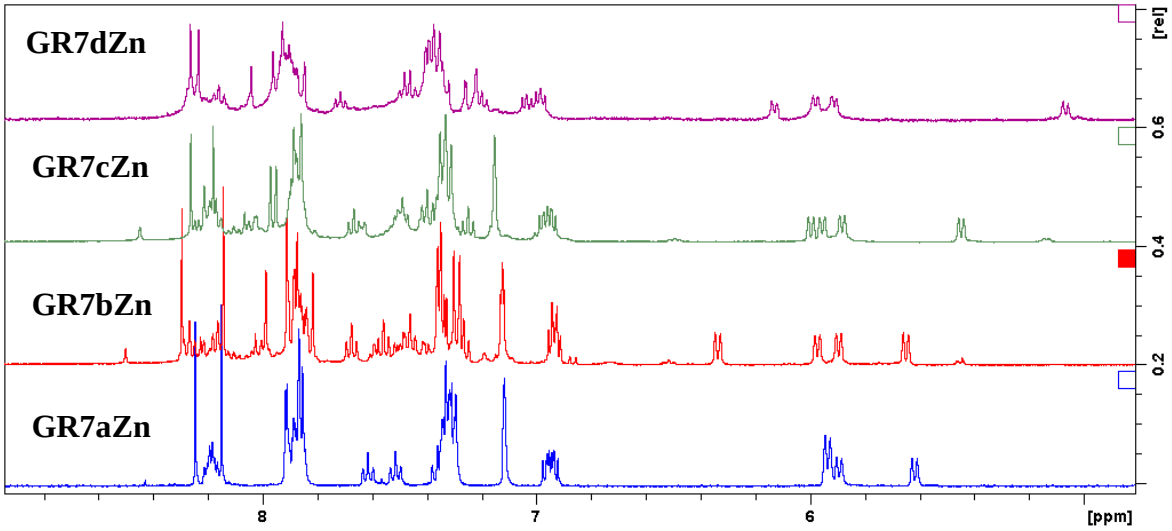

Figure E2.1: The ^{1}H NMR spectra of folded grids with different alkyl chain as a linker. The **GR7aZn** was measured after its recrystallization (v.d. Diisopropyl ether into acetonitrile). The spectra of other grids are initial assemblies according the standard procedure for grid formation.

DOSY measurement of GR7xZn complexes:

Complex	Solvent	T (K)	V molecule (angstrom3)
7a(Zn)	CD3CN	298	10463
7a(Zn)	CD3CN	298	6760
7b(Zn)	CD3CN	298	10864
7b(Zn)	CD3CN	298	7207
7c(Zn)	CD3CN	298	10353
7c(Zn)	CD3CN	298	6385

***GR7eZn*:**

^{1}H NMR (400MHz, CD_3CN): δ 8.41 (s, 1H); 8.28 (t, J = 7.6, 1H); 8.24 (t, J = 7.6, 1H); 8.15 (s, 1H); 8.05 (s, 2H); 7.94-7.87 (m, 8H); 7.63 (t, J= 7.7, 2H); 7.39-7.28 (m, 8H); 6.98-6.95 (m, 2H); 6.50 (s, 4 H); 5.96 (d, J=7.4, 1H); 5.91 (d, J=7.4, 1H); 5.78 (d, J=7.8, 1H); 5.72 (d, J=7.4, 1H); 5.08-4.80 (m, 4H); 3.61 (s, 3H); 3.56 (s, 3H); 3.54 (s, 3H); 3.50 (s, 3H);

^{1}H NMR spectrum of GR7eZn (Figure E2.2)

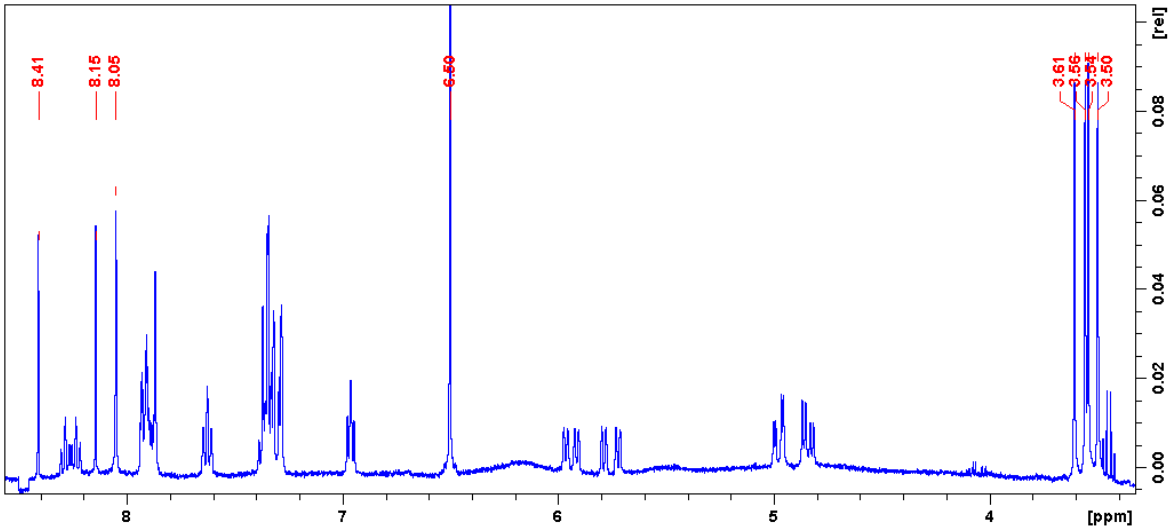

Figure E2.2.: Nicely resolved ^{1}H NMR of **GR7eZn**

GR7fZn –^{1}H NMR is broad.

ESI-MS: 1269.339, calc.: 1267.3396 $[(C_{62}H_{54}N_{16}O_2)(CF_3SO_3)Zn]^+$ and 1269.3423 $[(C_{62}H_{54}N_{16}O_2)_2(CF_3SO_3)_2Zn_2]^{2+}$)

Synthesis of the compound GR17*:

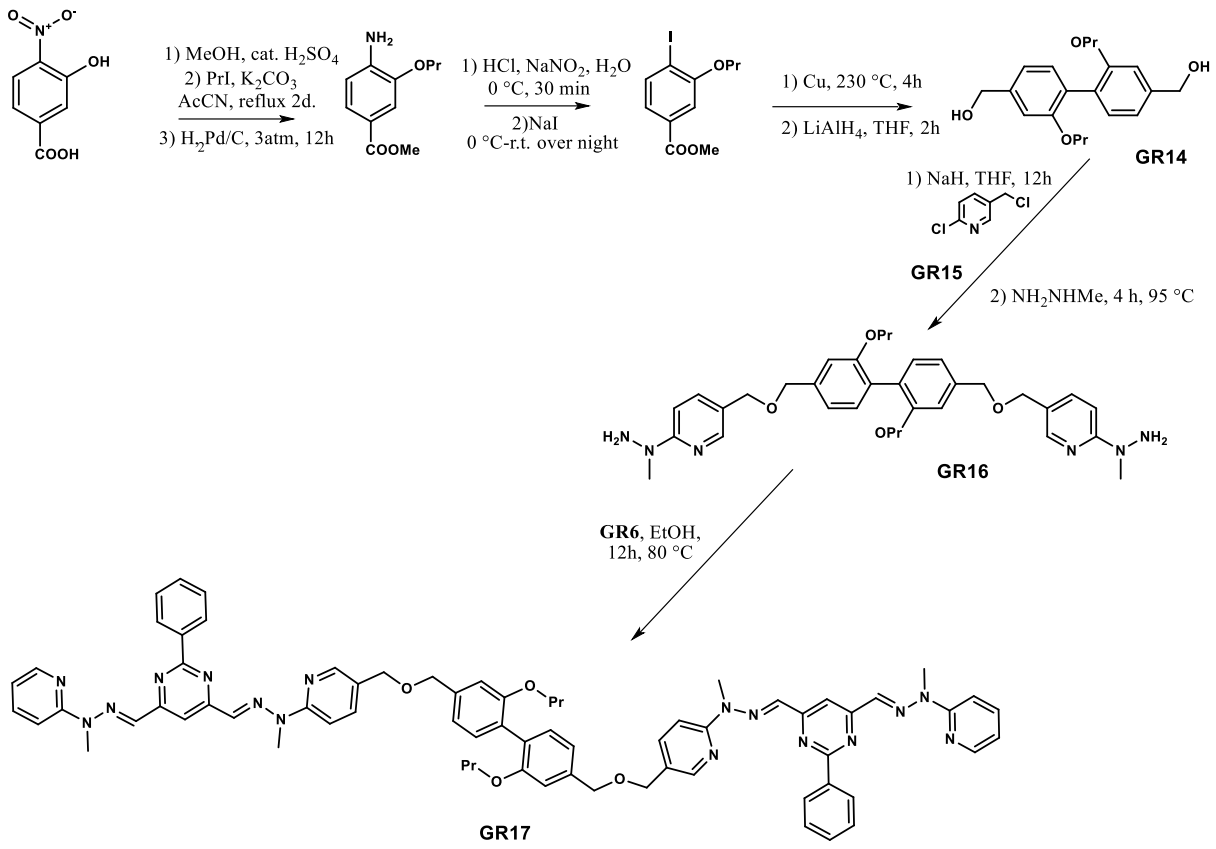

*Steps up to GR14 were done according the following report:

Rizzacasa, M.Z.; Sargent, M. V. *Australian Journal of Chemistry*, **1988**, 41, 1087-1097

GR14: Off-white powder.

^{1}H NMR (400MHz, $CDCl_3$): δ 7.25 (d, J=7.8, 2H); 7.00 (s,2H); 6.96 (d, J=7.8, 2H); 4.73 (s,4H); 3.91 (t, J=6.6, 4H); 1.67 (m, 4H); 0.89 (t, J=7.4, 6H)

^{13}C NMR: 156.82, 141.21, 131.70, 127.34, 118.37, 110.65, 69.85, 65.55, 22.58, 10.51

MS-ESI: 353.1705, calc. :353.1723 ($M+Na^+$)

***GR15*:**

The compound was synthesized according the standard procedure alkylation of aliphatic alcohols and was obtained as colourless oil in 27 % yield.

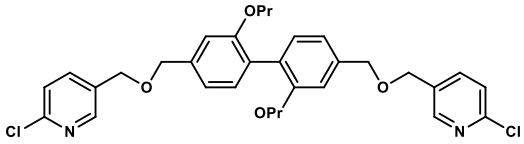

^{1}H NMR: δ 8.40 (d, J=2.3, 2H); 7.72 (dd, J=2.3, J=8.2, 2H); 7.35 (d, J=8.2, 2H); 7.25 (d, J=8.2, 2H); 6.94-6.96 (m, 4H); 4.61 (s,4H); 4.59 (s, 4H); 3.89 (t, 4H); 1.66 (sex, 4H); 0.88 (t, 6H);

Ms-ESI: 581.1892, calc.: 581.1968 ($M+H^+$)

GR16:

The compound was synthesized according the standard procedure for preparation of hydrazine derivatives and was obtained as off-white powder in >90 % yield.
^{1}H NMR (400MHz, DMSO): 7.99 (d, J=2.3, 2H); 7.46 (dd, J=2.3, J=8.6, 2H); 7.13 (d, J=8.6, 2H); 7.09 (d, J= 7.4, 2H); 6.93 (s, 2H); 6.88 (d, J=7.4, 2H); 4.53 (brs, 4H); 4.49 (s, 4H); 4.37 (s,4H); 3.83 (t, J=6.3, 4H); 3.19 (s, 6H); 1.52 (sex, 4H); 0.79 (t, J=8.0, 4H);

^{13}C NMR: 161.95; 165.51; 147.49; 139.36; 137.89; 131.39; 126.97; 121.44; 119.36; 111.53; 107.52, 71.34, 69.71, 69.51, 40.75, 22.54, 10.80,

Ms-ESI: 601.3432; calc.: 601.3497($M+H^+$)

GR17:

Synthesized according the general synthetic procedure for **GR7x**. Obtained as yellow solid powder in >90 % yield.

^{1}H NMR (400MHz, DMSO): 8.55-8.53 (m, 2H); 8-38 (s, 1H); 8.30-8.31 (m, 2H); 7.89 (t, J= 8.6, 2H); 7.81 (s, 2H); 7.75 (d, J=8.6, 1H); 7.7 (t, J= 7.6, 1H); 7.57-7.51 (m, 3H); 7.26 (s, 1H); 6.97 (m, 2H); 6.91 (t, J=5.8, 1H); 4.61(s, 2H); 4.59 (s, 2H); 4.49 (s, 4H); 3.89 (t, J=6.5, 2H); 3.81 (s, 3H); 3.80 (s, 3H); 1.65 (q, J=6.9, 2H); 0.87 (t, J=7.2, 3H);

ESI-MS: 1199.5819, calc.: 1199.5839 ($M+H^+$)

GR17Zn: ^{1}H NMR (400MHz, CD_3CN): Broad

6.2.2 The synthesis of rigid ligands for grid of grids (RGR5, RGR9)

Synthesis of the compound RGR5*:

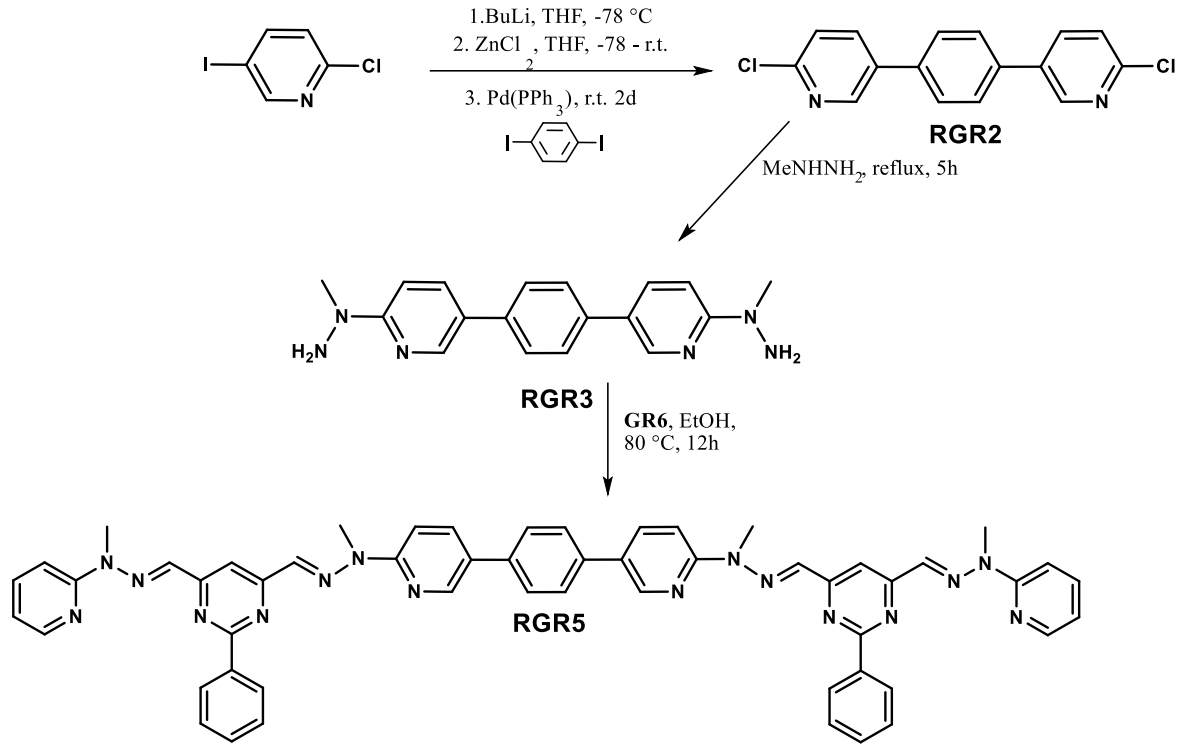

RGR2:

Baxter, P. N. W. *J. Org. Chem.*, **2000**, *65*, 1257–1272

RGR3:

The compound was synthesized according the standard procedure for preparation of hydrazine derivatives. The **RGR3** hydrazine also precipitated from the reaction mixture upon cooling.

^{1}H NMR (400MHz, DMSO): δ 8.40 (d, J = 2.7, 1H); 7.82 (dd, J = 2.3, J = 8.99, 1H); 7.64 (s, 2H); 7.22 (d, J = 8.6, 1H); 4.61 (s, 2H); 3.24 (s, 3H)

ESI-MS: 321.1837, calc.: 321.1822 ($M+H^+$);

RGR5:

The compound was synthesized according the standard procedure for alkylation of aliphatic hydroxyls. The ligand was obtained as off-white powder in >90% yield.
The compound is almost insoluble in DMSO and $CDCl_3$ therefore its ^1H NMR have very low resolution.

ESI-MS: 919.4147, calc: 919.4164 ($M+H^+$)

RGR5Zn:

^1H NMR: very broad.
ESI-MS: Inconclusive with bad resolution.

Synthesis of the ligand RGR9

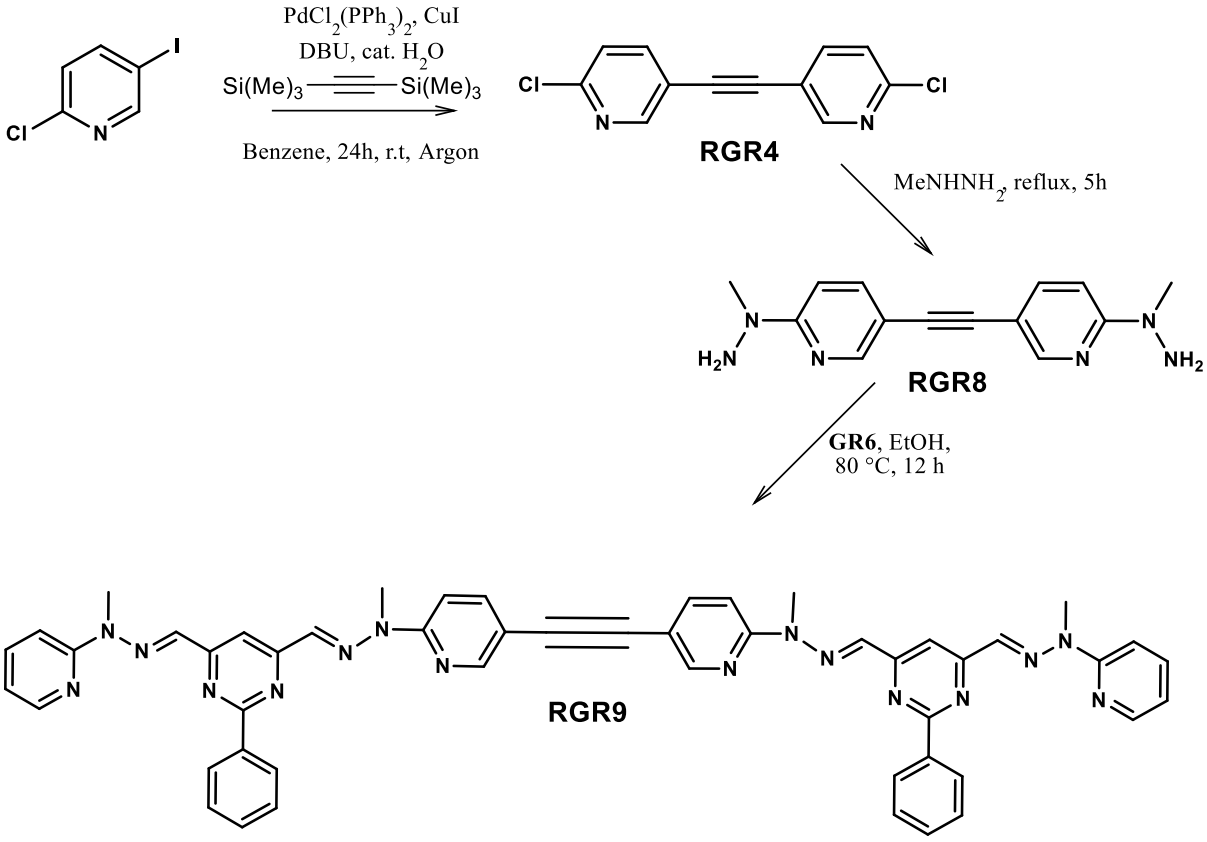

***RGR4*:**

Baxter, P. N. W. *J. Org. Chem.*, **2000**, *65*, 1257–1272

RGR8:

The compound was synthesized according the standard procedure for preparation of hydrazine derivatives. The **RGR8** hydrazine also precipitated from the reaction mixture upon cooling

^{1}H NMR (400MHz, DMSO): δ 8.15 (d, J=2.4, 1H); 7.54 (dd, J=2.2, J=8.8, 1H); 7.13 (d, J=9, 1H); 4.68 (s, 2H); 3.23 (s, 3H)

MS-ESI: 269.1516, calc.: 269.1509 ($M+H^+$)

RGR9:

The compound was synthesized according the standard procedure for alkylation of aliphatic hydroxyls. The ligand was obtained in >90 % yield.

^{1}H NMR (400MHz, $CDCl_3$): 8.54-51 (m, 2H); 8.48 (d, J=1.5, 1H); 8.37 (s, 1H); 8.31 (d, J= 3.9, 1H); 7.87-7.77 (m, 5H); 7.72 (dt, 1H); 7.53-7.51 (m, 3H); 6.94 (t, J=5.6, 1H); 3.80 (s, 3H); 3.79 (s, 3H);

MS-ESI: 867.3819, calc.: 867.3851 ($M+H^+$)

RGR9Zn:

^{1}H NMR: Very broad spectrum with $Zn(OTf)_2$

6.2.3 Synthesis of the basic grids with laterally functionalised ligands

Basic ligands and grids with classic functional groups

Synthesis of the ligand GR23

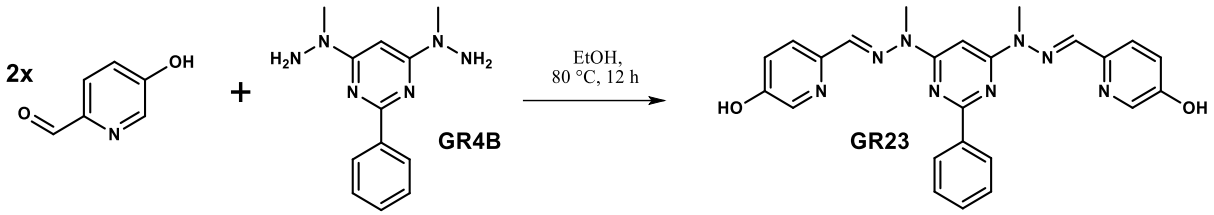

GR23:

Synthesized according the general procedure for hydrazone formation. Obtained as white solid in >90 % yield.

^{1}H-NMR (400MHz, DMSO): 10.30 (s, 2H); 8.45-8.48 (m, 2H); 8.21 (d, J=2.7, 2H); 7.95 (d, J=8.5, 2H); 7.90 (s, 2H); 7.70 (s,1H); 7.54 (t, j=3.4,3H); 7.34 (dd, J=2.7, J=8.5, 2H); 3.77 (s, 6H);

ESI-MS: 455.1941, calc.: 455.1938 ($M+H^+$)

M.p.: 341-343 °C (decomposition)

GR23Zn:

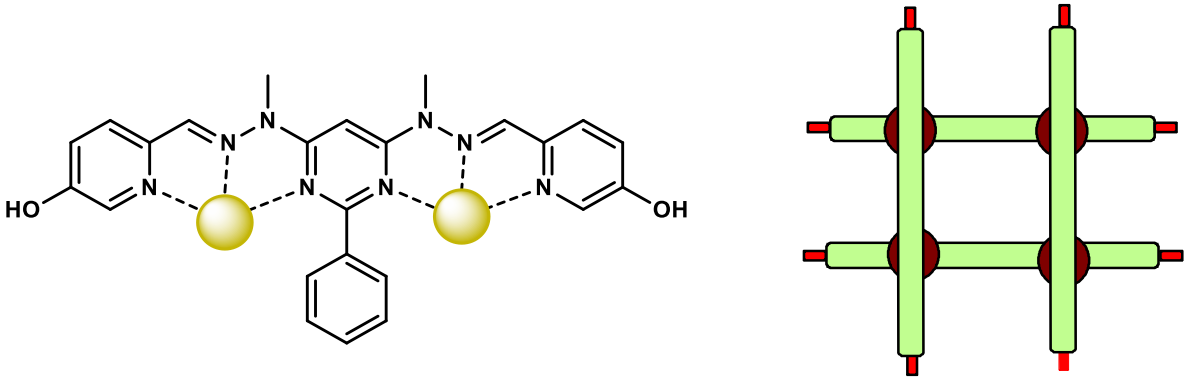

^{1}H-NMR (400MHz, CD_3CN): 10.82 (brs, 2H); 7.99 (s, 2H); 7.93 (t, J=7.6, 1H); 7.70 (t,J=7.3); 7.51 (d, J=8.5, 2H); 7.26 (dd, J=2.7, J=8.5, 2H); 7.12-7.17 (m, 3H); 6.76 (s, 1H); 6.44 (d, J=7.6, 1H); 5.62 (d, J=7.6, 1H); 3.61 (s, 6H);

^{13}C-NMR (CD_3CN): 166.11; 158.18; 157.06; 139.37; 138.18; 135.88; 135.49; 132.32; 130.48; 129.15; 128.55; 128.33; 125.56; 122.72; 122.42; 119;54; 33.18

MS-ESI: 941.7446, calc.: 941.7386 ($L_4M_4^{3+}$)

Synthesis of diamine ligand (GR26)

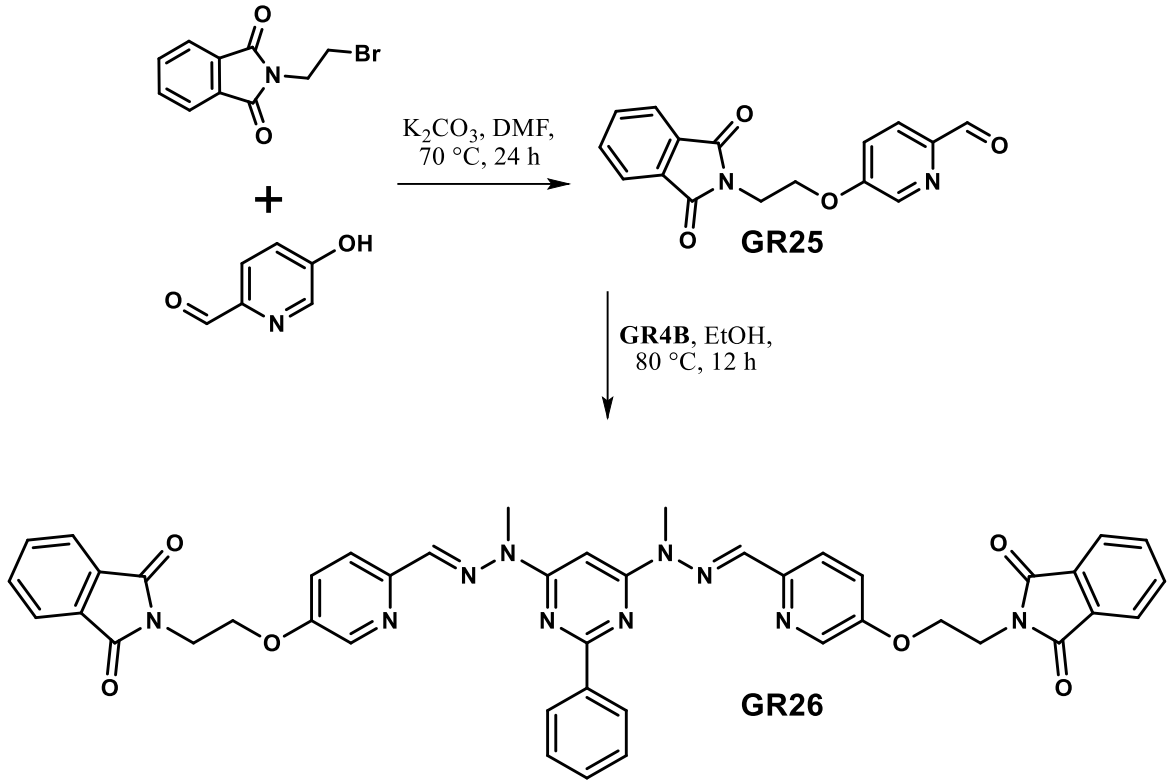

GR25:

Synthesized by the modified synthetic procedure for the alkylation aromatic alcohols. After evaporation of DMF, the residue was dissolved in CH_2Cl_2 and washed with water. The organic phase was collected and water phase was re-extracted two times withCH_2Cl_2. The organic phase was evaporated and the crude product purified by flash chromatography on silica (gradient of EtOAc: Petrol ether 1:4 to 2:1). The product was obtained as white solid in 63 % yield.

^{1}H-NMR (400MHz, $CDCl_3$): 10.02 (s, 1H); 8.45 (d, J=2.7, 1H); 7.99 (d, J=8.8, 1H); 7.94 (q, J=2.8, 2H); 7.80 (q, J=2.8, 2H); 7.35 (dd, J=8.6, J=2.6 ,1H); 7.34 (dd, J=2.7, J=8.5, 2H); 4.43 (t, J=5.6, 2H); 4.22 (t, J=5.6, 2H);

^{13}C NMR: 36.88, 65.44, 120.80, 123.25, 123.54, 131.89, 134.28, 138.73, 146.70, 157.69, 168.04, 191.92

ESI-MS: 297.0825, calc: 297.0870 ($M+H^+$)

M.p.: 139-140 °C

GR26:

^{1}H-NMR: Bad solubility in $CDCl_3$, (characterised in a form of Zn(II) complex)

ESI-MS: 801.2843, calc. 801.2892 ($M+H^+$)

GR26Zn:

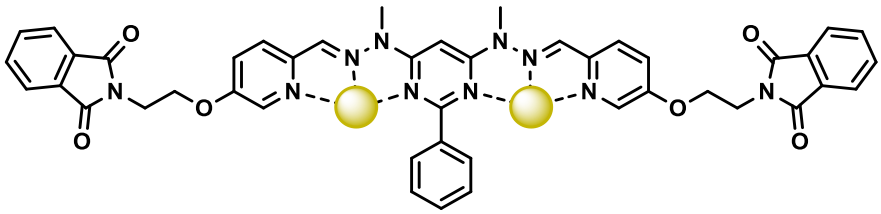

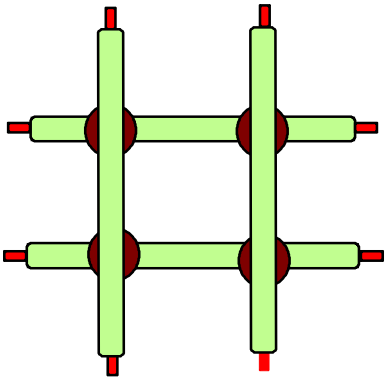

^{1}H-NMR(400MHz, CD_3CN): 8.07 (t, J=7.4, 1H); 8.01 (s, 2H); 7.82 (t, J=7.4, 2H); 7.77 (brs, 8H); 7.63 (d, J=8.5, 1H); 7.44 (dd, J=8.8, J=2.7, 2H); 7.27 (t, J=7.6, 1H); 7.15 (d, J=2.4, 2H); 6.81 (s, 1H); 6.48 (s, 1H); 5.68 (s, 1H); 4.17-4.10 (m, 4H); 3.73-3.69 (m, 4H); 3.68 (s, 6H);
^{13}C NMR (CD_3CN): 33.16, 35.89, 122.03, 122.47, 122.72, 124.11, 128.00, 128.48, 128.88, 130.52, 131.53, 132.53, 134.15, 135.06, 137.00, 139.13, 139.27, 156.87, 157.66, 165.98, 167.61,

GR27:

When a deprotection of **GR26** was carried out by standard method with hydrazine, the compound decomposed.

Second method, heating the ligand **GR26** in a mixture of H_2O/EtOH with 20x weight of KOH provided only partial hydrolysis of the phatilimide (**GR27**).

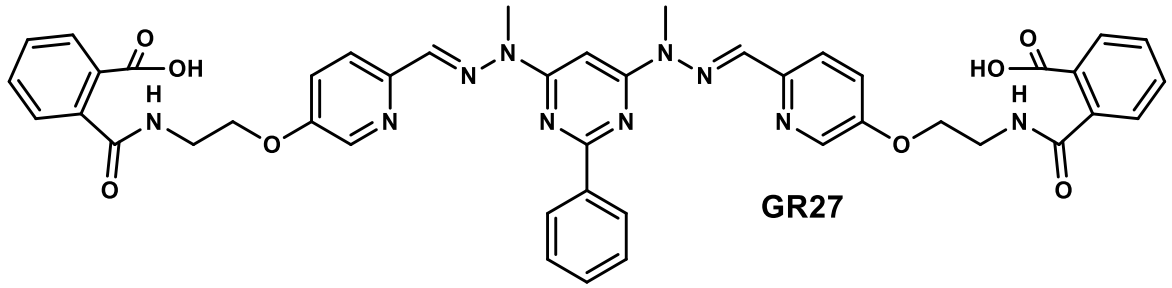

^{1}H-NMR (400MHz, $CDCl_3$): 8.49-8.46 (m, 2H); 8.41+8.40 (2xs or d, 2H); 7.99 (d, J=8.5, 2H); 7.96 (s, 2H); 7.80-7.76 (m, 4H); 7.67 (s, 1H); 7.53-7.56 (m, 4H); 7.42-7.44 (m, 2H); 7.32 (dt, 2H); 7.24 (dt, 2H); 4.28 (t, j=5.8,4H) 3.80 (s, 6H); 3.64 (m, 4H);

ESI-MS: 837.31, calc.: 837.31 ($M+H^+$)

Synthesis of simple grids with ester (GR29, GR28) or carboxylic functional groups (GR30, GR31)

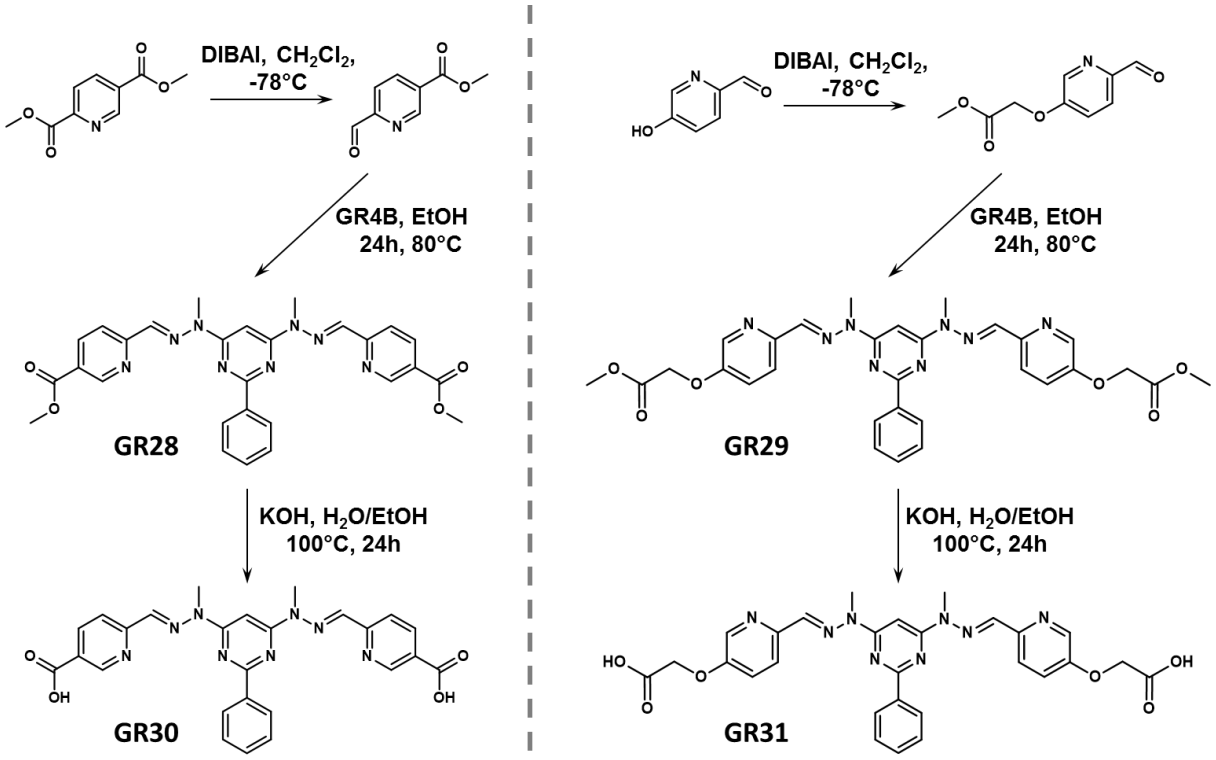

JHGR28:

^{1}H-NMR (400MHz, $CDCl_3$): 9.27 (s, 2H); 8.55-8.53 (m, 2H); 8.43-8.46 (m,2H); 8.27 (d, J=8.2, 2H); 8.07 (s, 2H); 7.88 (s, 1H); 7.54-7.56 (m, 3H); 4.07 (s, 6H) 3.93 (s, 6H);

GR28Zn:

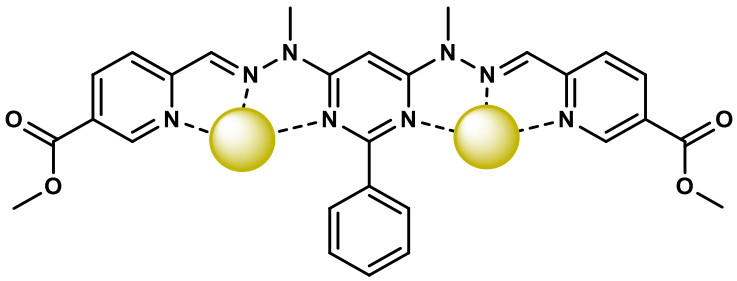

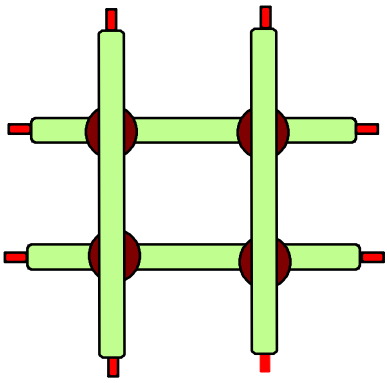

^{1}H-NMR (400MHz, $CDCl_3$): 8.39 (dd, J=1.8, J=7.9, 2H); 8.19 (s, 2H); 8.13 (t, J=7.4, 1H); 7.92 (t, J=7.4, 1H); 7.89-7.88 (m, 2H); 7.81 (d, J=7.9, 2H); 7.30 (t, J=7.4, 3H); 6.99 (s, 1H); 6.44 (d, J=7.3, 1H); 5.59 (d, J=7.6, 1H); 3.76 (s, 6H) 3.75 (s, 6H);

GR30:

Deprotection was carried out according the standard ester deprotection method. The **GR30** was obtained as white solid with 87 % yield.

^{1}H-NMR (400MHz, DMSO): 9.13 (s, 2H); 8.48-8.51 (m, 2H); 8.39 (d, J = 7.9, 2H); 8.16 (d, J = 7.9, 2H); 8.04 (brs, 2H); 7.78 (s, 1H); 7.57 (m, 3H); 3.86 (s, 6H)

GR30Zn:

Very insoluble complex of uncertain composition.

Blue fluorescence

GR29:

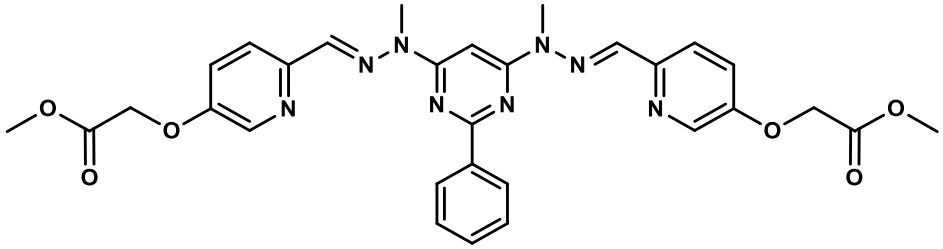

^{1}*H-NMR (400MHz, DMSO):* 8.47 (m, 2H); 8.38 (m, 2H); 7.98 (d, J=8.8, 2H); 7.94 (s, 2H); 7.69 (s, 1H); 7.65-7.6 (m, 2H); 7.57 (m, 3H); 5.03 (s, 4H); 3.78 (s, 3H); 3.75 (s, 3H);

GR29Zn:

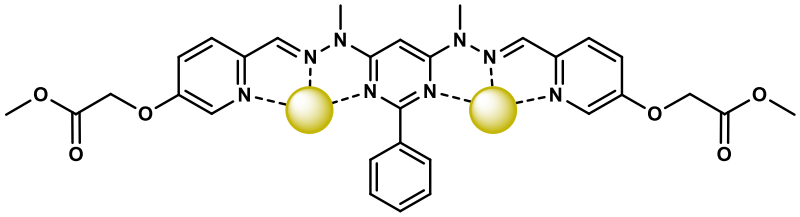

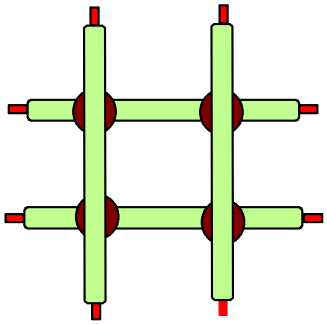

^{1}*H-NMR (400MHz, CD_3CN):* 7.99 (t, J = 7.6, 1H); 7.95 (s, 2H); 7.78 (t, J = 7.5, 2H); 7.64 (d, J = 8.6, 2H); 7.92 (t, J = 7.4, 1H); 7.38 (dd, J = 2.7, J = 8.8, 2H); 7.31 (d, J = 2.7, 2H); 7.30 (t, J = 7.4, 3H); 7.18 (t, J = 7.6, 1H); 6.73 (s, 1H); 6.42 (d, J = 7.3, 1H); 5.51 (d, J = 7.6, 1H); 4.63 (s, 4H); 3.67 (s, 6H) 3.63 (s, 6H);

Synthesis of basic bishydrazone ligand with two aldehyde groups (GR33)

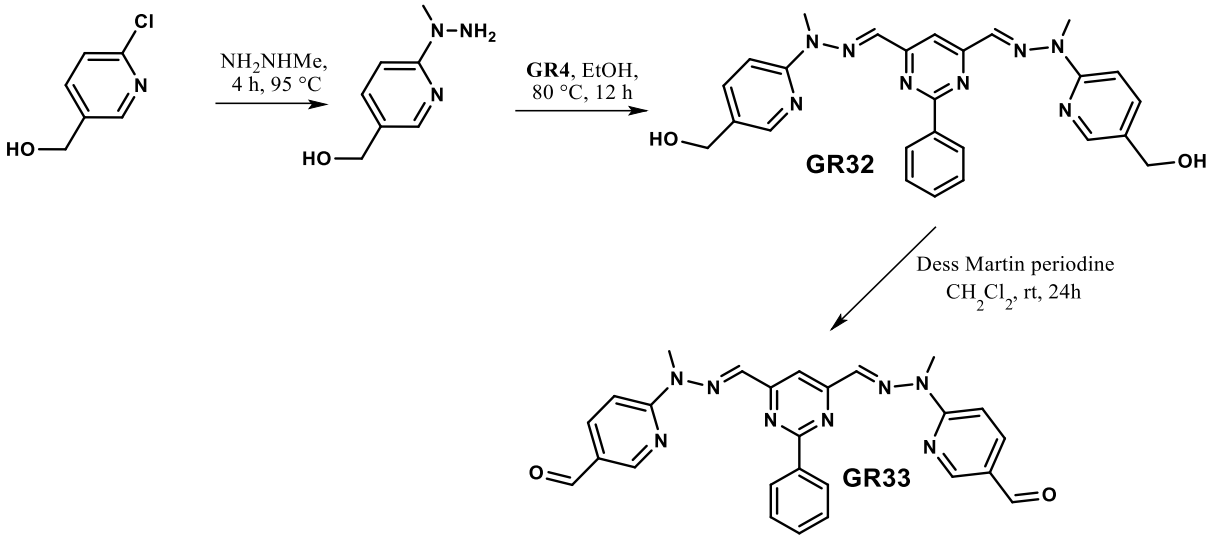

GR32:

Synthesized according the standard procedure for hydrazone formation. The product was obtained as orange powder with >90 % yield.

^{1}H-NMR (400MHz, DMSO): 8.54-8.49 (m, 2H); 8.26-8.24 (m, 3H); 7.80-7.78 (m, 6H); 7.57-7.55 (m, 3H); 5.23 (t, J=5.7, 2H); 4.50 (d, J=5.5, 4H); 3.73 (s, 6H);

^{13}C NMR: 164.09, 162.28, 156.18, 146.10, 137.88, 137.66, 133.15, 131.42, 131.24, 129.04, 128.27, 109.67, 108.09, 60.79, 30.59;
ESI-MS: 505.2095, calc.: 505.2071 ($M+Na^{+}$)

GR32Zn:

Compound doesn't form clean complex. There are signs of grid formation, but there is also a lot of hydrolysis.

GR33:

The compound was prepared according to standard procedure for Dess-Martin oxidation. The product was filtered off the reaction mixture as yellow solid in 83% yield.

^{1}H-NMR (400MHz, DMSO, 80°C): 10.00 (s, 2H); 8.82 (d, J=1.9, 2H); 8.55-8.52 (m, 2H); 8.33 (s, 1H); 8.22 (dd, J=8.6, 2H); 8.07 (brs, 2H); 7.96 (d, J=8.6, 2H); 7.57-7.59 (m, 3H); 3.85 (s, 6H);

ESI-MS: 501.1718, calc.: 501.1758 ($M+Na^{+}$)

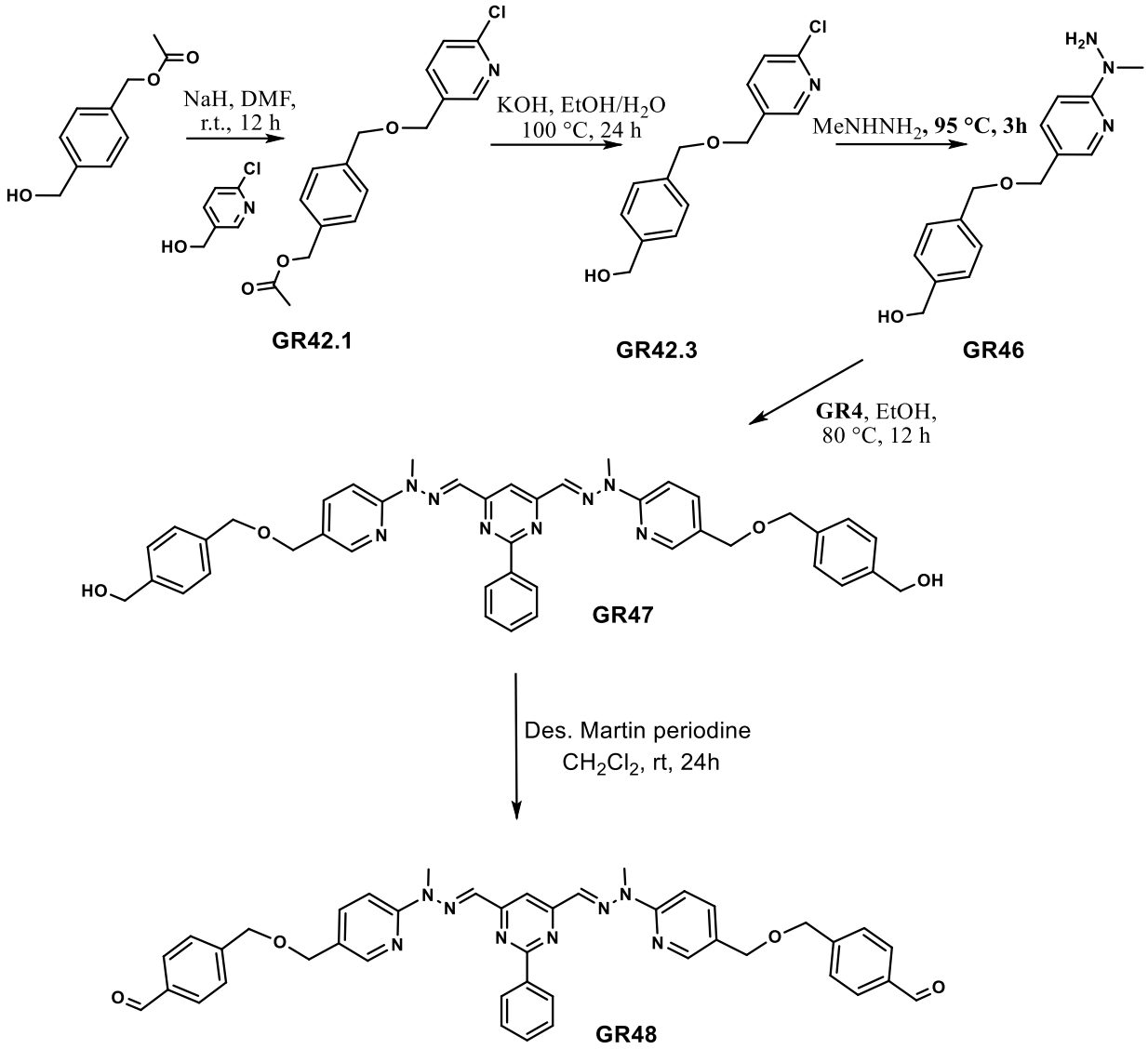

GR42.1:

4-Hydroxymethylbenzyl acetate (1 eq.) was added to the round bottom flask and dissolved in dry DMF. To this flask 4 eq. of NaH were added, the mixture was stirred for 15 min. and 5-(chloromethyl)-2-chloropyridine (1 eq.) was added. The reaction mixture was then stirred for 24 h. After that, DMF was evaporated under vacuo, and the crude product obtained by extraction with CHCl3 from water and evaporation of organic phase. The pure **GR42.1.** was obtained silica chromatography with EtOAc/petrolether gradient from 1:4 to 2:1. Yield 55 %.

^{1}H-NMR (400MHz, $CDCl_3$): 8.35 (d, J=2.4, 1H); 7.67 (dd, J=2.4, J=8.2, 1H); 7.36 (bs, 4H); 7.32 (d, J= 8.2, 1H); 5.11 (s, 2H); 4.56 (s, 2H); 4.53 (s, 2H); 2.10 (s, 3H);

JHGR42.3:

This product was obtained by general ester deprotection procedure. Yield 83%.

^{1}H-NMR (400MHz, $CDCl_3$): δ 8.35 (d, J=2.4, 1H); 7.67 (dd, J=2.4, J=8.2, 1H); 7.38-7.31 (m, 5H); 5.11 (s, 2H); 4.71 (s, 2H); 4.58 (s, 2H); 4.53 (s, 2H)

^{13}C NMR: δ 150.66, 148.73, 150.71, 138.39, 136.92, 132.80, 128.09, 127.19, 124.19, 72.44, 68.59, 65.05

ESI-MS: 264.0809, calc.: 264.0786 ($M+H^+$)

GR46:

This compound was obtained by standard procedure for hydrazine formation. Yield >90%.

^{1}H-NMR (400MHz, DMSO): 7.99 (d, 1H); 7.47 (dd, J=2.3, J=8.7, 1H); 7.32-7.27 (m, 4H); 7.15 (d, J= 8.5, 1H); 5.16 (t, J=5.5, 1H); 4.56 (s, 2H); 4.49 (d, J=4.49, 2H); 4.45 (s, 2H); 4.41 (s, 2H); 4.35 (s, 2H); 3.2 (s, 3H);

^{13}C NMR: 161.93, 147.41, 142.17, 137.82, 137.24, 127.8, 126.80, 121.48, 107.51, 71.18, 69.53, 63.16

GR47:

This compound was obtained by standard method for hydrazone preparation.

^{1}H-NMR (400MHz, DMSO): 8.49-8.51 (m, 2H); 8.28 (d, J=1.2, 2H), 8.25 (s, 1H); 7.79-7.85 (m, 6H); 7.55-7.57 (m, 3H); 7.32-7.27 (m, 8H); 5.16 (t, J=5.6, 2H); 4.52 (s, 4H); 4.50 (s, 4H); 4.48 (d, 4H); 4.41 (s, 2h); 4.35 (s, 2H); 3.74 (s, 6H);

^{13}C NMR: 164.10, 162.26, 156.66, 147.16, 142.30, 138.85, 137.63, 137.01, 133.62, 131.27, 129.06, 128.28, 127.89, 127.40, 126.84, 124.29, 109.89, 108.42, 71.68, 69.07, 63.15, 30.58

GR47Zn:

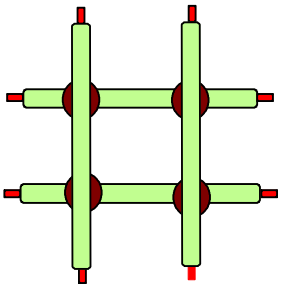

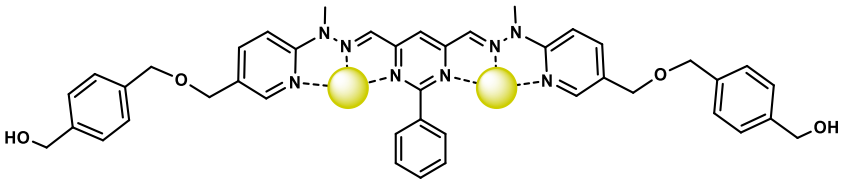

[1]H-NMR(400MHz, DMSO): 8.18 (t, J= 6, 1H); 8.13 (s, 1H), 8.25 (s, 1H); 7.83-7.85 (m, 4H); 7.53 (t, J=7.7, 1H); 7.34 (t, J=7.3, 1H); 7.28, 7.26 (2xs, 6H); 7.13 (d, J=7.9, 4H); 7.08 (d, J=1.8, 2H); 5.87 (t, J=6.12, 2H); 4.54 (d, J=5.4, 4H); 4.32 (s, 4H); 4.16 (s, 4H); 3.46 (s, 6H); 3.32 (t, J=5.6, 2H);

[13]C NMR: 166.87, 158.78, 149.92, 145.17, 143.31, 142.85, 137.55, 135.96, 134.80, 133.55, 131.31, 130.69, 129.87, 128.80, 128.57, 127.85, 124.62, 123.75, 122.86, 120.56, 112.80, 73.36, 68.23, 64.39, 35.21

GR48:

This compound was obtained by Standard Dess-Martin method as yellow powder in 75 % yield.

[1]H-NMR (400MHz, DMSO): 10.00 (s, 2H); 8.55-8.5 (m, 2H), 8.34 (d, J=1.5, 2H); 8.28 (s, 1H); 7.92-7.83 (m, 9H); 7.61-7.58 (m, 1H); 4.661 (s, 4H); 4.59 (s, 4H); 3.77 (s, 6H);

GR48Zn: From unknown reasons the ligand did not provide clean grid assembly.

6.2.4 Synthesise of extended dialdehyde ligand GR67, its complexes and decoration with other imines.

Dynamic assembly of GR67Zn:

The dialdehyde 2 eq. **GR40**, dihydrazine 1 eq. **GR4B** and 1eq. of $Zn(OTf)_2$ were added to NMR tube and dissolved in acetonitrile. The resulting mixture was heated at 70 °C for 12 h and analysed by ^{1}H NMR. (*Figure S2.2*)

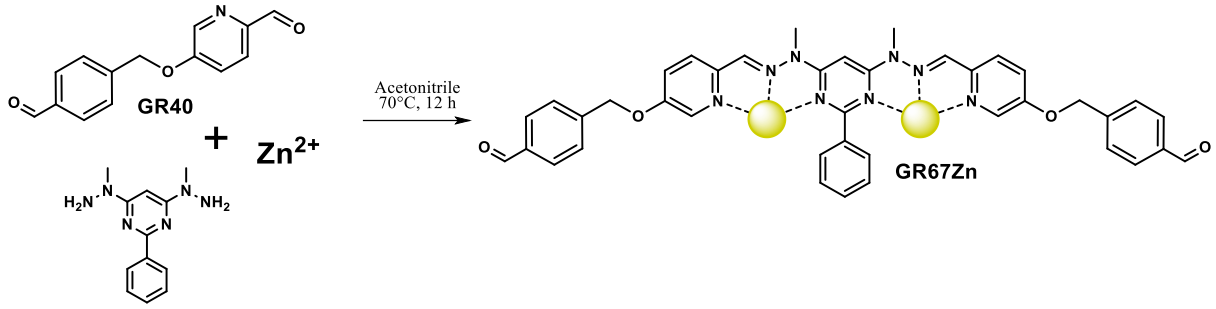

GR40:

^{1}H-NMR (400MHz, $CDCl_3$): 10.47 (s, 1H); 10.00 (s, 1H); 8.53 (brs, 1H); 7.98-7.93 (m, 3H); 7.61 (d, 2H); 7.36 (dd, J=2.7, J=8.8, 1H); 5.29 (s, 2H)

ESI-MS: 264.0718, calc.: 264.0631 ($M+Na^+$)

Dynamic and classic assembly of GR67Zn (Figure E2.3)

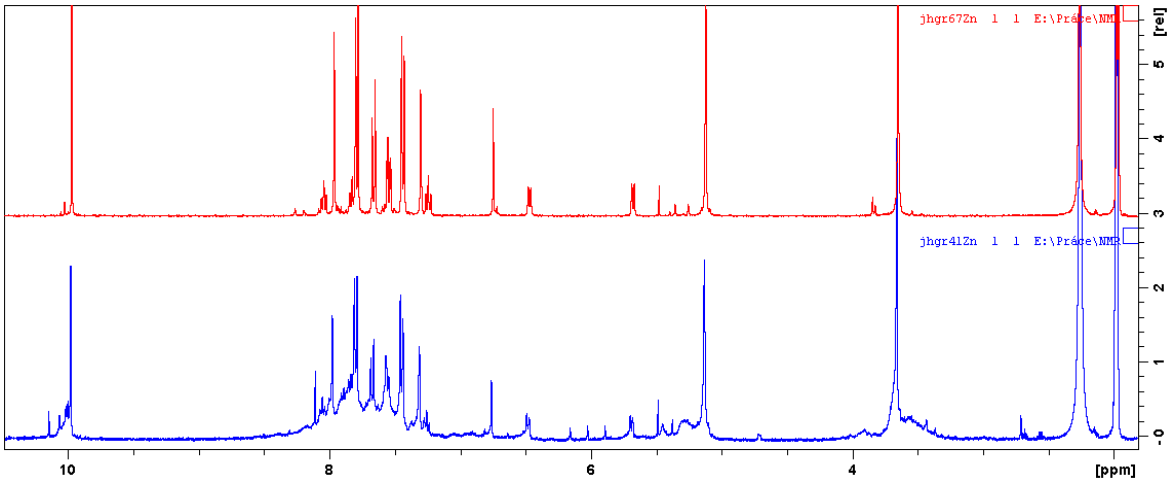

Figure E2.3: Bottom: Dynamic assembly of **GR67Zn** from components. **Top**: The assembly of the grid **GR67Zn** from the preformed ligand **GR67**.

Bottom up synthesis of dialdehyde ligand GR67 its Zn(II) complex and imine decoration of aldehydes in the GR67Zn complex

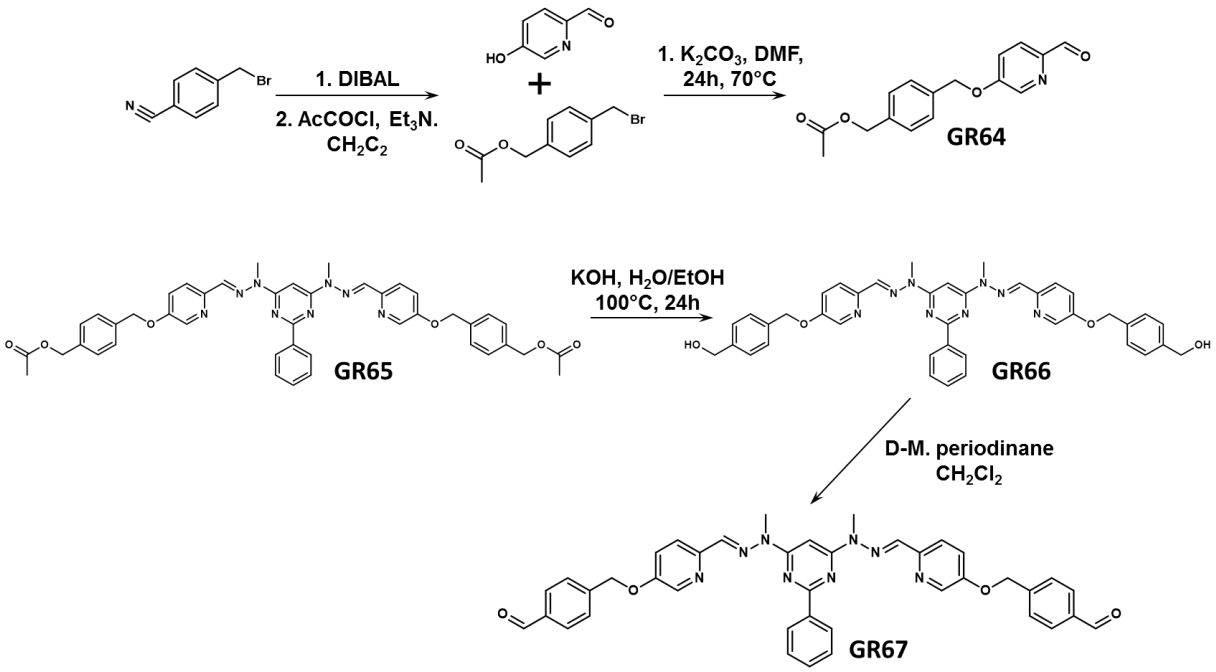

GR64:

Synthesized the standard synthetic procedure for the alkylation of aliphatic hydroxyls a ehite powder in yield 74 %.

^{1}H-NMR (400MHz, DMSO): 9.89 (s, 1H);8.56 (d, J = 2.7, 1H); 7.94 (d, J = 8.7, 1H); 7.66 (dd, J = 2.8, J = 8.7, 1H); 7.49 (d, J = 8.1, 2H); 7.41 (d, J = 8.1, 2H); 5.33 (s, 2H); 5.08 (s, 2H); 2.06 (s, 3H);

^{13}C NMR (DMSO): 191.96; 170.21; 157.89; 145.84; 138.99; 136.32; 135.57; 128.19; 128.07; 123.50; 121.57; 69.76; 65.09; 20.69;

GR65:

Synthesized according to standard procedure for hydrazone hydrazone formation in a yield >90 %.

^{1}H-NMR (400MHz, CDCl$_3$): 8.50-8.46 (m, 2H); 8.35 (d, J = 2.3, 2H); 8.09 (d, J = 8.80, 2H); 7.86 (s, 2H); 7.76 (s, 1H); 7.49-7.44 (m, 7H); 7.39 (d, 4H); 7.29 (dd, J = 2.3, J = 8.7, 2H); 5.19 (s, 4H); 5.11 (s, 4H); 3.80 (s, 6H); 2.10 (s, 3H);

^{13}C NMR (DMSO): 170.95; 163.34; 162.34; 154.63; 148.65; 138.39; 136.43; 136.13; 130.43; 128.85; 128.38; 128.20; 127.97; 123.33; 120.29; 86.77; 70.42; 65.99; 29.85; 21.13;

ESI-MS: 779.3451, calc.: 779.3426 ($M+H^+$)

GR65Zn:

This compound was prepared according the standard grid complex formation.

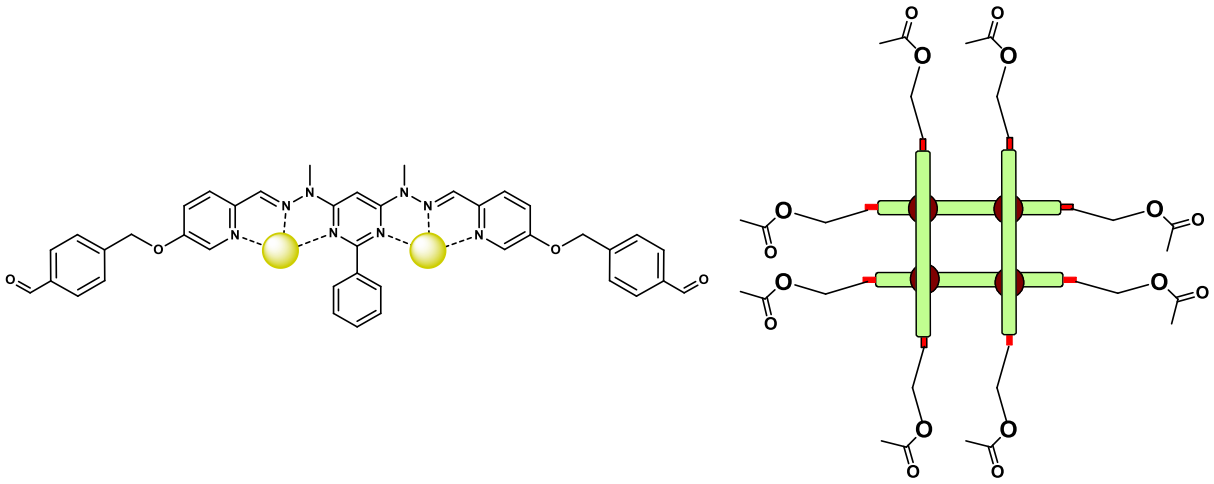

^{1}H-NMR (400MHz, CD_3CN): 7.99 (t, J = 7.6, 1H); 7.90 (s, 2H); 7.78 (t, J = 7.78, 1H); 7.63 (d, J = 8.7, 2H); 7.5 (dd, J = 2.6, J = 8.8, 2H); 7.29-7.18 (m, 10H); 6.68 (s, 1H); 6.43 (d, J = 7.2, 1H); 5.64 (dd, J = 7.5, 1H); 5.04 (s, 4H); 5.00 (s, 4H); 3.59 (s, 6H); 2.03 (s, 6H);

^{13}C NMR (CD_3CN): 171.53; 167.17; 159.23; 158.08; 140.27; 138.11; 137.78; 136.39; 135.85; 133.71; 130.16; 129.87; 129.19; 128.85; 124.62; 123.38; 71.55; 66.26; 34.30; 21.08;

ESI-MS: 13373.9388, calc.: 1373.9363 $[(GR65)_4Zn_4(OTf)_5]^{3+}$;

GR66:

The compound was prepared according the standard ester deprotecting method.

^{1}H-NMR (400MHz, DMSO): 8.47-8.44 (m, 2H); 8.43 (d, J = 2.7, 2H); 7.98 (d, J = 8.6, 2H); 7.92 (s, 3H); 7.68-7.11 (m, 3H); 7.55-7.53 (m, 3H); 7.45 (d, J = 8.3, 4H); 7.33 (J = 8.4, 4H); 5.29 (s, 4H); 5.20 (t, J = 5.7, 2H); 4.49 (d, J = 5.7, 4H); 3.77 (s, 6H);

^{13}C NMR (DMSO): 193.17; 167.21; 159.00; 158.11; 142.60; 140.33; 140.23; 138.02; 137.39; 136.40; 133.77; 131.68; 130.67

ESI-MS: 695.3147, calc.: 695.3199 ($M+H^{+}$)

GR66Zn:

This compound was prepared according the standard grid complex formation.

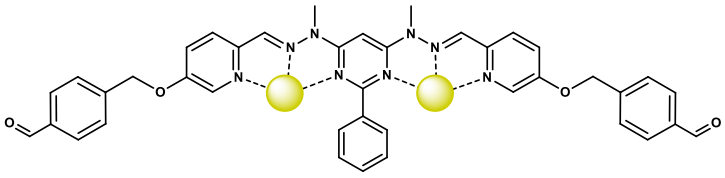

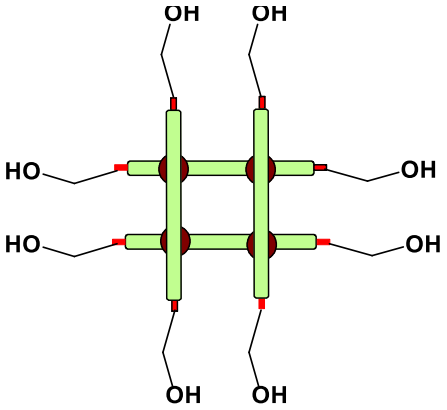

^{1}H-NMR (400MHz, CD_3CN): 7.99 (t, J = 7.5, 1H); 7.89 (s, 2H); 7.77 (t, J = 7.5, 1H); 7.64 (d, J = 8.7, 2H); 7.52 (dd, J = 2.7, J = 8.8, 2H); 7.24 (d, J = 8.0, 4H); 7.21-7.17 (m, 7H); 6.67 (s, 1H); 6.42 (d, J = 7.3, 1H); 5.63 (d, J = 7.6, 1H); 5.00 (s, 4H); 4.54 (d, J = 5.7, 4H); 3.59 (s, 6H); 3.38 (t, J = 5.8, 2H);

ESI-MS: 1261.8993, calc.: 1261.9079 $[(GR66)_4Zn_4(OTf)_5]^{3+}$;

GR67:

This compound was synthetized according the standard Dess-Martin method in a yield 68%.

^{1}H-NMR (400MHz, DMSO): 10.00 (s, 2H); 8.47-8.44 (m, 4H); 8.00 (d, J = 8.9, 2H); 7.94-7.92 (m, 6H); 7.72-7.68 (m, 7H); 7.51-7.55 (m, 3H); 5.44 (s, 4H); 3.77 (s, 6H);

ESI-MS: 691.2825, calc.: 691.2886 ($M+H^{+}$);

GR67Zn:

This compound was prepared according the standart grid coplex formation as it is described for simple grids with Zn(II).

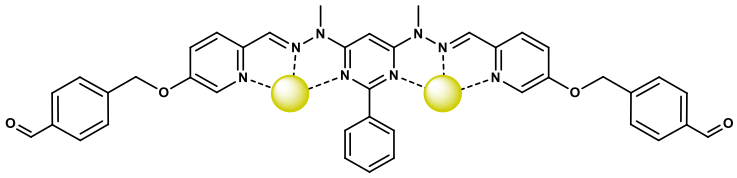

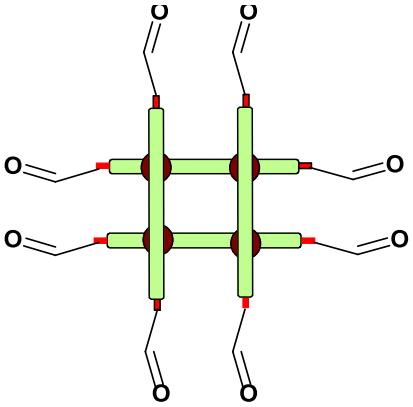

^{1}H-NMR (400MHz, CD_3CN): 9.94 (s, 2H); 8.01 (t, J = 7.6, 1H); 7.93 (s, 2H); 7.79 (t, J = 7.5, 1H); 7.76 (d, J = 8.3, 4H); 7.63 (d, J = 8.6, 2H); 7.52 (dd, J = 2.7, J = 8.7, 2H); 7.41 (d, J = 8.1, 4H); 7.27 (d, J = 2.7, 2H); 7.21 (t, J = 7.6, 1H); 6.72 (s, 1H); 6.44 (d, J = 7.8, 1H); 5.64 (d, J = 7.6, 1H); 5.09 (s, 4H); 3.62 (s, 6H);

^{13}C NMR (CD_3CN): 193.17; 167.21; 159.00; 158.11; 142.60; 140.33; 140.23; 138.02; 137.39; 136.40; 133.77; 131.68; 130.67; 130.19; 129.9; 129.19; 128.72; 124.85; 71.03;34.39;

ESI-MS: 1256.8542, calc.: 1256.8523 $[(\mathbf{GR67})_4Zn_4(OTf)_5]^{3+}$;

GR67Ag:

This compound was prepared according the standard grid complex formation.

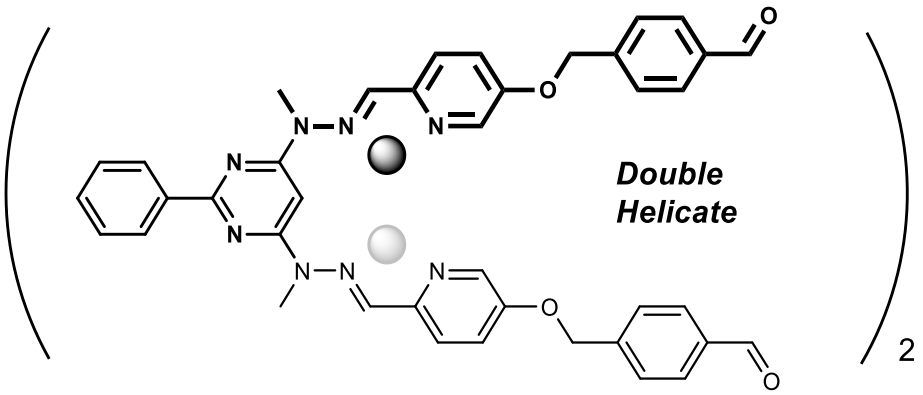

^{1}H-NMR (400MHz, CD_3CN): 9.97 (s, 2H); 8.34 (d, J = 7.1, 2H); 7.91(s, 2H); 7.75 (d, J = 8.2, 4H); 7.69-7.66 (m, 4H); 7.55 (dd, J = 2.8, J = 8.7, 2H); 7.46 (t, J = 7.2, 1H); 7.36 (t, J = 7.5, 2H); 7.20-7.18 (m, 5H); 4.76 (s, 4H); 3.57 (s, 6H)

^{13}C NMR (CD_3CN): 193.22; 162.70; 162.62; 156.91; 144.86; 142.85; 139.89; 138.39; 138.04; 137.32; 132.08; 130.55; 129.61; 128.97; 128.86; 127.42; 125.42; 70.83; 32.18;

Four following **GR67Zn grids with functionalized aldehyde groups were all prepared according the standard decoration procedure.*

Decorated grids from GR67Zn

GR67Zn+n-butylamine*:

This compound was prepared according the standard decoration procedure.

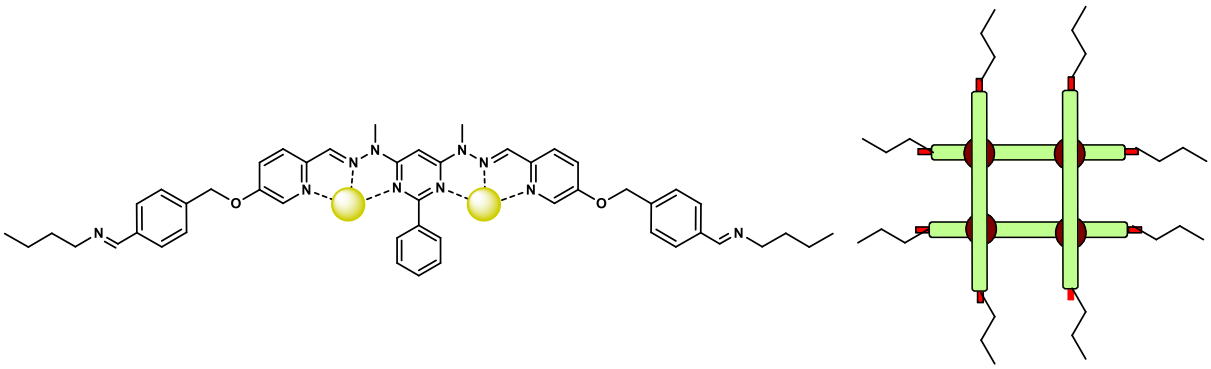

^{1}H-NMR (400MHz, CD_3CN): 8.27 (s, 2H); 8.02 (t, J = 7.6, 1H); 7.93 (s, 2H); 7.81 (t, J = 7.5, 1H); 7.65-7.62 (m, 6H); 7.52 (dd, J = 2.7, J = 8.7, 2H); 7.28-7.25 (m, 6H); 7.21 (t, J = 7.6,

1H); 6.91 (d, J = 8.2, 4H); 6.73 (s, 1H); 6.58 (d, J = 8.3, 4H); 6.45 (d, J = 7.8, 1H); 5.66 (d, J = 7.6, 1H); 5.07 (s, 4H); 3.63 (s, 6H); 3.59 (t, J = 6.6, 4H); 2.72 (t, J = 7.1, 4H); 1.64 (p, J = 7.3, 4H); (last triplet is hidden behind the peaks of free *n*-butylamine)

GR67Zn+p-toluidine*:

This compound was prepared according the standard decoration procedure.

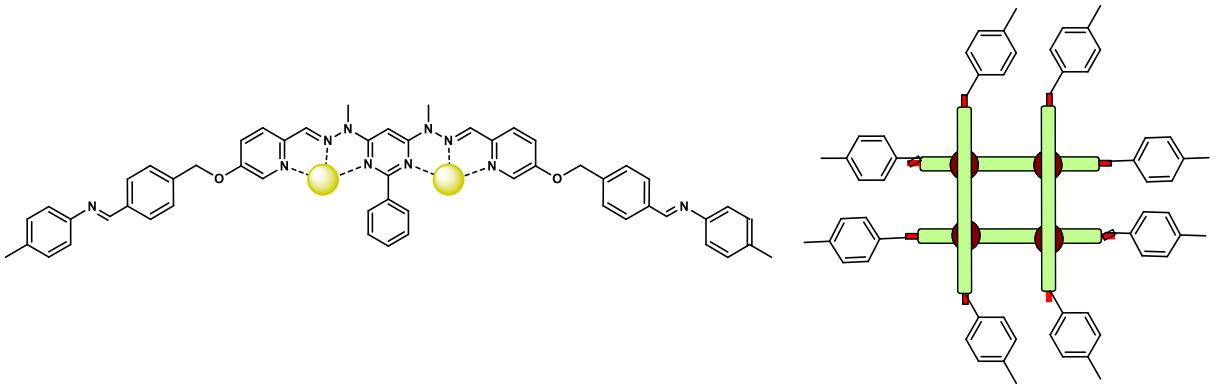

^{1}*H-NMR (400MHz, CD_3CN)*: 8.47 (s, 2H); 8.00 (t, J = 7.6, 1H); 7.91 (s, 2H); 7.80-7.77 (m, 5H); 7.64 (d, J = 8.6, 2H); 7.55-7.52 (m, 2H); 7.32 (d, J = 7.9, 4H); 7.28-7.19 (m, 4H); 7.21 (t, J = 7.6, 1H); 7.16 (d, J = 7.6, 4H); 7.08 (d, J = 8.2, 4H); 6.71 (s, 1H); 6.43 (d, J = 7.3, 1H); 5.62 (d, J = 7.2, 1H); 5.08 (s, 4H); 3.62 (s, 6H); 3.59 (t, J = 6.6, 4H); 2.33 (s, 6H);

GR67Zn+1-(N-methyl)-1-phynylhydrazine*:

This compound was prepared according the standard decoration procedure.

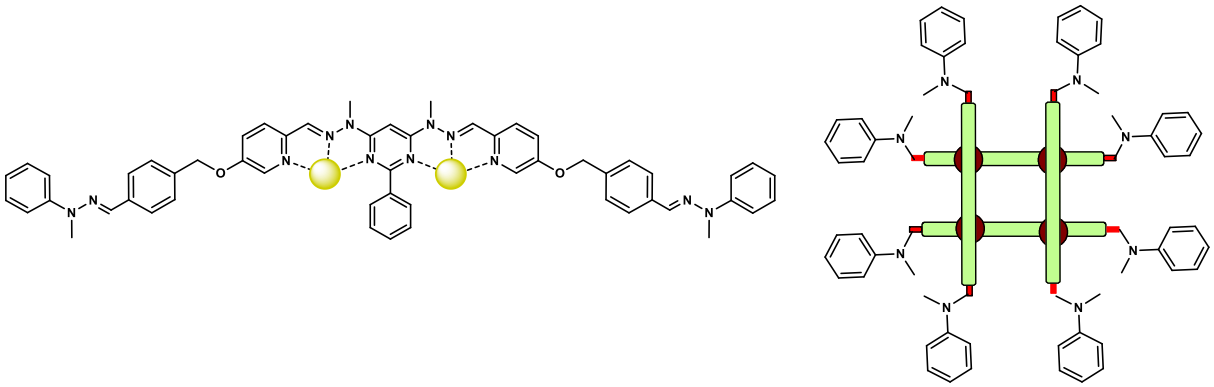

^{1}*H-NMR (400MHz, CD_3CN)*: 8.02 (t, J = 7.6, 1H); 7.89 (s, 2H); 7.79 (t, J = 7.5, 1H); 7.64-7.6 (m, 6H); 7.53 (s, 2H); 7.49 (dd, J = 2.7, J = 8.7, 2H); 7.41-7.38 (m, 4H); 7.34-7.28 (m, 5H); 7.24-7.19 (m, 13H); 7.17-7.13 (m, 1H); 7.04-7.01 (m, 6H); 6.94-6.90 (m, 2H); 6.76-6.71 (s, 4H); 6.65-6.59 (m, 1H); 6.43 (d, J = 7.3, 1H); 5.65 (d, J = 7.5, 1H); 5.02 (s, 4H); 3.62 (s, 6H); 3.36 (s, 6H);

GR67Zn+2-(2-Aminoethoxy)ethylamine (GR67ZnIm1) (Figure E2.5)*:

This compound was prepared according the standard decoration procedure. A lot of precipitate formed shortly after addition of diamino to the GR67Zn. Therefore, before measuring NMR of decorated grid, the solution was filtered through the wool stuck in Pasteur pipet.

^{1}H-NMR (400MHz, CD_3CN): 8.13 (s, 2H); 7.93 (s, 2H); 7.72 (t, J = 7.5, 1H); 7.67 (d, J = 8.6, 2H); 7.53-7.50 (m, 3H); 7.43 (d, J = 8.05, 4H); 7.24-7.20 (m, 6H); 7.09 (t, J = 7.4, 1H); 6.64 (s, 1H); 6.35 (d, J = 7.4, 1H); 5.30 (d, J = 7.3, 1H); 4.90 (q, J = 11.0, 4H); 3.55 (m,) this multiplet is mixed with the peaks of free Bis(2-aminoethyl) Ether

^{1}H NMR spectra of GR67Zn with aliphatic diamine – intraconnected grids

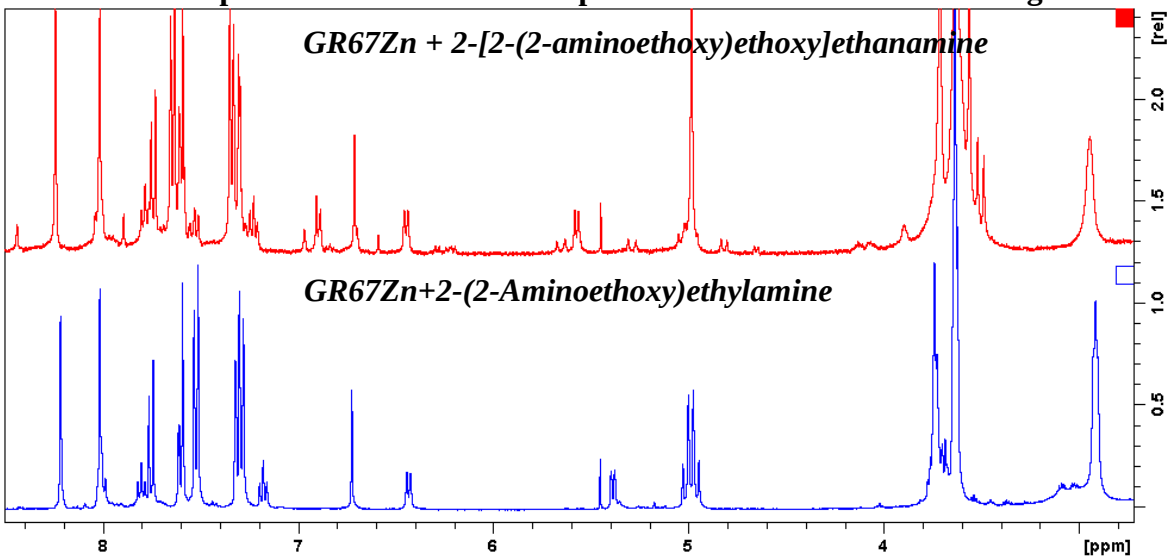

Figure E2.4.: Comparison of the unknown grid (proposed structure below Figure E1.5) after addition of 2-(2-Aminoethoxy)ethylamine (**GR67ZnIm1**, **Bottom**) and 2-[2-(2-aminoethoxy)ethoxy]ethanamine; **Top**) to the **GR67Zn**. Also, formation of large quantities of a precipitate of unknow constitution was observed as well.

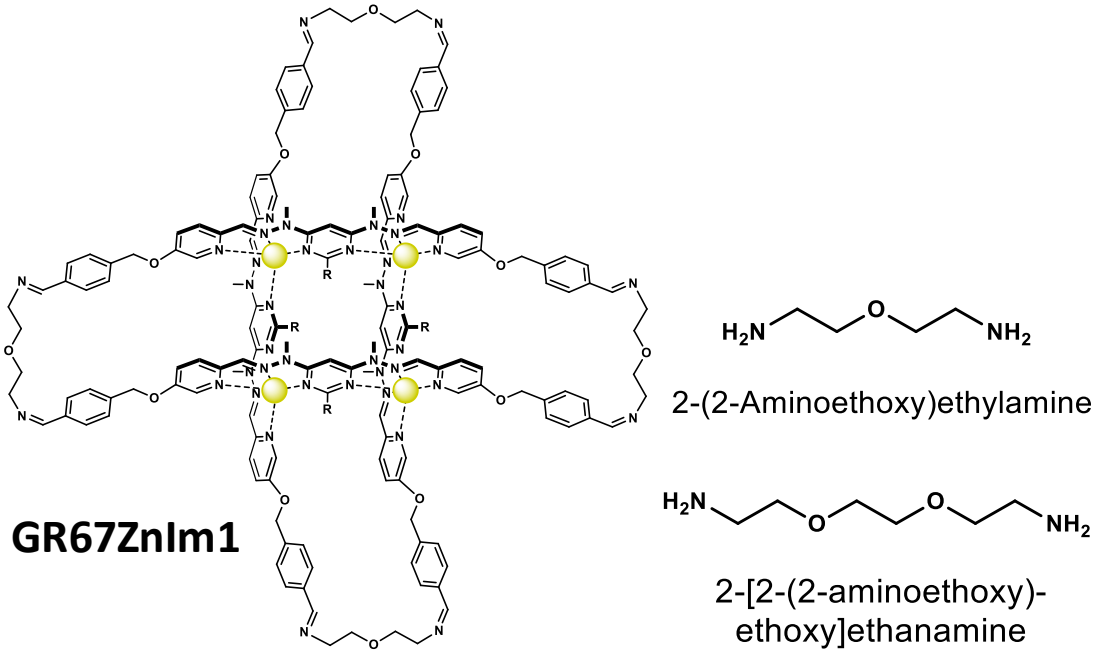

Figure E1.5.: Depiction of the proposed structure of observed unknown grid from the Figure E1.4. and structures of used diamines.

6.2.5 Synthesis of the aldehyde functionalized grids (GR70(B)Zn, GR71(B)Zn, GR72(B)Zn)

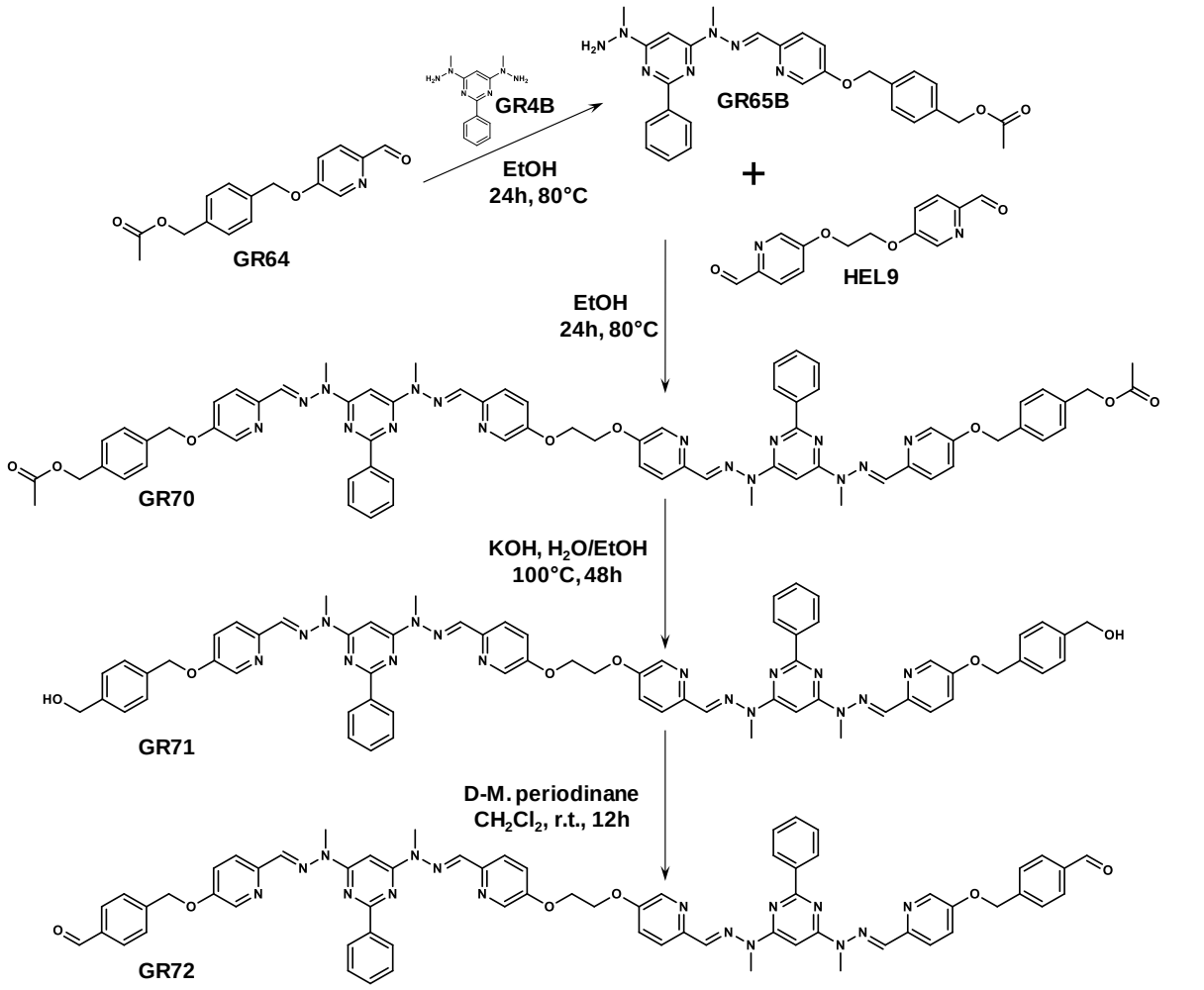

Folded grids: + 2 eq. $Zn(OTf)_2$

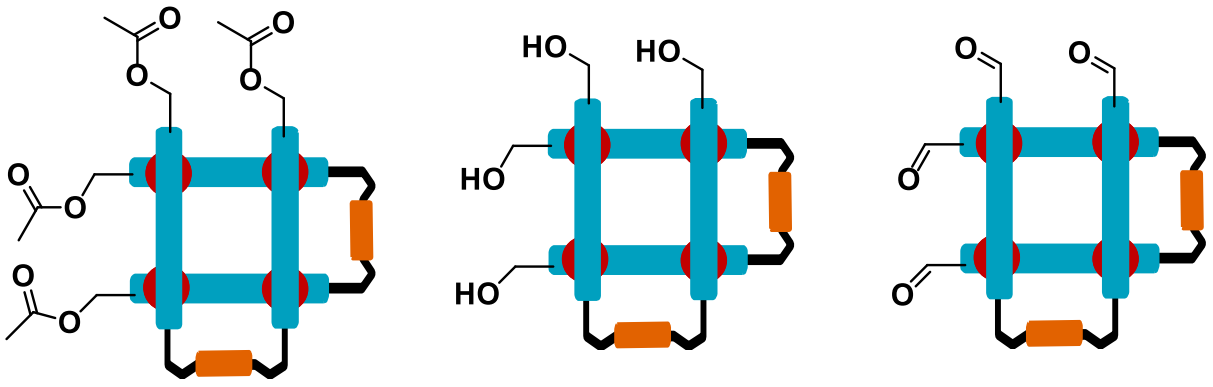

GR70Zn **GR71Zn** **GR72Zn**

OR

GR70BZn **GR71BZn** **GR72BZn**

Synthesis of the functionalized ligands:

GR65B:

The compound **GR65B** was prepared by mixing the dihydrazine **GR4B** and aldehyde **GR64** in 1:1 ratio. The mixture was left to stir at room temperature for 12 h. After that period, newly formed white precipitate was filtered and dissolved in little amount of acetonitrile and purified by the reverse phase chromatography with the gradient water/acetonitrile 95/5 to 5/95. The compound **GR65B** was obtained as white powder in 42 % yield. Such obtained pure product was then used in a following work.

^{1}H-NMR (400MHz, $CDCl_3$): 8.46-8.44 (m, 2H); 8.33 (d, J = 2.8, 1H); 7.99 (d, J = 8.8, 1H); 7.83 (s, 1H); 7.47-7.39 (m, 7H); 7.32 (dd, J = 2.8, J = 8.8, 1H); 6.92 (s, 1H); 5.17 (s, 2H); 5.12 (s, 2H); 4.29 (brs, 2H); 3.78 (s, 3H); 3.43 (s, 3H); 2.11 (s, 3H);

ESI-MS: 512.2391, calc.: 512.2405 ($M+H^+$);

GR70:

The ligand **GR70** was prepared according the modified standard procedure for the formation of hydrazones. After the 24 h of heating at reflux the mixture of **GR65B** and **HEL9** (Chapter 2) the white precipitate was filtered. However, some unreacted starting materials were present according the ^{1}H NMR. Therefore, additional purification by precipitation from hot DMF had to be included in the procedure. Filtration of the precipitate provided **GR70** in sufficient purity for the next step.

^{1}H-NMR (400MHz, $CDCl_3$): 8.50-8.48 (m, 4H); 8.36 (s, 2H); 8.32 (s, 1H); 8.11-8.05 (m, 4H); 7.81-7.86 (m, 4H); 7.73 (s, 2H); 7.50-7.35 (m, 16H); 5.15 (s, 4H); 5.06 (s, 4H); 4.53 (s, 4H); 3.77 (s, 12H); 2.05 (s, 3H);

ESI-MS: 1259.5303, calc.: 1259.5322 ($M+H^+$);

GR70B:

The ligand **GR70B** was prepared according the same modified standard procedure for the formation of hydrazones as the previous ligand **GR70**. After 24 h of heating at reflux the

mixture of **GR65B** and **HEL9B** (Chapter 2) the white precipitate was filtered. However, some unreacted starting materials were present according the ^{1}H NMR. Therefore, additional purification by precipitation from hot DMF had to be included in the procedure. Filtration of the precipitate provided **GR70B** in sufficient purity for the next step.

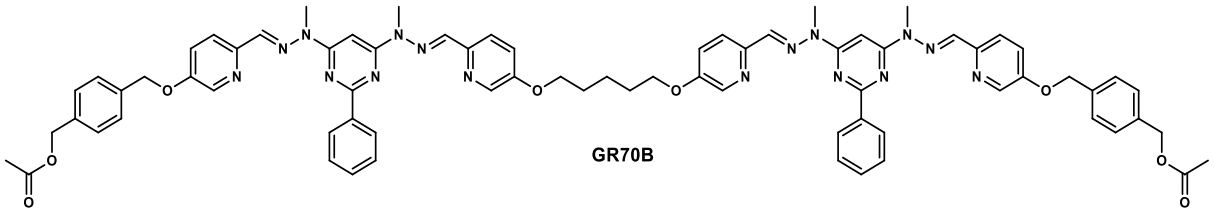

^{1}H-NMR (400MHz, $CDCl_3$): 8.49-8.46 (m, 4H); 8.34 (d, J = 2.8, 2H); 8.26 (d, J = 2.6, 2H); 8.06 (dd, J = 3.6, J = 8.7, 4H); 7.80 (d, J = 4.8, 4H); 7.73 (s, 2H); 7.50-7.46 (m, 10H); 7.42 (d, J = 8.0, 4H); 7.26-7.18 (m, 4H); 5.17 (s, 4H); 5.12 (s, 4H); 4.15 (t, J = 6.18, 4H); 3.77 (s, 6H); 3.73 (s, 6H); 2.10 (s, 6H); 1.97 (p, J = 7.0, 4H); 1.83-1.74 (m, 2H);

^{13}C NMR ($CDCl_3$): 170.94; 163.21; 162.24; 154.84; 154.50; 148.69; 148.36; 138.37; 136.45; 136.21; 136.14; 135.83; 130.37; 128.84; 128.35; 128.22; 127.94; 123.28; 122.94; 120.25; 120.17; 86.70; 70.33; 68.39; 65.97;29.78; 22.59; 21.11;

ESI-MS: 1301.5776, calc.: 1301.5792 ($M+H^+$);

GR71:

This ligand was obtained by the standard procedure for ester deprotection.

Only very broad ^{1}H NMR was obtained from $CDCl_3$ and DMSO.

GR71B:

This ligand was obtained by the standard procedure for ester deprotection.

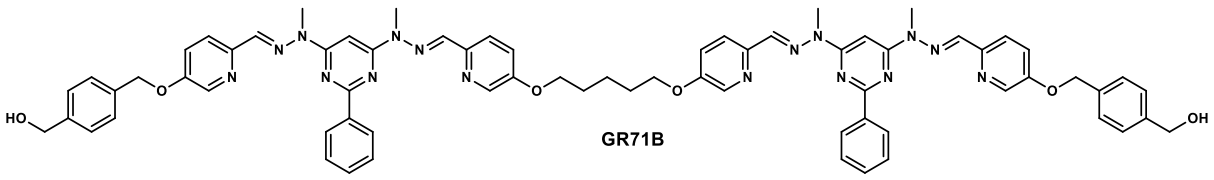

Only very broad ^{1}H NMR was obtained from $CDCl_3$ and DMSO due to the low solubility of the ligand. Therefore, the ligand was used directly for next step.

GR72:

This ligand was obtained by the standard procedure for Dess-Martin oxidation.

^{1}H-NMR (400MHz, $CDCl_3$): 9.89 (s, 2H); 8.45-8.40 (m, 4H); 8.30 (d, J = 2.6, 2H); 8.25 (d, J = 2.6, 2H); 8.06-7.97 (m, 4H); 7.87-7.76 (m, 9H); 7.65 (s, 2H); 7.59-7.50 (m, 4H); 7.45-7.37 (m, 7H); 7.27-7.24 (m, 4H); 5.15 (s, 4H); 4.49 (s, 4H); 3.70 (s, 12H);

^{13}C NMR: 191.69; 163.25; 162.33; 154.49; 154.22; 149.92; 142.81; 138.31; 136.33; 135.77; 130.45; 130.24; 128.38; 128.18; 127.83; 127.61; 123.63; 123.11; 120.30; 120.22; 86.74; 69.87; 67.49; 29.82

ESI-MS: 1171.4791, calc.: 1171.4798 ($M+H^+$);

GR72B:

This ligand was obtained by the standard procedure for Dess-Martin oxidation.

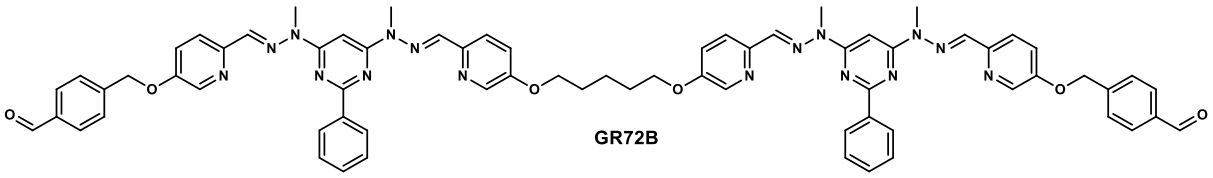

^{1}H-NMR (400MHz, $CDCl_3$): 10.03 (s, 2H); 8.49-8.45 (m, 4H); 8.34 (d, J = 2.6, 2H); 8.25 (d, J = 2.6, 2H); 8.08-8.04 (m, 4H); 7.94 (d, J = 7.96, 4H); 7.79 (d, J = 4.7, 4H); 7.72 (s, 2H); 7.64 (d, |J = 7.6, 4H); 7.54-7.47 (m, 10H); 7.65 (s, 2H); 5.25 (s, 4H); 4.19-4.14 (m, 8H); 3.78 (s, 6H); 3.73 (s, 6H); (the rest of aliphatic -CH_2- from the linker is hidden behind the water signal)

Aldehyde functionalised Zn(II) folded grids:

All the complexes below were prepared according the standard procedure for the grid formation.

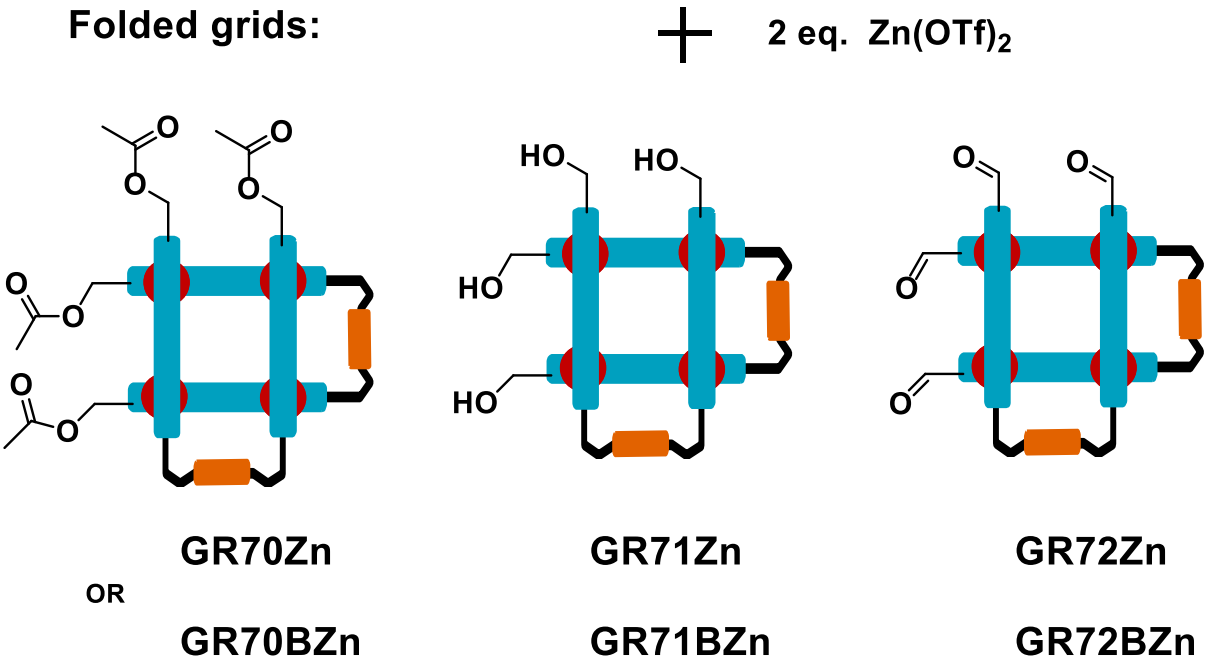

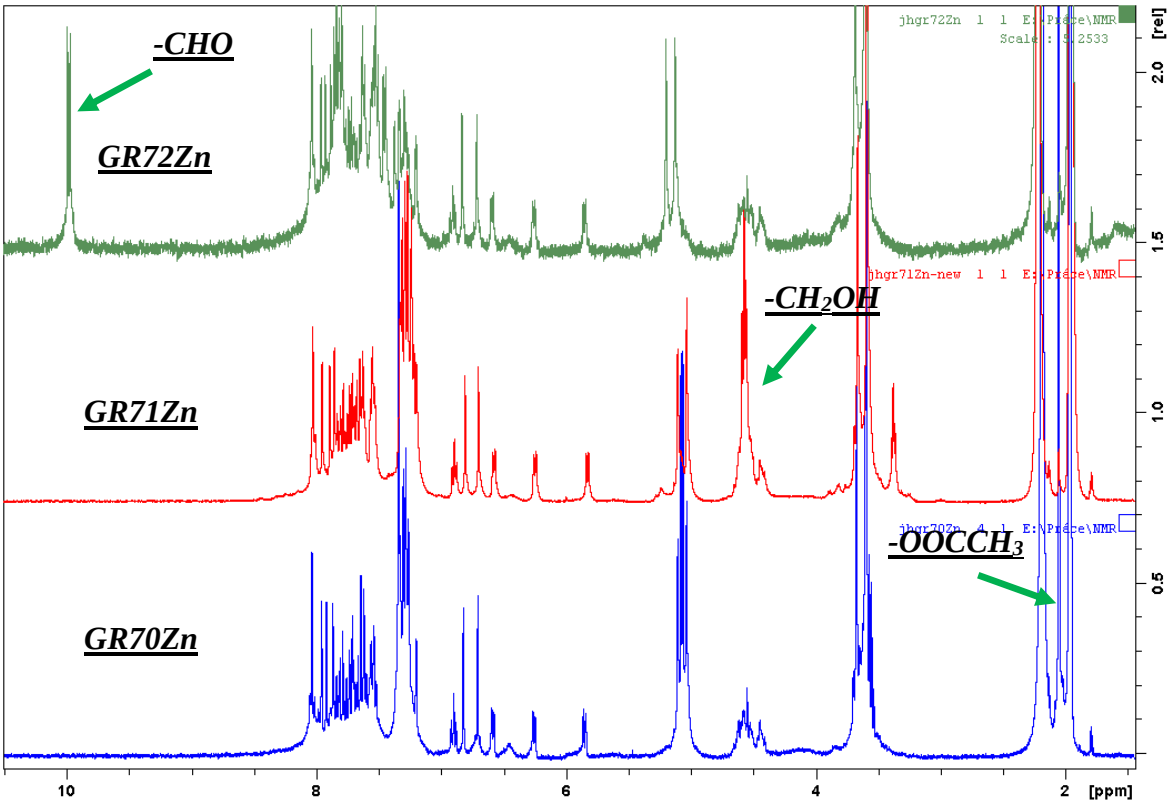

Figure E2.6: ^{1}H NMR of different folded Zn(II) grids with ester group (**GR70Zn**), hdyroxymethyl group (**GR71Zn**) and finally with aldehyde group (**GR72Zn**).

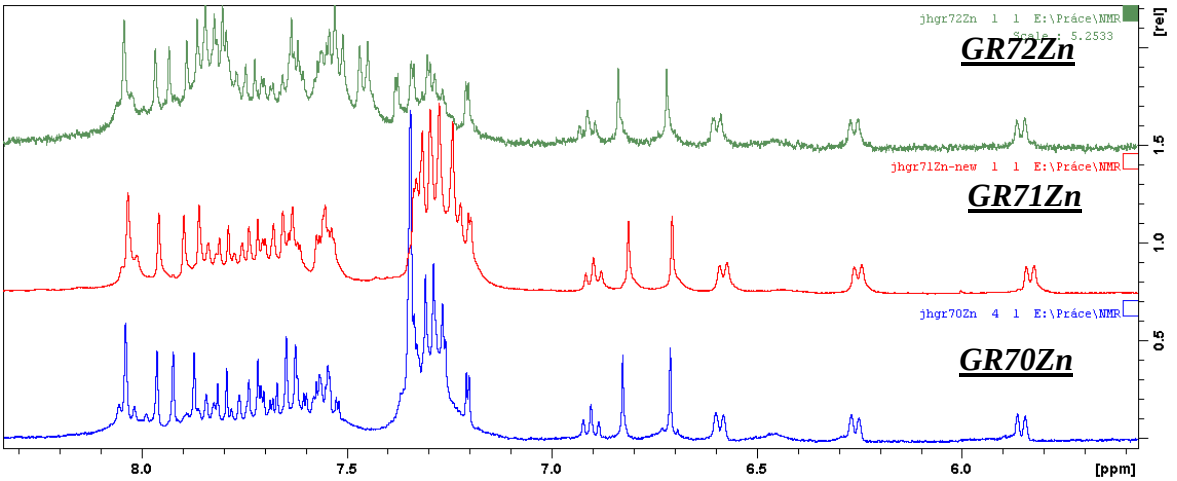

Figure E2.7: The zoomed in aromatic region of the **GR70Zn** (**Bottom**), **GR71Zn** (**Middle**), **GR72Zn** (**Top**). It is possible to clearly see the grid formation from the characteristic signals of protons from pyrimidine phenyl, which arise from its restricted rotation within the grid packing. It is also possible to see differentiation of the ligands within the grid from the doubled protons from the pyrimidine. Unfortunately, so far it was not possible to deconvolute and assign the signals in the region between 7 and 8.2 ppm. ESI-MS results, supporting the folded grid formation are given below in the text.

GR70Zn:

^{1}H-NMR (400MHz, CD_3CN): *Figure S1.4. and Figure S1.5*

..

ESI-MS: 1175.1738, calc.: 1175.1740 ($[(\mathbf{GR70})_2Zn_4(OTf)_5]^{3+}$);

GR71Zn:

^{1}H-NMR (400MHz, CD_3CN): *Figure S1.4. and Figure S1.5*

ESI-MS: 1119.1617, calc.: 1119.1598 ($[(\mathbf{GR71})_2Zn_4(OTf)_5]^{3+}$);

GR72Zn:

^{1}H-NMR (400MHz, CD_3CN): *Figure S1.4. and Figure S1.5*

ESI-MS: 1116.4706, calc.: 1116.4722 ($[(\mathbf{GR72})_2Zn_4(OTf)_5]^{3+}$);

GR70BZn:

^{1}H-NMR (400MHz, CD_3CN): 8.01 (t, J = 7.6, 2H); 7.92-7.87 (m, 10H); 7.77 (t, J = 7.4, 4H); 7.66-7.55 (m, 8H); 7.54-7.49 (m, 4H); 7.45-7.40 (m, 4H); 7.31-7.16 (m, 28H); 6.98 (t, J = 7.5, 2H); 6.75 (s, 2H); 6.68 (s, 2H); 6.64 (d, J = 7.3, 2H); 6.37 (d, J = 7.3, 2H); 5.77 (d, J = 7.4, 2H); 5.05 (s, 4H); 5.04 (s, 4H); 5.03 (s, 4H); 5.01 (s, 4H); 4.27-4.00 (m, 8H); 3.62 (s, 6H); 3.61 (s, 6H); 3.58 (s, 12H); 2.03 (2xs, 12H); 1.75-1.69 (m, 4H); 1.58-1.48 (m, 6H); 1.31-1.29 (m, 2H);

^{13}C NMR (CD_3CN): 171.55; 167.31; 166.77; 159.37; 159.27; 158.88; 158.80; 158.24; 158.11; 157.95; 157.88; 141.19; 140.96; 140.83; 14063; 140.26; 140.18; 140.07; 138.14; 138.01; 137.81; 137.29; 137.18; 136.45; 135.90; 135.85; 133.71; 133.36; 131.80; 131.59; 130.33; 130.14; 130.01; 129.83; 129.32; 129.20; 128.93; 128.54; 124.71; 124.63; 123.75; 123.61; 123.69; 120.56; 87.82; 87.55; 71.58; 69.35;66.27; 34.29; 34.23; 34.16; 34.08; 27.76; 27.05; 21.94; 21.08;

ESI-MS: 1203.2114, calc.: 1203.2054 ([(**GR70B**)$_2$Zn$_4$(OTf)$_5$]$^{3+}$);

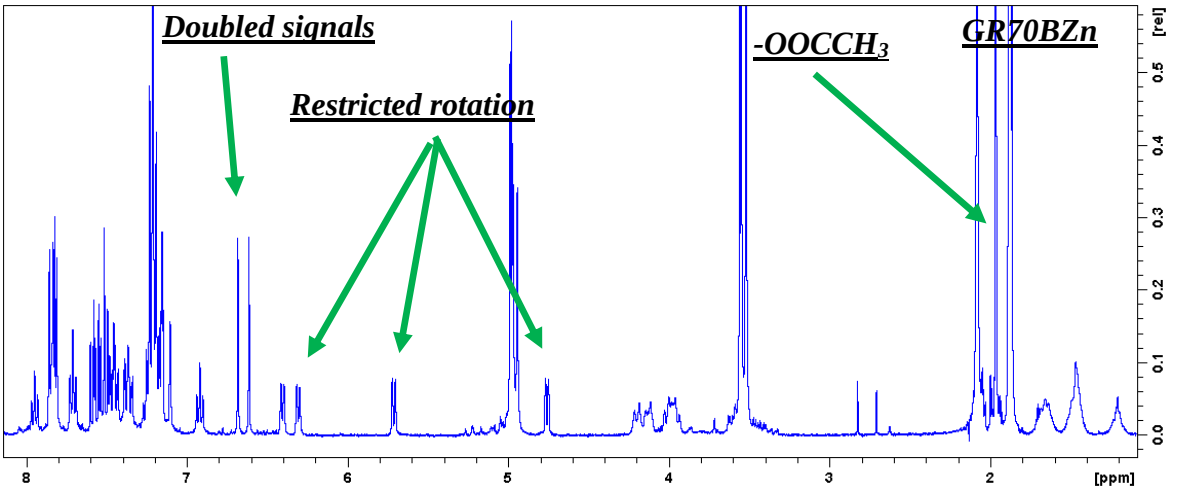

Figure E2.8: ^{1}H NMR spectrum of most likely folded grid structure made of ligand **GR70B**.

GR72BZn:

Better resolved spectrum is needed for detail description of the complex. However, the formation of the grid is certain.

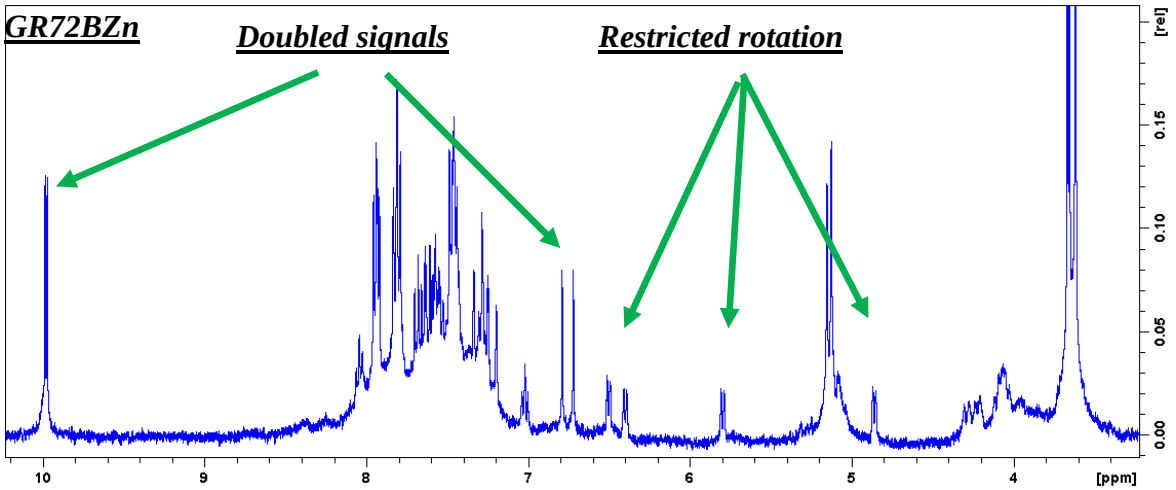

Figure E2.9.: ^{1}H NMR spectrum of most likely folded grid structure made of ligand **GR72B**. Unfortunately, the deconvolution and complete assignment wasn't yet possible.

6.3 Dynamic Helicates

6.3.1 Hydrazone and imine based binuclear helicates

Preparation of (JRHel7)Zn_2

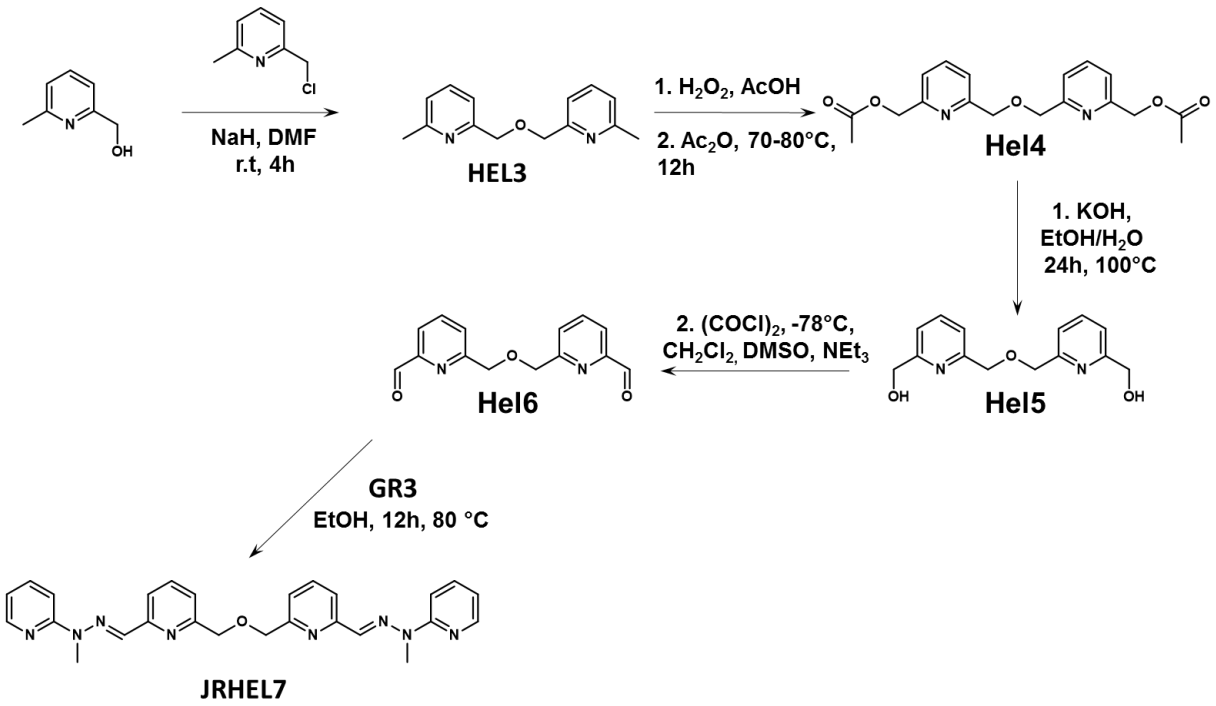

*Compounds **HEL3**, **HEL4**, **HEL5** were prepared according the procedure in the following literature:

Newcomb, M.; Gokel, G. W.; Cram, D. J. *J. Am. Chem. Soc.*, **1974**, 96, 6810-6811

Weber, E.; Josel, H.-P.; Puff, H. Franken, S. *J. Org. Chem.*, **1985**, 50, 3125-3132

HEL3:

^1H NMR (400 MHz, $CDCl_3$): δ 7.59 (t, J=7.6, 2H); 7.33 (d, J=7.8, 2H); 7.06 (d, J=7.4, d); 4.74 (s, 4H); 2.55 (s, 6H);

HEL4:

^{1}H NMR (400 MHz, $CDCl_3$): δ 7.73 (t, J=7.6, 2H); 7.47 (d, J=7.8, 2H); 7.26 (d, J=7.8, d); 5.20 (s, 4H); 4.77 (s, 4H); 2.15 (s, 6H);

HEL5:

^{1}H NMR (400 MHz, $CDCl_3$): δ 7.71 (t, J=7.6, 2H); 7.42 (d, J=7.6, 2H); 7.15 (d, J=7.9, 2H); 4.79 (s, 4H); 4.76 (s, 4H);

HEL6:

To the round bottom flask was equipped with septum, evacuated and purged with N_2. The CH_2Cl_2 (5 ml, dry solvent) solution containing oxalyl chloride ($(COCl)_2$, 176 μl, $2x10^{-3}$ mol) and dry DMSO (400 μl) were inserted through the septum via syringe and cooled to -78 °C. Next, the **HEL5** (100 mg, $3.8x10^{-4}$mol) CH_2Cl_2 in CH_2Cl_2 (3 ml) was inserted via syringe into the flask the mixture was stirred for 30 min, the Et_3N was added (1 ml) and reaction mixture was then let to reach room temperature. Addition of water, extraction with CH_2Cl_2, and chromatography on silica (EtOAc/Petrol ether gradient 1:10 to 2:1) furnished pure dialdehyde **HEL6**.

^{1}H NMR (400 MHz, $CDCl_3$): δ 10.02 (s, 2H); 7.89-7-84 (m, 3H); 7.73 (dd, J=7.9, 2H); 4.86 (s, 4H);

JRHEL7

The ligand **JRHEL7** was prepared according the standard procedure for hydrazone formation.

^{1}H NMR (400 MHz, CD_3CN): 8.44 (s, 2H); 8.15 (s, J = 7.9, 2H); 7.85-7.80 (m, 4H); 7.43 (d, J = 7.9, 2H); 7.34-7.31 (m, 2H); 7.28 (d, J = 8.7, 2H); 6.88-6.84 (m, 2H); 4.44 (d, J = 15.3, 2H); 3.83 (s, 6H); 3.57 (d, 15.3, 2H);

^{13}C NMR (100 MHz, CD_3CN): 159.54; 152.61; 148,05; 145.55; 143.35; 134.78; 128.19; 125.07; 120.3; 111.54; 69.74; 34.64

Preparation of the complexes of GR9e and GR9f

GR9e:

Ligand **GR9e** was prepared from the compound **GR5e** according the standard procedure for hydrazone formation.

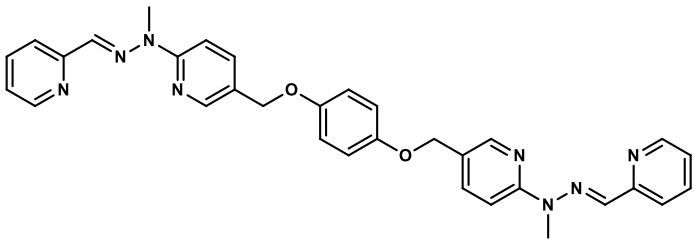

^{1}H NMR (400 MHz, $CDCl_3$): δ 8.57 (d, J=5.1, 2H); 8.27 (d, J=2.3, 2H); 8.02 (d, J=7.8, 2H), 7.78-7.67 (m, 8H); 7.27-7.17 (m, 2H); 6.91 (s, 4H); 4.96 (s, 4H); 3.70 (s, 6H);

^{13}C NMR *(100 MHz, $CDCl_3$)*: 157.39, 155.21, 153.05, 149.12, 146.68, 137.77, 136.40, 134.94, 124.71, 122.56, 119.37, 116.08, 109.97, 68.36, 29.79,

ESI-Ms: 581.2442, calc.: 581.2384 ($M+Na^+$);

Elemental Analysis**:** (%): N 20.13, C 68.45, H 5.42; (Calc.: N 20.06, C 68.80, H 5.41)

GR9e+Zn(II):

Two complexes in approximately 1:1 ratio can be found in the acetonitrile solution of **GR9E** and $Zn(OTf)_2$ (1:1) after 12 h at 70 °C.

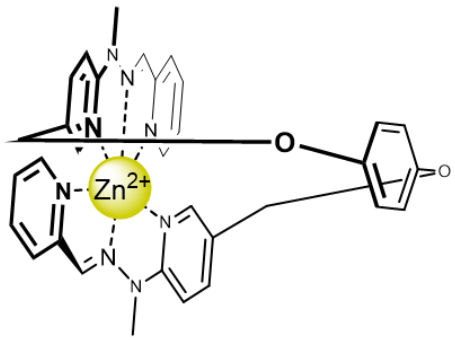

(GR9e)Zn

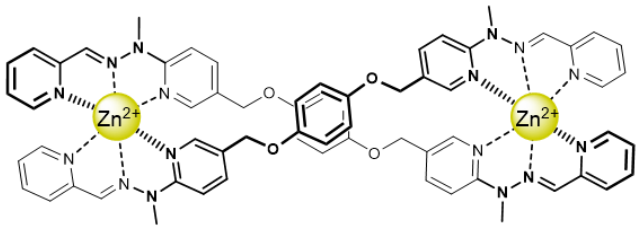

$(GR9e)_2Zn_2$

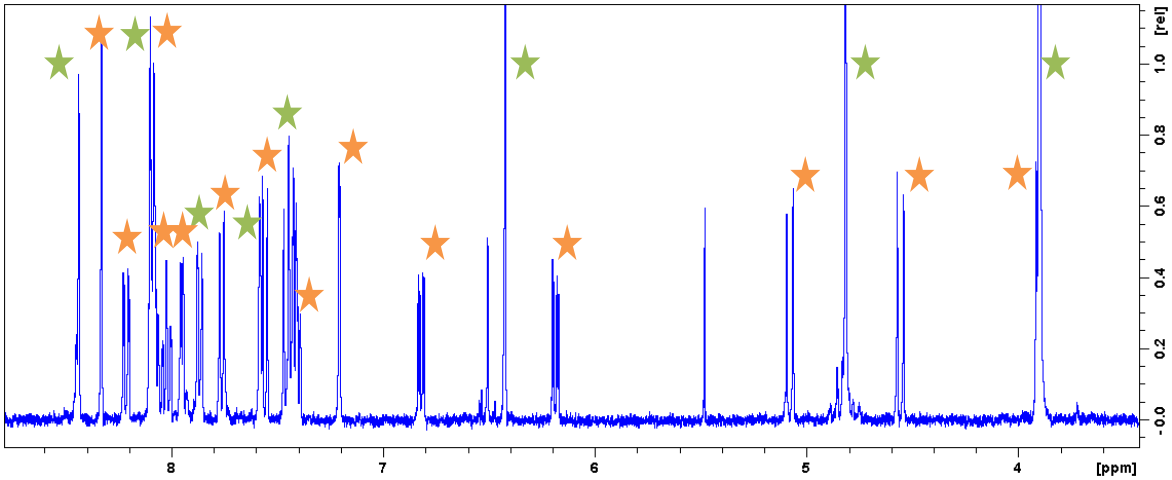

Figure E.3.1.: Equilibrated mixture of two complexes. **Green star**: Double helical **(GR9e)$_2$Zn$_2$**; **Orange star**: Peaks of the simple complex **(GR9e)Zn**.

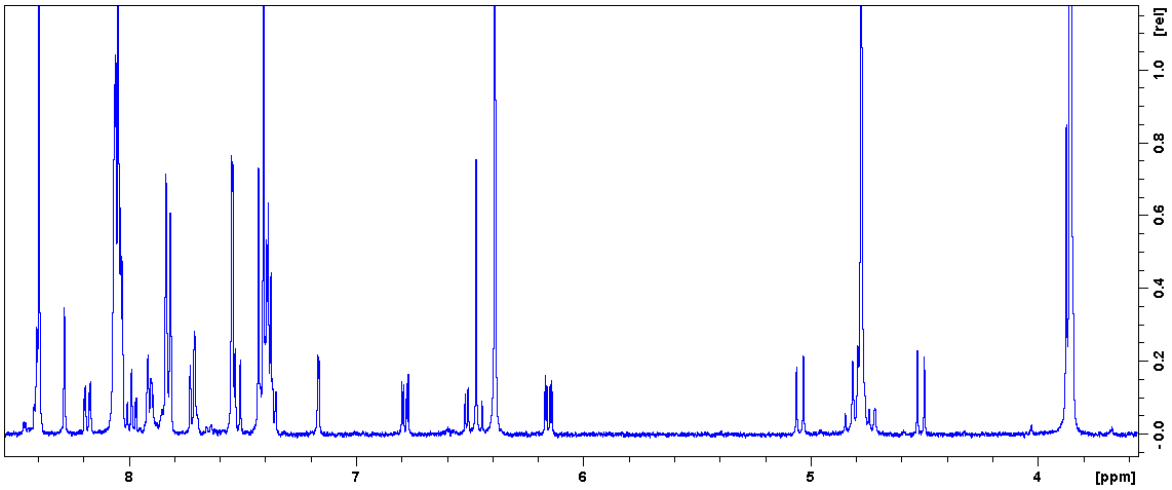

Figure E3.2.: ^{1}H NMR of dissolved crystal in CD_3CN. The same batch of crystals was used to determine structure of **(GR9e)$_2$Zn$_2$**. Therefore, the set of peaks with higher intensity (**Green star**, Figure S2.1.) was assigned to double helicate **(GR9e)$_2$Zn$_2$** and the other set of peaks (**Orange star**, Figure S2.2.) with lower intensity was assign to simple complex **(GR9e)Zn**.

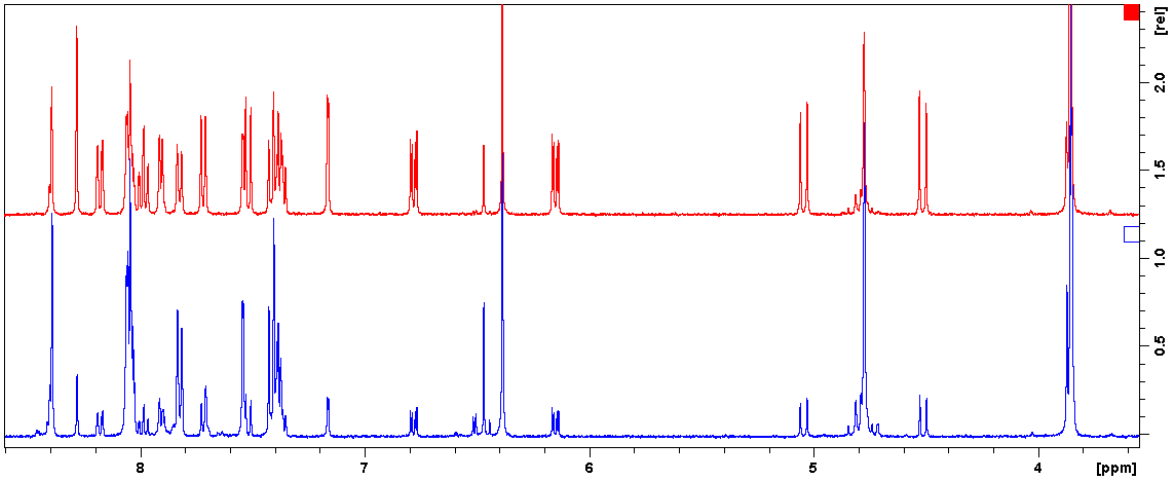

Figure E3.3.: Bottom: The spectrum of **(GR9e)$_2$Zn$_2$** after dissolution of the crystals; **Top**: The same sample after 15 h at room temperature.

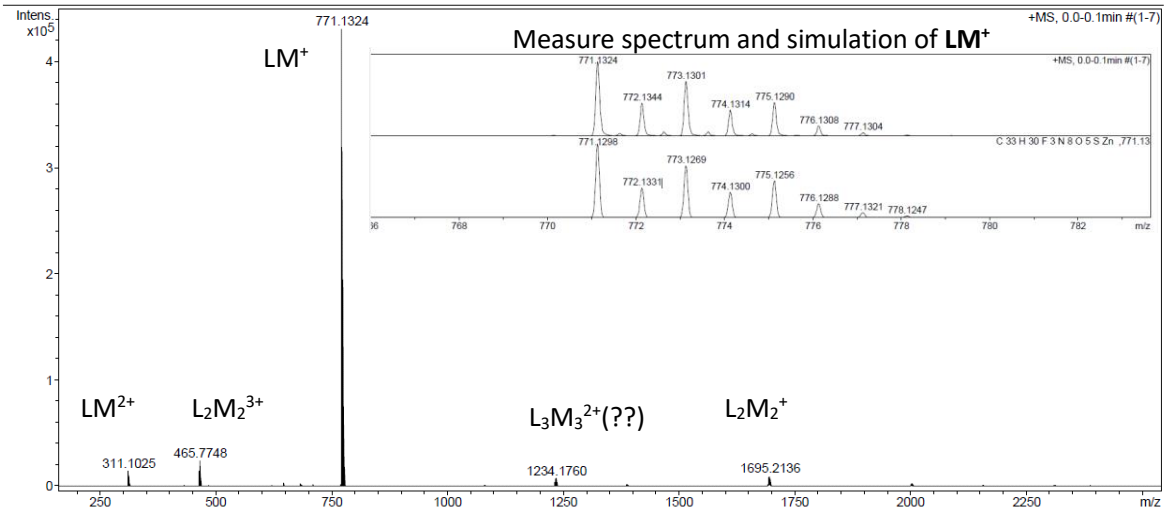

Figure E3.4.: ESI-MS spectrum of the Zn(II) complexes of **GR9e**.

Table E3.1.

Sample	***Solvent***	***Temp.*** *(°C)*	**Diffussion** (m^2/s)	**Volume** ($Å^3$)	**Calculated Volume*** ($Å^3$)
(**GR9E**)$_2$Zn$_2$	CD_3CN	298	$8{,}87 \times 10^{-10}$	1370	1300
(**GR9E**)Zn	CD_3CN	298	$6{,}35 \times 10^{-10}$	3737	4200

**Based on the distances in the crystal structure.*

(GR9e)$_2$Zn$_2$ (Green star):

^{1}H NMR (400MHz, $CDCl_3$): δ 8.39 (s, 2H); 8.06-8.03 (m, 6H); 7.83 (d, J=7.5, 2H), 7.54 (d, J = 1.7, 2H); 6.39 (s, 2H); 4.78 (s, 4H); 4.71 (s, 6H);

ESI-Ms: 1695.2196, calc.:1695.2084 ($L_2M_2^+$ = [(**GR9e**)$_2$Zn$_2$(OTf)$_3$]$^+$)

(GR9e)$_2$Fe$_2$:

Two complexes in approximately 1:1 ratio can be found in the acetonitrile solution of **GR9E** and $Fe(BF_4)_2$ (1:1) after 12 h at 70 °C.

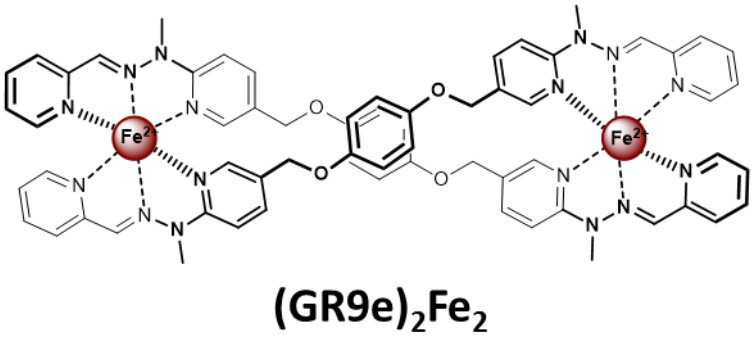

(GR9e)$_2$Fe$_2$

^{1}H NMR (400 MHz, CD_3CN): 9.35 (s,2H); 7.83 (d, J= 7.6, 2H); 7.71-7.76 (m, 4H); 7.60 (d, J= 5.5, 2H); 7.25 (d, J=1.6, 2H); 7.09 (dt, J=2.4, 2H); 7.05 (d, J=8.8, 2H); 6.21 (s,4H); 4.68 (d, J=13.4, 2H); 4.27 (s, 6H);

^{13}C NMR (100 MHz, CD_3CN,): 159.077; 156.82; 152.84; 151.22; 148.85; 143.20; 140.30; 138.50; 129.94; 126.10; 125.23; 116.50; 108.06; 65.99; 35.18;

ESI MS: 763.1371, calc.: 763.1358 ($L_2M_2^{2+}$ = [(**GR9e**)$_2$Fe$_2$(OTf)$_2$]$^{2+}$)

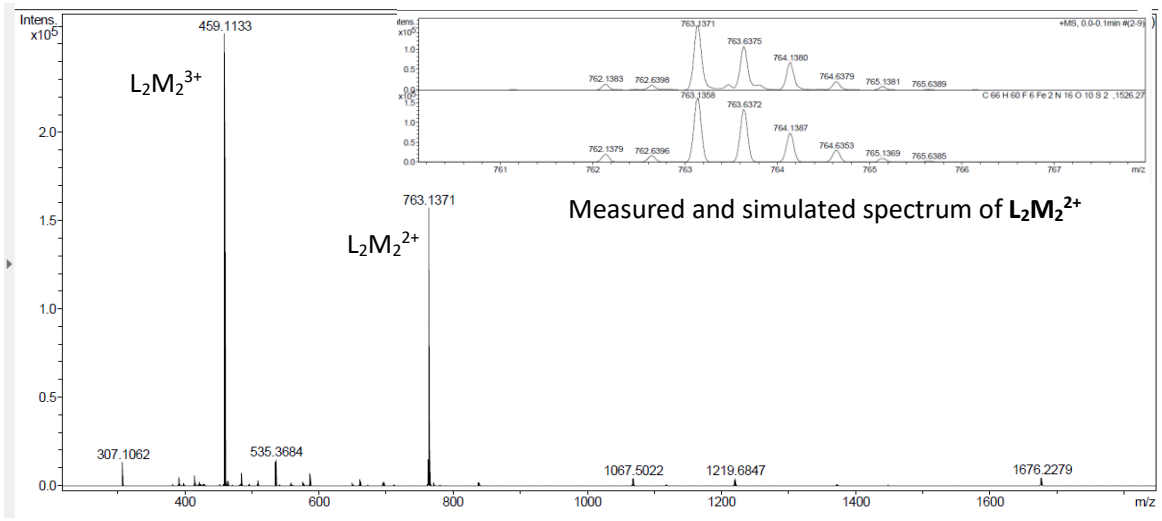

Figure S3.5.: ESI-MS spectrum of the Fe(II) complexes of **GR9e**.

GR9e+Cd:

Two complexes in approximately 1:1 ratio can be found in the acetonitrile solution of **GR9E** and $Cd(OTf)_2$ *x* 6 DMSO (1:1) after 12 h at 70 °C.

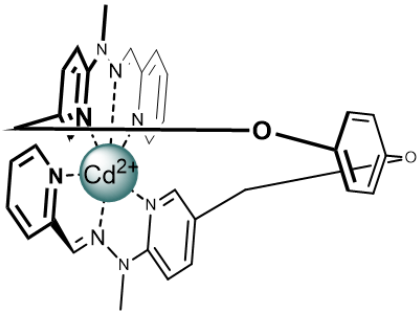

(GR9e)Cd

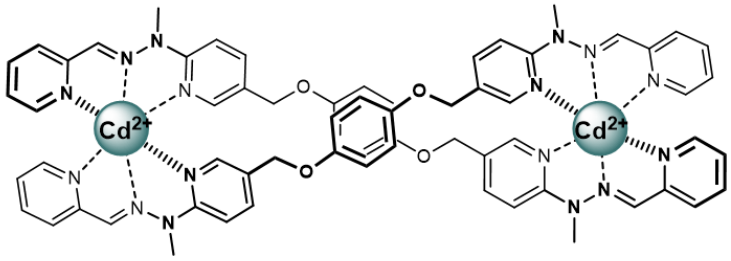

$(GR9e)_2Cd_2$

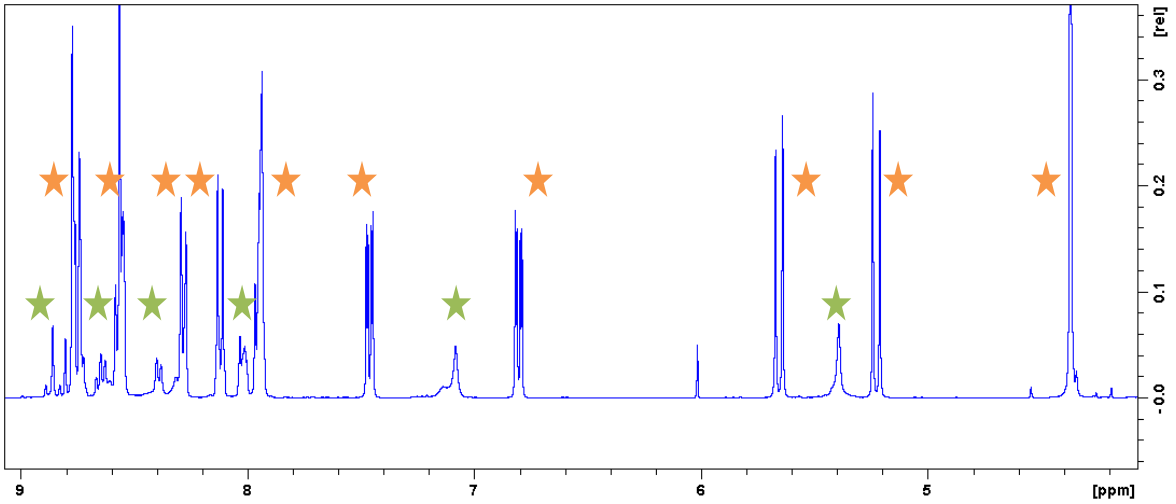

Figure E3.6: Equilibrated mixture of two complexes (4:1). **Orange star**: Peaks of the simple complex **(GR9e)Cd**; **Green star**: Double helicate **$(GR9e)_2Cd_2$**;

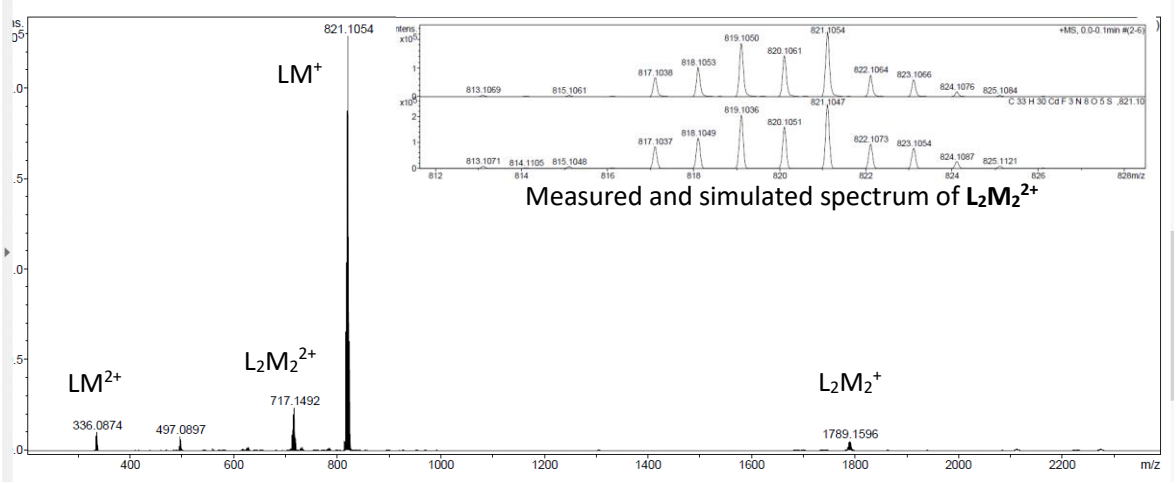

Figure E3.8.: ESI-MS spectrum of the Cd(II) complexes of **GR9e**.

$(GR9e)_2Cd_2$ (orange stars)

^1H NMR (400 MHz, CD_3CN): 8.24 (s, 2H); 8.22 (dd, J=1.9, J=8.9, 2H); 8.05-8.00 (m, 4H); 7.75 (d, J=8.2, 2H); 7.59 (d, J=8.8, 2H); 7.44-7.39 (m, 4H); 6.92 (dd, J=2.9, J=8.6, 2H); 6.27 (dd, J=2.9, J=8.7, 2H); 5.12 (d, J=12.5, 2H); 4.69 (d, J=12.5, 2H); 3.84 (s, 6H);

^{13}C NMR (100 MHz, CD_3CN): 154.36, 153.22, 150.29, 149.37, 148.59, 145.13, 142.27, 135.10, 127.97, 127.69, 124.79, 122.36, 112.17. 71.99, 34.60,

ESI-MS: 821.1054, calc.: 821.1047 (LM^+ = [(**GR9e**)Cd(OTf)]$^+$)

GR9f:

Ligand **GR9f** was formed from compound **GR5f** according the standard procedure for hydrazone formation.

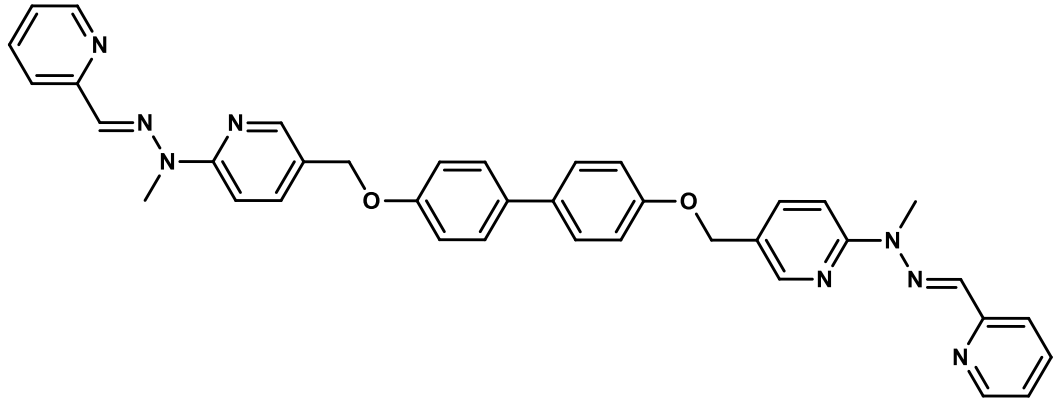

^{1}H NMR (400 MHz, $CDCl_3$): 8.57 (d, J=5.1, 2H); 8.31 (dd, J=1.9, 2H); 8.04 (d, J=8.2, 2H); 7.82 (s, 2H); 7.59 (d, J=8.8, 2H); 7.79 (d, J=8.6, 2H); 7.74 (m, 4H); 7.48 (d, J=9.0, 4H); 7.24-7.20 (m, 2H); 7.03 (d, J=9.0, 4H); 5.05 (s, 4H); 3.72 (s, 6H); 3.84 (s, 6H);

*^{13}C NMR (100 MHz, $CDCl_3$):*157.75, 157.42, 155.11, 148.95, 146.70, 137.77, 136.55, 134.77, 133.83, 127.81, 124.57, 122.58, 119.43, 115.23, 110.04, 67.75, 29.82

ESI-MS: 635.2836, calc.: 635.2877 ($M+H^+$)

$(GR9f)_2Zn_2$:

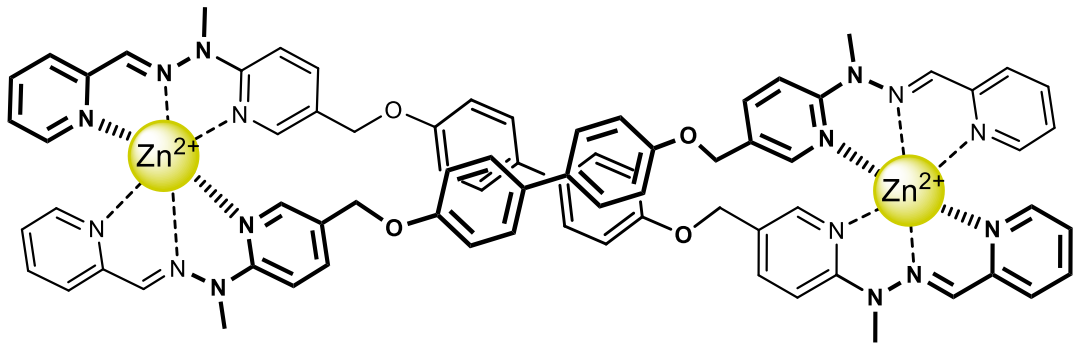

^{1}H NMR (400MHz, CD_3CN): 8.41 (s, 2H); 8.06 (d, J=7.0, 4H); 7.87-7.82 (m, 4H); 7.64 (d, J=2.3, 2H); 7.46-7.38 (m, 4H); 7.27 (d, J=9.0, 4H); 6.64 (d, J=9.0, 4H); 4.76 (d, J=12.5, 2H); 4.66 (d, J=12.5, 2H); 3.89 (s, 6H);

^{13}C NMR: .156.56, 151.84, 148.21, 147.34, 144.67, 142.09, 141.59, 134.33, 132.53, 128.10, 127.25, 126.95, 126.88, 126.38, 115.88, 115.43, 110.11, 65.25, 33.23

ESI-Ms: 849.1543, calc.: 849.1601 ($L_2M_2^{2+}$ = [(**GR9e**)$_2$Zn$_2$(OTf)$_2$]$^{2+}$))

DOSY NMR:

Sample	***Solvent***	***Temp.*** *(°C)*	**Diffussion** (m^2/s)	**Volume** ($Å^3$)	**Calculated Volume*** ($Å^3$)
GR9FZn	CD3CN	298	$5{,}77x10^{-10}$	4984	5700

(GR9f)$_2$Fe$_2$:

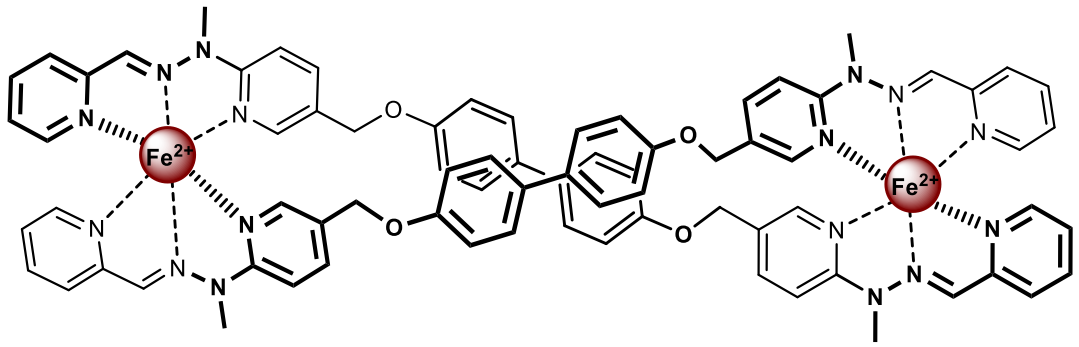

^1H NMR (400MHz, $CDCN_3$): 9.38 (s, 2H); 7.84 (d, J=7.6, 2H); 7.76 (t, J=7.1, 2H); 7.61 (d, J=5.2, 2H); 7.51 (dd, J= 1.3, J=8.6, 2H); 7.39 (s, 2H); 7.27-7.23 (m, 4H); 7.12-7.05 (m, 4H); 6.6 (d, J=8.8, 4H); 4.71 (d, J=12.5, 2H); 4.62 (d, 12.5, 2H); 4.36 (s, 6H);

^{13}C NMR (100MHz, $CDCN_3$): 160.07; 157.95; 157.39; 153.89; 150.4; 144.23; 141.69; 139.53; 133.44; 130.61; 127.89; 127.14, 126.24; 123.38; 120.83; 116.54; 109.02; 66.19; 36.30;

ESI-MS: 1828.2816, calc.: 1828.2816 (L_2M^+)

(GR9f)$_2$Cd:

^1H NMR (400 MHz, CD_3CN): 8.30 (s, 2H); 8.17 (d, J=4.6, 2H); 8.08 (dt, 2H); 7.94 (d, J=8.8, 2H); 7.84-7.79 (m, 4H); 7.49-7.44 (m, 4H); 7.29 (d, J=8.5, 4H); 6.69 (d, J=8.5, 4H); 4.82 (d, J=12.5, 2H); 4.77 (d, J=12.5, 2H); 3.82 (s,6H);

^{13}C NMR: 157.69, 153.75, 150.82, 148.93, 146.98, 142.85, 142.52, 135.27, 133.70, 128.81, 128.27, 128.11, 128.09, 127.72, 123.34, 120.79, 116.30, 111.75, 66.43, 34.59;

ESI-MS: 691.2297, calc.: 691.2327 (L_2M^{2+}= [(**GR9e**)$_2$Cd]$^{2+}$)

Preparation of the HEL10a and HEL10c based complexes

Synthesis of ***5-hydroxy-2-pyridinecarboxaldehyde*:***

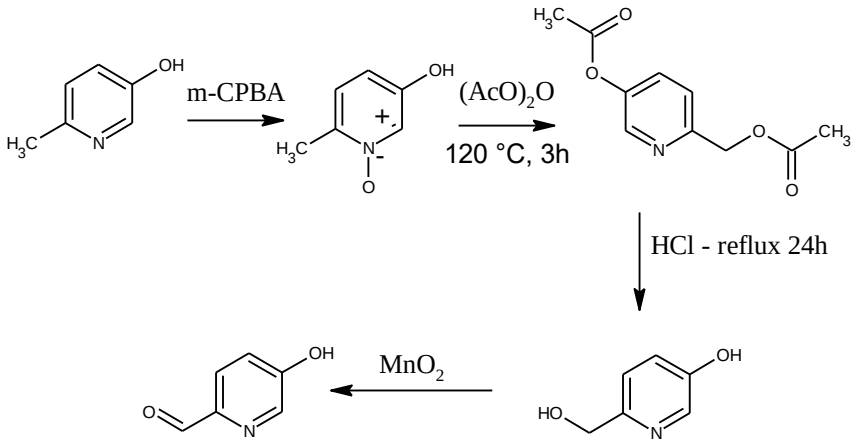

*The synthesis was done according the procedure described in the following literature:
Seredyuk, M.; Gaspar, A. B.; Ksenofontov, V.; Galyametdinov, Y.; Kusz, J.; Guetlich, P. *J. Am. Chem. Soc.*, **2008**, *130*, 1431-1439

HEL9:

The procedure was done according the standard procedure for alkylation of aromatic alcohols. The pure **HEL9** was obtained from crude product after DMF evaporation by trituration with hot water, dissolution in hot methanol and precipitation upon cooling the solution in fridge.

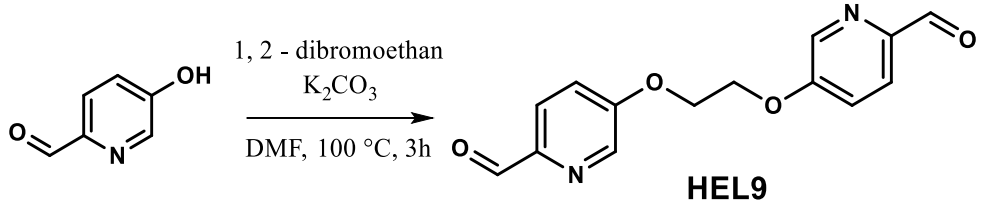

^{1}H NMR (400 MHz, DMSO): 9.90 (s, 2H); 8.55 (d, 2H); 7.96 (d, 2H); 7.67 (dd, 2H); 4.61 (s, 4H);

^{13}C NMR (100 MHz, DMSO): 192.47, 158.34, 146.43, 139.24, 123.98, 121.82, 67.53

ESI-MS: 295.0702, calc: 295.0689 ($M+Na^+$)

*Elemental Analysis***:** (%): N 10.41, C 61.11, H 4.49; (Calc.: N 10.29, C 61.76, H 4.44)

M.p.: 204.5-205.3 °C

HEL10a:

The ligand was prepared according the standard procedure for hydrazone formation.

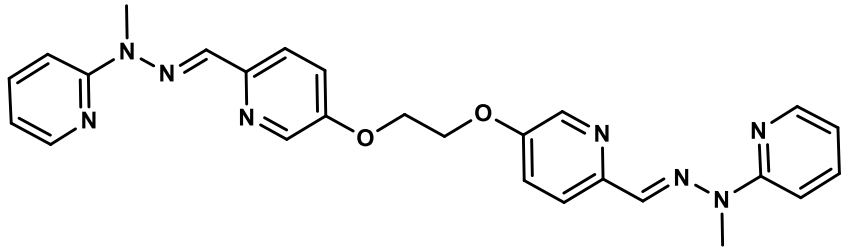

^{1}H-NMR (400 MHz, $CDCl_3$): 8.32 (d, J=3.1, 2H); 8.24 (d, J=3.9, 2H); 8.01 (d, J=9.8, 2H); 7.76 (s,2H); 7.72 (d, J=8.6, 2H); 7.61 (dt, 2H); 7.34 (dd, J=2.9, J=8.8, 2H); 6.81 (t, 2H); 4.46 (s,4H); 3.69 (s,6H);

^{13}C-NMR (100 MHz, $CDCl_3$): 157.49, 154.17; 148.96; 146.97; 137.54; 136.20; 134.27; 122.92; 120.04; 115.90; 109.95; 67.05; 29.62

ESI-Ms: 505.2040, calc.: 505.2071 ($M+Na^+$)

M.p.: 249.2-250.5 °C

(HEL10a)$_2$Zn$_2$:

The complex was prepared by mixing 1 eq. of **HEL10a** (0.006 mmol) and 1 eq. of $Zn(OTf)_2$ (0.006 mmol) in CD_3CN (0.5 ml) in NMR tube and subsequent heating at 70 °C for 12 h.

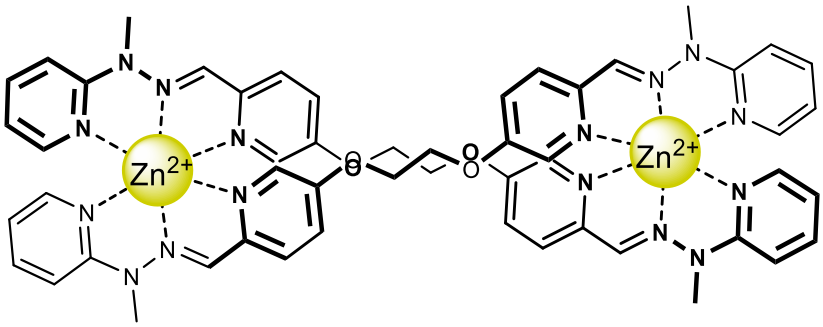

^{1}H-NMR (400 MHz, CD_3CN): 8.48 (s, 2H); 7.90 (dt, 2H); 7.81 (d, J=9.1, 2H); 7.70-7.65 (m, 4H); 7.57 (d, J=2.7, 2H); 7.36 (d, J=8.8, 2H); 6.92 (m, 2H); 4.42 (d, J=10.3, 2H); 4.25 (d, J=11.2, 2H); 3.86 (s, 3H);

^{13}C-NMR (100 MHz, CD_3CN): 158.28, 158.10, 153.32, 153.22, 146.92, 146.45, 143.56, 143.16, 141.55, 140.97, 139.48, 139.31, 135.07, 131.66, 127.86, 125.96, 124.44, 119.42, 119.33, 110.85, 110.79, 68.79, 68.64, 34.04, 33.61

ESI-MS: 695.1021, calc.: 695.0985 ($L_2M_2^{2+}$);

(HEL10a)$_2$Fe$_2$:

The complex was prepared by mixing 1 eq. of **HEL10a** (0.006 mmol) and 1 eq. of $Fe(BF_4)_2$ (0.006 mmol) in CD_3CN (0.5 ml) in NMR tube and subsequent heating at 70 °C for 12 h.

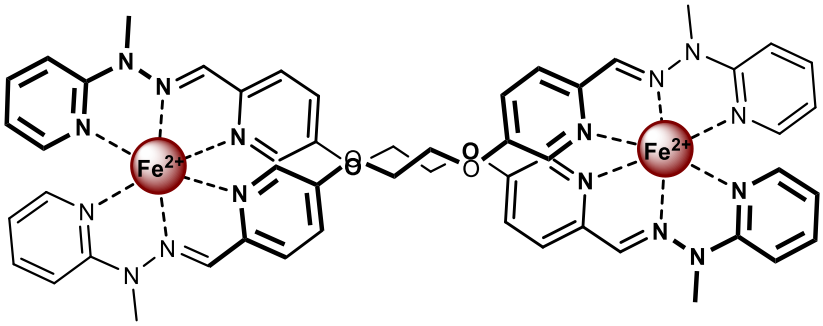

^{1}H-NMR (400 MHz, CD_3CN): 9.62 (s, 2H); 7.89 (s, 2H); 7.66 (t, 2H); 7.48 (brs, 4H); 7.09 (s, 2H); 7.04 (d, J=8.5, 2H); 6.77 (brt, 2H); 4.33 (brs, 8H); 4.16 (d, J=9.1, 2H)

^{13}C-NMR (CD$_3$CN): 158.80, 156.90, 152.69, 151.23, 143.87, 143.73, 141.49, 126.59, 122.22, 120.59, 108.64, 68.80, 36.19

ESI-MS: 687.1095, calc.: 687.1044 ($L_2M_2^{2+}$)

(HEL10a)$_2$Cd$_2$:

The complex was prepared by mixing 1 eq. of **HEL10a** (0.006 mmol) and 1 eq. of Cd(OTf)$_2$ 6x DMSO (0,006 mmol) in CD$_3$CN (0.5 ml) in NMR tube and subsequent heating at 70 °C for 12 h.

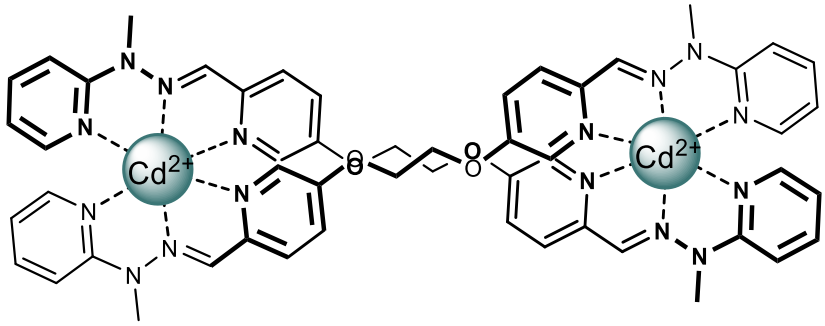

^{1}H-NMR (400 MHz, CD$_3$CN): 8.29 (s, 2H); 7.93-7.82 (m, 6H); 7.75-7.68 (m, 4H); 7.34 (d, J=8.6, 2H); 6.96 (t, 2H); 4.47 (d, J=10.5, 2H); 4.30 (d, J=10.5, 2H); 3.74 (s, 6H);

^{13}C-NMR (100 MHz, CD$_3$CN): 157.98, 154.01, 147.8, 142.92, 141.94, 140.98, 134.79, 128.80, 124.86, 119.15, 111.40, 68.35, 34.29

ESI-Ms: 744.0726, calc.: 744.0734 ($L_2M_2^{2+}$)

HEL10C:

The ligand was prepared from compound **HEL9** according the standard procedure for hydrazone formation.

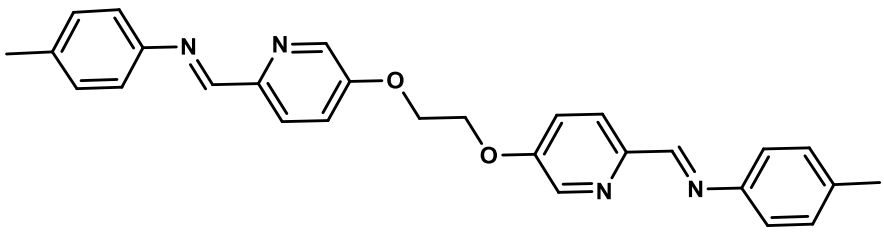

^{1}H-NMR (400 MHz, DMSO): 8.55 (s, 2H); 8.48 (dd, J=0.78, J=2.7, 2H); 8.15 (d, J=7.8, 2H); 7.64 (dd, 2H); 7.24 (brs, 4H); 4.58 (s, 4H); 2.34 (s, 6H);

ESI-MS: 451.2153, calc.: 451.2129 ($M+H^+$)

M.p.: 198.3-199.5 °C

(HEL10c)$_3$Zn$_2$:

The complex was prepared by mixing 1 eq. of **HEL10c** (0.006 mmol) and 0.75 eq. of $Zn(OTf)_2$ (0.004 mmol) in CD_3CN (0.5 ml) in NMR tube and subsequent standing at r.t. for 12 h.

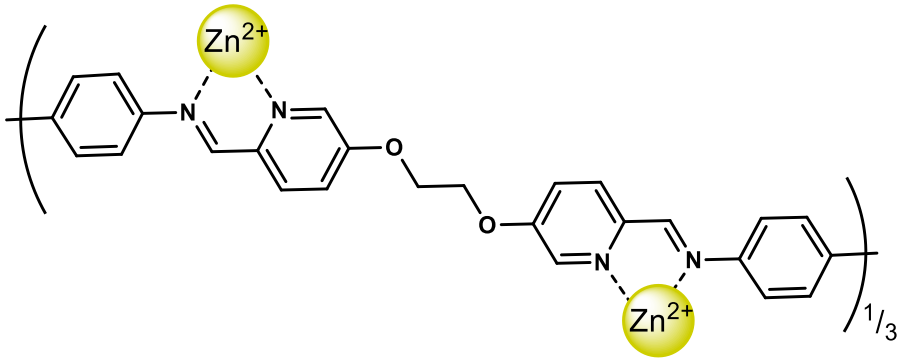

^{1}H-NMR (400 MHz, CD_3CN): 8.47 (s, 2H); 8.21 (d, J=8.6, 2H); 7.94 (dd, J=2.9, J=8.7, 2H); 7.45 (d, J=2.8, 2H); 7.09 (d, J=7.9, 4H); 6.23 (d, J=8.4, 4H); 4.59 (t, J=8.6, 2H); 4.55 (t, J=8.6, 2H); 2.35 (s, 6H)

^{13}C-NMR (100 MHz, CD_3CN): 168.22, 168.06, 164.96, 150.21, 144.92, 144.63, 143.65, 137.81, 137.65, 135.16, 127.92, 126.87, 73.01, 25.30

ESI-MS: 890.1878, calc.: 890.1882 ($L_3M_2^{2+}$)

(HEL10c)$_3$Fe$_2$:

The complex was prepared by mixing 1 eq. of **HEL10c** (0.006 mmol) and 0.75 eq. of $Fe(BF_4)_2$ (0.004 mmol) in CD_3CN (0.5 ml) in NMR tube and subsequent standing at r.t. for 12 h.

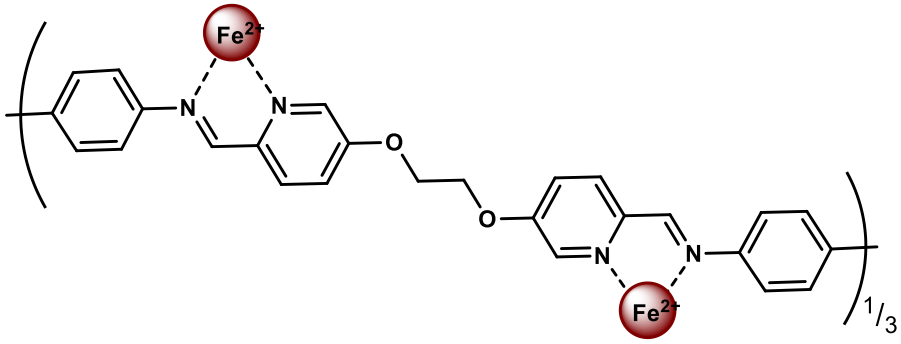

^{1}H-NMR (400 MHz, CD_3CN): 8.65 (brs, 2H); 8.43 (brs, 2H); 7.87 (brs, 2H); 7.00 (d, J=7.31, 4H); 6.92 (s, 2H); 5.34 (d, J=6.7, 2H); 4.60 (brs, 2H); 4.48 (brs, 2H); 2.33 (s, 6H);

^{13}C-NMR (100MHz, CD_3CN): 172.90, 159.92, 151.55, 148.72, 145.96, 139.24, 132.82, 130.27, 122.18, 121.62, 68.57, 20.67

ESI-MS: 655.0968, calc.: 655.0922 ($L_3M_2^{2+}$)

(HEL10c)$_3$Cd$_2$:

The complex was prepared by mixing 1 eq. of **HEL10c** (0.006 mmol) and 0.75 eq. of $Cd(OTf)_2$ x 6 DMSO (0.004 mmol) in CD_3CN (0.5 ml) in NMR tube and subsequent standing at r.t. for 12 h.

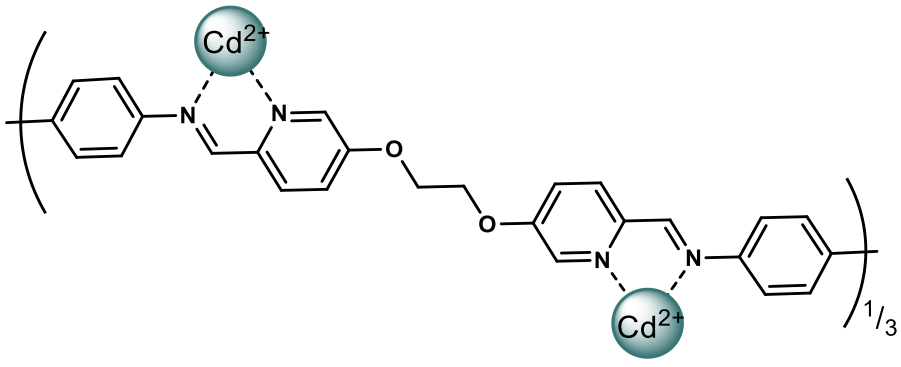

^{1}H-NMR (400 MHz, CD_3CN): 8.70 (s, 2H); 8.18 (d, J=8.6, 2H); 7.88 (dd, J=2.8, J=8.7, 2H); 7.65 (d, J=2.8, 2H); 7.07 (d, J=8.1, 4H); 6.70 (d, J=8.2, 4H); 4.55 (t, J=8.2, 2H); 4.51 (t, J=8.2, 2H); 2.30 (s, 6H);

^{13}C-NMR (100 MHz, CD_3CN): 162.79, 160.31, 145.67, 141.38, 140.57, 139.83, 134.11, 131.07, 123.32, 122.61, 68.48, 20.96

ESI-Ms: 937.1662, calc.: 937.1644 ($L_3M_2^{2+}$)

(HEL10c)$_2$Cu$_2$:

The complex was prepared by mixing 1 eq. of **HEL10c** (0.006 mmol) and 1 eq. of Cu(OTf) (0.006 mmol) in CD_3CN (0.5 ml) in NMR tube and subsequent standing at r.t. for 12 h.

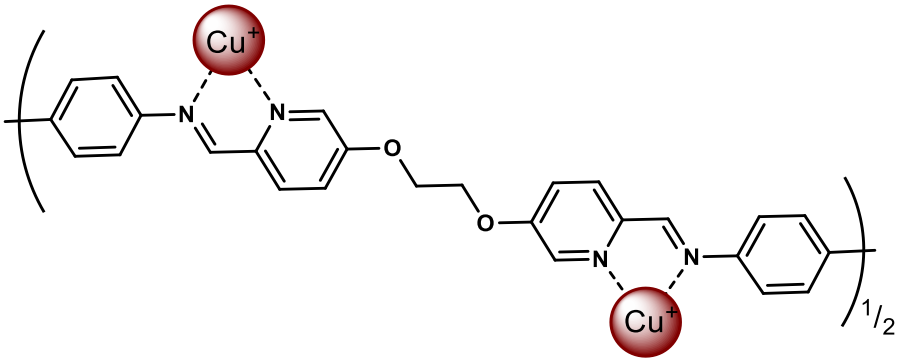

^{1}H-NMR (400 MHz, CD_3CN): 9.02 (s, 2H); 8.23 (d, J= 2.7, 2H); 7.99 (d, J=8.6, 2H); 7.68 (dd, J=2.9, J=8.8, 2H); 7.34 (d, J=8.2, 4H); 7.15 (d, J=8.2, 4H); 4.52 (s, 4H); 2.29 (s, 6H);

^{13}C-NMR (100 MHz, CD_3CN): 158.71, 156.16, 144.50, 144.46, 139.60, 139.19, 130.04, 128.89, 122.22, 120.24, 67.11, 20.02

ESI-Ms: 513.1386, calc.: 513.1346 ($L_2M_2^{2+}$)

The imine exchange in (HEL10c)$_3$Zn$_2$

To freshly prepared complex (**HEL10c)$_3$Zn$_2$** were added 2 eq. (in respect to ligand **HEL10c**) of 4-methoxybenzylamine or 2-(1-methylhydrazinyl) pyridine in CD_3CN and the ^{1}H NMR was

measured. In case of 4-methoxybenzylamine the mixture was then let to stand at room temperature. In the case of 2-(1-methylhydrazinyl) Pyridine the reaction mixture was heated at 70 °C.

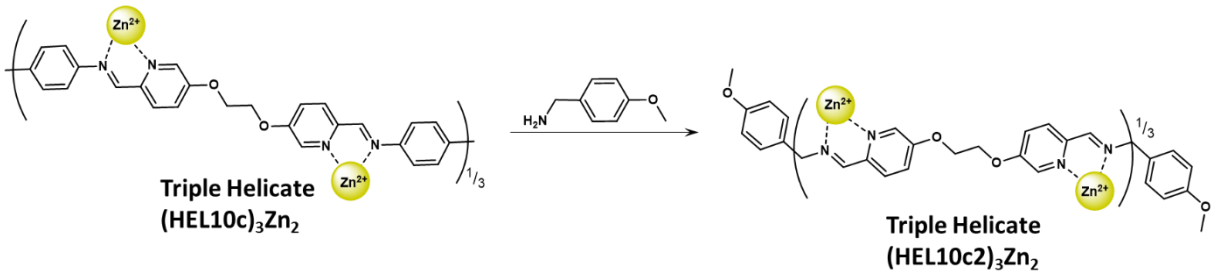

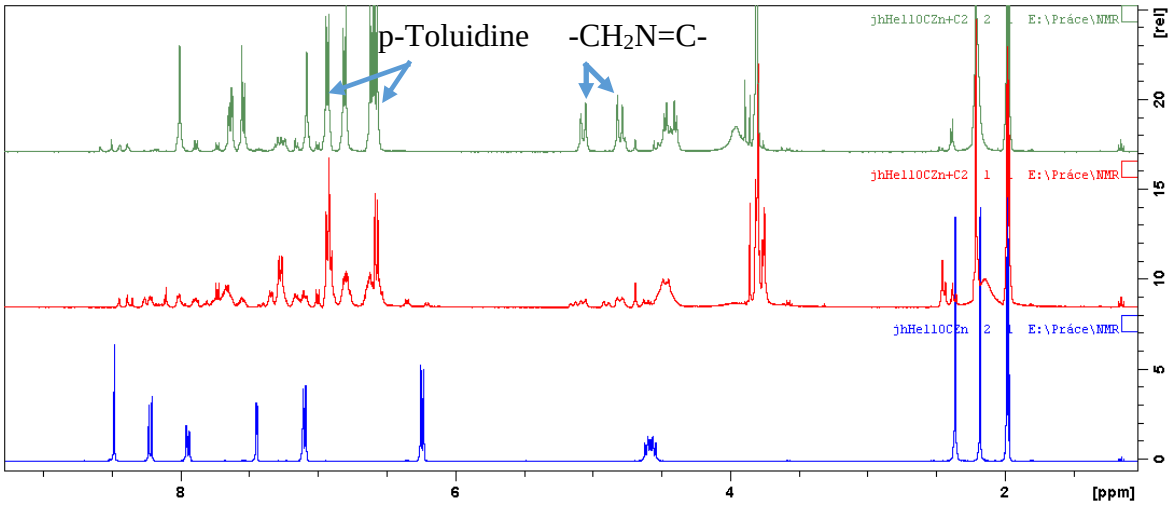

Figure E3.9.: The ^{1}H NMR (CD_3CN) spectra of **(HEL10c)$_3$Zn$_2$** exchange process with 4-methoxybenzylamine. **Bottom:** (**HEL10c)$_3$Zn$_2$** (Triple helicate); **Middle:** freshly mixed (**HEL10c)$_3$Zn$_2$** + 4-methoxybenzylamine; **Top:** Newly formed triple helicate with 4-methoxybezylimine (marked a new set of enantiotopic benzylic protons) and free *p*-toluidine

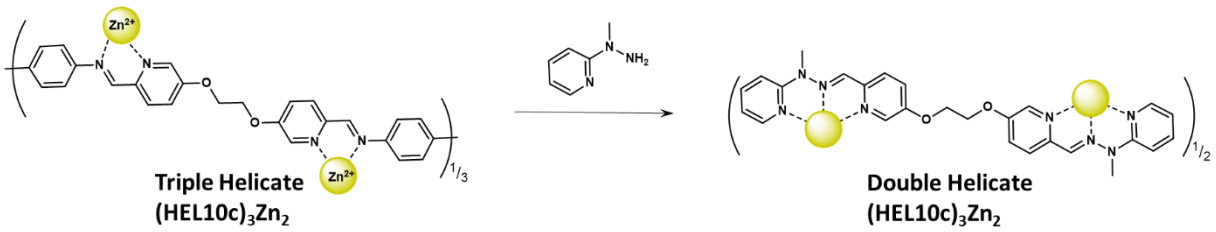

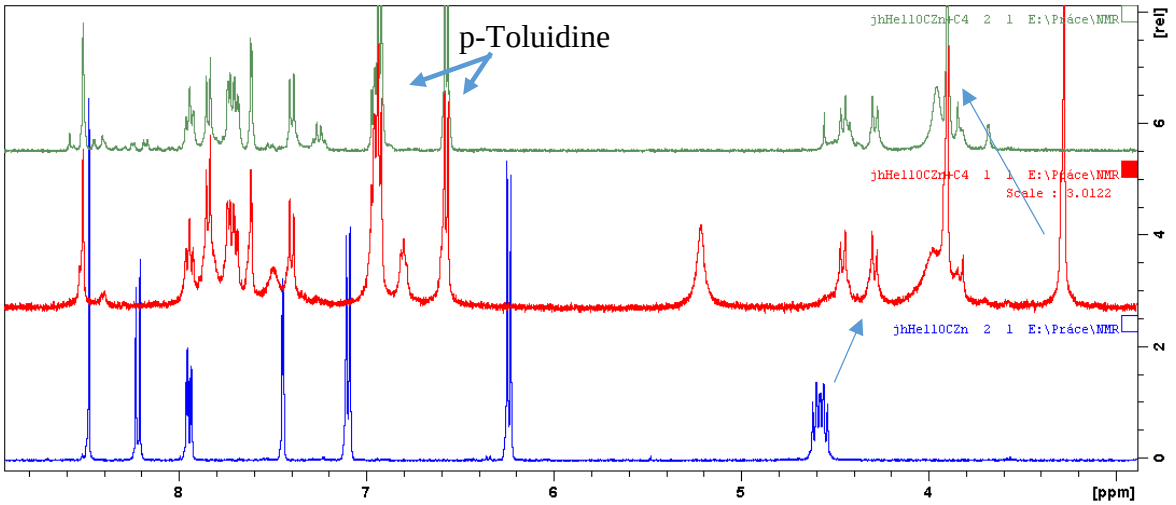

Figure E3.10.: The ^{1}H NMR (CD_3CN) spectra of **HEL10cZn** exchange process with, 2-(1-methylhydrazinyl) Pyridine; B**ottom: HEL10cZn** (Triple helicate); **Middle:** freshly mixed **HEL10cZn** + 2-(1-methylhydrazinyl) Pyridine.; **Top:** Newly formed **$(HEL10a)_2Zn_2$** (Double helicate) and free p-toluidine after 2 h at room temperature.

Metal exchange:

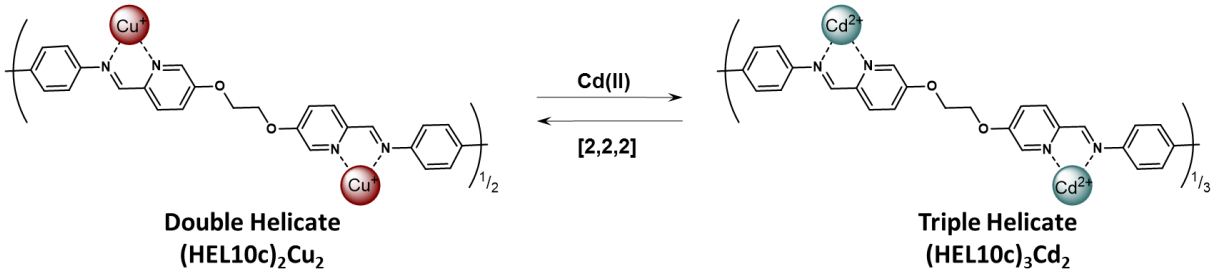

To freshly prepared complex **(HEL10c)**$_2Cu_2$ (0.006 mmol of Cu^+) was added an equimolar amount of $Cd(OTf)_2$ x 6 DMSO (0.006 mol, 0.2 M) in CD_3CN and ^{1}H NMR was immediately measured. Carefully weighted [2,2,2] cryptand (0.006 mmol, 2.25 µg) was then added to the solution. The mixture was shaken and ^{1}H NMR immediately measured.

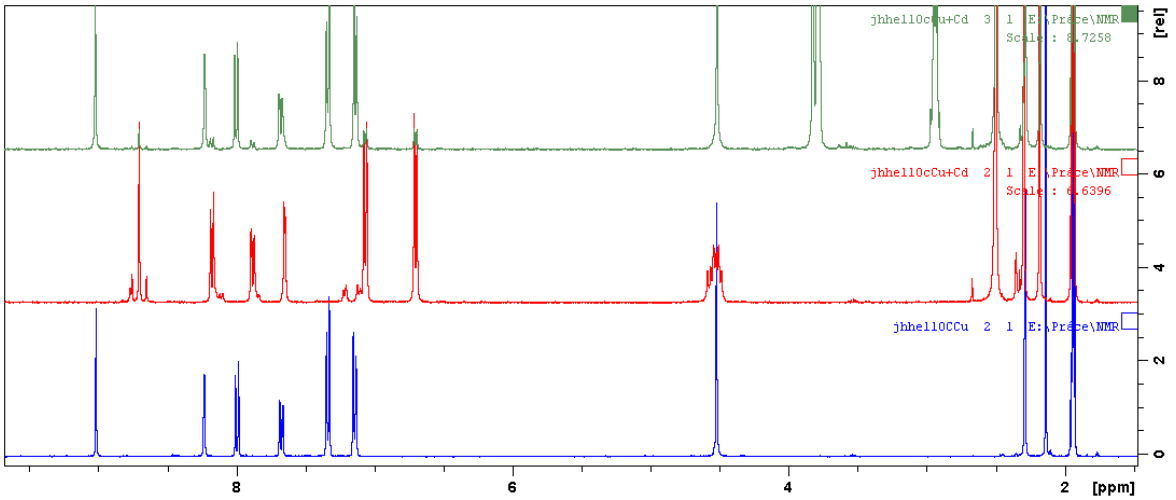

Figure E3.11: The ^{1}H NMR (CD_3CN) spectra of metal-exchange in **$(HEL10c)_2Cu_2$** for $Cd(OTf)_2$ x 6 DMSO and back to Cu(OTf). **Bottom: $(HEL10c)_2Cu_2$** (Double helicate); **Middle:** Immediate exchange of Cu(I) for Cd(II) and reconstitution of the complex into triple helical **$(HEL10c)_3Cd_2$**. **Top:** Addition of [2,2,2] cryptand removes Cd(II) from the helicate resulting in reformation of initial double helical **$(HEL10c)_2Cu_2$** forms with the Cu(I) from the solution.

6.3.2 Heterotopic ligands and multi-metal helicates

Preparation of the ligand CN13 and its complexes

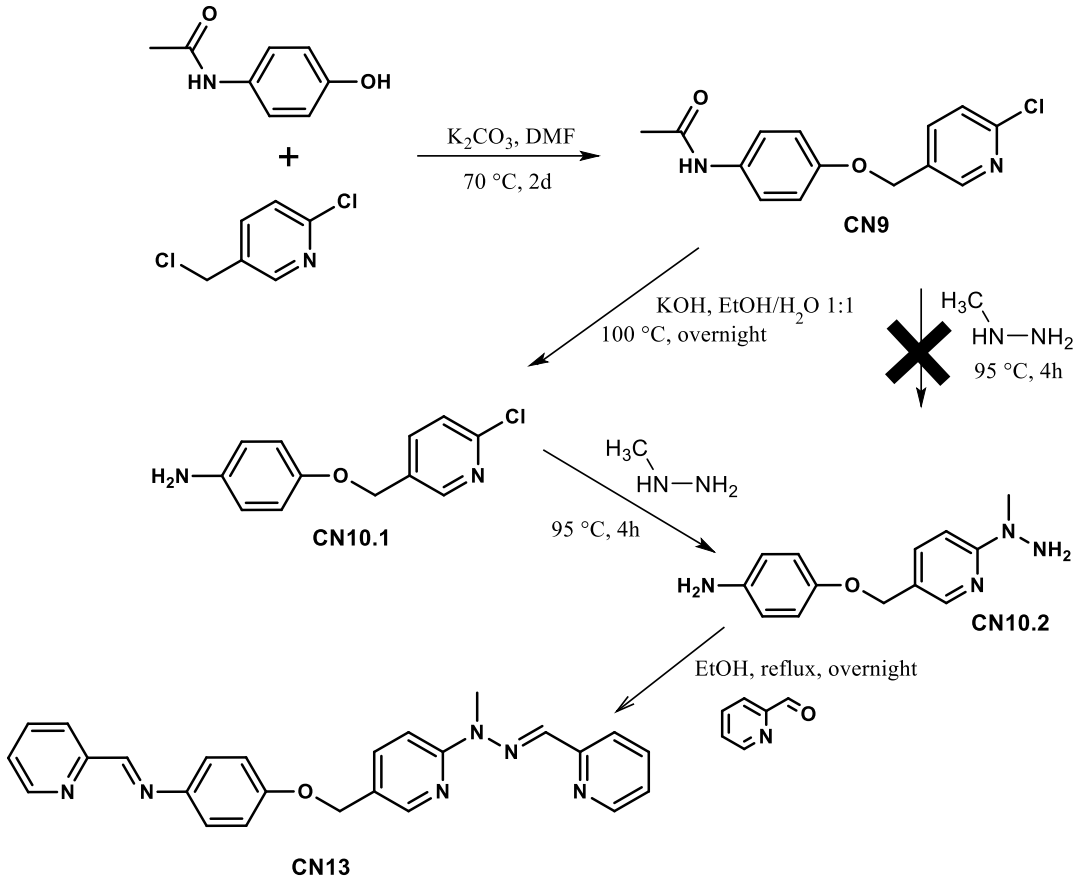

CN9*:

*John H. Hutchinson, J. H.; Li, Y.; Arruda, J. M.; Baccei, Ch.; Bain, G.; Chapman, Ch.; Correa, L.; Darlington, J.; King, Ch. D.; Lee, K.; Lorrain, D.; Prodanovich, P.; Rong, H.; Santini, A.; Stock, N.; Prasit, P.; Evans J. F. *J. Med. Chem*., **2009**, 52, 5803-5815

^{1}H NMR (400 MHz, DMSO): 9.79 (s, 1H); 8.50 (d, J = 2.3, 1H); 7.93 (dd, J = 8.22, J = 2.35, 1H); 7.55 (d, J = 8.6, 1H); 7.48 (d, J = 9.0, 2H); 6.95 (d, J = 9.0, 2H); 5.11 (s, 2H); 2.0 (s, 3H);

^{13}C NMR (100MHz, DMSO): 24.23, 66.73; 115.4; 120.95; 124.60; 132.89; 133.56; 139.71; 149.60; 150.15; 154.07; 168.19;

ESI-MS: 277.0726, calc.: 277.0738 ($M+H^+$)

Elemental Analysis**:** N 9.89, C 60.61, H 4.83; (Calc.: N 10.12, C 60.77, H 4.74)

M.p.: 170.5-173 °C

CN10.1:

The compound **CN10.1** was prepared according to the standard procedure for ester deprotection.

^{1}H NMR (400MHz, DMSO,): 8.46 (d, J = 2.3, 1H); 7.90 (dd, J = 2.3, J = 8.2, 1H); 7.54 (d, J = 8.2, 1H); 6.74 (d, J = 9.0, 2H); 6.52 (d, J = 9.0, 2H); 5.00 (s, 2H); 4.67 (s, 2H);

^{13}C NMR (100 MHz, DMSO): 149.94; 149.57; 149.50; 143.41; 139.64; 133.41; 124.53; 116.41; 115.31; 67.17

ESI-MS: 257.042, calc.: 257.042 ($M+Na^+$);

CN10.2:

The compound **CN10.2** was prepared according the standard procedure for preparation of hydrazine derivatives and was used immediately into next step.

^{1}H NMR (DMSO, 400MHz); 8.03 (d, J = 2.3, 1H); 7.49 (dd, J = 2.3, J = 8.2, 1H); 7.13 (d, J = 9.0, 1H); 6.69 (d, J = 8.6, 2H); 6.49 (d, J = 8.6, 2H); 4.76 (s, 2H); 4.59 (brs, 2H); 4.54 (brs, 2H); 3.18 (s, 3H);

CN13:

The ligand **CN13** was prepared according the standard procedure for the hydrazone formation.

^{1}H NMR (400 MHz, $CDCl_3$); 8.70 (d, J = 4.3, 1H); 8.63 (s, 1H); 8.57 (d, J = 4.3, 1H); 8.30 (1H, J = 1.9, 1H); 8.19 (d, J = 8.2, 1H); 8.03 (d, J = 7.8, 1H); 7.77-7.82 (m, 3H); 7.70-7.73 (m, 2H); 7.31-7.37 (m, 3H); 7.18-7.21 (m, 1H); 7.03 (d, J = 9.0, 2H); 5.03 (s, 2H); 3.71 (s, 3H);

^{13}C NMR (100 MHz, $CDCl_3$): 158.51; 157.91; 157.47; 155.16; 154.85; 149.65; 149.04; 146.70; 144.14; 137.73; 136.59; 136.41; 134.96; 124.82; 124.35; 122.68; 122.54; 121.66; 119.38; 115.52; 110.00; 67.93; 29.77;

ESI-MS: 423.190, calc.: 423.193 ($M+H^+$)

M.p.: 167-169 °C

$(CN13)_2AgZn$:

The complex ***$(CN13)_2AgZn$*** was prepared by mixing 1 eq. of **CN13** ($1x10^{-6}$ mol), 1 eq. of $Zn(OTf)_2$ ($1x10^{-6}$ mol) and 1 eq. of $Ag(BF_4)$ ($1x10^{-6}$ mol) in CD_3CN (0.5 ml) in NMR tube and subsequent standing in the dark at r.t. for 12 h. Following complexes were prepared according the same procedure, just with appropriate metal cations.

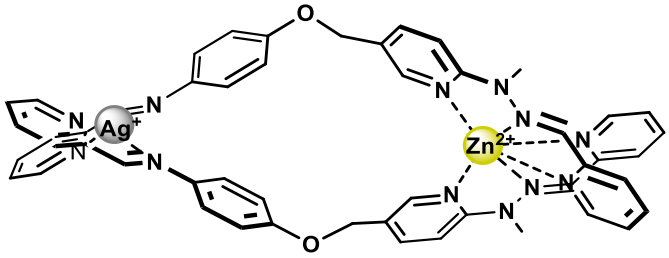

^{1}H NMR (400 MHz, CD_3CN): 8.80 (s, 1H); 8.69 (d, J = 4.6, 1H); 8.45 (s, 1H); 8.16-8.11 (dt, 1H); 8.07-8.02 (m, 2H); 7.99 (dd, J = 2.2, J = 8.8, 1H); 7.88-7.84 (m, 1H); 7.77 (d, J = 1.6, 1H); 7.70-7.67 (m, 1H); 7.42-7.36 (m, 2H); 7.33 (d, J = 9.0, 2H); 6.82 (d, J = 9.0, 2H); 4.94 (s, 2H); 3.88 (s, 3H);

^{13}C NMR (100 MHz, CD_3CN): 159.14; 157.57; 152.99; 152.42; 150.89; 149.17; 148.36; 145.85; 142.53; 141.97; 140.49; 135.40; 129.90; 129.03; 128.88; 127.87; 127.42; 125.03; 124.88; 116.82; 111.01; 66.95; 34.22;

ESI-MS: 1254.160, calc.: 1254.160 ($\mathbf{L_2MN}^+$ = [(**CN13**)$_2$Zn(OTf)Ag(BF_4)]$^+$)

Elemental Analysis: N 11.99, C 43.86, H 3.39; (Calc.: N 11.98, C 44.51, H 3.16)

DOSY NMR:

Sample	***Solvent***	***Temp.*** *(°C)*	**Diffussion** (m^2/s)	**Volume** (Å^3)	**Calculated Volume*** (Å^3)
CN13ZnAg	CD3CN	298	6.93x10^{-10}	2873	2700
CN13ZnCu	CD3CN	298	6.89 x10^{-10}	2923	2700

(CN13)ZnCu:

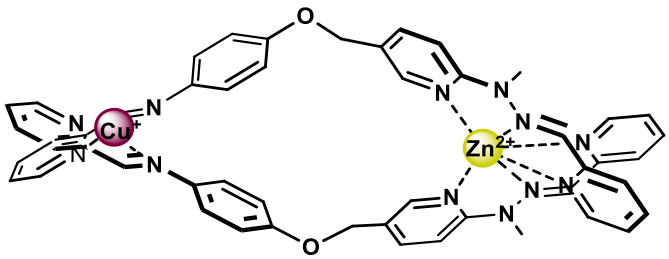

ESI-MS: 1272.146, calc.: 1272.132 ($\mathbf{L_2MN}^+$ = [(**CN13**)$_2$Zn(OTf)$_2$Cu]$^+$)

(CN13)Fe:

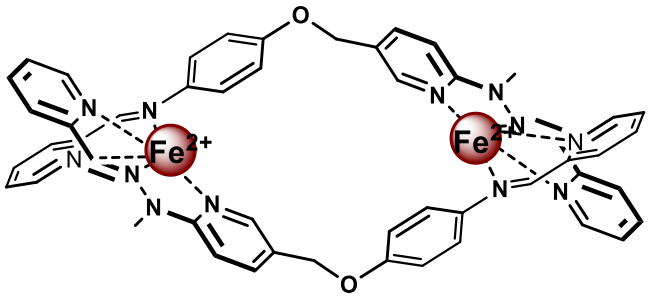

ESI-MS: 1217.25, calc.: 1217.25 ($\mathbf{L_2M_2}^+$ = $[(\mathbf{CN13})_2Fe_2(BF_4)_3]^+$)

(CN13)Cu:

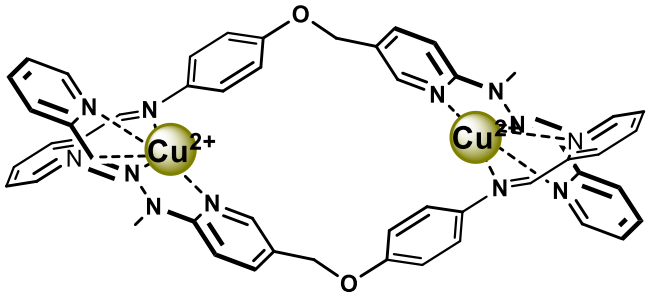

ESI-MS: 1407.12, calc. : 1407.12 ($\mathbf{L_2M_2}^+$ = $[(\mathbf{CN13})_2Cu_2(PF_6)_3]^+$)

(CN13)Pb:

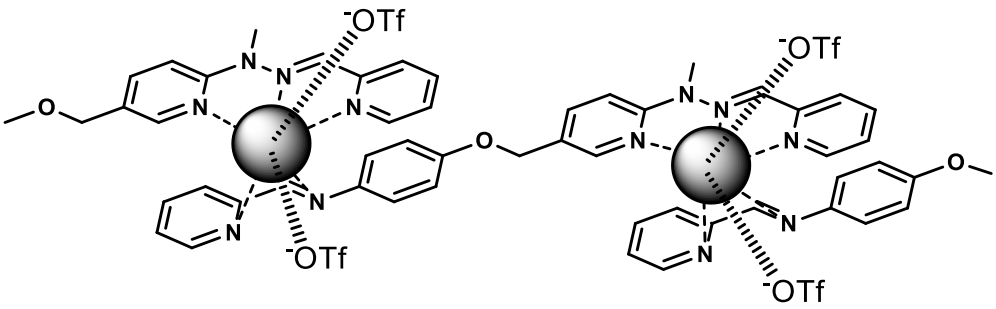

The compound was characterised only by crystal structure.

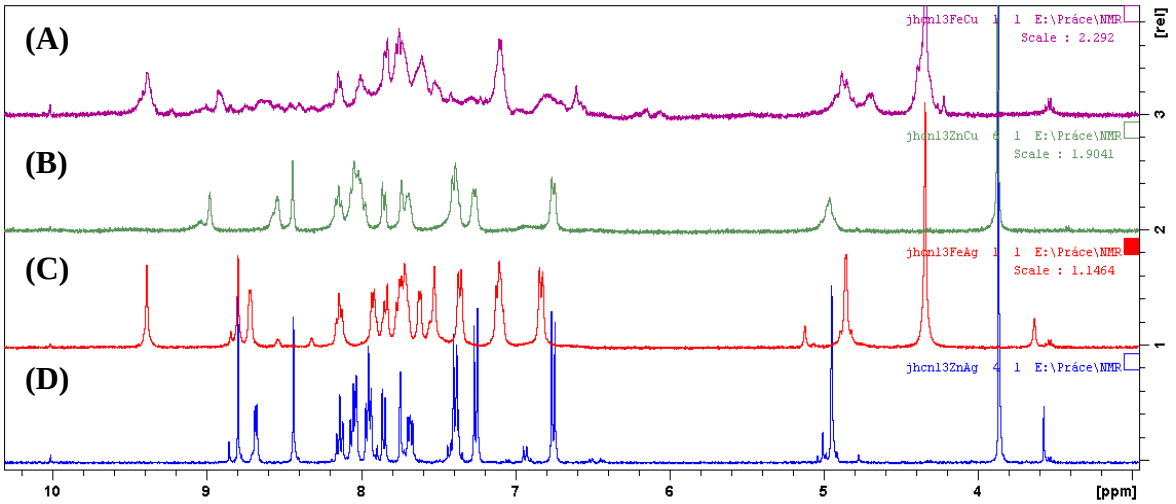

Figure E.3.12.: ^{1}H NMR spectra of: (**A**) (**CN13**)$_2$Fe(OTf)$_2$Cu(OTf); (**B**) (**CN13**)$_2$Fe(OTf)$_2$Ag(BF$_4$); (**C**) (**CN13**)$_2$Fe(OTf)$_2$Cu(OTf); (**D**) (CN13)$_2$Zn(OTf)$_2$Ag(BF$_4$) (**(CN13)$_2$AgZn**);

Preparation of the ligand CN26 and its complexes

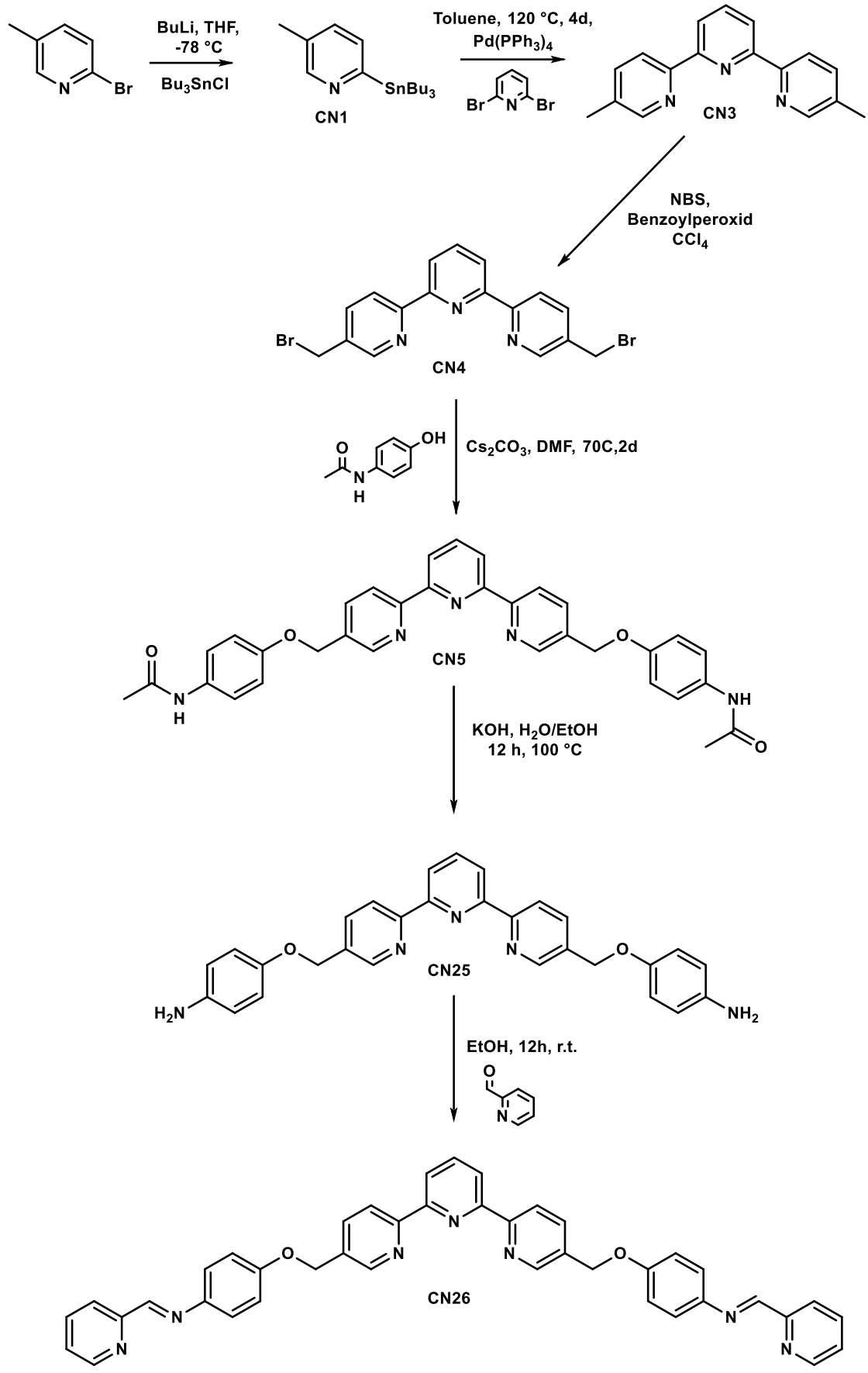

CN1 - Köytepe, S.; Erdoğan, S.; Seçkin T. *J. Hazard. Mater.*, **2009**, 162, 695–702

CN3 - Heller, M.; Schubert, U. S. *J. Org. Chem.*, **2002**, 67, 8269-8272

CN4 - Marquis, A.; Smith, V.; Harrowfield, J.; Lehn, J.-M.; Herschbach H.; Sanvito R.; Leize-Vagner, E.; van Doesselaer, A. *Chem. Eur. J.*, **2006**, 12, 5632-5641

***CN5*:**

The compound **CN5** was prepared according the standard procedure for alkylation of aromatic alcohols.

^{1}H NMR (400 MHz, DMSO): 9.80(s, 2H); 8.79 (d, J = 2.0, 2H)8.65 (d, J = 8.1, 2H); 8.45 (d, J = 7.8, 2H); 8.11 (t, J = 7.8, 1H); 8.07 (dd, J=2, J =8.3, 2H); 7.50 (d, J = 9.0, 4H); 7.00 (d, J = 9, 4H); 5.21 (s, 4H), 2.00 (s,6);

^{13}C NMR (100 MHz, DMSO): 24.25; 31.13; 67.44; 79.61; 115.42; 120.93; 121.24; 133.49; 133.83; 137.29; 139.02; 149.20; 154.23; 155.07; 155.16; 168.20;

MS-ESI: 582.2061, calc.: 582.2112($M+Na^+$)

M.p.: 244.7-246.7 °C

CN25:

The compound **CN25** was prepared according the standard ester deprotection procedure.

^{1}HNMR (400 MHz, DMSO): 8.75 (d, J = 2, 2H); 8.63 (d, J = 7.83, 2H); 8.44 (d, J = 7.8, 2H); 8.10 (t, J = 7.8, 1H); 8.03 (dd, J = 2.0, J = 8.2, 2H); 6.77 (d, J = 8.7, 4H); 6.52 (d, J = 8.6, 4H); 5.09 (s, 4H); 4.65 (s, 4H);

^{13}C NMR (100 MHz, DMSO): 155.10; 154.99; 149.76; 149.10; 143.37; 138.99; 137.18; 134.38; 121.16; 120.86; 116.45; 115.32; 67.94

MS-ESI: 476.2069, calc.: 476.2081($M+H^+$)

M.p.: 162.4-164.4 °C

CN26:

^{1}HNMR (400 MHz, DMSO): 8.77 (d, J=1.8, 2H); 8.63-8.70 (m, 6H); 8.47 (d, J = 7.8, 2H); 8.19 (d, J = 7.8, 2H); 7.94-7.97 (m, 2H); 7.80 (dt, 1H); 7.33-7.36 (m, 6H); 7.06 (d, J = 8.8, 4H), 5.20 (s, 4H);

MS-ESI: 654.2541, calc.: 654.2621 ($M+H^+$)

M.p.: 222.4-225 °C

(CN26)$_2$Zn:

The complex **(CN26)$_2$Zn** was prepared by mixing 1 eq. of **CN26** (0.006 mmol) and 1 eq. of $Zn(OTf)_2$ (0.006 mmol) in CD_3CN (0.5 ml) in NMR tube and subsequent heating at 70 °C for 2 h.

MS-ESI: 686.2228, calc.: 686.2258 (**L$_2$M^{2+}** = [(**CN26**)$_2$Zn]$^{2+}$)

(CN26)$_2$ZnAg$_2$:

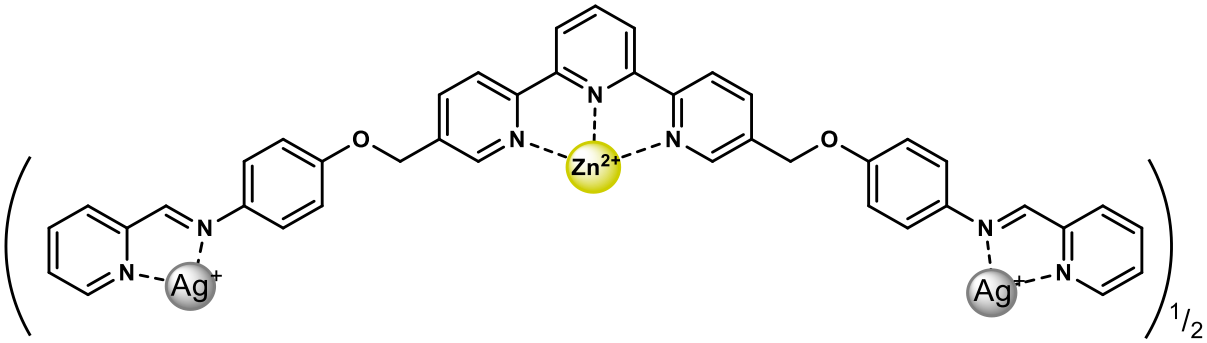

The complex **(CN26)$_2$ZnAg$_2$** was prepared by mixing 1 eq. of **CN26** (0.006 mmol), 1 eq. of $Zn(OTf)_2$ (0.006 mmol) and 2 eq. of $Ag(BF_4)$ (0.012 mmol) in CD_3CN (0.5 ml) in NMR tube and subsequent standing in the dark at r.t. for 12 h. Following complexes were prepared according the same procedure, just with appropriate metal cations.

MS-ESI: 912.1163, calc.: 912.1107 (**L**$_2$**MN**$_2^{2+}$ = [(**CN26**)$_2$Zn(OTf)Ag$_2$(BF$_4$)]]$^{2+}$)

Sample	***Solvent***	***Temp.*** *(°C)*	**Diffussion** (m^2/s)	**Volume** (Å^3)	**Calculated Volume*** (Å^3)
(**CN26**)ZnAg$_2$	CD3CN	298	-	6959	7.200*

*Calculated based on crystal structure of similar trinuclear double helicate (**MAF10**)$_2$Zn$_3$.

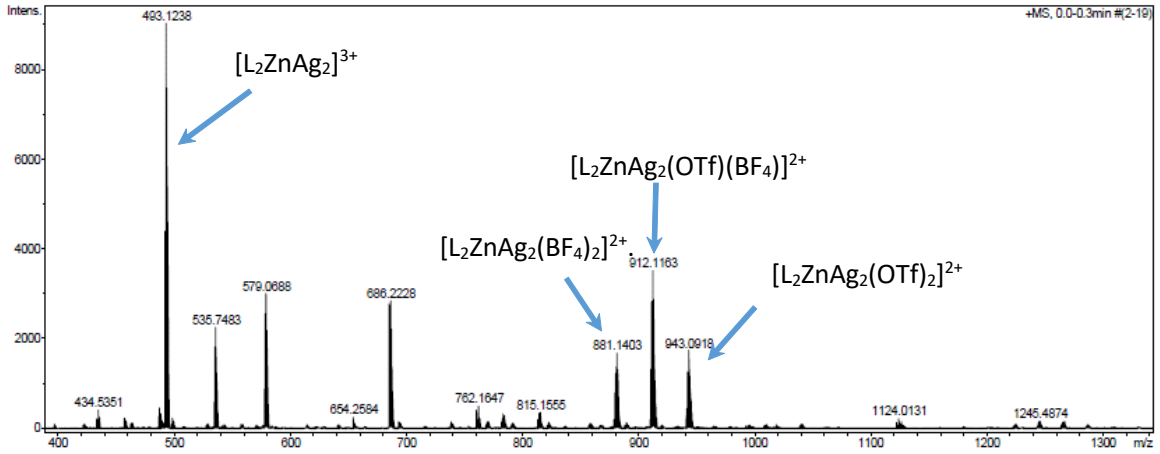

Figure E3.13.: The ESI-MS spectrum of acetonitrile solution of **(CN26)$_2$ZnAg$_2$**.

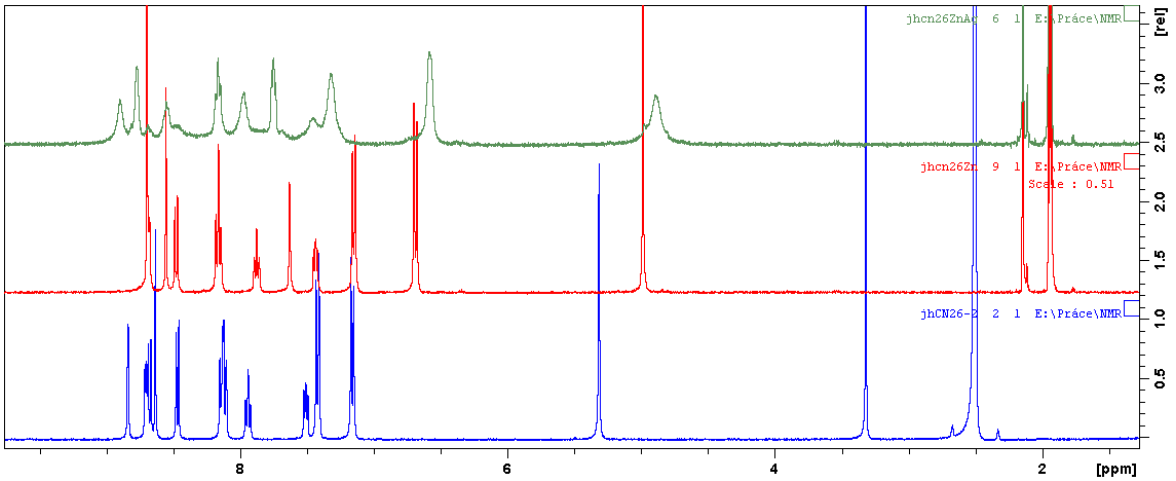

Figure SE.14: The ^{1}H NMR spectra of: Bottom: ligand **CN26** (DMSO); Middle: "Cross" complex **CN26Zn** (CD$_3$CN, (**CN26**)$_2$Zn(OTf)$_2$*);* Top: full trinuclear complex (CN26)$_2$ZnAg$_2$ (CD$_3$CN, (**CN26**)$_2$Zn(OTf)$_2$Ag$_2$(BF4)$_2$)

The ligands AS53, MAF10, MAF13 and its complexes

The following ligands were synthesized in collaboration with other colleagues. The final characterisation of complexes was then made in different groups. Our group participated mainly in the synthesis of starting building blocks and final crystallization.

AS53:

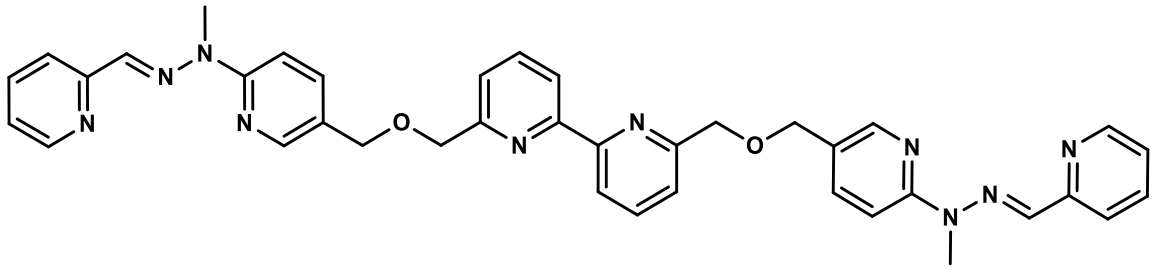

^{1}H NMR (400 MHz, CD_3CN): 8.52 (d, J = 3.9, 2H); 8.27-8.21 (m, 5H); 7.99 (d, J = 7.9, 2H); 7.93 (t, J = 7.6, 2H); 7.81-7.71 (m, 9H); 7.49 (d, J = 7.6, 2H); 7.29-7.25 (m, 2H); 4.67 (s, 4H); 4.59 (s, 4H); 3.62 (s, 6H);

^{13}C NMR (100 MHz, CD_3CN): 157.86; 156.92; 155.48; 146.82; 138.15; 137.50; 126.31; 122.63; 121.39; 120.04; 119.89; 110.21; 73.18; 70.13; 30.23;

$(AS53)_2Zn_2Cu$ and $(AS53)_4Zn_6$:

Crystal structures in appendice

MAF10:

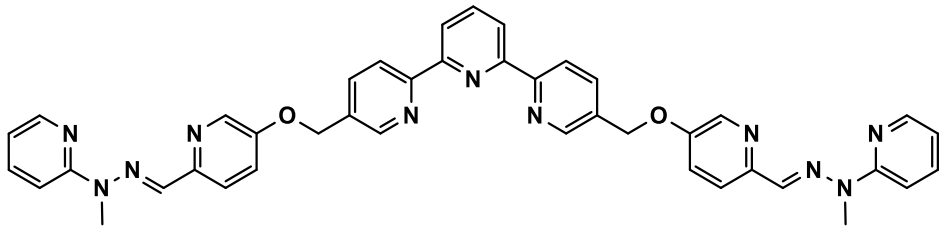

^{1}H NMR (400 MHz, CD_3CN): 8.86 (d, J = 1.7, 2H); 8.69 (d, J = 8.0, 2H); 8.47 (d, J = 7.8, 2H); 8.23-8.20 (m, 2H); 8.15-8.11 (m, 3H); 8.01 (d, J = 8.8, 2H); 7.76 (s, 2H); 7.72-7.69 (m, 4H); 7.60 (dd, J = 2.9, J = 8.9, 2H); 6.90-6.86 (m, 2H); 5.40 (s, 4H); 3.63 (s, 6H);

(MAF10)$_2$Zn$_3$:

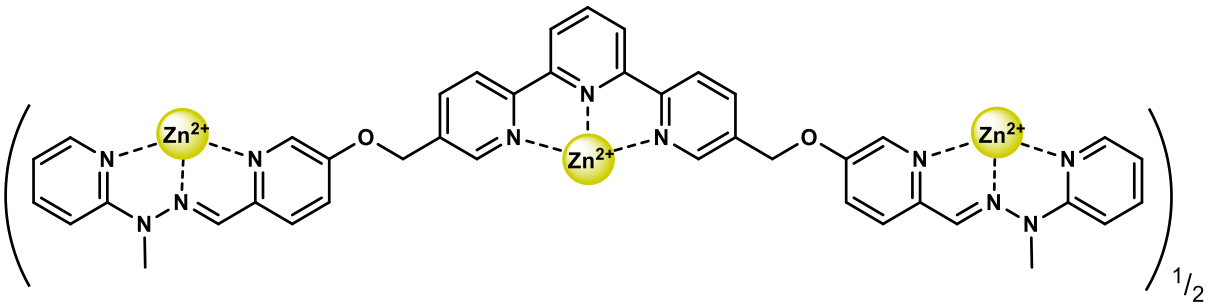

^{1}H NMR (400 MHz, CD$_3$CN): 8.96-8.74 (m, 3H); 8.59 (d, J = 8.2, 2H); 8.51 (s, 2H); 8.09 (dd, J = 1.9, J = 8.3, 2H); 7.96-7.91 (m, 2H); 7.90 (d, J = 8.68, 2H); 7.68-7.66 (m, 2H); 7.43-7.39 (m, 4H); 7.16 (d, J = 2.7, 2H); 7.96-7.93 (m, 2H); 5.27 (d, J = 15.2, 2H); 5.06 (d, J = 15.2, 2H); 3.91 (s, 6H);

(MAF13)$_2$ZnCu$_2$:

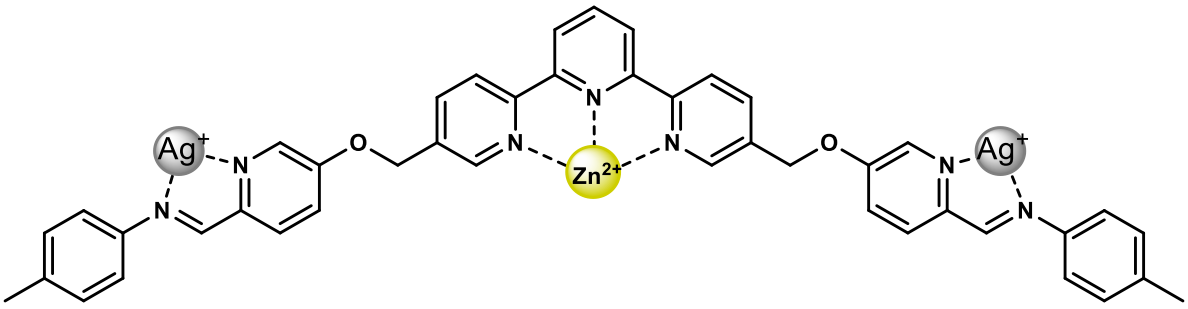

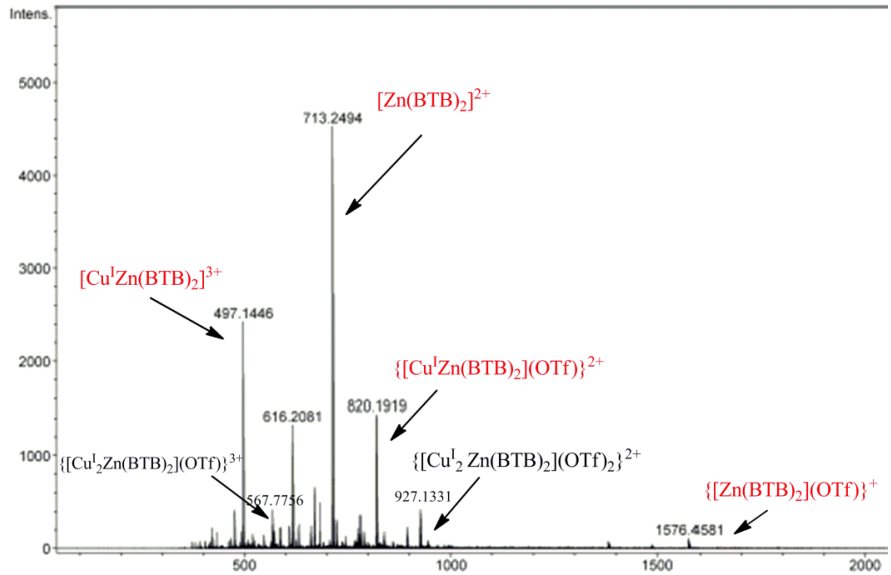

Figure S3.16.: The ESI-MS spectrum of acetonitrile solution of (**MAF13**)$_2$ZnCu$_2$. ((**MAF13**)$_2$Zn(OTf)$_2$Cu$_2$(OTf)$_2$);

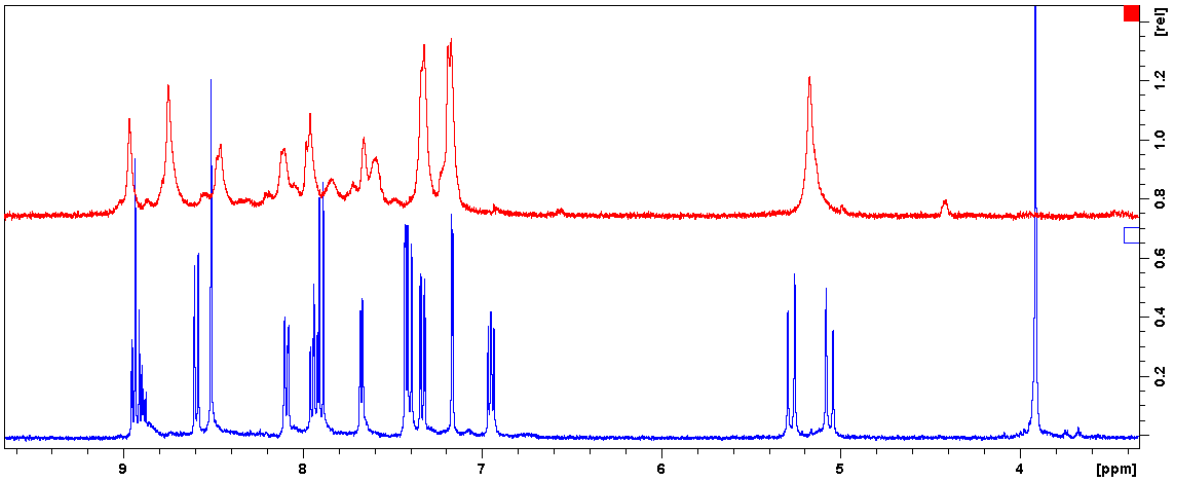

Figure E3.17.: The ^{1}H NMR spectra (CD_3CN) of: **Bottom**: (**MAF13**)$_2Zn_3$ ((**MAF13**)$_2Zn_3(OTf)_6$*);* **Top**: **(MAF13)**$_2ZnCu_2$ ((**MAF13**)$_2Zn(OTf)_2Cu_2(OTf)_2$);

Appendices :

Crystallographic data of determined crystal structures

$(GR9f)_2Zn_2$

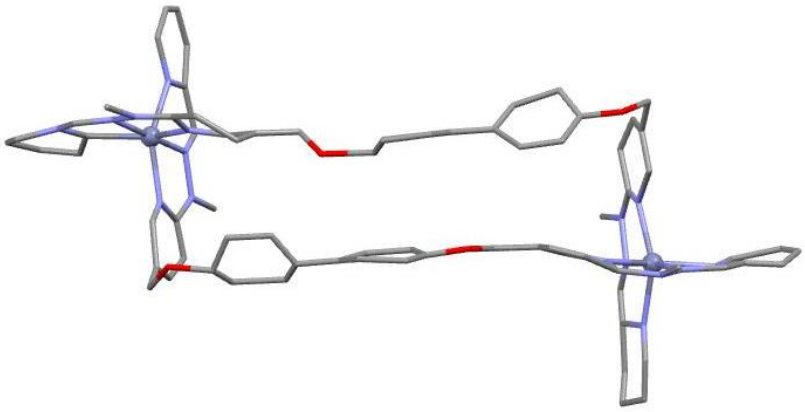

This structure could not be solved due to poor quality of the crystals grown. It has been included in this work as it is nevertheless an experimental proof that a double helicate can be obtained with the corresponding ligand **GR9f**.

(JRHEL7)Zn_2 **[Zn^{II}_2(HEL7)(MeCN)(CF_3SO_3)$_4$]·(MeCN)**

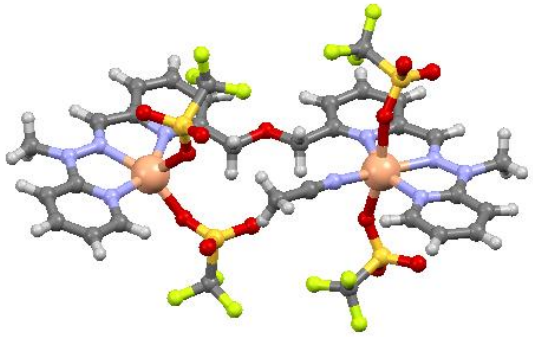

Bond precision: C-C = 0.0044 Å Wavelength = 0.71073

Cell: a = 19.5604(9) b = 15.2149(6) c = 32.8467(14)
α = 90° β = 95.158(1)° γ = 90°

Temperature: 173 K

Volume (Å^3)	9735.9(7)
Crystal system	Monoclinic
Space group	C2/c
Hall group	-C2yc
Moiety formula	$C_{32}H_{29}F_{12}N_9O_{13}S_4Zn_2$, C_2H_3N
Sum formula	$C_{34}H_{32}F_{12}N_{10}O_{13}S_4Zn_2$
M (g.mol^{-1})	1275.72
D (g.cm^{-3})	1.741
Z	8
Mu (mm^{-1})	1.273
F000	5136.0
F000'	5147.71
h,k,l max	25,20,43
Nref	11827
Tmin,Tmax	0.795,0.903
Tmin'	0.683

Correction method = Semi-empirical from equivalents
AbsCorr = Multi-scan

Data completeness = 0.999 Theta(max) = 28.048

R_1 (reflections) = 0.0483 (8744) wR_2 (reflections) = 0.1175 (11816)

S = 1.030 Npar = 698

$(GR9e)_2Zn_2$ **$[Zn^{II}_2(GR9e)_2]\cdot(CF_3SO_3)_4$**

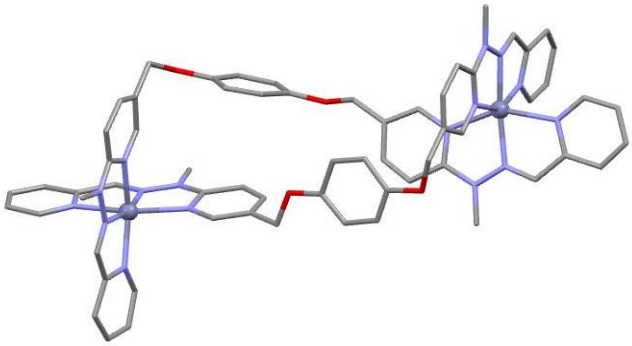

Bond precision: C-C = 0.0253 Å Wavelength = 0.71073

Cell: a = 14.380(3) b = 14.380(3) c = 34.574(7)
α = 90° β = 90° γ = 120°

Temperature: 173 K

Volume (Å^3)	6192(3)
Crystal system	Trigonal
Space group	$P3_221$
Hall group	$P3_22$"
Moiety formula	$C_{64}H_{60}N_{16}O_4Zn_2$, $4(CF_3O_3S)$
Sum formula	$C_{68}H_{60}F_{10}N_{16}O_{14}S_4Zn_2$
M (g.mol^{-1})	1774.34
D (g.cm^{-3})	1.428
Z	3
Mu (mm^{-1})	0.773
F000	2718.0
F000'	2722.58
h,k,l max	18,18,45
Nref	9987

Correction method = Not given
Data completeness = 1.77/0.99 Theta(max) = 28.015
R_1 (reflections) = 0.0856 (4534) wR_2 (reflections) = 0.2424(9853)
S = 0.929 Npar = 510

$(HEL10a)_2Fe_2$ **$[Fe_2(HEL10a)_2]\cdot(CF_3O_3S)_4\cdot(CH_3NO_2)_2$**

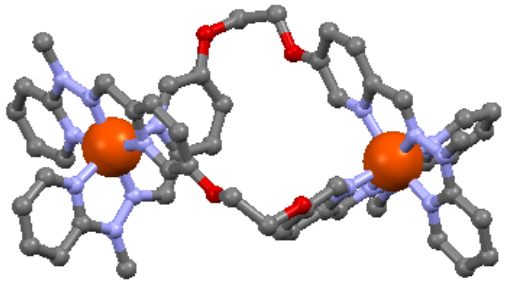

Bond precision: C-C = 0.0141 Å Wavelength = 0.71073

Cell: a = 12.2257(7) b = 14.8578(8) c = 23.7331(13)

α = 97.598(1)° β = 103.210(1)° γ = 98.335(1)°

Temperature: 173 K

Volume ($Å^3$)	4091.0(4)
Crystal system	Triclinic
Space group	P-1
Hall group	-P1
Moiety formula	$C_{52}Fe_2N_{16}O_4$, 3(CF_3O_3S), CF_2O_3S, 2(CH_3NO_2)
Sum formula	$C_{60}F_{12}Fe_2N_{19}O_{20}S_4$
M ($g.mol^{-1}$)	1774.73
D ($g.cm^{-3}$)	1.441
Z	2
Mu (mm^{-1})	0.559
F000	1754.0
F000'	1757.47
h,k,l max	16,19,31
Nref	20002
Tmin,Tmax	0.842,0.902
Tmin'	0.842

Correction method = Semi-empirical from equivalents
AbsCorr = Multi-scan

Data completeness = 0.995 Theta(max) = 28.126

R_1 (reflections)= 0.1775 (12761) wR_2 (reflections)= 0.5016 (19898)

S = 1.955 Npar = 1030

$(HEL10c)_3Fe_2$ **$[Fe_2(HEL10c)_3]\cdot(CF_3O_3S)_4\cdot(CH_3CN)_5$**

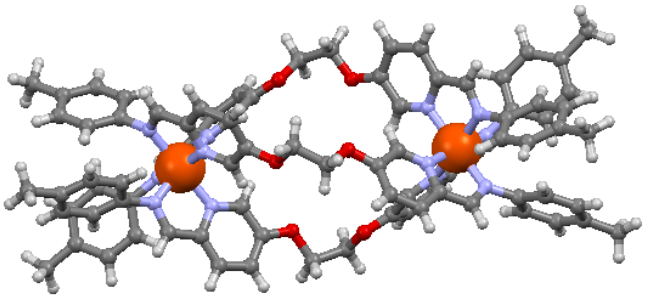

Bond precision: C-C = 0.0066 Å Wavelength = 0.71073

Cell: a = 13.531(3) b = 19.448(4) c = 23.943(5)
α = 98.257(4)° β = 104.362(5)° γ = 91.739(5)°

Temperature: 173 K

Volume (Å^3)	6026(2)
Crystal system	Triclinic
Space group	P-1
Hall group	-P1
Moiety formula	$C_{84}H_{78}Fe_2N_{12}O_6$, 4($CF_3O_3S$), 5($C_2H_3N$)
Sum formula	$C_{98}H_{93}F_{12}Fe_2N_{17}O_{18}S_4$
M (g.mol^{-1})	2264.84
D (g.cm^{-3})	1.248
Z	2
Mu (mm^{-1})	0.393
F000	2336.0
F000'	2339.61
h,k,lmax	18,26,32
Nref	30726
Tmin,Tmax	0.868,0.906
Tmin'	0.822

Correction method = Semi-empirical from equivalents
AbsCorr = Multi-scan

Data completeness = 0.960 Theta(max) = 28.552

R_1(reflections) = 0.0798 (17401) wR_2 (reflections) = 0.2557 (29504)

S = 1.033 Npar = 1341

(CN13)Pb **$[Pb_2(CN13)(CF_3O_3S)_2]\cdot(CH_3Cl)$**

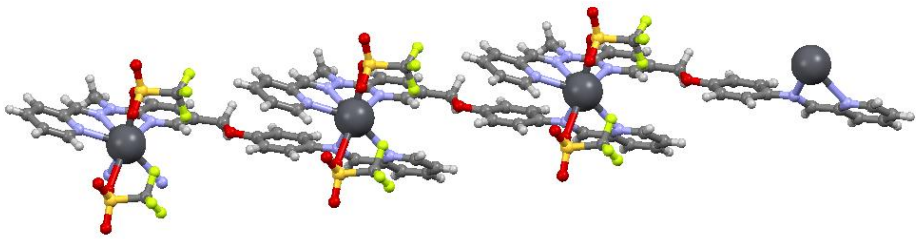

Bond precision: C-C = 0.0050 Å Wavelength = 0.71073

Cell: a = 10.1602(4) b = 11.5923(5) c = 16.0441(7)

α = 72.305(1)° β = 86.855(1)° γ = 82.028(1)°

Temperature: 173 K

Volume (Å^3)	1782.71(13)
Crystal system	Triclinic
Space group	P-1
Hall group	-P1
Moiety formula	$C_{27}H_{22}F_6N_6O_7PbS_2$, $CHCl_3$
Sum formula	$C_{28}H_{23}Cl_3F_6N_6O_7PbS_2$
M (g.mol^{-1})	1047.19
D (g.cm^{-3})	1.951
Z	2
Mu (mm^{-1})	5.159
F000	1016.0
F000'	1011.22
h,k,lmax	13,15,21
Nref	9508
Tmin,Tmax	0.544,0.662
Tmin'	0.353

Correction method = Semi-empirical from equivalents
AbsCorr = Multi-scan

Data completeness = 0.994 Theta(max) = 29.030

R_1reflections) = 0.0279 (8219) wR_2(reflections) = 0.0638 (451)

S = 1.041 Npar = 479

$(AS53)_2Zn_2Cu$ **$[Zn_2Cu(AS53)_2]\cdot(CF_3O_3S)_5\cdot(CH_3CN)_3$**

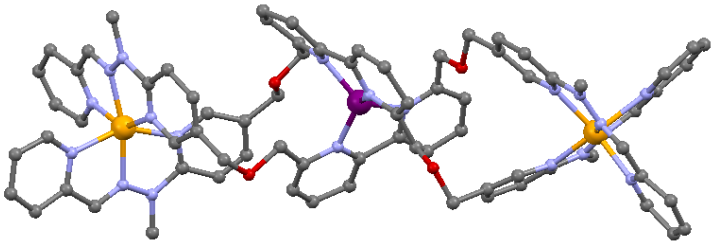

Bond precision: C-C = 0.0127 Å Wavelength = 1.54178

Cell: a = 22.5308(6) b = 15.2122(3) c = 32.8914(9)
α = 90° β = 105.227(2)° γ = 90°

Temperature: 130 K

Volume (Å^3)	10877.5(5)
Crystal system	Monoclinic
Space group	$P2_1/c$
Hall group	-P2ybc
Moiety formula	$C_{76}H_{71}CuN_{20}O_4Zn_2$, 5($CF_3O_3S$), 3($C_2H_3N$)
Sum formula	$C_{87}H_{80}CuF_{15}N_{23}O_{19}S_5Zn_2$
M (g.mol^{-1})	2391.38
D (g.cm^{-3})	1.460
Z	4
Mu (mm^{-1})	2.501
F000	4876.0
F000'	4878.71
h,k,lmax	26,17,38
Nref	17610
Tmin,Tmax	0.511,0.722
Tmin'	0.309

Correction method = Semi-empirical from equivalents
AbsCorr = Integration

Data completeness = 0.946 Theta(max) = 63.052

R_1 (reflections) = 0.0985 (10481) wR_2 (reflections) = 0.2987 (6658)

S = 1.067 Npar = 1342

$(AS53)_4Zn_6$ **$[Zn_6(AS53)_4]\cdot(CF_3O_3S)_{12}\cdot(CH_3CN)_{11}\cdot(C_6H_{14}O)_4$**

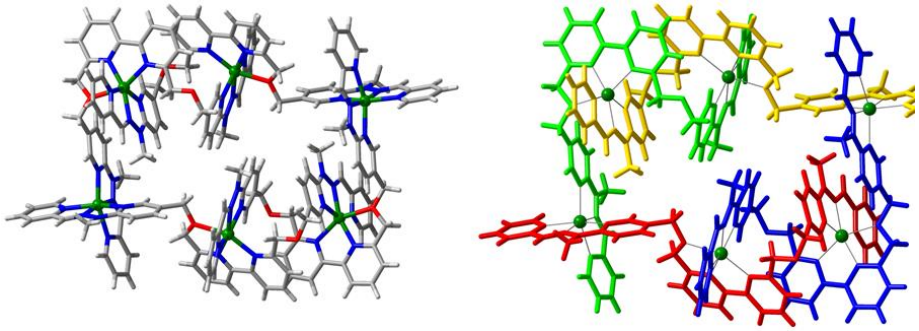

Bond precision: C-C = 0.0100 Å Wavelength = 0.71073

Cell: a = 21.6899(3) b = 25.0840(3) c = 24.4738(3)
α = 90° β = 110.599(1)° γ = 90°

Temperature: 150 K

Volume (Å^3)	12464.1(3)
Crystal system	Monoclinic
Space group	$P2_1/n$
Hall group	-P2yn
Moiety formula	$C_{152}H_{144}N_{40}O_8Zn_6$, 12($CF_3O_3S$), 4($C_6H_{14}O$), 11($C_2H_3CN$)
Sum formula	$C_{210}H_{229}F_{36}N_{51}O_{52}S_{12}Zn_6$
M (g.mol^{-1})	5760.51
D (g.cm^{-3})	1.535
Z	2
Mu (mm^{-1})	0.781
F000	5916.0
F000'	5925.58
h,k,lmax	27,31,31
Nref	26875
Tmin,Tmax	0.816,0.836
Tmin'	0.816

Correction method = Semi-empirical from equivalents
AbsCorr = Integration

Data completeness = 0.978 Theta(max) = 26.880

R_1 (reflections) = 0.0765 (19324) wR_2 (reflections) = 0.2415 (26285)

S = 1.028 Npar = 1506

$(MAF10)_2Zn_3$ **$[Zn_3(MAF10)_2]\cdot(CF_3O_3S)_6\cdot(CH_3CN)_3$**

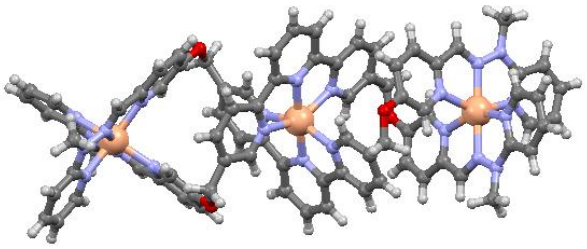

Bond precision: C-C = 0.0101 Å Wavelength = 0.71073

Cell: a = 19.3162(7) b = 42.6419(15) c = 14.3295(5)
α = 90° β = 106.592(1)° γ = 90°

Temperature: 173 K

Volume (Å^3)	11311.5(7)
Crystal system	Monoclinic
Space group	$P2_1/c$
Hall group	-P 2ybc
Moiety formula	$C_{82}H_{70}N_{22}O_4Zn_3$, 6($CF_3O_3S$), 3($C_2H_3N$)
Sum formula	$C_{94}H_{79}F_{18}N_{25}O_{22}S_6Zn_3$
M (g.mol^{-1})	2641.36
D (g.cm^{-3})	1.551
Z	4
Mu (mm^{-1})	0.850
F000	5368.0
F000'	5377.32
h,k,lmax	25,56,18
Nref	27392
Tmin,Tmax	0.815,0.934
Tmin'	0.775

Correction method = Semi-empirical from equivalents
AbsCorr = Multi-scan

Data completeness = 0.999 Theta(max) = 28.033

R_1 (reflections) = 0.0950 (17231) wR_2 (reflections) = 0.2660 (27352)

S = 1.025 Npar = 1460

GR23Zn **$[Zn_4(GR23)_4]\cdot(CF_3O_3S)_8\cdot(CH_3CN)_4$**

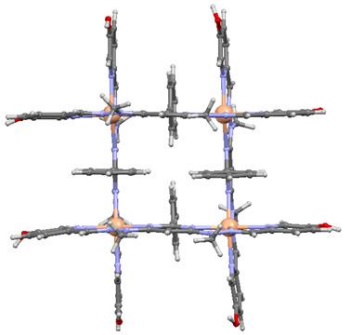

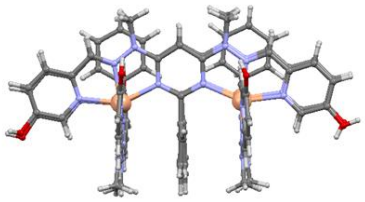

Bond precision: C-C = 0.0121 Å Wavelength = 0.71073

Cell: a = 18.226(8) b = 21.929(9) c = 24.168(10)
α = 93.752(8)° β = 103.191(9)° γ = 111.352(7)°

Temperature: 173 K

Volume (Å^3)	8641(6)
Crystal system	Triclinic
Space group	P-1
Hall group	-P1
Moiety formula	$C_{96}H_{88}N_{32}O_8Zn_4$, 8($CF_3O_3S$), 4($C_2H_3N$)
Sum formula	$C_{112}H_{100}F_{24}N_{36}O_{32}S_8Zn_4$
M (g.mol^{-1})	3436.33
D (g.cm^{-3})	1.321
Z	2
Mu (mm^{-1})	0.741
F000	3488.0
F000'	3494.20
h,k,lmax	24,29,32
Nref	45021
Tmin,Tmax	0.780,0.875
Tmin'	0.743

Correction method = Semi-empirical from equivalents
AbsCorr = Multi-scan

Data completeness = 0.930 Theta(max) = 28.782

R_1 (reflections)= 0.1127 (17113) wR_2 (reflections) = 0.3515 (41854)

S = 0.989 Npar = 1698

GR28Zn(corner) **$[Zn_3(GR28)_2(CH_3CN)_2]\cdot(CF_3O_3S)_{12}\cdot(CH_3CN)_7$**

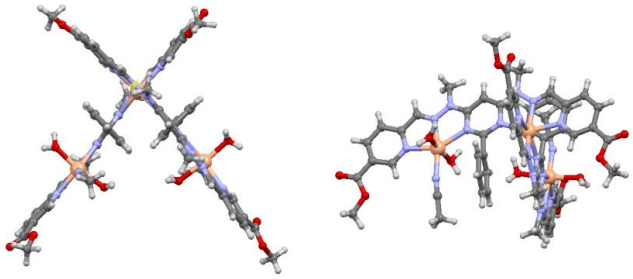

Bond precision: C-C = 0.0119 Å Wavelength = 1.54186

Cell: a = 14.9561(4) b = 17.3331(4) c = 21.9451(5)
α = 86.527(2)° β = 72.532(2)° γ = 72.001(2)°

Temperature: 120 K

Volume (Å^3)	5157.8(2)
Crystal system	Triclinic
Space group	P-1
Hall group	-P1
Moiety formula	2($C_{60}H_{66}N_{18}O_{12}Zn_3$), 12($CF_3O_3S$), 2($C_2H_3N$), 7($C_2H_3N$)
Sum formula	$C_{150}H_{159}F_{36}N_{45}O_{60}S_{12}Zn_6$
M (g.mol^{-1})	5013.29
D (g.cm^{-3})	1.614
Z	1
Mu (mm^{-1})	3.004
F000	2550.0
F000'	2553.92
h,k,lmax	16,19,24
Nref	15539
Tmin,Tmax	0.611,0.637
Tmin'	0.555

Correction method = Semi-empirical from equivalents
AbsCorr = Integration

Data completeness = 0.958 Theta(max) = 60.421

R_1 (reflections) = 0.0787 (10946) wR_2 (reflections) = 0.2327 (14887)

S = 1.088 Npar = 1335

GR67Zn **refinement incomplete**

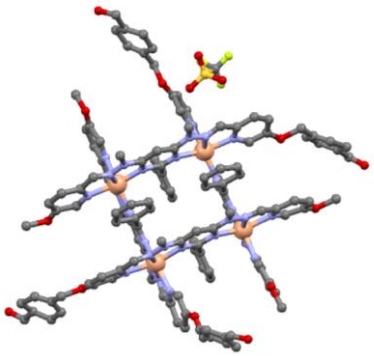

Bond precision: C-C = 0.0339 Å Wavelength = 1.54178

Cell: a = 22.1231(7) b = 40.157(2) c = 42.9782(18)
α = 90° β = 90° γ = 90°

Temperature: 173 K

Volume (Å^3)	38182(3)
Crystal system	Orthorombic
Space group	Fddd
Hall group	-F2uv2vw
Moiety formula	$C_{132}N_{32}O_{12}Zn_4$, 4(CF_3O_3S)
Sum formula	$C_{136}F_{12}N_{32}O_{24}S_4Zn_4$
M (g.mol^{-1})	3083.48
D (g.cm^{-3})	1.073
Z	8
Mu (mm^{-1})	1.594
F000	12192.0
F000'	12194.44
h,k,lmax	26,47,51
Nref	8461
Tmin,Tmax	0.699,0.762
Tmin'	0.394

Correction method = Semi-empirical from equivalents
AbsCorr = Multi-scan

Data completeness = 0.970 Theta(max) = 66.661

R_1 (reflections) = 0.2040 (3893) wR_2 (reflections) = 0.5432 (8205)

S = 1.797 Npar = 479

GR67AgOTf

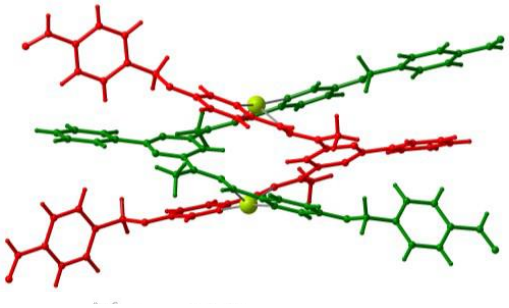

Bond precision: C-C = 0.0087 Å Wavelength = 0.71073

Cell: a = 32.7082(7) b = 19.4524(4) c = 29.0297(7)
α = 90° β = 107.092(2)° γ = 90°

Temperature: 153 K

Volume (Å^3)	17654.5(7)
Crystal system	Monoclinic
Space group	C2/c
Hall group	-C2yc
Moiety formula	$C_{161.60}H_{138.40}Ag_4N_{32.80}O_{16}$, 4($CF_3O_3S$), 5.2($C_2H_3N$)
Sum formula	$C_{176}H_{154}Ag_4F_{12}N_{38}O_{28}S_4$
M (g.mol^{-1})	4037.10
D (g.cm^{-3})	1.519
Z	4
Mu (mm^{-1})	0.579
F000	8240.0
F000'	8231.40
h,k,lmax	42,25,37
Nref	19653
Tmin,Tmax	0.946,0.966
Tmin'	0.870

Correction method = Semi-empirical from equivalents
AbsCorr = Integration

Data completeness = 0.982 Theta(max) = 27.186

R_1 (reflections) = 0.0723 (15198) wR_2 (reflections) = 0.1563 (19299)

S = 1.215 Npar = 1177

GR67ZnHydr **refinement incomplete**

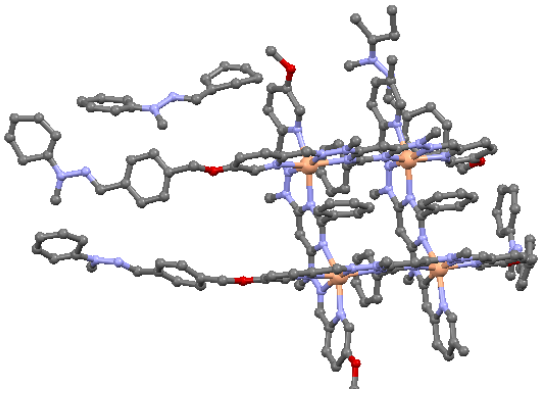

Bond precision: C-C = 0.0417 Å Wavelength = 0.71073

Cell: a = 24.190(5) b = 24.529(5) c = 25.655(5)
α = 112.530(5)° β = 99.319(5)° γ = 98.628(5)°

Temperature: 173 K

Volume (Å^3)	13494(5)
Crystal system	Triclinic
Space group	P-1
Hall group	-P1
Moiety formula	$C_{163}N_{39}O_6Zn_4$, $C_{14}N_2$, CF_3O_3S, 0.5(O_6S_2), CF_2O_2S
Sum formula	$C_{186}F_9N_{43}O_{22}S_7Zn_4$
M (g.mol^{-1})	3845.27
D (g.cm^{-3})	0.946
Z	2
Mu (mm^{-1})	0.464
F000	3812.0
F000'	3817.65
h,k,lmax	32,32,34
Nref	66294

Correction method = Not given

Data completeness = 0.981 Theta(max) = 28.175

R_1 (reflections) = 0.2666 (11775) wR_2 (reflections) = 0.6638 (65055)

S = 1.353 Npar = 1105

GR7eZn **refinement incomplete**

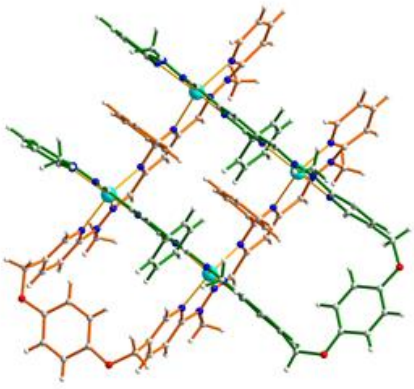

Bond precision: C-C = 0.0129 Å Wavelength = 1.54186

Cell: a = 29.2453(6) b = 19.5477(5) c = 30.1463(6)
α = 90° β = 96.636(2)° γ = 90°

Temperature: 150 K

Volume (Å^3)	17118.5(7)
Crystal system	Monoclinic
Space group	C2/c
Hall group	-C2yc
Moiety formula	$C_{112}H_{100}N_{32}O_4Zn_4$, 8($CF_3O_3S$)
Sum formula	$C_{120}H_{100}F_{24}N_{32}O_{28}S_8Zn_4$
M (g.mol^{-1})	3412.37
D (g.cm^{-3})	1.324
Z	4
Mu (mm^{-1})	2.378
F000	6928.0
F000'	6937.70
h,k,lmax	32,21,33
Nref	12709

Correction method = Not given

Data completeness = 0.980 Theta(max) = 60.000

R_1 (reflections) = 0.1321 (7271) wR_2 (reflections) = 0.3765 (12459)

S = 1.335 Npar = 799

GR7cZn **refinement incomplete**

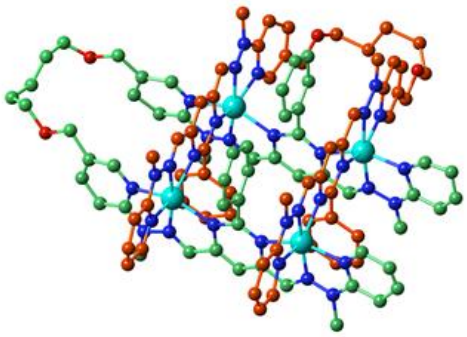

Bond precision: C-C = 0.0409 A Wavelength = 1.54178

Cell: a = 30.7104(16) b = 19.9836(9) c = 24.9340(12)
α = 90° β = 103.273(3)° γ = 90°

Temperature: 173 K

Volume (Å^3)	14893.3(13)
Crystal system	Monoclinic
Space group	C2/c
Hall group	-C2yc
Moiety formula	$C_{110}N_{32}O_4Zn_4$, 4(CF_3O_3S)
Sum formula	$C_{114}F_{12}N_{32}O_{16}S_4Zn_4$
M (g.mol^{-1})	2691.26
D (g.cm^{-3})	1.200
Z	4
Mu (mm^{-1})	1.925
F000	5312.0
F000'	5310.14
h,k,lmax	36,23,29
Nref	13068
Tmin,Tmax	0.566,0.857
Tmin'	0.440

Correction method = Not given

Data completeness = 0.986 Theta(max) = 66.337

R_1 (reflections) = 0.3002 (5196) wR_2 (reflections) = 0.6971 (12891)

S = 2.392 Npar = 741

GR50AB-Z **refinement incomplete**

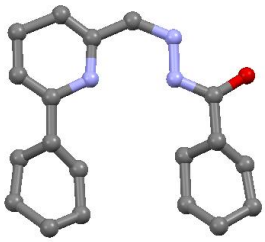

Bond precision: C-C = 0.0251 Å Wavelength = 0.71073

Cell: a = 34.916(4) b = 10.8433(14) c = 7.7682(10)
α = 90° β = 90.162(3)° γ = 90°

Temperature: 173 K

Volume (Å^3)	2941.1(6)
Crystal system	Monoclinic
Space group	$P2_1/c$
Hall group	-P2ybc
Moiety formula	$C_{66}N_6O_2$, 2($C_{27}N_3O$)
Sum formula	$C_{120}N_{12}O_4$
M (g.mol^{-1})	1673.32
D (g.cm^{-3})	1.890
Z	2
Mu (mm^{-1})	0.119
F000	1672.0
F000'	1672.70
h,k,lmax	46,14,10
Nref	7137
Tmin,Tmax	0.980,0.986
Tmin'	0.964

Correction method = Not given

Data completeness = 0.994 Theta(max) = 28.023

R_1 (reflections) = 0.2622 (4794) wR_2 (reflections) = 0.6414 (7096)

S = 2.726 Npar = 274

Jan HOLUB

Generation of Coordination Architectures from Dynamic Covalent Ligand Libraries

Résumé

La Chimie Dynamique Combinatoire basée sur les liaisions imines (-C=N-), avec l'aide de la chimie de coordination, donne accès à différentes types d'architectures metallosupramoléculaires et de réseaux dynamiques fonctionnels. Le travail effectué au cours de cette thèse traite de ces deux aspects. Dans un premier temps des structures de types grilles moléculaire et de type hélicate ont été synthétisés, à l'aide de métaux donnant une coordination octahédrale ou tétraédrale, et leurs propriétés dans un environnement dynamique ont été étudiées. Dans un deuxième temps des réseaux dynamiques, présentant des relations agoniste/antagoniste à travers l'échange des constituants aldéhydes et amines/hydrazines réseau, ont été étudiés. Ces systèmes permettent, à travers l'amplification d'un ou plusieurs constituants, une rééquilibration du réseau permettant l'implémentation de fonction tel que l'apprentissage et la prise de décision pour ces systèmes chimiques adaptifs. Un nouveau système, est présenté et étudié ici, permettant une redistribution stable même après le retrait du stimuli métallique (ajout/retrait d'un métal), permettant à ce système de réaliser un processing d'information : apprentissage, stockage, rappel et effacement.

Mots-clés: Chimie Dynamique Covalente, Imine, Grilles, Helices, Système Responsive, Hydrazone

Résumé en anglais

Dynamic Combinatorial Chemistry of imine-based dynamic covalent bonds (-C=N-), under the governance of coordination chemistry, can lead to different matallosupramolecular architectures and responsive functional systems. In this work these two aspects have been approached. Grids and helicates architectures based on aldehydes and amines/hydrazines backbones have been synthesised, in order to probe their behaviour in a dynamic network environment, using both octahedral and tetrahedral coordinating metal cations. Dynamic systems can be also represented by dynamic networks that define agonistic and antagonistic relationships between different constituents linked through component exchange. These networks can be switched through amplification of the best fittest constituent(s) in a dynamic set, allowing to access higher level functions such as training, learning, and decision making for adaptive chemical systems. A novel multi responsive system, able to be trained for information storage, has been studied, exhibiting a stable distribution even after removal of the metal stimuli, making this system able to perform information processing operations: training, storage, recall, and erase.

Keywords: Dynamic Covalent Chemistry, Imine, Grid, Helicate, Responsive system, Hydrazone